University of Southampton
Faculty of Natural and Environmental Sciences

Structural studies on the interaction between eukaryotic elongation factor 2 kinase (eEF2K) and calmodulin (CaM)

Kelly Hooper

Thesis for the Degree of Doctor of Philosophy

June 2015

UNIVERSITY OF SOUTHAMPTON

ABSTRACT

FACULTY OF NATURAL AND ENVIRONMENTAL SCIENCES

Biological Sciences

Doctor of Philosophy

Structural studies on the interaction between eukaryotic elongation factor 2 kinase (eEF2K) and calmodulin (CaM)

Kelly Hooper

Eukaryotic elongation factor 2 kinase (eEF2K) critically regulates translation elongation by controlling the activity of eEF2, which catalyses the translocation reaction of the ribosome. eEF2K phosphorylates eEF2 and prevents its binding to the ribosome to inhibit translation elongation.

eEF2K is activated by elevated Ca^{2+} levels via calmodulin (CaM), although the molecular mechanism of activation is not understood. A conserved region at the N-terminus of eEF2K has been shown to be a key interaction site for CaM.

A peptide corresponding to the CaM binding region of eEF2K ($eEF2K_{82-100}$) as well as longer eEF2K fragments to represent the full-length protein have been studied to dissect the molecular mechanism of eEF2K activation by Ca^{2+}/CaM. Nuclear magnetic resonance (NMR) spectroscopy has been used to determine the binding site and the mechanism of peptide recognition and the three-dimensional solution structure of the Ca^{2+}/CaM: $eEF2K_{82-100}$ complex has been elucidated. These investigations revealed important roles for particular residues within the CaM binding region of eEF2K and in CaM itself and also resulted in a model for eEF2K activation that involves residues in the kinase domain, as well as the CaM binding region. The elucidation of this protein complex structure provides a vital tool in the study of eEF2K function, critical in cancer biology.

Table of Contents

List of Figures

List of Tables

Academic Thesis: Declaration of Authorship

I, Kelly Hooper

declare that the thesis entitled "Structural studies on the interaction between eukaryotic elongation factor 2 kinase (eEF2K) and calmodulin (CaM)" and the work presented in the thesis are both my own, and have been generated by me as the result of my own original research. I confirm that:

- this work was done wholly or mainly while in candidature for a research degree at this University;
- where any part of this thesis has previously been submitted for a degree or any other qualification at this University or any other institution, this has been clearly stated;
- where I have consulted the published work of others, this is always clearly attributed;
- where I have quoted from the work of others, the source is always given. With the exception of such quotations, this thesis is entirely my own work;
- I have acknowledged all main sources of help;
- where the thesis is based on work done by myself jointly with others, I have made clear exactly what was done by others and what I have contributed myself;
- parts of this work have been published as:

XIE, J., MIKOLAJEK, H., PIGOTT, C. R., HOOPER, K. J., MELLOWS, T., MOORE, C. E., MOHAMMED, H., WERNER, J. M., THOMAS, G. J. & PROUD, C. G. 2015. Molecular Mechanism for the Control of Eukaryotic Elongation Factor 2 Kinase by pH: Role in Cancer Cell Survival. *Molecular and Cellular Biology,* 35**,** 1805-24.

Signed: ……..

Date:……..

Acknowledgements

Firstly, I would like to thank Joern Werner for his supervision throughout this project and for his advice and knowledge along the way. I would also like to thank Chris Proud for his continued support and for introducing me to the project.

Thanks goes to Geoff Kelly, Alain Oregioni and Tom Frenkiel at the MRC Biomedical NMR centre at the National Institute for Medical Research (Mill Hill, London) for access to NMR time on the 700 and 950 MHz spectrometers, as well as their help and guidance. Also to Dmitri Svergun and Peter Konarev for the chance to collect SAXS data at the DORIS III beamline (PETRA III storage ring) at Deutsches Elektronen-Synchrotron (DESY), EMBL in Hamburg. I would also like to thank Matt Crump and Chris Williams from the University of Bristol for advice on using Aria for NMR structure calculation.

My biggest thank you goes to Halina Mikolajek for her continual help, advice and support– we got through it together in the end! Without her I don't think this would have been possible. Another big thank you is owed to Stuart Findlow for his (almost) limitless amount of patience with me – you can have some peace now! I would also like to thank all members of the structural biology groups past and present for making the last three years so enjoyable, especially Louise Bolton, Curtis Phippen, Matt Rodrigues and Andy Hutchin.

To all the great friends I have met along the way, thank you! And another thank you to all my friends and family who have both listened in sympathy when it all went wrong and celebrated with me when it started going right - even though they had no idea what I was going on about most of the time!

My last special thank you goes to my family and my fiancé Michael Buggy for putting up with the ups and downs over the last few years – I couldn't have done it without you all.

Abbreviations

ATP	Adenosine triphosphate
CaM	Calmodulin
CaMK	Calmodulin kinase
ChaK	Channel kinase
CSP	Chemical shift perturbation
eEF	Eukaryotic elongation factor
eEF2K	Eukaryotic elongation factor 2 kinase
ePK	Eukaryotic protein kinase
EF	Edema factor
GTP	Guanosine triphosphate
GDP	Guanosine diphosphate
ITC	Isothermal titration calorimetry
MST	Microscale thermophoresis
MHCK A	Myosin heavy chain kinase A
MLCK	Myosin light chain kinase
mTOR	Mammalian target of rapamycin
mRNA	Messenger ribonucleic acid
NMR	Nuclear magnetic resonance
PKA	Protein kinase A
P_i	Phosphate
PRE	Paramagnetic relaxation enhancement
RDC	Residual dipolar couplings
RMSD	Root mean squared deviation
SAXS	Small angle X-ray scattering
tRNA	Transfer ribonucleic acid

Chapter 1. Introduction and Literature Review

1.1 Motivation

This project focuses on a protein involved in the regulation of protein synthesis known as eukaryotic elongation factor 2 kinase (eEF2K). It is an atypical protein kinase (Redpath et al., 1996) that is classed as an α-kinase due to the presence of an α-kinase catalytic domain (Ryazanov et al., 1997). eEF2K is a major regulator of translation elongation (Redpath et al., 1993) and as such plays a vital role in the cell. As a consequence of its involvement in protein synthesis, eEF2K has been implicated in some cancers (Wu et al., 2006, Parmer et al., 1999, Bagaglio et al., 1993) and is thought to be a potential target for cancer intervention. It is regulated by a number of key signalling pathways and kinases that phosphorylate eEF2K to result in its activation or inactivation depending on the needs of the cell (Browne et al., 2004, Browne and Proud, 2004, Knebel et al., 2001).

The eEF2K protein is currently the focus of investigations to determine how it regulates translation, how it in turn is regulated and its interactions with substrate. There has been substantial progress in examining the intricacies of eEF2K regulation through biochemical analysis (Pigott et al., 2012, Browne et al., 2004, Browne and Proud, 2004, Pyr Dit Ruys et al., 2012).

It is known that Ca^{2+}/CaM must bind to eEF2K to produce an active kinase that can phosphorylate substrate (Redpath et al., 1996). However, the molecular details of this interaction including the recognition, binding and subsequent activation processes are less studied and thus remain largely unknown. This interaction is especially interesting in terms of a mechanism of CaM: target interactions as eEF2K contains a non-canonical (Rhoads and Friedberg, 1997) CaM recognition sequence that is not recognised as a conventional CaM target by sequence databases (Pigott et al., 2012).

The structural details of this interaction are vital to determining the mechanism of activation of eEF2K and consequently a possible intervention point for selectively controlling this kinase in cancer treatment. Targeting eEF2K is beneficial due to the fact that it contains an unusual α-kinase domain, rather than a conventional kinase domain, which is shared between all other

kinases throughout the proteome. Further work would be needed to ensure that only eEF2K in cancer cells is specifically targeted, as it is a vital protein in normal cell physiology. Specific drug delivery methods may be useful, especially in terms of glioblastoma and breast cancer. It is hoped that development of an eEF2K inhibitor, or a compound that affects eEF2K's mechanism of action in some other way, will be beneficial in the treatment of cancer. The ability to target eEF2K therefore represents an unmet medical need. In addition, studying this system will provide insight into what is likely to be a rare mechanism of CaM: target recognition and binding.

1.2 Aims

The aim of this project was to gain structural insight into the interaction between Ca^{2+}/CaM and eEF2K and understand how this results in the activation of eEF2K. Further, we have investigated this interaction in terms of an unusual mechanism of CaM: target recognition. Biophysical techniques including isothermal titration calorimetry (ITC), small angle X-ray scattering (SAXS) and solution nuclear magnetic resonance (NMR) spectroscopy, were used to study the binding of CaM to eEF2K and to address the questions surrounding the mechanism of activation and regulation of eEF2K by CaM.

1.3 Experimental strategy

A short peptide corresponding to the CaM binding region of eEF2K (residues 82-100) was employed to investigate the interaction between eEF2K and CaM using NMR and also to study the structure of CaM bound to $eEF2K_{82-100}$. This, rather than full-length eEF2K, was used for NMR studies because it is much smaller and therefore suitable for solution phase structural studies.

In addition, eEF2K fragments have been developed using a parallel cloning technique. These fragments differ in length and so contain different regions of the protein, thus varying in the functional domains they contain. They are used to investigate the precise roles of the different domains and the effects they have on the activity and function of the protein, especially the binding of CaM to eEF2K and the way in which Ca^{2+} modulates this interaction and elicits activation of eEF2K. In this way we can study the molecular mechanism that governs the activation of eEF2K.

1.4 Ca^{2+} signalling and calmodulin

1.4.1 Ca^{2+} signalling

Ca^{2+} is an essential element for cells to carry out many biological functions and as such has a unique role in cell signalling. It is able to fulfil this unique role because the intracellular Ca^{2+} concentration is extremely low, approximately 10^{-7} M, compared to the extracellular concentration, which is 10^4 times higher (Chin and Means, 2000). As a result, the influx of Ca^{2+} ions in response to certain stimuli has a significant influence on the cell and so is an extremely effective method of transmitting signals and causing cellular effects.

Ca^{2+} is often described as a universal but extremely versatile intracellular signal as a result of the fact that numerous and varied cellular processes are controlled by the simple action of an increase in concentration of a single ion. This is possible as cells can make use of many signalling components, termed the Ca^{2+} signalling toolkit, which can be assembled in different combinations to create a vast range of spatial and temporal Ca^{2+} signals that can regulate diverse cellular processes. There are four functional units involved in a calcium signalling event. Firstly, signalling is triggered by a stimulus that generates Ca^{2+} mobilising signals, which activate mechanisms that cause Ca^{2+} to enter the cytoplasm. Upon entering the cell, or as a result of release from intracellular stores, Ca^{2+} binds to Ca^{2+} binding proteins, which then go on to affect numerous Ca^{2+} sensitive cellular processes. To complete the signal, there are off mechanisms, such as pumps and exchangers, which remove the excess Ca^{2+} from the cytoplasm to restore the cells resting state. These four components of the Ca^{2+} signalling network and their identities within a cell are demonstrated in Figure 1 (Berridge et al., 2000).

Critical to this process of Ca^{2+} signalling is the ability of Ca^{2+} binding proteins to translate the information from transient Ca^{2+} signals into the desired cellular outcome. Some of these proteins, such as protein kinase C, are directly bound by Ca^{2+} for regulation whilst others act as second messengers or intermediaries to couple the Ca^{2+} signals to the desired cellular or biochemical change. These proteins may respond to Ca^{2+} binding by functioning as Ca^{2+} buffers or Ca^{2+} transporters and thus not undergoing any significant

conformational change, as is the case for parvalbumin and calbindin. Conversely, another group of these proteins, which includes calmodulin and troponin C, experience a Ca^{2+} induced conformational change upon binding. This results in them being able to recognise their own target proteins and consequently induce the necessary cellular response (Chin and Means, 2000).

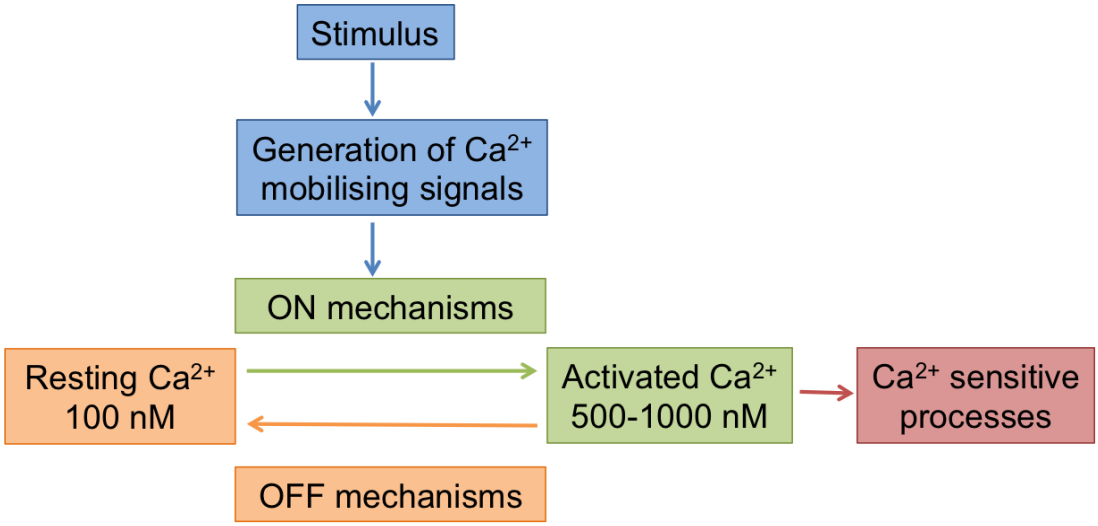

Figure 1. Components of the Ca^{2+} signalling network.
Stimuli act to generate Ca^{2+} mobilising signals (blue) that act on various ON mechanisms to trigger an increase in the intracellular concentration of Ca^{2+} (green). The increased level of Ca^{2+} stimulates various Ca^{2+} sensitive processes to trigger many different cellular pathways (pink). The response is terminated by OFF mechanisms that restore the resting levels of Ca^{2+} (orange). Figure adapted from (Berridge et al., 2000)

1.4.2 Role of calmodulin

CaM is a vital molecule within all eukaryotic cells that has significant roles in signalling pathways involved in the regulation of many of the crucial cellular processes concerned with growth, proliferation and movement. It acts as an intracellular Ca^{2+} sensor or Ca^{2+} binding protein to translate Ca^{2+} signals into a necessary biochemical change. CaM is one of the most prominent and well-studied Ca^{2+} binding proteins and is the first responder to a Ca^{2+} signal.

A transient rise in Ca^{2+} within a cell results in the binding of four Ca^{2+} ions to CaM. The affinities of each of these binding events has a K_d of $5x10^{-7}$ M to $5x10^{-6}$ M, which is within the range of intracellular Ca^{2+} concentrations (10^{-7}-10^{-6} M). If the affinity was much higher than this ($K_d<10^{-7}$ M) then the protein would act as a Ca^{2+} buffer and sequester any excess Ca^{2+}, whilst if the affinity

was much lower (K_d>10^{-5} M) then the protein would be unable to detect Ca^{2+} changes in the relevant range and so could not function as a Ca^{2+} binding protein. The binding of Ca^{2+} to CaM results in drastic conformational changes that results in the release of substantial free energy and the ability of CaM to convert the Ca^{2+} binding event into biochemical processes (Chin and Means, 2000). The details surrounding this conformational change and how this signal is translated into a downstream effect will be discussed in the following sections.

The availability and localisation of CaM are also important during a Ca^{2+} signalling event. CaM constitutes at least 0.1% of the total protein within a cell (Chin and Means, 2000), with rapidly growing cells expressing even higher concentrations. However, it has been estimated that the total concentration of CaM-binding proteins is approximately 2-fold higher than the total concentration of CaM in cells (Persechini and Cronk, 1999, Sanabria et al., 2008). The formation of CaM complexes with target proteins occurs throughout the cell as there are cytosolic, nuclear and membrane proteins that can bind CaM in both its Ca^{2+}-bound and Ca^{2+}-free forms., and these interactions of CaM with its target proteins affect its mobility through the cytoplasm (Lubyphelps et al., 1995, Kim et al., 2004). For example, a CaM-binding protein termed regulator of CaM signaling (RCS) can increase its affinity for CaM when phosphorylated and act as a competitive inhibitor of other CaM-activated enzymes (Rakhilin et al., 2004). CaM can therefore be thought of as limiting in its role as a messenger. The generally accepted model is that CaM is sequestered by its targets in basal conditions and Ca^{2+} signals activate downstream targets to which CaM is already bound or redistribute it to nearby targets with higher affinity for the Ca^{2+}-saturated form of CaM.

1.4.3 Structure of calmodulin

CaM is a relatively small molecule of 148 amino acid residues and approximately 17 kDa. It contains four EF-hand motifs to which Ca^{2+} ions bind. An EF-hand motif consists of two perpendicularly arranged α-helices joined by an interhelical loop, which is able to form a single Ca^{2+} binding site that binds one Ca^{2+} ion (Ikura, 1996). The loop of the EF-hand motif consists of twelve

residues, five of which contribute directly to providing oxygen ligands to the Ca^{2+} ion whilst the remaining atoms provide hydrogen bonding via the backbone and side chain NH groups to stabilise the geometry of the loop. This results in coordination of the Ca^{2+} ion by seven oxygen atoms in a pentagonal bipyrimidal configuration, as shown in Figure 2. A single oxygen atom from the amino acid residues at positions X, Y, Z and –Y, as well as two oxygen atoms from the residue at position –Z, contribute to the coordination of the Ca^{2+} ion. In addition, a water molecule located at position –X completes the coordination sphere (Strynadka and James, 1989, Waltersson et al., 1993, Biekofsky et al., 1998). In addition, the residues adjacent to these coordinating residues are key and also often highly conserved in terms of the two glycine residues either side of the aspartate or asparagine residue at position Z. These enable the correct positioning of the coordinating residues to enable the binding of Ca^{2+} by creating a loop due to the fact that glycine has the smallest side chain. Although these glycine residues do not contact the Ca^{2+} ion, they are critical for successful Ca^{2+} binding and demonstrate how well optimised and "perfectly designed" CaM is.

(A)

	X		Y		Z		-Y		-X			-Z
I	20											31
	ASP	LYS	ASP	GLY	ASP	GLY	THR	ILE	THR	THR	LYS	GLU
II	56											67
	ASP	ALA	ASP	GLY	ASN	GLY	THR	ILE	ASP	PHE	PRO	GLU
III	93											104
	ASP	LYS	ASP	GLY	ASN	GLY	THR	ILE	SER	ALA	ALA	GLU
IV	129											140
	ASP	ILE	ASP	GLY	ASP	GLY	GLN	VAL	ASN	TYR	GLU	GLU

(B)

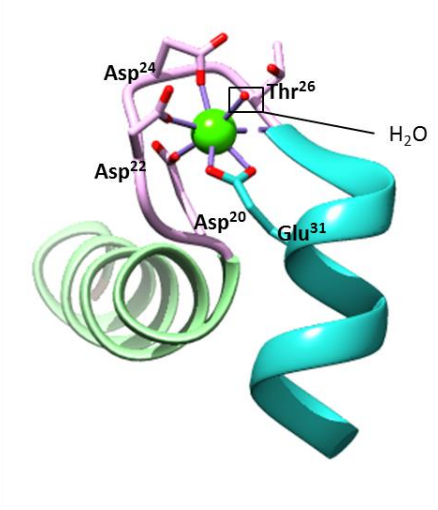

Figure 2. Ca^{2+} coordination by the four Ca^{2+} binding sites in CaM.
Amino acid sequences of the four Ca^{2+} binding sites in CaM (A) and the location and positioning of the coordinating residues from the first Ca^{2+} binding site of CaM (B). The residues responsible for Ca^{2+} coordination are shown in red in (A) and are indicated on the structure of the first Ca^{2+} binding site of CaM in (B). This site consists of helix A (green), the interconnecting loop (pink) and helix B (blue) to form the first EF-hand motif. PDB ID: 1CLL. (A) is adapted from (Waltersson et al., 1993).

Two EF-hand motifs form an N-terminal domain, with low affinity sites for Ca^{2+}, whilst the other two combine to form a C-terminal domain with high affinity for Ca^{2+}. The C-terminal domain of CaM has a 3-5 fold higher affinity for Ca^{2+} than the N-terminal domain of CaM, providing cooperativity for Ca^{2+} binding and additional discrimination for Ca^{2+} recognition for the concentrations of Ca^{2+} within the cell (Chin and Means, 2000). These two globular domains are connected by a short linker, which in the crystal structure

is alpha helical but which solution data has shown to be flexible (Barbato et al., 1992). The structure of Ca^{2+}/CaM is shown in Figure 3.

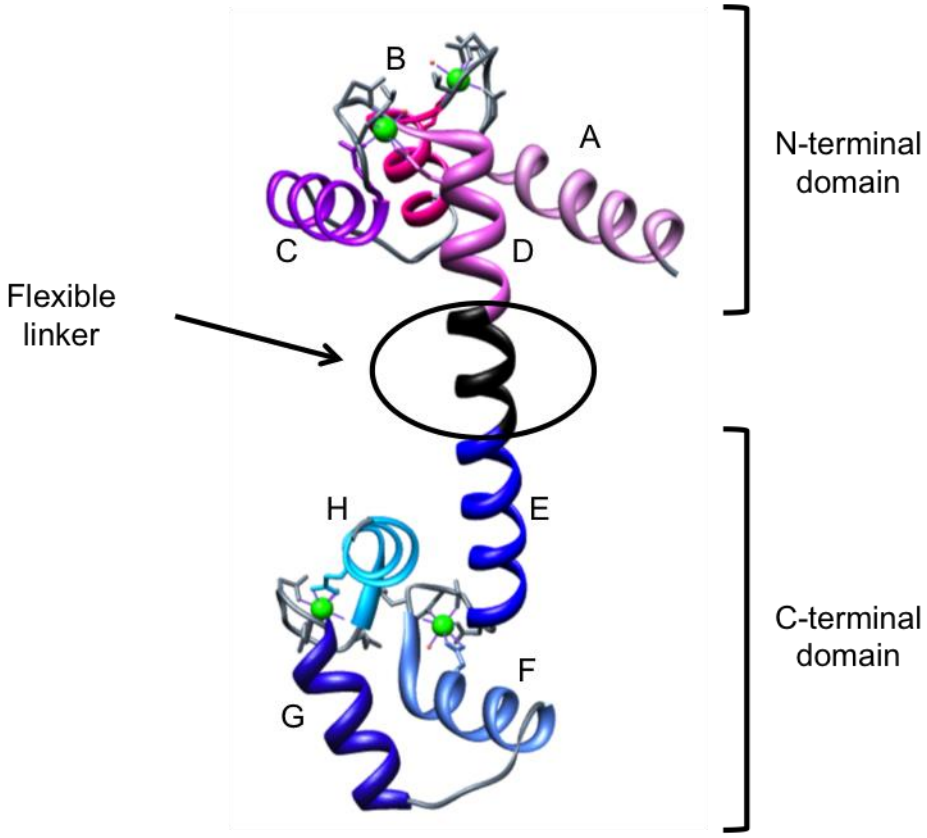

Figure 3. Structure of Ca^{2+}/CaM solved by X-ray crystallography.
An N-terminal globular domain (pinks), containing two EF-hand motifs is linked to a C-terminal globular domain (blues) containing a further two EF-hand motifs. Each domain binds to two Ca^{2+} ions (green). In the crystal structure the two domains are connected by a long α-helix (the central helix) however residues 77-81 (black) have been shown by data from solution NMR to be non-helical and flexible. PDB ID: 1CLL (solved by X-ray crystallography).

The structure of CaM has been determined in both the Ca^{2+} bound (Ca^{2+}/CaM) and Ca^{2+} free (apo-CaM) states. Solution NMR was used to solve the structure of apo-CaM (Zhang et al., 1995) due to its flexible nature whilst X-ray crystallography was suitable for elucidation of the Ca^{2+}/CaM structure (Babu et al., 1985). There are a number of major differences in the arrangement of the helices between the two structures; however, their secondary structure is essentially identical. They both contain two globular domains consisting of four α-helices (A, B, C and D in the N-terminal domain and E, F, G and H in the C-terminal domain) and a short antiparallel β-sheet. Solution data including

secondary chemical shifts of $^{13}C_{\alpha}$ atoms, backbone amide hydrogen exchange experiments (Spera, 1991) and circular dichroism studies suggest that apo-CaM has higher flexibility than Ca^{2+}/CaM and is described as having a highly dynamic nature (Yamniuk and Vogel, 2004).

The major differences between the two structures of CaM are due to significant changes in helix packing and arrangement. In apo-CaM the two helices of each EF-hand are arranged in an almost antiparallel configuration but upon Ca^{2+} binding this changes to an almost perpendicular arrangement as shown in Figure 4 (Zhang et al., 1995). Therefore, it seems that upon Ca^{2+} binding, there is significant structural rearrangement causing specific and dramatic changes to the domain structures and organization due to alterations in the interhelical angles of the EF-hand motifs (Chin and Means, 2000).

The antiparallel organisation of the helices in apo-CaM results in this structure being described as adopting a 'closed' conformation, whilst Ca^{2+}/CaM is described as being in an 'open' conformation. Comparison studies of the structures of Ca^{2+}/CaM and apo-CaM by M.B. Swindells and M. Ikura further identified the C-terminal domain of apo-CaM as being in a 'semi-open' state, independent of any interactions with Ca^{2+} or target peptide. This demonstrated that the N- and C-terminal domains of CaM respond in different ways to the loss and gain of Ca^{2+} and may also explain the difference in Ca^{2+} affinities between the two domains (Swindells and Ikura, 1996).

The differences in structures as shown by NMR and X-ray crystallography are also shown by small angle X-ray scattering (SAXS) studies on CaM. These demonstrate that in the presence of $Ca^{2+,}$ CaM exists as an elongated molecule, whilst in the absence of Ca^{2+}, the CaM molecule is shorter (Seaton et al., 1985).

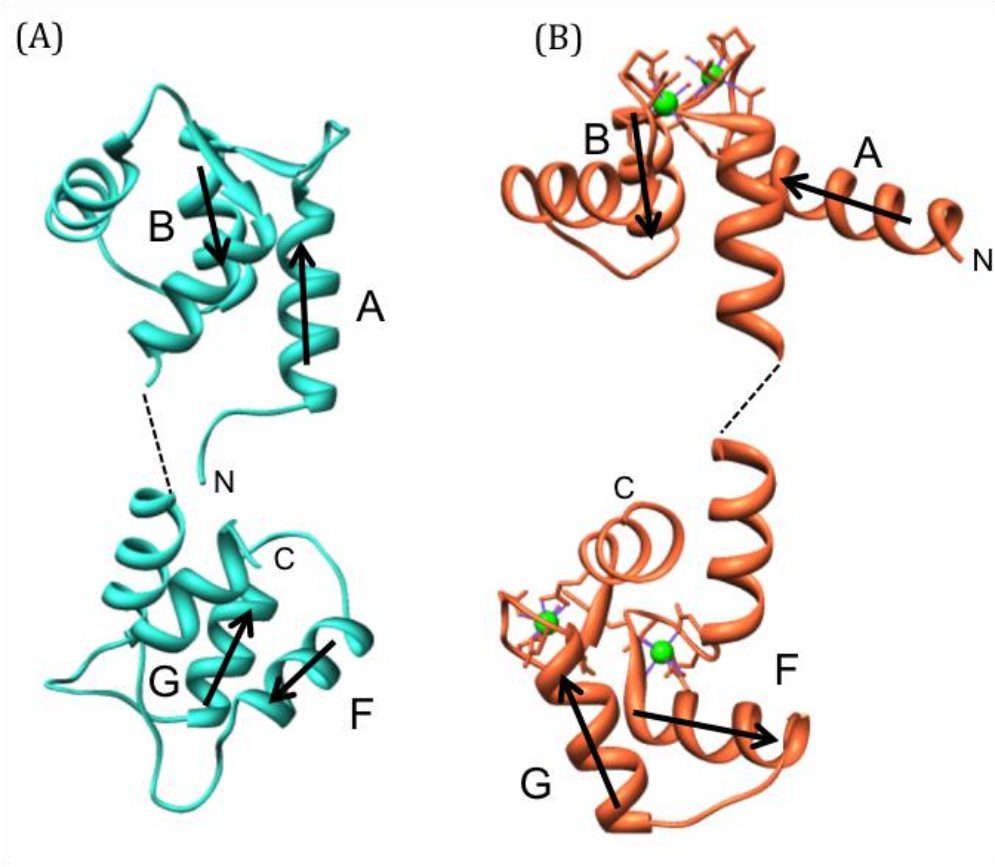

Figure 4. Structural differences between apo-CaM and Ca^{2+}/CaM .
Solution structure of apo-CaM (PDB ID: 1CFD) (A) and crystal structure of Ca^{2+}/CaM (PDB ID: 1CLL) (B). Arrows demonstrate the change in orientation and arrangement of helices A and B in the N-terminal domain and helices F and G in the C-terminal domain. The flexible linker has been removed for clarity and replaced with a dotted line.

1.4.4 Calmodulin target recognition

Once CaM has bound Ca^{2+} ions and undergone conformational change it is able to translate this into a biochemical event that affects cellular processes. One of the key methods through which CaM does this is to bind to target proteins to affect them and influence signalling pathways in this manner. It does this by recognizing and binding certain motifs in target proteins. There are a large number of diverse proteins that CaM can interact with and regulate, although the interactions between CaM and Ca^{2+}/CaM-dependent protein kinases are particularly well characterized and understood.

Structural studies of the interaction between CaM and target peptides often results in a classic wraparound structure. The two domains of CaM are both involved in the interaction as the central flexible linker bends in a hinge-

like manner, allowing the two globular domains to come close together and engulf the CaM binding region (Meador et al., 1992). The structural details of CaM in complex with target peptides and proteins will be discussed in detail in sections 1.4.4.2 and 1.4.4.3.

There are two main methods of describing the mechanism by which CaM binds to target proteins. Initially, theories were put forward involving static structures that are influenced by conformational switches to trigger biological responses. According to this explanation, conformational changes in CaM that occur upon Ca^{2+} binding facilitate its interaction with biological targets. The movement of helices and structural rearrangement within the domains leads to the exposure of hydrophobic patches on the surface of CaM, which are buried in apo-CaM (Ikura, 1996, Zhang et al., 1995, Kuboniwa et al., 1995). The interhelical angles in each EF-hand become large resulting in the formation of deep clefts in each domain, lined with hydrophobic residues. These hydrophobic patches are responsible for interacting with target proteins to trigger a biological response, in most cases this is by activating them (Laporte et al., 1980). The exposure of hydrophobic residues upon Ca^{2+} binding is shown in Figure 5, using the methionine residues as an example. This description of events was suggested due to comparisons between the Ca^{2+} bound and Ca^{2+} free CaM structures which showed significant differences that were attributed to the presence or absence of Ca^{2+} (Chin and Means, 2000, Ikura, 1996). This has since been challenged and developed but is still often cited in the literature and therefore warrants an explanation here.

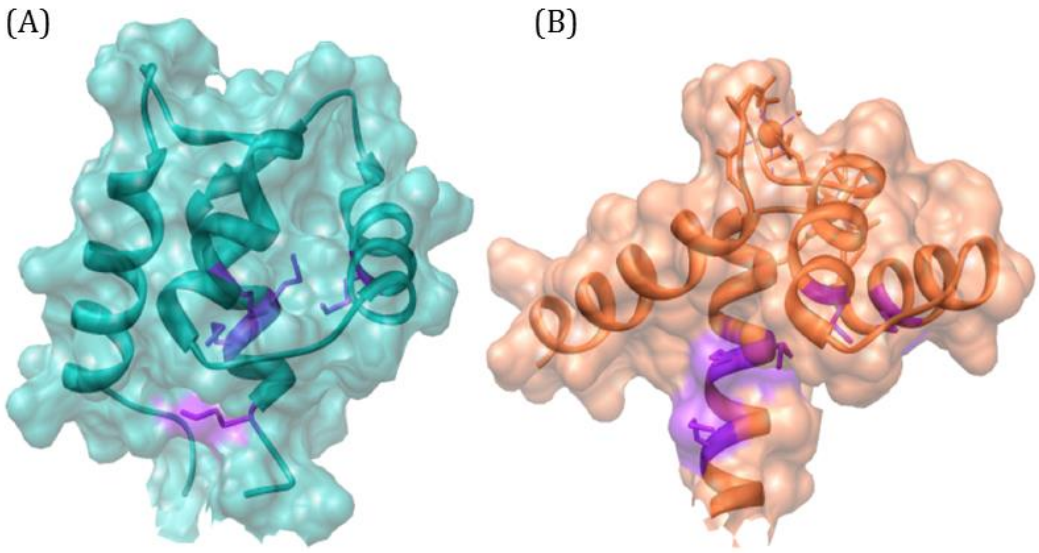

Figure 5. Exposure of hydrophobic residues upon Ca^{2+} binding.
In apo-CaM (A) methionine residues are buried and the majority are not exposed to solvent. In Ca^{2+}/CaM (B) these residues are exposed to solvent and available for interaction with target proteins. Only the N-terminal domain is shown for clarity but similar events occur in the C-terminal domain.

The previous explanation describes an induced fit mechanism of protein: ligand interactions (Koshland, 1958) whereby the interaction between a protein (CaM) and a ligand (Ca^{2+} first and then the target protein or peptide) induces conformational change in the protein. It is now accepted that a number of systems follow the conformational selection paradigm (Ma et al., 1999). According to this model there are a number of conformations of a dynamically fluctuating protein from which the ligand selects the one that is compatible with binding and shifts the conformational ensemble towards this state. This idea is extensively supported by experimental work involving X-ray crystallography, cryo-electron microscopy, kinetic studies, single molecule fluorescence and especially NMR, which show an ensemble of conformational states of free protein that includes conformations of the bound state of the protein (Csermely et al., 2010).

It is often the case that the distinction between induced fit and conformational selection models is not discrete. Indeed, Anthis et al demonstrated that CaM is subject to interplay between these two models. Paramagnetic relaxation enhancement (PRE) NMR spectroscopy investigated transient states of apo-CaM that are sparsely occupied. They found that CaM

samples a range of compact structures (populated at 5–10%) and that Ca^{2+} dramatically alters the distribution of these configurations in favour of states resembling the peptide-bound structure. When bound to Ca^{2+}, CaM shows an innate propensity to form the physiologically active compact structures (Anthis et al., 2011). Further NMR data from Gsponer et al (2008) produced an ensemble of the different conformational states of Ca^{2+}/CaM and found that this included a range of structures that resembled the structure of Ca^{2+}/CaM bound to a target peptide from myosin light chain kinase (MLCK). These ensembles are shown in Figure 6. In addition, further analysis of their ensemble showed that correlated motions within the Ca^{2+}/CaM state direct the structural and dynamic fluctuations towards a complex-like state (Gsponer et al., 2008).

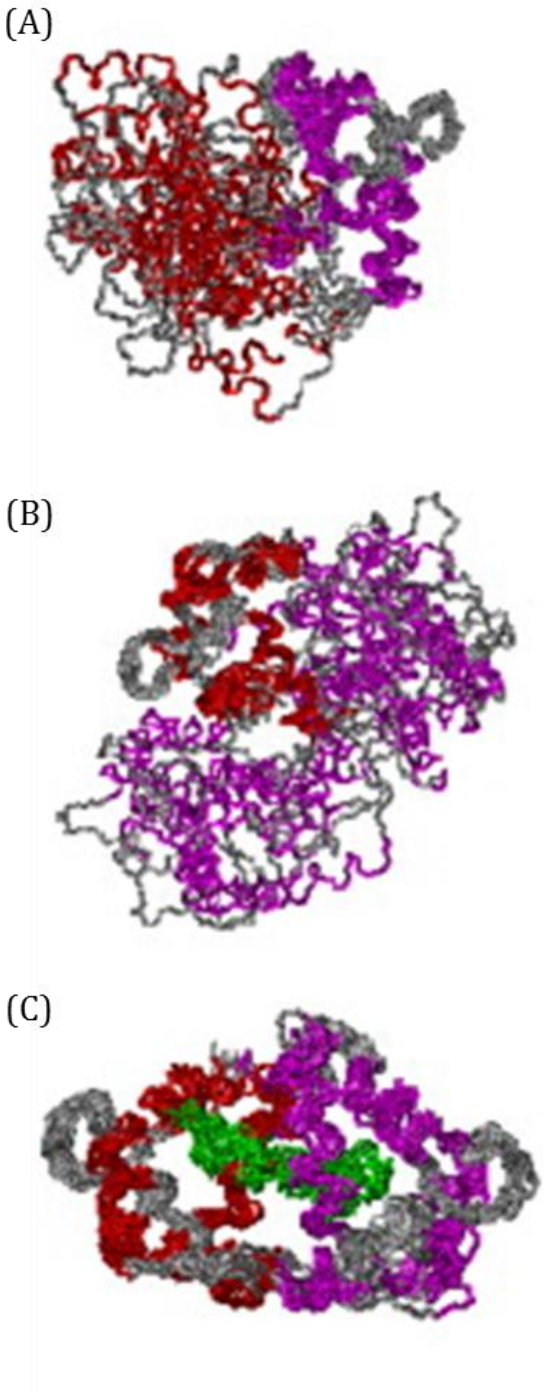

Figure 6. Structural ensembles of conformational states of free and MLCK bound Ca^{2+}/CaM.

Ensemble of structures representing the Ca^{2+}/CaM state aligned against their N-terminal domains, shown in magenta (A) and against their C-terminal domains, shown in red (B). An ensemble of structures representing the CaM: MLCK peptide complex state, with the peptide shown in green (C). PDB ID's: 2K0E (Ca^{2+}/CaM) and 2K0F (Ca^{2+}/CaM bound to peptide from MLCK). Figure taken from (Gsponer et al., 2008).

1.4.4.1 Calmodulin targets

The list of proteins that are affected either directly or indirectly by CaM binding in response to calcium signalling is vast and constantly growing. These proteins are often termed CaM effector proteins as they are responsible for carrying out the various roles of CaM within the cell. Some of the most highly characterised of these targets are proteins involved in protein phosphorylation, including CaM dependent adenylyl cyclases, protein kinases and phosphodiesterases. In addition, CaM also regulates ion channels, the plasma membrane Ca^{2+} pump and the ryanodine receptor among many other targets (Chin and Means, 2000)

1.4.4.2 Calmodulin binding motifs

CaM can bind to an extensive number of target proteins in the cell. The vast majority of these proteins contain a CaM binding region that interacts directly with CaM and conforms to standard sequence motifs. There are 4 major classes of recognition motifs termed the IQ motif and the 1-14, 1-10 and 1-16 motifs which are so called based on the position of hydrophobic residues in the sequence (Rhoads and Friedberg, 1997). The IQ motif is unusual in that it is often responsible for binding to CaM in a Ca^{2+} independent manner (Rhoads and Friedberg, 1997, Bahler and Rhoads, 2002). Each of these also contains further subclasses based on the common features of hydrophobic anchor residues interspersed with positively charged residues, as shown in Figure 7.

The CaM binding regions of proteins consist of 16-25 amino acid residues and, although they share little homology in their primary sequences, many have the propensity to form a basic amphiphilic α-helix, that is an α-helix with opposing polar and nonpolar faces oriented along the helix. This can be shown by a helical wheel representation, as in Figure 7, whereby basic and polar residues are distributed on one side of the helix and hydrophobic residues on the opposite side. Studies using small peptides that correspond to the CaM binding regions of proteins have shown that they have little structure in solution but still adopt an α-helical conformation upon Ca^{2+}/CaM binding (Padre and Stull, 2000).

(A)

Motif name	Motif sequence	Known targets
1-5-8-14	(FILVW)xxx(FAILVW)xx(FAILVW)xxxxx(FILVW)	Sodium calcium exchanger
1-8-14	(FILVW)xxxxxx(FAILVW)xxxxx(FILVW)	Neuronal nitric oxide synthase
1-8-14 basic	(RK)(RK)(RK)(FILVW)xxxxxx(FAILVW)xxxxx(FILVW)	Myosin light chain kinase
1-14	(FILVW)xxxxxxxxxxx(FILVW)	Ryanodine receptor 1
1-5-10	xxx(FILVW)xxxx(FAILVW)xxxx(FILVW)	Heat shock protein 90
1-5-10 basic	(RK)(RK)(RK)(FAILVW)xxxx(FILV)xxxx(FILVW)	CaM dependent kinase II
1-10	(FILVW)xxxxxxxx(FILVW)	Inositol triphosphate 3 kinase
1-16	(FILVW)xxxxxxxxxxxxx(FILVW)	CaM dependent kinase kinase
IQ	(FILV)Qxxx(RK)Gxxx(RK)xx(FILVWY)	L-type calcium channel
IQ-like	(FILV)Qxxx(RK)xxxxxxxx	Voltage-gated sodium channel

(B)

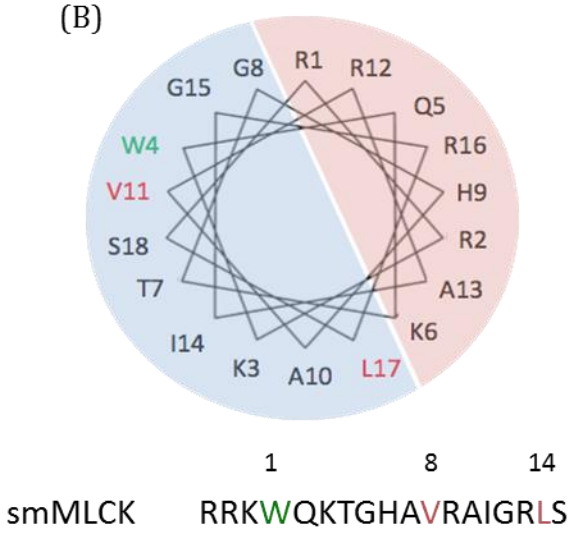

Figure 7. Putative CaM binding regions of proteins.

Table of the conserved sequences of the putative CaM binding motifs with examples of protein targets known to contain them (A). Helical wheel representation of the CaM binding region from smooth muscle myosin light chain kinase (smMLCK) (B). The key anchor residue is coloured green and the other hydrophobic amino acids involved in CaM binding are coloured red. The red shading demonstrates the side of the helix with polar amino acid residues and the blue shading the side of the helix with hydrophobic amino acid residues. Table from (Kovalevskaya et al., 2013).

1.4.4.3 Structures of CaM bound to target peptides

The majority of the published structures of CaM bound to target involve a synthetic peptide analogue rather than the full-length protein itself. This synthetic peptide corresponds to the CaM binding region of the target protein.

The Protein Data Bank (Bernstein et al., 1977) contains a number of structures (48 structure hits on 15th April 2014) of CaM bound to these target peptides. Analysing these structure hits shows that the target peptide forms an

α-helix within the CaM: peptide complex. The majority of structures show a similar overall shape and domain organisation with a classical wraparound structure.

An example of this is the crystal structure of Ca^{2+}/CaM bound to a peptide from smMLCK (ARRKWQKTGHAVRAIGRLSS) (Meador et al., 1992). The structure is compact with the N- and C-terminal domains in close association, creating a tunnel for the target peptide that allows both domains to engulf and interact with the target peptide. This is indicative of the classic wraparound structure, as is shown in Figure 8. The compact nature of this structure allows the hydrophobic patches from each domain of CaM to come together and form a hydrophobic arc that interfaces with the hydrophobic side of the peptide. Residues Trp^5 and Thr^8 of the peptide occupy the hydrophobic pocket of C-terminal domain whilst Ala^{14}, Ile^{15} and Leu^{18} occupy the N-terminal domain patch.

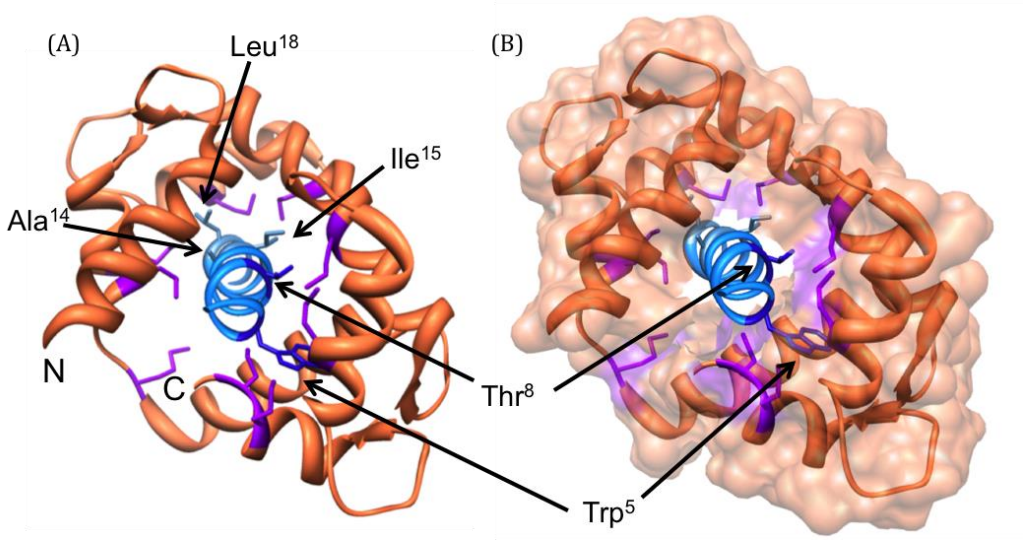

Figure 8. Crystal structure of Ca^{2+}/CaM bound to a peptide corresponding to the CaM binding region of smMLCK.

Ca^{2+}/CaM (orange) bends at the central flexible linker to allow the N- and C-terminal domains to come into close association and interact with the peptide from smMLCK (blue). Methionine residues of CaM (purple), which contribute to the hydrophobic binding patches line the interaction site and make contact with the peptide. Trp^5 and Thr^8 of the peptide (dark blue) bind to the C-terminal domain whilst Ala^{14}, Ile^{15} and Leu^{18} (light blue) occupy the N-terminal domain. Ribbon representation (A) and surface representation (B). PDB ID: 1CDL.

Further structural investigations using these short target peptides have revealed diversity in CaMs mechanisms of target recognition, interaction and activation. The vast majority of the complex structures show a bending of the central flexible linker to allow both domains of Ca^{2+}/CaM to make contact with the peptide. The organisation of the two domains with respect to each other is thus very similar across the different complexes. This is demonstrated in Figure 9, where structures of Ca^{2+}/CaM bound to two different target peptides have been overlaid. It is evident that the overall structures are remarkably similar but that there are some differences in the helix orientations in the individual domains. This differs for those structures of apo-CaM in complex with target peptide, in which case only one domain is often involved in binding (Kumar et al., 2013).

One major difference seen in the case of the small peptides is that, depending on the protein target they are able to bind in different orientations. In some examples, such as CaMKII, the N-terminal of the peptide interacts with the C-terminal domain of CaM, whilst in CaMKK the N-terminal domain of the peptide interacts with the N-terminal domain of CaM (Osawa et al., 1999). In addition the two domains of CaM can be located different distances apart in the complex structures. When bound to a peptide from CaMKII, the two domains are located one helical turn closer together in space compared to its structure when bound to the MLCK peptide, resulting in a more compact structure. These differences are illustrated in Figure 9.

The ability to bind the peptides in different orientations and also the other differences across the structures of CaM: peptide complexes, such as the variation in helix orientations within the two domains, demonstrate a structural plasticity of CaM. This is necessary to enable CaM to recognise and bind to its varied targets and bring about its variety of biological effects.

It should be noted that applying observations based on the complexes of these small target peptides may not necessarily be suitable for studying further functions of the full-length target protein. For example, differences have been shown between the Ca^{2+}/CaM: MLCK peptide complex and the Ca^{2+}/CaM: MLCK enzyme complex. It has been shown that Ca^{2+} has a higher affinity for the peptide complex compared to the enzyme complex (Peersen et al., 1997) and

small angle X-ray scattering (SAXS) has shown that there are differences between the Ca^{2+} dependent interaction of CaM with the peptide and with full-length MLCK enzyme (Heller et al., 2003, Krueger et al., 2001). It is thought that this could be due to inherent conformational flexibility in a short, isolated peptide compared to in the context of a large protein. It is therefore important to consider this when studying CaM: peptide complexes. Another example of the differences between peptide- and protein-bound CaM complexes has been shown for death associated protein kinase (DAPK). In this case the peptide-bound complex conforms to the classic wraparound structure of CaM, whilst the full length protein-bound complex shows CaM to be in a much more extended conformation. In addition to interactions with the CaM binding region of DAPK, both domains of CaM also make extensive contacts with the DAPK catalytic domain (de Diego et al., 2010, Tidow and Nissen, 2013).

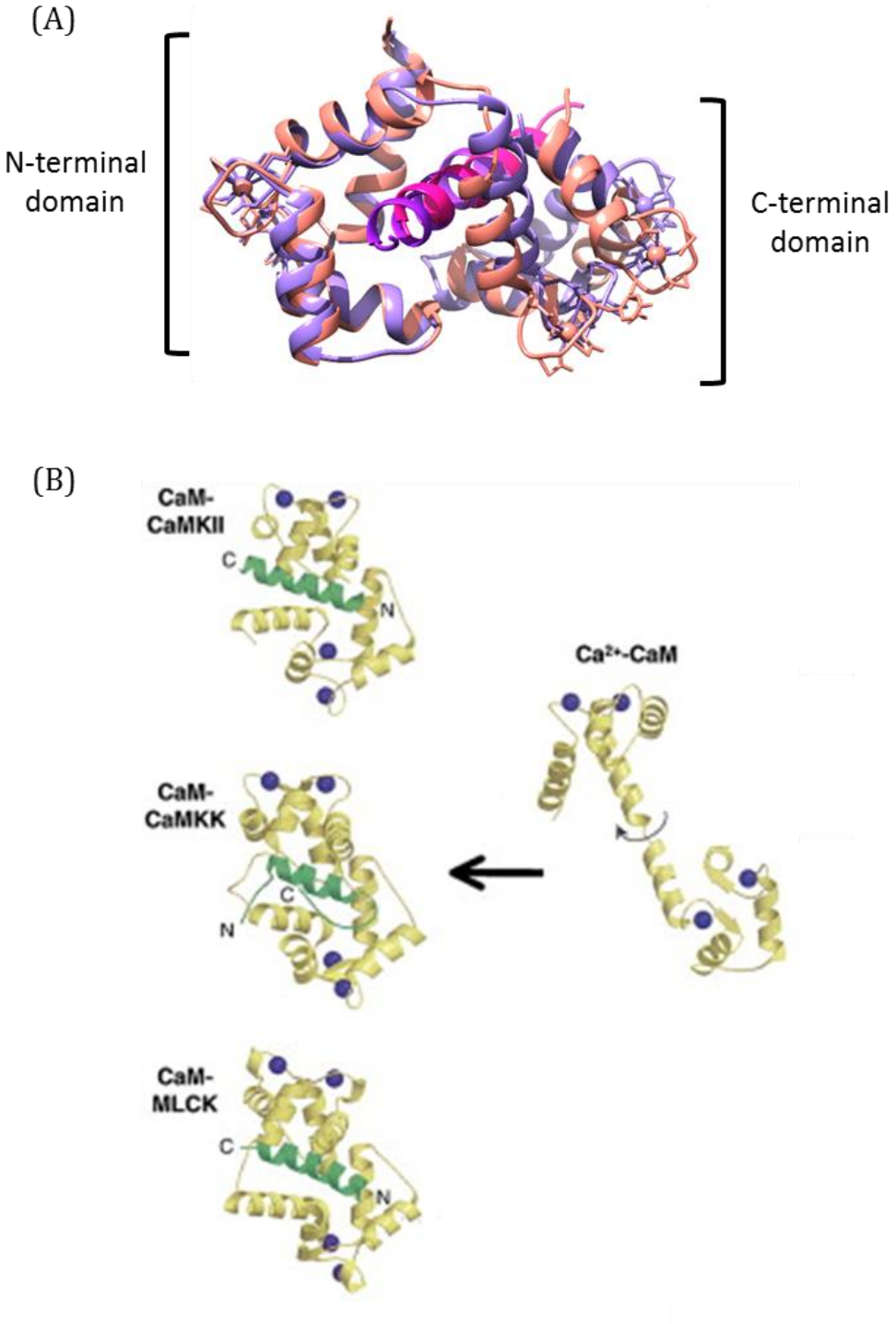

Figure 9. Binding of Ca^{2+}/CaM to target peptides.

Structures of two Ca^{2+}/CaM: peptide complexes overlaid to give an RMSD of 0.7Å (A). PDB ID: 2F3Y is shown in pinks and PDB ID: 1CDL is shown in purples. Structures of Ca^{2+}/CaM in complex with target peptides show similar but distinct recognition and interaction modes (B). (B) taken from (Hoeflich and Ikura, 2002).

1.4.4.4 Structures of CaM bound to target proteins

The determination of structures of Ca^{2+}/CaM bound to some of its full-length protein targets further showed great differences in the recognition and interaction with CaM binding motifs, as shown in Figure 10.

These structures did not show CaM to adopt the collapsed, compact wraparound structure that is achieved by bending of the central flexible linker to interact with short peptide targets. Instead, CaM remains in a largely open conformation. In the case of the structure of the CaM-edema factor (EF) complex four discrete regions of EF form a surface that recognizes an extended conformation of CaM (Drum et al., 2002). Another example, of Ca^{2+}/CaM bound to the gating domain of a Ca^{2+} activated K^{+} channel, is shown in Figure 10. In this complex, the CaM binding domain consists of two long alpha helices, a1 (residues 413-440) and a2 (residues 446-489), connected by a loop (residues 441-445), which is considerably longer than any of the target peptides studied. Two of these CaM binding domains form a dimer which is bound to two CaM molecules in such a way that each molecule of CaM contacts both subunits of the CaM binding domain dimer to form a highly elongated complex (Schumacher et al., 2001).

From these structures, especially that of the CaM-EF complex (Drum et al., 2002), modes of action were determined that differed from the classic mechanism, whereby CaM binding induces conformational change to relieve autoinhibition from a pseudosubstrate autoinhibitory domain, which will be described in Section 1.4.5. In contrast, the activation of EF by CaM is complex and involves rearrangement of key switches to create an active site from an area that is solvent exposed when CaM is not bound (Grabarek, 2005), namely the rotation of a helical domain away from the catalytic core in order to stabilise a disordered loop for enzyme activation (Drum et al., 2002).

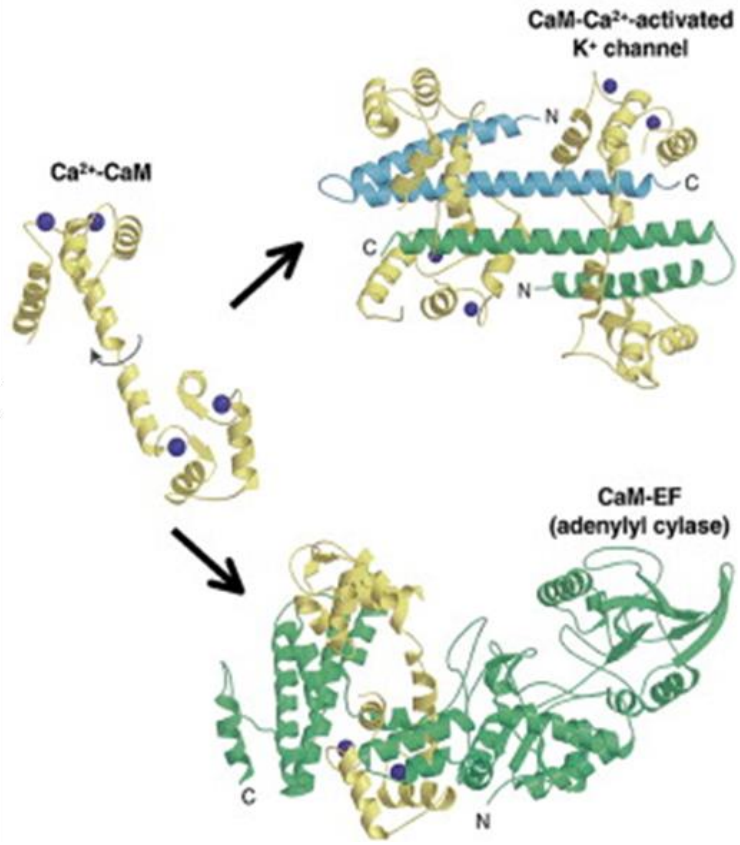

Figure 10. Structures of Ca^{2+}/CaM binding to full-length protein targets.
The interaction between Ca^{2+}/CaM and full-length proteins is more complex, with CaM adopting an open conformation rather that a compact and collapsed wraparound structure as is seen upon interaction with small peptide targets. Taken from (Hoeflich and Ikura, 2002).

1.4.5 Calmodulin target regulation

The exposure of hydrophobic residues on CaM results in the release of a considerable amount of biochemical energy that is transduced into an effect. Depending on the target this effect is different and could result in activation or deactivation of the target protein.

In a review article, Chin and Means classified CaM binding proteins into six categories depending on their modes of regulation by CaM in the absence and presence of Ca^{2+}. The first of these classes binds essentially irreversibly to CaM, whether Ca^{2+} is bound or not, and therefore CaM essentially acts as a subunit of the protein. Phosphorylase kinase is an example of this group, which can bind apo-CaM but is activated in response to Ca^{2+} binding. A second group, which includes neuromodulin, can also bind to apo-CaM but dissociate reversibly in the presence of Ca^{2+}. The third class contains myosin light chain

kinase, which is extensively used in CaM binding studies. This group forms low-affinity and inactive complexes with CaM at low concentrations of Ca^{2+} when CaM may be partially or completely in the apo-form but at high concentrations of Ca^{2+} the complexes formed are of high affinity and the kinase is activated. There are a further class of CaM effector proteins that bind to Ca^{2+}/CaM and are consequently inactivated, including select members of the G protein-coupled receptor (GPCR) family. A fifth group, which mainly contains a family of proteins termed the Ca^{2+}/CaM dependent protein kinases, exhibits the conventional behaviour of being activated by Ca^{2+}/CaM. The sixth group is a subset of the fifth whereby CaM binding promotes their regulation by a further kinase, CaM kinase kinase (Chin and Means, 2000).

Studies focussing on the fifth group of CaM effector proteins, the Ca^{2+}/CaM dependent protein kinases, have provided the most information on the mechanisms that underlie CaM target regulation. In the case of the majority of Ca^{2+}/CaM dependent protein kinases, this involves triggering conformational changes within the target protein to release a pseudosubstrate autoinhibitory domain (Goldberg et al., 1996). This will be further discussed in Section 1.6.6.
Given the vast number of CaM-binding proteins, the different roles these CaM effector proteins are responsible for in the cell and the different mechanisms of regulation by which these effector proteins are controlled it seems remarkable that a single molecule, CaM, is uniquely responsible for eliciting all of these different responses.

1.5 eEF2K and translation elongation

1.5.1 Role of eEF2K

eEF2K is a critical regulator of translation elongation as a consequence of its ability to phosphorylate eEF2, its only known natural substrate, in response to various stimuli and signalling pathways. It is also able to phosphorylate an alternative artificial substrate, known as the MH-1 peptide, which corresponds to the myosin heavy chain kinase A phosphorylation site in Dictyostelium myosin heavy chains. This is an ability that is exploited for in vitro studies on eEF2K. As previously discussed, eEF2K is an unusual protein

kinase whose activity is affected by a number of signalling pathways but mostly it is dependent on Ca^{2+}/CaM for activation.

1.5.2 Process of protein translation

Protein synthesis involves a number of processes and reactions that are collectively termed translation. There are three main stages of translation known as initiation, elongation and termination which are well reviewed in (Sonenberg and Hinnebusch, 2009) and I have briefly summarised here.

The initiation stage of eukaryotic protein synthesis is a multi-step process, facilitated and regulated by a series of protein factors known as eukaryotic initiation factors (eIFs) which all have specific roles. The overall aim of this process is to correctly assemble and position the 80S ribosome, with the initiator methionyl tRNA (Met-$tRNA_i$) loaded in the P site, at the AUG initiation codon of the mRNA to be translated. This initiates translation and allows the elongation and termination stages of protein synthesis to continue. Throughout translation initiation, eIFs are required for in the formation of various complexes to facilitate progress through the pathway.

Peptide chain elongation follows initiation and involves the sequential addition of further amino acids to form a polypeptide chain that can fold into a three-dimensional protein able to carry out its biological function. A key step of this process is translocation, which results in movement of the ribosome along the mRNA by one codon and also the movement of tRNAs from the A and P sites to the P and E sites respectively. As in translation initiation, there are protein factors that aid in driving the elongation process called eukaryotic elongation factors or eEF's.

Once the last amino acid has been added in the elongation stage and a stop codon is reached the translation process must be terminated through a series of steps catalysed by release factors. These release factors are responsible for recognizing the stop codon in the ribosomal A site and are then involved in triggering the cleavage and dissociation of the polypeptide chain from the ribosome (Sonenberg and Hinnebusch, 2009).

1.5.3 Translation elongation

Following translation initiation, the Met-tRNA$_i$ is located at the ribosomal P site, meaning that the A site is free to receive an incoming aminoacyl-tRNA. This first elongator aminoacyl-tRNA is brought to the ribosome by eEF1A. Once it is correctly positioned at the A site, there follows a ribosome-mediated GTP hydrolysis reaction, resulting in the release of GDP-bound eEF1A. Nucleophilic attack by the lone pair of electrons on the amino nitrogen of the aminoacyl-tRNA at the A site on the carbonyl carbon of the Met-tRNAi in the P site initiates the condensation reaction that results in peptide bond formation to join the two amino acids linked to the tRNA molecules. The reaction that follows is termed the translocation reaction, as it involves the aminoacyl-tRNA's in the A and P sites moving to the P and E sites respectively in two stages. Significant large-scale movements within the ribosome accompany this translocation, as the ribosome changes from the pre-translocational to the post-translocational state to receive further incoming aminoacyl-tRNA's into a free A site. It requires eEF2, which acts by a GTPase switch mechanism (Spahn et al., 2004).

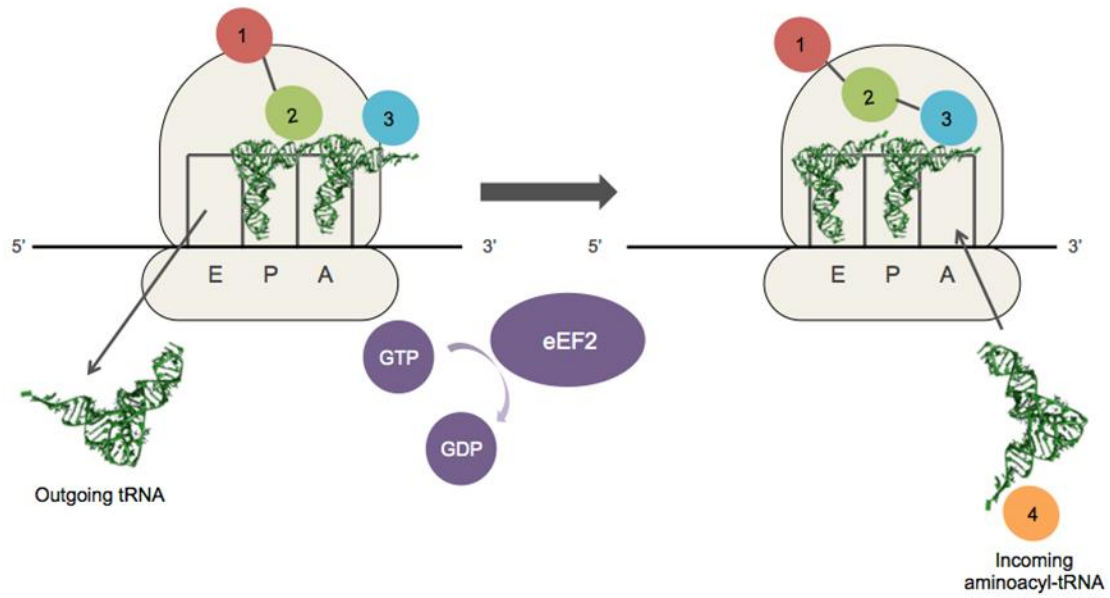

Figure 11. The process of translocation in translation elongation.
eEF2 functions as a GTPase to aid in the translocation process whereby the tRNAs bound at the A and P sites of the ribosome are moved to the P and E sites, freeing the A site for the next incoming aminoacyl-tRNA. The first amino acid in the peptide chain is coloured red, the second is coloured green and the third, which is being added to the chain, is coloured blue.

1.5.3.1 Role of eEF2 in translation elongation

eEF2 is the factor that mediates translocation. It is structurally and functionally homologous to its bacterial and archael counterparts termed EF-G and aEF2 respectively and in addition it also displays extremely high sequence conservation within the mammalian kingdom (Jorgensen et al., 2006).

It is a 100 kDa monomeric protein (Price et al., 1991) of 827 amino acid residues that consists of five structural domains, termed I-V (Spahn et al., 2004). These five domains are involved in binding to the ribosome and upon binding have been shown to change their relative orientations. eEF2 also binds and interacts with GTP, which subsequently undergoes GTP hydrolysis; the relative domain orientations have been shown to change as a result of this reaction (Jorgensen et al., 2003).

Its role in translation elongation is as a GTPase, to aid in the translocation process responsible for movement of tRNA's from the A and P sites to the P and E sites so that peptide chain elongation may continue. Cryo-EM studies (Taylor et al., 2007) have mapped the domain movements of eEF2 and the structural re-arrangements that occur within the ribosome during the translocation reaction. These studies showed that a pronounced ratchet-like subunit re-arrangement (RSR) occurs in the eEF2 and ribosome complex that is suggested to play a role in the translocation of tRNAs.

These events are triggered by GTP hydrolysis on eEF2 that causes conformational change within eEF2. This breaks the contact between the mRNA and tRNA and the ribosome to result in the necessary tRNA translocation (Taylor et al., 2007). Once GTP hydrolysis occurs, GDP-eEF2 is released and it is thought that this release reverses the conformational changes caused by GTP-eEF2 binding to the ribosome (Wilden et al., 2006). As a result the A site is made available for another incoming aminoacyl-tRNA, allowing peptide elongation to continue.

1.5.3.2 Regulation of translation elongation

The process of translation elongation consumes a large amount of energy, with at least four high energy bonds consumed for each amino acid added to the chain. Therefore, under conditions of increased energy demand or

decreased energy supply it is important and advantageous that the cell can divert the energy necessary for protein translation to other, more vital process (Browne and Proud, 2004). The rate of peptide chain elongation thus depends on the cellular conditions and indeed, changes in the elongation rate are observed at different physiological conditions and in response to certain stimuli. Regulatory mechanisms are clearly important to match the requirements of the cell with the energy supply.

These regulatory mechanisms can be long term and involve changes in the cellular levels of translation factors and ribosomes. Primarily, however, the regulation mechanisms involve rapid changes in the activity or in the association of components of the translational machinery. This involves covalent modification of the two elongation factors responsible for controlling the progression through the elongation stage of translation (Proud, 2007). eEF1 has been shown to undergo methylation and phosphorylation (Ryazanov et al., 1991). However, it is eEF2 modifications, namely phosphorylation, which are considered to be majorly responsible for regulating the rate of translation elongation.

eEF2 can be phosphorylated on Thr^{56} by eEF2K (Redpath et al., 1993, Price et al., 1991). When eEF2 is phosphorylated in this way, its activity and ability to bind to the ribosome is inhibited and thus the rate of peptide chain elongation is reduced. This phosphorylation by eEF2K and the subsequent decrease in translation elongation is triggered by a number of stimuli, mostly associated with cellular stress. These include increases in cytoplasmic Ca^{2+} levels, as eEF2K is classed as a Ca^{2+}/CaM dependent protein kinase, nutrient and amino acid depletion (Wang et al., 1998) and reductions in cellular ATP (McLeod and Proud, 2002). Consequently, a number of signalling pathways are involved in controlling the activity of eEF2K, and subsequently the activity of eEF2, in order to coordinate the rate of translation elongation with the physiological state of the cell.

1.5.4 Domain structure of eEF2K

The three-dimensional structure of eEF2K has not been elucidated. However, analysis of the primary sequence of eEF2K allowed the identification

of several domains, which have been studied to determine their roles for eEF2K function (Diggle et al., 1999, Pavur et al., 2000). A depiction of this domain organisation is shown in Figure 12.

An alpha kinase catalytic domain is located near the N-terminus with a CaM binding region immediately N-terminal to this. The role of the region at the extreme N-terminus is unknown but it is largely unstructured. Close to the C-terminus there are four predicted alpha helical regions that resemble Sel 1-like repeats. These repeats are found in some other proteins, such as Sel1, Hrd3, Nif1, Chs4 and Shc1, which are involved in the regulation of cell division and differentiation. The repeats themselves are thought to provide a platform for protein interactions and be important in signal transduction pathways (Pigott et al., 2012, Mittl and Schneider-Brachert, 2007). C-terminal to the Sel1-like repeats is a highly conserved region necessary for phosphorylation of its substrate eEF2 and the MH-1 peptide, possibly because it is responsible for interacting with its substrate eEF2 (Diggle et al., 1999). A conserved linker region, which is predicted to be unstructured, is present between the N-terminal catalytic and C-terminal Sel 1-like repeats (Pigott et al., 2012).

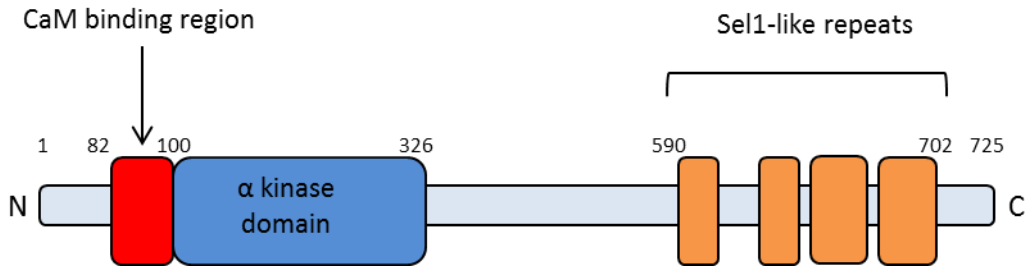

Figure 12. Domain organisation of eEF2K.
The CaM binding region (red) is located near the N-terminus, preceeding the atypical α kinase domain (blue). A region consisting of four sel1-like repeats is located near the C-terminus and is important for eEF2 phosphorylation.

The interplay between these domains is critical for the function of eEF2K and some significant work has been carried out and is underway to dissect their roles. It has been shown by recent truncation studies that the region at the extreme N-terminus (residues 1-75) and the linker (residues 357-477) are not necessary for the intrinsic activity of eEF2K. In fact, fragments which did not contain the extreme N-terminal residues (residues 1-75) were found to have

higher activity than those which did, suggesting an inhibitory role for these residues. The region containing the Sel 1-like repeats was shown to be vital for phosphorylation of the substrates; both eEF2 and the MH-1 peptide (Pigott et al., 2012).

1.5.4.1 CaM binding region of eEF2K

eEF2K contains a CaM binding region close to the N-terminus, immediately prior to the alpha kinase domain (residues 74-100). Studies involving mutational analysis (Diggle et al., 1999) and CaM binding assays (Pavur et al., 2000) have determined that this region is responsible for CaM binding in eEF2K. However, it is not recognised as containing a sequence corresponding to one of the typical, known CaM binding motifs discussed in Section 1.4.4.2. A region near to the C-terminus (residues 514-526) is identified by a CaM target database (http://calcium.uhnres.utoronto.ca/ctdb/ctdb/home) to contain a sequence that does conform to one of the accepted CaM binding sequence motifs. However, it has been shown that a fragment of eEF2K consisting of residues 490-725 cannot bind CaM and that the entire C-terminal region of eEF2K is dispensable for the control of eEF2K by Ca^{2+}/CaM (Pigott et al., 2012).

1.5.5 eEF2K activity

The rate of translation elongation is coupled to the energetic state of the cell, as described in Section 1.5.3.2. In turn, this means that eEF2K activity also reflects the cellular state and as such it will be activated if the rate of protein translation needs to be reduced and deactivated if protein translation should proceed. This is achieved by the regulation mechanisms outlined in Section 1.5.6.

As mentioned, eEF2K is activated by Ca^{2+}/CaM. Once Ca^{2+}/CaM is bound to eEF2K it can carry out autophosphorylation to further alter its activated state, either to induce Ca^{2+} independent activity (at Ser^{500}) or to activate substrate recognition (at Thr^{348}). This further regulation by autophosphorylation is discussed in Section 1.5.6.3.

eEF2K is then responsible for phosphorylation of its substrate, eEF2, to bring about the desired biological effect of blocking its binding to the ribosome

to decrease the rate of peptide translation elongation. eEF2K phosphorylates eEF2 at Thr^{56}. Other phosphorylation sites have been identified on eEF2 and are listed on Phosphosite, (www.phosphosite.org), however it is only Thr^{56} which is phosphorylated by eEF2K to affect translation.

Once activated, eEF2K can also phosphorylate the MH-1 peptide in vitro. This property is useful for studying eEF2K activity.

1.5.6 Regulation of eEF2K

eEF2K is a major regulator of translation elongation and therefore the process of protein synthesis within cells. As a large amount of energy is consumed during protein synthesis, it must be tightly regulated and so the cell balances eEF2K activity with ATP availability.

Some of the major signalling pathways have an influence on eEF2K activity; the mTOR pathway and AMPK pathway are the central sensors of cellular nutrients and energy levels (Browne and Proud, 2004). In addition, the presence of Ca^{2+}/CaM also affects the activity of eEF2K, resulting in its activation (Palfrey, 1983, Nairn and Palfrey, 1987, Redpath et al., 1993, Mitsui et al., 1993).

With the exception of its activation by Ca^{2+}/CaM, this regulation is achieved by ubiquitination and phosphorylation, which can either increase or decrease eEF2K activity depending on the original stimulus and pathway involved.

1.5.6.1 Activation of eEF2K by Ca^{2+}/CaM

Ca^{2+}/CaM binds to a region of eEF2K near the N-terminus to activate the kinase so that it can phosphorylate eEF2. The importance of CaM binding in the activation of eEF2K is demonstrated when the protein is phosphorylated at Ser^{78}, adjacent to the CaM binding domain. Phosphorylation here inhibits the binding of CaM and thus inhibits eEF2K activity. This therefore demonstrates the fact that eEF2K activation is dependent on CaM interactions (Browne and Proud, 2004).

It is suggested in the literature that the binding of Ca^{2+}/CaM may in some way relieve autoinhibition by the CaM binding domain and thus trigger autophosphorylation to fully activate eEF2K. This mechanism has been

suggested as the known structures of other members of the Ca^{2+}/CaM dependent protein kinase family are activated in this manner, as discussed in Section 1.6.6. In addition, Piggott et al found that the extreme N-terminus of eEF2K, adjacent to the CaM binding region, seems to act in an inhibitory manner with respect to eEF2K activity (Pigott et al., 2012). However, the structure of eEF2K is not yet known and the mechanism by which CaM activates eEF2K is therefore not understood.

1.5.6.2 Regulation of eEF2K by ubiquitination and degradation

The stability of eEF2K can be regulated by the ubiquitin-proteasome system (Kruiswijk et al., 2012, Arora et al., 2005, Wang et al., 2015). It is a relatively short-lived protein with a half-life of less than 6 hours, which is ubiquitinated before the involvement of the proteasome in degradation. Heat shock protein 90 (Hsp90) is involved in stabilising eEF2K and so a balance between the association of eEF2K with Hsp90 and degradation by the ubiquitin-proteasome pathway is indicated as maintaining the cellular levels of eEF2K (Arora et al., 2005).

This degradation is activated in response to genotoxic stress, whereby eEF2K is first activated by AMPK-mediated phosphorylation to induce a temporary decrease in translation rate. Following this, eEF2K is targeted for proteasome-dependent degradation by a ubiquitin ligase through a phosphodegron that includes an autophosphorylation site. This shows an important link between the DNA damage response and translation (Kruiswijk et al., 2012).

Further work has shown that other cellular stresses, such as acidosis and cell treatment with 2-deoxyglucose, also result in eEF2K degradation. In these cases though, a phosphodegron is not required. It was found however, that kinase-dead and other activity-deficient mutants of eEF2K are stabilised, including a mutant lacking a critical autophosphorylation site (Thr^{348}), that is thought to be reuired for eEF2K to adopt ts active conformation. Together these results indicate that eEF2K must be active in order to be targeted for degradation by the proteasome. Small molecule eEF2K inhibitors did not

stabilise the protein, which has important implications in targeting eEF2K in cancer therapy (Wang et al., 2015).

1.5.6.3 Regulation of eEF2K by cell signalling pathways

The mTOR and AMPK cell signalling pathways are important for the regulation of eEF2K activity. Their effects on eEF2K activity is summarised in Figure 13.

mTORC1 is activated by signalling through the mTOR signalling pathway in response to growth factors and nutrients to promote cell growth and proliferation. It is therefore involved in increasing the rate of translation as a response to these pro-growth signals. One of the ways in which it does this is by promoting the phosphorylation of eEF2K at a number of residues to cause a decrease in its activity and therefore stimulate translation elongation. Some of these phosphorylation sites have been characterised. For example, Ser^{359} is phosphorylated in response to mTORC1, thus inhibiting the activity of eEF2K. It has been shown that it is cdc2/cyclin B which phosphorylates this residue in response to mTORC1, and also p38 MAPKδ (Knebel et al., 2001). It is thought that this control by cdc2/cyclin B plays a role in mitotic cells to inactivate eEF2K and thus keep eEF2 phosphorylation low and so encourage the translation of certain mRNA's (Knebel et al., 2001, Smith and Proud, 2008). The p70 S6 kinases, which are regulated by mTOR, phosphorylate eEF2K at a conserved serine, Ser^{366}, thus inactivating it (Wang et al., 2001). Phosphorylation at Ser^{78} is important for the activation of eEF2K by Ca^{2+}/CaM as phosphorylation here negatively influences the binding of CaM to eEF2K. This phosphorylation is regulated in response to insulin, also in an mTOR dependent manner, although the protein kinase directly responsible for this phosphorylation event is not known (Browne and Proud, 2004).

In contrast to the mTOR pathway, AMPK is known to phosphorylate protein targets to cause a decrease in energy consumption and therefore increase the energy supply in cells. Browne et al (2004) showed that AMPK is directly responsible for the phosphorylation of Ser^{398}, which results in an increase in eEF2 phosphorylation, indicative of an increase in eEF2K activity (Browne et al., 2004).

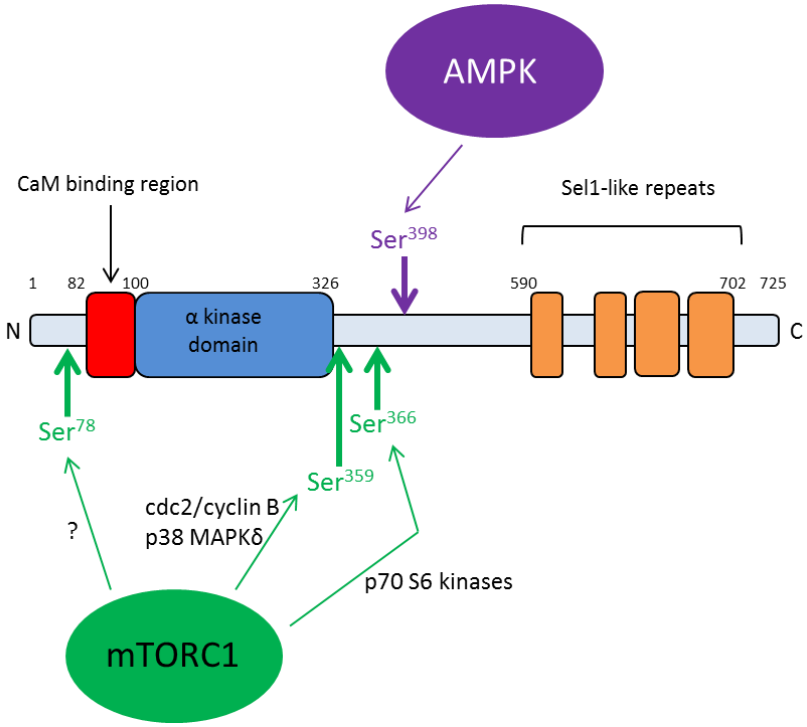

Figure 13. Regulation of eEF2K by cell signalling pathways.
Phosphorylation of serine residues of eEF2K is controlled by two cell signalling pathways. The mTOR signalling pathway increases the rate of translation by activating a number of protein kinases which in turn phosphorylate Ser^{78}, Ser^{359} and Ser^{366} to decrease eEF2K activity (all shown in green). The AMPK signalling pathway directly phosphorylates Ser^{398} of eEF2K to cause an increase in eEF2K activity (shown in purple).

1.5.6.4 Modulation of eEF2K activity by pH

Acidification (decrease in cellular pH) is associated with a number of physiological and pathological processes such as high intensity exercise, diabetic ketoacidosis and in malignant solid tumours (Fitts, 1994, Kraut and Madias, 2010, Neri and Supuran, 2011). These conditions are characteristic of increased energy demand and so are associated with mechanisms that turn off processes that require large amounts of energy, such as protein synthesis.

eEF2K is activated by low pH (Dorovkov et al., 2002), which provides a mechanism for inhibiting protein synthesis. Data indicates that acidic conditions promote the binding of eEF2K to CaM and thereby enhance eEF2K activity (Dorovkov et al., 2002, Pigott et al., 2012). The CaM binding region of eEF2K contains three highly conserved histidine residues, whose side chains can ionize around neutral pH. There is also a single histidine residue in CaM and two highly conserved histidine residues in the ATP-binding region of eEF2K. It

is thought that these histidine residues are critical for the control of eEF2K activity in response to pH (Xie et al., 2015).

1.5.6.5 Autophosphorylation of eEF2K

There are multiple autophosphorylation sites on eEF2K including, Thr^{348}, Thr^{353}, Ser^{366}, Ser^{445}, Ser^{78} (Pyr Dit Ruys et al., 2012) Ser^{474} and Ser^{500} (Tavares et al., 2012). Autophosphorylation at these sites, except for at Ser^{78}, is stimulated by Ca^{2+}/CaM and can have positive or negative effects on eEF2K, causing an increase or decrease in its effects (Tavares et al., 2012). These autophosphorylation sites are summarised in Figure 14.

Thr^{348} phosphorylation has been shown to be necessary for activity against substrate. This is predicted to be because, when phosphorylated, Thr^{348} can act as a ligand for a P_i pocket; in a similar mechanism to that demonstrated for MHCK A by Thr^{825} (Crawley et al., 2011). This suggests that autophosphorylation may be a prerequisite for eEF2K activity (Pyr Dit Ruys et al., 2012).

Ser^{500} autophosphorylation is associated with Ca^{2+} independent activity of eEF2K. This suggests a mechanism to explain how eEF2K possesses significant activity after the Ca^{2+} signal has finished and the concentration of Ca^{2+} returns to basal levels (Redpath et al., 1993, Tavares et al., 2012).

Ser^{78} is phosphorylated by an unknown kinase in response to insulin; however, it is also autophosphorylated at low levels in vivo and in vitro (Pyr Dit Ruys et al., 2012) thus impairing the interaction between eEF2K and CaM.

Ser^{366} was identified as a major site of autophosphorylation by Pyr dit Ruys et al (2012), who determined that phosphorylation here impairs the activation of eEF2K in response to Ca^{2+} ions. Thus it seems that phosphorylation here acts to desensitise eEF2K to activation by Ca^{2+}/CaM rather than affecting the interaction itself. It is therefore thought that this autophosphorylation may act to turn off eEF2K following its activation in response to cellular stress.

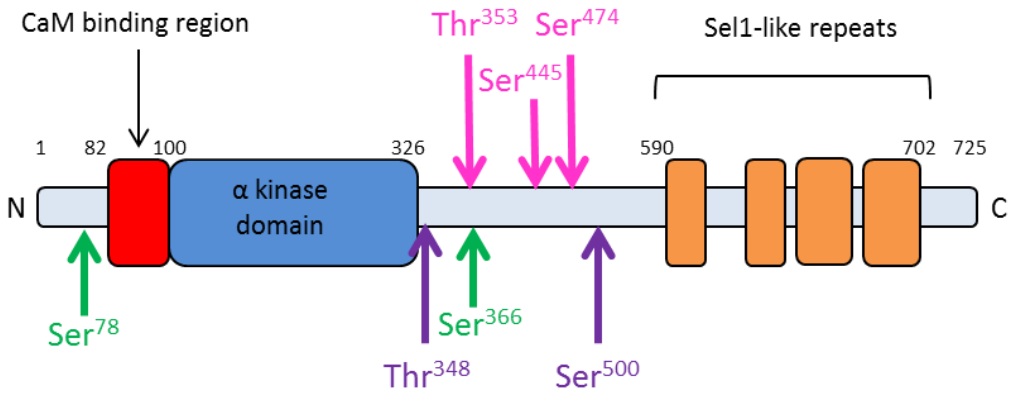

Figure 14. Autophosphorylation of eEF2K.

There are a number of autophosphorylation sites on eEF2K. Autophosphorylation at Ser^{78} and Ser^{366} impair the activation of eEF2K (coloured green), whilst autophosphorylation at Thr^{348} is thought to be necessary for eEF2K activity and autophosphorylation at Ser^{500} promotes Ca^{2+} independent eEF2K activity (coloured purple). Three other autophosphorylation sites have been identified (coloured pink) but their roles remain undetermined.

1.5.7 eEF2K in human disease

eEF2K plays a crucial role in regulating protein synthesis at the elongation stage of translation. It is itself heavily regulated due to its critical position as a regulator of protein synthesis, a process that must remain controlled within cells. eEF2K has thus been heavily implicated in human diseases, namely in glioblastoma and other malignancies but also in Alzheimer's disease (Li et al., 2005) and a number of other conditions.

It was shown that eEF2 phosphorylation in proliferating glioma cells is either absent or markedly decreased compared to normal glial cells as a result of diminished eEF2K activity (Bagaglio et al., 1993). There is also evidence that eEF2K may be important in linking growth factor signalling, protein synthesis and proliferation in human breast cancer (Parmer et al., 1999).

Most significantly, it is reported that eEF2K is involved in the positive regulation of autophagy in tumour cells and thus may promote cell survival in conditions of nutrient derivation (Wu et al., 2006). It therefore may be part of a survival mechanism in glioblastoma and other cancers, especially those with solid tumours, whereby eEF2K protects cancer cells from nutrient starvation. It has been shown that cancer cells cope with nutrient starvation and adapt to

poor nutrient availability by switching on eEF2K, likely via the AMPK pathway (Leprivier et al., 2013).

Autophagy plays a vital role in cell growth and differentiation, development and homeostasis, where cell components are degraded by the lysosomal machinery (Meijer and Codogno, 2004). As a result, it is usually tightly regulated in normal cells. Autophagy has been implicated in cancer as it has been demonstrated to become unregulated, with an especially important role in established tumours. It has been shown that autophagy can be increased, decreased or remain the same in different types of cancers and tumours and at different stages (Ogier-Denis and Codogno, 2003). If cells cannot activate autophagy, protein synthesis occurs at a much greater rate than protein degradation, leading to increased cellular growth – characteristic of tumour cells. However, the activation of autophagy can also benefit tumour cells to guarantee their survival under extreme conditions such as nutrient starvation (Cuervo et al., 2005).

eEF2K regulates protein synthesis, which is a process that consumes large amounts of energy; also it lies downstream of mTORC1, which is a known regulator of autophagy. Wu et al (2006) presented evidence that eEF2K can act as the link between mTORC1 and autophagy. They showed that eEF2K can induce increased autophagy and thus protect cancer cell viability and promote survival under conditions of nutrient deprivation. They also demonstrated that silencing eEF2K expression caused the autophagic response to nutrient deprivation to decrease.

Similarly to nutrient starvation, oxygen starvation (hypoxia) also imposes a stress on many cells, impairing ATP production by mitochondria. Hypoxia is especially important in highly oxidative tissues such as heart muscle and brain during cardiac ischemia or stroke. One important mechanism by which cells can respond to inadequate oxygen (hypoxia) involves the regulation of proteins by proline hydroxylation. Proline hydroxylation is catalysed by prolyl hydroxylases, which require oxygen as a co-substrate. In the absence of oxygen, proline hydroxylation will therefore be impaired. It has been shown that eEF2K is activated during hypoxia or upon inhibition of prolyl hydroxylases. And that eEF2K is inhibited by its hydroxylation on a highly

conserved proline residue, restricting its activity during normoxia. During hypoxia, when proline hydroxylation is impaired, eEF2K becomes more active to inhibit protein synthesis, thus protecting cells from hypoxia (Moore et al., 2015).

eEF2K has also been implicated in Alzheimer disease. The levels of a number of translational control elements have been studied in Alzheimer disease brains. Li et al (2005) found that levels of phosphorylated eEF2K were significantly increased when compared to controls and they suggested that this change could contribute to upregulating the translation of tau, a key protein in Alzheimer's disease pathology (Li et al., 2005). mTOR-dependent signalling has been implicated in a number of diseases, including other neurodegenerative diseases such as Parkinson's and Huntington's (Li et al., 2005).

1.6 Protein kinases

1.6.1 Phosphorylation by protein kinases

Protein kinases (in concert with protein phosphatases) mediate the majority of signal transduction in eukaryotic cells. They are involved in controlling many cellular processes such as metabolism, transcription, cell cycle progression, apoptosis, differentiation and cytoskeletal rearrangement and cell movement (Manning et al., 2002b).

Protein kinases are enzymes that modify other proteins by a process termed protein phosphorylation, an essential mechanism for the control of various cellular processes and signalling pathways. Protein phosphorylation involves the transfer of a phosphate group from an ATP molecule to a serine, threonine or tyrosine residue of a protein target, thus modifying protein activity. Protein kinases catalyse this reversible phosphotransfer reaction on a vast number of diverse protein substrates whilst protein phosphatases can remove the phosphate group and therefore reverse the modification.

The process of protein phosphorylation on serine residues was first discovered in 1955 with glycogen phosphorylase (Fischer and Krebs, 1955, Sutherland and Wosilait, 1955). However, it was not until the discovery of cyclic AMP dependent protein kinase (cAMPK), now termed protein kinase A (PKA), and tyrosine phosphorylation that a host of other protein kinases were

identified, leading to the acceptance of a general role for protein kinases in the regulation of numerous cellular processes (Johnson et al., 1998).

Eukaryotic protein kinases (ePKs) are now known to constitute 1.5-2.5% of all eukaryotic genes (Manning et al., 2002a) whilst the completion of the human genome project saw the identification of 518 putative protein kinases, comprising approximately 1.7% of all human genes (Manning et al., 2002b).

1.6.2 Evolution and classification of protein kinases

The ePKs comprise one of the largest superfamilies of homologous proteins, related by their catalytic kinase domains. A superfamily is defined as a group of proteins that share structure, sequence and functional features, suggesting that they are derived from a common ancestor protein (Murzin et al., 1995).

Most protein kinases belong to this single superfamily as they contain a highly conserved protein kinase catalytic core domain. They are then further classified into a hierarchy of groups, families and subfamilies, originally by Hanks and Hunter (Hanks and Hunter, 1995) and then extended by Manning et al (2002a). This is demonstrated for the human kinome in Figure 15, showing the nine groups of the family and within these a vast number of families and subfamilies classified according to kinase domain sequence similarity as well as knowledge concerning sequence similarity and domain structure, biological functions and classification of yeast, worm and fly kinomes (Manning et al., 2002b).

Although there is a relatively high degree of sequence conservation and a number of structural similarities between the members of the ePK superfamily, there is some variation between their structures, even within the largely conserved protein kinase catalytic core (Scheeff and Bourne, 2005). This is reflected in the division of the ePK superfamily into a number of separate families, which are in turn grouped based on their structural folds; the protein kinases in a certain fold group have a catalytic core with highly similar architecture and structures (Cheek et al., 2005). The result is a large superfamily of protein kinases that differ in their structural features, probably as a consequence of the structurally and functionally diverse nature of their

substrates, their specificities and different regulatory mechanisms. The structural diversity allows for specific interactions with the vast array of protein kinase targets (Scheeff and Bourne, 2005).

In addition to ePKs, 13 atypical protein kinase families have been identified which have biochemical kinase activity but lack sequence similarity and show different degrees of structural homology to the ePKs (Manning et al., 2002b). eEF2K is an atypical protein kinase, belonging to the alpha kinase family.

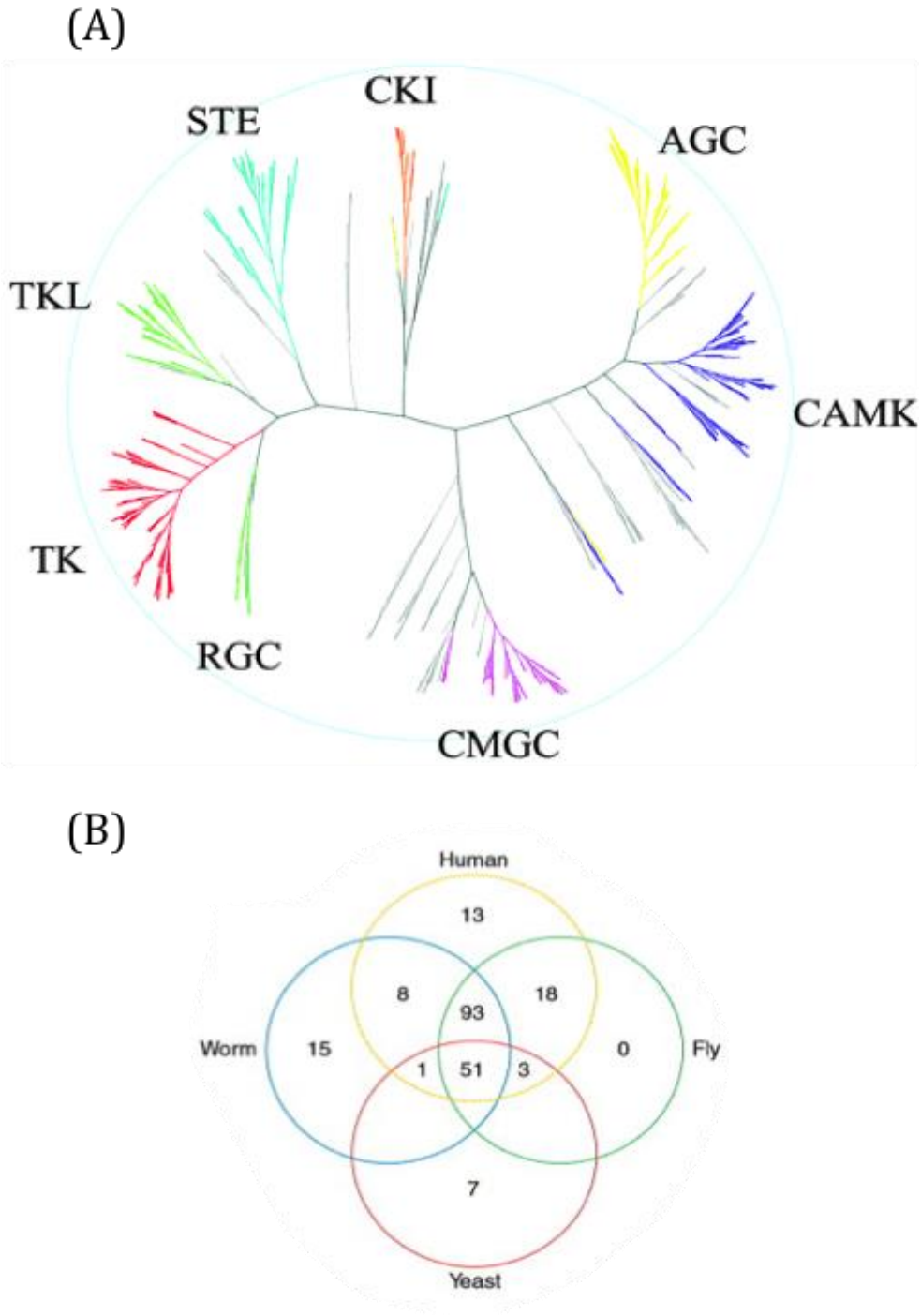

Figure 15. Classification of protein kinases

Dendrogram of ePK domains from human kinome (A) and distribution of the kinase subfamilies among human, fly, yeast and worm genomes (B). Kinase families refer to: serine/threonine kinases (STE), casein kinases (CK1), protein kinase A, G and C families (AGC), Ca^{2+}/CaM dependent protein kinases (CAMK), CMGC family includes cyclin-dependent kinases, mitogen-activated protein kinases, glycogen synthase kinases and CDK-like kinases, receptor guanylate cyclases (RGC), tyrosine kinases (TK), Tyrosine kinase-like kinases (TKL). Figure taken from (Manning et al., 2002a) and (Manning et al., 2002b).

1.6.3 Protein kinase catalytic core domain

ePK sequence comparisons and structure elucidation reveal a protein kinase catalytic core domain with common architecture that is largely conserved both in sequence and structure throughout the superfamily. This region consists of approximately 250-300 amino acid residues (Hanks et al., 1988) and is responsible for the catalytic activity of protein kinases.

1.6.3.1 Structure of the Protein kinase catalytic core

The consensus structure of the protein kinase catalytic core is often depicted using protein kinase A (PKA) as a standard; this was the first protein kinase to have its structure solved (Knighton et al., 1991b). It consists of two lobes, an N-terminal lobe and a C-terminal lobe, that create a deep cleft at the interface of the two lobes where the ATP binding region is located and the phosphor-transfer reaction occurs. The N-terminal lobe is smaller and comprised primarily of a five-stranded antiparallel β-sheet, whilst the larger C-terminal lobe is mostly α-helical with a single β-sheet at the domain interface. The structure of PKA is shown in Figure 16.

The C-terminal lobe is involved mainly with protein binding and catalysis, as well as containing several residues that interact with ATP. The N-terminal lobe is also associated with nucleotide binding and contains the highly conserved glycine-rich loop (also termed the P-loop) with the Gly-x-Gly-x-x-Gly (GXGXXG) motif that binds to ATP. Most of the invariant and highly conserved amino acid residues are located at the sites of nucleotide binding and catalysis, which converge at the domain interface. The catalytic loop and the activation loop in the C-terminal lobe and the catalytic triad, composed of the side chains of Lys^{72}, Asp^{184} and Glu^{91}, are further examples of highly conserved features in the protein kinase catalytic core (Knighton et al., 1991b). The functional roles of these conserved features will be discussed in terms of the catalytic mechanism in Section 1.6.3.2.

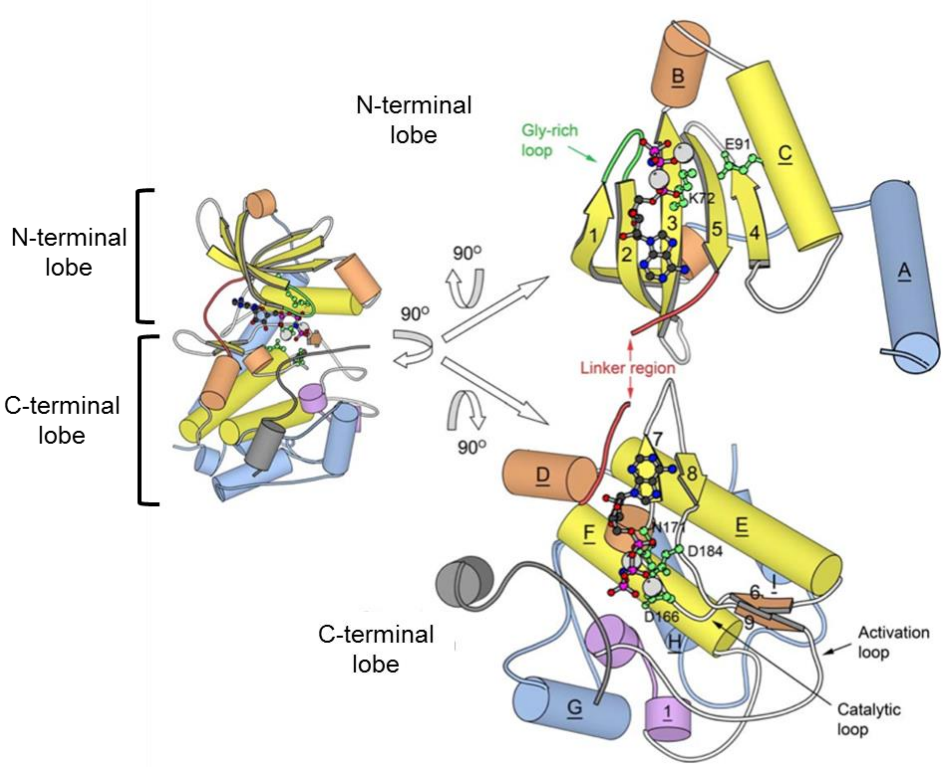

Figure 16. Structure of the kinase catalytic core domain of PKA.

The structure of PKA is bilobal, with an N-terminal lobe consisting mostly of β-sheet (arrows) and a C-terminal lobe that is primarily made up of α-helices (cylinders). The expanded views shown on the right were achieved according to the rotations shown by the arrows to demonstrate the locations of the highly conserved regions of the protein kinase catalytic core at the interface between the two lobes. The activation and catalytic loops are shown with arrows in the C-terminal lobe and the glycine rich lobe is shown in green in the N-terminal lobe. Those residues that are highly conserved and critical, including the catalytic triad, are also shown in green and labelled. Figure adapted from (Scheeff and Bourne, 2005).

1.6.3.2 Catalytic mechanism of conventional ePKs

Conventional ePKs are responsible for protein phosphorylation, which involves the transfer of a phosphate group from an ATP molecule to a serine, threonine or tyrosine residue of a protein target. The protein kinase catalytic core domain catalyses this reversible phosphotransfer reaction through three separate roles. The domain binds and orientates the ATP phosphate donor with a divalent cation, usually Mg^{2+} or Mn^{2+}, and also binds and orientates the protein substrate to form the ternary complex. This is followed by transfer of the γ-phosphate from the donor, ATP, to the acceptor hydroxyl on serine, threonine or tyrosine residues of the protein substrate (Hanks and Hunter, 1995). An outline of this reaction scheme is shown in Figure 17.

Structural studies of protein kinase A (PKA) with bound inhibitors and nucleotides (Bossemeyer, 1995, Knighton et al., 1991c, Zheng et al., 1991, Knighton et al., 1991a) have led to the elucidation of functional roles for the highly conserved residues and regions of the protein kinase catalytic core domain. These are explained and shown on a structure of PKA bound to ATP and a peptide substrate in Figure 17.

The N-terminal lobe contains the consensus motif Gly-x-Gly-x-x-Gly-x-Val, which is located in a loop region between the first and second β-strands and is thus often termed the Gly-rich loop. This loop is inherently flexible and is described as acting as a clamp to anchor the non-transferable phosphates of ATP (Taylor et al., 1992, Zheng et al., 1991). The backbone amides at positions 4, 5 and 6 of this motif form hydrogen bonds with the β-phosphate oxygens of the ATP molecule, whilst positions -1 and 8 contribute to a hydrophobic pocket that encloses the adenine ring (Hanks and Hunter, 1995).

There are two conserved, charged residues in the N-terminal lobe, Lys^{72} and Glu^{91}. In the ternary complex, Lys^{72} comes close to the α- and β-phosphates of ATP. These two residues are part of the stable scaffolding of the core structure, located in the middle of a β-strand and α-helix respectively. It is likely therefore that they provide a docking site for ATP, together with the hydrophobic pocket that binds the adenine ring. Once the nucleotide is bound, the Gly-rich loop can clamp it firmly into its proper position (Taylor et al., 1992)

The catalytic loop, located in the C-terminal lobe in a loop region between β-sheets 6 and 7, contains two invariant residues, Asp^{166} and Asn^{171}, as well as two highly conserved residues, Arg^{165} and Lys^{168}. Asp^{166} within the loop serves as a catalytic base to correctly position and accept the proton from the hydroxyl group of the substrate, then also to facilitate the rapid release of the phosphorylated target once phosphotransfer has taken place. Asn^{171} is located on the other side of the loop, and its side chain is responsible for stabilising the loop by hydrogen bonding to the backbone carbonyl of Asp^{166}. Asn^{171} is also nearby to the side chain of another conserved residue, Asp^{184}, which forms part of the catalytic triad along with Lys^{72} and Glu^{91} of the N-terminal lobe (Taylor et al., 1992) Asp^{184} chelates the Mg^{2+} ions that bridge the β-and γ-phosphates of

the ATP, therefore orientating the γ-phosphate for transfer (Hanks and Hunter, 1995)

An activation loop is present in the C-terminal domain following β-strand 9. Many protein kinases are known to be activated by phosphorylation of residues in this loop, for example, PKA requires phosphorylation at Thr^{197} for maximum kinase activity (Steinberg et al., 1993).

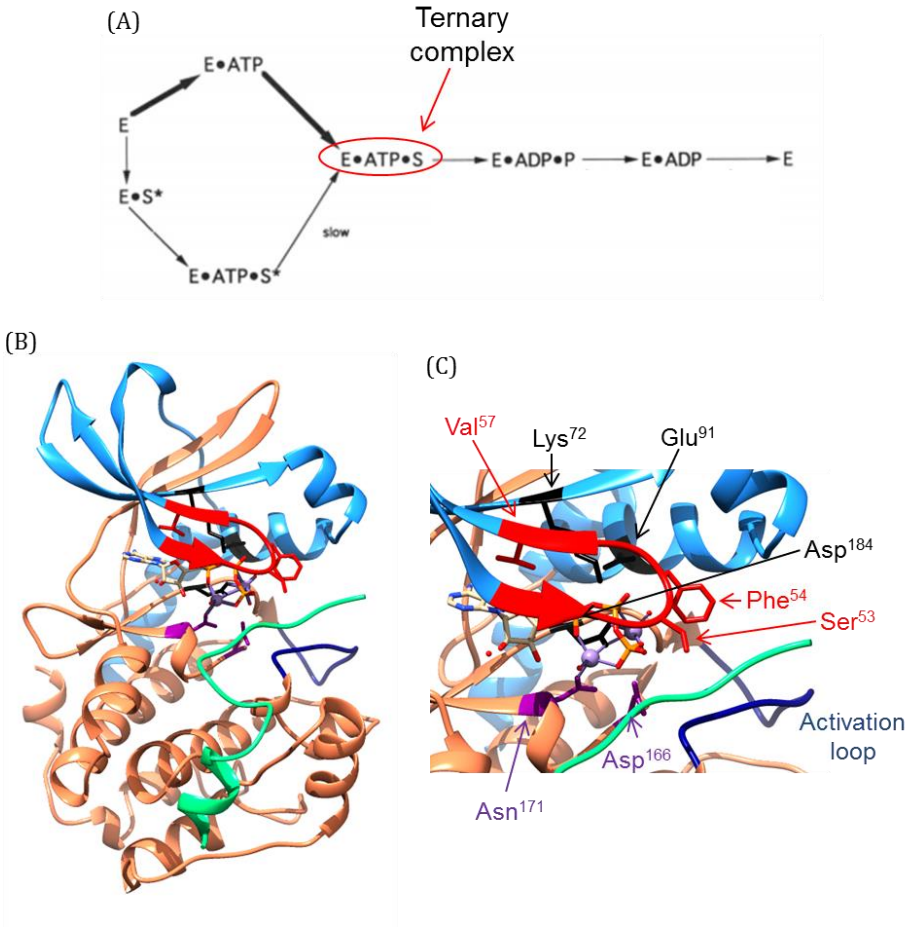

Figure 17. Catalytic mechanism of protein kinases depicted using protein kinase A.

Reaction pathway for catalysis by protein kinases (A). Structural representation of the location of residues and regions important for catalysis in protein kinase A with full catalytic core domain shown (B) and a zoomed in view of the interface of the two lobes (C). The N-terminal lobe is coloured blue, the C-terminal lobe is coloured orange and the bound peptide substrate is coloured green. There are two Mn^{2+} ions bound which are coloured lilac and a bound ATP molecule is also shown. Residues important for catalysis and discussed in the text have their atoms shown. The Gly-rich loop is coloured red, the three residues which form the catalytic triad are coloured black, two invariant residues in the catalytic loop are coloured purple and the activation loop is coloured navy. PDB ID: 1ATP. (A) taken from (Madhusudan et al., 1994).

1.6.4 Atypical protein kinases

Atypical protein kinases lack sequence homology with the protein kinase catalytic core of the conventional ePKs. They have modified structural folds and do not share many of the conserved kinase features (Scheeff and Bourne, 2005), however, although they lack sequence homology with ePKs, they do have some structural features in common (Manning et al., 2002a). In fact the overall architecture of the protein kinase domain is often the same but with some differing structural details (Ye et al., 2010).

1.6.5 Alpha kinases

The alpha kinases are a family of atypical protein kinases that demonstrate very little sequence similarity to conventional ePKs. They share an alpha kinase catalytic domain; the sequence of which is conserved between the members of the family, as shown in Figure 18, but does not share any significant homology to the conserved protein kinase catalytic core domains of conventional ePKs (Ryazanov et al., 1999).

There are, however, functional counterparts in the active site of alpha kinases for many of the highly conserved residues responsible for catalysis in conventional ePKs (Ye et al., 2010), suggesting that there is a common but distant ancestor and evolutionary history between the alpha kinases and conventional ePKs (Crawley and Cote, 2009).

Genes encoding these protein kinases classified as alpha kinases are present in a diverse range of organisms, with six being present in humans (Drennan and Ryazanov, 2004). There are three alpha kinases that have been studied most intensely and as a result are the best characterised; myosin heavy chain kinase A (MHCK A) from *Dictyostelium discoideum*, channel kinase (ChaK) or transient receptor potential melastatin-like 6 and 7 (TRPM6 and TRPM7) and eukaryotic elongation factor 2 kinase (eEF2K). There are now crystal structures available for MHCK A (Ye et al., 2010) and ChaK (Yamaguchi et al., 2001).

Much of the early work on alpha kinases focused on MHCK A from *Dictyostelium* and revealed the unusual feature of this family that resulted in the collective term alpha kinases. It was discovered that MHCK A, as well as other

members of the family, have an unusual tendency to phosphorylate serine and threonine residues in alpha helices. This is in contrast with conventional protein kinases, which usually have a preference for phosphorylating target residues within the context of loops, turns or regions with an irregular structure (Ryazanova et al., 2004). It has since been shown in recent studies (Clark et al., 2008) that some members of the family are able to phosphorylate residues that are not located in alpha helices, however, the name alpha kinases still remains (Middelbeek et al., 2010). Examples of this are two channel kinases termed TRPM6 and TRPM7 which can also phosphorylate the three mammalian alpha-helical assembly domains of their substrates, myosin II heavy chain isoforms (MHCK-A, B, and C) but also the non-helical C-terminus of these substrates (Clark et al., 2008).

The crystal structures of the alpha kinase catalytic domains of MHCK A and ChaK revealed a number of conserved features present in the alpha kinase family. Comparison of the two structures demonstrates that they both share an overall similarity in terms of their secondary structure and architecture. Sequence alignment of the catalytic domains of the alpha kinase family reveals that secondary structural elements are maintained, indicating a common structure for the alpha kinase catalytic domain. In addition, the key catalytic residues of the active site are positioned in almost precisely the same locations in space in both the MHCK A and ChaK alpha kinase domains (Ye et al., 2010). However, there are some significant differences in the structures of alpha kinase domains compared to the kinase domains of conventional ePKs, especially in the C-terminal lobe. The crystal structure of ChaK revealed that this lobe shares a marked similarity to the structure of a group of metabolic enzymes that contain an ATP grasp fold.

An example of these similarities and differences in protein structure between alpha kinase domains and the kinase domains of conventional ePKs concerns a particular characteristic feature of conventional ePKs, which is the presence of a conserved GXGXXG motif. This motif is positioned within the glycine rich loop in the N-terminal lobe and is important for binding the phosphates of ATP. Alpha kinases contain a similar conserved glycine rich motif (Ryazanov et al., 1997), however, it is located in a different region in alpha

kinases compared to ePKs. In alpha kinases this motif is located at the extreme C-terminus of the catalytic core in a loop that structurally resembles the activation loop in conventional ePKs and is therefore likely to be involved in peptide substrate recognition (Middelbeek et al., 2010, Yamaguchi et al., 2001). Consequently the activation loop and thus the C-terminal lobe of alpha kinases differ substantially from the structure of conventional ePKs.

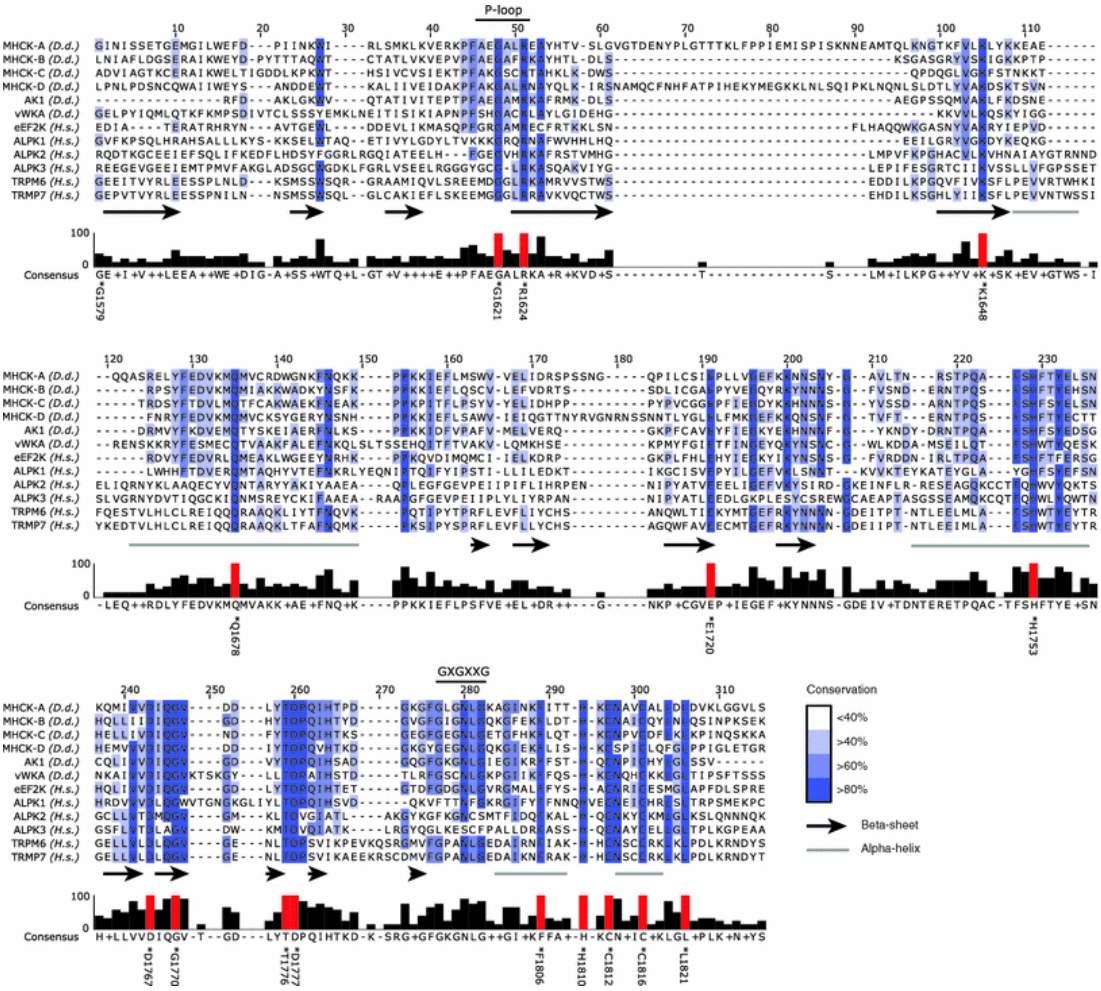

Figure 18. Sequence alignment of *Dictyostelium* and human alpha kinases.

Dictyostelium and human alpha kinase amino acid sequences aligned using ClustalW2 sequence alignment software. Those sequences used correspond to the alpha kinase domain of human TRPM7 (residues 1579-1830). The blue shading shows the conservation of specific amino acid residues and a bar chart underneath shows the alignment, where red bars represent fully conserved residues. Figure taken from (Middelbeek et al., 2010).

1.6.5.1 MHCK A

MHCK A is often referred to as the prototypical alpha kinase (Cote et al., 1997). Its role within the cell involves phosphorylation of the myosin II tail to

disrupt myosin II bipolar filament assembly and thus inhibit processes such as cytokinesis (Crawley et al., 2011). The crystal structure of the alpha kinase catalytic domain of MHCK A was solved in complex with various ATP derivatives in 2010 (Ye et al., 2010). This work revealed an overall architecture that is similar to that known for the kinase catalytic core domains of conventional ePKs but differs in the precise structural details. Similarly the structure was found to consist of N- and C-terminal lobes, which in addition also have similar compositions to the conventional ePKs. The N-terminal lobe is composed mainly of an antiparallel β-sheet, formed from seven β-strands whilst the C-terminal lobe is made up of three α-helices as well as a short stretch of antiparallel β-strands. There are however some topological differences in the C-terminal lobe compared to conventional ePKs.

In MHCK A the two lobes are connected and supported by a central α-helix of 21 amino acid residues that runs from the top to the bottom of the domain. A cleft is consequently formed at the interface between the two lobes; which is where the ATP molecule binds. In the case of MHCK A the active site is relatively open in nature and extends to the right of the bound ATP, forming an active site pocket. The structure of the alpha kinase catalytic domain of MHCK A with structural features highlighted is shown in Figure 19. This active site pocket is regulated by a C-terminal glycine-rich loop, termed the N/D loop, which controls access to the pocket by binding to Mg^{2+} ions and changing conformation. The crystal structure revealed that the catalytic alpha kinase domain also tightly binds a zinc atom as well as two Mg^{2+} ions. The Zn^{2+} ion is required for stability whilst the binding of Mg^{2+} ions, one to the active site pocket and one to the centre of the N/D loop, is regulatory. In addition, a phosphate (P_i) molecule binds to a region termed the P_i pocket, which is a highly basic site in the C-terminal lobe (Ye et al., 2010).

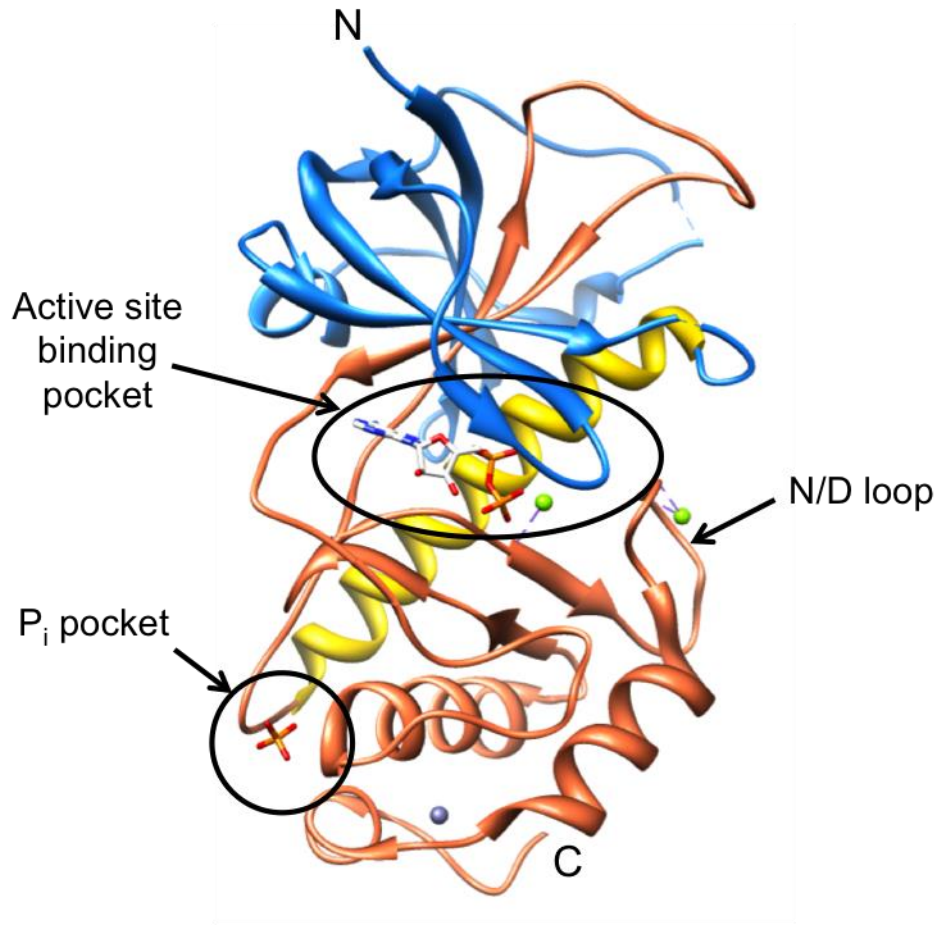

Figure 19. Structure of the alpha kinase catalytic domain of MHCK A.

The structure of the alpha kinase catalytic domain of MHCK A is similar to that of conventional ePKs. It has an N-terminal lobe composed mainly of a β-sheet (blue) and a C-terminal lobe consisting mainly of α-helices (orange) with a short stretch of β-strands. In contrast to conventional ePKs it has a central α-helix that runs from the top to the bottom (yellow). The active site binding pocket is formed at the interface between the two lobes and access to this is regulated by the C-terminal N/D loop, which binds a Mg^{2+} ion (green sphere). ADP is bound in the active site. Another Mg^{2+} ion binds in the active site and there is also a Zn^{2+} ion in the C-terminal lobe (grey sphere). PDB ID: 3PDT.

There is some evidence that the alpha kinase catalytic mechanism may differ in an important way from the conventional ePKs. Ye et al (2010) found that when the kinase domain of MHCK A was crystallized in the presence of a peptide substrate an invariant residue in the catalytic loop, Asp^{766}, was phosphorylated, indicating that the alpha kinases may carry out their phosphorylation reaction through an aspartylphosphate intermediate.

In addition, it was shown that autophosphorylation is vital to the function of MHCK A and causes the kinase activity to increase 50-fold. Crawley

et al (2011) found that a particular residue, Thr^{825}, is a key autophosphorylation site required for the activity of MHCK A. They proposed a mechanism by which autophosphorylated Thr^{825} acts as a ligand for the P_i pocket to induce conformational change and convert MHCK A into its high activity state.

Sequence alignments of the alpha kinase family indicate that eEF2K and other members may also be regulated by this mechanism (Crawley et al., 2011). In eEF2K, Thr^{348} has been identified. The mechanism and conservation among the alpha kinase family is shown in Figure 20. Tavares et al (2014) show that Thr^{348} plays a similar role in eEF2K as Thr^{825} in MHCK A. Ca^{2+}/CaM binding to eEF2K enhances the ability of eEF2K to autophosphorylate, resulting in the phosphorylation of Thr^{348} which binds to a conserved basic pocket in the kinase domain. In this way, Thr^{348} autophosphorylation appears to control the catalytic output of active eEF2K (Tavares et al., 2014).

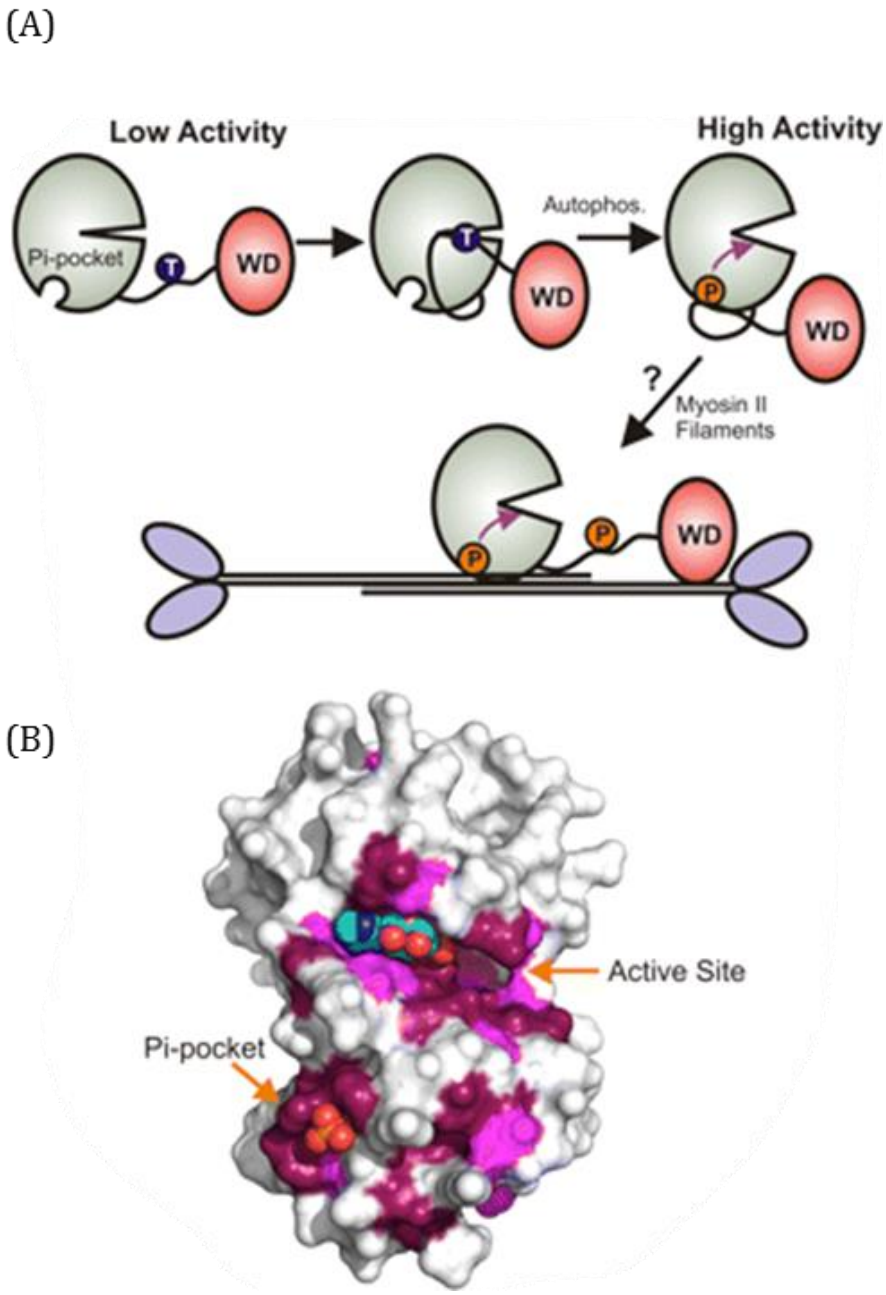

Figure 20. Proposed activation mechanism for the alpha kinase family.

Model for the activation of MHCK A, showing only the alpha kinase catalytic domain (green) and WD-repeat domain (red). When the P_i pocket is empty the kinase has low activity. Autophosphorylation of Thr^{825}, which is located in the disordered sequence that connects the two domains shown, provides a ligand for the P_i pocket. This induces a conformational change (purple arrow) that converts the domain into a high activity state (A). The conservation of amino acids among the alpha kinase family was mapped onto a structure of MHCK A (PDB ID: 3KLM) using the ConSurf server. A multiple sequence alignment of 20 MHCK homologues was performed and invariant residues coloured purple and highly conserved residues coloured violet. The P_i pocket, the active site and the N/D loop are all highly conserved, indicating a common activation mechanism among the family (B). Figure taken from (Crawley et al., 2011).

1.6.5.2 ChaK (or TRPM6 and TRPM7)

Transient receptor potential melastatin-like (TRPM6 and TRPM7) ion channels, often known as channel kinases (ChaK), are permeable to Ca^{2+} and Mg^{2+} ions and are therefore believed to be involved in regulating the influx of Ca^{2+} ions in mammalian cells (Ryazanova et al., 2001). They are novel in that they combine an ion channel domain with an intrinsic alpha kinase catalytic domain and so are able to phosphorylate themselves as well as other proteins on threonine residues. Sequence analysis showed that the kinase domain of ChaK has little detectable sequence similarity to that of conventional ePKs, however, similarly to MHCK A, its crystal structure demonstrates significant structural similarity to the kinase domain of conventional ePKs. It consists of two lobes, which have an overall secondary structure similar to that described for conventional ePKs and exemplified by PKA, although the C-terminal lobe shows some topological differences. The nucleotide binds at the interface between the two lobes in a similar manner to that demonstrated for other kinases. Similar to MHCK A, there are a number of residues key for catalysis which are conserved between ePKs and ChaK. The similarities and differences between the structures of the catalytic domains of ChaK and PKA and the locations of conserved residues are demonstrated in Figure 21.

There are also a number of conserved structural and functional features with the other members of the alpha kinase family. This is especially evident when comparing the crystal structure of the alpha kinase domain of MHCK A with that of ChaK. As in MHCK A, there is an invariant aspartate residue, Asp^{1765}, that plays a role in catalysis. The exact role played by this residue in ChaK is not precisely the same as that seen by the invariant aspartate in MHCK A, as ChaK is not thought to catalyse phosphotransfer via an aspartate intermediate but instead by a mechanism similar to that used by conventional ePKs (Yamaguchi et al., 2001).

The structure also revealed similarities to a group of metabolic enzymes that contain ATP-grasp domains. Yamaguchi et al (2001) determined that there is marked structural similarity between ChaK and conventional ePKs in the N-terminal lobe but that the structure of the C-terminal lobe of ChaK shows significant differences. Instead, the C-terminal lobe has key features that are

more similar to the corresponding lobe of enzymes with ATP-grasp folds. For example, the kinase domain of ChaK does not contain the catalytic loop, which is a defining feature of conventional ePK kinase domains. In contrast, Asp^{1765}, which is important for catalysis, is located on a continuous beta strand (Yamaguchi et al., 2001).

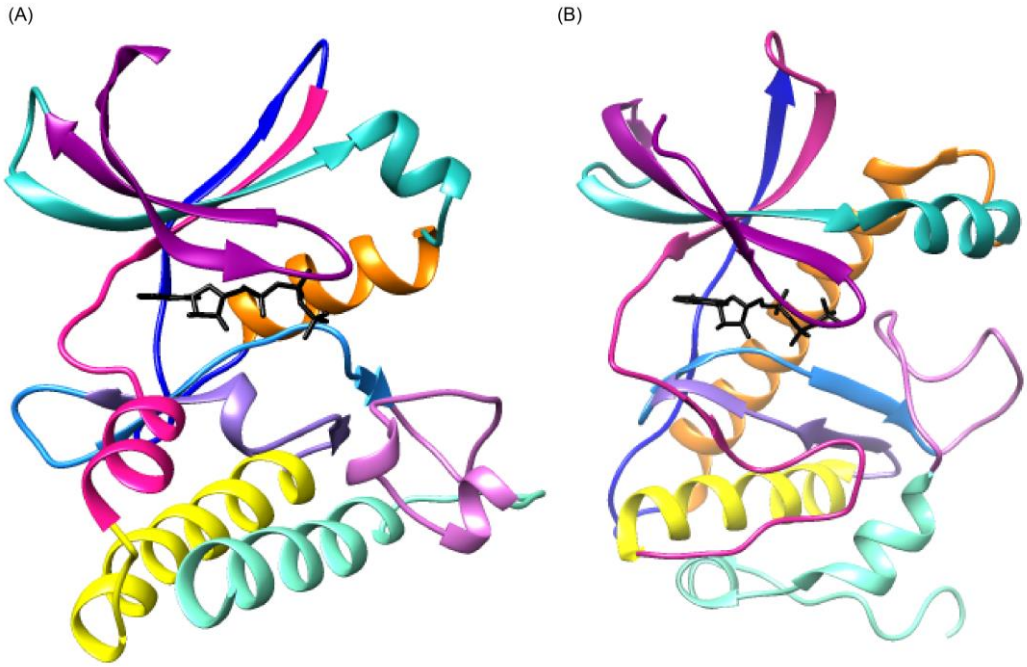

Figure 21. Comparison of the structures of the alpha kinase catalytic domain of ChaK and the catalytic core domain of PKA.

The structure of the alpha kinase catalytic domain of ChaK (A) and the structure of the kinase catalytic core domain of PKA (B). Some of the key amino acid residues involved in catalysis are highlighted, demonstrating conservation across the two structures. There are a number of structural similarities within the N-terminal lobes but some structural differences within the C-terminal lobes, especially the location of the key aspartate residue, shown in dark blue. Figure adapted from (Drennan and Ryazanov, 2004).

1.6.6 Ca^{2+}/CaM dependent protein kinases

There is another family of protein kinases termed the Ca^{2+}/CaM-dependent protein kinases. Only one member of the alpha kinase family, eEF2K, is classified as a Ca^{2+}/CaM dependent protein kinase (Palfrey, 1983), as well as being termed an alpha kinase. This is due to its dependence on CaM for activation and to carry out its role within cells and is therefore also referred to as CaM kinase III. In addition, the family also includes phosphorylase kinase,

myosin light chain kinase (MLCK) and CaM kinases I, II, and IV, which all belong to the conventional ePK family. These kinases can then be further grouped depending on whether they have a single substrate, in the case of phosphorylase kinase, MLCK and eEF2K, or whether they are multifunctional with several substrates like CaM kinase I, II and IV.

This family of protein kinases has an overall domain architecture, which is common between most members, except eEF2K, and which has a number of variations on the common structure. This conserved domain structure, shown in Figure 22, consists of an N-terminal kinase domain followed by an autoinhibitory domain that overlaps with a CaM binding domain. Some also contain a C-terminal association domain that is required for multimerisation (Hook and Means, 2001).

eEF2K differs markedly from the other members of the family in terms of the domains it consists of and the arrangement of these domains. It does not contain the usual overlapping autoinhibitory and CaM binding domain at the C-terminus but instead has a CaM binding domain at the N-terminus, preceding the kinase domain. It is yet to be determined whether this domain has an autoinhibitory function. In addition, the catalytic domain of eEF2K bears very little resemblance in sequence to the catalytic core domains of the other Ca^{2+}/CaM dependent protein kinases, which are all well conserved among the family and with other conventional ePKs.

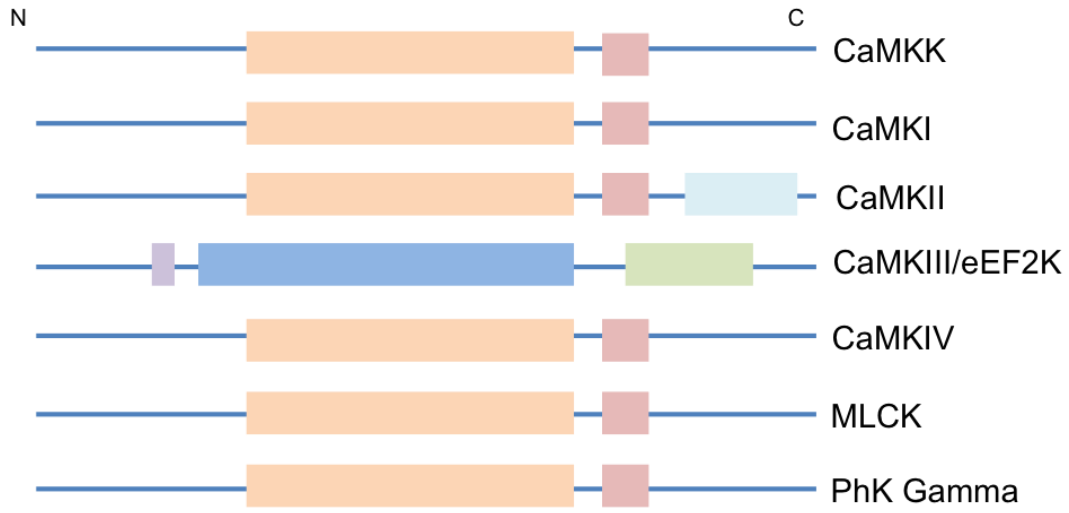

Figure 22. Domain structures of members of the Ca^{2+}/CaM dependent protein kinase family.

The domain architecture of the Ca^{2+}/CaM dependent protein kinase family is conserved among all members of the family, except for eEF2K (or CaM kinase III). The conserved kinase domains are shown in orange, whilst the kinase domain of eEF2K is shown in dark blue to indicate its difference. The autoinhibitory and CaM binding domains are shown in red for the majority of the kinases although it should be noted that the CaM binding region of eEF2K is situated near the N-terminus and is coloured purple. The additional domain in CaM kinase II is shown in light blue and the one in eEF2K is shown in green. Figure adapted from (Swulius and Waxham, 2008) and not drawn to scale.

There is a high degree of conservation of the key amino acid residues involved in the phosphotransferase reaction between Ca^{2+}/CaM dependent protein kinases and conventional ePKs. It is therefore believed that Ca^{2+}/CaM dependent protein kinases carry out catalysis by the same basic mechanism as conventional ePKs. In addition, the catalytic domain demonstrates significant structural similarity to the common fold of the catalytic core domain of ePKs (Swulius and Waxham, 2008), as demonstrated by the crystal structures of CaM kinase I (Goldberg et al., 1996) and CaM kinase II (Rellos et al., 2010).

1.6.6.1 Autoinhibition of Ca^{2+}/CaM dependent protein kinases

The majority of kinases in the Ca^{2+}/CaM dependent protein kinase family appear to share similar general mechanisms of action, in terms of their catalysis and thus the process by which they perform the phosphotransfer reaction. In addition, they also share a similar method of regulation, whereby their activation is dependent on the binding of Ca^{2+}/CaM.

The basal levels of Ca^{2+} are low (see Section 1.4), which means there is little Ca^{2+} available to bind to Ca^{2+} binding proteins such as CaM. Consequently, there are few Ca^{2+}/CaM complexes in cells (Chin and Means, 2000) and thus the Ca^{2+}/CaM dependent kinases are inactive. These kinases remain inactivated as a result of autoinhibition in the resting state. The classic, bi-lobed structure of the protein kinase catalytic core is followed by a regulatory domain which contains both an autoinhibitory and an overlapping CaM binding domain. It is believed that autoinhibition is achieved by a pseudosubstrate mechanism involving the autoinhibitory domain, which prevents phosphotransfer by the enzyme. The autoinhibitory domains of the Ca^{2+}/CaM dependent kinases achieve this by either blocking the binding of substrate, distorting the catalytic site or a combination of both of these effects. When Ca^{2+} levels increase within the cell as a result of specific cell signalling events, the Ca^{2+} ions will bind to CaM and form Ca^{2+}/CaM complexes. These complexes can bind to the kinases at their CaM binding regions, disrupting the interactions between the autoinhibitory and the catalytic domains. Consequently the autoinhibition is lifted as the pseudosubstrate autoinhibitory domain is removed from the substrate binding site and the kinase is activated (Swulius and Waxham, 2008).

This mechanism is demonstrated by the crystal structure of CaMKI that has been determined in the autoinhibited form (Goldberg et al., 1996). The regulatory region at the C-terminus forms a helix-loop-helix that crosses the two domains of the catalytic core domain of the enzyme to make multiple inhibitory interactions. The first helix and the loop disrupt the substrate binding site whilst the second helix causes conformational change in the ATP binding region, most notably the Gly-rich loop, to obstruct the binding pocket, as shown in Figure 23. In addition, a section of the CaM binding region points away from the catalytic core domain and is thus made available for an interaction with CaM (Goldberg et al., 1996).

This general mechanism is thought to be true for all of the kinases in the family, except for eEF2K, which varies in its sequence and therefore probably also in its mechanism of action and regulation. Relatively little is known about eEF2K in comparison to the other Ca^{2+}/CaM dependent protein kinases.

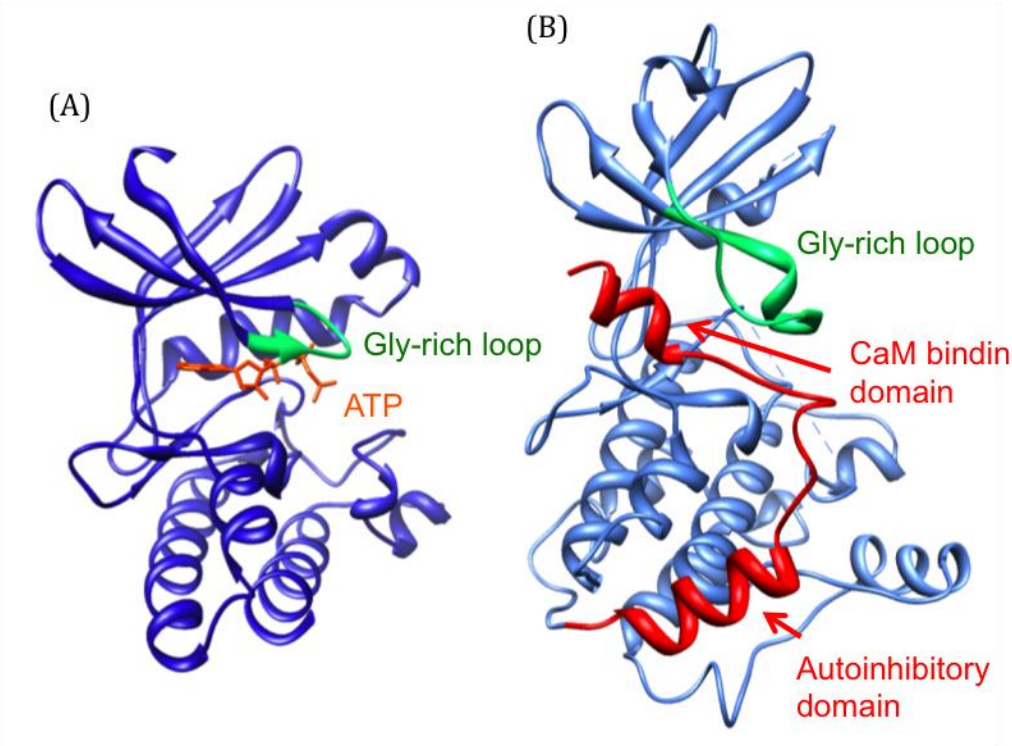

Figure 23. Autoinhibited structure of CaMKI compared to an active structure of PKA.

The structure of the kinase catalytic core of PKA with ATP bound (orange) in an active state (A) and the structure of CaMKI in an autoinhibited state (B). The regulatory region of CaMKI is shown in red and forms a helix-loop-helix that binds across the catalytic domain. This distorts the Gly-rich loop (shown in green). The difference in conformation of the Gly-rich loop is evident between the two structures. PDB IDs: 1ATP (PKA) and 1A06 (CaMKI).

1.7 Studying protein structure and function

1.7.1 Nuclear magnetic resonance (NMR)

The first demonstrations of NMR were published in 1946 by two separate groups almost simultaneously; Bloch, Hansen and Packard from Stanford University (Bloch et al., 1946) and Purcell, Torey and Pound (Purcell et al., 1946) working at Harvard University for which they were jointly awarded the Nobel Prize for Physics in 1952. Their early work has now evolved into a vital experimental technique with vast applications in a number of fields including chemistry, physics, biology, medicine, archaeology and many more (Andrew, 1984).

NMR is extremely useful in the determination of atomic structure, accounting for over 10,000 structures in the Protein Data Bank as of 2013 (Bernstein et al., 1977). Although X-ray crystallography remains the most

popular experimental method for solving three-dimensional structures of proteins, NMR is able to provide information on many aspects of protein science including insight into protein dynamics.

There are numerous textbooks and lecture series' available with well explained and detailed descriptions of NMR theory and the vast number of NMR experiments available. Some of these have been used throughout this study and should be referred to for details on NMR theory that will not be covered in the scope of this literature review (Cavanagh, 1996, Freeman, 1987, Hore, 1995, Keeler, 2010, Rattle, 1995). Spin Dynamics by Malcolm Levitt offers an up to date and especially thorough explanation of NMR theory (Levitt, 2001).

This study has made use of a number of classical NMR features, namely chemical shift, J-coupling and dipolar coupling as well as chemical exchange. These shall be discussed in some detail in the following sections.

1.7.1.1 Chemical shifts

The signals detected by the NMR spectrometer are the resonance frequencies of each nucleus. The resonance frequency (ω) of a nucleus is determined mainly by the strength of the magnetic field (B_0) and the gyromagnetic ratio (γ) as shown in Equation 1.

$$\boldsymbol{\omega = \gamma B_0} \qquad \textbf{Equation 1}$$

This means that at a given field strength all protons will resonate at a very similar frequency and in the same way all ^{13}C nuclei will resonate at a similar frequency to each other but which is different from that of protons.

However, the observed resonance frequencies also depend to some degree on the local chemical environment of each nucleus. This means that each nucleus (in a different environment) will differ slightly from the standard values and therefore from each other. This difference in resonance frequencies is termed the chemical shift and it is very important for the analysis of NMR data to distinguish between nuclei in different chemical environments, meaning for example, that the Cα of glycine will be characteristic and different from the Cα of other amino acid residues. It also means that there will be separate signals for each of the protons in a protein.

The chemical shift arises because of the local distribution of electrons at each nucleus. This is because the external magnetic field (B_0) induces motion of the electrons that generates a secondary local magnetic field (B') at each nucleus. This can either enhance or oppose the main magnetic field in an effect called nuclear shielding. As a result, the field that is actually experienced by a nucleus (B) in a molecule such as a protein differs slightly from the external magnetic field. Therefore this net magnetic field at the location of a nucleus depends on the external magnetic field and the secondary field and can be given by Equation 2 whereby σ is the constant of proportionality between B_0 and B' termed the shielding constant.

$$\boldsymbol{B = B_0 - B' = B_0(1 - \sigma)} \qquad \textbf{Equation 2}$$

As a result of nuclear shielding the resonance frequency of a nucleus becomes:

$$\boldsymbol{\nu = \frac{\gamma B_0(1-\sigma)}{2\pi}} \qquad \textbf{Equation 3}$$

The size and sign of this shielding constant are determined by the local electronic structure of the molecule near to the nucleus, meaning that the resonance frequency of a nucleus is characteristic of its local chemical environment.

To make the resonance frequencies easier to interpret and to remove the influence of the external magnetic field strength on the values, the chemical shift is defined as the difference in resonance frequencies between the nucleus of interest and a reference nucleus. A dimensionless parameter δ is used, with δ values given in parts per million (ppm) and being independent of the strength of the external magnetic field:

$$\boldsymbol{\delta = 10^6 \frac{\nu - \nu_{ref}}{\nu_{ref}}} \qquad \textbf{Equation 4}$$

The chemical shift of a nucleus is thus characteristic of its local chemical environment. This is extremely useful in order to interpret NMR spectra. The

chemical shift can be used as a probe to monitor changes in the local chemical environment of individual resonances in response to an effect. One of the key uses of this is in the investigation of ligand binding. NMR spectra can be measured of proteins in the absence and presence of a ligand and the chemical shift monitored. As discussed, a change in chemical shift is indicative of a change in chemical environment and thus identifies those amino acid residues of the protein which are affected by ligand binding and likely to be involved in the interaction. A review by Williamson (2013) summarises the use of chemical shift perturbations to characterise ligand binding (Williamson, 2013).

In addition, the chemical shift also reports on the local secondary structure. The chemical shifts of particular nuclei, including HN, Hα, Cβ, CO and N, but especially Cα nuclei, reflect the secondary structure. Depending on the secondary structure, phi and psi backbone torsion angles will be different and characteristic. The chemical shift of these nuclei can be used to predict phi and psi angles to anticipate the presence of an α-helix, β-strand or disordered region. The prediction of phi and psi angles is based on the analysis of secondary chemical shifts, which are the differences between chemical shifts and their corresponding random coil value. These secondary chemical shifts correlate with the different types of protein secondary structure. Programmes such as TALOS-N (Shen and Bax, 2013) and DANGLE (Cheung et al., 2010) are therefore used that compare the secondary shifts of a given residue to a database of 200 proteins to extract secondary structural information from a resonance assignment.

1.7.1.2 Spin-spin coupling

The appearance of an NMR spectrum is not determined solely by the chemical shifts of the nuclei. There is another effect that arises due to the fact that nuclei themselves are a source of local magnetic fields that affect the energies of other nuclei. These are termed spin-spin couplings and can be separated into dipolar couplings and J-couplings (also known as scalar couplings).

Dipolar couplings arise because each nuclear spin is magnetic and generates a magnetic field. This field covers the surrounding space and will thus

affect any other nuclear spins in the area. As a result any given nuclear spin will experience the magnetic field generated by any other nuclear spins located close by in space, as shown in Figure 24. The dipolar coupling interaction is mutual and as such a second nuclear spin will interact with the magnetic field generated by a first nuclear spin and in addition the first nuclear spin will also experience a magnetic field generated by the second nuclear spin.

A dipolar coupling occurs through space making it very useful for studies of molecular structure through nuclear overhauser effect spectroscopy (NOESY) and rotating overhauser effect spectroscopy (ROESY) experiments. NOE (nuclear overhauser effect) experiments are extremely useful to gain information about protein interactions and for structure determination to identify nuclei that have a dipolar coupling and are therefore close in space. We are able to exploit the dipolar coupling as it results in an NOE. The NOE occurs as a result of cross relaxation, whereby two dipolar coupled nuclear spins relax together to cause cross-relaxation and thus the transfer of spin polarisation between spins. This leads to the identification of two spins which have a dipolar coupling.

Dipolar couplings are measured and used extensively in solid state NMR. In solution state NMR the dipolar couplings average out to zero due to the rotational motion of the molecules. However, become useful in anisotropic liquids, such as liquid crystals, where there will be a preferential molecular orientation and the dipolar couplings do not average out. This permits the measurement of residual dipolar couplings (RDC's), which provide information on molecular orientation. RDC's are described in further detail in Section 1.7.1.4.

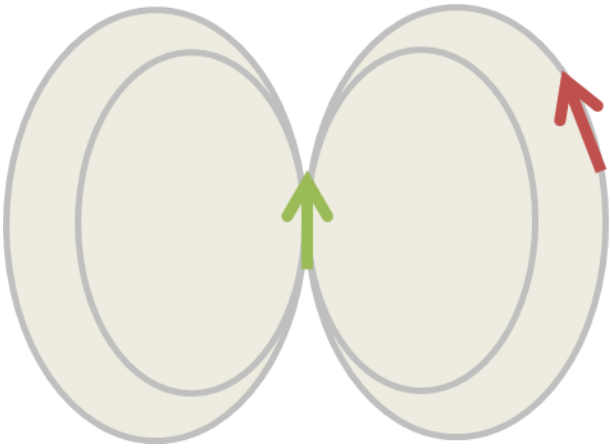

Figure 24. Origin of dipole-dipole couplings.
A magnetic field is generated by one nuclear spin, represented with the green arrow. This causes another spin, represented with the red arrow, to be affected and to experience and interact with this generated magnetic field.

In contrast J-coupling is mediated by the electrons involved in chemical bonding. As a result nuclear spins can be coupled together in an isotropic liquid. This is due to the influence of the electrons involved in the chemical bonds on the magnetic fields present between nuclear spins. Two spins will consequently only have a measurable J-coupling if they are linked together through a small number of bonds and therefore J-coupling is termed an indirect, through-bond coupling that is exclusively intramolecular. The J-coupling becomes important in the design of NMR experiments so that magnetisation can be transferred via these couplings to dictate what is seen on the resultant NMR spectra. For example, a one bond J-coupling occurs between the ^{1}H and ^{15}N nuclei of the amide in the peptide bond, which is exploited for the collection of ^{1}H-^{15}N-HSQC experiments. Some further examples will be described in Section 1.7.5 for the NMR experiments used in this study.

1.7.1.3 Chemical exchange

NMR spectroscopy permits the monitoring of the exchange of a nucleus between environments, either as a result of a chemical reaction or interaction or a conformational change. Chemical exchange can reveal protein motions on the millisecond to microsecond timescale. This chemical exchange may be slow, fast or intermediate depending on the exchange rate (K_{ex}) between the two different nuclear environments. The type of chemical exchange witnessed is

also dependent on the frequency separation of the resonances corresponding to the two nuclear environments.

Two-site exchange

A two-site exchange reaction, whereby a nuclear spin transfers between two chemical environments with different chemical shifts (termed site and site B) is shown in Equation 5. This is the simplest example of chemical exchange and can be used to define the exchange rate constant (K_{ex}), as shown in Equation 6. The forward first-order kinetic rate constant (k_1) describes the forward reaction from site A to site B, whilst k_{-1} is the reverse first-order kinetic rate constant. ρ_a is the equilibrium population of site A and ρ_b is the equilibrium population of site B. K_{ex} is therefore dependent on the rates of the forward and reverse reactions and also whether the populations of the two sites are the same (symmetrical two-site exchange) or whether they are significantly different (asymmetric two-site exchange) (Millet et al., 2000, Cavanagh, 1996).

$$A \underset{k_{-1}}{\overset{k_1}{\rightleftharpoons}} B \qquad \textbf{Equation 5}$$

$$K_{ex} = k_1 + k_{-1} = \frac{k_1}{\rho_b} = \frac{k_{-1}}{\rho_a} \qquad \textbf{Equation 6}$$

The two sites (A and B) have different chemical shift frequencies termed ω_a and ω_b, meaning that there is a chemical shift difference frequency ($\Delta\omega$) defined in Equation 7. The effect of the exchange process on the NMR spectrum and the classification of either a slow, medium or fast exchange regime is dependent on this difference in chemical shift frequency and the exchange rate.

$$\Delta\omega = \omega_a - \omega_b \qquad \textbf{Equation 7}$$

For symmetrical two-site exchange (A⇌B), whereby the equilibrium population is equal between the two sites, this can be simply visualised and is demonstrated in Table 1 and Figure 25. If there is slow exchange, meaning a small K_{ex}, there will be two discrete peaks of equal intensity at two resonance

frequencies (ω_a and ω_b), corresponding to the two different nuclear environments. This will mean that K_{ex} is much less than the frequency separation of the two resonances. As K_{ex} increases the two lines will broaden and eventually merge into a single flat resonance, indicating intermediate exchange and that K_{ex} has a similar magnitude to the difference in resonance frequencies. Greater increase in K_{ex} will yield fast exchange and produce an NMR spectrum with a single sharp resonance at the mean frequency of the two nuclear environments ($\rho_a\omega_a+\rho_b\omega_b$). In the case of fast exchange, where K_{ex} is large, the frequency separation of the two resonances will be extremely small or zero.

Table 1. Classification of slow, intermediate and fast exchange regimes with contributions from exchange rate and chemical shift difference frequency.

Exchange regime	Characterisation
Slow	$K_{ex} << \Delta\omega$ or $K_{ex}/\Delta\omega < 1$
Intermediate	$K_{ex} \approx \Delta\omega$ or $K_{ex}/\Delta\omega \approx 1$
Fast	$K_{ex} >> \Delta\omega$ or $K_{ex}/\Delta\omega > 1$

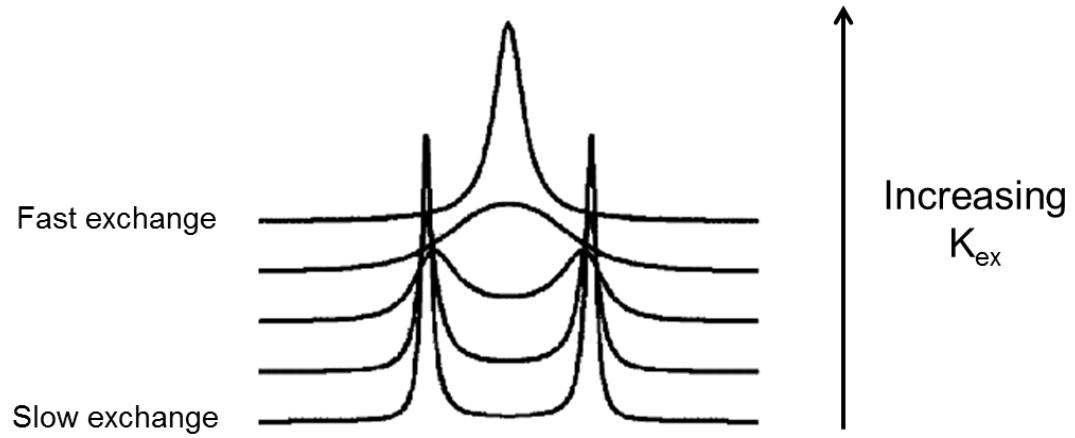

Figure 25. Representation of symmetrical two-site exchange.

When a system is in slow exchange there will be two peaks of equal intensity visible at the resonance frequency of each different environment on an NMR spectrum. As K_{ex} increases these two peaks will broaden and coalesce. If K_{ex} increases further then fast exchange will be witnessed and there will be a single sharp peak present at the mean resonance frequency between the two environments.

If there is asymmetric chemical exchange or exchange with more than two sites then the NMR spectra produced are not as simple to interpret. For asymmetric chemical exchange in the slow exchange limit the two resonances will not be of equal intensity and will broaden at different rates. In fast exchange the mean resonance frequency will be weighted towards the environment with the larger population. This is demonstrated in Figure 26. In many situations the populations of the two sites are unequal and asymmetric chemical exchange is evident.

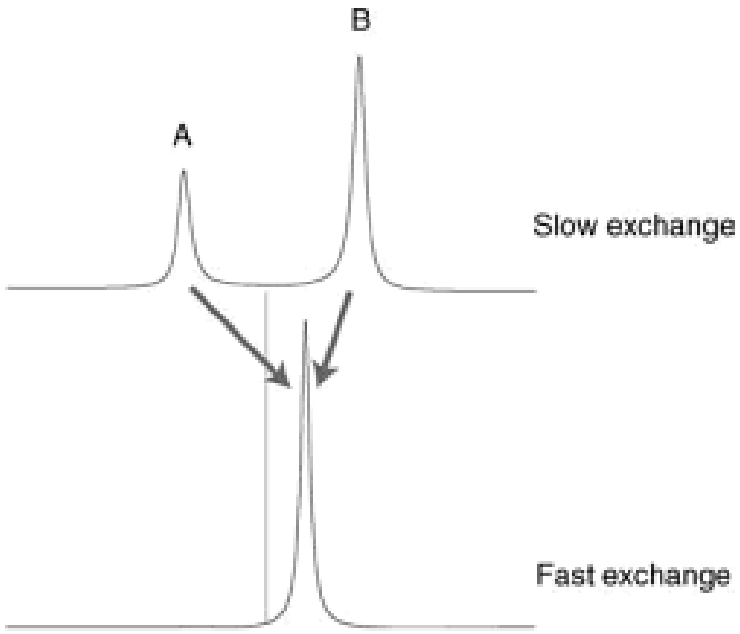

Figure 26. Representation of asymmetric two-site exchange.
When the populations of two states in slow exchange are different the two resonances will have different peak intensities. In the case of fast exchange the single mean resonance will be weighted towards the state with the larger population. Figure taken from (Levitt, 2001).

NMR titrations are performed to analyse chemical exchange. In these experiments the concentration of one component of the interaction (usually protein) is kept constant whilst the concentration of the second component (usually interacting ligand) is gradually increased. In the case of two-site exchange we are looking at a reaction such as that shown in Equation 8, where P denotes protein and L denotes ligand.

$$P + L \underset{k_{-1}}{\overset{k_1}{\rightleftharpoons}} PL \qquad \textbf{Equation 8}$$

The changes in resonance frequencies are monitored by HSQC experiments so that their line shape behaviour as a result of increasing amounts of ligand can be monitored. Detailed lineshape analysis can yield kinetic and thermodynamic parameters. If the system is in fast exchange then an approximation is made that assumes a normalised shift of the exchange averaged peak is a measure of the saturation of the bound complex. In slow exchange the peak intensities are used as an approximation of the saturation of the bound complex.

Multiple site exchange

The system being studied may not necessarily be governed by two-site exchange. Instead, the reaction mechanism may involve a number of steps and result in multiple-site exchange. The principles previously discussed apply to this multiple-site exchange; however, the effects on the NMR spectrum and the necessary interpretation are more complex. This is not well covered in the text books and literature but is important in terms of the interaction studied in this thesis and so will be described.

Work by Kovrigin (2012) analysed multi-state spectral patterns in NMR titrations and compared these line shapes to those from a two-site model. He was able to show that various models of three-site exchange display distinguishing features with regards to the experimental line shapes produced. Six different three-state binding mechanisms were studied, of which I will discuss two. There are shown in equation 9, where A and B denote ligand binding steps and coupled transitions respectively. In this case R represents receptor but could be generalised to any protein.

$$\underset{A}{\overset{}{}}\quad\underset{B}{\overset{}{}} \qquad\qquad \underset{A}{\overset{}{}}\quad\underset{B}{\overset{}{}}$$

$$(\mathbf{1})R + L \rightleftharpoons RL \rightleftharpoons R * L \qquad (\mathbf{2})2R + 2L \rightleftharpoons 2RL \rightleftharpoons (RL)_2 \qquad \textbf{Equation 9}$$

When A and B have the same exchange characteristics and are thus both in the fast exchange limit, the line shapes in the titration are represented by a single peak moving from the initial to the final positions. This is similar to the case for a two-site exchange model. However, Figure 27 shows that the addition of a second step in the binding mechanism also in fast exchange results in dramatic line broadening. This has the effect of making the line shapes appear indicative of intermediate exchange, therefore suggesting slower kinetics than are true for the system. If both A and B are in slow exchange with significant populations in each state then a three state binding mechanism is easier to identify. A peak at the frequency of free receptor will disappear, as two new peaks appear at the separate frequencies of the 2 different bound states (RL and R*L for binding mechanism 1 or RL and $(RL)_2$ for binding mechanism 2).

Figure 27 also demonstrates titration patterns that would be seen if A and B are in opposite exchange regimes. Binding mechanism 1 represents the induced fit mechanism (Koshland, 1958), whereby the bound complex (RL) rearranged into a more tightly bound species (R*L). When A is in slow exchange and B is in fast exchange, the two bound forms behave as if they were a single species and so we see a fast exchange weighted average resonance that increases in intensity as the titration progresses. Reversing the exchange characteristics so that A is in fast exchange and B is in slow exchange, we see that as the titration progresses the resonance corresponding to R disappears and shifts while the peak corresponding to R*L increases in intensity at a single resonance frequency. Similar but distinct observations are seen for binding mechanism 2 and are also shown in Figure 27.

Overall it seems that three site binding mechanisms can produce spectra and line shapes that are complex. When the exchange characteristics of both processes in the mechanism are the same the spectra may appear characteristic of intermediate exchange in a two-site system. Three site binding mechanisms may however be recognised if the two processes are in opposing exchange regimes by the characteristic patterns shown in Figure 27. Resonances may disappear/appear and shift resulting in curved peak patterns.

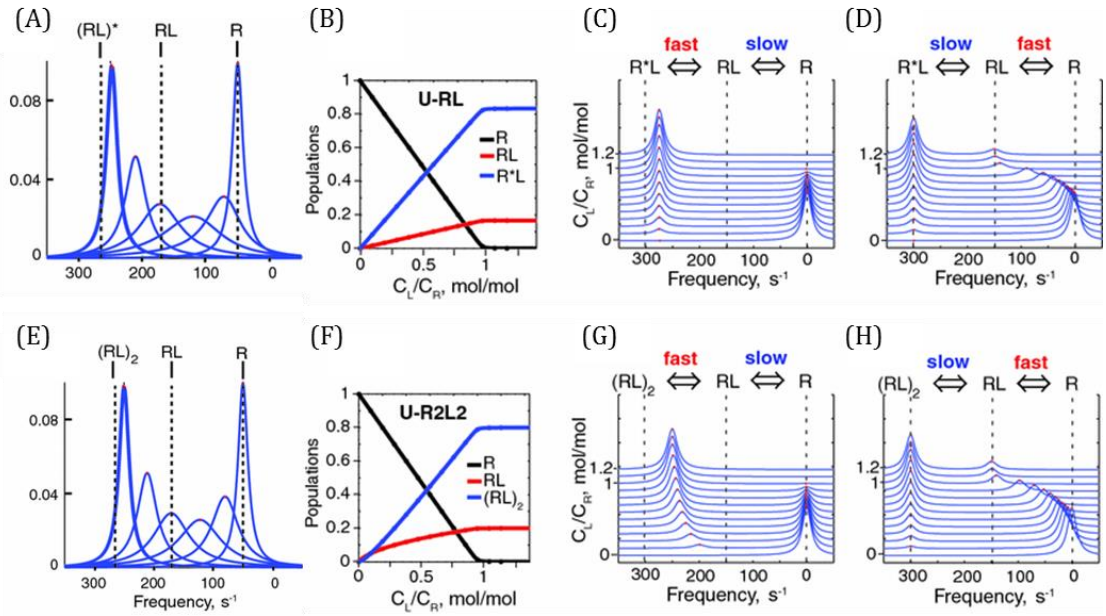

Figure 27. Line shapes and titration patterns from three-state binding mechanisms.

Line shapes (A and E) and titration patterns (B-D and F-H) for three state binding mechanism 1 (A-D) and 2 (E-H). Line shapes representative of three state binding mechanism 1 (A) and 2 (E) in fast exchange. The evolution of populations during the titration for binding mechanism 1 (B) and 2 (F). Variation and ambiguity of NMR titration patterns from three state binding mechanism 1 (C and D) and2 (G and H) in mixed exchange regimes. Line shapes and titration patterns simulated by LineShapeKin according to equilibrium and rate constants detailed in (Kovrigin, 2012). Figure adapted from (Kovrigin, 2012).

1.7.1.4 Residual Dipolar Couplings

The measurement of Residual Dipolar Couplings (RDCs) is important for studying molecular orientation in proteins. They are measured when the protein molecule is partially aligned as a result of being prepared in an alignment media such as bicelles, Pf1 phage, liquid crystals or polyacrylamide gel.

The alignment of the protein is described by means of an alignment tensor. This description of alignment consists of 3 Euler angles, which describe the orientation, as well as 2 magnitudes. Together these parameters represent the alignment of the protein in the laboratory frame and they are summarised in Figure 28. The three Euler angles (α, β and γ) characterise the angles between the X, Y and Z axes of the alignment tensor, whilst the magnitudes (Aa and Ar) represent the axial and rhombic components of the tensor.

The alignment tensor allows the interpretation of RDCs to specify long-range orientation restraints by providing a reference coordinate system. These reference coordinate axes are determined according to the molecular alignment and so for each internuclear (NH) vector, there is a corresponding cone of possible orientations, all related to a common reference coordinate system.

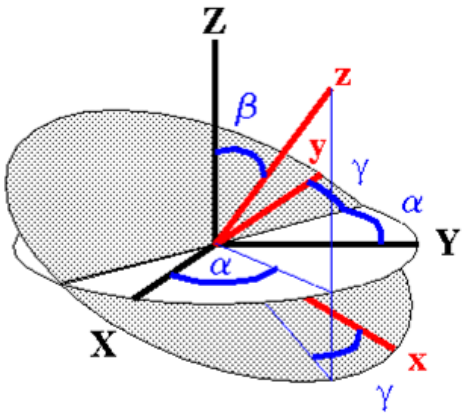

Figure 28. The alignment tensor

Representation of the alignment tensor (red) with respect to the laboratory frame (black). The 3 Euler angles are shown in blue.

1.7.1.5 Studying proteins by NMR

NMR spectroscopy is unique as a technique that can be used to study the atomic structure and dynamics of proteins in solution. Unlike X-ray crystallography, NMR spectroscopy can provide information on molecular motion in proteins and protein flexibility. Three-dimensional protein structures can be solved by NMR and structural information can be gained for use in conjunction with other biophysical techniques.

Isotopic labelling of proteins

For a nucleus to be visible on an NMR spectrum it must possess nuclear spin. Whether or not a nucleus possesses nuclear spin depends on the number of protons and neutrons it has and therefore different elements and even different isotopes of the same element have different nuclear spins, as shown in Table 2. Isotopes which have zero spin cannot be studied by NMR. Proton (^{1}H) NMR is possible for studying proteins as this isotope has spin ½ and spin ½ nuclei are the most readily detectable by NMR. However, the naturally

abundant forms of carbon and nitrogen, ^{12}C and ^{14}N respectively, are not spin ½ and so they must be replaced by their isotopes which are spin ½ - ^{13}C and ^{15}N. This is achieved by isotopic labelling, whereby proteins are overexpressed in *E. coli* that is grown on minimal media containing ^{15}N ammonium salts as the only nitrogen source and/or ^{13}C glucose as the only carbon source.

Table 2. Nuclear spin and percentage natural abundance of isotopes relative to protein NMR.

Isotope	Spin	Natural abundance (%)
^{1}H	½	99.9885
^{2}H	1	0.0115
^{12}C	0	98.93
^{13}C	½	1.07
^{14}N	1	99.632
^{15}N	½	0.368

Studying the atomic structure of proteins by NMR spectroscopy

NMR spectroscopy can be used to study the structures of proteins in solution at the atomic level. It is possible to solve three-dimensional protein structures by NMR, although a lot of structural information can also be gained through NMR studies without structure calculation.

Resonance assignment, which involves determining the chemical shifts of the atoms in a protein, is relatively time consuming but can yield a wealth of information and is important for the interpretation of further experiments. A set of triple resonance, three-dimensional NMR experiments are collected and analysed to determine the chemical shifts of the protein backbone. Further NMR experiments can then be conducted to assign the other atoms in amino acid side chains. Once all resonances are assigned spectra can be compared and chemical shift perturbations calculated to provide information on amino acids involved in interactions.

NOE measurements provide distance restraints that are needed for structure calculation but can also provide details on protein interactions, as NOEs are only measured between atoms within a certain spatial distance. Their

measurement can therefore determine which amino acids are closely located in space and therefore likely to interact.

Orientation restraints can also be determined by NMR in the form of RDC (residual dipolar coupling) measurements to provide information on protein structure based on the calculation of alignment tensors. For multi-domain proteins this means it is possible to define the orientation of these domains with respect to each other.

Solving the three-dimensional solution structure of a protein

NMR can be used to solve the three-dimensional structure of a protein in solution and has been used to determine over 10,500 structures in the Protein Data Bank (September 2014).

The traditional method for solving structures with NMR involves assigning NOE cross peaks between pairs of spatially proximal atoms. As mentioned previously, an NOE occurs as a result of cross relaxation, whereby two dipolar coupled nuclear spins relax together to cause the transfer of spin polarisation between spins. This results in the presence of a cross peak on the NMR spectrum that corresponds to the chemical shifts of two spins (atoms) which are close in space, usually within 5Å. The intensity/volume of these cross peaks is related to the distance between the two atoms and is approximately proportional to $1/r^6$, where r is the inter-proton distance. The assignment of these NOE cross peaks thus results in the production of a list of distance restraints for a given protein. This list can be integrated into structure calculation software, which performs restrained molecular dynamics (RMD) simulations, with a simulated annealing procedure to produce three-dimensional protein structures.

An RMD simulation aims to solve Newtons equation of motion, as shown in Equation 10, where F is the force, m is the mass and a is the acceleration of an atom, i.

$$\boldsymbol{F_i = m_i a_i} \qquad \textbf{Equation 10}$$

The force is related to the potential energy (V), which is the sum of a number of individual energy terms, as outlined in Equation 11. The first five terms comprise the empirical energy terms that describe the physical interactions between atoms. This includes bond lengths (V_{bond}), bond angles (V_{angle}) and dihedral angles ($V_{dihedral}$) as well as non-bonding interactions, defined by the van der Waals (V_{vdw}) and electrostatic ($V_{coulumb}$) terms. The last term, V_{NOE}, represents the NMR experimental data in the form of NOE distance restraints. This energy value will be high if the distance is too large or too small in relation to the distance determined from the intensity/volume of the NOE cross peak. Thus, its value will be close to 0 if the physical distance corresponds to the distance described by the NOE.

$$\boldsymbol{V_{total} = V_{bond} + V_{angle} + V_{dihedral} + V_{vdw} + V_{coulumb} + V_{NOE}}$$

Equation 11

1.7.1.6 NMR experiments

Heteronuclear single quantum correlation (HSQC) spectroscopy

The HSQC experiment is an important and widely used tool in the study of protein structure and dynamics in the field of biological NMR. It is a relatively simple two-dimensional experiment that can reveal significant information on the structure and dynamics of proteins as well as insight into the interactions between proteins and also interactions with peptides and ligands.

It detects protons correlated to a heteronucleus such as ^{15}N (in a ^{1}H-^{15}N-HSQC) or ^{13}C (in a ^{1}H-^{13}C-HSQC) by magnetisation transfer using an INEPT (insensitive nuclei enhanced by polarisation transfer) sequence (Morris and Freeman, 1979). This sequence allows the transfer of magnetisation from a sensitive nucleus with a high gyromagnetic ratio to an insensitive nucleus with a low gyromagnetic ratio through the J-couplings. In this way, magnetisation is transferred from a proton nucleus to either a ^{15}N or ^{13}C nucleus, depending on the experiment. During the evolution period the ^{15}N nuclei acquire a frequency label specific to nitrogen (i.e. the ^{15}N chemical shift) and this labelled magnetisation is transferred back to the protons by a second INEPT sequence where it is detected. As a result the detected signal from the heteronucleus will

be increased, overcoming issues with the lower sensitivity of the ^{15}N and ^{13}C nuclei. The INEPT sequence is therefore an important building block used in a number of different NMR experiments as it provides the ability to detect NMR signals on the nucleus with the highest gyromagnetic ratio and thus highest sensitivity. As such, experiments can be recorded with maximum sensitivity.

The resulting ^{1}H-^{15}N-HSQC spectrum is two-dimensional with ^{1}H measured in the direct dimension (x axis) and ^{15}N in the indirect dimension (y axis). Resonances appear on the spectrum for each NH correlation in the protein being measured. Therefore a signal is present for each backbone NH in the protein and as a result there will effectively be one resonance for each amino acid present. Proline is the exception to this as it doesn't have a free NH and so does not produce a signal on the spectrum. In addition, the NH_2 groups from asparagine and glutamine side chains also produce signals, as well as the NH from the indole ring of tryptophan residues.

Here, ^{1}H-^{15}N-HSQC experiments have been conducted to investigate interactions between CaM and eEF2K$_{82\text{-}100}$ by comparing the ^{1}H-^{15}N-HSQC spectra of free CaM to that for eEF2K$_{82\text{-}100}$-bound CaM. This is possible because the position of the CaM resonances on the spectrum corresponding to the frequency of the chemical shift of a particular NH have been assigned. As the chemical shift is representative of the local chemical environment of a nucleus any differences in chemical shift between HSQC spectra of the free CaM and the eEF2K$_{82\text{-}100}$-bound state are indicative of an interaction.

^{1}H-^{13}C-HSQC experiments are collected in a similar manner and produce similar spectra. The differences arise from the fact that magnetisation is transferred from protons to ^{13}C nuclei rather than ^{15}N. As a result the resonances that appear on the spectrum correspond to CH correlations and therefore signals are present for each CH in the protein. There are a large number of CH_2 and CH_3 groups present in a protein and so ^{1}H-^{13}C-HSQC spectra can be difficult to assign. In this study we make use of the fact that resonances corresponding to methyl (CH_3) groups give particularly strong signals that appear in a particular region of the spectrum and thus limit our analysis to these resonances. ^{1}H-^{13}C-HSQC experiments have also been conducted to

investigate interactions between CaM and eEF2K$_{82-100}$ by comparing the ^{1}H-^{13}C-HSQC spectra of free CaM to that for eEF2K$_{82-100}$-bound CaM.

HNCA

The HNCA experiment is a triple resonance NMR experiment used primarily for backbone assignment in conjunction with further triple resonance experiments. It links the chemical shifts of the HN of a particular amino acid residue to the chemical shift of its Cα and also the Cα of the previous residue (Kay et al., 1990).

Magnetisation is passed from ^{1}H (HN) to ^{15}N and then transferred to the ^{13}Cα via the N-Cα J-coupling before being passed back again to the ^{15}N and ^{1}H for detection. This magnetisation transfer pathway is shown in Figure 29. A three-dimensional spectrum is produced as the chemical shift evolves for $^{1}H^{N}$, $^{15}N^{H}$ and ^{13}Cα. There will be two Cα peaks present on the spectrum because the ^{15}N is coupled to both its own Cα and also the Cα of the preceding residue. However, the coupling to its own Cα is stronger (as it is a one-bond J-coupling) and so has a greater intensity on the spectrum, meaning that they can be distinguished from each other.

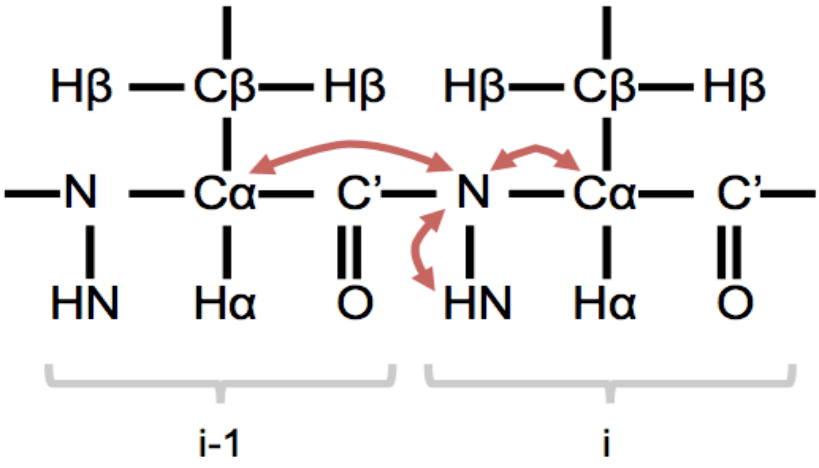

Figure 29. Magnetisation transfer pathway of the HNCA experiment.
Magnetisation is transferred from the HN to N and then to both the Cα of the preceding residue (i-1) and the directly bonded Cα (i) via the J-coupling. It is then passed back to H and HN for detection. This allows the chemical shift to evolve on HN, N and Cα producing a three-dimensional spectrum.

HNCACB

The HNCACB experiment is a triple resonance NMR experiment that produces a three-dimensional spectrum, similar to an HNCA except that an HNCACB also contains Cβ resonances (Grzesiek and Bax, 1992b). This experiment is also used for backbone assignment and in collaboration with CBCA(CO)NH and HSQC experiments these constitute the standard set of experiments for backbone assignment.

Magnetisation is transferred from ^{1}Hα to ^{13}Cα and also from ^{1}Hβ to ^{13}Cβ, and this is then passed to ^{13}Cα as well. The chemical shift is evolved simultaneously on Cα and Cβ so that they appear in one dimension on the spectrum. Magnetisation is then passed to ^{15}N and then ^{1}H (HN) for detection and these chemical shifts are also evolved. This magnetisation transfer pathway is shown in Figure 30. ^{15}N is passed magnetisation from both its own Cα and also the Cα from the previous residue, meaning that for each HN there will be two Cα's and two Cβ's present on the spectrum. Similarly to the HNCA experiment the peaks corresponding to the Cα's and Cβ's from the previous residue will have weaker intensities than those from the residue itself.

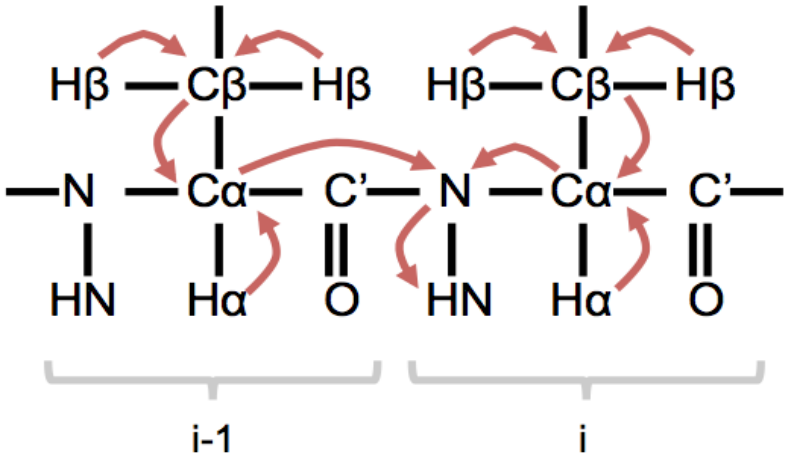

Figure 30. Magnetisation transfer pathway of the HNCACB experiment.
Magnetisation is transferred from Hβ to Cβ and from Hα to Cα. The magnetisation on Cβ is then passed to Cα before being transferred to N and HN for detection. The magnetisation is transferred to N and HN (i) from the Cα of i and i-1. The chemical shift evolves simultaneously on Cα and Cβ and also on HN and N.

CBCA(CO)NH

The CBCA(CO)NH experiment is another triple resonance experiment that is used closely with the HNCACB experiment for backbone assignment (Grzesiek and Bax, 1992a). It links the chemical shifts of the HN of a particular amino acid to the Cα and Cβ chemical shifts of the preceding amino acid.

The magnetisation transfer pathway, shown in Figure 31, is initially the same as for the HNCACB experiment as magnetisation is transferred from ^{1}Hα to ^{13}Cα and also from ^{1}Hβ to ^{13}Cβ, and this is then passed to ^{13}Cα as well. It is then passed to ^{13}CO and then to the ^{15}N and ^{1}H (HN) of the next amino acid residue in the sequence for detection. As for the HNCACB experiment, the Cα and Cβ chemical shifts are evolved simultaneously and the chemical shifts of ^{15}N and ^{1}H are also evolved. The chemical shift of ^{13}CO is not evolved and so has no corresponding peaks on the resultant spectrum.

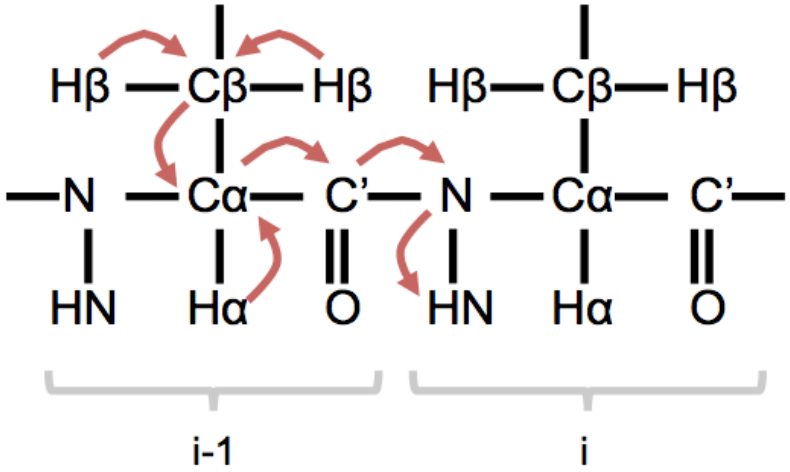

Figure 31. Magnetisation transfer pathway of the CBCA(CO)NH experiment.

Magnetisation is transferred from Hβ to Cβ and from Hα to Cα. The magnetisation on Cβ is then passed to Cα before being transferred to CO (all on i-1) and then to N and HN (i) for detection. The chemical shift evolves simultaneously on Cα and Cβ and also on HN and N.

H(CCO)NH

The H(CCO)NH experiment is used in the assignment of side chains to obtain the chemical shifts of hydrogen's in amino acid side chains. A three-dimensional spectrum is produced that links the chemical shift of the HN of a

particular amino acid residue to the chemical shifts of the hydrogen's in the side chain of the preceding amino acid residue (Montelione et al., 1992).

Magnetisation is transferred from the ^{1}H nuclei in the amino acid residue side chain to the attached ^{13}C nuclei. This is then transferred between the ^{13}C nuclei in the side chain by isotropic ^{13}C mixing before being passed to the ^{13}CO and then to the ^{15}N and ^{1}H (HN) of the next amino acid residue in the sequence for detection. The chemical shift is evolved simultaneously on all of the side chain hydrogen nuclei and also the chemical shifts of ^{1}H and ^{15}N are evolved. The carbon chemical shifts are not evolved and therefore the resultant spectrum has one ^{15}N dimension and two ^{1}H dimensions.

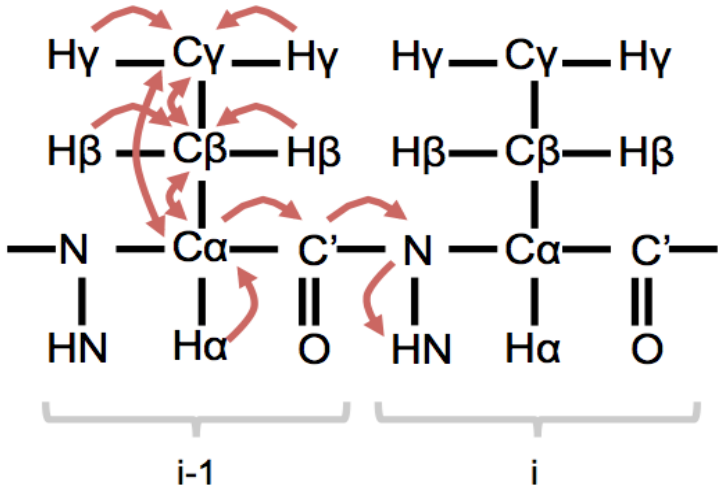

Figure 32. Magnetisation transfer pathway of the H(CCO)NH experiment.
Magnetisation is transferred from the side chain hydrogen nuclei to their attached carbons for isotropic ^{13}C mixing. The magnetisation is then passed to the CO (all on i-1) and then to N and HN (i) for detection. The chemical shift evolves simultaneously on the hydrogen's in the side chain and also on HN and N.

HCCH-TOCSY

The HCCH-TOCSY experiment is used for side chain assignment as it can yield the chemical shifts of the hydrogen and carbon atoms in the side chains. A three-dimensional spectrum is produced in which all of the hydrogen side chain chemical shifts are visible, linked to the chemical shifts of the carbon nuclei of the amino acid residue.

Magnetisation is transferred from the side chain hydrogen nuclei to the attached carbon nuclei, as in the H(CCO)NH experiment. Isotropic ^{13}C mixing follows before the magnetisation is transferred back to the side chain hydrogen nuclei for detection.

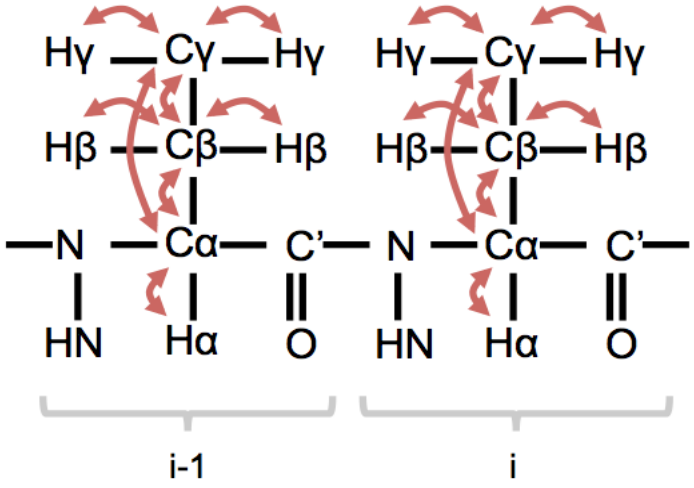

Figure 33. Magnetisation transfer pathway of the HCCH-TOCSY experiment.

Magnetisation is transferred from the side chain hydrogen nuclei to their attached carbons for isotropic ^{13}C mixing (i). It is then passed to N and HN (i) for detection. The chemical shift evolves on all nuclei that experience magnetisation transfer.

hbCBcgcdceHE and hbCBcgcdHD

The hbCBcgcdceHE and hbCBcgcdHD spectra are used to assign the Hδ and Hε atoms in the rings of aromatic residues. The experiments provide correlations between the sidechain Cβ and ring Hδ and Hε chemical shifts. The approach developed by Yamazaki et al (1993) is based exclusively on the transfer of magnetisation via scalar couplings (Yamazaki et al., 1993).

^{15}N-NOESY-HSQC

The ^{15}N-NOESY-HSQC experiment can be used to obtain NOE restraints for structure calculations and also to help with resonance assignment of the methyl groups of methionine residues (Marion et al., 1989b, Marion et al., 1989a). The three-dimensional spectrum yields cross peaks between the chemical shifts of all of the amide groups in each amino acid residue and all spatially proximal proton resonances in the protein.

Magnetisation is exchanged between all of the hydrogens in a given amino acid and also in neighbouring residues. This exchange is achieved using the NOE, meaning that it occurs through space rather than via J-couplings as with the previously described NMR experiments.

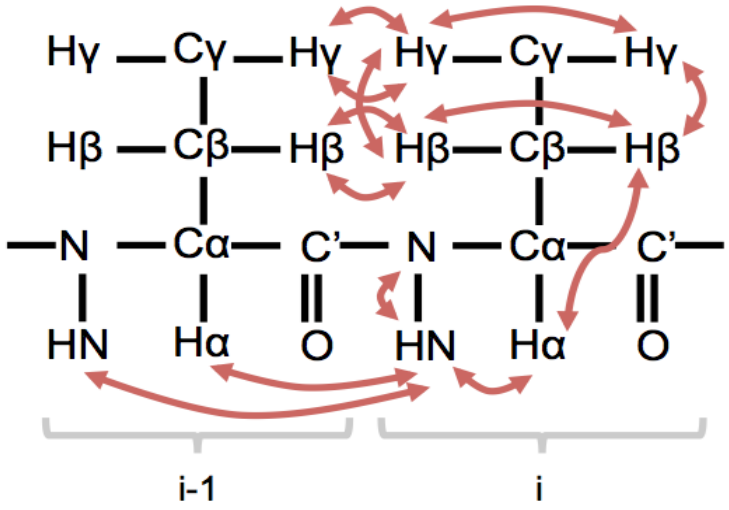

Figure 34. Magnetisation transfer pathway of the ^{15}N-NOESY-HSQC experiment.

Magnetisation is exchanged between all of the hydrogen's via the NOE. It is then transferred to ^{15}N and back to ^{1}H for detection. The chemical shift evolves on all nuclei that experience magnetisation transfer.

^{13}C-NOESY-HSQC

The ^{13}C-NOESY experiment can be used to obtain NOE restraints for structure calculations and also to help with resonance assignment. The spectrum can be centred on either the aromatic or aliphatic carbons, depending on the groups of interest. The three-dimensional spectrum produced links the chemical shift of each ^{13}C, ^{1}H group to all hydrogens nearby in space.

Magnetisation is exchanged between all of the hydrogens in a given amino acid and also in neighbouring residues. This exchange is achieved using the NOE, meaning that it occurs through space rather than via J-couplings as described for ^{15}N-NOESY-HSQC.

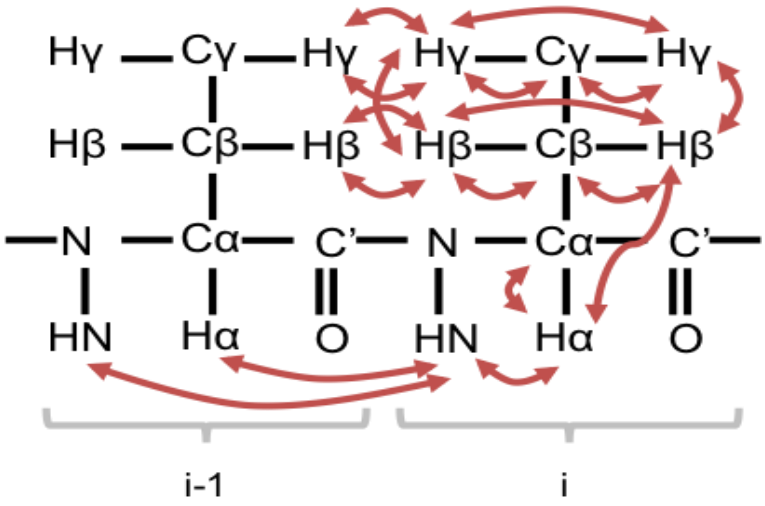

Figure 35. Magnetisation transfer pathway of the ^{13}-NOESY-HSQC experiment.

Magnetisation is exchanged between all of the hydrogen's via the NOE. It is then transferred to neighbouring ^{13}C nuclei and back to ^{1}H for detection. The chemical shift evolves on all nuclei that experience magnetisation transfer.

^{15}N/^{13}C filtered NOESY and ^{15}N/^{13}C filtered and ^{13}C edited NOESY

In a ^{15}N/^{13}C filtered NMR experiment ^{1}H-signal from the ^{15}N and ^{13}C labelled protein is suppressed using heteronuclear J-couplings (Otting and Wuthrich, 1990). This leaves signal originating from protons that are bonded to ^{12}C and ^{14}N nuclei, (the unlabelled protein) for assignment of the unlabelled peptide. The ^{15}N/^{13}C filtered ^{13}C edited three-dimensional NOESY combines the filtering in one spectral dimension with the heteronuclear editing in an additional dimension to measure NOEs between an unlabelled and labelled protein and generate intermolecular distance restraints (Ikura and Bax, 1992, Robertson et al., 2009, Zwahlen et al., 1997).

1.7.2 Small Angle X-ray Scattering

Small angle X-ray scattering (SAXS) is a biophysical technique that allows the study of biological macromolecules in solution, including proteins, nucleic acids and their complexes. Specifically, and in the case of this thesis, it can be used to investigate protein structure and protein interactions. SAXS is especially useful because the protein does not need to be crystallised (as for X-ray crystallography), so can be studied in solution and also is not limited by molecular weight. The resolution of SAXS data is typically limited to tens of

Angstroms, which is lower than the atomic resolution of X-ray crystallography and NMR but well suited to studying the arrangement of protein complexes.

In a SAXS experiment the intensity of X-ray photons that are scattered off molecules in solution is recorded as a function of the scattering angle. This scattering profile provides information on the shape of the molecules. This can be used to estimate some key parameters such as the radius of gyration (R_g), molecular weight (M_w) and maximum extend of the molecules in question (D_{max}).

The radius of gyration is a measure for the overall size of a macromolecule, which is computed as the root mean square distance of the parts from the centre of mass of the molecule (Lipfert and Doniach, 2007). It therefore refers to the distribution of components around an axis and so gives information on the size of a molecule. Since the scattering profile at very small angles can be approximated by an exponential decay using the Guinier approximation, one can create a linear Guinier plot, the slope of which estimates the R_g.

In a SAXS experiment the M_w is estimated using the scattering intensity at zero angle (I_0), which is the total scattering derived from all distance correlations within the volume of the molecule. It is therefore proportional to the solution concentration and to the number of atoms in the particle. Again, the I_0 is determined from the Guinier plot as it corresponds to the x-axis intercept. The I_0 is usually given in arbitrary units, however when a standard (such as BSA) is used then I_0 can be used to estimate the M_w (Konarev et al., 2006).

The D_{max} refers to the maximum diameter of the scattering particle and can be obtained from the first zero value of the distance distribution function – p(r). This is derived from the scattering curve by a Fourier transform. The distance distribution function represents the distribution of distances between all pairs of atoms within the particle, weighted by the respective electron densities (Vachette, 2010) and hence encodes characteristic features of the shape of the particle, as illustrated in Figure 356(C).

The process of data analysis from the original SAXS scattering curve to the elucidation of the key parameters from Guinier plot and distance distribution function is shown in Figure 36. In the ATSAS data analysis package

(Konarev et al., 2006) the overall data quality is estimated by comparison of Rg values over a range of different scattering angles and the extrapolation of the data towards a zero scattering angle. In an ideal scattering curve none of the low angle data points would be discarded and the estimation of Rg would be independent of the window of scattering angles. It would therefore be assigned a quality factor of 100 %. Less consistent data would be penalized with a lower %. Automated data processing pipelines in ATSAS consider quality scores above 50% to be acceptable (Petoukhov et al., 2007).

High quality data can then be subjected to *ab initio* modeling providing a 3D bead-model of the shape of the protein in question using the program DAMAVER (Volkov and Svergun, 2003). If atomic structures of the components of the scattering particle are available their three-dimensional arrangement can be determined with rigid body modeling using the program CORAL (Petoukhov and Svergun, 2005)

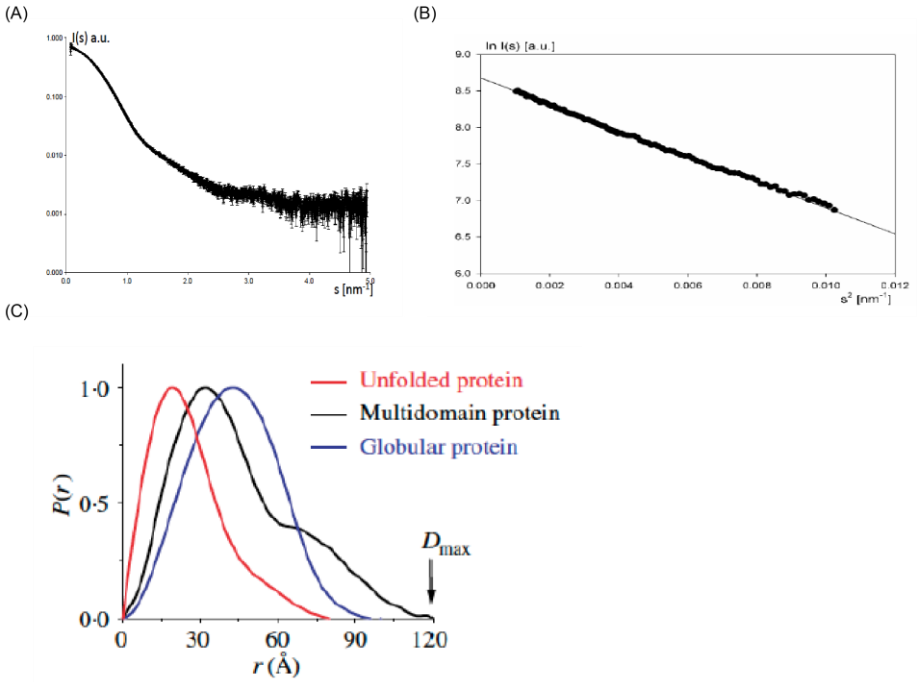

Figure 36. SAXS data analysis plots.

A scattering intensity profile is produced initially (A) that shows the intensity as a function of the scattering angle. The Guinier plot (B) is produced from the values in the scattering intensity profile and a distance distribution function (C) is produced by Fourier transform of the scattering intensity profile. The distance distribution function is characteristic of the shape/structure of the protein, as is shown for three different protein conformations. Adapted from (Putnam et al., 2007, Roessle, 2012).

1.7.3 Isothermal Titration Calorimetry

Isothermal titration calorimetry (ITC) is a technique for studying molecular interactions by directly measuring the absorption or release of heat in chemical reaction that is triggered by the mixing of two components. In the case of protein interactions his allows the determination enthalpy (ΔH) and entropy changes (ΔS) upon binding and hence the derivation of binding affinity. (Leavitt and Freire, 2001). In addition, ITC can be used to determine the stoichiometry of an interaction. .

In a typical experiment, one of the reactants (ligand/protein) is titrated into the reaction cell, which contains the second reactant/protein. Each time the ligand is added a chemical reaction (binding event) occurs, which is manifested in the release or absorption of a certain amount of heat. This heat (q_i) is proportional to the amount of ligand (L) that binds to the protein in a particular injection and is characteristic of the binding enthalpy. This is shown in Equation 12, where v is the volume of the reaction cell, ΔH is the enthalpy change and ΔL_i is the increase in concentration of bound ligand after the i^{th} injection.

$$\boldsymbol{q_i = v \times \Delta H \times \Delta L_i} \qquad \textbf{Equation 12}$$

The heat at each titration step is measured by the amount of power (microcalories per second) needed to compensate the change in temperature in the sample cell over the time interval required to return the system to equilibrium. With each injection of reactant produces a time dependent signal corresponding to the required power. The total heat per injection is then obtained by calculating the area under each peak.

As the titration proceeds, the amount of free, uncomplexed protein in the reaction cell decreases until complete saturation of the binding sites is achieved. The magnitude of the peaks therefore becomes progressively smaller until it remains constant and the peaks are of similar size that ideally should be zero. Non-zero signals under saturating protein ligand conditions typically arise from heat of dilution effects when the buffers in the sample cell are not in thermodynamic equilibrium with the buffer in the titration syringe. The functional form of ΔL_i differs depending on the specific binding model of the

system being studied. For the simplest model in which the protein has a single binding site, where K_a is the binding constant, ΔH is the enthalpy change. [P] is the concentration of protein and [L] is the concentration of free ligand, the heat can be written as follows:

$$\boldsymbol{q_i = v \times \Delta H \times [P] \times \left(\frac{K_a[L]_i}{1 + K_a[L]_i} - \frac{K_a[L]_{i-1}}{+ K_a[L]_{i-1}}\right)}$$

Equation 13

Analysis of the data yields ΔH (enthalpy change) and ΔG (via K_a), which in turn permits the calculation of ΔS (conformational entropy change) using the standard thermodynamic expression.

$$\boldsymbol{\Delta G = \Delta H - T\Delta S}$$ **Equation 14**

Thus, considerable information can be gained about protein interactions using ITC.

1.7.4 Microscale thermophoresis

Another technique has also been used in this thesis to study the binding of two molecules and quantify the biomolecular interaction. It measures the motion of molecules along microscopic temperature gradients and detects changes in their hydration shell, charge and size. An infrared laser induces the temperature gradient and the molecules movement is detected and quantified either by using covalently attached dyes, fluorescent fusion proteins or intrinsic tryptophan fluorescence. Throughout the experiment the concentration of the fluorescent molecule is kept constant whilst the concentration of the binding partner is increased.

Before the infrared laser is switched on, the molecules are distributed evenly and will diffuse freely in solution. Switching on the laser causes the molecules to experience a thermophoretic force in the temperature gradient and will typically move out of the heated spot. In the steady state the molecule flow is counterbalanced by ordinary mass distribution but after turning off the laser, the molecules will diffuse back in order to re-establish a homogeneous

distribution. These three stages (fluorescence signal before turning on laser, thermophoresis of molecules and back diffusion after switching laser off) are recorded for each sample with varying concentrations of ligand. The changes in thermophoretic properties are recorded as a change in fluorescence intensity (Seidel et al., 2013),

Chapter 2. Materials and Methods

2.1 Recipes

A number of buffers have been used throughout this project and their recipes are described here.

LB Media (1 L) pH 7.5 – 10 g Tryptone, 5 g NaCl, 5 g Yeast Extract

Minimal M9 Media (1 L) pH 7.4 – 6 g Na_2HPO_4, 3 g KH_2PO_4, 0.5 g NaCl, 1 mL 1 M $MgSO_4$, 0.3 mL 1 M $CaCl_2$**.** After autoclaving: 1 g NH_4Cl or 1 g $^{15}NH_4Cl$ or 1 g (both Goss Scientific), 3 g Glucose or 2 g ^{13}C-Glucose, 1 mL 1 mg/ml Biotin (in H_2O or D_2O), 1 mL 0.1 mg/ml Thiamine (in H_2O or D_2O), 10 mL Trace Elements

Lysis buffer – 50 mM HEPES pH 7.5, 300 mM NaCl, 1 mM β-mercaptoethanol (if used for eEF2K fragments), 5 % glycerol

Ni binding buffer – 50 mM HEPES pH 7.5, 300 mM NaCl, 20 mM imidazole, 1 mM β-mercaptoethanol (if used for eEF2K fragments), 5 % glycerol

Ni wash buffer – 50 mM HEPES pH 7.5, 500 mM NaCl, 40 mM imidazole, β-mercaptoethanol (if used for eEF2K fragments), 5 % glycerol

Ni elution buffer – 50 mM HEPES pH 7.5, 150 mM NaCl, 250 mM imidazole, 1 mM β-mercaptoethanol (if used for eEF2K fragments), 5 % glycerol

Low salt SP column buffer – 50 mM HEPES pH 7.5, 75 mM NaCl, 1 mM β-mercaptoethanol, 5 mM $MgCl_2$

High salt SP column buffer – 50 mM HEPES pH 7.5, 1 M NaCl, 1 mM β-mercaptoethanol, 5 mM $MgCl_2$

$CaCl_2$ containing phenyl Sepharose buffer – 20 mM Bis-Tris pH 6.8, 150 mM KCl, 1 mM $CaCl_2$

EDTA containing phenyl Sepharose buffer – 20 mM Bis-Tris pH 6.8, 150 mM KCl, 1 mM EDTA

Gel filtration buffer (CaM) – 25 mM Bis-Tris pH 6.8, 150 mM KCl

NMR sample buffer – 25 mM Bis-Tris pH 6.8, 150 mM KCl, either 10 mM $CaCl_2$ or 2 mM EGTA, 6 % (v/v) D_2O

SDS-PAGE 12 % gel

	Stacking Gel	Running Gel
Protogel 33 % acrylamide	0.66 ml	3.33 ml
dH_2O	2.9 ml	3.33 ml
0.3 % SDS, 3 M Tris pH 8.45	1.24 ml	3.33 ml

TEMED	10 µl	10 µl
Ammonium persulphate	25 µl	50 µl

SDS-PAGE sample buffer - 2.5 mL 1 M Tris pH 6.8, 4 mL 20 % SDS, 40 mg Bromophenol Blue, 2 mL Glycerol, 1 mL dH_2O, 860 µl β-mercaptoethanol

SDS-PAGE running buffers - Cathode Buffer (1 L): 100 mM Tris pH 8.2, 100 mM Tricine, 0.1 % SDS. Anode Buffer (1 L): 200 mM Tris pH 8.9

Activity assay buffer – 50 mM Mops pH 7.0, 16.7 ng/µl CaM (unless omitted), 5 mM $MgCl_2$, 14 mM β-mercaptoethanol, 0.67 mM $CaCl_2$, 2 mM EDTA, 0.4 mM EGTA, 0.1 mM PMSF

All reagents and chemicals were purchased from Sigma-Aldrich and Melford, unless otherwise stated.

2.2 Bacterial protein expression

$^{15}N/^{13}C$ labelled CaM and unlabelled eEF2K fragments for NMR studies was expressed, as well as unlabelled CaM for other biophysical and biochemical experiments. Plasmid maps are shown in Figure 37 for CaM and Figure 38 for eEF2K fragments. All protein expression work was performed under sterile conditions using sterilized media and solutions.

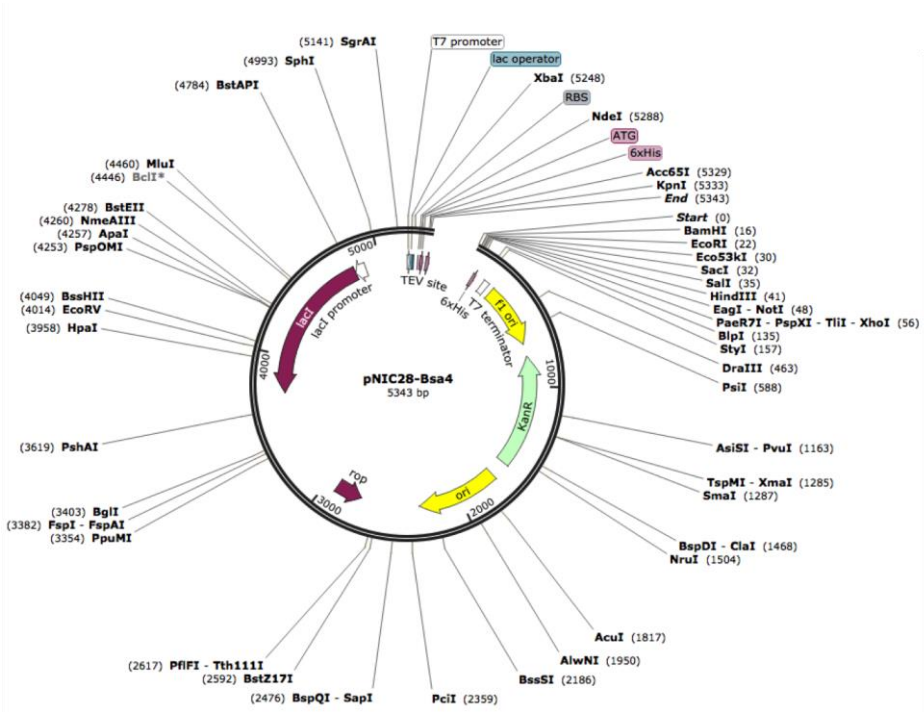

Figure 37. Plasmid map of pNIC28-Bsa4 used for CaM expression.

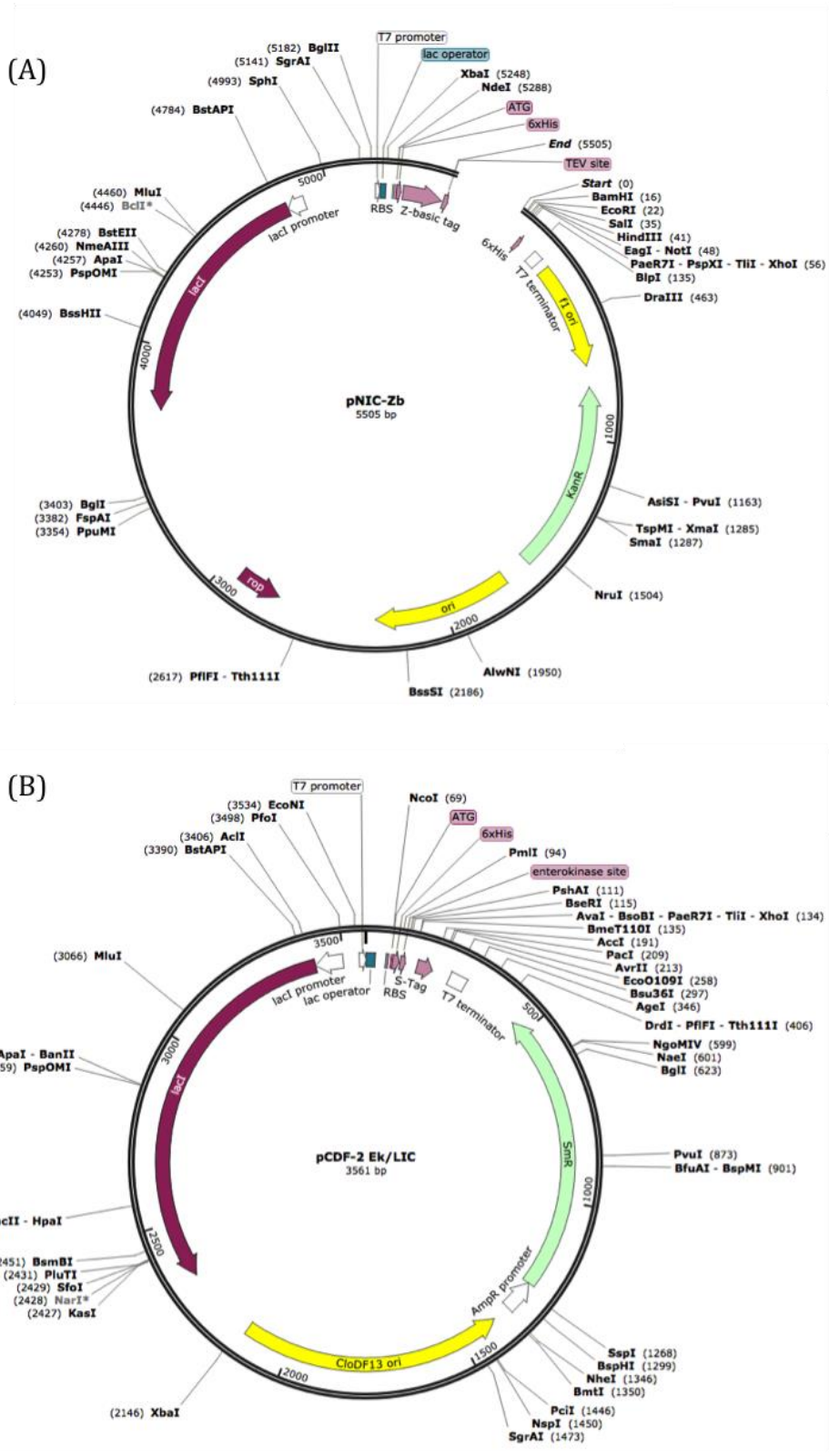

Figure 38. Plasmid map for pNIC-Zb and pCDF2-LIC used for eEF2K fragment expression.

2.2.1 Transformation

The vector containing the insert for the desired protein construct was transformed into BL21-CodonPlus(DE3)-RIPL *E. coli* cells (Agilent technologies). A pNIC28-Bsa4 vector contains the CaM insert and confers kanamycin resistance. An N-terminal eEF2K fragment (pNIC-Zb vector) was co-expressed with a C-terminal eEF2K fragment (pCDF-LIC vector). All vectors were sourced from the Structural Genomics Consortium (SGC), Oxford. The successful co-expression of both of these eEF2K fragments confers resistance to spectinomycin and kanamycin.

DNA was added to the competent cells and placed on ice for 30 min. Heat shock was performed at 42 °C for 45 seconds and the samples were placed on ice for a further 2 min. LB (Luria broth) media was added and the samples incubated at 37°C with shaking for one hour. Transformed *E. coli* were streaked onto LB agar plates supplemented with desired antibiotic to a final concentration of 50 μg/ml and incubated overnight at 37 °C.

2.2.2 Starter cultures in LB media

A colony was picked from the LB agar plate following successful transformation and used to inoculate 50 mL LB supplemented with desired antibiotic to a final concentration of 50 μg/mL. This was then incubated at 30 °C with shaking (170 rpm) overnight.

2.2.3 Scaled up cultures (unlabelled) in LB media

The starter cultures were scaled up the following day. 1 L of LB was supplemented with desired antibiotic and inoculated with starter culture. This was incubated at 37 °C with shaking (170 rpm) until the OD_{600} reached 0.6-0.9 (measured using ThermoScientific Nanodrop 2000c spectrophotometer). Isopropyl β-D-1-thiogalactopyranoside (IPTG) was added to a final concentration of 1 mM to induce protein expression and the cultures were incubated at 18 °C with shaking (170 rpm) overnight. This protein expression strategy is shown in Figure 39.

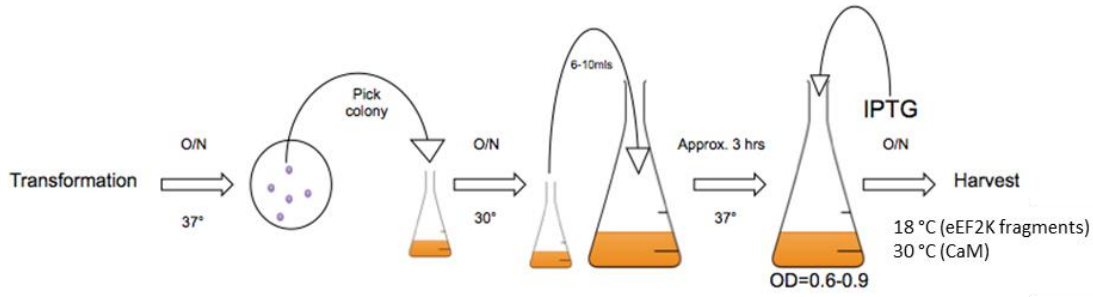

Figure 39. Protein expression method.

Transformation was performed and a colony was picked to be cultured for a small-scale starter culture. This was then scaled up to 1L growths until an OD_{600} of 0.6-0.9 was reached when IPTG was used to induce protein expression.

2.2.4 Scaled up cultures for $^{15}N/^{13}C$ labelling in minimal media

The starter culture was centrifuged at 2500 rpm for 10 min and the pellet re-suspended in sterile minimal M9 media. This was then added to the litre of M9 media supplemented with desired antibiotic to a final concentration of 50 µg/ml and incubated at 37 °C with shaking (170 rpm) until the OD_{600} reached 0.6-0.9 when IPTG was added to a final concentration of 1mM to induce protein expression. The cultures were then incubated at 18 °C with shaking (170 rpm) overnight.

2.2.5 Harvest

Cultures were centrifuged for 20 min at 5000 rpm and the supernatant discarded. The pellet was collected, re-suspended in lysis buffer and then stored at -20 °C.

2.3 Protein purification

Different purification strategies were employed for CaM and eEF2K fragments. Both undergo affinity chromatography using Ni-NTA as an initial step; they then differ in the concentration step with a phenyl Sepharose column used for CaM purification and an SP Sepharose ion-exchange column used for purification of the eEF2K fragments. Cleavage of the His_6 purification tag was the same for both proteins and both were gel filtered.

2.3.1 Cell lysis

Celll pellets were thawed and re-suspended in cell lysis buffer. Cell lytic reagent (Sigma-Aldrich), β-mercaptoethanol (if used for eEF2K fragments) and

protease inhibitors (cOmplete ULTRA tablets, mini, EDTA-free from Roche) were added and the suspension transferred to a sonication vessel. The cells were sonicated for 5 min with 10-second pulses and 30 second off intervals. They were then centrifuged for 40 min at 16000 rpm and the supernatant collected.

2.3.2 Affinity chromatography

Ni-NTA agarose (Generon) was applied to a bench column (Bio-Rad) and washed with dH_2O then binding buffer. The supernatant following cell lysis was incubated with the Ni-NTA agarose and the flow through from the column collected. The Ni-NTA agarose was washed with 6 CV (column volumes) of binding buffer, followed by 3 CV of wash buffer and lastly 3 CV of binding buffer again. The protein bound to the Ni-NTA agarose was eluted in elution buffer and added to a small amount of either low salt SP column buffer (for eEF2K fragments) or phenyl Sepharose column buffer containing $CaCl_2$ (for CaM) to dilute the imidazole.

2.3.3 Ion exchange chromatography

eEF2K fragments were further purified and concentrated by ion exchange chromatography as the next step in protein purification. A 5 mL SP Sepharose column (GE Healthcare) was attached to an AKTA Prime Plus (GE Healthcare) and equilibrated with low salt SP column buffer. The Ni-NTA elute was loaded at 1 mL/min, via a 50 mL loading superloop, on to the column. The absorbance was monitored at 280 nm and 10 mL fractions were collected until the absorbance had stabilized at the baseline. The fraction size was decreased to 5 mL and 20 % high salt SP column buffer was applied to the column. Once the absorbance had stabilized, 100% high salt SP column buffer was applied to elute the protein. The absorbance at 280 nm was monitored to identify the fractions containing eluted protein. These were analysed by sodium dodecyl sulphate polyacrylamide gel electrophoresis (SDS-PAGE) and pooled together.

2.3.4 Hydrophobic interaction chromatography

CaM was further purified and concentrated by hydrophobic interaction chromatography as the next step in protein purification. A phenyl Sepharose

column (GE Healthcare) was equilibrated with $CaCl_2$ containing phenyl Sepharose buffer. The Ni-NTA elute was loaded at 1 mL/min, via a 50 mL loading superloop, on to the column. The absorbance was monitored at 280 nm and 10 mL fractions were collected until the absorbance had stabilized at the baseline. A one step gradient of 100% EDTA containing phenyl Sepharose buffer was applied to the column to elute the bound protein and the fraction size volume was decreased to 5 mL. Monitoring the absorbance at 280 nm identified the fractions containing eluted protein; these were then analysed by SDS-PAGE and appropriate fractions were pooled together.

2.3.5 Cleavage of protein purification tag and dephosphorylation of eEF2K fragments

Protein purification tags were removed by cleavage with TEV (tobacco etch virus) protease (provided by Dr Halina Mikolajek). 140 µL of 3 mg/ml TEV protease was added to the 20 mL elute from hydrophobic interaction chromatography (CaM) or ion exchange chromatography (eEF2K fragments) and incubated overnight at room temperature. Cleavage was assessed by SDS-PAGE.

Lambda phosphatase (provided by Dr Halina Mikolajek) was added (approximately 200 units/20 µl of reaction mixture), where 1 unit corresponds to the amount of enzyme that hydrolyses 1 µmol of *p*-nitrophenyl phosphate per min at pH 9.8 and 37°C) at the same time as TEV when purifying eEF2K fragments to remove phosphate groups that are added as a result of autophosphorylation. $MnCl_2$ was added with the lambda phosphatase in order for it to function as Mn^{2+}-dependent protein phosphatase.

2.3.6 Size exclusion chromatography/gel filtration

A Superdex 75 column (GE Healthcare) was attached to an AKTA purifier (GE Healthcare) and equilibrated with relevant gel filtration buffer. For CaM this buffer was as listed in Section 2.1 and for the eEF2K fragments this was varied depending on the technique performed with the resulting sample. The elute from hydrophobic interaction chromatography (CaM) or ion exchange chromatography (eEF2K fragments) was concentrated using a viva spin with a 10 kDa (CaM) or 30 kDa (eEF2K fragments) MW cutoff membrane (Sartorius)

and loaded on to the column at 1 ml/min with 2 mL fractions collected. The absorbance at 280 nm was monitored as well as the conductance. The fractions containing protein were pooled, the concentration measured using NanoDrop and stored at 4 °C.

2.4 Protein analysis and characterization

SDS-PAGE analysis was used throughout the protein expression and purification process to monitor protein quality and yield. Mass spectroscopy was also used to determine the molecular weight of both proteins following expression and purification. The kinase activity of the eEF2K fragments was monitored by radioactive kinase activity assays. Two methods were utilized, one using eEF2 as the substrate of eEF2K and one with the MH-1 peptide.

2.4.1 SDS-PAGE

A Bio-Rad mini protein 3 system was used for SDS-PAGE analysis with a 4% stacking and 10% running gel. 4X sample buffer was added to the samples before boiling to denature the protein and centrifuging at 13,200 rpm for 2 min. Samples were then loaded onto the gel and this was run at 160 V for 35 min. Gels were stained with InstaBlue stain (Generon) and imaged with a gel imager.

2.4.2 Mass spectrometry

Purified protein (30 µL, 20 µM) was desalted on a 0.5 mL micro-spin column packed with Bio-Gel P-6 (Bio-Rad Laboratories) equilibrated in deionized H_2O and centrifuged at 1000 x g for 4 min. Mass spectra were recorded on a VG Quattro II triple quadrupole mass spectrometer (Fisons Instruments) with an electospray source. Desalted protein in water (5µl,20µM) was mixed with an equal volume of acetonitrile 2% formic acid and injected into the electrospray probe in a stream of acetonitrile/H_2O (50/50) at a flow rate of 10 µL/min. Spectra were recorded in the positive ion mode between 750-1500 *m/z* using the following instrument settings: capillary 3500 V, sample cone 35 V, source temperature 80^o C. Typically, 50 spectra were combined and deconvoluted using the maximum entropy algorithm, MaxEnt™ (Micromass, Altrincham, UK) to give relative molecular mass spectra over the ranges 17,500

– 18,500 Da at 1 Da resolution. Spectra were externally calibrated using NaI/CsI spectra recorded under identical conditions immediately after each sample.

2.4.3 Activity Assay

Using eEF2 as substrate:

Assays of eEF2K activity were performed in activity assay buffer. Reactions, in a total volume of 40 µl, contained 1 µg of purified eEF2 and were initiated by adding [γ-^{32}P] ATP (final concentration 0.1 mM, 1 µCi per reaction). Reactions were incubated at 30 °C for 30 min and then SDS-PAGE sample buffer was added. The samples were immediately heated at 95 °C for 5 min and products were analysed by SDS-PAGE. The gels were stained with Coomassie Brilliant Blue and de-stained with destain/fixing solution (50% (v/v) methanol and 10% (v/v) acetic acid). Gels were then placed on Whatman 3MM paper, covered with Saran wrap and dried on a vacuum gel dryer. Radioactivity was detected using a phosphorimager (Typhoon, GE Healthcare).

Using MH-1 peptide as substrate:

Assays of eEF2K activity against the MH-1 peptide were performed in activity assay buffer by a similar method, except that analysis involved spotting samples from the reaction mixture on to phosphocellulose paper (P81, Whatman). Filters were immediately placed in 300 mL of 75 mM orthophosphoric acid and washed three times. They were then rinsed in ethanol and dried. Radioactivity was determined using Cerenkov counting.

2.4.4 Isothermal titration calorimetry (ITC)

Isothermal titration calorimetry measurements were carried out using a VP-ITC MicroCalorimeter (GE Healthcare Bio-Sciences) at 25°C. CaM and the $eEF2K_{82-100}$ peptide were prepared and dialyzed in the same buffer (20 mM PIPES, 150 mM KCl, pH 6.8 with either 10 mM $CaCl_2$, or 2 mM EGTA). Ligand was titrated into protein solution at molar ratios of 20:1 corresponding to approximately 500 µM ligand (peptide) and 25 µM protein (CaM). Each experiment consisted of a first injection of 1 µl followed by approximately 50 injections of 4 µl of peptide solution into the cell containing CaM, while stirring at 310 rpm. Control titrations (peptide into buffer) using the same titration schedule were measured and subtracted from the protein experiments. Data

acquisition and analysis were performed using the VP-ITC analysis script in the Origin Scientific Graphing and Analysis software package (OriginLab). Data analysis was performed by generating a binding isotherm and best fit using the following parameters: N (number of sites), Δ H (enthalpy of system in cal/mol), Δ S (entropy of system in cal/mol/deg), and K (binding constant in M^{-1}). Following data analysis, K (M^{-1}) values were converted to K_d (μM). Data are expressed as mean values from experimental repeats, with an error calculated as the standard deviation.

2.4.5 Microscale thermophoresis (MST)

MST analysis was performed using a Monolith NT.115 instrument (NanoTemper technologies) using apo-CaM and $eEF2K_{82-100}$ peptide and using a Monolith NT LabelFree using Ca^{2+}/CaM and $eEF2K_{82-100}$. Each of these was performed in triplicate. The method was provided by NanoTemper technologies and is outlined in their report(NanoTemper, 2013a, NanoTemper, 2013b).

Fluorescent labelling method:

A fluorescent label (NT-647) was covalently attached to CaM via NHS coupling using the L001 Monolith NT.115 protein labelling kit (NanoTemper technologies). The fluorescent dye carries a reactive NHS-ester group that modifies primary amines present in amino acids like lysine. The assay was performed in buffer containing 25 mM Bis-Tris pH 6.8, 150 mM KCl, 2 mM EGTA and 0.05% Tween. The concentration of NT-647 labelled apo-CaM was kept constant (50 nM), while the concentration of the non-labelled $eEF2K_{82-100}$ peptide was varied between 137 nM - 4.5 mM. A dilution series was prepared to produce 16 samples of different concentrations before the fluorescently labelled CaM was added. The samples were loaded into MST NT.115 standard glass capillaries and the MST analysis was performed using the Monolith NT.115. MST curves of the raw data were recorded for each capillary, which the NanoTemper analysis software package uses to produce a binding curve and then fit the data to give a K_d.

Label free method:

The sample preparation and experiment procedure are the same for the label free method of MST, except that a protein labelling kit is not used as CaM

does not need to be fluorescently labelled. Instead the tryptophan containing molecule, the $eEF2K_{82-100}$, was kept at a constant concentration and a serial dilution of Ca^{2+}/CaM was prepared. The assay was performed in buffer containing 50 mM Tris pH 7.6, 150 mM NaCl, 10 mM $MgCl_2$, 10 mM $CaCl_2$ and 0.05% Tween-20.

2.4.6 Small angle X-ray scattering (SAXS)

2.4.6.1 Sample preparation and data collection

SAXS data was collected on the DORIS III beamline (PETRA III storage ring) at Deutsches Elektronen-Synchrotron (DESY), EMBL in Hamburg.

For the SAXS experiments, CaM and $eEF2K_{82-100}$ were dialysed into a buffer containing 50 mM HEPES pH 7.5, 150 mM NaCl and 5 mM $MgCl_2$. Measurements were carried out with CaM in the presence and absence of the peptide in either 10 mM CaCl (for Ca^{2+}/CaM) or 2 mM EGTA (for apo-CaM) at varying concentrations ranging between 1.8 and 7 mg/ml at 25 ˚C. The corresponding buffer was always used for a blank experiment.

2.4.6.2 Analysis of SAXS data

Programs from the ATSAS package (Konarev et al., 2006) were used for data analysis. The molecular weight was estimated by comparing the scattering I (0) to that of a standard solution of bovine serum albumin (BSA). The distance distributions were obtained using GNOM (Svergun, 1992) and further used for *ab initio* modelling in DAMMIF (Franke and Svergun, 2009). DAMAVER (Volkov and Svergun, 2003) was used to align *ab initio* models and create an averaged model. The calculations of the theoretical solution scattering of different crystal structures was carried out using CRYSOL (Svergun et al., 1995). SUPCOMB (Kozin and Svergun, 2001) was used to produce an overlay of the *ab initio* and rigid body models.

Rigid body modelling of Ca^{2+}/CaM in the presence of $eEF2K_{82-100}$ was carried out using CORAL (Petoukhov and Svergun, 2005). The N-terminal domain of CaM was defined as residues 4-77 and the C-terminal domain as residues 82-148. Residues 1-3 and 78-81 were termed as unknown. The PDB files outputted from module as a result of RDC measurements were used and

edited to contain the residues listed above. A simulated annealing protocol via CORAL was used to find the optimal positions of the two domains of CaM based on the scattering curve. The angular step in degrees was set to 0 to fix the domain orientations of Ca^{2+}/CaM with respect to each other according to the alignment derived from the RDC data.

2.5 NMR spectroscopy

2.5.1 NMR experimental parameters

NMR experiments were performed at the Southampton NMR Centre at the University of Southampton at a temperature of 298 K (25 °C), unless otherwise stated. All spectra, unless otherwise mentioned, were recorded at 600 MHz at a temperature of 298 K with a spectral width of 10 kHz on a Varian INOVA-600 instrument fitted with a Z-gradient cold probe. The ^{1}H NMR chemical shifts were referenced to the residual H_2O signal at 4.78 ppm. Standard BioPack triple resonance and heteronuclear-edited experiments were used with a recycle delay of 1 second. Water suppression was achieved for the triple resonance and ^{1}H-^{15}N-HSQC experiments by gradient enhanced echo sequences, whilst ^{1}H-^{13}C-HSQC experiments were affected by gradients for water suppression. Experimental parameters are listed in the Appendix (Appendices 1-6).

NMR spectra were processed using NMRPipe with water deconvolution, mild resolution enhancement and linear prediction (Delaglio et al., 1995). All analysis of NMR spectra and resonance assignment was carried out using the CcpNmr suite (Vranken et al., 2005).

2.5.2 Resonance assignment

Following purification $^{15}N/^{13}C$ labelled CaM was highly concentrated in the gel filtration buffer containing 25 mM Bis-Tris and 150 mM KCl using a Vivaspin concentrator (10 kDa Mw cut-off membrane). NMR samples were prepared in 300 µl in Shigemi tubes. For resonance assignment experiments a 1 mM CaM sample concentration was used. To acquire spectra of Ca^{2+}/CaM, 10 mM $CaCl_2$ was added to the sample, whilst for apo-CaM 2 mM EGTA was added. For the resonance assignment of CaM bound to $eEF2K_{82\text{-}100}$ a ten-fold excess (10 mM) of $eEF2K_{82\text{-}100}$ was used to ensure saturation of the bound state. For the

three-dimensional structure calculation of the Ca^{2+}/CaM: $eEF2K_{82-100}$ complex, the backbone and side chain atoms were assigned using data collected at a 1:1 ratio (1 mM) of CaM to $eEF2K_{82-100}$, as discussed in Section 2.5.8. D_2O (6 %) was added to all samples and the pH was checked and adjusted to pH 6.8 as necessary.

The triple resonance experiments for the assignment of backbone and side chain resonances of CaM were acquired at the Southampton NMR centre at the University of Southampton. An additional data set at a temperature of 315 K was recorded to aid in the assignment of apo-CaM bound to $eEF2K_{82-100}$. The data for Ca^{2+}/CaM backbone assignment were acquired with a Z-gradient room temperature triple resonance probe whilst all other data was acquired with a coldprobe (both Agilent). The ^1H NMR chemical shifts were referenced to the residual H_2O signal at 4.78 ppm. Standard BioPack triple resonance and heteronuclear-edited experiments were used. For detailed experimental parameters see appendices 1-4.

The resonance assignment was carried out using the CcpNmr suite (Vranken et al., 2005).

Table 3. NMR experiments used for the resonance assignments of CaM in four different conditions.

Ca^{2+}/CaM	Ca^{2+}/CaM in the presence of ten-fold excess $eEF2K_{82-100}$	apo-CaM	apo-CaM in the presence of ten-fold excess $eEF2K_{82-100}$
^1H-^{15}N-HSQC	^1H-^{15}N-HSQC	^1H-^{15}N-HSQC	^1H-^{15}N-HSQC
^1H-^{13}C-HSQC	^1H-^{13}C-HSQC	^1H-^{13}C-HSQC	^1H-^{13}C-HSQC
HNCACB	HNCA	HNCACB	HNCA
CBCA(CO)NH	HNCACB	H(CCO)NH	HNCACB
H(CCO)NH	CBCA(CO)NH	^{15}N-TOCSY	CBCA(CO)NH
^{15}N-TOCSY	H(CCO)NH	^{15}N-NOESY HSQC	H(CCO)NH
^{15}N-NOESY HSQC	^{15}N-NOESY HSQC	HCCH-TOCSY	^{15}N-NOESY HSQC
HCCH-TOCSY	HCCH-TOCSY		HCCH-TOCSY

2.5.3 Chemical shift perturbation analysis

Combined chemical shift perturbations (CSPs) were calculated from ^1H-^{13}C-HSQC spectra using the following equation, where d is the difference in

chemical shift (δ) in ppm between the free and the bound state, δ is the chemical shift in ppm and α is a scaling factor (0.3) to combine the chemical shift perturbations on different nuclei (Williamson, 2013):

$$\Delta\boldsymbol{\delta} = \sqrt{\frac{\mathbf{1}}{\mathbf{2}}\left[\,\boldsymbol{\delta}_{\boldsymbol{H}}^{\mathbf{2}} + \left(\boldsymbol{\alpha}\,\cdot\,\boldsymbol{\delta}_{\boldsymbol{C}}^{\mathbf{2}}\right)\right]} \qquad \textbf{Equation 125}$$

This same equation can be used to calculate CSPs from ^{1}H-^{15}N-HSQC spectra, however, a different scaling factor of 0.14 is used in this case due to the different chemical shift ranges of carbon and nitrogen.

CSPs were classified as either small, medium or large by eye from bar charts which show CSP plotted against residue number. For apo-CaM, small CSPs were determined as those smaller than 0.3 but larger than 0.05, medium range CSPs as those between 0.3 and 0.9, and any CSPs over 0.9 were classified as large. For Ca^{2+}/CaM, small CSPs were determined as those with a value between 0.03 and 0.15, whilst those between 0.15 and 0.5 are classified as medium, and any above 0.5 as large.

It should be noted that molecular graphics and analyses were performed with the UCSF Chimera package. Chimera is developed by the Resource for Biocomputing, Visualization, and Informatics at the University of California, San Francisco (supported by NIGMS P41-GM103311) (Pettersen et al., 2004).

2.5.4 Peptide titration

2.5.4.1 Sample preparation and data collection

Two 0.1 mM samples of CaM were prepared in 25 mM Bis-Tris, 150 mM KCl, 10 mM $CaCl_2$, pH 6.8. One sample was supplemented with eEF2K$_{82\text{-}100}$ peptide to 2 mM (20:1 ratio), and the pH adjusted to 6.8.

The eEF2K$_{82\text{-}100}$ peptide titration was carried out at the Southampton NMR centre. The ^{1}H NMR chemical shifts were referenced to the residual H_2O signal at 4.78 ppm. Standard BioPack heteronuclear-edited experiments were used. For detailed experimental parameters see Appendix 5.

Gradient enhanced ^{1}H-^{15}N-HSQC and ^{1}H-^{13}C-HSQC spectra were recorded on each of the two samples before aliquots of the sample containing eEF2K$_{82\text{-}100}$ peptide were added to the CaM only sample to achieve peptide to

protein ratios of 0:0, 0.05:1, 0.1:1, 0.15:1, 0.2:1, 0.3:1, 0.4:1, 0.6:1, 0.8:1, 1:1, 1.5:1, 2:1, 3:1, 4:1, 6:1, 10:1 and 20:1. At each titration point, further ^{1}H-^{15}N-HSQC and ^{1}H-^{13}C-HSQC spectra were recorded, which were processed using NMRPipe with water deconvolution, mild resolution enhancement and linear prediction (Delaglio et al., 1995) and were further analysed with the CcpNmr suite (Vranken et al., 2005).

2.5.4.2 Analysis of peptide titration

Analysis of the peptide titration data was carried out in collaboration with Zenawi Welderufael and Dr Ilya Kuprov, using software developed in Dr Ilya Kuprov's research group (School of Chemistry, University of Southampton). This software is called Spinach (Hogben et al., 2011) and a brief explanation by Dr Ilya Kuprov of the theory behind it is included below.

Each ^{1}H-^{15}N-HSQC spectra from the peptide titration experiment was theoretically calculated using Spinach, according to the description below. These spectra were fitted to experimental spectra using the least square method (Marquardt, 1963) to obtain χ^2 – the value of the function evaluated as the parameters passed over to the objective function. The least square method minimizes the difference between the experiment and the theory. The optimized parameters are K_d – the dissociation constant, K_{dis} – the effective dissociation, ^{1}H and ^{15}N relaxation constants, and intensity multiplier.

The objective function was minimized using Nelder-Mead simplex method (Nelder and Mead, 1965). The method minimizes a function of several variables by computing a simplex from an initial estimate, which evaluates the function at the points and reflects the worst value in the centroid of the other points. The objective function, which is the least square function, computes the square of the difference between the theory and experimental spectra as given in Equation 16.

$$\chi^2(a,b) = \sum_{n=1}^{N}\left(\left(\text{spec\_exp}\right)_n - \left(\left(\text{spec\_theo}\left(\text{parameters}\right)\right)_n\right)\right)^2 \qquad \textbf{Equation 136}$$

Where $\chi^2(a,b)$ is the value of the function at the parameters, spec_exp - the experimental spectra, while spec_theo(parameters) is the theoretical

spectra with the parameters to be optimized and $_N$ is the number of iterations of the titration. In the fitting process K_d was initially fixed and the fitting was run for the other four parameters, and then K_d was varied from result obtained from previous fitting run.

Brief explanation of Spinach

Theoretical calculation of the HSQC spectra in the presence of chemical exchange was carried out using Spinach v1.5 (Hogben et al., 2011) for a collection of standalone N–H pairs. To model spin dynamics in the presence of a unimolecular chemical reaction

$$\mathrm{A} \underset{k_-}{\overset{k_+}{\rightleftharpoons}} \mathrm{B} \qquad \textbf{Equation 147}$$

Spinach uses the following equation of motion:

$$\frac{d}{dt}\begin{pmatrix}\hat{\rho}_\mathrm{A}\\ \hat{\rho}_\mathrm{B}\end{pmatrix} = -i\begin{pmatrix}\hat{\hat{H}}_\mathrm{A}+i\hat{\hat{R}}_\mathrm{A} & 0\\ 0 & \hat{\hat{H}}_\mathrm{B}+i\hat{\hat{R}}_\mathrm{B}\end{pmatrix}\begin{pmatrix}\hat{\rho}_\mathrm{A}\\ \hat{\rho}_\mathrm{B}\end{pmatrix} + \begin{pmatrix}-k_+\hat{\hat{E}} & k_-\hat{\hat{E}}\\ -k_-\hat{\hat{E}} & k_+\hat{\hat{E}}\end{pmatrix}\begin{pmatrix}\hat{\rho}_\mathrm{A}\\ \hat{\rho}_\mathrm{B}\end{pmatrix} \qquad \textbf{Equation 158}$$

where $\hat{\rho}_{\mathrm{A,B}}$ are density matrices of the spin systems of chemical species A and B, $\hat{\hat{H}}_{\mathrm{A,B}}$ are their spin Hamiltonian commutation superoperators, $\hat{\hat{R}}_{\mathrm{A,B}}$ are their relaxation superoperators, $\hat{\hat{E}}$ is a unit superoperator and $k_\pm$ are the reaction rates. The formalism given for the case of two chemical species in Equation 18 is a special case of a more general implementation of chemical kinetics in Spinach, which operates in the direct product of spin state space and chemical state space.

The spin part of the problem contains 254 N–H pairs and was therefore handled using the restricted state space approximation (Kuprov, 2008). Because a collection of standalone N–H pairs is assumed in this case, state space restriction to two-spin orders connecting directly coupled spins is in this case exact. A single spin pair in Liouville space yields a 16-dimensional problem and therefore the total dimension of the matrices in Equation 18 is 254 x 16 x 2 =

8128 – small enough to be handled comfortably by the sparse matrix functionality implemented in Spinach.

The HSQC spectra were computed using standard Spinach functionality with pulse sequence and acquisition parameters matched to the experimental values. Theoretical spectra were fitted to the experimental data using the least squares method with the error functional minimization performed by the Nelder-Mead Simplex algorithm.

2.5.5 NMR analysis of an eEF2K$_{82-100}$ peptide with an additional ATCUN motif

The binding mode and therefore the orientation of eEF2K$_{82-100}$ can be determined by NMR. An eEF2K$_{82-100}$ peptide construct was used that contains an additional ATCUN (amino terminal Cu^{2+}(Ni^{2+})-binding) motif, consisting of three amino acid residues (Gly-Ser-His) that coordinate Cu^{2+} with very high affinity. Cu^{2+} is paramagnetic, which means that binding of Cu^{2+} to the ATCUN motif causes broadening and the disappearance of NMR signals (Mal et al., 2002).

Samples of $^{15}N/^{13}C$ labelled CaM (0.1 mM) were prepared in 25 mM Bis-Tris, 150 mM KCl, 10 mM $CaCl_2$, pH 6.8 with 1 mM eEF2K$_{82-100}$ containing the additional ATCUN motif at the N-terminus. A gradient enhanced ^{1}H-^{15}N-HSQC spectrum was collected before the addition of 2 mM $CuSO_4$ when a second gradient enhanced ^{1}H-^{15}N-HSQC spectrum was collected. For detailed experimental parameters see Appendix 5.

NMR spectra were processed using NMRPipe with water deconvolution, mild resolution enhancement and linear prediction (Delaglio et al., 1995). All analysis of NMR spectra was carried out using the CcpNmr suite (Vranken et al., 2005).

Comparison of the two spectra led to the identification of NMR signals that disappear upon the addition of Cu^{2+} and thus those residues located near to the N-terminus of eEF2K$_{82-100}$.

2.5.6 NMR studies of eEF2K fragments

eEF2K and CaM were expressed and purified as outlined in Section 2.2. NMR samples were prepared in 400 µl and transferred to Bruker shaped tubes.

The eEF2K fragments were prepared at 100 μM with 20 μM ^{15}N- and ^{13}C-labelled CaM in a buffer containing 20mM HEPES pH 7.5, 150 mM KCl, 5 mM $MgCl_2$ and either 10 mM $CaCl_2$ or 2 mm EGTA with 5 % (v/v) D_2O.

NMR experiments were acquired at the MRC Biomedical NMR Centre at the National Institute for Medical Research (Mill Hill, London). All spectra were recorded at 700 MHz at a temperature of 298 K with a spectral width of 14.084 kHz on a Bruker Avance-700 instrument fitted with a triple resonance PFG cryoprobe. The ^1H NMR chemical shifts were referenced to the residual H_2O signal at 4.78 ppm. Spectra were measured using standard Bruker pulse programs.

NMR spectra were processed using NMRPipe with water deconvolution, mild resolution enhancement and linear prediction (Delaglio et al., 1995). All analysis of NMR spectra was carried out using the CcpNmr suite (Vranken et al., 2005).

2.5.7 RDC measurements and analysis

The dependence of RDCs on the relative orientations of amide bonds in a molecule provides powerful constraints on the solution structures. RDCs were used to investigate the relative orientations of the CaM domains in the CaM: eEF2K82$_{-100}$ complex. The RDCs define an alignment tensor that describes axial (Aa) and rhombic components (Ar) and three rotation angles (Euler angles α, β, γ) that give the orientation of the tensor with respect to the molecular frame. The interdomain orientation of the complex in solution is determined by rotating the molecular frames of the N- and C-terminal domains such that the alignment tensors of the two domains are co-linear.

RDC measurements were collected with a ten-fold excess of eEF2K$_{82-100}$ to CaM and also at a 1:1 ratio of CaM and eEF2K$_{82-100}$.

2.5.7.1 NMR sample preparation

For RDC measurements at a 1:10 ratio of CaM to eEF2K$_{82-100}$, a 0.5 mM sample of CaM was prepared with 5 mM eEF2K$_{82-100}$ in 25 mM Bis-Tris, 150 mM KCl, pH 6.8 containing either 10 mM $CaCl_2$ for isotropic data collection. The aligned sample was prepared using liquid crystals from hexaethylene glycol monododecyl ether (C12E6) and hexanol (Ruckert and Otting, 2000). Hexanol

was added to C12E6 until the solution became opalescent, indicating the formation of liquid crystals. The sample used for isotropic data collection was added to this mixture and transferred to an NMR tube for anisotropic data collection.

For RDC measurements at a 1:1 ratio of CaM to $eEF2K_{82-100}$ a 1 mM sample of CaM was prepared with 1 mM $eEF2K_{82-100}$ in 25 mM BisTris, 150 mM KCl, pH 6.8 containing either 10 mM $CaCl_2$ The aligned sample was prepared by adding a pre-dried 600 µl volume, 5 mm diameter, 5% polyacrylamide gel to the sample used for isotropic data collection and allowing the gel to soak up the sample and swell for at least 24hrs at room temperature. The gels were inserted into a 5 mm NMR tube for anisotropic data collection.

2.5.7.2 NMR experiments

RDC data was acquired at the Southampton NMR centre at the University of Southampton. All spectra were recorded at 600 MHz at a temperature of 298 K with a spectral width of 10 kHz on a Varian INOVA-600 instrument fitted with a Z-gradient cold probe.

A series of eleven $^{1}J_{NH}$-modulated ^{1}H-^{15}N-HSQC experiments (Tjandra et al., 1996) were collected with incremental dephasing delay values (0.001, 0.002, 0.004, 0.005, 0.006, 0.007, 0.009, 0.010, 0.011, 0.012 and 0.013 seconds) for both the isotropic and anisotropic samples.

2.5.7.3 Analysis

NMR spectra were processed using NMRPipe (Delaglio et al., 1995) and analysed using the CcpNmr suite (Vranken et al., 2005). Assignments were transferred to each ^{1}H-^{15}N-HSQC spectrum collected for the isotropic and anisotropic samples with the different dephasing delay values. The intensity of each assigned peak was determined and plotted against the dephasing delay value for the isotropic and anisotropic data separately. MATLAB was used to fit the data to the following curve where *a* is the initial peak intensity, *b* accounts for any imperfection in π pulses during the experiment, r_2 is the relaxation rate and where J_{NH} (J-coupling value) is equal to approximately -92 Hz under isotropic conditions:

$$f(x) = a(-b + \cos(\pi \cdot 2 \cdot J_{NH} \cdot x))\exp(-2\left(\frac{x}{T_2}\right)) \qquad \textbf{Equation 169}$$

This was performed for each residue from both the isotropic and anisotropic data, producing fit curves and values for *a*, *b* and the J-coupling for each assigned residue following 100 iterations. The J-coupling value for each residue was thus determined under isotropic and anisotropic conditions. Subtraction of the isotropic J-coupling value from the anisotropic J-coupling value yielded the RDC value.

Errors were also calculated using MATLAB. An additional series of 100 artificial intensity data points were created based on a Gaussian distribution about the original, measured intensity data point using the baseline noise in the spectra to determine the width of the distribution. These were then fitted according to Equation 19 by the same method as previously described to generate a corresponding series of *a*, *b* and the J-coupling values. The standard deviation of these 100 additional values gave the error for each measurement. The MATLAB script for the fitting regime calculation of J-couplings and the error calculation was kindly written by Alistair Bailey and Neil Dalchau.

RDC values measured for the Ca^{2+}/CaM: $eEF2K_{82\text{-}100}$ complex were analysed using Module 1.0 (Dosset et al., 2001) to generate alignment tensors. Ca^{2+}/CaM was analysed as a whole molecule and also as two individual modules, representing the N- and C-terminal domains. The N-terminal domain was defined as module 1 and contained residues 1-73 and the C-terminal domain was defined as module 2 and contained residues 81-148. The flexible linker region (residues 74-80) was not included in the modular analysis. The experimental RDC values for the Ca^{2+}/CaM: $eEF2K_{82\text{-}100}$ complex were compared to back-calculated RDC values determined from a selection of atomic structures of other CaM: peptide complexes from the RCSB Protein Data Bank. The overall fit and correlation between the experimental and back-calculated RDC values was assessed for each CaM: peptide complex to determine which structure best represented that of the Ca^{2+}/CaM: $eEF2K_{82\text{-}100}$ complex. A χ^2 value was determined for each residue on the agreement between the experimental and back calculated values which led to the removal of outliers if

they were located in regions of the protein structure that were likely to be flexible, for example, the Ca^{2+} coordinating loops.

An alignment tensor was generated following each fit for the individual modules. Errors were calculated by Monte Carlo analysis of 500 simulations. The two modules were aligned according to the two alignment tensors to determine the orientation of the two modules with respect to each other. Degenerate 180° rotations about each axis of the alignment tensor were performed to determine the four possible orientations of module 1 relative to module 2. These were outputted as separate PDB files for the N- and C-terminal domains.

2.5.8 Solution structure calculation

The solution structure of the Ca^{2+}/CaM: $eEF2K_{82\text{-}100}$ complex was determined at a 1:1 ratio of Ca^{2+}/CaM to $eEF2K_{82\text{-}100}$. Previous resonance assignments were carried out with a ten-fold excess of $eEF2K_{82\text{-}100}$ and so the assignment of data collected under stoichiometric conditions was required.

2.5.8.1 Resonance assignment

Resonance assignment was carried out on a sample containing 1 mM purified $^{15}N/^{13}C$ labelled CaM and 1 mM $eEF2K_{82\text{-}100}$ peptide from China Peptides (Shanghai, China). This sample was prepared in a 300 µl Shigemi tube with 25 mM Bis-Tris pH 6.8, 150 mM KCl and 10 mM $CaCl_2$.

The triple resonance experiments for the assignment of backbone and side chain resonances of CaM were acquired at the Southampton NMR centre at the University of Southampton. NMR experiments to assign the protons of aromatic rings were also collected here. The ^1H NMR chemical shifts were referenced to the residual H_2O signal at 4.78 ppm. Standard BioPack triple resonance and heteronuclear-edited experiments were used. For detailed experimental parameters see appendices 1-4.

Two-dimensional $^{15}N/^{13}C$ filtered NOESY and TOCSY experiments were collected at the MRC Biomedical NMR centre at the National Institute for Medical Research (Mill Hill, London) on a Bruker Avance III HD at 700 MHz spectrometer fitted with a triple resonance PFG cryoprobe. These were used to assign the $eEF2K_{82\text{-}100}$ peptide.

The resonance assignment was carried out using the CcpNmr suite (Vranken et al., 2005).

2.5.8.2 Secondary structure assignment

Talos-N (Shen and Bax, 2013) was used to predict and assign the secondary structure of the Ca^{2+}/CaM: $eEF2K_{82-100}$ complex. Talos-N predicts the backbone torsion/dihedral angles using secondary chemical shifts.

2.5.8.3 NOE assignment

^{13}C-NOESY HSQC and ^{15}N-NOESY HSQC spectra were used to assign NOE cross peaks. These spectra were collected with the same sample described in Section 2.5.8.1. The ^{15}N-NOESY HSQC spectrum was collected at the Southampton NMR Centre at the University of Southampton. The ^{1}H NMR chemical shifts were referenced to the residual H_2O signal at 4.78 ppm. The ^{13}C-NOESY HSQC spectrum was acquired at the MRC Biomedical NMR centre at the National Institute for Medical Research (Mill Hill, London) on a Bruker Avance III HD at 700 MHz spectrometer fitted with a triple resonance PFG cryoprobe.

A three-dimensional $^{15}N/^{13}C$ filtered NOESY was collected at the Southampton NMR centre at the University of Southampton. Cross peaks were assigned between CaM and $eEF2K_{82-100}$ to create intermolecular distance restraints for the complex.

The NOE assignment was carried out using the CcpNmr suite (Vranken et al., 2005).

Table 4. NMR experiments used for the resonance and NOE assignment of the Ca^{2+}/CaM: $eEF2K_{82-100}$ complex.

Resonance assignment of Ca^{2+}/CaM	^{1}H-^{15}N-HSQC ^{1}H-^{13}C-HSQC HNCACB CBCA(CO)NH H(CCO)NH ^{15}N-TOCSY ^{15}N-NOESY HSQC HCCH-TOCSY hbCBcgcdceHE hbCBcgcdHD HNCO

Resonance assignment of eEF2K$_{82-100}$	2D CN FIL NOESY 2D CN FIL TOCSY
NOE assignment	^{15}N-NOESY HSQC ^{13}C-NOESY HSQC 3D NOESY CN FIL

2.5.8.4 Structure calculations

The NMR solution structure calculation was carried out using Aria 2.3 (Rieping et al., 2007) and Crystallography and NMR system 1.3 (CNS) (Brunger et al., 1998).

Aria, which stands for ambiguous restraints for iterative assignment, is software used for automated NOE assignment and NMR structure calculation. It is, in theory, capable of fully automating the assignment process and has the potential to determine the cross peak assignments on a NOESY spectrum when provided with only an unassigned peak list and chemical shift table. It uses an iterative structure calculation scheme that utilises CNS to perform the molecular dynamics simulations and simulated annealing steps in the calculation. Aria is responsible for analysing the resulting conformers following each calculation step to update and improve the restraint lists for the next stage in the calculation. Aria can receive input directly from the CcpNmr suite (Vranken et al., 2005) and also output results into an existing CcpN project.

For the calculation of the structure of the Ca^{2+}/CaM: eEF2K$_{82-100}$ complex, the auto-assignment function of Aria was not used. NOE's were assigned manually and instead, we made use of the floating chirality assignment function, which focuses on the difficulty in assigning chemical shifts at a prochiral centre. This was useful for the treatment and assignment of methyl groups, as it tests both alternatives during the structure calculation.

NOE distance restraint tables were made in CcpN, using the inbuilt function, following the standard protocol. The peak intensity scaling factor is defined such that the reference intensity, which defaults to the peak list's average volume, exactly corresponds to the reference distance (default 3.2 Å). The upper and lower bounds of the distance restraints are calculated as fractional differences from the calculated target distance (the default fractional

error is 0.20 Å). The resulting restraint tables were then incorporated into Aria directly in the case of the ^{15}N-NOESY and ^{13}C-NOESY spectra for the intra-CaM restraints and also the filtered NOESY for the intra-peptide restraints. The restraint table for the intermolecular distances between CaM and eEF2K$_{82\text{-}100}$ was created in CcpN and exported as a text file to be input for Aria. This was edited to give a distance of 5 Å, a lower error limit of 3.5 Å and an upper error limit of 0.5 Å for each restraint.

In addition, a restraint table was created to maintain the four Ca^{2+} ions of CaM in their correct orientations in the Ca^{2+} coordinating loops. The 6 coordinating atoms in CaM for each loop were determined based on previously determined Ca^{2+}/CaM structures in the PDB, as shown in Table 5. A distance of 2.4 Å with upper and lower limits of 0.2 Å was given for each restraint.

Table 5. Ca^{2+} coordination in CaM, including residues and atoms.

Residue	Atom
20	OD2
22	OD2
24	OD1
26	O
31	OE1, OE2
56	OD1
58	OD1
60	OD1
62	O
67	OE1, OE2
93	OD2
95	OD1
97	OD1
99	O
104	OE1, OE2
129	OD1
131	OD2
133	OD2
135	O
140	OE1, OE2

Dihedral restraints generated by Talos-N (Shen and Bax, 2013) were also included in the calculations to provide further information on secondary structure for the calculation.

Hydrogen bonds were added at later stages of the calculation, once a converged fold had been established. These were determined based on the structures produced and in concordance with previously determined Ca^{2+}/CaM structures in the PDB. Helices in CaM structures are of the same length and so hydrogen bonds were assigned for the Ca^{2+}/CaM: eEF2K_{82-100} complex based on their presence and location in the helices of known CaM structures. Although there are differences between the three-dimensional structures of different CaM: target complexes, the helices are consistent. Only those H-bonds were chosen which were in the centre of helices, whilst those at the boundaries were not included in case of inconsistencies here.

During the structure calculation eight iterations were performed, followed by water refinement. For each iteration 20 structures were produced, with the eight lowest energy structures carried forward into the following iteration. For the final structure calculation, 100 structures were calculated in iteration eight and the twenty lowest structures were carried forward into the water refinement to create an ensemble. The final structure calculation was carried out with 10,000 refine steps and 50,000 cool steps.

The iCING server (Doreleijers et al., 2012) was used to validate the protein structure ensemble and the results were compared to existing structure ensembles for CaM: target peptide structures in the PDB.

2.5.9 pH titration

A pH titration was carried out to investigate the pKa values for histidine residues in eEF2K_{87-100}. All NMR experiments were recorded at 600 MHz at a temperature of 298 K on a Varian INOVA-600 instrument fitted with a z-gradient cold probe (Agilent technologies). 1D proton spectra were recorded with an acquisition time of 0.4s using 1D sequence with WATERGATE water suppression as implemented in Biopack (Agilent Technologies). The ^{1}H resonances were referenced to TSP at 0 ppm and processed with mild

resolution enhancement and water deconvolution in VnmrJ3.1 (Agilent Technologies).

Samples of synthetic peptides corresponding to eEF2K$_{78-100}$ (China peptides, Shanghai) were prepared in D_2O buffer containing 25 mM Bis-Tris, 150 mM KCl and 10 mM $CaCl_2$. A set of 28 1D spectra were recorded over a pH range of 4.8-8.9 by the addition of sodium deuteroxide and deuterium chloride. The chemical shifts of the CH_2 protons of the imidazole side chains of the three histidine residues were determined with an accuracy of 0.02ppm. The data were fitted to the Hill equation (Markley, 1973) using a Hill coefficient of 1 and allowing the pKa to vary using the non-linear fitting routines in Grace (Grace Development Team). The pKa values were corrected by 0.04 units to account for the isotope effect of D_2O (Krezel and Bal, 2004). Using the above method the pKa of the imidazole ring of histidine was determined to be 6.13 in a separate titration.

Chapter 3. Expression, purification and characterisation of CaM and eEF2K fragments

3.1 Introduction

CaM and eEF2K fragments have been expressed and purified for use in this study. ^{15}N-^{13}C labelled CaM was produced for NMR studies whilst unlabelled CaM and eEF2K fragments were also produced. In the absence of structural data, a modular approach was pursued, with the aim to determine roles and affects associated with different regions of the proteins.

A number of eEF2K fragments have been used and are shown in Table 6. They consist either of residues from the N-terminal portion of eEF2K or from the C-terminal portion and differ in the functional regions of eEF2K that they contain.

Table 6. The eEF2K fragments used in this study with their corresponding amino acid residues and the functional regions that each contains.

eEF2K fragment	Residues	Region(s) contained
N-eEF2K$_{48-336}$	48-336	CaM binding, Kinase
N-eEF2K$_{74-332}$	74-342	CaM binding, Kinase
N-eEF2K$_{100-336}$	100-336	Kinase
C-eEF2K$_{490-725}$	490-725	Sel 1-like
eEF2K$_{82-100}$	82-100	CaM binding

The N-terminal fragments contain the regions of interest for this study, the CaM binding region and alpha kinase domain. However, in order to produce soluble protein they must be co-expressed and purified with C-eEF2K$_{490-725}$ (Pigott et al., 2012). In addition to the eEF2K fragments, a short peptide corresponding to the CaM binding region of eEF2K (residues 82-100) was also used in this study, detailed in grey in Table 6. This peptide was not expressed in *E. coli* and purified but was synthesised by solid phase methods and purchased from China Peptides. A schematic representation of the eEF2K fragments and the functional regions they contain is shown in Figure 40.

The eEF2K fragments were investigated using NMR and other biophysical techniques to gain insight into the molecular mechanism of

activation of eEF2K in response to Ca^{2+}/CaM. In addition, $eEF2K_{82-100}$ in particular, was used to investigate an unusual CaM-binding region and the mechanism of CaM target recognition.

In order to analyse the NMR data collected, CaM was assigned in four different conditions; Ca^{2+}/CaM, apo-CaM, Ca^{2+}/CaM bound to $eEF2K_{82-100}$ and apo-CaM bound to $eEF2K_{82-100}$. The protein backbone resonances were assigned and also some of the side chain resonances in order to further define interaction sites on CaM for $eEF2K_{82-100}$.

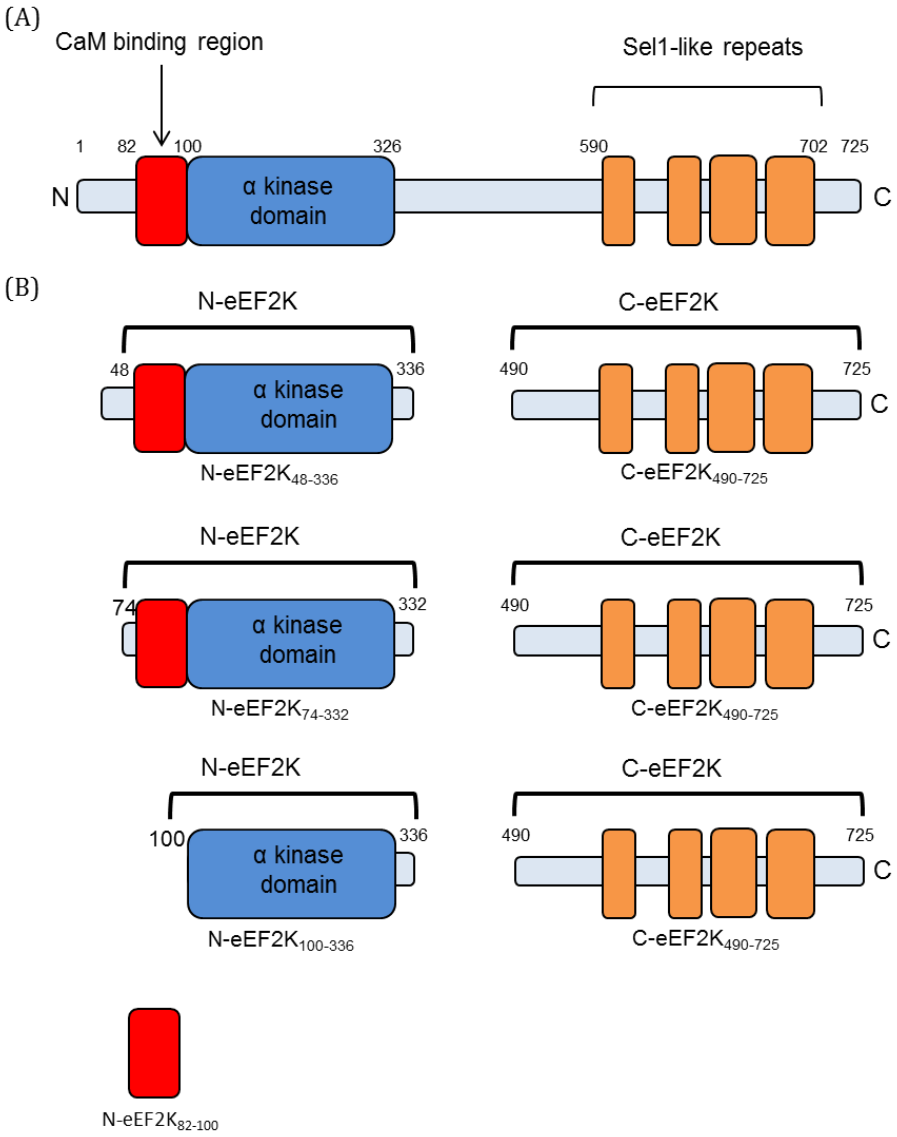

Figure 40. Representation of the eEF2K fragments used in this study.

Domain organisation of eEF2K (A). Schematic representation of each eEF2K fragment and the functional regions that each contains (B). The CaM binding region is shown in red, the α-kinase domain is blue and the Sel 1-like domain is orange. The residue numbers are labelled.

3.2 Production and characterisation of CaM

3.2.1 Expression and purification of CaM

To study the structure of CaM by NMR spectroscopy it must be ^{13}C and ^{15}N labelled during protein expression before purification. A vector containing the CaM coding region was transformed into competent *E. coli* and expressed according to the protocol outlined in 2.2.3. CaM expressed well, producing a high yield of stable protein (approximately 40 mg/mL) that is evident above the *E. coli* background, as shown in Figure 41.

A robust purification strategy has been employed for CaM that involves an initial affinity chromatography step using a Ni-NTA column to remove the majority of the other proteins expressed by *E. coli*. Hydrophobic interaction chromatography using a phenyl Sepharose column exploits the mechanism by which CaM interacts with calcium to provide a highly specific interaction with the column resin. Figure 41 shows that this purification step yields pure CaM, requiring only the cleavage of the His_6 purification tag by TEV protease and gel filtration to remove this cleaved tag. There is a band on the gel following the purification step with phenyl Sepharose (lane 7), just below the band that corresponds to CaM before tag cleavage, which indicates there is some CaM present where the tag has already been cleaved. The band seen on the gel for purified CaM is of the correct molecular weight, which was further confirmed by mass spectrometry (Section 3.2.2).

The high yield, stability and purity of the CaM produced are all important factors to allow NMR spectroscopy studies as high concentrations of stable and pure protein are needed to achieve the high quality of NMR spectra necessary for resonance assignment and analysis.

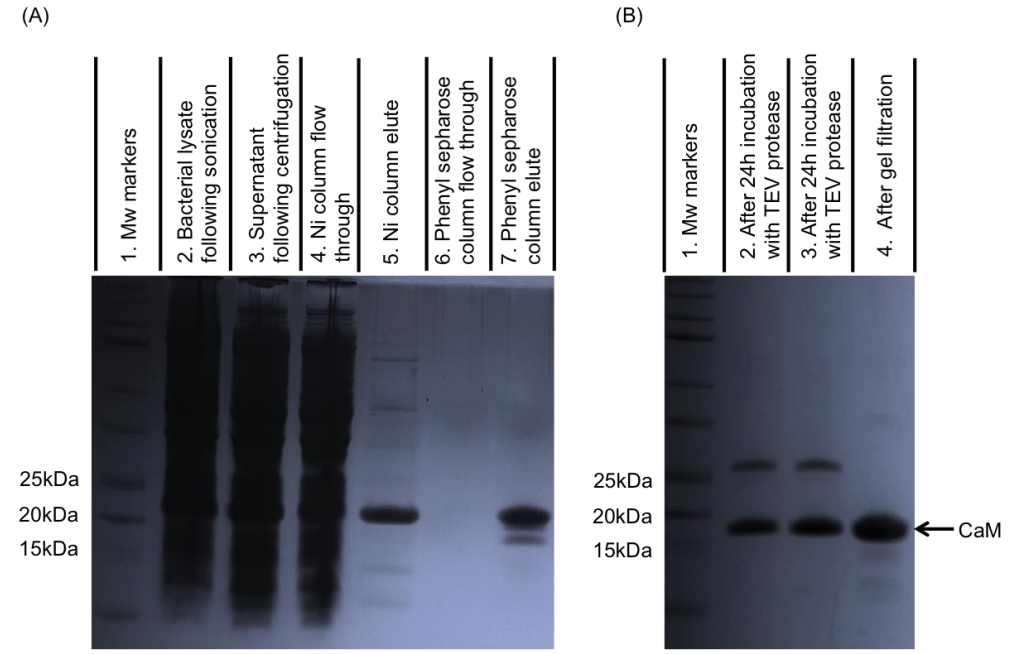

Figure 41. SDS-PAGE gel of expression and purification of CaM.

(A) SDS-PAGE gel of purification of CaM before gel filtration. This includes: cell lysis (lane 2), centrifugation (lane 3), affinity chromatography with Ni-NTA resin (lanes 4 and 5), hydrophobic interaction chromatography with a phenyl Sepharose column (lane 6) and digestion with TEV protease (lane 7). (B) SDS-PAGE gel of protein sample following TEV digestion (lanes 2 and 3) and gel filtration (lane 4).

3.2.2 Mass spectrometry of CaM

Mass spectrometry was performed by Neville Wright at the University of Southampton to check the precise molecular weight of the purified CaM. The spectrum shown in Figure 42 was collected from a sample of purified Ca^{2+}/CaM. A strong peak corresponding to 17,818 Da is identified. This corresponds to ^{15}N-^{13}C labelled Ca^{2+}/CaM, which has a theoretically calculated Mw of 17,772 Da (including His_6 purification tag and increased Mw for isotopic labelling) and thus confirms the presence of full-length CaM bound to calcium ions.

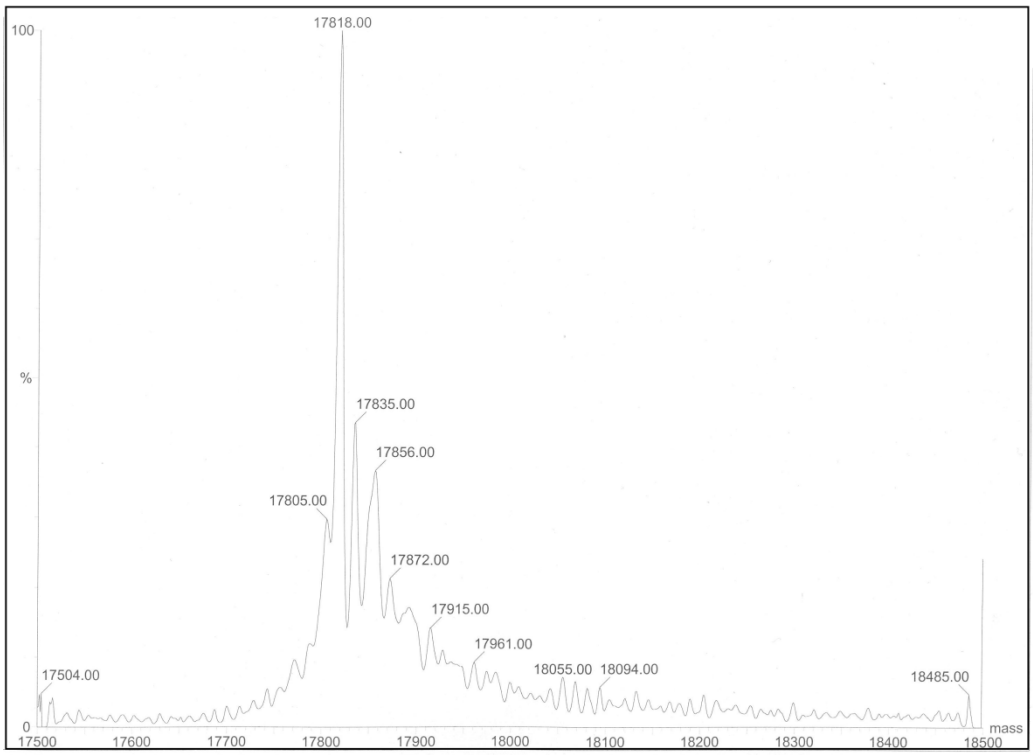

Figure 42. Mass spectrum of ^{13}C-^{15}N labelled Ca^{2+}/CaM.

Mass spectrum of doubly labelled Ca^{2+}/CaM collected with a U-3010 spectrometer using the positive ion mode with the mass to charge ratio (M/z) analysed between 750 and 1500. A strong peak is identified at 17818 Da.

3.3 Production and characterisation of eEF2K fragments

3.3.1 Expression and purification of eEF2K fragments

To produce soluble eEF2K, a fragment of the N-terminal region containing the kinase domain is co-expressed with a fragment of the C-terminal region containing the Sel1-like domain. The N-terminal fragments were cloned into pNIC-Zb vectors containing an N-terminal Z-tag and an N-terminal polyhistidine tag whilst the C-terminal fragment, C-eEF2K$_{490-725}$, was cloned into the pCDF vector.

Both vectors, one containing the N-terminal fragment insert and one containing the C-terminal fragment insert, were co-transformed into competent *E. coli* cells and the fragments were expressed according to the protocol outlined in 2.2.3. SDS-PAGE analysis demonstrates that expected bands for the co-expressed N-eEF2K$_{48-336}$ and C-eEF2K$_{490-725}$ fragments are observed above the *E. coli* background, as shown in Figure 43.

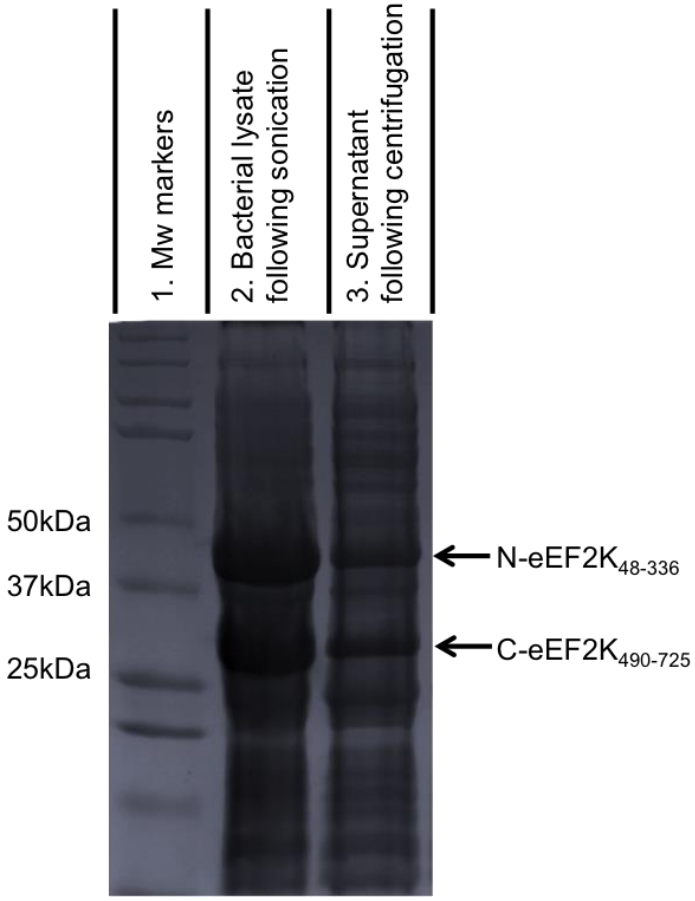

Figure 43. SDS-PAGE gel of expression of eEF2K fragments.
Samples were collected after cell lysis by sonication and following subsequent centrifugation. Bands are present for both eEF2K fragments, above the *E. coli* background, indicating successful induction. This is an example trace from a purification of N-eEF2K$_{48-336}$ and C-eEF2K$_{490-725}$.

A purification strategy has been optimised for the eEF2K fragments. The first stage in purification uses Ni-NTA resin for affinity chromatography, facilitated by the presence of a polyhistidine tag. This is followed by an ion-exchange chromatography step, which is highly specific and produces pure and concentrated protein due to the presence of a positively charged Z-tag on the N-terminal eEF2K fragments, as shown in Figure 44. Another advantage of this purification step is that it ensures the N- and C-terminal eEF2K fragments are present at a 1:1 molar ratio. This eliminates the possibility of there being an excess of one of the fragments as C-eEF2K$_{490-725}$ often expresses more strongly than the N-terminal eEF2K fragments.

Fractions identified to contain eEF2K fragments were incubated with TEV protease to cleave the protein purification tags and Lambda Phosphatase

and $MnCl_2$ to dephosphorylate the eEF2K fragments. Size exclusion chromatography/gel filtration was used to separate the cleaved tag from the eEF2K fragments so that they could be used for further studies. In this step larger proteins elute first, as the smaller ones are maintained within the resin for longer and therefore eluted later, as shown in Figure 41.

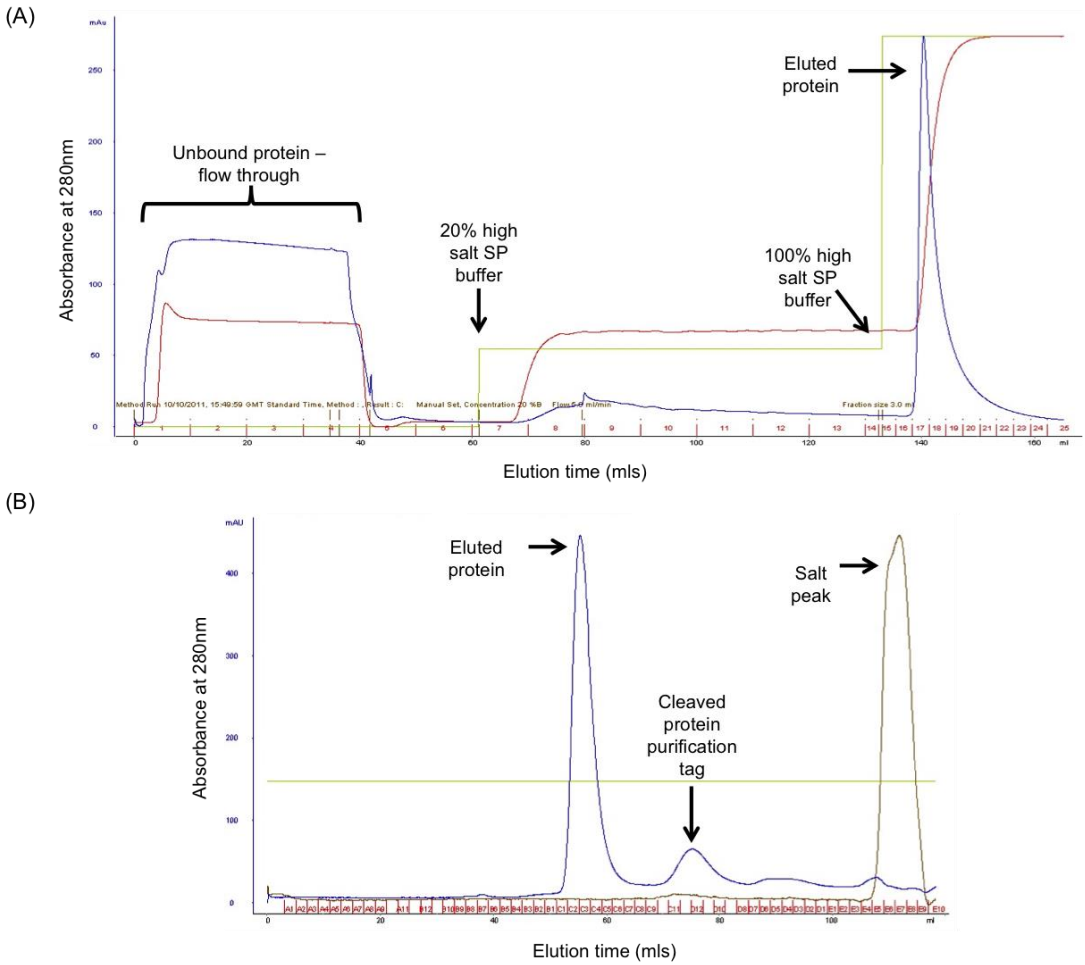

Figure 44. Ion exchange chromatography and gel filtration traces from the purification of eEF2K fragments.

(A) Ion exchange chromatography trace. The blue trace indicates the absorbance readings at 280nm and therefore demonstrates the presence of protein. The red trace indicates the conductance. The green lines denote the changes in buffer concentrations. This is an example trace from a purification of N-eEF2K$_{48-336}$ and C-eEF2K$_{490-725}$. (B) Gel filtration trace. The blue trace indicates the absorbance readings at 280nm and therefore demonstrates the presence of protein. The large peak shows the elution of eEF2K fragments whilst the second, smaller peak shows the elution of the cleaved protein purification tags. The red trace indicates the conductance. This is a sample trace from a purification of N-eEF2K$_{48-336}$ and C-eEF2K$_{490-725}$.

SDS-PAGE was used throughout the purification stages to monitor the process and determine purity, as shown in Figure 45.

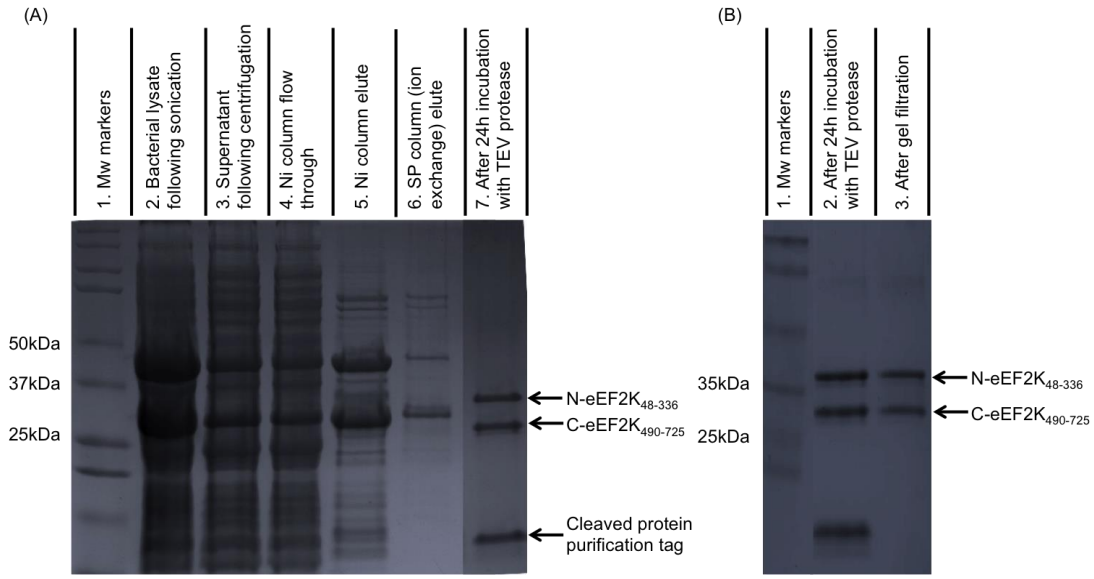

Figure 45. SDS-Page gel of expression and purification of eEF2K fragments. (A) SDS-PAGE gel of purification of eEF2K fragments before gel filtration. This includes: cell lysis (lane 2), centrifugation (lane 3), affinity chromatography with Ni-NTA resin (lanes 4 and 5), ion exchange chromatography with an SP Sepharose column (lane 6) and digestion with TEV protease (lane 7). (B) SDS-PAGE gel of protein sample following gel filtration. Arrows indicate the positions of the two fragments of eEF2K that are co-expressed, as well as the cleaved protein purification tag. This is an typical gel from a purification of N-eEF2K$_{48-336}$ and C-eEF2K$_{490-725}$.

3.3.2 Activity of eEF2K fragments

A radioactive kinase assay was used to determine the activity of the eEF2K fragments expressed and purified from *E. coli*. It was important to know whether these eEF2K fragments could bind CaM and become activated to phosphorylate substrate and thus function in a similar way to the wild-type enzyme.

Two N-terminal fragments were analysed, N-eEF2K$_{48-336}$ and N-eEF2K$_{100-336}$, and both were co-expressed with C-eEF2K$_{490-725}$. N-eEF2K$_{48-336}$ contains the full-length α-kinase domain as well as the CaM binding region whilst N-eEF2K$_{100-336}$ does not contain the CaM binding region. The activity of these were analysed in the presence and absence of calcium and then compared to that determined for wild-type eEF2K, as shown in Figure 46. The activity

conditions were as described by Pigott et al with optimised concentrations of Mg^{2+} and ATP, as well as CaM and eEF2K (Pigott et al., 2012).

In the case of wild-type eEF2K, very high Cerenkov counts were recorded in the presence of Ca^{2+}/CaM, indicating a high level of kinase activity. In the presence of apo-CaM the enzyme was inactive. N-eEF2K$_{48-336}$ (in the presence of C-eEF2K$_{490-725}$) demonstrates similar results, with no activity detected in the absence of calcium. It is active in the presence of Ca^{2+}/CaM although the Cerenkov counts measured were over ten-fold lower than for wild-type eEF2K, meaning that this fragment is considerably less active than the wild-type. N-eEF2K$_{100-336}$ shows no activity in the presence of either Ca^{2+}/CaM or apo-CaM, presumably due to the fact that there is no CaM-binding region present. CaM is therefore unable to bind and activate eEF2K to phosphorylate substrate.

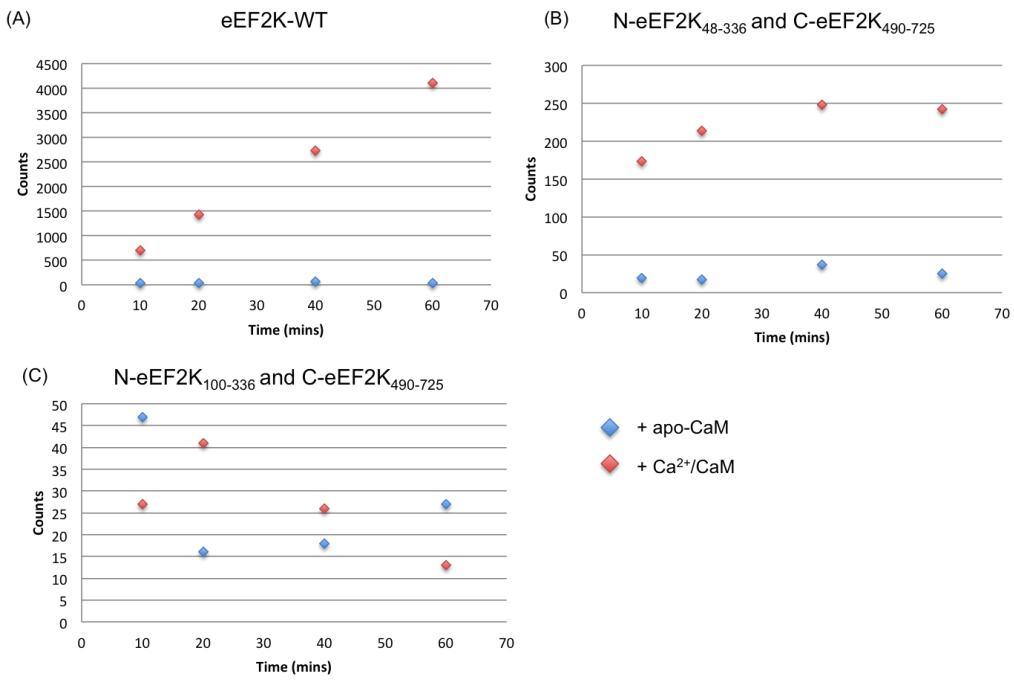

Figure 46. Activity of eEF2K fragments compared to eEF2K-WT analysed by radioactive kinase assay.

Activity of eEF2K fragments and eEF2K-WT determined by radioactive kinase assay using MH-1 as the eEF2K substrate. Phosphorylation of MH-1 by eEF2K was monitored over a series of time points (0-60 min) and measured by Cerenkov counting. (A) Kinase activity of eEF2K-WT, (B) Kinase activity of N-eEF2K$_{48-336}$ and (C) Kinase activity of N-eEF2K$_{100-336}$. Buffer conditions are as described in Section 2.4.3 and all experiments were collected in a single assay.

3.4 Resonance assignments for CaM

NMR experiments yield significant information on protein interactions but to analyse this NMR data, resonance assignments of the protein are needed. Resonance assignment involves determining the chemical shifts of the atoms in the protein and thus which peaks on an NMR spectrum correspond to which atom in the protein. CaM has previously been assigned and is listed on the Biological Magnetic Resonance Data Bank (BMRB), but it has not yet been assigned in the presence of a peptide from eEF2K.

CaM was assigned in four states to aid in the analysis of NMR experimental data and gain understanding of the interaction between CaM and eEF2K. Ca^{2+}/CaM and apo-CaM have been assigned in their free states and also when bound to $eEF2K_{82\text{-}100}$. Although Ca^{2+}CaM has been assigned by a number of groups previously, it was re-assigned here in the same conditions as for the $eEF2K_{82\text{-}100}$ bound-Ca^{2+}/CaM. Assignments of apo-calmodulin are not available on the BMRB. The chemical shift tables are found in the Appendix (Appendices 7-10). Each of these conditions yields distinct and characteristic ^{1}H-^{15}N-HSQC and ^{1}H-^{13}C-HSQC spectra.

The protein backbone atoms, including the N-H, Cα and Cβ resonances, were assigned initially and this was followed by the assignment of some side chain atoms. It was found that analysis of the ^{1}H-^{15}N-HSQC spectra alone did not provide sufficient information on the binding of $eEF2K_{82\text{-}100}$ to CaM and so the amino acid side chains that contain methyl groups were assigned in addition to the protein backbone. The region of ^{1}H-^{13}C-HSQC spectra that contains peaks corresponding to the methyl groups of aliphatic residues is the clearest area of a ^{1}H-^{13}C-HSQC spectrum and therefore the easiest to assign and interpret. Assigning these side chain atoms means we can get a clearer idea of the amino acid residues of CaM responsible for interaction, as it is these atoms that will largely contact $eEF2K_{82\text{-}100}$. Also, the backbone N-H resonances are particularly sensitive to distal effects such as large-scale structural changes and so it is less reliable to define an interaction site by studying these.

3.4.1 Backbone assignment

A combination of triple resonance NMR experiments was used to assign the backbone resonances of Ca^{2+}/CaM, Ca^{2+}/CaM bound to $eEF2K_{82\text{-}100}$, apo-CaM and apo-CaM bound to $eEF2K_{82\text{-}100}$. HNCACB experiments were collected and utilised for the assignment of each CaM state in conjunction with ^{1}H-^{15}N-HSQC experiments. CBCA(CO)NH and HNCA data were also collected and aided in the assignment of some of the CaM states. This yielded the chemical shifts of N, HN, Cα and Cβ atoms from the protein backbones.

HNCACB experiments alone were sometimes sufficient to assign resonances of the protein backbone of some CaM states. This was possible as the spectrum displays two peaks corresponding to the Cα and Cβ of a particular amino acid residue and also another two peaks for the Cα and Cβ of the preceding residue. This makes a method of sequential assignment possible. Strips were produced that correspond to the chemical shift of the nitrogen atom of the amide (NH) bond. These strips therefore contain peaks for the Cα and Cβ chemical shifts of the corresponding residue, which appear with a relatively strong intensity. They also contain peaks with weaker intensities that represent the Cα and Cβ chemical shifts of the previous residue. It was therefore possible to sequentially link strips by connecting the strong peaks of one strip to the weak peaks of another strip. These strong to weak connections were identified as both peaks have the same carbon chemical shift, thus indicating that both peaks correspond to the same carbon atom. The sequential assignment method is demonstrated in Figure 47.

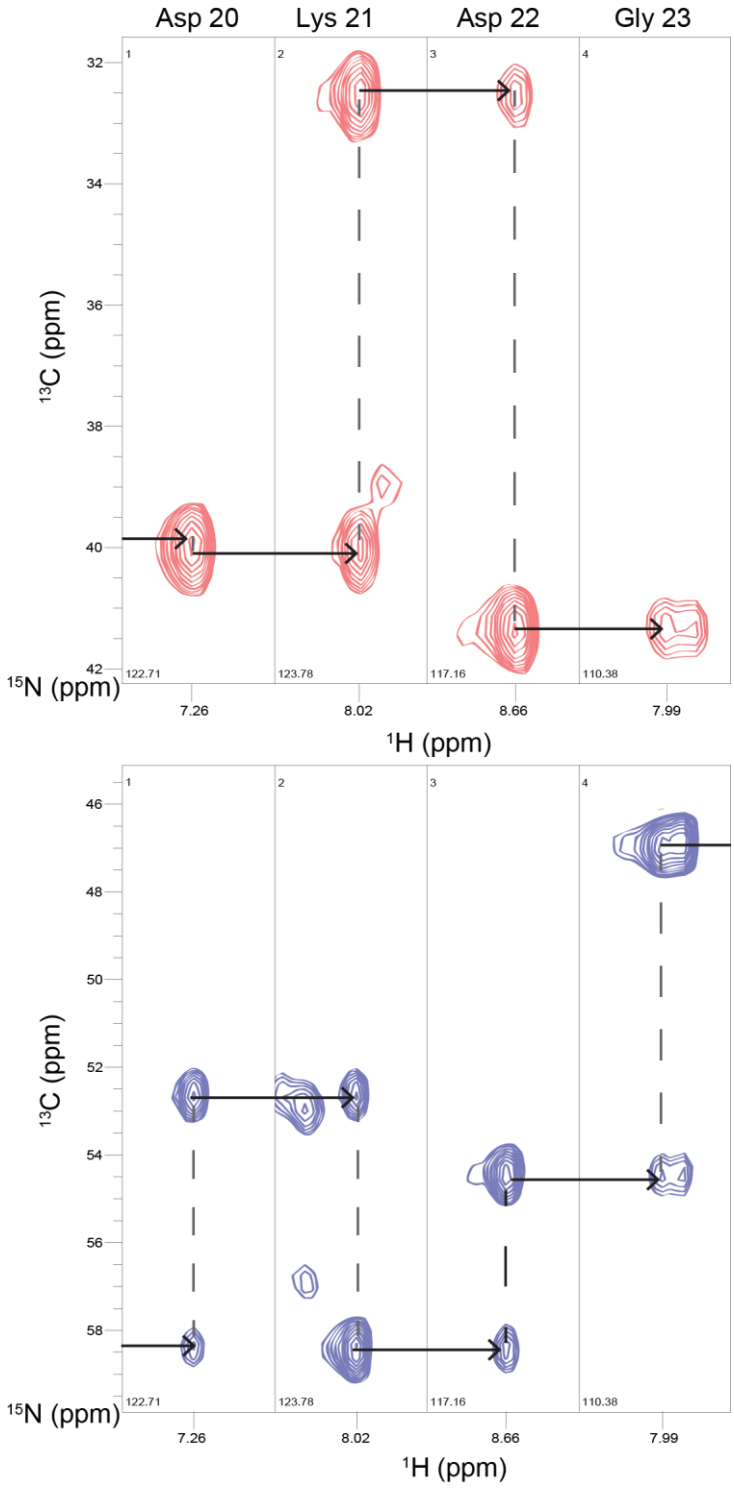

Figure 47. Representative strip plot from HNCACB experiment on apo-CaM.

Representative HNCACB strips for the sequential assignment of residues Asp[20], Lys[21], Asp[22], Gly[23]. The region of the spectra containing the Cα chemical shifts are shown at the bottom with the peaks in blue and the region of the spectra containing the Cβ chemical shifts are shown at the top with the peaks in red. Arrows show the linkages between strips, connecting the strong peak in strip i-1 to the weak peak in strip i. Dashed lines represent the visualisation of the linking between the strong and weak peaks in an individual strip.

When using the HNCACB experiment alone for backbone resonance assignment there can be some ambiguity, especially if the signal-to-noise ratio is relatively low. Employing the HNCA and CBCA(CO)NH experiments can help to relieve some of this uncertainty. The HNCA experiment has a higher sensitivity and therefore produced spectra with a greater signal to noise ratio compared to the HNCACB experiment. By overlaying the HNCA experiment with the HNCACB experiment linkages can be discovered in the Cα region where the HNCA spectrum has a higher quality and then transferred to the Cβ region using the HNCACB. The CBCA(CO)NH experiment produces a spectrum with peaks only for the Cα and Cβ resonances of the preceding amino acid residue. This means that when the HNCACB and CBCA(CO)NH spectra are overlaid, the CBCA(CO)NH peaks will appear on top of the weak peaks in the HNCACB spectra, as shown in Figure 48. This is therefore extremely helpful in distinguishing between the two peaks on an HNCACB strip as to which one corresponds to residue i and which is representative of i-1. It is also useful if the signal to noise ratio of the HNCACB spectrum is low, causing the weaker peaks corresponding to the i-1 residue to be indistinguishable from the noise.

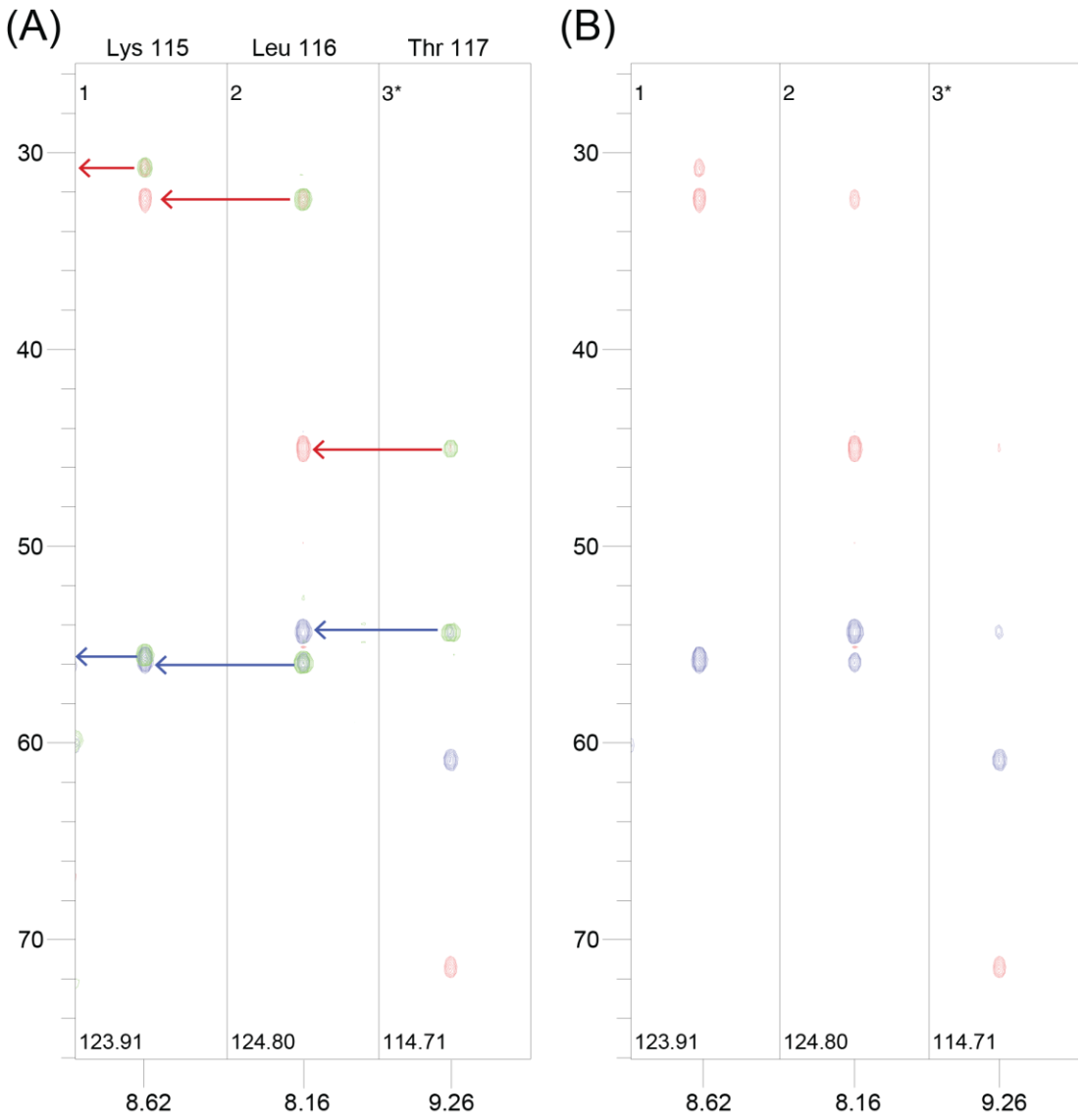

Figure 48. Representative strip plot from HNCACB and CBCA(CO)NH experiments on Ca^{2+}/CaM.

(A) Overlay strip plot of HNCACB (red for Cβ region and blue for Cα region) and CBCA(CO)NH (green) spectra for the sequential assignment of residues Lys^{115}, Leu^{116} and Thr^{117}. Red and blue arrows indicate the sequential backward linkages between strips, connecting the weak HNCACB peak with an overlaying CBCA(CO)NH peak in strip i to the strong peak that does not have an overlaying CBCA(CO)NH peak in strip i-1. (B) Identical strip plot with CBCA(CO)NH spectrum removed so that only the HNCACB spectrum is visible.

3.4.2 Side chain assignment

Following on from the protein backbone assignment, further NMR experiments are needed to assign the side chain resonances of amino acid residues. For this project, it is the methyl groups of the amino acid side chains that were most important and so the side chains of those amino acids containing methyl groups were assigned primarily using H(CCO)NH, HCCH-

TOCSY and ^{15}N-NOESY spectra. The H(CCO)NH and HCCH-TOCSY experiments were used together to assign the methyl groups in alanine, leucine, isoleucine, valine and threonine, whilst the remaining amino acid containing a methyl group, methionine, required the use of the ^{15}N-NOESY experiment.

The chemical shifts of N-H resonances (determined from assigning the protein backbone resonances) were identified on the H(CCO)NH spectrum for each amino acid residue. On the corresponding ^{15}N plane in the three-dimensional spectrum and at the relevant proton chemical shift, a strip of peaks will be present for the resonances of protons in the spin system of the residue side chain. These peaks provide the proton chemical shifts and the HCCH-TOCSY was then used to identify the carbon chemical shifts of the atoms in the side chain.

The use of the HCCH-TOCSY spectrum to assign spin systems is shown in Figure 49. The Cα and Cβ chemical shifts were known from the backbone assignment and also some of the side chain proton chemical shifts were now known from the H(CCO)NH experiment. On the carbon plane that corresponds to the Cα chemical shift of a particular amino acid residue a strip of cross peaks from the diagonal was present at the proton shifts determined from the H(CCO)NH experiment. Similarly there was also a strip of cross peaks on the carbon plane corresponding to the Cβ chemical shift with the peaks present in the same positions. Correlations between the cross peaks were marked and used to determine the chemical shifts of the carbon atoms in the residue side chain. These were identified by locating planes with strips of cross peaks in the same positions. The peak that appears on the diagonal indicates the carbon atom to which this proton is bonded. For example, the Hα peak will appear on the diagonal on the carbon plane that corresponds to the chemical shift Cα.

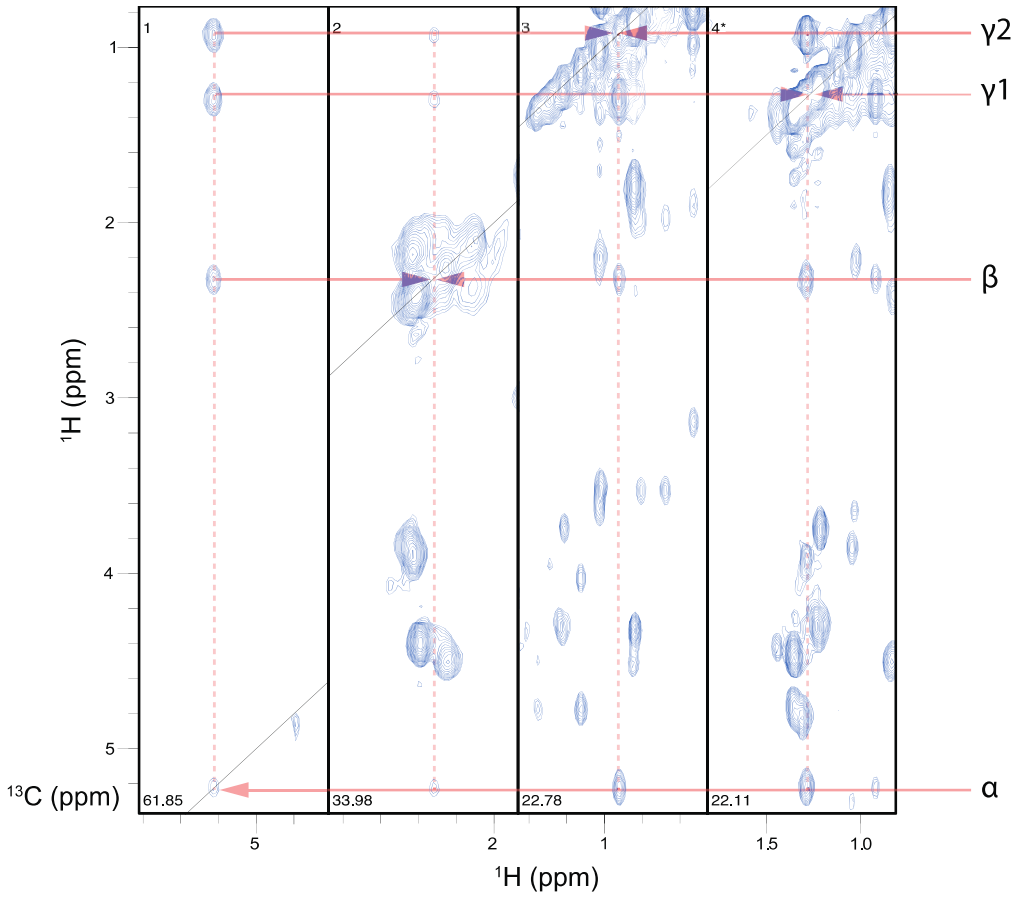

Figure 49. Representative strip plot from HCCH-TOCSY experiment on Ca^{2+}/CaM.

Representative HCCH-TOCSY strips for residue Val[136]. Proton cross peaks are present for each side chain proton and appear in a strip (marked by dashed red lines) from the diagonal on each carbon plane. The peak on the diagonal corresponds to the proton bonded to the carbon atom at the particular carbon chemical shift, as shown by the red arrows.

The resonances of atoms in the methyl group of methionine side chains could not be assigned using these spectra, as there is a sulphur atom within the carbon chain. This means that magnetisation transfer through chemical bonds cannot occur via this sulphur to reach the methyl group in the experiments already discussed for side chain assignment. Therefore another experiment is used which transfers magnetisation through space that is termed the ^{15}N-NOESY experiment. This is a very crowded spectrum and so is relatively difficult to analyse and interpret. The assigned N-H resonances from the protein backbone assignment were used to navigate to the corresponding nitrogen plane chemical shift where a strip of cross peaks from the diagonal will be present at the frequency of the known proton shift. These peaks will represent

all resonances within a particular distance from the starting amino acid residue, one of which will represent the chemical shift of the methyl group proton.

3.4.3 Resonance assignment of Ca^{2+}/CaM

The protein backbone ^{13}C, ^{15}N and ^{1}H resonances of Ca^{2+}/CaM were 100% assigned using the method outlined in Section 3.4.1. All peaks corresponding to backbone N-H's on the ^{1}H-^{15}N-HSQC of Ca^{2+}/CaM, shown in Figure 47, are assigned. Prolyl residues do not have a backbone N-H and so no peaks are present on the spectrum for Pro^{43} and Pro^{66}. All Cα and Cβ resonances are also assigned for each amino acid residue, including the two prolines.

The ^{1}H-^{15}N-HSQC spectrum of Ca^{2+}/CaM has an excellent signal to noise ratio and shows well-dispersed peaks of similar intensity, indicating a correctly folded and stable protein. The HNCACB spectrum was of high quality and for the majority of amino acid residues would have been sufficient for assignment, although a CBCA(CO)NH was also used to reduce any ambiguity.

All of the amino acid residues containing methyl groups have also been assigned for Ca^{2+}/CaM. The ^{1}H-^{13}C-HSQC, shown in Figure 51, has a good signal to noise ratio, especially in the region containing resonances from methyl groups within the protein, and every peak in this region could be assigned to a separate methyl group of Ca^{2+}/CaM.

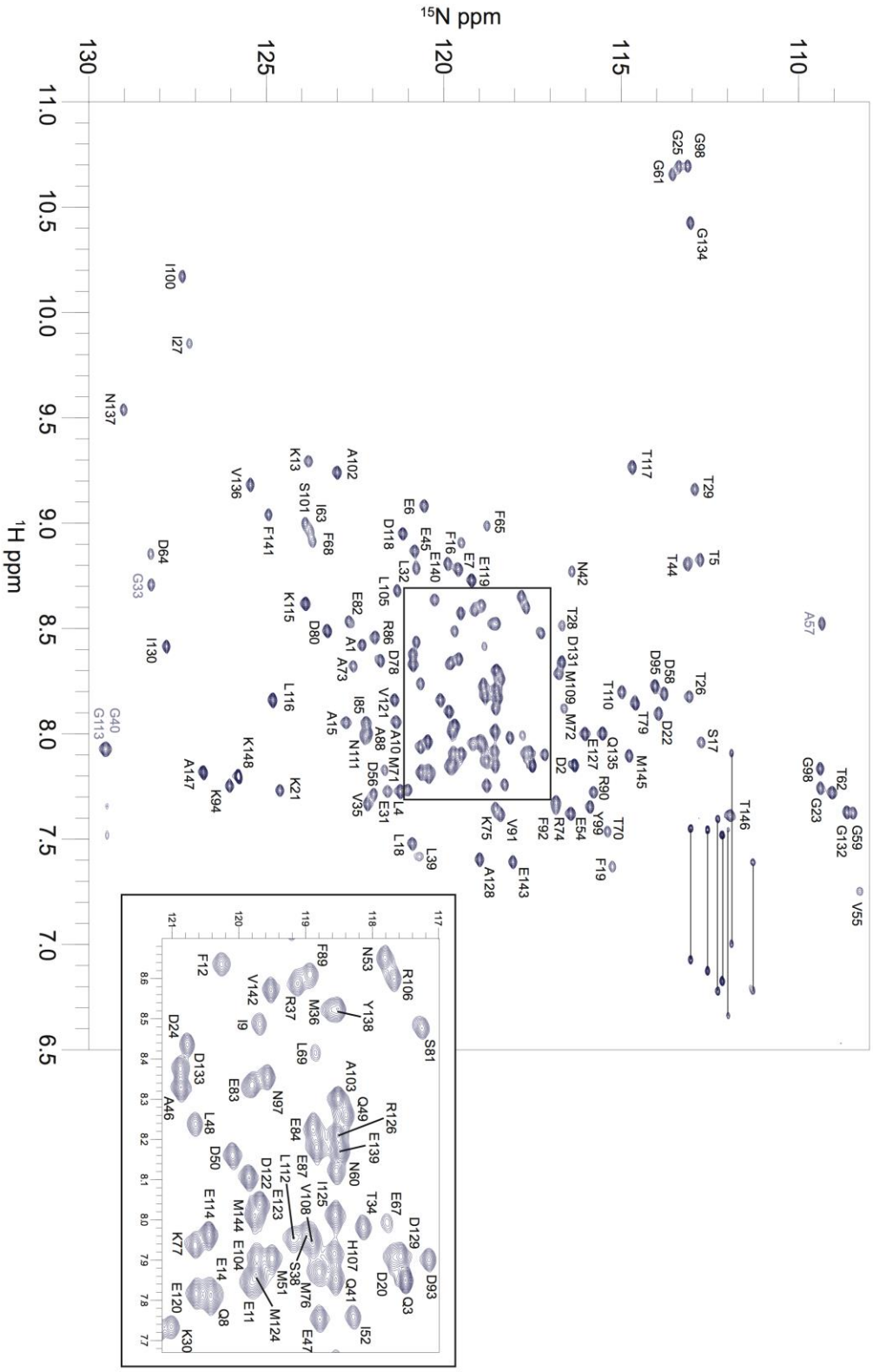

Figure 50. Assigned ^{1}H-^{15}N-HSQC spectrum of Ca^{2+}/CaM.

^{1}H-^{15}N-HSQC spectrum of Ca^{2+}/CaM with peaks labelled as a result of resonance assignment, according to the amino acid residue they represent. Pairs of peaks that correspond to side chain NH_2 groups are marked with joining solid lines. Those peaks which have been folded are labelled in grey. Buffer conditions are as described in Section 2.5.2.

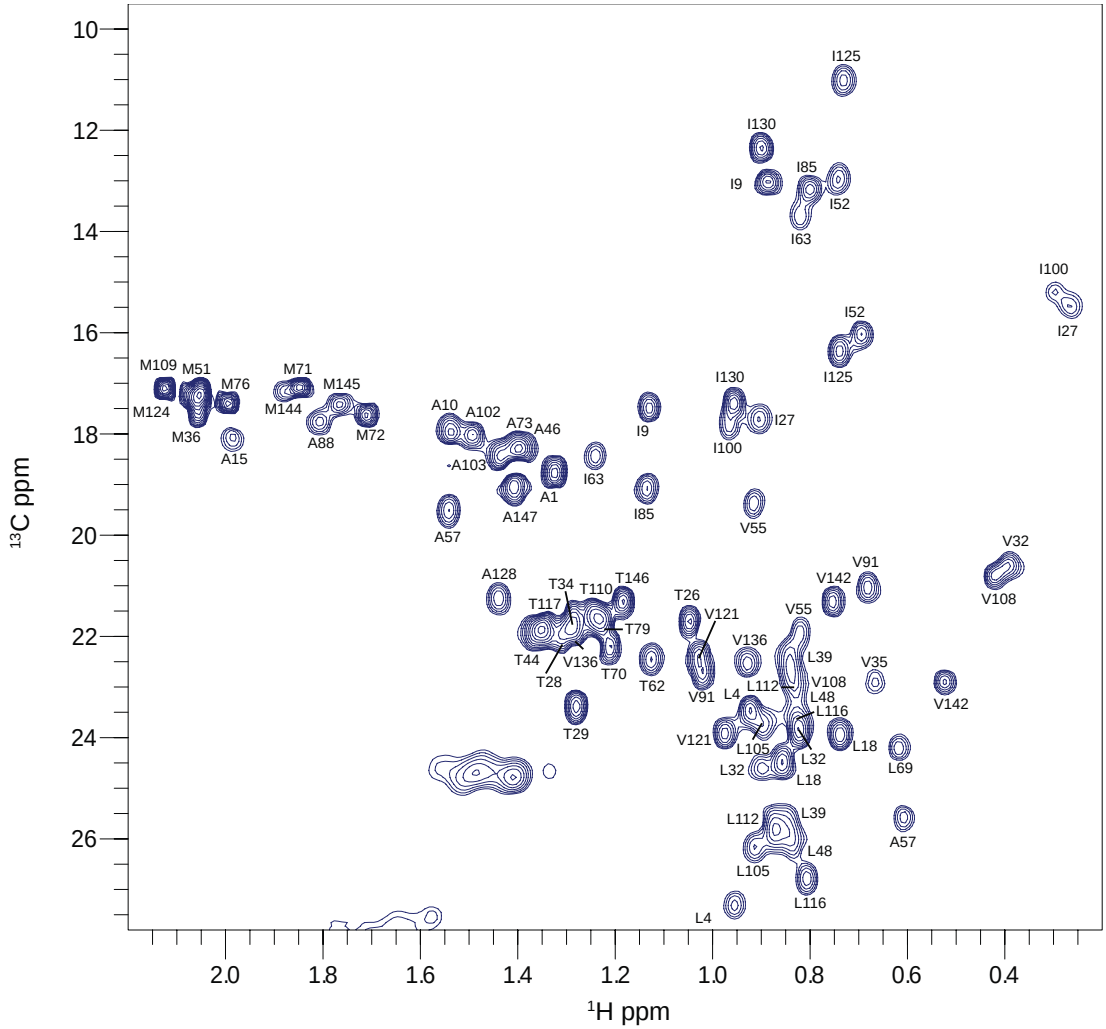

Figure 51. Assigned ^{1}H-^{13}C-HSQC spectrum of Ca^{2+}/CaM.

Region of the ^{1}H-^{13}C-HSQC spectrum that contains resonances of methyl groups of Ca^{2+}/CaM with peaks labelled as a result of resonance assignment. The side chain assignment was not stereo-specific and so those amino acid residues containing two methyl groups have two peaks, which have both been labelled with the amino acid and sequence position. Buffer conditions are as described in Section 2.5.2.

3.4.4 Resonance assignment of Ca^{2+}/CaM bound to eEF2K$_{82-100}$ (1:10 ratio)

Ca^{2+}/CaM was also assigned when bound to eEF2K$_{82-100}$. The NMR assignments were collected with a ten-fold excess of eEF2K$_{82-100}$ to CaM in order to ensure that the bound state of Ca^{2+}/CaM was populated.

The protein backbone was 98% assigned, with three amino acid residues in addition to the two proline residues, being unassigned. The first amino acid residue of Ca^{2+}/CaM, Ala^{1}, could not be assigned, as well as Arg^{37} and Glu^{84}. The most likely reason for the fact that Ala^{1} could not be assigned is that it is the first amino acid in the structure and thus it is probably relatively flexible in solution.

Arg^{37} and Glu^{84} could not be assigned due to the signal to noise ratio of the HNCACB spectrum, which could not be improved by the use of an additional HNCA spectrum.

The ^{1}H-^{15}N-HSQC spectrum of the Ca^{2+}/CaM: $eEF2K_{82-100}$ complex has a good signal to noise ratio and contains the expected number of peaks for the protein size. The signal to noise ratio of the HNCACB spectrum was relatively poor compared to those collected for other conditions and therefore a HNCA spectrum was used in addition for the backbone assignment. For the majority of amino acid residues this method was suitable, resulting in 98% of the N-H correlations on the ^{1}H-^{15}N-HSQC spectrum being assigned, as shown in Figure 52.

Side chain atom assignment of those amino acid residues that have a methyl group was also successful through the use of H(CCO)NH, HCCH-TOCSY and ^{15}N-NOESY spectra. The Ala^{1} methyl resonance could not be assigned as the backbone N-H was unknown. Also, Thr^{26}, Thr^{62} and Thr^{79} could not be assigned due to the fact that many of the resonances were overlapping, meaning that they could not be unambiguously assigned. The ^{1}H-^{13}C-HSQC spectrum was well resolved and the majority of peaks could be assigned, as shown in Figure 53. However, there were six peaks that could not be assigned, which are highlighted in Figure 53. The chemical shifts of these peaks mean that they are unlikely to correspond to the threonine residues whose side chain atoms could not be assigned and this was confirmed by the H(CCO)NH and HCCH-TOCSY spectra. It is possible that they represent doubled peaks, meaning they occur as a result of a methyl group being in two states throughout the experiment. This will generate two separate peaks on the spectrum as the atoms exist in two chemical environments, resulting in two distinct chemical shifts.

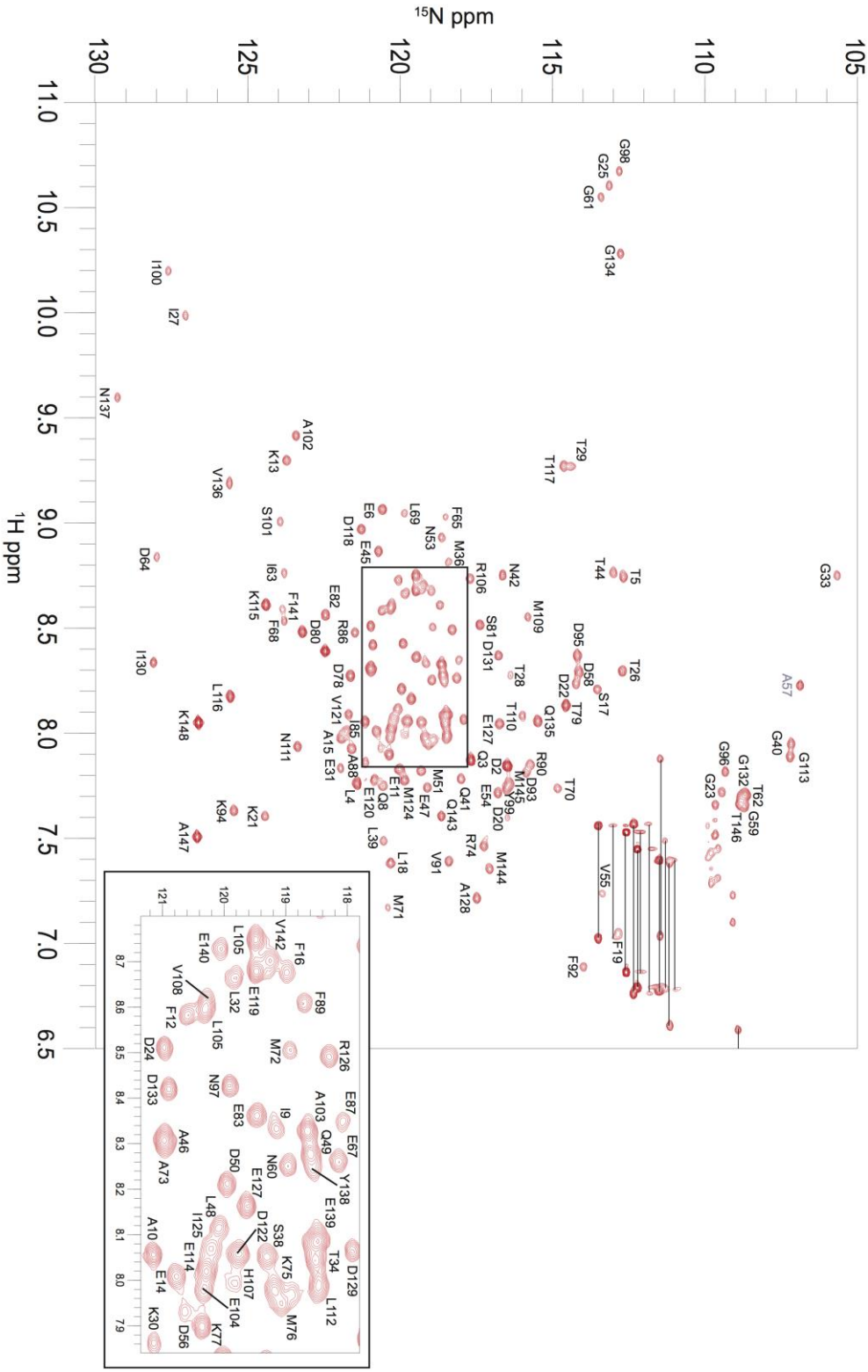

Figure 52. Assigned ^{1}H-^{15}N-HSQC spectrum of the Ca^{2+}/CaM: eEF2K$_{82\text{-}100}$ complex.

^{1}H-^{15}N-HSQC spectrum of the Ca^{2+}/CaM: eEF2K$_{82\text{-}100}$ complex with peaks labelled as a result of resonance assignment, according to the amino acid residue they represent. Pairs of peaks that correspond to side chain NH_2 groups are marked with joining solid lines. Those peaks that have been folded are labelled in grey. Buffer conditions are as described in Section 2.5.2.

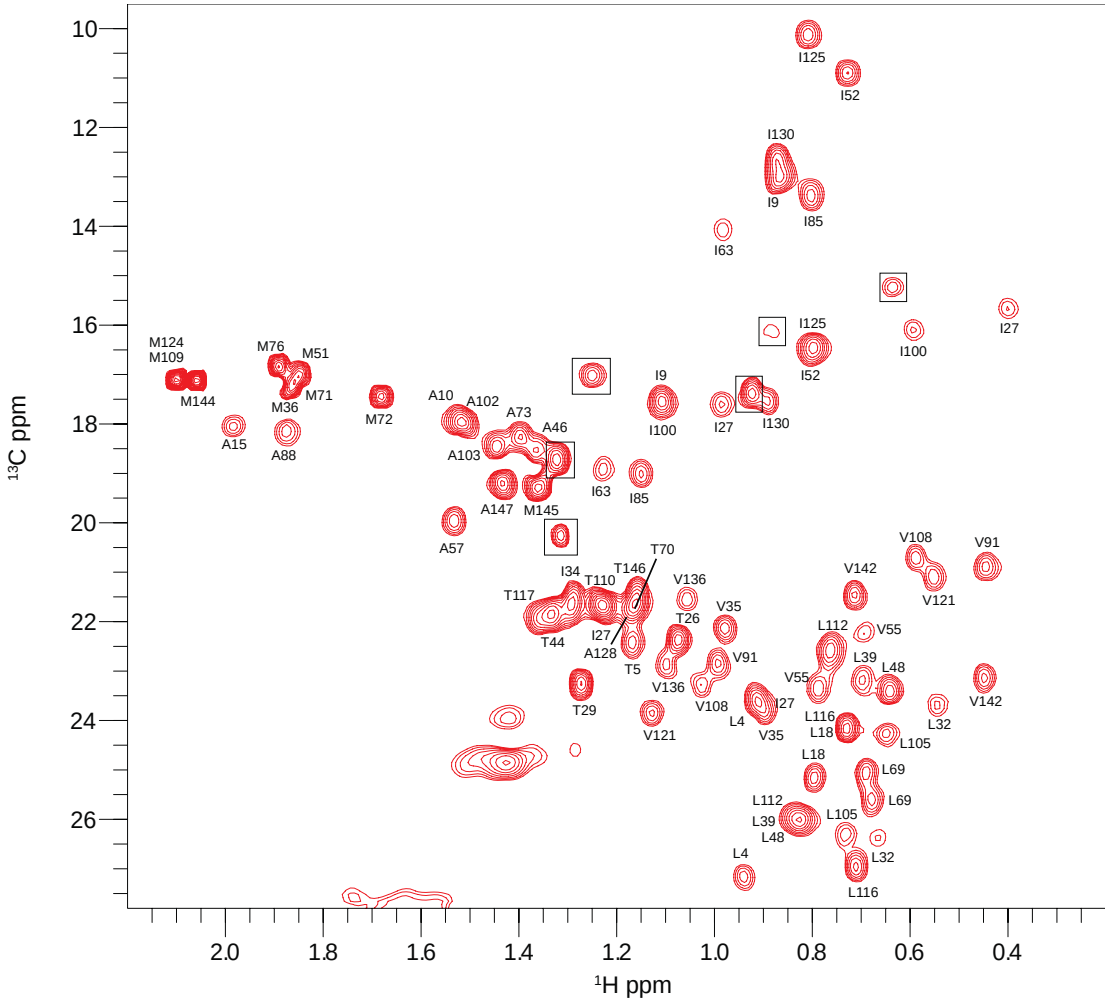

Figure 53. Assigned ^{1}H-^{13}C-HSQC spectrum of the Ca^{2+}/CaM: $eEF2K_{82\text{-}100}$ complex.

Region of the ^{1}H-^{13}C-HSQC spectrum that contains resonances of methyl groups of the Ca^{2+}/CaM: $eEF2K_{82\text{-}100}$ complex with peaks labelled as a result of resonance assignment. The side chain assignment was not stereo-specific and so those amino acid residues containing two methyl groups have two peaks that have both been labelled with the amino acid and sequence position. Those peaks that could not be assigned have been highlighted with black boxes. Buffer conditions are as described in Section 2.5.2.

3.4.5 Resonance assignment of apo-CaM

Apo-CaM was assigned in the presence of EGTA to aid in determining whether $eEF2K_{82\text{-}100}$ can bind to CaM in the absence of calcium. There are four distinct glycyl residues in CaM that have unusual chemical shifts and which show characteristic chemical shift changes between the calcium bound and calcium free states. They are located towards the far left hand side of the spectrum at approximately 10 ppm in the proton dimension. For Ca^{2+}/CaM there are four resonances present corresponding to Gly^{25}, Gly^{61}, Gly^{98} and Gly^{134},

which are involved in calcium binding. For apo-CaM only two of these resonances are present, which correspond to Gly^{25} and Gly^{61}, both of which are located in the N-terminal domain. The fact that we only resonances of these two glycine residues could be observed in this region of the ^{1}H-^{15}N-HSQC spectrum means that all calcium has been efficiently removed from the sample and therefore achieves a true representation of apo-CaM.

The protein backbone was 95% assigned, with residues Asp^{122}, Glu^{123}, Met^{124}, Glu^{140}, Phe^{142} and Gln^{143} being unable to be assigned. The reason for these residues not being assigned is due to ambiguity on the HNCACB spectrum meaning that sequential assignment for these two short regions, 122-124 and 140-143 could not be achieved. The quality of the ^{1}H-^{15}N-HSQC was good and is shown with the assignments labelled in Figure 54.

In terms of the side chain atoms, the majority of peaks on the ^{1}H-^{13}C-HSQC spectrum were assigned except for one, as shown in Figure 55. The side chains of Leu^{39}, Ala^{128} and Thr^{146} could not be assigned via the H(CCO)NH and HCCH-TOCSY due to some uncertainty as a result of overlapping resonances. The backbone atoms of Met^{124} were unable to be assigned; meaning the resonances of its side chain atoms could also not be determined. The side chain resonances of Val^{142} were assigned on the HCCH-TOCSY. However, there seemed to be no clear corresponding peak on the ^{1}H-^{13}C-HSQC spectrum. This is probably due to overlapping peaks in that region of the spectrum. The one peak in the ^{1}H-^{13}C-HSQC spectrum that could not be assigned is in the region that contains methionine methyl group resonances and so it is likely that this peak represents the unassigned Met^{124} methyl group.

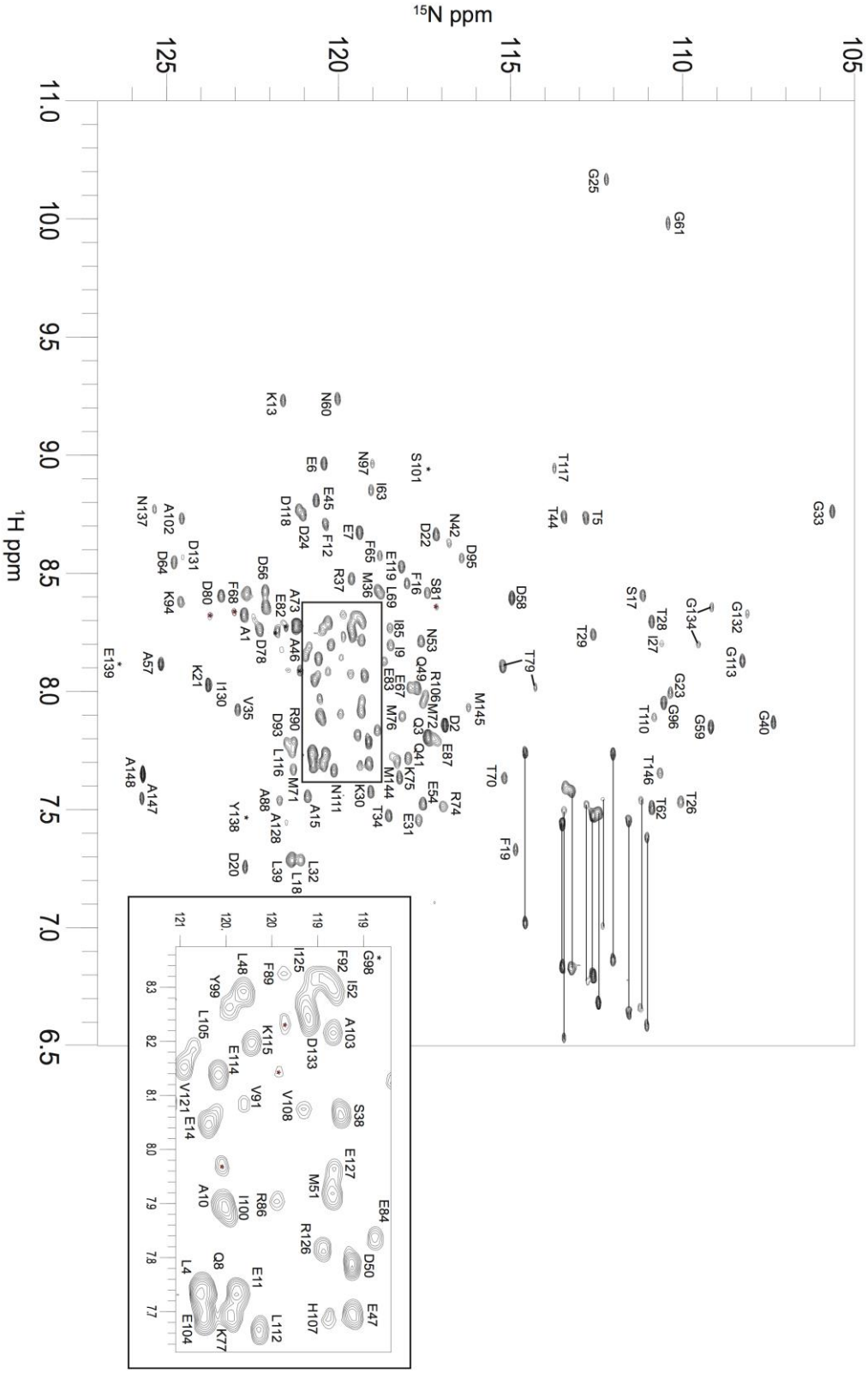

Figure 54. Assigned ^{1}H-^{15}N-HSQC spectrum of apo-CaM.

^{1}H-^{15}N-HSQC spectrum of apo-CaM with peaks labelled as a result of resonance assignment, according to the amino acid residue they represent. Pairs of peaks that correspond to side chain NH_2 groups are marked with joining solid lines. Those peaks that have been folded are labelled in grey. * represent unassigned peaks. Buffer conditions are as described in Section 2.5.2.

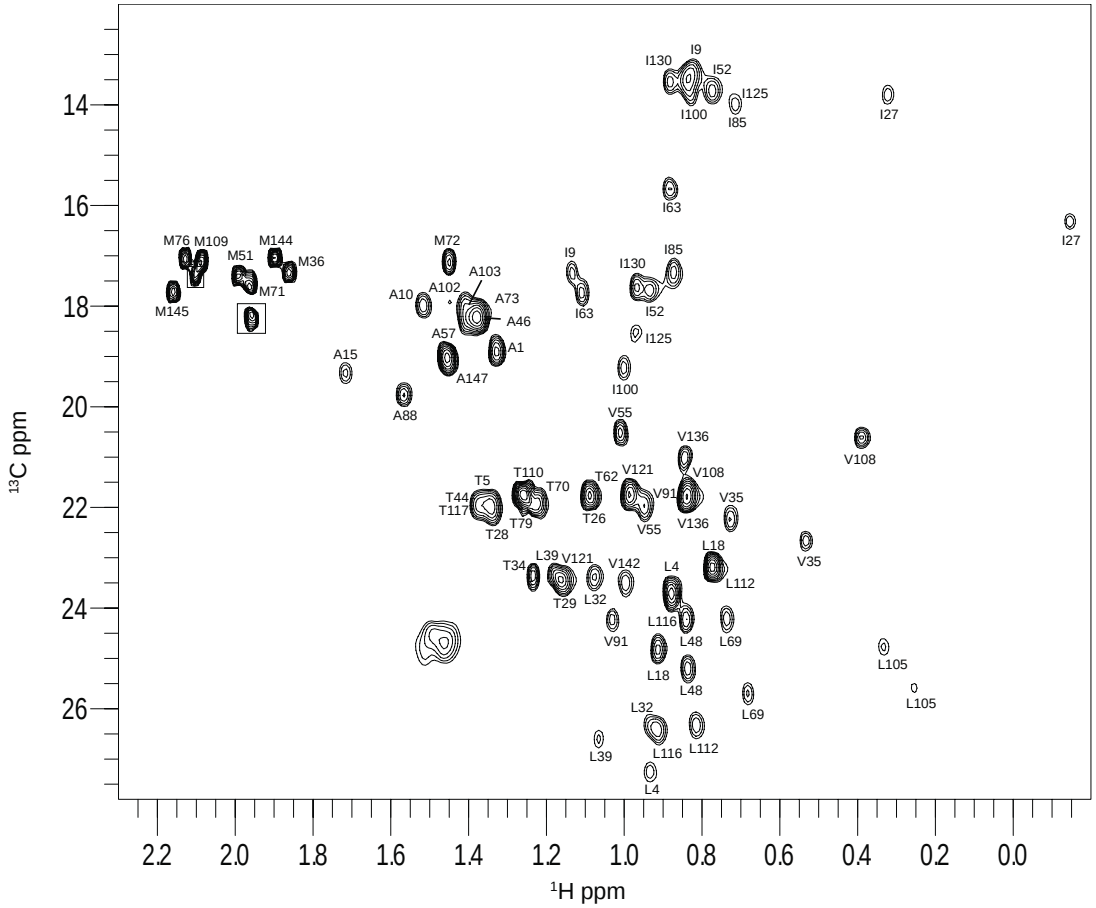

Figure 55.Assigned ^{1}H-^{13}C-HSQC of apo-CaM.

Region of the ^{1}H-^{13}C-HSQC spectrum that contains resonances of methyl groups of apo-CaM with peaks labelled as a result of resonance assignment. The side chain assignment was not stereo-specific and so those amino acid residues containing two methyl groups have two peaks that have both been labelled with the amino acid and sequence position. Those peaks that could not be assigned have been highlighted with black boxes. Buffer conditions are as described in Section 2.5.2.

3.4.6 Resonance assignment of apo-CaM bound to eEF2K$_{82\text{-}100}$ (1:10 ratio)

There were some differences between NMR spectra of apo-CaM and apo-CaM in the presence of a ten-fold excess of eEF2K$_{82\text{-}100}$ and therefore this apo-CaM: eEF2K$_{82\text{-}100}$ complex was also assigned.

A ^{1}H-^{15}N-HSQC spectrum is produced with generally well-dispersed peaks of similar intensity, indicative of a correctly folded and stable protein complex. This is shown in Figure 56. There is a region towards the centre of the spectrum where there is a high density of peaks, making it more difficult to interpret than the other assigned CaM states. This made the assignment process more challenging and for this reason a second data set was collected at 42 °C, which helped to increase the resolution and quality of the spectrum. The

majority of backbone resonances were assigned using the original data set with the 42 °C data being used at the end to gain some extra clarity and thus assign some additional amino acid residues. This strategy resulted in 90% of the backbone resonances of apo-CaM: eEF2K$_{82-100}$ being assigned. Asp^{22}, Thr^{62}, Asp^{64}, Phe^{65}, Asp^{84}, Glu^{104}, Glu^{120}, Val^{121}, Arg^{126}, Glu^{127}, Asp^{133}, Tyr^{138}, Glu^{139}, Glu^{140} and Phe^{141} were the residues that could not be assigned. A number of these C-terminal residues could also not be assigned in apo-CaM or are adjacent to and surrounding the region which couldn't be assigned. Asp^{84} could not be assigned in the Ca^{2+}/CaM: eEF2K$_{82-100}$ complex. The fact that they could not be assigned in more than one CaM state may imply something about the nature of these particular residues that is consistent between conditions. For example, they could be positioned in flexible regions of the protein or exchanging rapidly between two states.

The side chain atoms of methyl group containing amino acid residues were also assigned, excluding Ile^{130} whose resonances could not be determined from the H(CCO)NH and HCCH-TOCSY spectra and Thr^{62} whose backbone resonances were also unassigned. The majority of peaks on the ^{1}H-^{13}C-HSQC spectrum, shown in Figure 57, could be assigned. There are three peaks that could not be assigned and similarly to the spectrum for Ca^{2+}/CaM some of these peaks are not likely to correspond to those side chain methyl groups, which remain unassigned. It is therefore possible that these peaks represent a second state for some of the already assigned methyl groups. In fact, the peak shown in Figure 57 that is highlighted by a black box towards the top right hand side of the spectrum has peaks present in the HCCH-TOCSY spectrum with proton chemical shifts that are the same as Ile^{100}. This is strong evidence that this peak corresponds to a second state of one of the methyl groups in Ile^{100}; also as it is of a weaker intensity than the labelled peak it likely has a lower population.

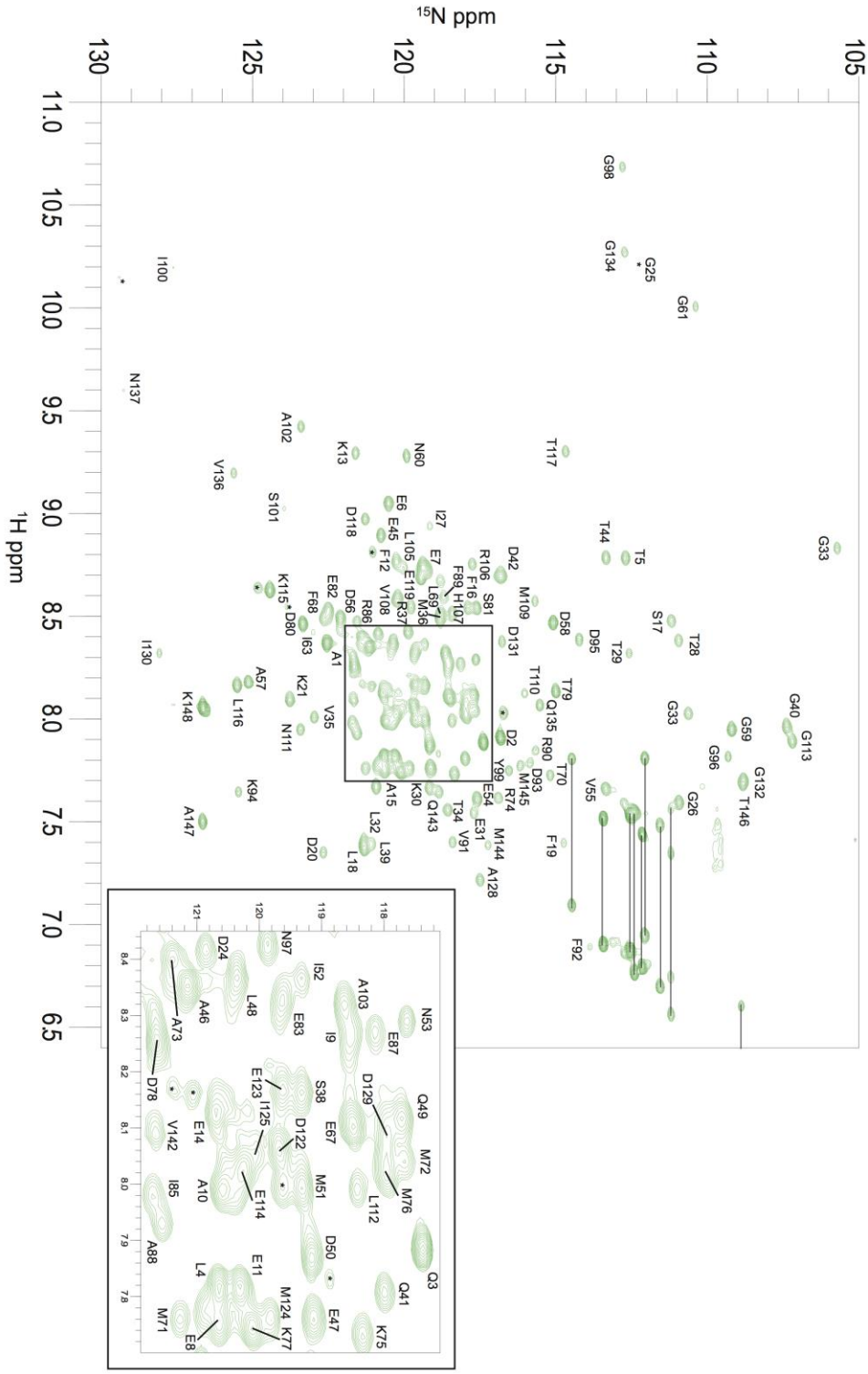

Figure 56. Assigned ^{1}H-^{15}N-HSQC spectrum of the complex of apo-CaM: eEF2K$_{82\text{-}100}$.

^{1}H-^{15}N-HSQC spectrum of the Ca^{2+}/CaM: eEF2K$_{82\text{-}100}$ complex with peaks labelled as a result of resonance assignment, according to the amino acid residue they represent. Pairs of peaks that correspond to side chain NH_2 groups are marked with joining solid lines. Those peaks that have been folded are labelled in grey. Buffer conditions are as described in Section 2.5.2.

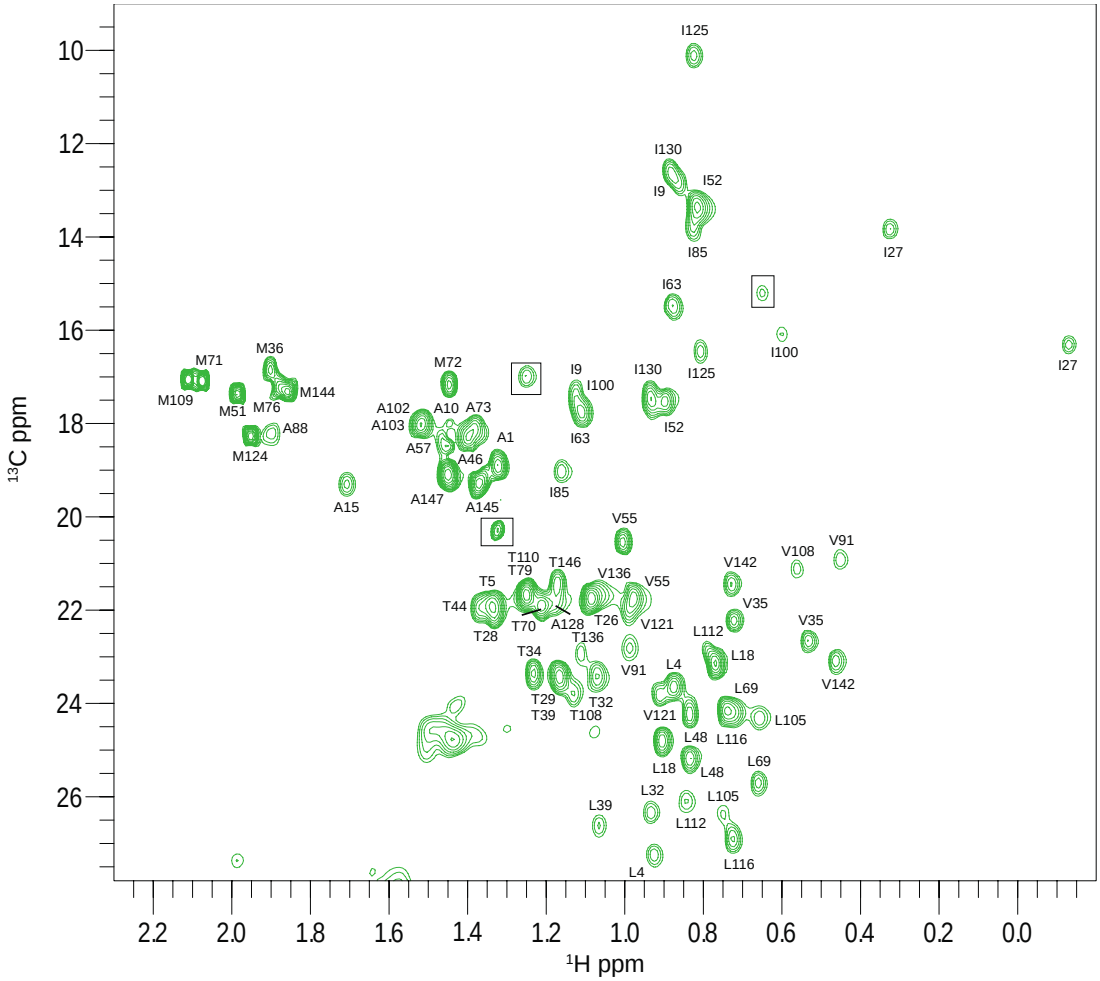

Figure 57. Assigned ^{1}H-^{13}C-HSQC spectrum of the apo-CaM: eEF2K$_{82\text{-}100}$ complex.

Region of the ^{1}H-^{13}C-HSQC spectrum that contains resonances of methyl groups of the apo-CaM: eEF2K$_{82\text{-}100}$ complex with peaks labelled as a result of resonance assignment. The side chain assignment was not stereo-specific and so those amino acid residues containing two methyl groups have two peaks that have both been labelled with the amino acid and sequence position. Those peaks that could not be assigned have been highlighted with black boxes. Buffer conditions are as described in Section 2.5.2.

3.5 Discussion

The yields and purity achieved for unlabelled and ^{15}N-^{13}C labelled CaM were high, allowing the completion of triple resonance experiments for the assignment of CaM in four states. This is shown by the mass spectrometry results and through analysis with SDS PAGE (Section 3.2). However, the yields obtained for each eEF2K fragment and from different purifications varied. Co-expression and purification of N-eEF2K$_{48\text{-}336}$ and C-eEF2K$_{490\text{-}725}$ resulted in relatively low yields and therefore required a large amount of culture to achieve the amounts necessary for biophysical characterization, especially by NMR and

ITC. There were also some issues with the stability of the N-eEF2K$_{48-336}$ fragment. For this reason some further fragments were investigated and N-eEF2K$_{74-332}$ was identified as a better candidate for biophysical studies. When co-expressed with C-eEF2K$_{490-725}$ these fragments are significantly more stable, can be stored at -20 °C for later use and also are produced at a much higher yield.

The activity of the eEF2K fragments was assessed in the presence and absence of Ca^{2+}. The fragments were compared to WT-eEF2K, which shows high levels of activity (reaching over 4000 Cerenkov counts after 60 min of assay) that increases linearly with time when incubated with Ca^{2+}/CaM but no detectable activity when incubated with apo-CaM. This is consistent with the earlier data (Pigott et al., 2012), which shows that Ca^{2+} is needed to elicit activation of eEF2K. N-eEF2K$_{74-332}$ and C-eEF2K$_{490-725}$ were used for the same activity assay under the same conditions, as described in Section 3.3.2. Upon incubation with Ca^{2+}/CaM the kinase fragments were active, although the Cerenkov counts measured were less than seen for the WT-eEF2K, reaching a maximum of 300 in 60 min. Again, there was no detectable kinase activity when the fragments were incubated with apo-CaM, suggesting that this eEF2K fragment has similar catalytic properties to the wild-type enzyme. N-eEF2K$_{100-336}$ and C-eEF2K$_{490-725}$ showed no activity (Cerenkov counts less than 50) in the presence of both Ca^{2+}/CaM and apo-CaM. As Ca^{2+}/CaM is present but cannot activate eEF2K, this suggests that CaM is unable to bind. This confirms again that region containing residues 74-100, which are missing in this fragment, are essential for CaM binding to eEF2K and thus kinase activation. This is in agreement with published data (Diggle et al., 1999, Pigott et al., 2012).

CaM has been assigned in four states. Both Ca^{2+}/CaM and apo-CaM have been assigned in the free state and also in complex with eEF2K$_{82-100}$, representing the CaM binding region of eEF2K. The backbone resonances of Ca^{2+}/CaM were assigned to 100%, Ca^{2+}/CaM: eEF2K$_{82-100}$ complex to 98%, apo-CaM to 95% and apo-CaM: eEF2K$_{82-100}$ complex to 90%. Side chain resonances have also been assigned in order to annotate the methyl group region of the corresponding ^{1}H-^{13}C-HSQC spectra. Assignment of these four states of CaM allowed chemical shift perturbation analysis as discussed in Chapter 4.

Chapter 4. Characterisation of the interaction between CaM and eEF2K

4.1 Introduction

There is little known about the mechanism by which calcium signalling results in Ca^{2+}/CaM activating eEF2K to block protein translation. Understanding the interaction between CaM and eEF2K is therefore crucial.

An interaction can be thought of as having two key aspects that can be investigated. A binding affinity (the dissociation constant - K_d) can be determined which provides information on the rate and strength of the interaction. Structural studies can determine the residues and regions of proteins important for the interaction. And together these two pieces of information can lead to the proposal of a mechanism for the interaction. Using the $eEF2K_{82-100}$ peptide we will mimic the interaction between CaM and eEF2K to study this binding event by NMR spectroscopy, ITC and MST and thus gain insight into this important binding and regulation mechanism.

The information gained from the resonance assignments of CaM in four states, outlined in Section 3.4, was used to study the binding of $eEF2K_{82-100}$ to CaM. Differences are identified between the four states of CaM that are evident in both the ^{1}H-^{15}N-HSQC and ^{1}H-^{13}C-HSQC spectra and which can be compared and analysed to provide information on which amino acid residues in Ca^{2+}/CaM and apo-CaM are likely to interact with $eEF2K_{82-100}$. This resulted in the elucidation of binding surfaces on CaM and consequently some insight into the mechanism of CaM binding to eEF2K.

It has also been shown by NMR spectroscopy that apo-CaM is able to interact to some extent with $eEF2K_{82-100}$. As mentioned in Section 3.4 this is shown by the fact that the characteristic fingerprint spectra of apo-CaM alone and apo-CaM in the presence of a ten-fold excess of $eEF2K_{82-100}$ are different. Similar analysis has therefore enabled the determination of the interaction site on apo-CaM for eEF2K. Comparison of these two interaction sites results in the conclusion that $eEF2K_{82-100}$ binds differently to Ca^{2+}/CaM than to apo-CaM, indicating differences in their mode of interaction. Further analysis, via an NMR

peptide titration allowed us to gain added understanding of the binding mechanism and more detail on the interaction.

It is important to note that, ^{1}H-^{15}N-HSQC spectra report on global changes of molecules and complexes (protein backbone), whilst ^{1}H-^{13}C-HSQC spectra are less sensitive to these global changes. In this Chapter methyl resonance assignments on ^{1}H-^{13}C-HSQC spectra are used to compare the different states of CaM. These are especially useful as methyl groups are able to rotate freely, making them much less sensitive to conformational (global) changes and therefore more accurate in the prediction of interacting residues and the proposal of binding surfaces.

To further investigate the binding of eEF2K$_{82\text{-}100}$ to CaM and to determine a binding affinity (K_d) for the interactions, isothermal titration calorimetry (ITC) and microscale thermophoresis (MST) were used. These results meant we could interpret our interaction data with higher accuracy and gain greater insight into the mechanism by which CaM binds to eEF2K and results in its activation.

4.2 Binding of eEF2K$_{82\text{-}100}$ to apo-CaM

4.2.1 Comparison of NMR spectra of apo-CaM and the apo-CaM: eEF2K$_{82\text{-}100}$ complex

By comparing the NMR spectra of free apo-CaM and apo-CaM in the presence of eEF2K$_{82\text{-}100}$, it is evident that there is an interaction in the absence of calcium. This is interesting as in many CaM and target interactions the CaM molecule needs to bind calcium ions before it can then in turn bind to other target proteins (Chin and Means, 2000). It seems, however, that apo-CaM can bind to the eEF2K$_{82\text{-}100}$ peptide.

An overlay of the ^{1}H-^{15}N-HSQC spectra of apo-CaM collected for the first and last titration points from the eEF2K$_{82\text{-}100}$ peptide shows that there are significant differences between the two. Changes in peak position between the two spectra indicate that the corresponding amino acid residues, known from completing the assignment, have a different local chemical environment when the eEF2K$_{82\text{-}100}$ peptide is present. This manifests in a difference in the chemical shifts seen when the NMR spectra are overlaid; a change in peak position. The

resulting implication is that those residues that experience a chemical shift change are involved in the interaction and have a role in binding.

In order to determine which amino acid residues of apo-CaM are involved in binding to eEF2K$_{82\text{-}100}$, overlays of ^{1}H-^{13}C-HSQC's are analysed to investigate the changes in the resonances of methyl groups in amino acid side chains. Similarly to the ^{1}H-^{15}N-HSQC spectra overlay it is evident that there is an interaction occurring as a number of peaks have changed their chemical shift in the presence of eEF2K$_{82\text{-}100}$. For apo-CaM, the majority of those peaks that move are C-terminal amino acid residues, suggesting that it is predominantly the C-terminal domain of apo-CaM that interacts with eEF2K$_{82\text{-}100}$. This is shown in Figure 58, where the changes in peak position of the isoleucine residues have been highlighted.

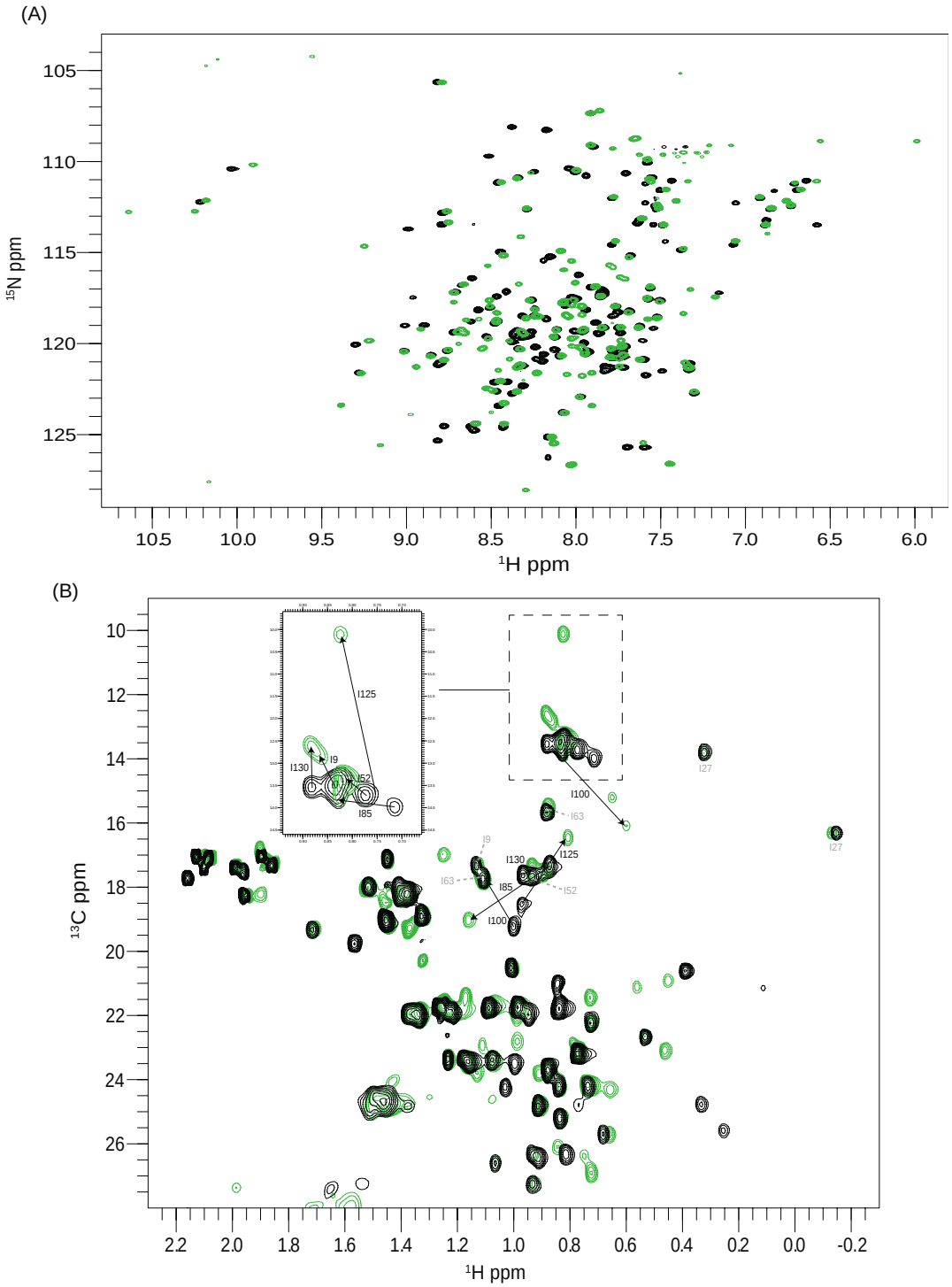

Figure 58. Overlay of ^{1}H-^{15}N-HSQC and ^{1}H-^{13}C-HSQC spectra of apo-CaM and the apo-CaM: eEF2K$_{82\text{-}100}$ complex.

^{1}H-^{15}N-HSQC spectra of apo-CaM (black) and the apo-CaM: eEF2K$_{82\text{-}100}$ complex (green) overlaid (A). ^{1}H-^{13}C-HSQC spectra of apo-CaM (black) and the apo-CaM: eEF2K$_{82\text{-}100}$ complex (green) overlaid with changes in peak position of isoleucine methyl group resonances upon addition of eEF2K$_{82\text{-}100}$ shown with arrows and those that do not change labelled in grey (B). Spectra correspond to the start and end points (20 fold excess of eEF2K$_{82\text{-}100}$) of the peptide titration. Buffer conditions are as described in Section 2.5.4.

Analysis of the changes in chemical shift, termed the CSPs, further suggests that it is primarily the C-terminal domain of apo-CaM that is responsible for interacting with $eEF2K_{82-100}$. The same analysis was performed as for Ca^{2+}/CaM in Section 4.3 to determine which CSPs are significant and is summarised in Figure 59. Residues in the C-terminal domain of CaM are greatly affected by the addition of $eEF2K_{82-100}$ as they have large CSPs. In contrast the CSPs experienced by amino acid residues in the N-terminal domain are much smaller or non-existent. Plotting those residues which have significant CSPs onto a known structure of apo-CaM (PDB ID: 1CFD) consolidates this. It therefore seems likely that $eEF2K_{82-100}$ interacts with apo-CaM via its C-terminal domain. Small CSPs are coloured grey and were determined as those smaller than 0.3 but larger than 0.05, medium range CSPs are coloured light green and are those between 0.3 and 0.9. Any CSPs over 0.9 were classified as large and are coloured dark green. These values were determined by eye from the bar chart in Figure 60.

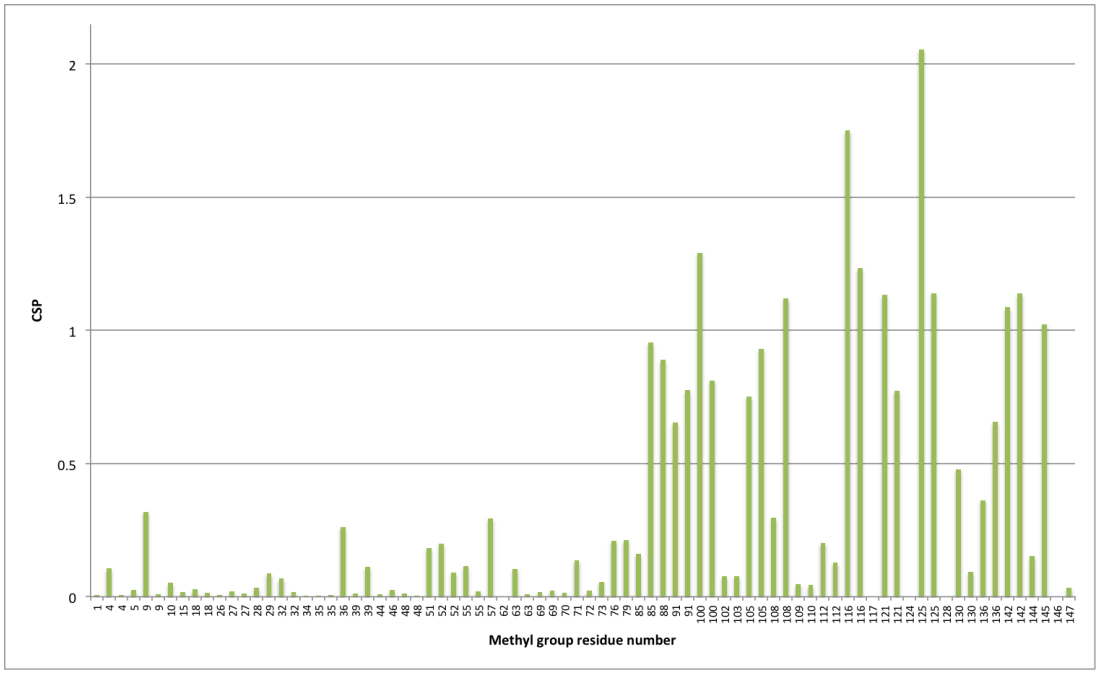

Figure 59. Significant CSPs in apo-CaM upon binding of $eEF2K_{82-100}$.
Bar chart showing the CSP values plotted against the amino acid sequence of CaM.

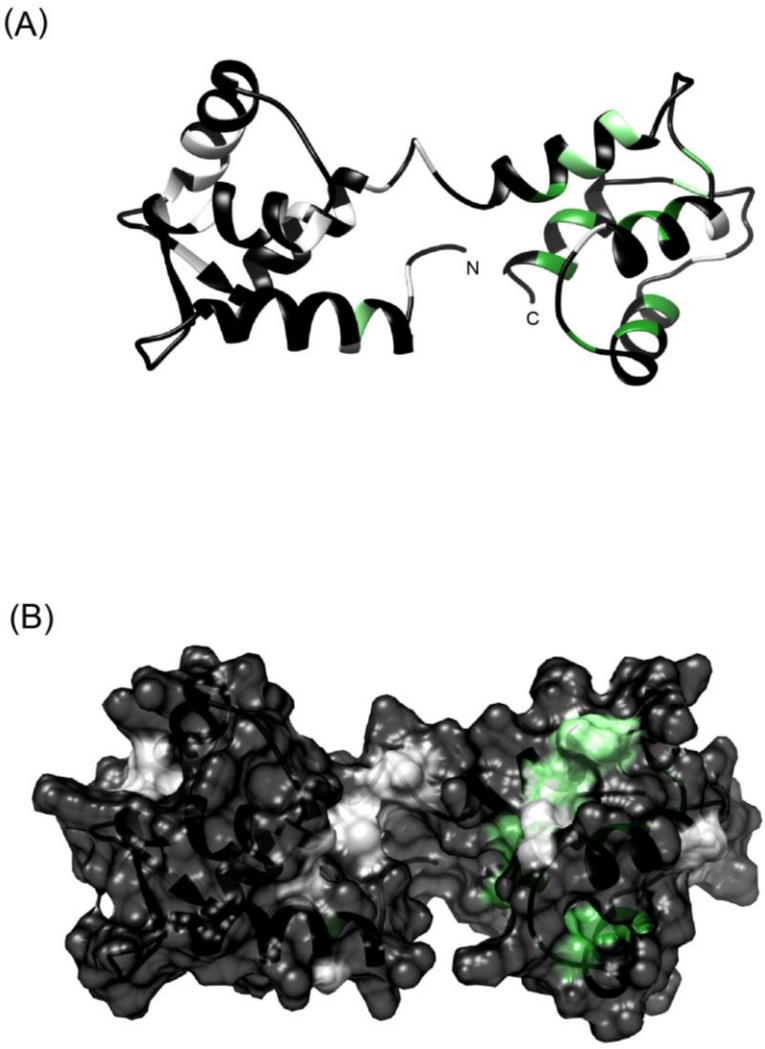

Figure 60. CSPs plotted onto structure of apo-CaM

Significant CSPs shown on a backbone ribbon representation of apo-CaM (A) and on a surface representation of apo-CaM (B) with the N terminal domain on the left and the C-terminal domain on the right. Those CSPs classified as small are coloured grey, medium as light green and large as dark green. PDB ID: 1CFD.

4.2.2 Mechanism of apo-CaM binding to eEF2K$_{82-100}$ from analysis of peptide titration

An NMR peptide titration was also carried out for apo-CaM to investigate the binding of eEF2K$_{82-100}$.

The majority of resonances of apo-CaM are in fast exchange for the interaction with eEF2K$_{82-100}$, suggesting that binding is relatively weak. However, similarly to the results for Ca^{2+}/CaM, there are a number of peaks which show multiple exchange characteristics. These are highlighted in Figure 60 and show fast exchange initially before changing to slow exchange at higher

peptide concentrations. This suggests that there is a binding mechanism that is more complex than a two-step binding equilibrium and also that this interaction is relatively weak.

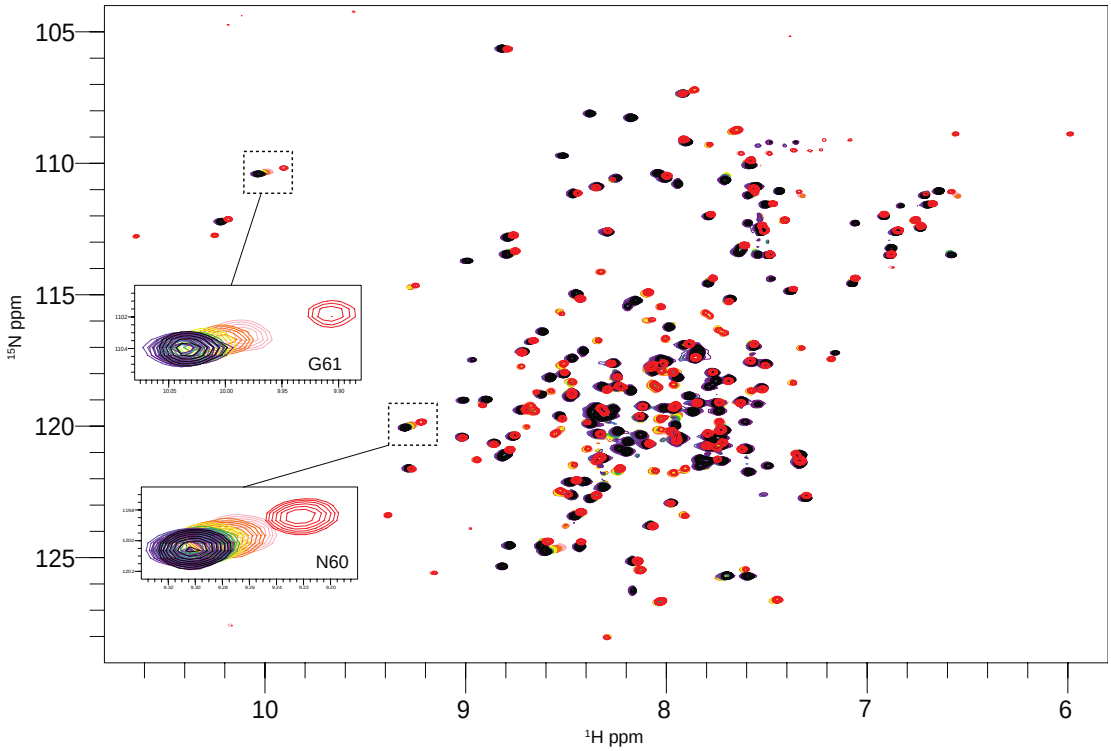

Figure 61. Apo-CaM binding to eEF2K$_{82\text{-}100}$.
Overlay of ^{1}H-^{15}N-HSQC spectra collected at each titration point during an NMR peptide titration of apo-CaM with eEF2K$_{82\text{-}100}$ peptide. The first titration point where the sample contains no peptide is shown in black, the last titration point corresponding to a 20-fold excess of peptide is shown in red and the titration points in between are shown in a colour range from dark to light. Buffer conditions are as described in Section 2.5.4.

4.2.3 Affinity of eEF2K$_{82\text{-}100}$ binding to apo-CaM

The affinity of the interaction between apo-CaM and eEF2K$_{82\text{-}100}$ was investigated using two methods to determine a K_d of binding. ITC was performed initially by Dr Halina Mikolajek but this technique was unable to yield a K_d measurement or detect binding. Binding of eEF2K$_{82\text{-}100}$ to apo-CaM was established by NMR, which as a technique is uniquely sensitive to weak interactions. Therefore MST was employed to measure the interaction and this technique could detect the weak binding and calculate a K_d value for the interaction. The K_d was determined by MST to be 1.38 mM +/- 86.2 µM, which is particularly low and therefore not likely to be physiologically relevant,

especially when we consider the large numbers of other proteins capable of interacting with CaM even in the absence of Ca^{2+}.

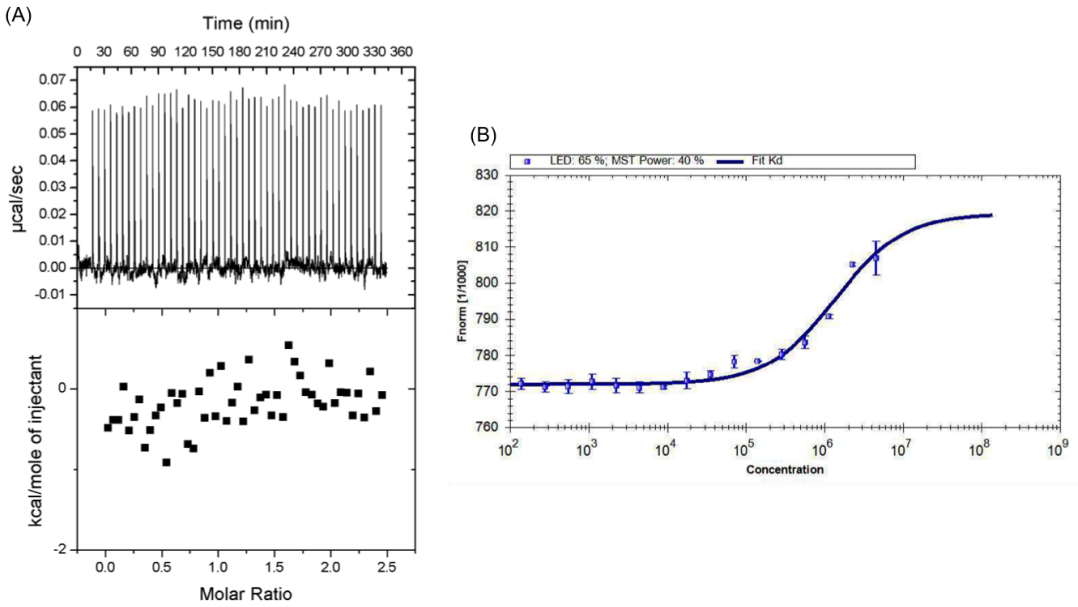

Figure 62. Binding of eEF2K$_{82\text{-}100}$ to apo-CaM

Calorimetric titrations of apo-CaM with the eEF2K peptide [82-100], showing the original titration curve (top) and the binding isotherm obtained (bottom) (A). MST binding curve of CaM and eEF2K$_{82\text{-}100}$ obtained from the L001 Monolith NT.115 (B). Buffer conditions are as described in Section 2.4.4 (ITC) and 2.4.5 (MST).

4.3 Binding of eEF2K$_{82\text{-}100}$ to Ca^{2+}/CaM

4.3.1 Comparison of NMR spectra of Ca^{2+}/CaM and the Ca^{2+}/CaM: eEF2K$_{82\text{-}100}$ complex

Comparing NMR spectra of free Ca^{2+}/CaM and of Ca^{2+}/CaM bound to eEF2K$_{82\text{-}100}$ has allowed the identification of amino acid residues in CaM which are influenced by the binding of eEF2K$_{82\text{-}100}$. Similarly to apo-CaM, the majority of peaks are located in different positions on each spectrum, indicating that there is an interaction occurring.

An overlay of the ^{1}H-^{15}N-HSQC spectra from the start and end points of the eEF2K$_{82\text{-}100}$ peptide titration shows significant changes on almost every ^{1}H-^{15}N resonance present, as shown in Figure 62. This would imply that all of the amino acid residues of CaM are involved in the interaction with eEF2K$_{82\text{-}100}$; or

that there is a global conformational change, whereby the protein changes structure.

For this reason, the amino acid side chains were chosen to map the potential binding sites. An overlay of the ^{1}H-^{13}C-HSQC spectra from the start and end points of the $eEF2K_{82\text{-}100}$ peptide titration is therefore more useful and is also shown in Figure 62. It can be seen that there are a number of resonances whose chemical shift does not change between the two spectra, indicating that they are not involved in the interaction. These peaks correspond mainly to the methyl groups of alanine and threonine residues, whilst the vast majority of those peaks corresponding to valine, leucine, isoleucine and methionine methyl groups experience at least some change in chemical shift. These chemical shift changes have been annotated with arrows in Figure 62 for the isoleucine methyl groups. Some of the changes are relatively small, in the range of 0.05 PPM in the proton dimension, whilst some are considerable, such as Ile^{100}, which changes by 0.4 PPM in the proton dimension.

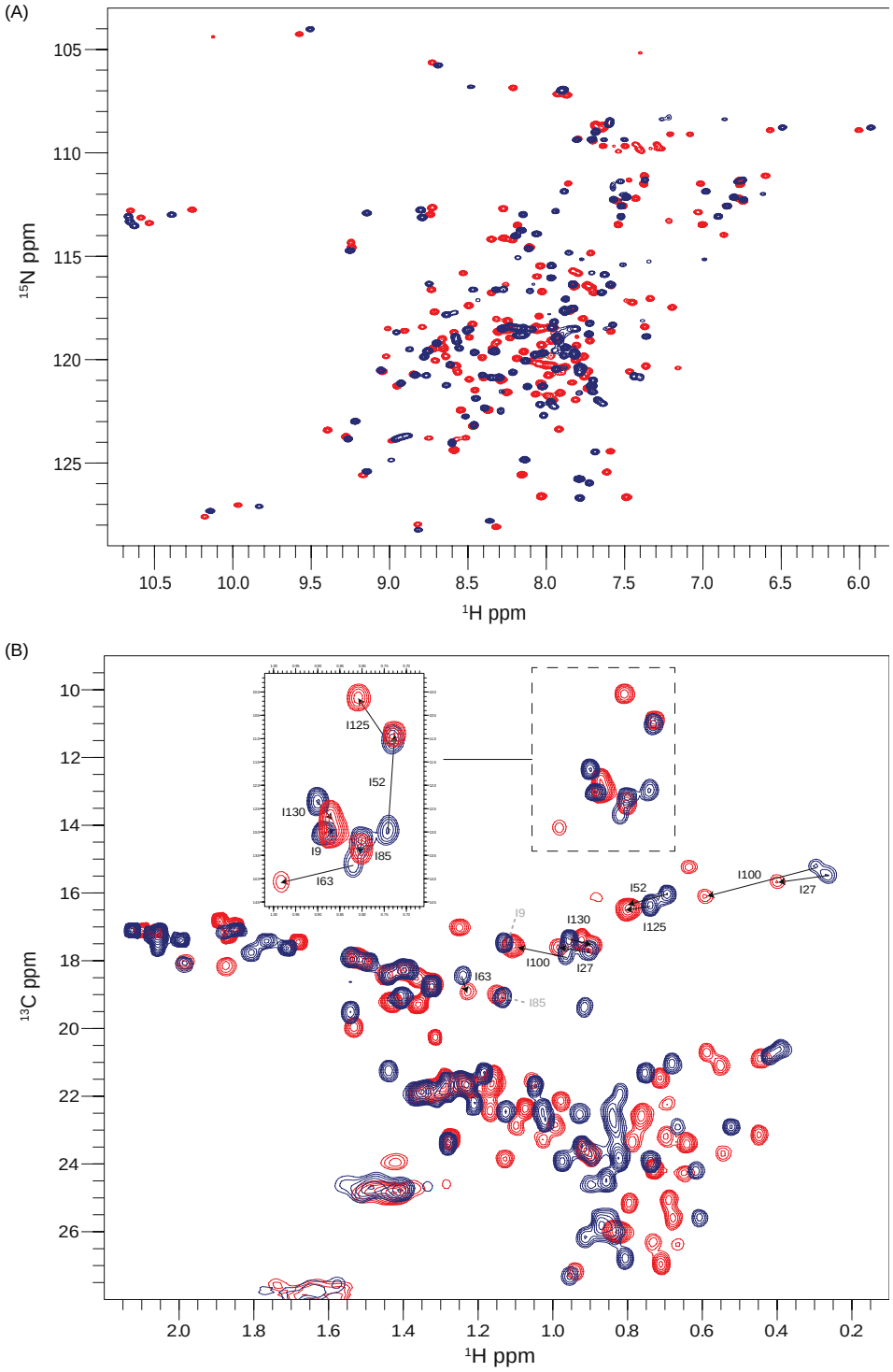

Figure 63. Overlay of ^{1}H-^{15}N-HSQC and ^{1}H-^{13}C-HSQC spectra of Ca^{2+}/CaM and the Ca^{2+}/CaM: eEF2K$_{82-100}$ complex.

^{1}H-^{15}N-HSQC spectra of Ca^{2+}/CaM (navy) and the Ca^{2+}/CaM: eEF2K$_{82-100}$ complex (red) overlaid (A). ^{1}H-^{13}C-HSQC spectra of Ca^{2+}/CaM (navy) and the Ca^{2+}/CaM: eEF2K$_{82-100}$ complex (red) overlaid with changes in peak position of isoleucine methyl group resonances upon addition of eEF2K$_{82-100}$ shown with arrows and those that do not change labelled in grey (B). Spectra correspond to the start and end points (20 fold excess of eEF2K$_{82-100}$) of the peptide titration. Buffer conditions are as described in Section 2.5.4.

An equation (described in Section 2.5.3) is used to combine the changes in both dimensions of the spectrum to produce a chemical shift perturbation (CSP) value that encompasses the changes in both the proton and heteronuclear chemical shifts. These values are plotted and it is evident that there are significant CSPs throughout both domains of CaM but that some residues in the N-terminal domain seem to experience the largest perturbations, as shown in Figure 63. As outlined in Section 2.5.4.2, CSPs were classified as being small, medium or large. Small CSPs were determined as those with a value between 0.03 and 0.15, whilst those between 0.15 and 0.5 were classified as medium, and any above 0.5 as large.

A published structure of Ca^{2+}/CaM (PDB ID: 1CLL) was used to visualise the location of those amino acid residues with significant CSPs, as shown in Figure 64. When viewed in this manner, the CSPs cluster into clear and contiguous surfaces, an observation that is consistent with the known mechanism by which CaM binds to its targets. Small CSPs are shown in light blue, medium in light pink and large in red.

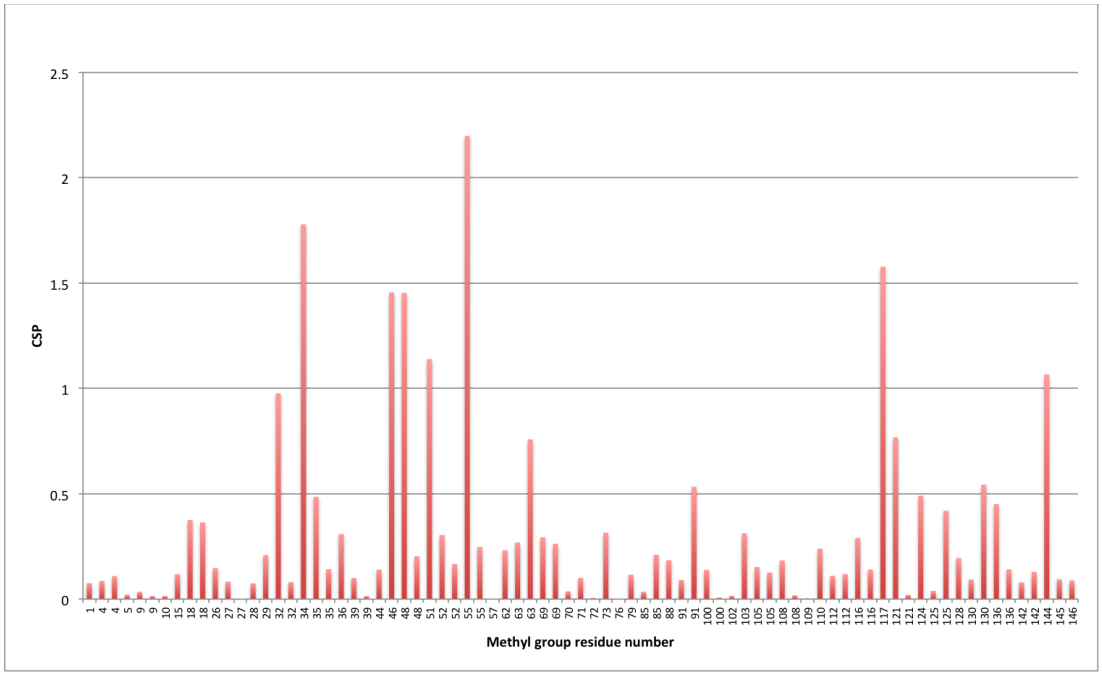

Figure 63. Significant CSPs in Ca^{2+}/CaM upon binding of $eEF2K_{82-100}$.
Bar chart showing the CSP values plotted against the amino acid sequence of CaM.

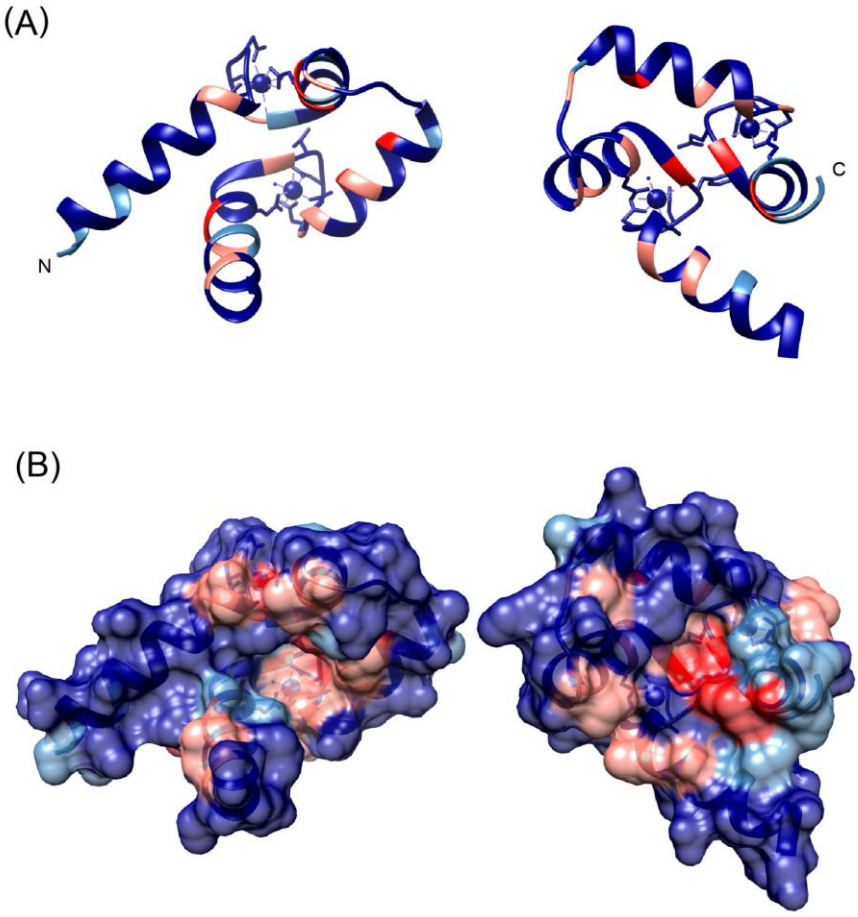

Figure 64. CSPs plotted onto structure of Ca^{2+}/CaM

Significant CSPs shown on a backbone ribbon representation (A) and surface representation (B) of Ca^{2+}/CaM with the N-terminal (left) and C-terminal (right) domains shown individually. Those CSPs classified as small are coloured in light blue, those classified as medium are light pink and those classified as large are shown in red. (PDB ID: 1CLL)

4.3.2 Mechanism of Ca^{2+}/CaM binding to $eEF2K_{82-100}$ from analysis of peptide titration

The mechanism by which Ca^{2+}/CaM binds to $eEF2K_{82-100}$ was investigated using an NMR peptide titration. HSQC spectra were collected of Ca^{2+}/CaM at increasing concentrations of $eEF2K_{82-100}$ so that peak movements could be analysed in greater detail. Overlaying all of the ^{1}H-^{15}N-HSQC spectra collected means we can follow the changes in Ca^{2+}/CaM peak position and intensity as the concentration of $eEF2K_{82-100}$ increases from zero to 20-fold excess. The exchange characteristics of the interaction can therefore be analysed. The different types of exchange and their implications are described

in Section 1.7.1. As discussed, the exchange characteristics of an interaction can provide information on the interaction strength as well as reaction rates and possible mechanistic insight into the interaction.

Overlaying ^{1}H-^{15}N-HSQC spectra for each of the titration points, as shown in Figure 65, demonstrates that there is a combination of slow and fast exchange. Some resonances clearly show slow exchange during the 0-20-fold excess concentration range, which is indicative of a tight interaction. In contrast there are also a small proportion of resonances that show fast exchange, characteristic of weak binding. In addition, there are a relatively large number of resonances that demonstrate both fast and slow exchange during the titration up to 20-fold excess of $eEF2K_{82\text{-}100}$. For example, for a number of peaks slow exchange is demonstrated up to approximately a 1:1 ratio of Ca^{2+}/CaM to $eEF2K_{82\text{-}100}$. However, as the titration continues and the concentration of $eEF2K_{82\text{-}100}$ continues to increase, the chemical shift still changes and the peaks on the spectrum show a pattern of movement that indicates fast exchange. There are also some examples where the peaks change direction in their movements during the course of the titration. For example, the peaks can be traced in one direction due to fast exchange up to a certain $eEF2K_{82\text{-}100}$ concentration but they then change direction and move differently until the end of the titration. Some examples of such peak movements and traces that show multiple exchange characteristics are shown in Figure 65 and are reminiscent of those discussed in Section 1.7.1. Those residues that show multiple exchange characteristics are often hard to map in two dimensions, and hence line shape analysis such as that by Kovrigen (2012) is unlikely to be successful (Kovrigin, 2012).

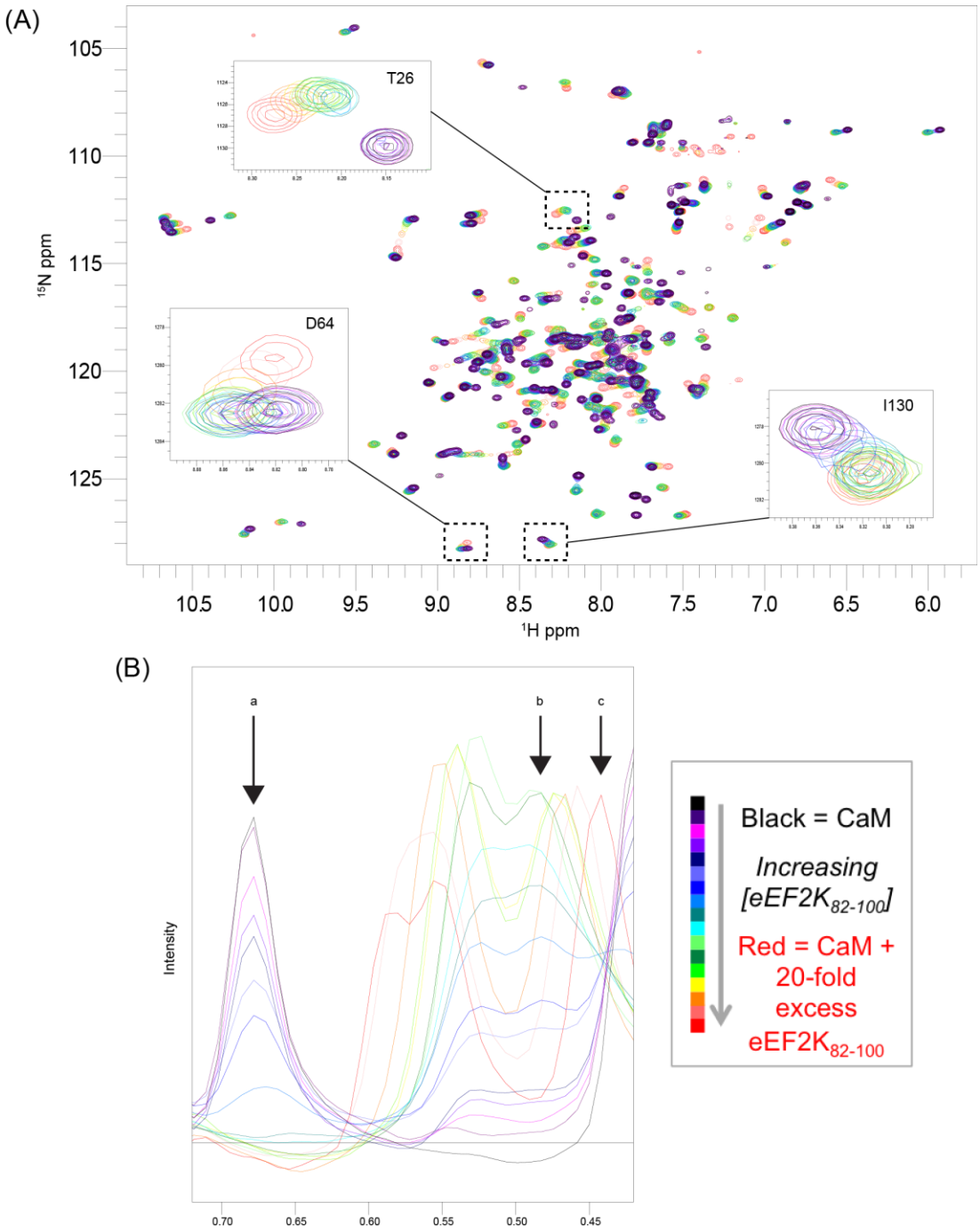

Figure 65. Ca^{2+}/CaM binding to $eEF2K_{82-100}$

Overlay of ^{1}H-^{15}N-HSQC spectra collected at each titration point during an NMR peptide titration of Ca^{2+}/CaM with $eEF2K_{82-100}$ peptide (A). Example one-dimensional trace from the NMR peptide titration of Val^{91}, which shows evidence of multiple exchange characteristics. Slow exchange is evident between a and b which then changes to fast exchange between b and c (B). The first titration point where the sample contains no peptide is shown in black, the last titration point corresponding to a 20-fold excess of peptide is shown in red and the titration points in between are shown in a colour range from dark to light, as shown in the legend. Buffer conditions are as described in Section 2.5.4.

The identity of the resonances in Ca^{2+}/CaM that are in fast or slow exchange upon $eEF2K_{82-100}$ binding were determined as well as those residues which show single or multiple exchange characteristics. Of those amino acid residues that show single exchange characteristics, the majority of residues in the N-terminal domain of Ca^{2+}/CaM are in fast exchange, whilst those in the C-terminal domain are mostly in slow exchange. This is visualised in Figure 66 and indicates that the C-terminal domain interacts more strongly and with a higher affinity with $eEF2K_{82-100}$ than the N-terminal domain.

Those residues that show multiple exchange characteristics are located primarily in the N-terminal domain of Ca^{2+}/CaM, whilst the majority of the residues in the C-terminal domain have a single exchange characteristic.

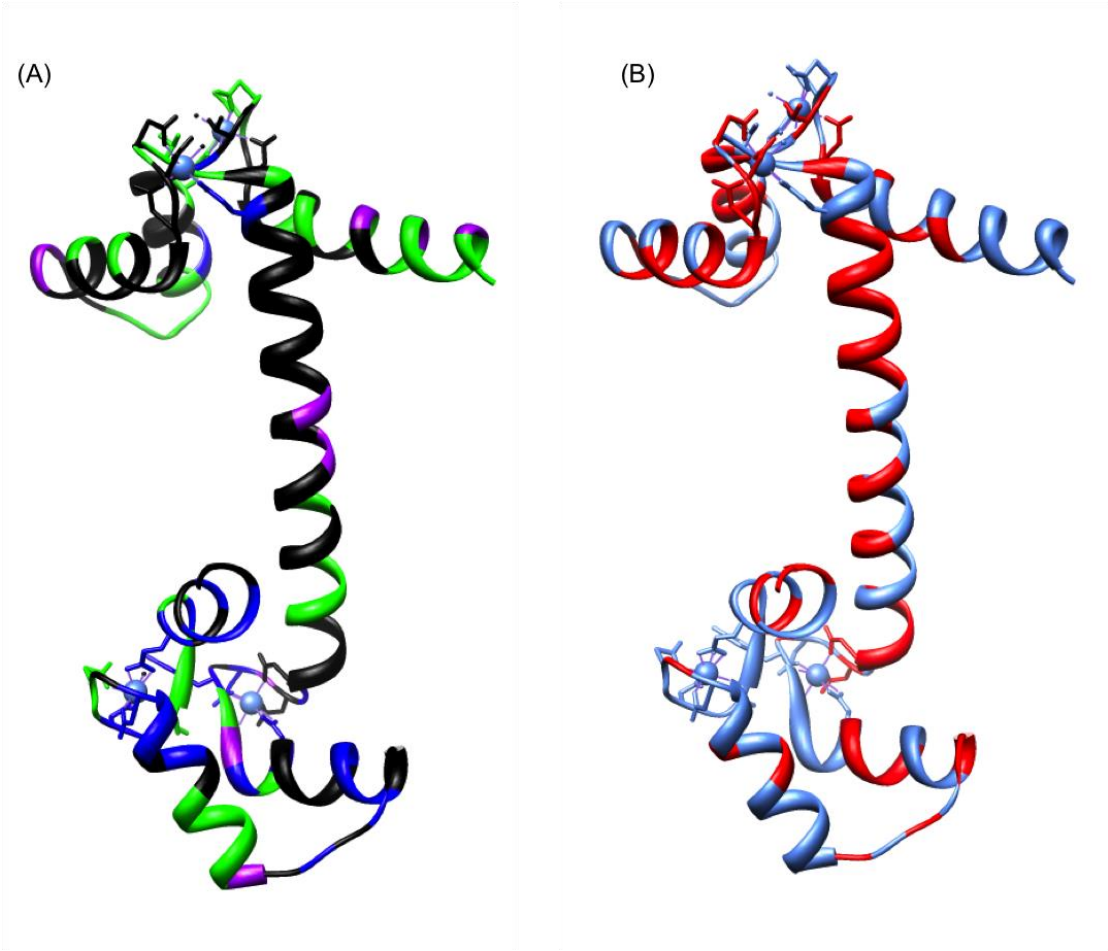

Figure 66. Exchange characteristics of amino acid residues in Ca^{2+}/CaM.
Amino acid residues of Ca^{2+}/CaM in slow exchange (blue), fast exchange (green) and intermediate exchange (purple). Those residues that show multiple exchange characteristics are shown in black (A). Amino acid residues of Ca^{2+}/CaM that show single (blue) and multiple (red) exchange characteristics (B). PDB ID: 1CLL.

The interesting observations from the peptide titration have started to be investigated in collaboration with Dr Ilya Kuprov and Zenawi Welderufael using Spinach (Hogben et al., 2011) as described in Section 2.5.4.2. Spectra were simulated and then fitted to the experimental data. The theoretically simulated spectra are shown in Figure 67 compared to the experimental spectra, demonstrating an accurate simulation. Another method for characterising possible multiple exchange characteristics was discussed in Section 1.7.1.3, however Spinach was used instead to overcome problems with two-dimensional data. LineShapeKin Simulation software (Kovrigin, 2012) is based on the analysis of line shape patterns, and therefore involves extracting one-dimensional traces representative of peak movements. With the CaM spectrum there are a number of overlapping peaks and so the extraction of these peak patterns is difficult. In addition, some of the unusual peak patterns are evident across the two dimensions and therefore extracting slices in either dimension does not represent the whole transition. For these reasons Spinach was decided as a method of choice, although it would still be interesting to use LineShapeKin on some of the peaks in the future.

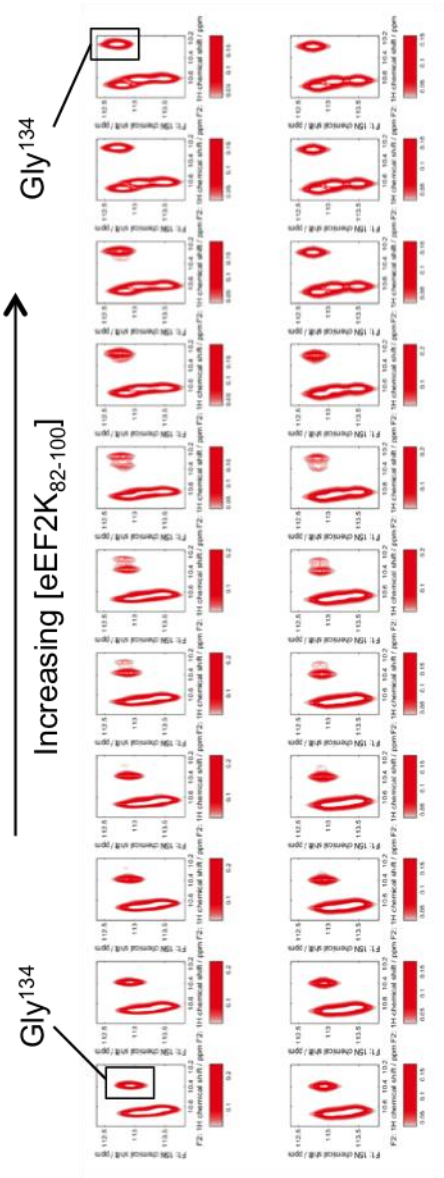

Figure 67. Experimental and Spinach calculated regions of ^{1}H-^{15}N-HSQC spectra from peptide titration.

Experimental (top row) and theoretically simulated (bottom row) regions of ^{1}H-^{15}N-HSQC spectra of Ca^{2+}/CaM titrated with $eEF2K_{82\text{-}100}$. Concentration of $eEF2K_{82\text{-}100}$ increases from left to right. The peak at the top right is Gly^{134}, which is being modelled here. The other three peaks correspond to three more glycine residues, although the mapping is concentrated on Gly^{134}. Figure produced by Zenawi Welderufael using SPINACH.

Dr Ilya Kuprov and Zenawi Welderufael carried out the fitting of these spectra, as described in Section 2.5.4.2. Initial results have confirmed that the majority of peaks do not fit model 1, which is a simple two-step reaction mechanism. The results for the fitting are summarised in Table 7. Single peaks or groups of peaks (depending on the location in the spectrum) were fit individually, and these corresponding residues are listed in the table. The k_{dis}

(effective dissociation) and k_d values are important for drawing conclusions. For the majority of residues the k_{dis} value is fairly constant (15.8-79.4). However, for some residues a significantly different value was determined, for example a value of $1.3x10^{-3}$ was determined for Asp^{64}. This is consistent with the fact that Asp^{64} is one of the residues highlighted for exhibiting unusual peak patterns in the titration (Figure 65). Thr^{44}, Thr^{29} and Leu^{32} also have significantly different values and show peak patterns not indicative of a one step binding mechanism. The values for the K_d are also interesting as they range from nM to μM.

The transverse relaxation rates for protons and nitrogen were also optimized during the fitting. For a 16.9 kDa protein such as CaM, overall rotational motion would predict a ^{15}N T_2 ($1/R_2$) of about 70 ms (Scheschonka et al., 2008) but the line shape derived T_2 value observed here may well report additional slow motions or magnetic susceptibility fluctuations. Importantly, during the NMR titration experiments this number was kept fixed to remove these effects from the line shape analysis. It should also be noted that an intensity multiplier value was used as a scaling factor to ensure that the experimental and theoretically calculated spectra had the same intensity.

Table 7. Spinach analysis of peptide titration data using a one step reaction mechanism model.

Residues	χ^2	k_{dis}	k_d (M)	R2p (Hz)	R2n (Hz)	Intensity multiplier – A
Gly^{25}, Gly^{61}, Gly^{98}, Gly^{134}	9.6	63.1	$8.19x10^{-9}$	80	29	0.58
Ile^{100}	$1x10^{-4}$	15.8	$9.53x10^{-9}$	26	15	
Ala^{102}, Lys^{13}, Val^{136}	3.9	63.1	$1.37x10^{-6}$	69	31	0.74
Leu^{116}, Ile^{130}	$1x10^{-4}$	25.1	$8.48x10^{-8}$	66	36	0.90
Lys^{21}, Lys^{148}, Lys^{94}, Ala^{148}	$1x10^{-4}$	31.6	$1.65x10^{-7}$	73	24	0.77
Ala^{128}, Leu^{18}, Leu^{39}	4.8	39.8	$9.55x10^{-7}$	69	44	0.61
Ile^{85}, Ala^{88}, Asn^{11}, Ala^{15},	5.1	63.1	$1.1x10^{-7}$	70	28	0.60

Gln^{143}, Val^{91}, Ala^{128}	2.8	79.4	$2.02x10^{-8}$	67	29	0.56
Thr^{79}, Asp^{22}, Asp^{95}, Thr^{26}	7.3	63.1	$8.27x10^{-7}$	63	27	0.75
Asn^{42}	1.4	50.1	$4.78x10^{-7}$	69	32	0.49
Asp^{64}	0.5	$1.3x10^{-3}$	$2.5x10^{-7}$	96	42	0.55
Asp^{118}, Leu^{32}, Glu^{45}	6.2	316	$2.23x10^{-6}$	57	28	0.86
Phe^{16}, Glu^{6}, Asp^{118}	7.1	0.8	$2.76x10^{-5}$	44	25	0.79
Thr^{5}, Thr^{44}	2.5	$2x10^{-3}$	$9.2x10^{-7}$	76	34	0.83
Thr^{29}, Thr^{117}	3.4	501.2	$2.34x10^{-6}$	76	34	0.72
Gly^{33}	1.9	79.4	$3.93x10^{-7}$	90	37	0.55
Ile^{27}	0.4	63.1	$1.01x10^{-6}$	82	41	0.48
Asp^{118}, Leu^{105}, Arg^{86}, Glu^{82}, Asp^{80}, Lys^{115}, Phe^{141}, Val^{136}, Ile^{63}, Ser^{101}	16.9	79.4	$7.04x10^{-7}$	69	33	0.64

4.3.3 Affinity of $eEF2K_{82-100}$ peptide binding to Ca^{2+}/CaM

Isothermal titration calorimetry was carried out by Dr Halina Mikolajek to determine a measurement of the binding affinity through the determination of the K_d. A K_d of 247 nM +/- 2 nM was determined for the binding of $eEF2K_{82-100}$ to Ca^{2+}/CaM, indicating a tight interaction between the $eEF2K_{82-100}$ peptide and Ca^{2+}/CaM.

As well as ITC, another technique was used independently to determine a measure of the K_d. Microscale thermophoresis was used to confirm the strength of the interaction between $eEF2K_{82-100}$ and Ca^{2+}/CaM. A value, of 417 nM +/- 38.2 nM, was calculated using this technique.

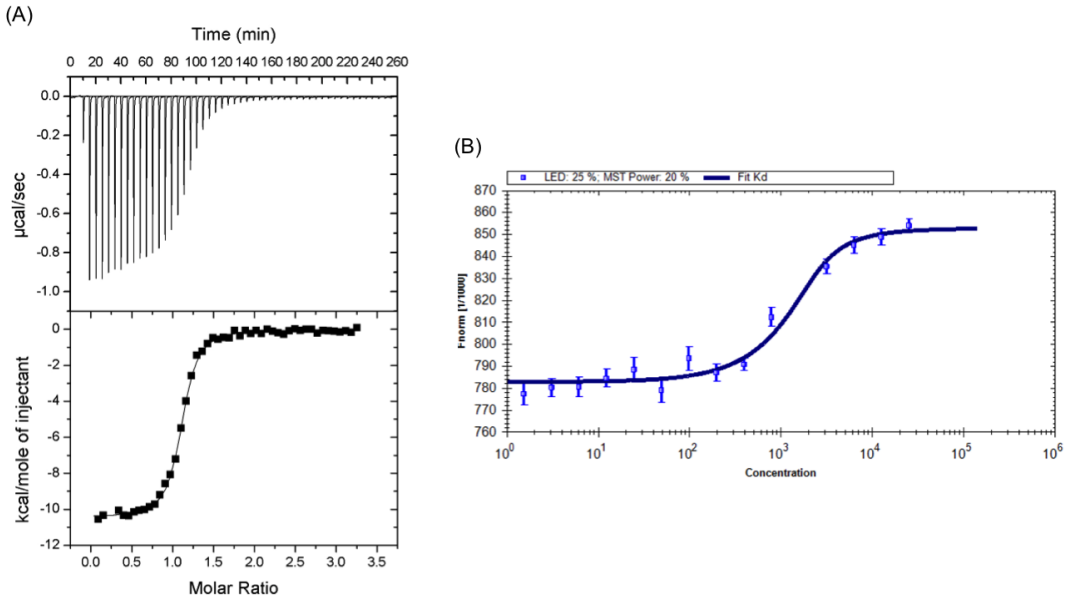

Figure 68. Binding of eEF2K$_{82\text{-}100}$ to Ca^{2+}/CaM.

Calorimetric titrations of Ca^{2+}/CaM with the eEF2K peptide [82-100], showing the original titration curve (top) and the binding isotherm obtained (bottom) (A). MST binding curve of CaM and eEF2K$_{82\text{-}100}$ obtained from the Monolith NT LabelFree (B). Buffer conditions are as described in sections 2.4.4 (ITC) and 2.4.5 (MST).

4.3.4 Binding mode and orientation of eEF2K$_{82\text{-}100}$ in the Ca^{2+}/CaM: eEF2K$_{82\text{-}100}$ complex

The structures of a number of CaM: peptide complexes have been solved by X-ray crystallography. The majority of these structures showed CaM to be in a closed, wraparound conformation with the peptide bound through the centre and therefore contacting both domains of CaM. These structures also revealed that the bound peptide can be orientated in two ways, either with the N-terminal region of the peptide bound to the N-terminal domain of CaM and the C-terminal region of the peptide bound to the C-terminal domain of CaM or vice versa.

The orientation of the eEF2K$_{82\text{-}100}$ peptide when bound to Ca^{2+}/CaM has been determined using NMR and a modified version of eEF2K$_{82\text{-}100}$, which contained a three residue N-terminal extension known as the ATCUN motif. This motif binds Cu^{2+} ions with very high affinity resulting in line broadening and peak disappearance in the NMR spectrum due to the paramagnetic properties of Cu^{2+} (Mal et al., 2002). This ATCUN motif is located at the N-

terminus of eEF2K$_{82-100}$, meaning that Cu^{2+} ions will bind here and thus only cause line broadening of residues located nearby. This meant that the amino acid residues of CaM which are located near the N-terminus of eEF2K$_{82-100}$ in the peptide bound complex could be identified and thus the orientation.

Overlaying the ^{1}H-^{15}N-HSQC spectra collected of the Ca^{2+}/CaM: eEF2K$_{82-100}$ complex in the absence and presence of $CuSO_4$ showed that a number of peaks disappeared upon the addition of $CuSO_4$, as shown in Figure 69. As this complex is assigned this led to the identification of a number of CaM residues, which hence were located near to the N-terminus of eEF2K$_{82-100}$. These were Thr^{44}, Glu^{47}, Leu^{48}, Gln^{49}, Asp^{50}, Glu^{54}, Met^{71}, Lys^{75}, Met^{76}, Asp^{80}, Ser^{81}, Glu^{82} and Thr^{117}. In addition, some peaks were identified which have a much lower intensity due to line broadening and therefore have almost disappeared. These correspond to Asn^{42}, Asn^{53}, Thr^{79} and Glu^{83}. These residues are all located in the N-terminal domain except for Thr^{117}, which may be an anomalous result as it is located far away from all of the other residues identified. Specifically, the residues identified are present in helix III, helix IV and the linker region, demonstrating that the N-terminus region of eEF2K$_{82-100}$ is bound to the N-terminal domain of CaM.

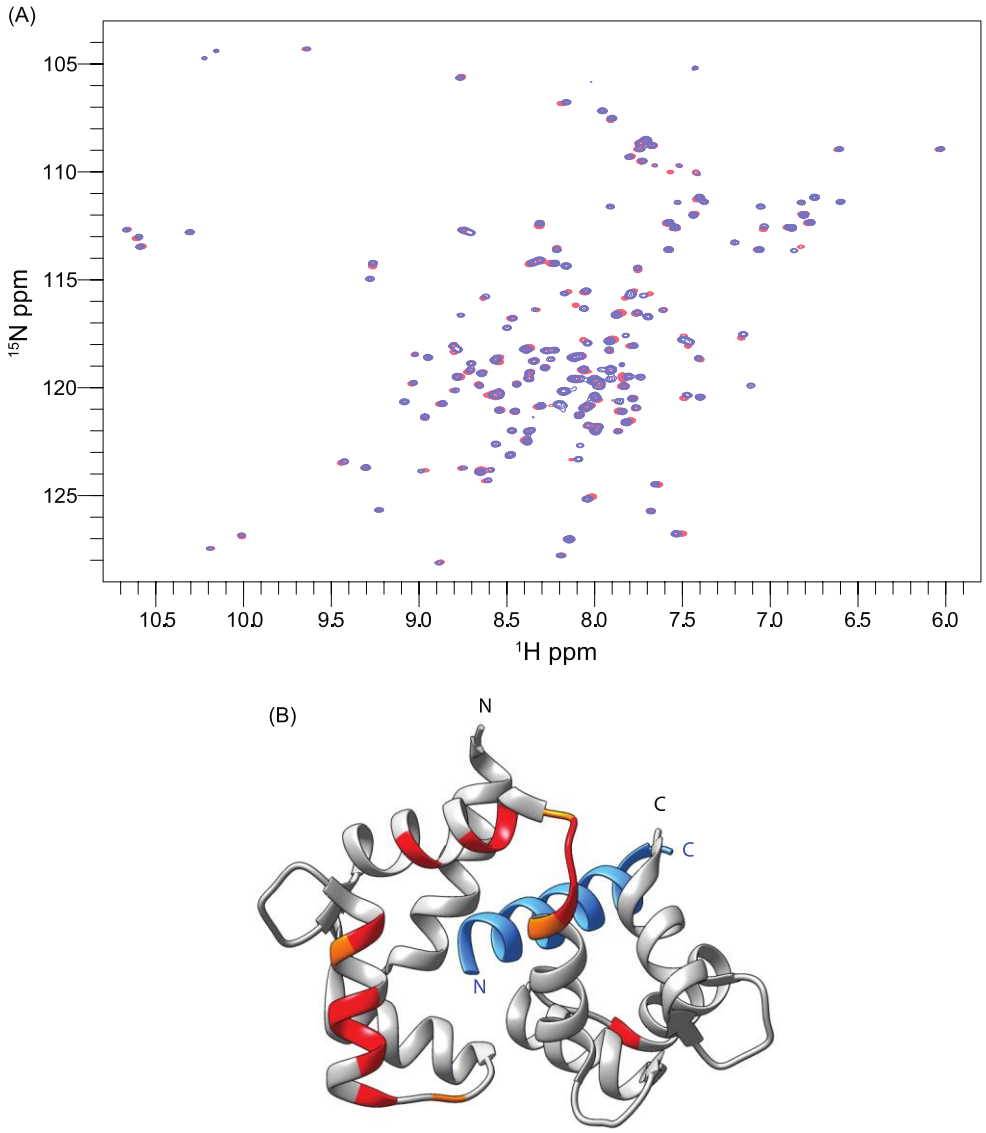

Figure 69. Orientation of eEF2K$_{82\text{-}100}$ in the Ca^{2+}/CaM: eEF2K$_{82\text{-}100}$ complex.
An eEF2K$_{82\text{-}100}$ peptide with an N-terminal extension corresponding to an ATCUN motif was used to determine the orientation of the peptide in the Ca^{2+}/CaM: eEF2K$_{82\text{-}100}$ complex. An overlay of ^{1}H-^{15}N-HSQC spectra collected in the absence and presence of Cu^{2+} allows the identification of those peaks that are broadened upon Cu^{2+} addition (A). The corresponding amino acid residues plotted onto a structure of Ca^{2+}/CaM bound to a target peptide. Those for which the NMR signal completely disappears upon Cu^{2+} addition are coloured red and those which almost disappear are coloured orange (B). Buffer conditions are as described in Section 2.5.5. PDB ID: 2F3Y.

4.4 Comparison of the binding modes of eEF2K$_{82\text{-}100}$ to CaM in the presence and absence of calcium

NMR spectra of the bound states of apo-CaM and Ca^{2+}/CaM can be overlaid to compare the apo-CaM: eEF2K$_{82\text{-}100}$ and Ca^{2+}/CaM: eEF2K$_{82\text{-}100}$ complexes. These comparisons are shown in Figure 70. In both case the end

point of the peptide titrations were used for comparison, when there was a 20-fold excess of $eEF2K_{82-100}$ compared to Ca^{2+}/CaM and apo-CaM. Given the binding constants determined for both of these interactions (with K_d values of 247 nM for Ca^{2+}/CaM binding to $eEF2K_{82-100}$ and 1.38 mM for apo-CaM binding to $eEF2K_{82-100}$) this ratio should be sufficient to occupy the bound state with Ca^{2+}/CaM: $eEF2K_{82-100}$ and apo-CaM: $eEF2K_{82-100}$ complexes formed.

It is evident that a number of resonances are located at the same chemical shift positions in both of the spectra, indicating that these amino acid residues are located in the same chemical environments in both complexes. This suggests that these residues interact with $eEF2K_{82-100}$ in the same way whether there is calcium present or not and therefore that the binding mode is conserved for apo-CaM and Ca^{2+}/CaM on these residues.

In Figure 70 the ^{1}H-^{15}N-HSQC spectra has been labelled to highlight some of the peaks which have the same chemical shift in both bound states. The vast majority of these correspond to amino acid residues of the C-terminal domain, strongly suggesting that $eEF2K_{82-100}$ binds to the same residues in the C-terminal domain of apo-CaM as in Ca^{2+}/CaM. This is consistent with the fact that $eEF2K_{82-100}$ binds by a conserved interaction to both apo-CaM and Ca^{2+}/CaM.

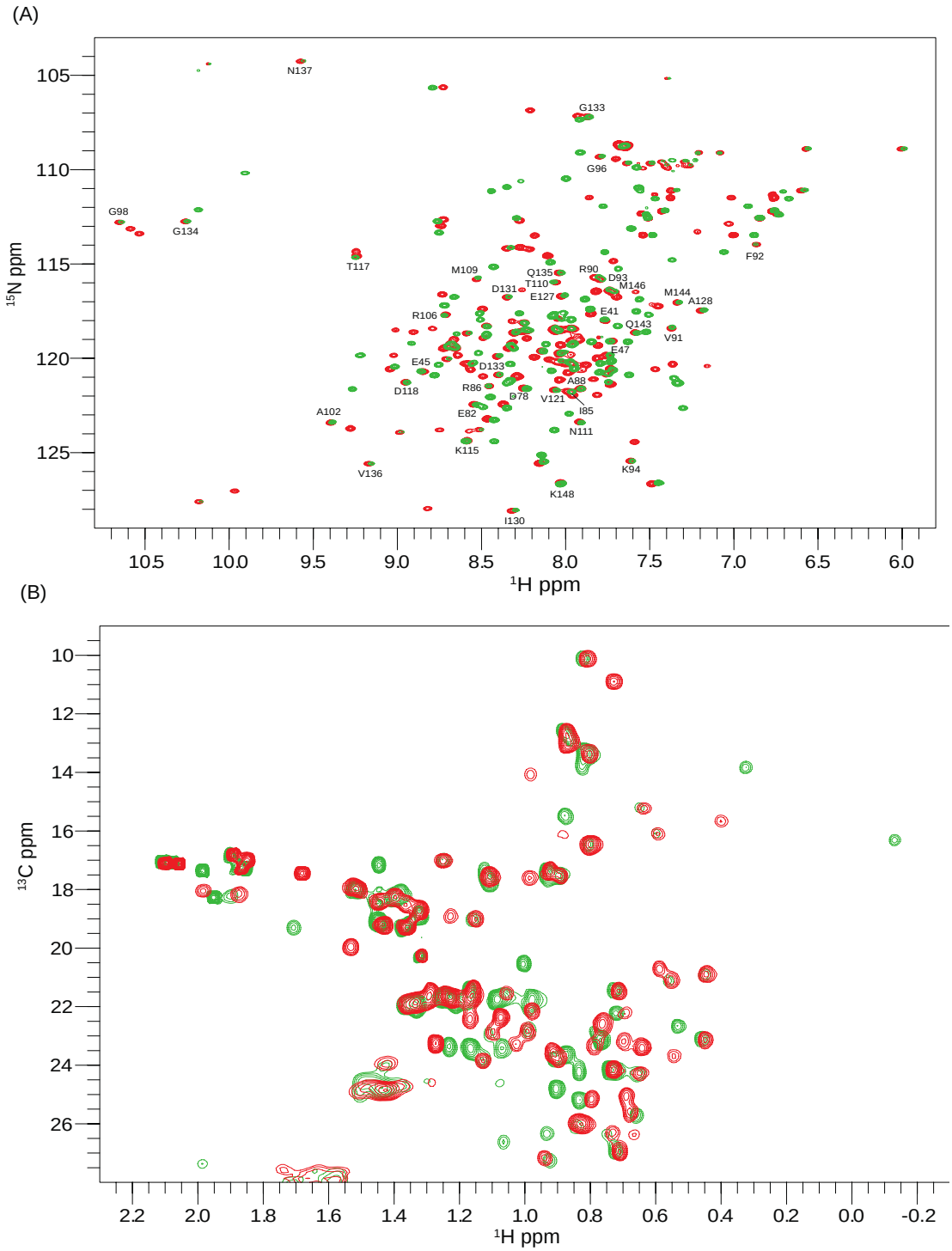

Figure 70.Comparison of eEF2K$_{82\text{-}100}$ binding to Ca^{2+}/CaM and apo-CaM.

^{1}H-^{15}N-HSQC spectra of the Ca^{2+}/CaM: eEF2K$_{82\text{-}100}$ complex (red) and the apo-CaM: eEF2K$_{82\text{-}100}$ complex (green) overlaid. Some of the residues whose peak positions are the same in both eEF2K$_{82\text{-}100}$ bound spectra are labelled (A). ^{1}H-^{13}C-HSQC spectra of the Ca^{2+}/CaM: eEF2K$_{82\text{-}100}$ complex (red) and the apo-CaM: eEF2K$_{82\text{-}100}$ complex (green) overlaid (B). Spectra correspond to the end points (20 fold excess of eEF2K$_{82\text{-}100}$) of peptide titrations with Ca^{2+}/CaM and apo-CaM. Buffer conditions are as described in Section 2.5.4.

4.5 Binding of eEF2K fragments to CaM

The interaction surfaces on Ca^{2+}/CaM and apo-CaM for $eEF2K_{82-100}$ have been defined, thus providing insight into the binding mechanism and possible structures of these complexes. In order to apply our findings to explaining the interaction between CaM and the eEF2K protein we have also examined some eEF2K fragments that represent full-length eEF2K. Throughout this study a number of eEF2K fragments have been investigated, as shown in Table 6 of Section 3.1.

These eEF2K fragments were expressed and purified as outlined in Section 3.3. Originally $eEF2K_{(48-336)(490-725)}$ was identified as a possible eEF2K fragment for use in structural studies, however, the yield was often low following expression and purification and there were problems with protein stability upon addition of CaM. This fragment contained the residues corresponding to the CaM binding region and so another eEF2K fragment was investigated that also contained this region but with fewer amino acid residues at the N-terminus. $eEF2K_{(74-342)(490-725)}$ was found to produce higher yields and be more suitable for NMR studies. Samples for these NMR studies were produced by Dr. Halina Mikolajek. Another eEF2K fragment was used for parallel NMR studies that did not contain the CaM binding region, $eEF2K_{(100-336)(490-725)}$.

A similar experimental strategy was employed for the eEF2K fragments as has been discussed for $eEF2K_{82-100}$, whereby NHSQC spectra were collected of CaM in the absence and presence of a five-fold excess of the eEF2K fragments. A 1:5 ratio of CaM to eEF2K fragments was used rather than a 1:10 ratio as was the case for experiments with $eEF2K_{82-100}$ as the amount of eEF2K fragments was limited to the yield obtained from a single expression and purification protocol. The experiments were collected for Ca^{2+}/CaM and apo-CaM.

The binding sites for $eEF2K_{82-100}$ on Ca^{2+}/CaM and apo-CaM have been determined and are discussed in sections 4.2.1 and 4.3.1. A similar analysis was carried out for the ^{1}H-^{13}C-HSQC spectra collected in the presence of the eEF2K fragments to determine the residues in Ca^{2+}/CaM and apo-CaM that are involved in binding to the eEF2K fragments. Ca^{2+}/CaM and apo-CaM in the

presence of these fragments have not been assigned because the samples do not remain intact for long enough or produce data of a high enough quality for the experiments necessary to carry out a full assignment. As a result, detailed chemical shift perturbation analysis cannot be carried out. However, Ca^{2+}/CaM and apo-CaM have been assigned and therefore the overlays of ^{1}H-^{13}C-HSQC spectra shown in Figures 71 and 72 can still reveal those residues that experience a change in chemical shift upon binding to the eEF2K fragments.

Figure 71 shows the NMR data collected for Ca^{2+}/CaM binding to the two different eEF2K fragments. Binding of Ca^{2+}/CaM to $eEF2K_{(74-342)(490-725)}$, which contains the CaM binding region, involves the same residues identified using $eEf2K_{82-100}$. There are also some additional changes with $eEF2K_{(74-342)(490-725)}$, which indicates there may be some additional interactions. The second eEF2K fragment used for NMR studies does not contain the CaM binding region, $eEF2K_{(100-336)(490-725)}$. The same experiments and analysis were performed to produce an overlay of ^{1}H-^{13}C-HSQC spectra. The spectrum produced upon addition of $eEF2K_{(100-336)(490-725)}$ differs from the reference spectrum of Ca^{2+}/CaM, demonstrating that there is binding of this fragment to Ca^{2+}/CaM, even though it does not contain the CaM binding region.

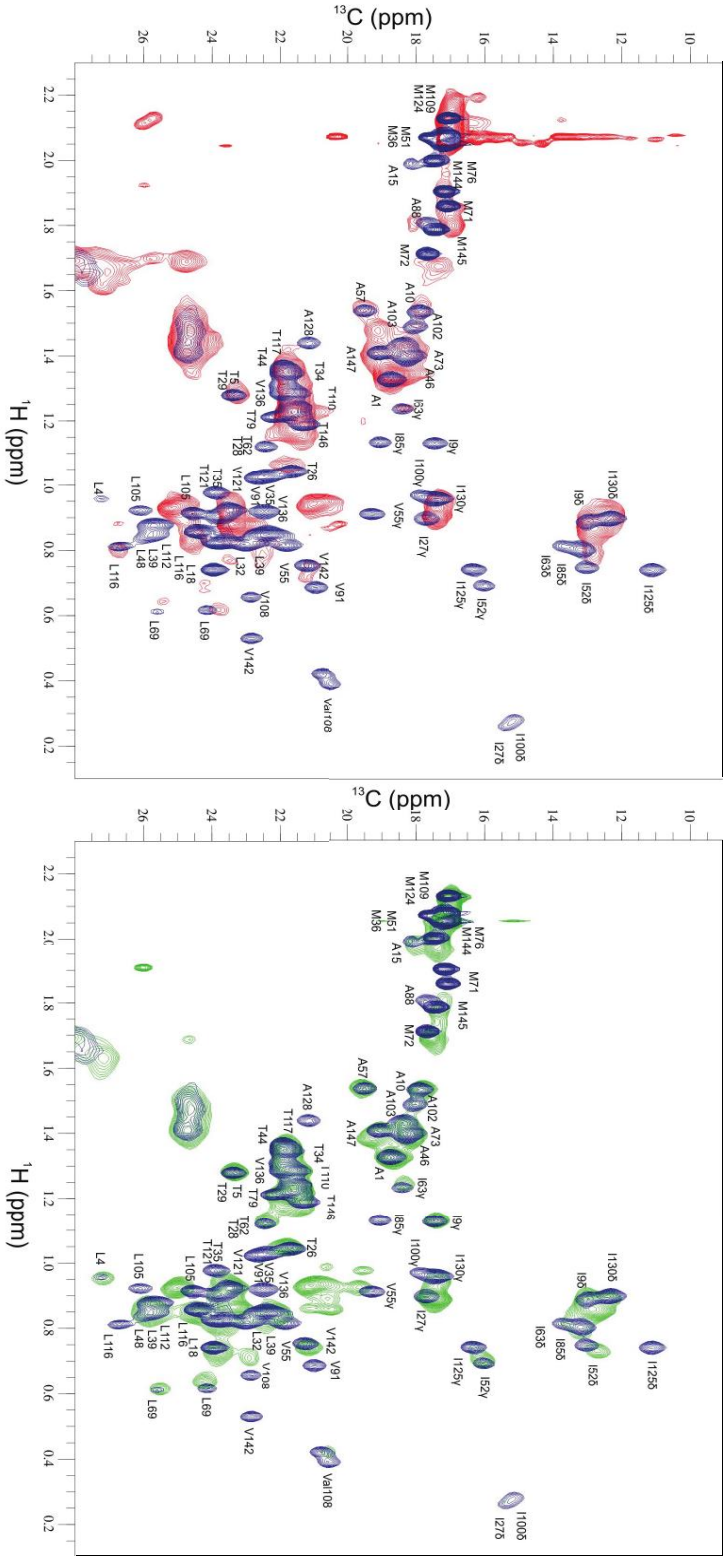

Figure 71. Overlay of ^{1}H-^{13}C-HSQC spectra of Ca^{2+}/CaM collected in the absence and presence of eEF2K fragments.

Overlay of ^{1}H-^{13}C-HSQC spectra of Ca^{2+}/CaM collected in the absence (navy) and presence of a five-fold excess of $eEF2K_{(74-342)(490-725)}$ (red). (A) Overlay of ^{1}H-^{13}C-HSQC spectra of Ca^{2+}/CaM collected in the absence (navy) and presence of a five-fold excess of $eEF2K_{(100-336)(490-725)}$ (green) (B). Buffer conditions are as described in Section 2.5.6.

The interaction of apo-CaM with the eEF2K fragments was also investigated using the same strategy and the results are shown in Figure 72. The conclusions from these overlays are similar to those found for Ca^{2+}/CaM. The residues identified as undergoing a change in chemical shift upon addition of $eEF2K_{(74-342)(490-725)}$ are similar to those residues determined as constituting the binding site for $eEF2K_{82-100}$.

The overlay of apo-CaM in the absence and presence of $eEF2K_{(100-336)(490-725)}$, which does not contain the CaM binding region, shows identical spectra with no chemical shift changes. This indicates that apo-CaM does not bind to the kinase domain alone and thus it only interacts with the CaM binding region.

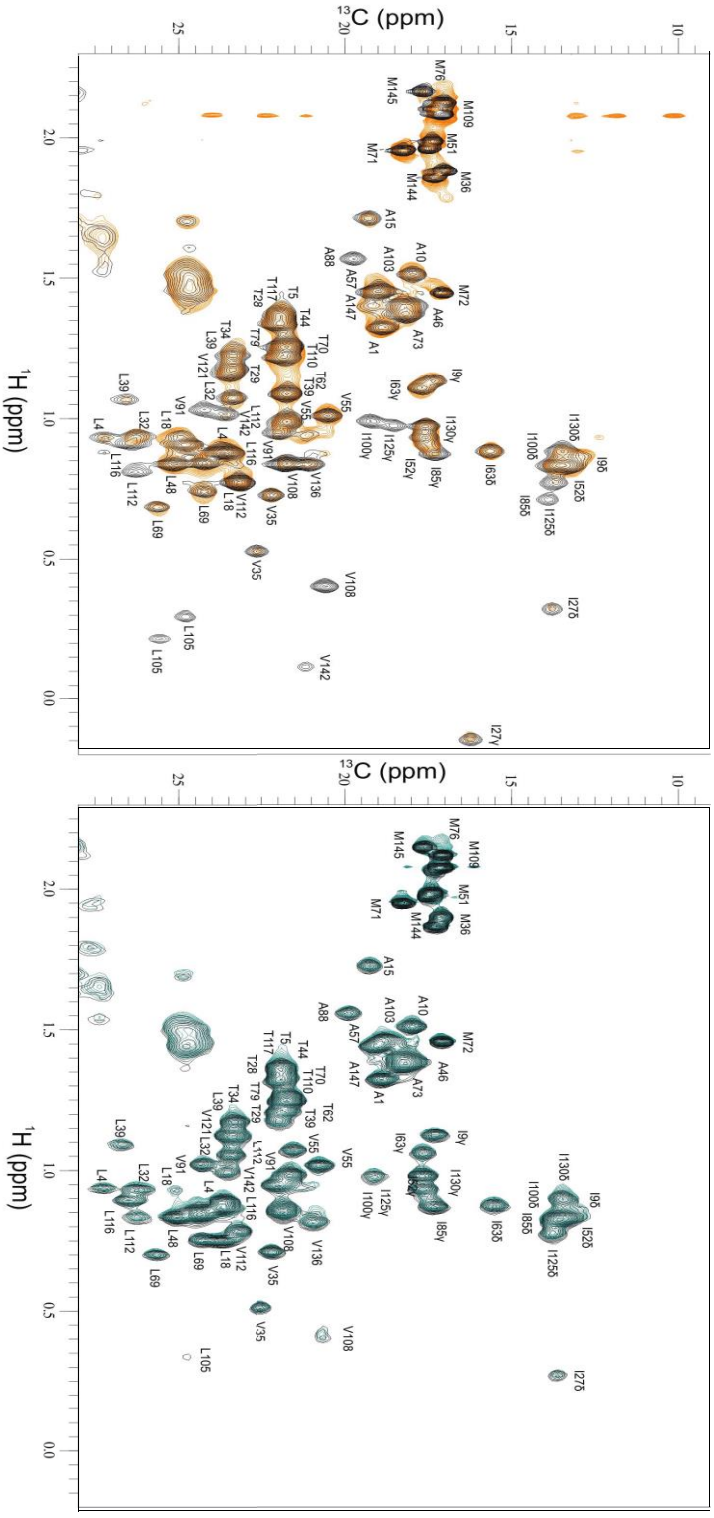

Figure 72. Overlay of ^{1}H-^{13}C-HSQC spectra of apo-CaM collected in the absence and presence of eEF2K fragments.

Overlay of ^{1}H-^{13}C-HSQC spectra of apo-CaM collected in the absence (black) and presence of a five-fold excess of eEF2K$_{(74-342)(490-725)}$ (orange) (A). Overlay of ^{1}H-^{13}C-HSQC spectra of Ca^{2+}/CaM collected in the absence (black) and presence of a five-fold excess of eEF2K$_{(100-336)(490-725)}$ (teal) (B). Buffer conditions are as described in Section 2.5.6.

4.6 Discussion

The CaM resonances have been assigned in four states to high levels of completeness. Both Ca^{2+}/CaM and apo-CaM have been assigned in the free state and also in complex with $eEF2K_{82\text{-}100}$, representing the CaM binding region of eEF2K.

It was therefore possible to perform CSP analysis across the free and bound states of CaM to identify residues important in $eEF2K_{82\text{-}100}$ binding. We found that it was not possible to identify an interaction site by analysing changes in the NH's of the protein backbone. This is likely because the N-H resonances that appear on a ^{1}H-^{15}N-HSQC spectra are sensitive to distal effects that may not occur nearby to the specific interaction site. This is especially true in alpha helices as conformational change and structural rearrangement can be transmitted through the helix, causing effects to be manifested in amino acid residues that are not involved directly in binding. The vast majority of the secondary structure of CaM consists of eight alpha helices and it is known to be a flexible molecule that has been shown to undergo some major conformational change and structural rearrangement upon target binding (Chin and Means, 2000), as discussed in Section 1.4. Overlays of ^{1}H-^{15}N-HSQC spectra of free Ca^{2+}/CaM and Ca^{2+}/CaM bound to $eEF2K_{82\text{-}100}$ show significant differences that make mapping of an interaction site in this manner not possible, likely for the reasons discussed above.

The side chains of amino acid residues were therefore analysed and used to identify binding surfaces instead. Side chain atoms will ultimately be responsible for much of the binding as it is here that interactions will form between CaM and $eEF2K_{82\text{-}100}$. This is shown again when considering an alpha helix as the side chains will point out of the alpha helix, available to make contacts, whilst the backbone atoms are maintained within the secondary structure. Amino acid side chains that contain methyl groups were assigned and used as probes for the interaction sites. The methyl group region on a ^{1}H-^{13}C-HSQC spectrum is well resolved and gives clear signals for interpretation. Also, CaM contains a high level of hydrophobic amino acid residues, located throughout the molecule in both domains and especially prominent in the regions known to interact with other peptide targets (Chin and Means, 2000).

The methyl groups are therefore good candidates for probing the interaction sites for $eEF2K_{82\text{-}100}$ on CaM.

The CSP analysis identified contiguous binding surfaces on both Ca^{2+}/CaM and apo-CaM. For Ca^{2+}/CaM, two interaction sites are present, one in each domain, whilst only the C-terminal domain of apo-CaM is significantly perturbed upon $eEF2K_{82\text{-}100}$ binding. This is consistent with findings in the literature whereby apo-CaM binds with its C-terminal domain to its targets. A key example of this is the MLCK peptide, which Anthis et al (2011) showed could interact with CaM in the absence of Ca^{2+} (apo-CaM) via its C-terminal domain (Anthis et al., 2011). It was found that the hydrophobic amino acid residues are those which appear to have large changes in chemical shifts, consistent with the fact that they are known to be important for CaM binding to its targets (Chin and Means, 2000). It is therefore not surprising that they are important in the interaction with $eEF2K_{82\text{-}100}$.

A peptide titration experiment with Ca^{2+}/CaM identified the presence of multiple exchange characteristics, implying that the interaction between Ca^{2+}/CaM and $eEF2K_{82\text{-}100}$ is more complex than a simple two-step binding equilibrium. If only single exchange characteristics were observed, such that each resonance only showed fast, slow or intermediate exchange, then this would imply that the interaction is simple with $eEF2K_{82\text{-}100}$ binding to Ca^{2+}/CaM in one step to produce the Ca^{2+}/CaM: eEF2K complex. However, as we see a high number of resonances demonstrating multiple exchange characteristics, this is not the case for this interaction and there must be a more complex binding equilibrium and mechanism of binding.

This has been shown with initial results from Spinach simulations to analyse the line shapes in two-dimensions. This is very much a work in progress and so only the initial results are presented in this thesis. Currently only model 1, which corresponds to a simple two-step binding equilibrium, has been evaluated. The results from this determined that this model did not fit some of the residues, as expected. Further analysis will trial different models, representing different reaction mechanisms to see whether these can better fit some of the unusual peak patterns.

With regard to slow and fast exchange characteristics, it is not surprising that there are more residues undergoing slow exchange in the C-terminal domain, as it has often been reported that the C-terminal domain of CaM has a higher affinity for its targets than the N-terminal domain (Crivici and Ikura, 1995). An anchor residue in the CaM binding domains of protein and peptide targets often binds to the C-terminal domain of CaM (Rhoads and Friedberg, 1997).

With regard to single and multiple exchange characteristics, the C-terminal domain contains residues that display single exchange characteristics whilst the N-terminal domain contains a number of residues with characteristics of multisite exchange. This could be consistent with a single $eEF2K_{82\text{-}100}$ peptide binding to Ca^{2+}/CaM to form the Ca^{2+}/CaM: $eEF2K_{82\text{-}100}$ complex at relatively low concentrations of peptide. A conformational change could occur which reveals a second weaker affinity binding site in the N-terminal domain of CaM, allowing a second peptide to bind. This would account for the single exchange characteristics in the C-terminal domain, as the peptide binds to this domain in a single step to form the Ca^{2+}/CaM: $eEF2K_{82\text{-}100}$ complex. This would also account for the multiple exchange characteristics in the N-terminal domain with the first exchange event corresponding to formation of the Ca^{2+}/CaM: $eEF2K_{82\text{-}100}$ complex and the second exchange event corresponding to the binding of a second peptide to the N-terminal domain. The first exchange characteristic we observe, at low concentrations of $eEF2K_{82\text{-}100}$, corresponds to the formation of the Ca^{2+}/CaM: eEF2K complex. The fact that we see additional changes as the $eEF2K_{82\text{-}100}$ concentration continues to increase, resulting in a second exchange characteristic, indicates a further interaction is occurring so that as the peptide concentration becomes higher than a 1:1 ratio between Ca^{2+}/CaM and $eEF2K_{82\text{-}100}$, a second peptide is able to bind to a second, weaker interaction site on Ca^{2+}/CaM. This would imply that the peptide titration up to approximately a 1:1 ratio reflects the formation of the stoichiometric Ca^{2+}/CaM: eEF2K complex.

In fact, there could be two possible explanations as to why multiple exchange characteristics are observed - either the high excesses of $eEF2K_{82\text{-}100}$ present at the end of the peptide titration the system is forced to form another,

different complex (as previously discussed) or the interaction mechanism must involve the formation of an intermediate. If an intermediate is formed the binding mechanism would also involve two steps. The first step is the formation of an intermediate, which corresponds to the stages between a and b in the one-dimensional trace shown for Val^{91} in Figure 65. In this example, and also for the peak movements of Thr^{26}, this stage is in slow exchange implying that the binding of $eEF2K_{82\text{-}100}$ to form this intermediate complex is relatively tight. There is then a second stage to the interaction whereby the intermediate complex becomes the final Ca^{2+}/CaM: $eEF2K_{82\text{-}100}$ complex. This likely involves conformational change and some structural rearrangement to allow additional and possibly different binding interactions to occur between the peptide and Ca^{2+}/CaM; this part of the interaction corresponds to the step between b and c in Figure 65.

It is important to determine which of these explanations is true in this case. Further study of the 1:1 complex of Ca^{2+}/CaM and $eEF2K_{82\text{-}100}$, rather than with a 20-fold excess of $eEF2K_{82\text{-}100}$, should help to resolve this, especially the determination of the solution structure of this 1:1 complex.

The orientation of the $eEF2K_{82\text{-}100}$ peptide in its complex with Ca^{2+}/CaM has been determined using an ATCUN peptide as described in Section 4.3.4. It was found that the N-terminal portion of the peptide interacts with the N-terminal domain of Ca^{2+}/CaM. This is consistent with the structure of Ca^{2+}/CaM in complex with a peptide from CAMKK in the literature (Osawa et al., 1999), although complex structures are available which show target peptides in both orientations. There are two tryptophan residues in the CaM binding region of eEF2K at positions 85 and 99. The orientation of $eEF2K_{82\text{-}100}$ in the manner discussed means that Trp^{99} is likely anchored to the C-terminal domain of CaM. This domain is often attributed to contain the high affinity binding site of Ca^{2+}/CaM (Crivici and Ikura, 1995).

ITC and MST were used to determine the affinity of the interactions between Ca^{2+}/CaM and apo-CaM and $eEF2K_{82\text{-}100}$. A high overall affinity was estimated by ITC (247 +/-2 nM) and MST (417+/-38.2 nM) for Ca^{2+}/CaM. The

two values for the K_d are different, probably due to differences in the methods performed. MST requires a fluorescent label to be attached, which could account for the differences in measurements seen. The K_d measured for apo-CaM by MST (1.38 +/-86.2 mM) reveals that the interaction between apo-CaM and $eEF2K_{82-100}$ is weak. This is also shown by results from the peptide titration of apo-CaM with $eEF2K_{82-100}$, which shows mainly fast exchange. Studying the apo-CaM interaction with eEF2K can still provide important information on the mechanism of recognition and binding, despite this weak interaction. As discussed, it is predominantly the C-terminal domain of apo-CaM that interacts with $eEF2K_{82-100}$ and it also seems that the C-terminal domain of Ca^{2+}/CaM interacts more strongly with $eEF2K_{82-100}$. Taken with the finding that the interaction mechanism on the C-terminal domain seems consistent for apo-CaM and Ca^{2+}/CaM this provides a possible explanation for the binding mechanism of CaM and $eEF2K_{82-100}$ and consequently the interaction between CaM and eEF2K in the cell. An interaction between eEF2K and the C-terminal domain is possible in the absence of calcium; however, activation of eEF2K requires the presence of calcium through a calcium signal. Therefore it is likely the additional involvement of the N-terminal domain of CaM that is seen when calcium is present that causes necessary conformational change to result in eEF2K activation.

In addition to $eEF2K_{82-100}$, some kinase fragments were used to represent full-length eEF2K and also to further dissect the roles the different domains play in the interaction and activation. Residues that experience a change in chemical shift upon $eEF2K_{82-100}$ addition are also affected upon addition of $eEF2K_{(74-342)(490-725)}$ suggesting that the recognition by Ca^{2+}/CaM of the eEF2K peptide and this eEF2K fragment are extremely similar. The fact that Ca^{2+}/CaM and apo-CaM recognition modes of both the eEF2K peptide and the eEF2K fragment containing the same CaM binding region, $eEF2K_{(74-342)(490-725)}$, are similar demonstrates that information gained on the interaction using the eEF2K peptide can be applied to eEF2K.

There are also some additional changes with $eEF2K_{(74-342)(490-725)}$ compared to $eEF2K_{82-100}$, indicating that there may be some additional

interactions between the kinase domain of eEF2K and Ca^{2+}/CaM. This means that the binding of Ca^{2+}/CaM to eEF2K is not dictated only by the CaM binding region and that additional contacts with residues in the kinase domain are important for the interaction. This could have implications on the activation mechanism of eEF2K by CaM. Our results show that Ca^{2+}/CaM can bind to only those residues that constitute the CaM binding region (residues 82-100) but that when the kinase domain is also present there are additional contacts with residues outside of the CaM binding region. These additional interactions through the kinase domain of eEF2K may be responsible for triggering the activation of eEF2K.

Binding of apo-CaM to eEF2K does not result in an active eEF2K that can phosphorylate substrate. The fact that no additional contacts between apo-CaM and the kinase domain of eEF2K are identified suggests that these interactions are necessary for the activation of eEF2K.

In conclusion, Chapter 4 presents results that compare the interaction of Ca^{2+}/CaM and apo-CaM with $eEF2K_{82-100}$. The binding mode is different in the absence and presence of Ca^{2+}, and this therefore provides insight into the binding and interaction between these two molecules.

Chapter 5. Insights into the structure of the Ca^{2+}/CaM: $eEF2K_{82-100}$ complex obtained from SAXS and RDC data

5.1 Introduction

Chapter 4 details the characterisation of the interaction between Ca^{2+}/CaM and $eEF2K_{82-100}$. However, further detail on the structural basis for this interaction is needed to better understand the conformational changes involved in the activation of eEF2K.

The three-dimensional structure of eEF2K remains unknown and as eEF2K is a large protein of 100 kDa, it is difficult to study this by NMR, especially at a level where resonance assignment and structure calculations are feasible. Therefore, we have investigated the three-dimensional structure of CaM bound to $eEF2K_{82-100}$ to further improve our understanding of this interaction and the regulation of eEF2K. Resonance assignments have been possible in this case, as shown in Section 3.4 with a ten-fold excess of $eEF2K_{82-100}$ and later in Chapter 6 at a 1:1 ratio of Ca^{2+}/CaM to $eEF2K_{82-100}$.

A combination of small angle X-ray scattering (SAXS) and NMR data was used to produce a structural model for the Ca^{2+}/CaM: $eEF2K_{82-100}$ complex. Residual dipolar coupling (RDC) measurements were determined by NMR for Ca^{2+}/CaM in the presence of a ten-fold excess of $eEF2K_{82-100}$ and SAXS data was also collected with this same excess of $eEF2K_{82-100}$. RDC measurements were used to determine the orientation of the two domains of Ca^{2+}/CaM with respect to each other. Analysis of the SAXS data was performed taking into account the relative domain orientations determined as a result of RDC measurements.

This same analysis was performed on data collected at a 1:1 ratio of Ca^{2+}/CaM and $eEF2K_{82-100}$. This meant that structural models were produced for both conditions to determine which condition better represented the natural state of the Ca^{2+}/CaM: $eEF2K_{82-100}$ complex.

5.2 Domain orientations of Ca^{2+}/CaM when bound to $eEF2K_{82-100}$ revealed by RDC analysis

A series of J-modulated ^{15}N-HSQC spectra at a 1:1 ratio and at a 1:10 ratio of Ca^{2+}/CaM to $eEF2K_{82-100}$ was collected for RDC data analysis under isotropic and anisotropic conditions. These spectra all had good signal to noise

ratios and the majority of peaks were present and located at the correct chemical shift positions, consistent with previous spectra. There were some differences in the spectra collected under anisotropic conditions, when the sample was aligned in a polyacrylamide gel. A Table showing the chemical shift differences between the resonances on spectra collected under isotropic and anisotropic conditions is shown in Appendix 11 for the 1:1 data and Appendix 12 for the 1:10 data. For the spectra collected at a 1:1 ratio, Thr^{70}, Val^{55} and His^{107} show the largest chemical shift difference between the two spectra, however, the maximum difference (for Thr^{70}) is 0.069 ppm, which is not significant. This meant that the resonances could be easily assigned, as it was clear which peak corresponded to which resonance.

The spectra collected at a 1:10 ratio however, were not as good quality, with a lower signal-to-noise ratio, meaning that it was much harder to distinguish peaks from each other. Also, the anisotropic spectra showed larger chemical shift differences between resonances, as shown in Appendix 11. In the case of this data, the maximum chemical shift difference was 0.33 ppm for Thr^{29}, which is considerably more than the value for the 1:1 data. There are also 14 resonances from the 1:10 ratio data set with chemical shift differences larger than the maximum chemical shift difference seen in for the 1:1 ratio data.

In addition, there were some difficulties in analysing these spectra for the calculation of RDCs via the fitting procedure outlined in Section 2.5.7.3. The central region of the Ca^{2+}/CaM ^{15}N-HSQC spectrum contains a large number of resonances in a small area. The majority of these are overlapped due to some degeneracy in chemical shifts in this region, and this was exacerbated under anisotropic conditions. This meant that peaks could not be picked and assigned to a single residue, as every residue does not have its own corresponding, individual peak. If a peak consists of more than one resonance it is difficult to interpret information from its intensity, as is needed for RDC determination. A single dipolar coupling measurement must be determined in both the isotropic and anisotropic data set in order for a residual dipolar coupling to be calculated. Consequently, a number of residues could not be included in the analysis and an accurate RDC measurement could not be determined for them. This is summarised in Appendices 11 and 12. Despite this, there were still a significant

number of peaks that could be included for each data set and this was sufficient for further analysis.

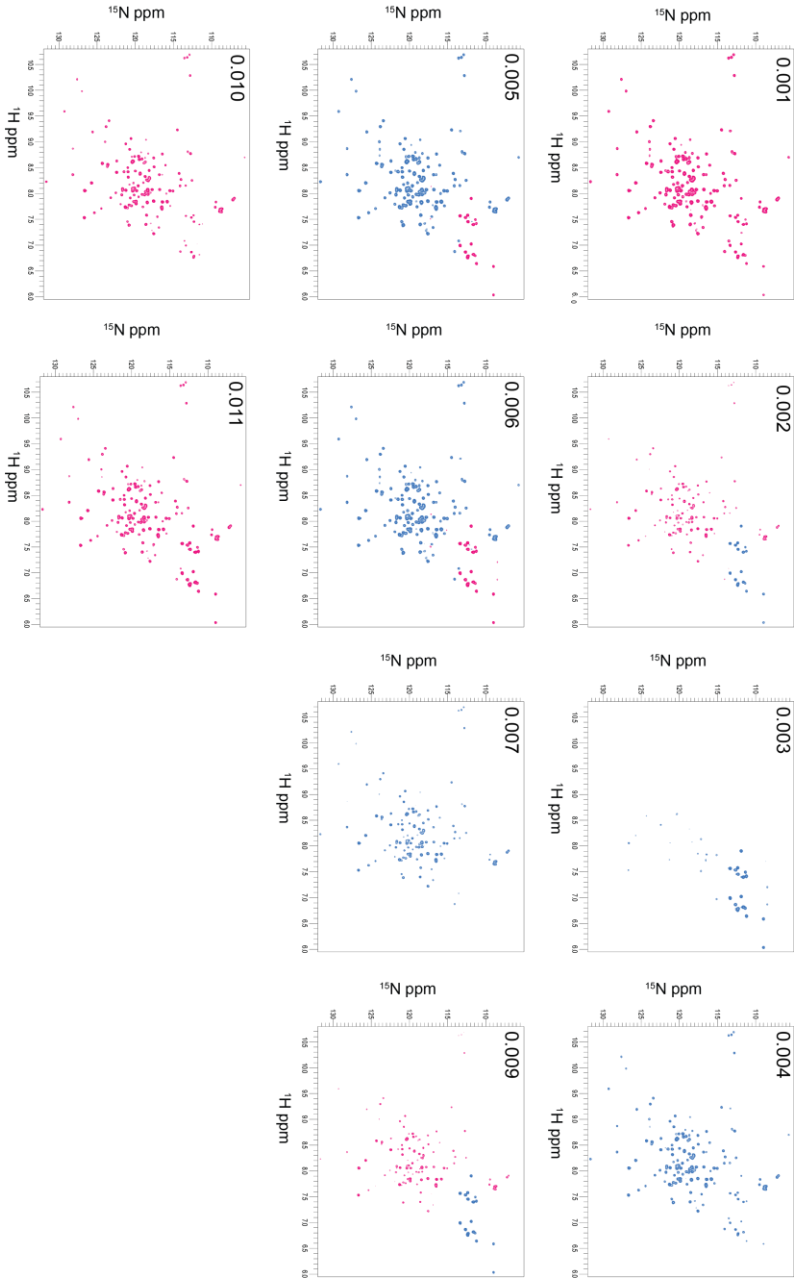

Figure 73. ^{15}N-HSQC spectra collected for the measurement of dipolar couplings.

Series of J-modulated ^{15}N-HSQC spectra collected with different dephasing delays (tauD). The dephasing delay (seconds) is indicated in the top left of each spectrum in seconds. These were collected in isotropic conditions for the sample containing a 1:1 ratio of Ca^{2+}/CaM and $eEF2K_{82\text{-}100}$. Positive contours are shown in pink and negative contours are shown in blue. Buffer conditions are as described in Section 2.5.7.

The RDC values for those residues that could clearly be attributed to a single resonance on the spectrum were determined through a non-linear fitting routine. This involved fitting the experimental data to a formula, as described in Section 2.5.7.3, using a script that is shown in Appendix 13 This analysis produced plots for each residue and determined the J-coupling values under isotropic and anisotropic conditions. These plots are shown in Figure 74, for the anisotropic data at the 1:1 ratio.

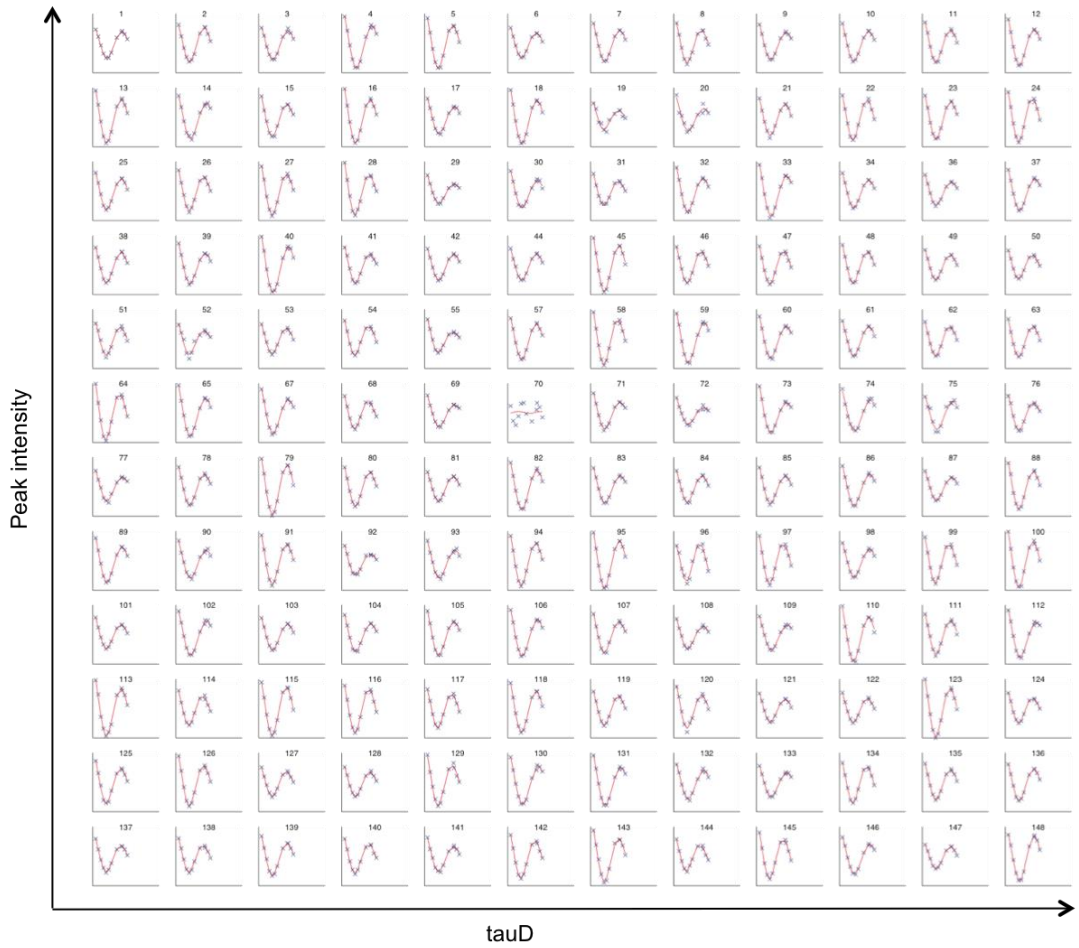

Figure 74. Data fitting for the measurement of dipolar couplings.
Series of plots showing an example overview of MATLAB simulations of data fitting for the measurement of dipolar couplings in anisotropic conditions for the sample containing a 1:1 ratio of Ca^{2+}/CaM and $eEF2K_{82\text{-}100}$. Peak intensity is plotted against tauD and the corresponding residue number is shown above each plot. Buffer conditions are as described in Section 2.5.8.

The determination of the J-couplings under isotropic and anisotropic conditions meant that the RDCs could be calculated, as the RDC is the difference

between these two J-coupling values. Tables containing the RDC values calculated for each residue of Ca^{2+}/CaM are shown in Appendix 14 for the data collected at a 1:1 ratio and in Appendix 15 for the data collected at a 1:10 ratio. In addition, the fitting of the curve to the experimental data also determined values for other parameters, aside from the J-couplings, which are also shown in Appendices 13 and 14. Values are given for the J-coupling (J_{NH}), initial peak intensity (a) and for any imperfection in π pulses during the experiment (b).

For all data sets, isotropic and anisotropic and at both ratios of Ca^{2+}/CaM and $eEF2K_{82-100}$, the r2 (relaxation rate) values generated from the curve fitting remain fairly constant, only differing by 0.02 in general between residues. The value corresponding to the imperfection of π pulses during the experiment also remains particularly constant throughout the curve fitting for each residue.

RDC values calculated from the data collected at a 1:1 ratio are considerably smaller than those values collected at a 1:10 ratio. This is due to the fact that different alignment media were used, meaning that the degree of alignment is different. The 1:1 ratio anisotropic data was collected in a polyacrylamide gel, whilst the 1:10 ratio anisotropic data was collected in liquid crystals. The polyacrylamide gel must align the protein less strongly than the liquid crystals. For the 1:1 data, the RDC values range from -9.29 to 7.59 Hz and for the 1:10 data the RDC values range from -30.43 to 32.58. This is shown in Figures 75 and 76.

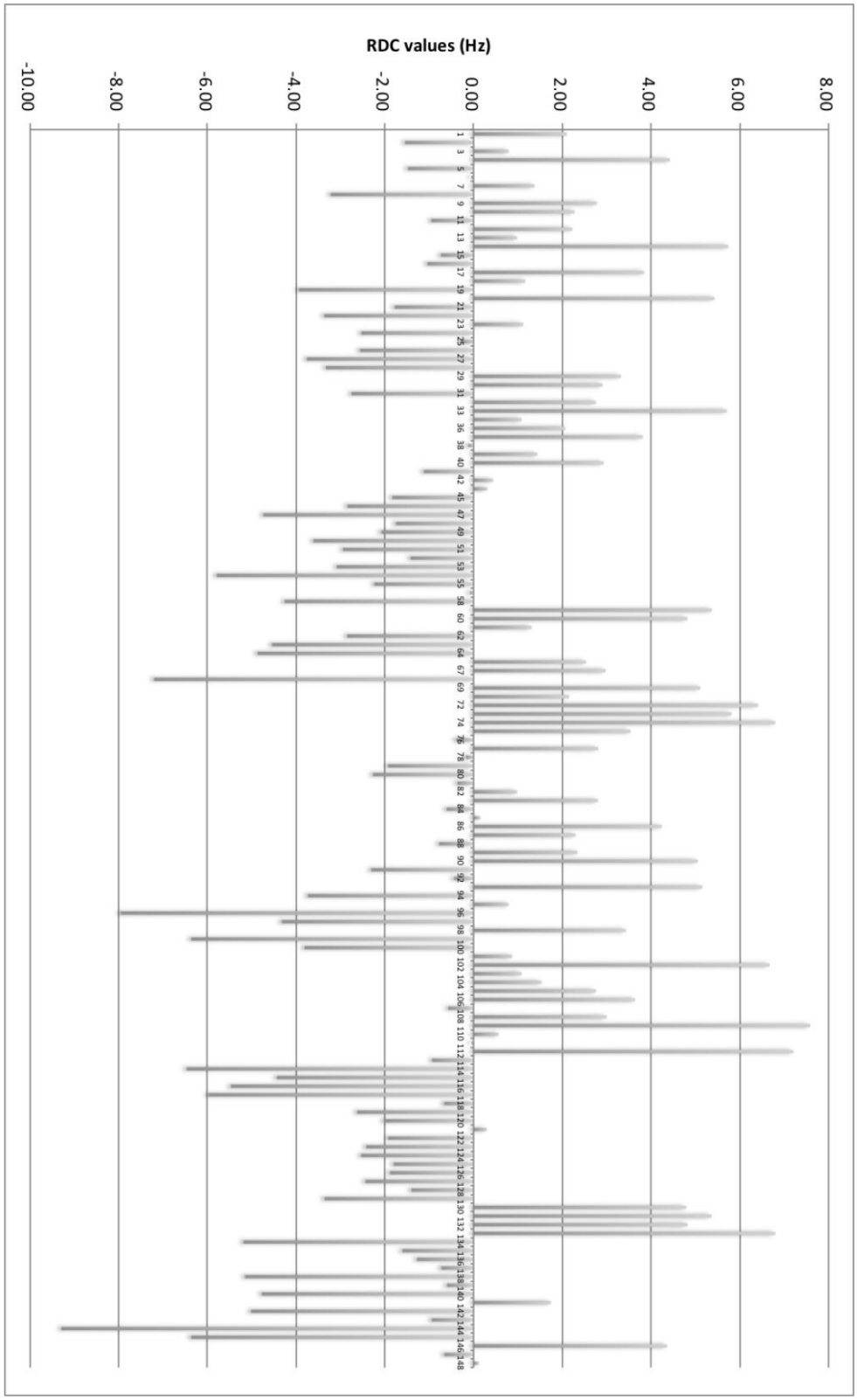

Figure 75. Chart of RDC values per residue for data collected at a 1:1 ratio of Ca^{2+}/CaM and $eEF2K_{82-100}$.

RDC value is plotted against residue number. Buffer and experimental conditions are as described in Section 2.5.7.

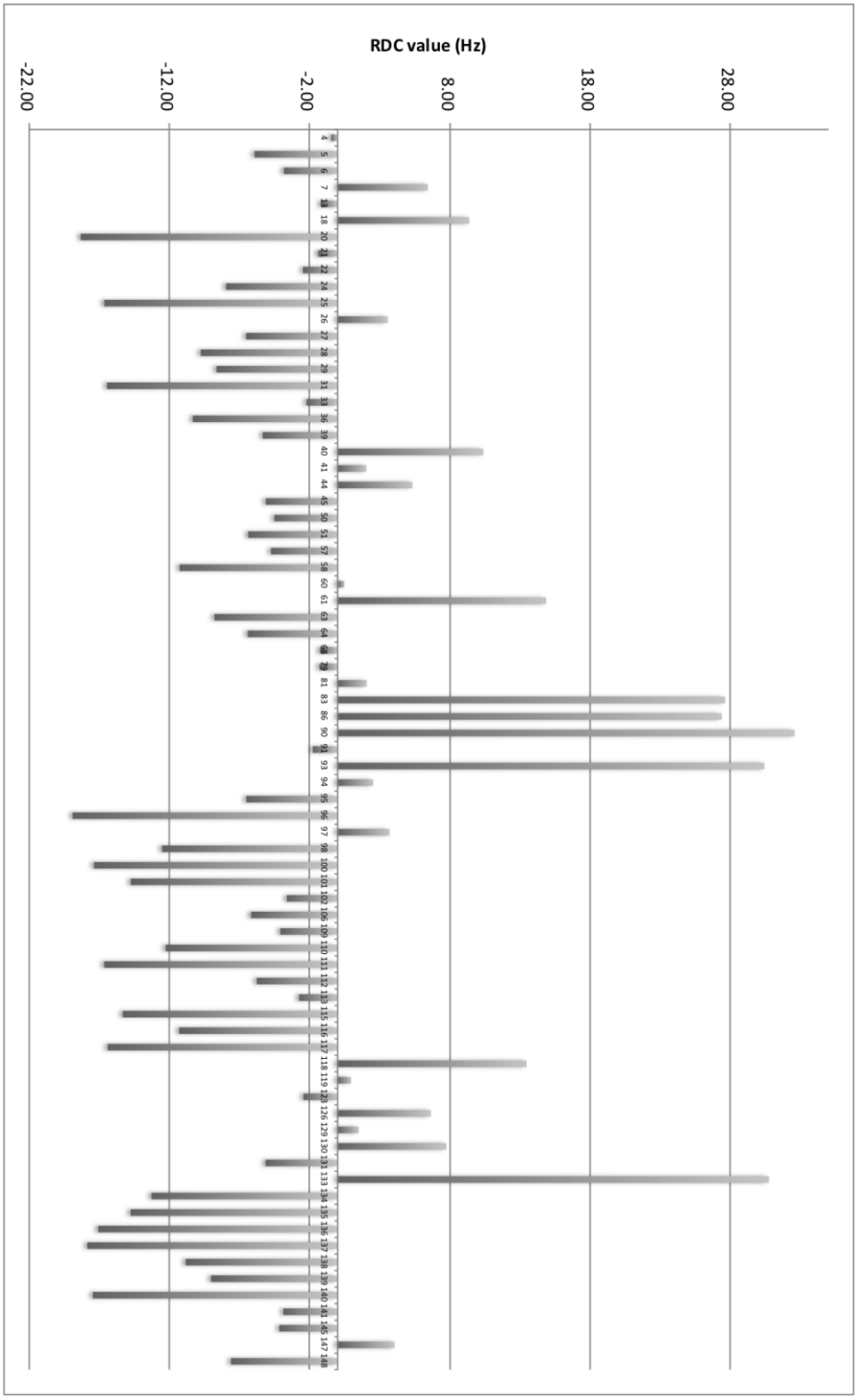

Figure 76. Chart of RDC values per residue for data collected at a 1:10 ratio of Ca^{2+}/CaM and $eEF2K_{82-100}$.

RDC value is plotted against residue number. Buffer and experimental conditions are as described in Section 2.5.7.

Experimental RDC values for the Ca^{2+}/CaM: $eEF2K_{82-100}$ complex were compared to back-calculated RDC values determined from a chosen structure of a CaM: peptide complex deposited in the PDB. A number of structures from the PDB were trialled initially to assess the overall fit and correlation between the experimental and back-calculated RDC values. These structures were selected as they contained different types of CaM recognition motif. Those chosen were - Ca^{2+}/CaM bound to a peptide from smooth muscle myosin light chain kinase (PDB ID: 1CDL) with a basic 1-8-14 motif, Ca^{2+}/CaM bound to a peptide from Ca^{2+}/CaM kinase kinase (PDB ID: 1IQ5) with a 1-16 motif, $Ca2^{+}$/CaM bound to a peptide from myristoylated alanine-rich C kinase substrate (MARCKS) (PDB ID: 1IWQ) with a 1 hydrophobic domain and Ca^{2+}/CaM bound to a peptide from the cardiac ca(v)1.2 calcium channel with a 1-16 (IQ) motif (PDB ID: 2F3Y). As discussed in Section 1.4.4.2, these motifs dictate the location of hydrophobic residues within the target motif.

A χ^2 value, which describes how the values differ from each other, was determined for each residue, for each module (domain of CaM) and for the structure as a whole, and these values are shown in Table 8 for some of the structures in the PDB that were tested. The N-terminal domain of CaM was defined as residues 1-73 and the C-terminal domain of CaM as residues 81-148, whilst the linker region (residues 74-80) was not included in this analysis.

Further analysis of the χ^2 values for each residue involved the selective removal of outliers to generate alignment tensors following each fit of the experimental and back calculated data. If a residue had a high χ^2 value and was located in a flexible region of the protein then it was removed. These regions were the loops, especially the Ca^{2+} coordinating loops, and the N- and C-termini of the protein. Those resides which were removed for the final analysis are shown in Appendix 14 for the data collected at a 1:1 ratio and Appendix 15 for the data collected at a 1:10 ratio. At the 1:1 ratio, the values for 93 residues were included in total, 49 in the N-terminal domain and 44 in the C-terminal domain. At a 1:10 ratio the values for 60 residues were included in total, 27 in the N-terminal domain and 32 in the C-terminal domain.

Table 8 shows that the Ca^{2+}/CaM: peptide complex whose back calculated values best fitted the data from the Ca^{2+}/CaM: $eEF2K_{82-100}$ complex was PDB ID: 2F3Y, as shown by the significantly lower χ^2 value. This structure from the PDB is a crystal structure of Ca^{2+}/CaM bound to the hydrophobic IQ domain of the cardiac ca(v)1.2 calcium channel (Fallon et al., 2005). This structure was therefore used for the rest of the analysis in Module 1.0 to determine the alignment tensor of each domain in CaM and thus the orientation of the two domains with respect to each other.

Table 8. χ^2 values per residue for different Ca^{2+}/CaM: target peptide complexes in the PDB, using data collected at a 1:1 ratio of Ca^{2+}/CaM and $eEF2K_{82-100}$.

	PDB ID: 1CDL	PDB ID: 1IQ5	PDB ID: 1IWQ	PDB ID: 2F3Y
N-terminal domain χ^2	14.54	8.08	12	5.88
C-terminal domain χ^2	14.83	11.09	12.22	9.43

The two domains of CaM were fit individually (as two separate modules) to give two alignment tensors. The accuracy of the fit is represented in a correlation plot, which shows the correlation between the experimental values and the back-calculated values for the RDCs. These plots, for the N- and C-terminal domains at both ratios, are shown in Figure 77. From these plots, the degree of correlation across both data sets at different ratios is fairly consistent. In the C-terminal domain, for data collected at a 1:1 ratio, there is one value that does not fit the correlation. The correlation coefficient for the N-terminal domain at a 1:1 ratio is 0.94 and for the C-terminal domain is 0.98. For the 1;10 date, the correlation coefficient for the N-terminal domain is 0.95 and for the C-terminal domain is 0.91.

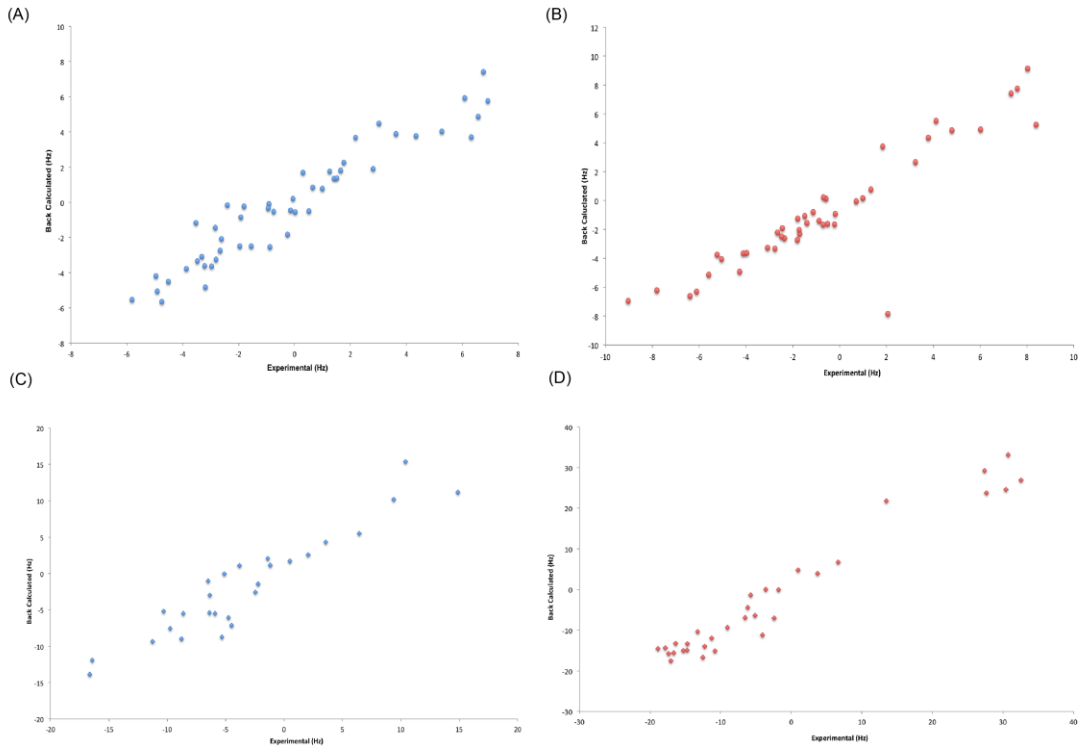

Figure 77. Correlation plots for experimental and back calculated RDC values.

Correlation plots for the N- (A) and C-terminal domain (B) of Ca^{2+}/CaM for data collected at a 1:1 ratio with $eEF2K_{82\text{-}100}$ and the N- (C) and C-terminal domain at a 1:10 ratio (D).

The details of these alignment tensors for both data sets are shown in Table 9. Section 1.7.1.4 describes the alignment tensor, which consists of 3 angles and 2 magnitudes. From Table 9 we can see that the strength of alignment, as described by Aa and Ar (the axial and rhombic components of the alignment tensor respectively), differs across the two domains of Ca^{2+}/CaM. This is the case for both the 1:1 and 1:10 ratio data and indicates that the domains of Ca^{2+}/CaM do not align as a single unit, suggesting that there are dynamics present between the domains. These values also show that the C-terminal domain aligns more strongly, as the Aa and Ar values are larger compared to the N-terminal domain. In terms of the angles of the alignment tensor, it is β that tells us most directly about the orientation of the molecule. It describes the angle between the alignment tensor and the laboratory frame, with respect to the Z-axis. In terms of the 1:1 data, this means that there would need to be approximately a 40 ° rotation between the N- and C-terminal

domains in order for them to align. For the 1:10 data this is similar, with approximately a 50 ° rotation required. The α and γ angles also differ across the two domains.

Table 9. Alignment tensor values for Ca^{2+}/CaM in the presence of $eEF2K_{82-100}$ at 1:1 and 1:10 ratios.

	1:1 ratio		1:10 ratio	
	N-terminal domain	C-terminal domain	N-terminal domain	C-terminal domain
α (°)	30.8 (± 1.6)	-41.0 (± 0.9)	-45.9 (± 4.3)	131.1 (± 2.4)
β (°)	104.6 (± 0.3)	57.9 (± 0.4)	72.3 (± 1.9)	128.4 (± 0.4)
γ (°)	81.4 (± 0.6)	52.8 (± 0.4)	-68.2 (± 8.0)	-168.9 (± 0.4)
Aa	3.5 (± 0.07)	4.7 (± 0.06)	6.7 (± 0.18)	14.9 (± 0.2)
Ar	1.0 (± 0.07)	1.8 (± 0.04)	4.0 (± 0.17)	1.6 (± 0.2)
χ^2 per residue	5.88	9.43	10.47	13.28

The two modules were aligned according to the two alignment tensors to determine the orientation of the two modules with respect to each other. The four degenerate alignments, generated by 180° rotations around the x-, y- and z-axes, were performed and are shown in Figure 78 for the data collected at a 1:1 ratio. For each data set, only two of the four models produced as a result of these degenerate rotations are possible. For the other two of the models, the two domains are orientated in such a way that the linker region could not possibly connect the two domains. The distance between residue 73, the last residue of the N-terminal domain, and residue 81, the first residue of the C-terminal domain, is too large for the linker region, which is 5 residues in length, to join the two domains. For the 1:1 data set, the two models which produce possible orientations have experienced no rotations and a 180° rotation about the z-axis, as shown in Figure 78 (A and D), whilst for the 1:10 data set it is 180° rotations about the x- and y-axes that produce possible models, as shown in Figure 79.

It should be noted at this stage that the x-axis of the N-terminal domain alignment tensor is very small, meaning that this tensor is not well defined. This

has implications for further analysis and use of the RDC data and will be discussed.

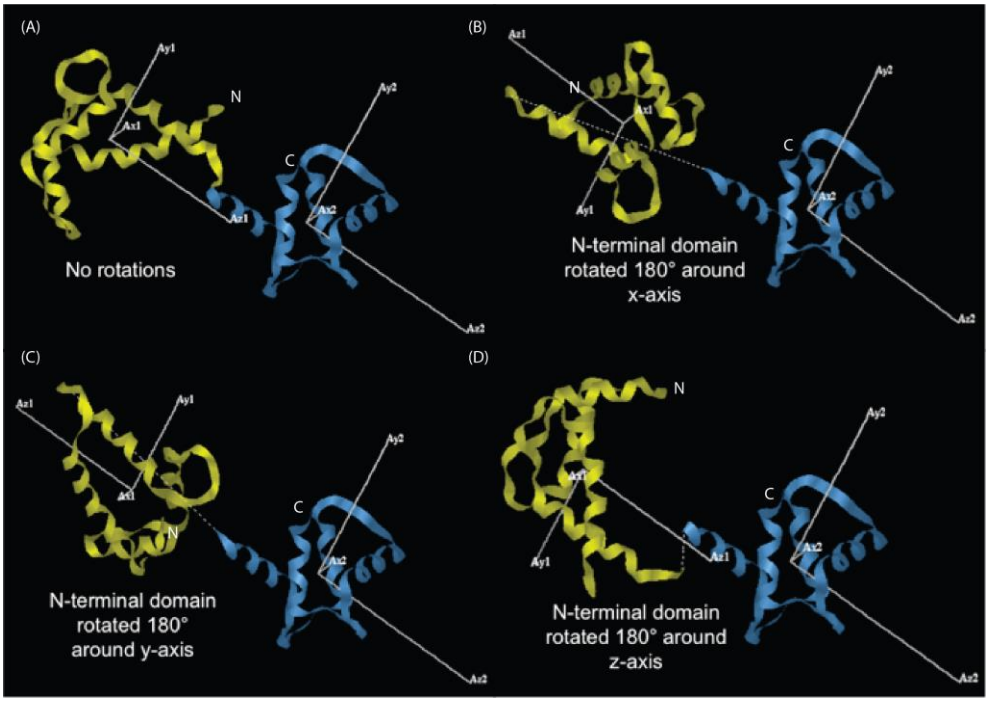

Figure 78. Four degenerate orientations of the two domains of CaM with respect to each other from 1:1 ratio data.

The four possible orientations are derived from four degenerate rotations. These rotations are defined from the alignment tensor values for Ca^{2+}/CaM in the presence of $eEF2K_{82\text{-}100}$ at a 1:1 ratio.

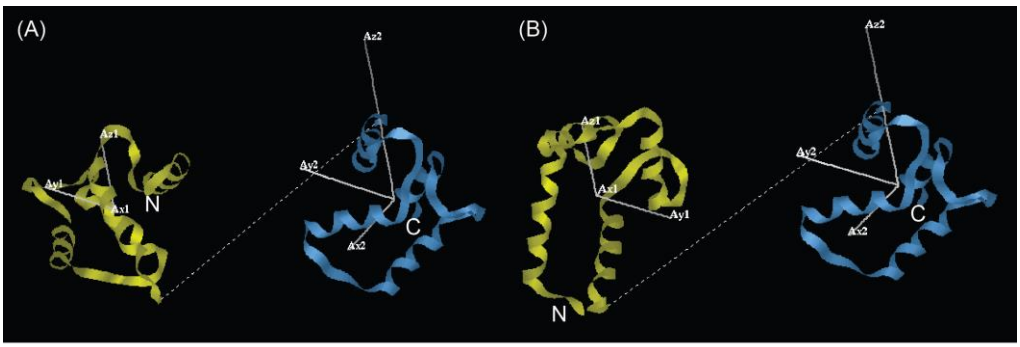

Figure 79. Two possible orientations of the two domains of Ca^{2+}/CaM with respect to each other from 1:10 ratio data.

Of the four degenerate orientations, only two are possible. A rotation of the N-terminal domain about the y-axis (A) and about the x-axis (B). These rotations are defined from the alignment tensor values for Ca^{2+}/CaM in the presence of $eEF2K_{82\text{-}100}$ at a 1:10 ratio.

5.3 Size and shape of the Ca^{2+}/CaM: eEF2K complex revealed by SAXS analysis

SAXS data were collected on the DORIS III beamline (PETRA III storage ring) at Deutsches Elektronen-Synchrotron (DESY), EMBL in Hamburg by Dr. Halina Mikolajek and analysed by the author, using the ATSAS software package (Konarev et al., 2006).

A series of experiments were conducted on samples at concentrations between 1.8 mg/mL and 7 mg/mL at both 1:1 and 1:10 ratios of Ca^{2+}/CaM to $eEF2K_{82-100}$. During experimental collection some parameters are calculated, as described and defined in Section 1.7.2 and shown for the Ca^{2+}/CaM and $eEF2K_{82-100}$ data in Table 10. These parameters include the radius of gyration (Rg), which is defined as the distance or distribution of the constituents of an object around an axis, which is at the centre of mass of the object. This is an important parameter that SAXS experiments can determine to approximate the size of an object. Firstly, because the Rg is sensitive to aggregates, determining Rg as a function of concentration provides information about aggregation. Secondly, once aggregation has been ruled out, Rg can give information on the size of an object, in this case the Ca^{2+}/CaM: $eEF2K_{82-100}$ molecule. In terms of Ca^{2+}/CaM, the Rg is useful as it can distinguish between an open and extended conformation, as is characteristic of free Ca^{2+}/CaM, and a closed and compact structure that is classically attributed to Ca^{2+}/CaM: peptide complexes.

Another parameter called the D_{max} was determined and is the point where the distance distribution (or pair correlation) function goes to zero and is described in Section 1.7.2. This corresponds to the maximum length of the object. The D_{max} can be used in conjunction with the Rg to give the first information on the shape of the molecule.

The experimental molecular weight (Mw) is also given as well as the volume in nm^3 of the molecule, which is further useful information to determine if there is aggregation in the sample. Information is also provided on the quality of the data collected, as described in Section 1.7.2. A quality score of above 50% is determined as acceptable. These parameters were taken into account to decide which concentrations and data sets to take through into further SAXS

analysis and to calculate a structural model. One data set at a 1:1 ratio and one data set at a 1:10 ratio were selected.

The concentration of 2.5 mg/mL was decided as the concentration to be carried forward for further analysis. At higher concentrations, the protein showed signs of aggregation. This can be seen for the data collected at 5 mg/mL and a 1:1 ratio (data ref: 6), which has a M_w of 35 kDa, significantly higher than would be expected for Ca^{2+}/CaM at 16.9 kDa and $eEF2K_{82-100}$ at 2.29 kDa. The scattering intensity at zero angle (I(0)) is particularly sensitive to aggregation, with an increased I(0) value being indicative of and evidence for aggregation. At 5 mg/mL, the I(0) increases significantly for the 1:1 data, indicating aggregation. An interesting point to note is that for the 1:10 data, at concentrations higher than 2.5 mg/mL the I(0) decreases, meaning that an increase in concentration yields a decrease in I(0). This differs from what is seen for the 1:1 ratio. A probable explanation for this is that there is significant scattering of the free peptide, due to the large excess in the sample, which is biasing the values more towards the small peptide than the larger Ca^{2+}/CaM. This could also explain the similar observations for the M_w and Vol, which also show a decrease as the concentration increases.

In addition, 2.5 mg/mL is also comparable across the two different ratios, as this concentration was collected at both 1:1 and 1:10 ratios. Through investigation of the quality scores, one of the sets of data collected for 1:1 ratio at 2.5 mg/mL was selected (data ref: 3) for comparison with the 2.5 mg/mL data for the 1:10 ratio (data ref: 7). Data ref 3 had the highest quality score than the other data files collected at the same concentration.

Table 10. SAXS parameters collected at 1:1 and 1:10 ratios of Ca^{2+}/CaM to $eEF2L_{82-100}$ and at varying concentrations.

	1:1						1:10			
	1.8mg/mL	2.5mg/mL			3.3mg/mL	5mg/mL	2.5mg/mL	3.5mg/mL	5mg/mL	7mg/mL
Data ref.	1	2	3	4	5	6	7	8	9	10
Rg (nm)	1.92 ± 0.04	1.98 ± 0.12	1.98 ± 0.08	1.97 ± 0.18	1.91 ± 0.02	2.00 ± 0.02	2.08 ± 0.14	2.00 ± 0.04	2.08 ± 0.05	2.04 ± 0.02
I (0)	21.71	19.27	19.42	17.58	22.29	37.71	18.67	11.02	15.8	11.3

Dmax (nm)	6.4	6	6	6.2	6	6.2	6.4	7.0	6.7	6.5
Vol (nm^3)	31	40	39	49	33	13	44	12	37	12
Mw (kDa)	20	18	18	16	21	35	17	10	15	11
Quality (%)	77	65	76	69	80	85	75	78	77	79

Rg and Dmax are larger for the data collected at a 1:10 ratio compared to a 1:1 ratio. The volume is also larger for the 1:10 ratio and so taken together this suggests that the size of the molecule at a 1:10 ratio is larger. Analysing the experimental scattering curves for both data sets in Figure 80, there is no evidence of aggregation at the concentrations chosen and we see that the curves are similar across the two data sets. The distance distribution functions are also shown in Figure 80 and demonstrate the characteristic shape of a dumbbell shaped molecule - a large first peak is followed by a smaller second peak. For the 1:1 data, the height of the first peak is twice the height of the second peak, which is located at twice the distance of the first peak. The second peak appears to be slightly smaller for the 1:10 data compared to the 1:1 data and is also located further away. This indicates that the two domains are located closer together in space when the ratio of Ca^{2+}/CaM to $eEF2K_{82-100}$ is 1:1, compared to when it is 1:10. At a 1:10 ratio the distance distribution function suggests the molecule is more extended, with the domains positioned further apart. This is consistent with the values in Table 11, which also suggest the Ca^{2+}/CaM: $eEF2K_{82-100}$ complex is larger and more extended when a ten-fold excess of $eEF2K_{82-100}$ is present.

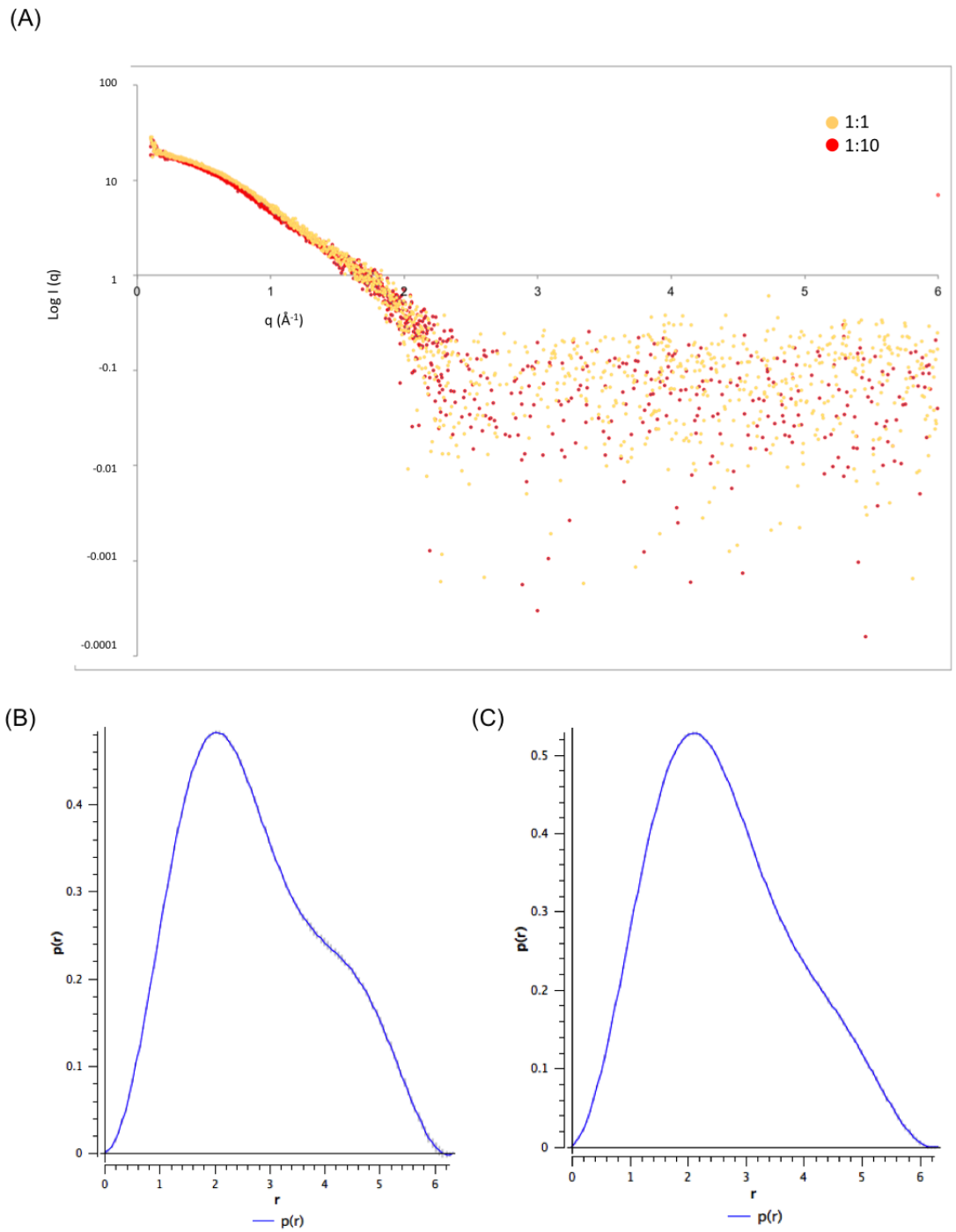

Figure 80. SAXS data at 1:1 and 1:10 ratios of Ca^{2+}/CaM to $eEF2L_{82\text{-}100}$.
Experimental scattering curves at a 1:1 ratio (orange) and at a 1:10 ratio (red) (A) and distance distribution functions at 1:1 (B) and 1:10 (C) ratios.

Theoretical Rg values can be calculated for structures of Ca^{2+}/CaM: target peptide complexes solved by X-ray crystallography. An Rg of 1.68 nm was calculated for a complex between Ca^{2+}/CaM and the hydrophobic IQ domain of the cardiac Ca(v)1.2 calcium channel (PDB ID: 2F3Y). This is significantly lower than the experimental Rg value determined for the Ca^{2+}/CaM: $eEF2K_{82\text{-}100}$

complex, as shown in Table 12. SAXS data was also collected for free Ca^{2+}/CaM, which showed an Rg value of 2.50 and is included in Table 12. The Rg for the Ca^{2+}/CaM: $eEF2K_{82-100}$ complex is therefore smaller than free Ca^{2+}/CaM but larger than other Ca^{2+}/CaM: target peptide complexes. This suggests that the size of the Ca^{2+}/CaM: $eEF2K_{82-100}$ complex is somewhere in between that of free Ca^{2+}/CaM and other known Ca^{2+}/CaM: target peptide complexes.

Table 11. Calculated and experimental Rg values for Ca^{2+}/CaM: target peptide complexes.

Ca^{2+}/CaM: target peptide complex	Experimental Rg (nm)	Calculated Rg (nm)
Ca^{2+}/CaM: $eEF2K_{82-100}$ complex (1:1 data)	1.98	-
Ca^{2+}/CaM: $eEF2K_{82-100}$ complex (1:10 data)	2.08	-
Ca^{2+}/CaM	2.50	-
Ca^{2+}/CaM: hydrophobic IQ domain of the cardiac Ca(v)1.2 calcium channel (2F3Y)	-	1.68

The ATSAS software package was used to perform modelling based on the SAXS scattering results for data collected at the 1:1 ratio and at the 1:10 ratio. *Ab initio* models were created using DAMMIF (Franke and Svergun, 2009) and DAMAVER (Volkov and Svergun, 2003), as described in Section 2.4.6.2. These models are shown in Figure 81. Consistent with the parameters shown in Table 10, the *ab initio* model for the data at a 1:1 ratio is slightly smaller than the model for the data at a 1:10 ratio.

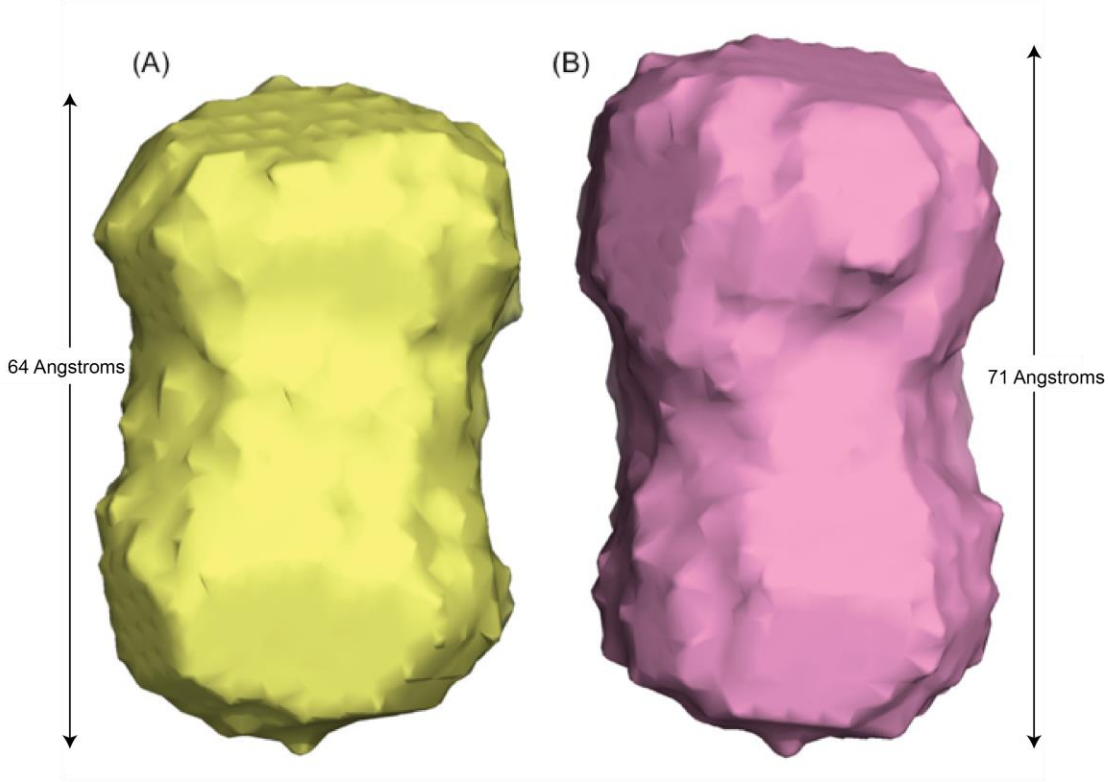

Figure 81. *Ab initio* models of Ca^{2+}/CaM.
Average *ab initio* model produced by DAMAVER from 10 models for Ca^{2+}/CaM at a 1:1 ratio with $eEF2K_{82-100}$ (A) and 1:10 ratio (B).

5.4 Combining SAXS and RDC data to study the Ca^{2+}/CaM: $eEF2K_{82-100}$ complex

The information gained from SAXS and RDC experiments was combined through the process of rigid body modelling. This was carried out using CORAL (Petoukhov and Svergun, 2005), which incorporated the domain orientations defined by RDC data with the scattering intensity from SAXS experiments.

Rigid body modelling was carried out for Ca^{2+}/CaM, whilst $eEF2K_{82-100}$ was not included in the modelling process. $eEF2K_{82-100}$ is only 19 residues in length with a Mw of 2.29 kDa and therefore does not have a great influence on the model due to the relatively low resolution of SAXS data. The resulting models are shown in Figure 82, with the rigid body and *ab initio* models overlaid. An NSD (normalised spatial discrepancy) value measures the fit of the rigid body model to the *ab initio* model. For the four models shown in Figure 82, the NSD value was between 0.95 and 0.97, meaning that the models were similar. Visually, some seem to fit better than others, as shown in Figure 82.

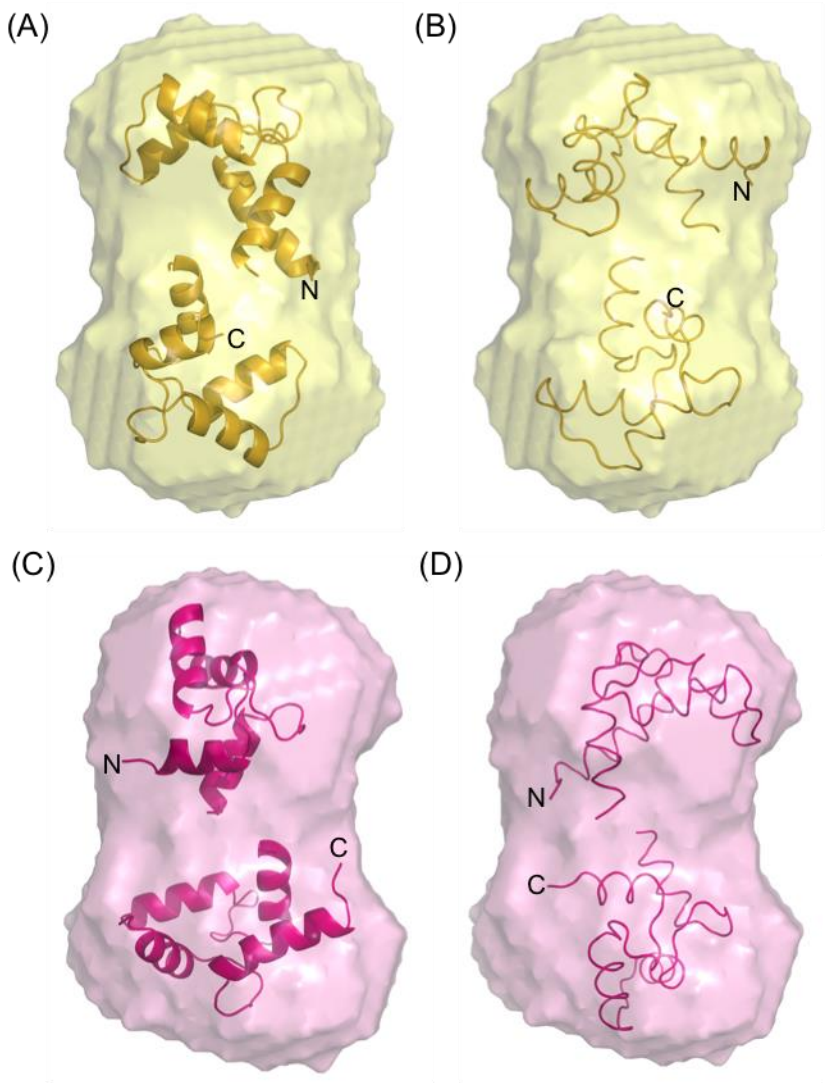

Figure 82. Overlays of rigid body and *ab initio* models of Ca^{2+}/CaM in the presence of $eEF2K_{82-100}$.

Overlays produced by SUPCOMB (Kozin and Svergun, 2001) from *ab initio* and rigid body models of the two possible orientations of the CaM domains with respect to each other for the 1:1 ratio (A and B) and 1:10 ratio (C and D) of Ca^{2+}/CaM and $eEF2K_{82-100}$. The two possible orientations are derived from RDC data and degenerate rotations based on the alignment tensors. No rotation (A), rotation about the z-axis (B), rotation about the y-axis (C) and rotation about the x-axis (D).

Residues of Ca^{2+}/CaM that show significant CSPs upon addition of a ten-fold excess of $eEF2K_{82-100}$ were mapped, as described in Section 4.3. In addition, a binding site has been mapped for the 1:1 data (Appendix 16). The location of these residues can be mapped on to the rigid body models produced from SAXS and RDC data to visualise the binding sites of the N- and C-terminal domains, as shown in Figure 83. For the 1:10 data the binding sites are facing away from

each other, which is inconsistent with the CSP data as the peptide would be unable to contact both binding sites, across the two domains. The domain orientations for the 1:1 data are more favourable, however the orientations are still not consistent with the CSP defined binding sites, unless the peptide is in an unusual configuration.

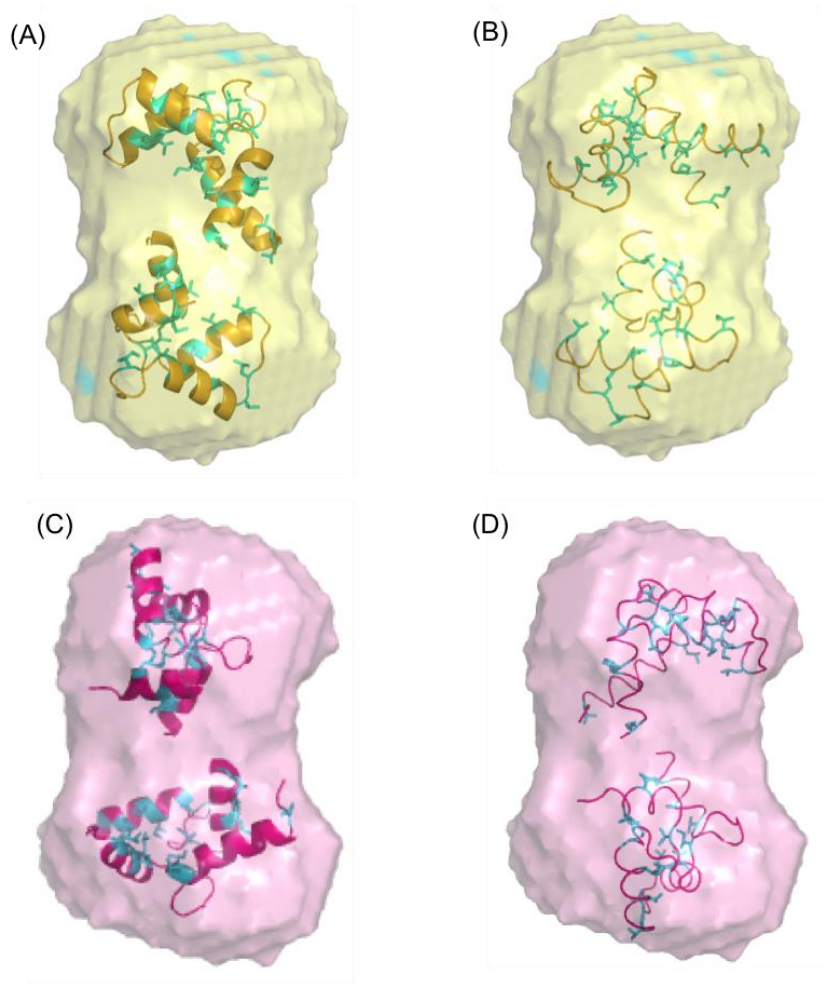

Figure 83. Overlays of rigid body and *ab initio* models of Ca^{2+}/CaM in the presence of $eEF2K_{82-100}$ with residues that show significant CSP's highlighted.

Overlays as in Figure 82 for the models of the two possible orientations of the CaM domains with respect to each other for the 1:1 ratio (A and B) and 1:10 ratio (C and D) of Ca^{2+}/CaM and $eEF2K_{82-100}$. The two possible orientations are derived from RDC data and degenerate rotations based on the alignment tensors and those residues that show significant CSP's are shown in cyan. No rotation (A), rotation about the z-axis (B), rotation about the y-axis (C) and rotation about the x-axis (D).

5.4.1 RDC and SAXS analysis using the NOE-derived structure of the Ca^{2+}/CaM: eEF2K_{82-100} complex

Chapter 6 will describe the elucidation of the three-dimensional structure of the Ca^{2+}/CaM: eEF2K_{82-100} complex determined by NMR structure calculation using NOEs. The same RDC and SAXS data analysis just described was carried out using the NOE-derived structure, rather than the crystal structure of Ca^{2+}/CaM bound to the hydrophobic IQ domain of the cardiac ca(v)1.2 calcium channel (PDB ID: 2F3Y).

The alignment tensor values determined, differed from those previously determined using the crystal structure for the same experimental data. Table 12 shows that the strength of alignment, as described by Aa and Ar, differs across the two domains of Ca^{2+}/CaM, when either the calculated structure or the reference structure from the Protein Data Bank are used. This indicates that the domains of Ca^{2+}/CaM do not align as a single unit, meaning that there are dynamics present between the domains, with the two domains able to move relative to each other. The χ^2 per residue is much higher for the NOE-derived structure, demonstrating that the correlation between the back-calculated and experimental RDC values is not as defined as for the crystal structure. This is also shown in Figure 84 by the correlation plots themselves, for the N- and C-terminal domains. Fr the N-terminal domain the correlation coefficient is 0.80 and for the C-terminal domain is 0.91.

Table 12. Alignment tensor values determined by correlation with the NOE-derived Ca^{2+}/CaM: eEF2K_{82-100} complex.

	Ca^{2+}/CaM bound to the hydrophobic IQ domain of the cardiac ca(v)1.2 calcium channel (PDB ID: 2F3Y)		**Ca^{2+}/CaM: eEF2K_{82-100} complex**	
	N-terminal domain	**C-terminal domain**	**N-terminal domain**	**C-terminal domain**
α (°)	30.8 (± 1.6)	-41.0 (± 0.9)	109.1 (± 1.1)	-171.0 (± 1.3)
β (°)	104.6 (± 0.3)	57.9 (± 0.4)	70.4 (± 0.8)	78.5 (± 0.4)
γ (°)	81.4 (± 0.6)	52.8 (± 0.4)	136.7 (± 0.6)	106.6 (± 0.7)
Aa	3.5 (± 0.07)	4.7 (± 0.06)	-2.4 (± 0.05)	3.3 (± 0.06)
Ar	1.0 (± 0.07)	1.8 (± 0.04)	-1.6 (± 0.04)	1.0 (± 0.06)
χ^2 per residue	5.88	9.43	18.60	14.86

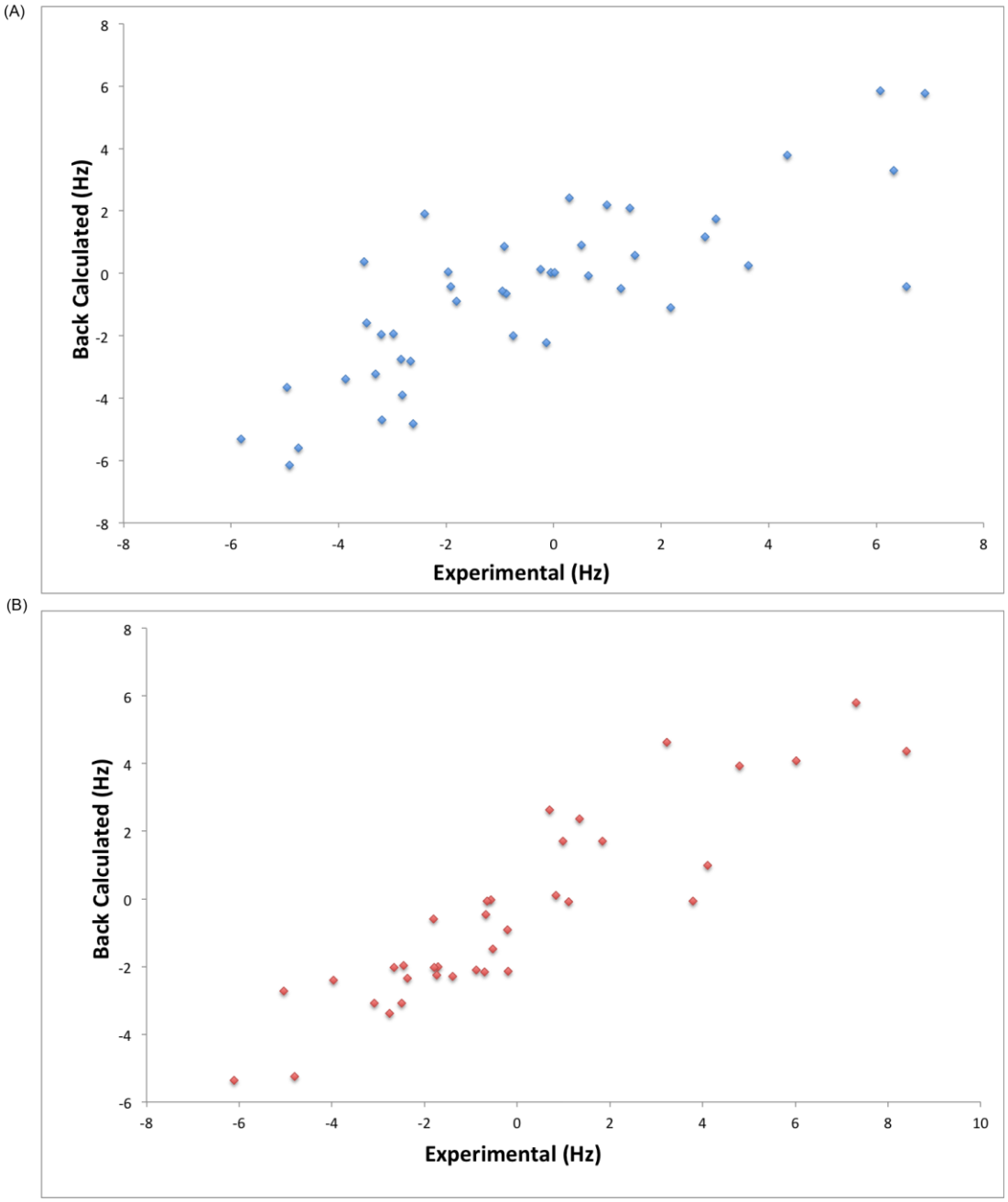

Figure 84. Correlation plots between experimental RDC values and back calculated values from the Ca^{2+}/CaM: $eEF2K_{82-100}$ complex.

Correlation plots for the N-terminal domain of Ca^{2+}/CaM (A) and the C-terminal domain (B). Back-calculated values obtained from calculated structure of the Ca^{2+}/CaM: $eEF2K_{82-100}$ complex.

The two modules were aligned according to the two alignment tensors to determine the orientation of the two modules with respect to each other. The four degenerate alignments, generated by 180° rotations around the x-, y- and z-axes, were performed and are shown in Figure 85. Only two of these

degenerate orientations are possible - no rotation and 180 ° rotation about the y-axis. It is these two models which can then be analysed further in combination with SAXS data to incorporate the domain orientations defined by RDC data with the scattering intensity from SAXS experiments. The x-axis is again especially small for the N-terminal domain alignment tensor, as was the case for the crystal structure derived tensor. This suggests that the alignment tensor is not well defined.

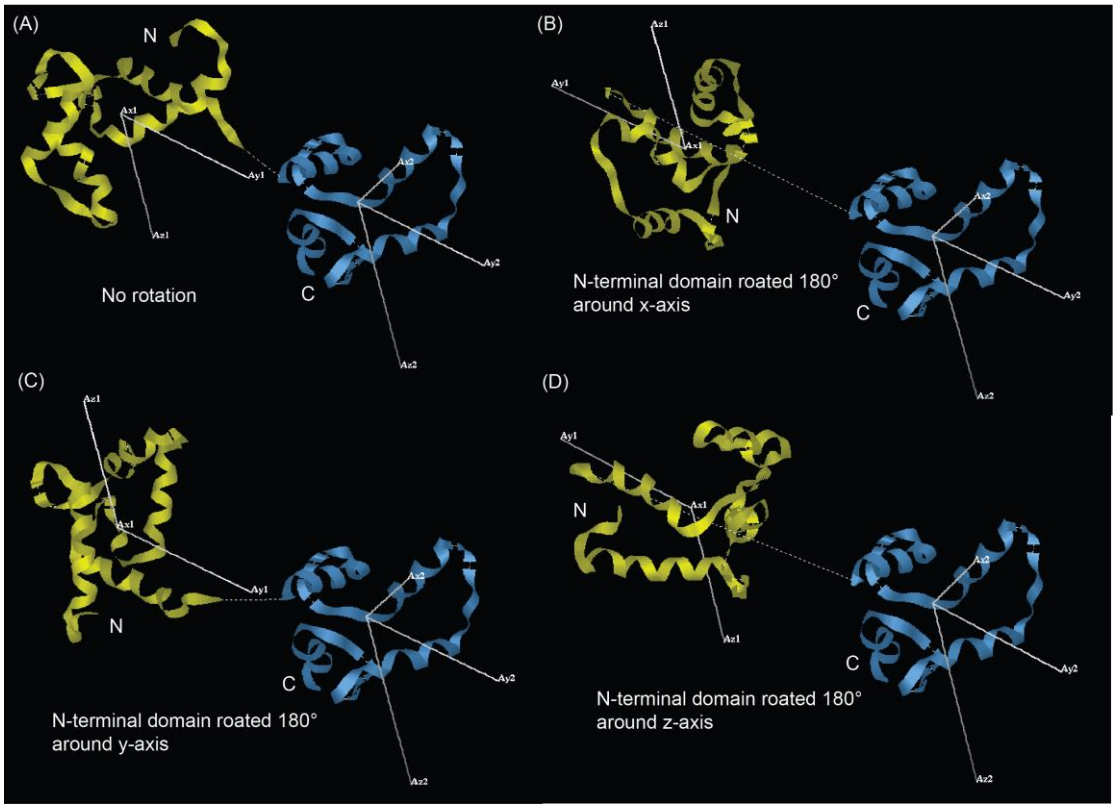

Figure 85. Four possible orientations of the two domains of CaM with respect to each other.

The four possible orientations are derived from four degenerate rotations. These rotations are defined from the alignment tensor values for Ca^{2+}/CaM in the presence of $eEF2K_{82\text{-}100}$ at a 1:1 ratio. Based on correlation with calculated structure of the Ca^{2+}/CaM: $eEF2K_{82\text{-}100}$ complex.

Rigid body modelling using CORAL (Petoukhov and Svergun, 2005) was carried out. The resulting models are shown in Figure 86, with the rigid body and *ab initio* models overlaid. An NSD (normalised spatial discrepancy) value measures the fit of the rigid body model to the *ab initio* model. For both overlays, shown in Figure 86, the NSD value was 0.96, indicating an acceptable fit.

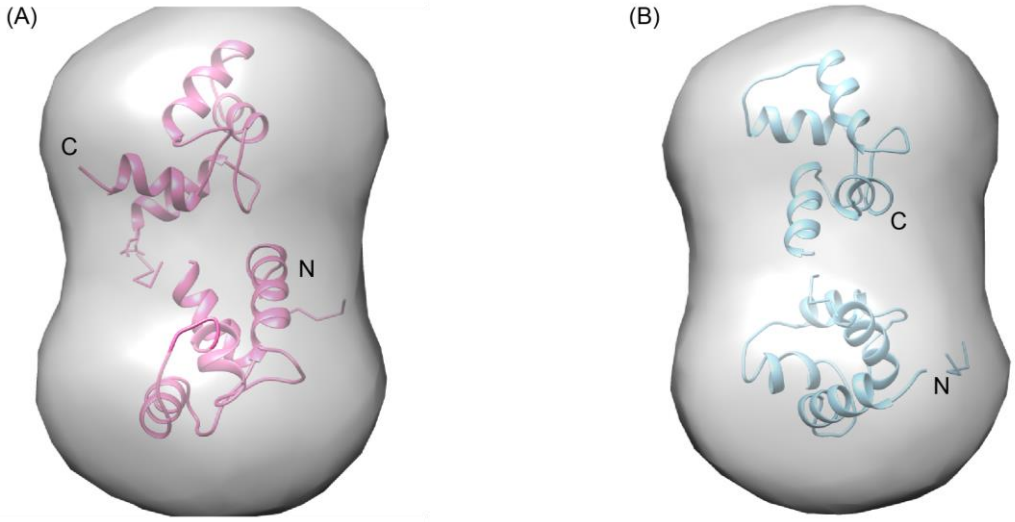

Figure 86. Overlays of rigid body and *ab initio* models of Ca^{2+}/CaM in the presence of $eEF2K_{82-100}$, using the calculated structure.

Overlays produced by SUPCOMB (Kozin and Svergun, 2001) from *ab initio* and rigid body models of the two possible orientations of the CaM domains with respect to each other. The two possible orientations are derived from RDC data and degenerate rotations based on the alignment tensors. No rotation (A), and rotation about the y-axis (B).

5.5 Discussion

This Chapter describes the first information on the structure of the Ca^{2+}/CaM: $eEF2K_{82-100}$ complex obtained by a combination of RDC NMR and SAXS data. The data were collected in both 1:1 and 1:10 ratios and differences were determined between the two data sets, suggesting that Ca^{2+}/CaM undergoes structural changes as the ratio of Ca^{2+}/CaM: $eEF2K_{82-100}$ increases above stoichiometric amounts.

As discussed, there was some difficulty in assigning all peaks on all spectra collected. This was especially true for the spectra collected under anisotropic conditions for the 1:10 data, where there were significant changes in chemical shift. A likely explanation for this is that the large excesses of peptide are interacting with the alignment medium. In the majority of cases there is little interaction between proteins and the chosen alignment medium, however, it has also been noted that proteins can interact with the medium (Higman et al., 2011, Chen and Tjandra, 2012, Tjandra and Bax, 1997). If some

of the peptide is interacting with the media then a ten-fold excess will not have been achieved and so the anisotropic spectrum will differ from the isotropic spectrum.

The RDC measurements were used to determine alignment tensors. The process of obtaining these alignment tensors involved eliminating measurements with low χ^2 values if they were in loop regions of the structure or in other regions likely to be different to the reference structure (PDB ID: 2F3Y). The argument for initial exclusion is the potential variability of the true structure compared to the trial structure for the alignment tensor determination. The effect of each deletion was checked to determine that the inclusion or exclusion did not greatly affect the alignment tensor but lowered the overall χ^2. Dynamics can also have an effect and can generate erroneous RDC values when interpreted against a rigid conformation. The key point is that the alignment tensor does not change significantly if these data are excluded, which is the case with the number of RDC values collected for both 1:1 and 1:10 data. There are also differences between the ways in which the two domains are orientated with respect to each other, hence the two domains were treated separately. Also, we know that the linker between the two domains of Ca^{2+}/CaM is flexible and so the two domains can be orientated independently of each other (Barbato et al., 1992, Chou et al., 2001).

The angles and magnitudes of the alignment tensor indicated that there are interdomain motions and dynamics between the two domains of Ca^{2+}/CaM when bound to $eEF2K_{82\text{-}100}$. This is a well-known feature of Ca^{2+}/CaM, with the interdomain motions having been studied by a number of different methods (Baber et al., 2001, Bertini et al., 2004, Gsponer et al., 2008). The alignment tensor also showed that the molecule aligned more strongly when a ten-fold excess of $eEF2K_{82\text{-}100}$ was present. This is consistent with the fact that larger RDC values were obtained in these conditions, probably as a result of the different alignment medium used compared to the 1:1 ratio data. It could also be consistent with the fact that SAXS data indicates a more elongated Ca^{2+}/CaM complex molecule in the 1:10 conditions, which may align better than a compact molecule.

The SAXS data sets taken through into the modelling stages and incorporation with the RDC measurements showed no sign of aggregation and had high quality scores, indicating that the data were also of high quality.

Ab initio modelling reflected the initial values taken directly from the raw SAXS data. The first interesting point about this data concerns the Rg values. Our SAXS data for the complex gives an Rg value of 1.98 nm for the 1:1 ratio data and 2.08 nm for the 1:10 data, however, this is not consistent with the classic wraparound structure seen for other Ca^{2+}/CaM and peptide complexes and discussed in Section 1.4.4.3. Rg values can be calculated in Chimera (Pettersen et al., 2004) for existing structures and for Ca^{2+}/CaM bound to the hydrophobic IQ domain of the cardiac Ca(v)1.2 calcium channel. (PDB ID: 2F3Y), this value is 1.69, significantly lower than the Rg values calculated from our SAXS data for the Ca^{2+}/CaM: $eEF2K_{82\text{-}100}$ complex. This suggests that the structure of the complex differs from the classic wraparound structure exhibited by other known Ca^{2+}/CaM complex structures. This is not entirely surprising considering the fact that eEF2K contains a CaM recognition sequence that is different from the canonical sequence seen in the vast majority of CaM binding targets. This structural difference is clearly seen following *ab initio* modelling that reveals a shape more consistent with the free Ca^{2+}/CaM structure. Calculating the Rg of PDB ID: 1CLL, an X-ray structure of free Ca^{2+}/CaM, gave a value of 2.24. This indicated that the size of the Ca^{2+}/CaM: $eEF2K_{82\text{-}100}$ complex is in between that of free Ca^{2+}/CaM and the classic wraparound Ca^{2+}/CaM: peptide complex. This is also consistent with results seen for come other CaM complexes, for example, the full length DAPK: CaM complex shows CaM to be in a much more extended conformation (de Diego et al., 2010).

The second interesting point about this data came from comparing the 1:1 and 1:10 ratio data. There are differences between the initial parameters, Rg, Dmax and volume, reflected at the *ab initio* modelling stage. The models produced for the 1:10 data are larger, although they both have the same overall shape. This indicates that as the concentration of $eEF2K_{82\text{-}100}$ increases, there are structural changes within Ca^{2+}/CaM. This is consistent with the observations from the peptide titration discussed in Section 4.3.2, where there

are additional changes in the NMR spectra after the 1:1 ratio is reached. There are also unusual peak patterns and exchange characteristic seen between the 1:1 and 1:10 ratios from the peptide titration, indicative of a more complex binding equilibrium than the simple two-step mechanism. Combining observations from the peptide titration and the differences seen in the SAXS data it seems possible that, as the concentration of $eEF2K_{82\text{-}100}$ increases to beyond the 1:1 ratio, the structure of Ca^{2+}/CaM is altered. As discussed in Section 4.6, this could be for two reasons, there could be a second peptide binding or there could be a binding mechanism involving an intermediate. Partial or double occupancy could be another consideration.

The RDC and SAXS data were combined through rigid body modelling, which positioned the possible domain orientations, derived from RDC data, into the *ab initio* model that represents the SAXS data. Two possible models were generated from each data set. When the two models representing the 1:10 data are examined, it can be seen that a single peptide could not contact both domains. This is because the binding sites in each domain, discussed in Section 4.3, are orientated in such a way that they are facing away from each other. A single peptide, which is 19 residues long, is therefore unlikely to cause the CSP's shown in Figure 83 on both domains at once. This suggests that, as concentrations of $eEF2K_{82\text{-}100}$ reach a ten-fold excess, the two domains open up and get further away from each other, allowing a peptide to bind to each domain. This is consistent with the SAXS parameters (Rg and Dmax) which suggest a more open conformation for Ca^{2+}/CaM. Looking at the models in Figure 83, two peptides, one bound to each domain, could cause the CSP's seen in Chapter 4, whereas one peptide could not. This is consistent with the differences in Rg and Dmax seen between the two different data sets and also with observations made during the peptide titration.

In the cell there will not be an excess of eEF2K to Ca^{2+}/CaM, as the concentration of eEF2K is much lower than free CaM. Black et al (2004) determined an intracellular available CaM concentration of 8.8 +/- 2.2 μM under resting conditions in a human kidney cell line (Black et al., 2004). In addition Ca^{2+}/CaM will interact with a large array of target proteins to initiate a

number of different cellular signalling pathways. The amount of eEF2K will thus never reach these excesses compared to free CaM in the cell and so this 1:10 complex, possibly with two peptides bound, is not representative of the biological interaction between eEF2K and Ca^{2+}/CaM. Initially, a ten-fold excess was used to ensure the bound state was reached. Results presented in Chapter 4, and here in Chapter 5, demonstrate that this is reached with equal amounts of $eEF2K_{82-100}$ and Ca^{2+}/CaM, and a stoichiometric complex is formed.

Alignment tensors were determined from the 1:1 RDC data using a crystal structure of Ca^{2+}/CaM bound to a target peptide with an IQ motif and an NOE-derived structure of the Ca^{2+}/CaM: $eEF2K_{82-100}$ complex. In both of these cases the x-axis of the N-terminal domain alignment tensor was very small. This means that the tensor is not well defined as the two other axis are liable to flip. This means that the domain orientations derived from these RDC data may not represent the correct interdomain orientations. Importantly, the domain orientations we see as a result of RDC measurements are inconsistent with our CSP analysis that defined binding sites in each of the CaM domains. These in turn reflect observations from previously determined CaM: target peptide complex structures. Also, Chapter 6 will detail the elucidation of an NOE-derived structure of the Ca^{2+}/CaM: $eEF2K_{82-100}$ complex, which differs from the domain orientations from RDC analysis. It seems likely therefore that in this case the RDC data are insufficient for the determination of an interdomain orientation.

RDC measurements were collected in one alignment media for each data set. Ideally, more than one alignment media should be used to obtain different alignment tensors for each data set. A study by Bax and Grishaev (2005) showed that when only one RDC is measured per residue, the model can be adjusted to fit these measurements. In this way the model may not reflect the correct structure or the couplings. (Bax and Grishaev, 2005). For this reason the RDC data were not included in further structural studies.

In conclusion, the combination of RDC and SAXS data of the Ca^{2+}/CaM: $eEF2K_{82-100}$ complex was insufficient to fully explain the interaction between

CaM and eEF2K. Importantly, there are also inconsistencies between the RDC and CSP data. The data presented in this chapter agrees with previous findings from the peptide titration that the 1:1 data better represents the physiological, stoichiometric complex, with one peptide bound to one molecule of Ca^{2+}/CaM. Therefore, further structural studies will focus on data collected with stoichiometric amounts of $eEF2K_{82-100}$ and Ca^{2+}/CaM to avoid driving the equilibrium into this second state, which likely represents two peptides bound to a single Ca^{2+}/CaM molecule.

Chapter 6. Solution structure of the Ca^{2+}/CaM: $eEF2K_{82-100}$ complex determined by NMR

6.1 Introduction

Three-dimensional protein structures provide a wealth of information. The structure of a protein complex is especially important in understanding protein interactions. The interaction between Ca^{2+}/CaM and eEF2K triggers the activation of eEF2K but what are the molecular details of this interaction? It is important to understand the interaction to learn about the mechanism of activation of eEF2K.

After having determined a number of characteristics of the interaction (Chapter 4) and the overall shape of the complex (Chapter 5) we proceeded to calculate the solution structure of the Ca^{2+}/CaM: $eEF2K_{82-100}$ complex.

Chapters 4 and 5 also show that data collected at a 1:1 ratio of Ca^{2+}/CaM and $eEF2K_{82-100}$ reflects the bound protein complex, therefore NMR data collected at this ratio was used for the solution structure calculation. We have elucidated the structure of the protein complex, providing insight into the atomic details of the binding of eEF2K to Ca^{2+}/CaM. This detailed information is extremely important in understanding the interaction and resultant activation of eEF2K.

The activation of eEF2K is an important process in cancer biology and has been proposed as a possible intervention point for developing new cancer therapies. Determining the structure of the complex is an important step in understanding the interaction between Ca^{2+}/CaM and eEF2K, providing information for drug discovery studies to try and develop a compound that could target this interaction in the treatment of cancer. Since the recognition motif does not conform to any known, canonical CaM-binding sequences, the structure is also interesting in terms of studying CaM: target interactions and may enhance our understanding of CaM target recognition in general.

Chapter 1, especially Section 1.5.6, described the how pH and hypoxia affect eEF2K activity. The elucidation of the three-dimensional structure of the Ca^{2+}/CaM: $eEF2K_{82-100}$ complex means that we can study these effects and provide a structural explanation for some of these observations.

Mechanistic studies in the laboratory of Prof. Chris Proud have investigated the effect of specific mutations in the CaM binding region of eEF2K, in order to study the mechanism of eEF2K activation and the effects of pH and hypoxia. A summary of those mutations and their effects on eEF2K activation and Ca^{2+}/CaM-binding is shown in Table 13. In this chapter, the three-dimensional structure of the Ca^{2+}/CaM: $eEF2K_{82-100}$ complex will be used to investigate the activity of eEF2K, in reference to these mutations and effects.

Table 13. Summary of eEF2K mutations in the CaM-binding region of eEF2K that have been studied, including their effects on eEF2K activity and CaM-binding.

Mutation	Effect on eEF2K activity	Effect on binding
W85A	Not determined	↓
W85G	DEAD	Not determined
W99A	↓	↓
P96A	↓	↓
P98A	↓	↓
H87K	↑	↑
H94K	↑	↑
H87A	↓	↓
H90A	↓	↓

6.2 Resonance assignment

6.2.1 Resonance assignment of Ca^{2+}/CaM bound to $eEF2K_{82-100}$ (1:1 ratio)

The first stage of an NMR structure calculation is to assign as many atoms as possible in the protein. In terms of a protein complex, this involves assigning both components - Ca^{2+}/CaM and $eEF2K_{82-100}$. Ca^{2+}/CaM was assigned in the bound form in Chapter 3, in the presence of a ten-fold excess of $eEF2K_{82-100}$, however, a resonance assignment is needed for the complex at a 1:1 ratio.

To assign the backbone and side chain resonances of Ca^{2+}/CaM, the same basic protocol was followed as described in sections 2.5.2 and 3.4. The backbone resonance assignment is shown in Figure 87.

Apart from the two proline residues, 100% of the backbone resonances have been assigned. For previous resonance assignments only those side chains containing methyl groups were assigned, as only these were needed for the CSP

analysis. For the structure calculation, as many assignments as possible are necessary. Of the protons in Ca^{2+}/CaM, 86% have been assigned, 79% of the carbon atoms and 82% of the nitrogen atoms.

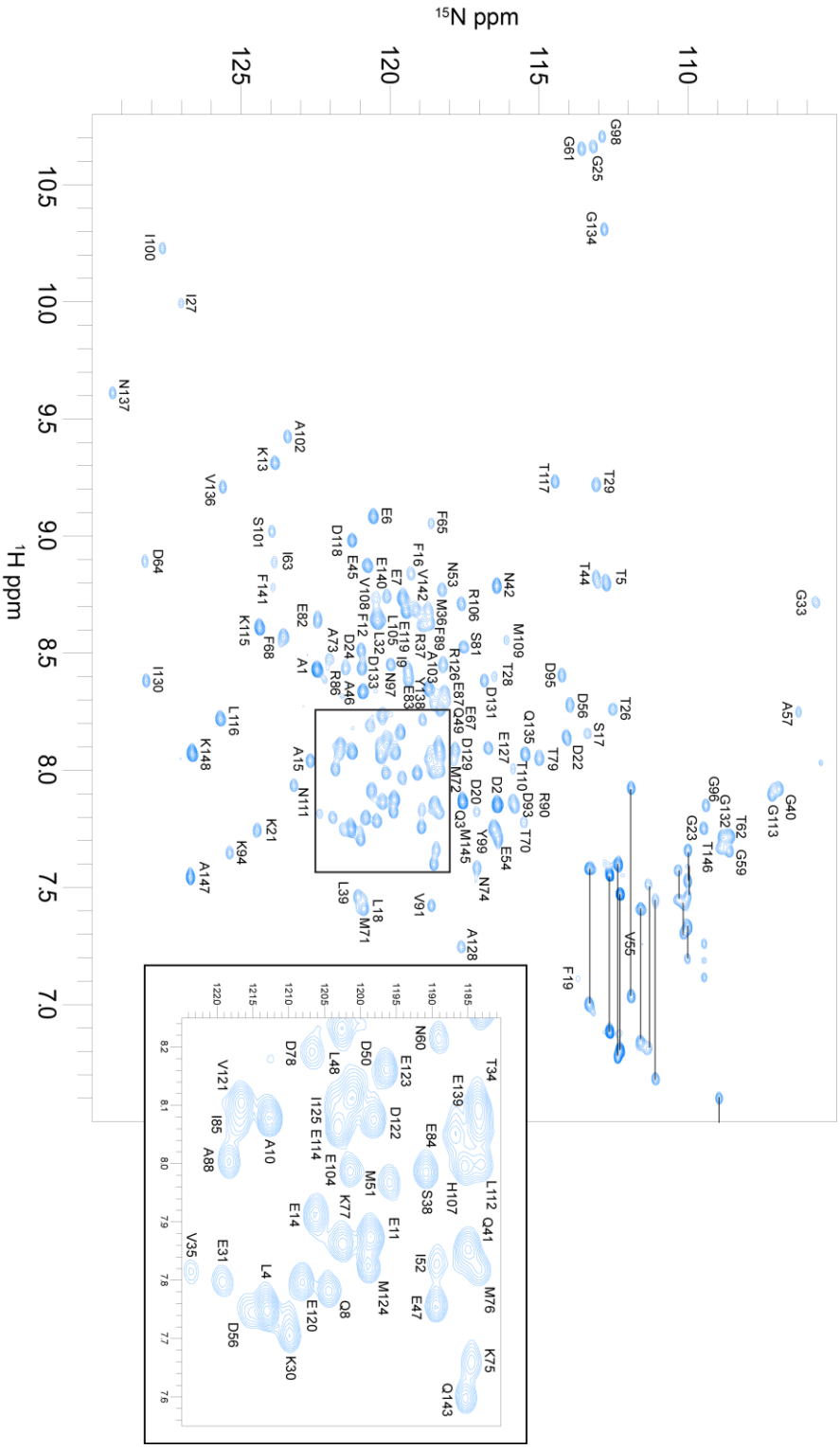

Figure 87. Assigned ^{1}H-^{15}N-HSQC spectrum of Ca^{2+}/CaM: eEF2K$_{82\text{-}100}$ complex (1:1 ratio)

^{1}H-^{15}N-HSQC spectrum of the Ca^{2+}/CaM: eEF2K$_{82\text{-}100}$ complex, at a 1:1 ratio, with peaks labelled as a result of resonance assignment, according to the amino acid residue they represent. Double peaks that correspond to side chain NH_2 groups are marked with joining solid lines. Those peaks which have been folded are labelled in grey. Buffer conditions are as described in Section 2.5.8.1.

The ^{1}H-^{15}N-HSQC and ^{1}H-^{13}C-HSQC spectra collected for the 1:1 Ca^{2+}/CaM: $eEF2K_{82-100}$ data are similar but distinct from those collected for the 1:10 data, as shown in Figure 88. The fact that there are differences between the spectra for the different ratios is consistent with the findings in Chapter 4 and Chapter 5. The differences indicate that the structure of the complex varies at the different peptide concentrations. The changes in peak position have been demonstrated for the ^{1}H-^{13}C-HSQC spectra overlay in Figure 88. The majority of methyl groups are located in the same positions in the two spectra. However, there are a significant number (labelled and shown with arrows) that change peak position between the two different peptide concentrations. All of these resonances correspond to residues of the N-terminal domain and linker region of Ca^{2+}/CaM. Again, this is consistent with observations made in Chapters 4 and 5.

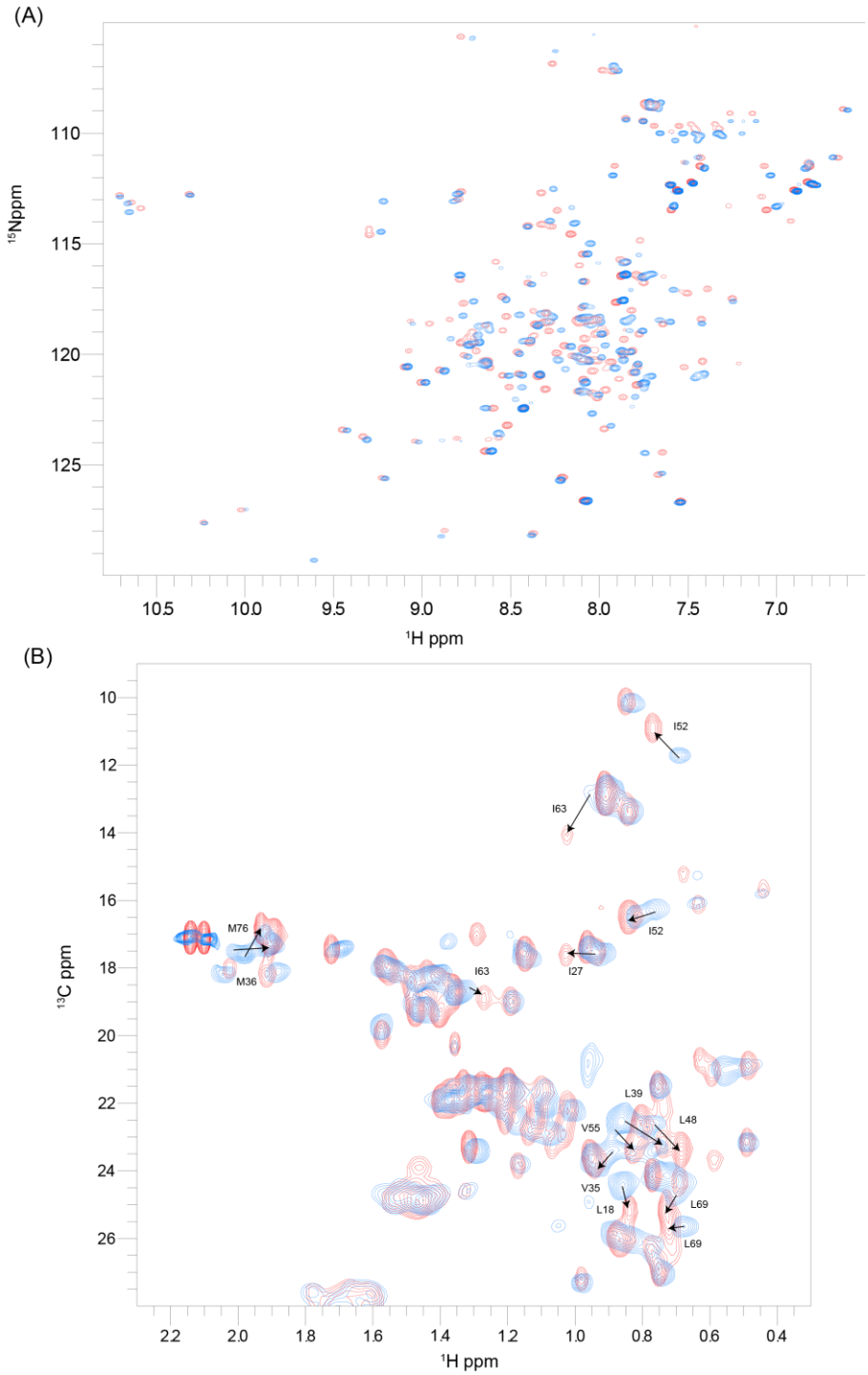

Figure 88. Overlay of ^{1}H-^{15}N-HSQC and ^{1}H-^{13}C-HSQC spectra of the Ca^{2+}/CaM: eEF2K$_{82\text{-}100}$ complex collected at 1:1 and 1:10 ratios of Ca^{2+}/CaM and eEF2K$_{82\text{-}100}$.

^{1}H-^{15}N-HSQC spectra of the Ca^{2+}/CaM: eEF2K$_{82\text{-}100}$ complex collected at a 1:1 ratio (blue) and 1:10 ratio (red) of Ca^{2+}/CaM and eEF2K$_{82\text{-}100}$ (A). ^{1}H-^{13}C-HSQC spectra of the Ca^{2+}/CaM: eEF2K$_{82\text{-}100}$ complex collected at a 1:1 ratio (blue) and 1:10 ratio (red) of Ca^{2+}/CaM and eEF2K$_{82\text{-}100}$ with those residues which experience a significant change in peak position labelled (B). Buffer conditions are as described in Section 2.5.8.1.

The side chain atom assignment was carried out as described in Section 3.4.2. In addition to this, the protons of aromatic side chains were assigned in order to accurately calculate the structure of the Ca^{2+}/CaM: $eEF2K_{82-100}$ complex. hbCBcgcdceHE and hbCBcgcdHD experiments were used which correlate the chemical shifts of the aromatic protons (hδ and hε) with the chemical shift of the Cβ atom, therefore if the Cβ atom was assigned and had a distinct chemical shift then the Hδ and Hε atoms could also be assigned. The result of this assignment is shown in Figure 89.

An interesting point to note from this spectrum is the presence of multiple peaks with a Cβ shift of approximately 30 ppm. Peaks corresponding to histidine residues will also be present on this spectrum and these peaks correspond to His^{107}, which has a Cβ shift of 29.96 ppm. The fact that there are multiple peaks here, when there is only a single histidine residue in Ca^{2+}/CaM, suggest that there is some conformational heterogeneity.

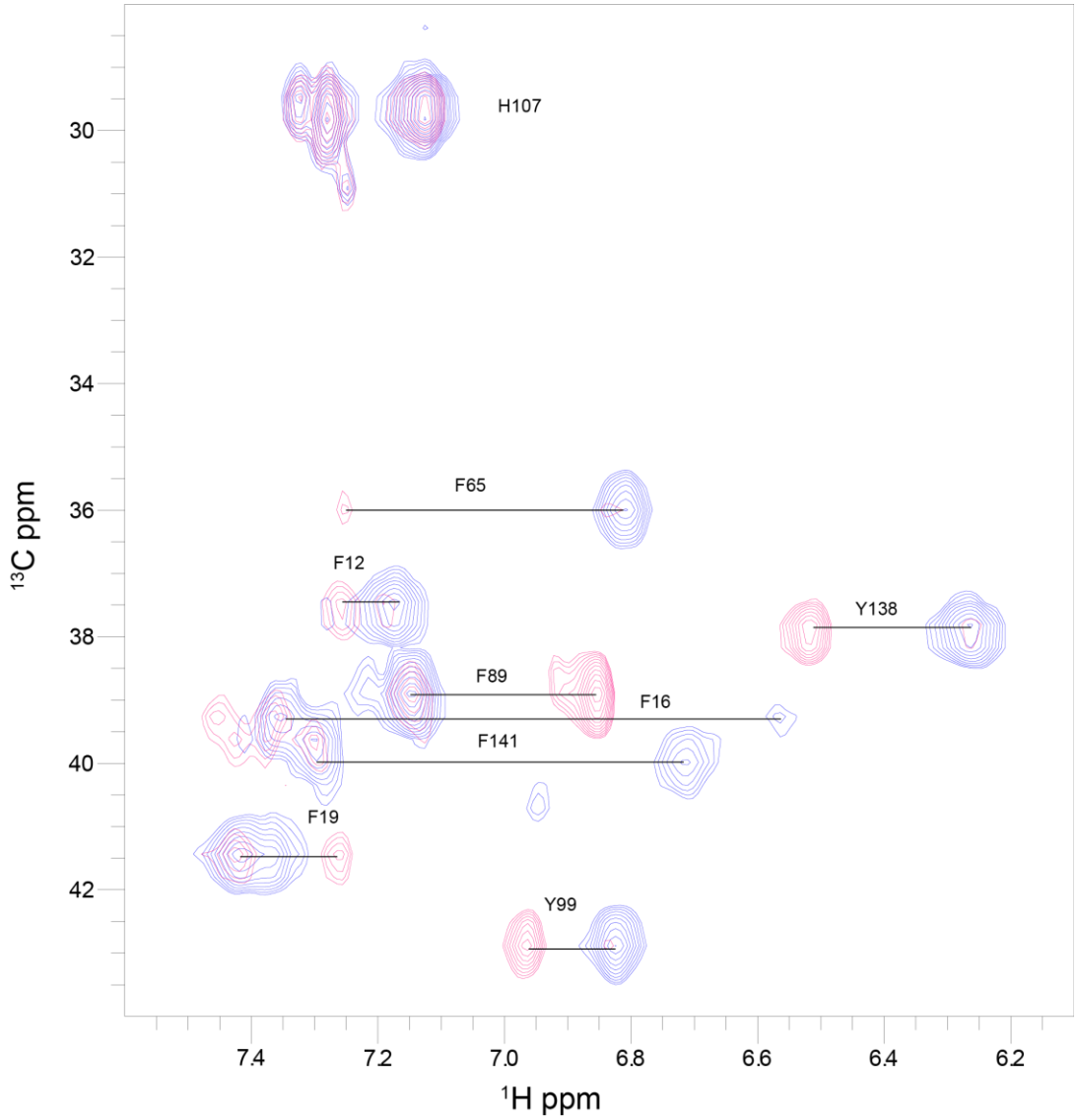

Figure 89. Assigned hbCBcgcdceHE and hbCBcgcdHD spectra.

hbCBcgcdceHE (pink) and hbCBcgcdHD (blue) spectra with those residues that could be assigned labelled. The hδ and hε peaks are joined by black lines and labelled with their corresponding residue. The peaks at the top of the spectrum represent His^{107}, which has a Cβ shift of 29.96.

6.2.2 Resonance assignment of eEF2K$_{82\text{-}100}$ bound to Ca^{2+}/CaM

Assigning the resonances of eEF2K$_{82\text{-}100}$ is more complex as the peptide is unlabelled and therefore cannot be detected by the conventional NMR methods previously described. Isotope-filtered experiments were used to eliminate signal from the ^{15}N and ^{13}C labelled Ca^{2+}/CaM to leave signal that originated from ^{12}C and ^{14}N nuclei, which corresponds to eEF2K$_{82\text{-}100}$ resonances. In this experiment, ^{15}N-H. ^{13}C-H, ^{14}N-H and ^{12}C-H resonances were excited but only (^{14}N)-H and (^{12}C)-H resonances were detected.

Two-dimensional proton NOESY and TOCSY experiments with $^{15}N/^{13}C$ filtering in F and F2 dimensions were used in combination to assign as many of the peptides proton resonances as possible. The process of assigning the resonances of $eEF2K_{82\text{-}100}$ is demonstrated in Figure 90. Initially, strips are identified which belong to individual atoms, as shown in Figure 90 by the dashed lines. Those NOESY peaks that do not have an overlaying TOCSY peak are then investigated to see whether they connect two strips together. These connections will be possible for the adjacent amino acid residue, as they will be close in space. Also, if the peptide is helical, then there will be through space connections at (i,i+3) (where i represents and amino acid residue). A number of these connections were identified, including (i,i+3), and these are shown in Figure 90 with solid arrows. Determining these connections meant that strips could be linked together and the resonances assigned.

Resonances were assigned for all residues in $eEF2K_{82\text{-}100}$, except for Met^{95}, Pro^{96} and Pro^{98}. The reason that these residues could not be assigned is due to the presence of prolines here. In total, 78% of the side chain protons were assigned. i+3 connections were identified for each residue throughout the peptide, up until Ala^{92}, which is the first residue to not connect to the residue at i+3. This strongly suggests that the N-terminal and central parts of $eEF2K_{82\text{-}100}$ form an α-helix and that, due to the presence of two proline residues at the C-terminal end of $eEF2K_{82\text{-}100}$, it seems likely that this region is unstructured or experiences multiple conformational states due to cis trans isomerisation.

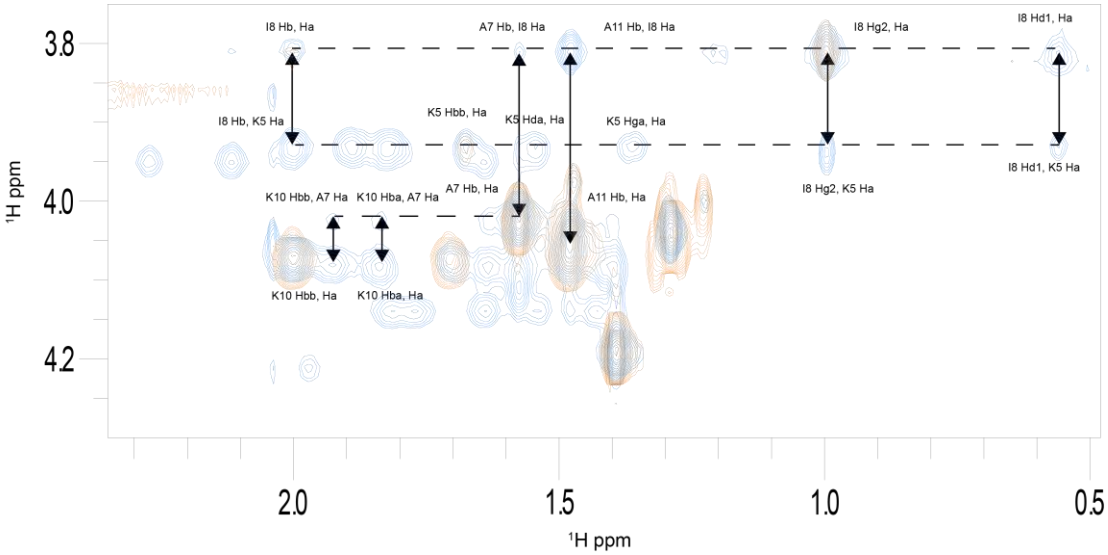

Figure 90. Assignment of proton resonances of eEF2K$_{82\text{-}100}$ using two-dimensional proton NOESY and TOCSY experiments with ^{15}N and ^{13}C filtering in F and F2 dimensions.

Overlay of NOESY (blue) and TOCSY (orange) experiments to demonstrate the method for assigning proton resonances of eEF2K$_{82\text{-}100}$ when bound to Ca^{2+}/CaM. Dotted lines represent the chemical shift of a proton – the top line represents Ile^{8} Hα, the middle line represents Lys^{5} Hα and the bottom line represents Ala^{7} Hα. The vertical arrows show the connections between the chemical shifts that enable assignment. These connections are present for the previous amino acid (i-1) and also, because eEF2K$_{82\text{-}100}$ is a helix, for i+3.

6.3 Secondary structure assignment

Dihedral restraints can aid in structure calculation and so the φ/ψ backbone torsion angles were predicted using TALOS-N (Shen and Bax, 2013). TALOS-N provides empirical prediction of protein backbone φ/ψ torsion angles, side chain χ1 torsion angles and secondary structure using a combination of six kinds (HN, Hα, Cα, Cβ, CO, N) of chemical shift assignments for a given sequence.

The majority of these chemical shifts had already been assigned, as outlined in Section 6.2.1; however, the CO resonances also needed assignment for inclusion in TALOS-N. A HNCO experiment was used for this, which is relatively simple to assign as it correlates the CO chemical shift to the HN chemical shift that has already been assigned. 134 CO resonances were assigned out of 148, resulting in a percentage assigned of 91%.

TALOS-N predicts the secondary structure of the protein based on the assigned chemical shifts. The results of this prediction are shown in Figure 91.

It is clear that there are 8 α-helices predicted for Ca^{2+}/CaM, which is consistent with the known structures of free and bound Ca^{2+}/CaM and is discussed in sections 1.4.3 and 1.4.4. In addition, TALOS-N predicts some small regions of β-strand, just before helices 2, 4, 6 and 8, which is again consistent with known structures of Ca^{2+}/CaM when bound to target peptides. There is also some prediction of a β-strand before helix 7, although this is not as highly predicted as for the other regions.

Importantly, TALOS-N also predicts the protein backbone φ/ψ torsion angles. This was successful for the majority of residues of Ca^{2+}/CaM in complex with $eEF2K_{82-100}$; however, there were some residues that could not be predicted as well as the others. Gln^{41} and Lys^{57} had predictions classified as generous, meaning that they could not be as sure of the prediction. Asp^{56}, Asp^{78}, Thr^{79}, Ser^{81} and Gly^{132} had predictions classified as ambiguous. For all other residues, the predictions were classified as strong. Those predictions that were not classified as strong were not included in the structure calculation. The Table of φ/ψ angles used in the structure calculation is shown in Appendix 18.

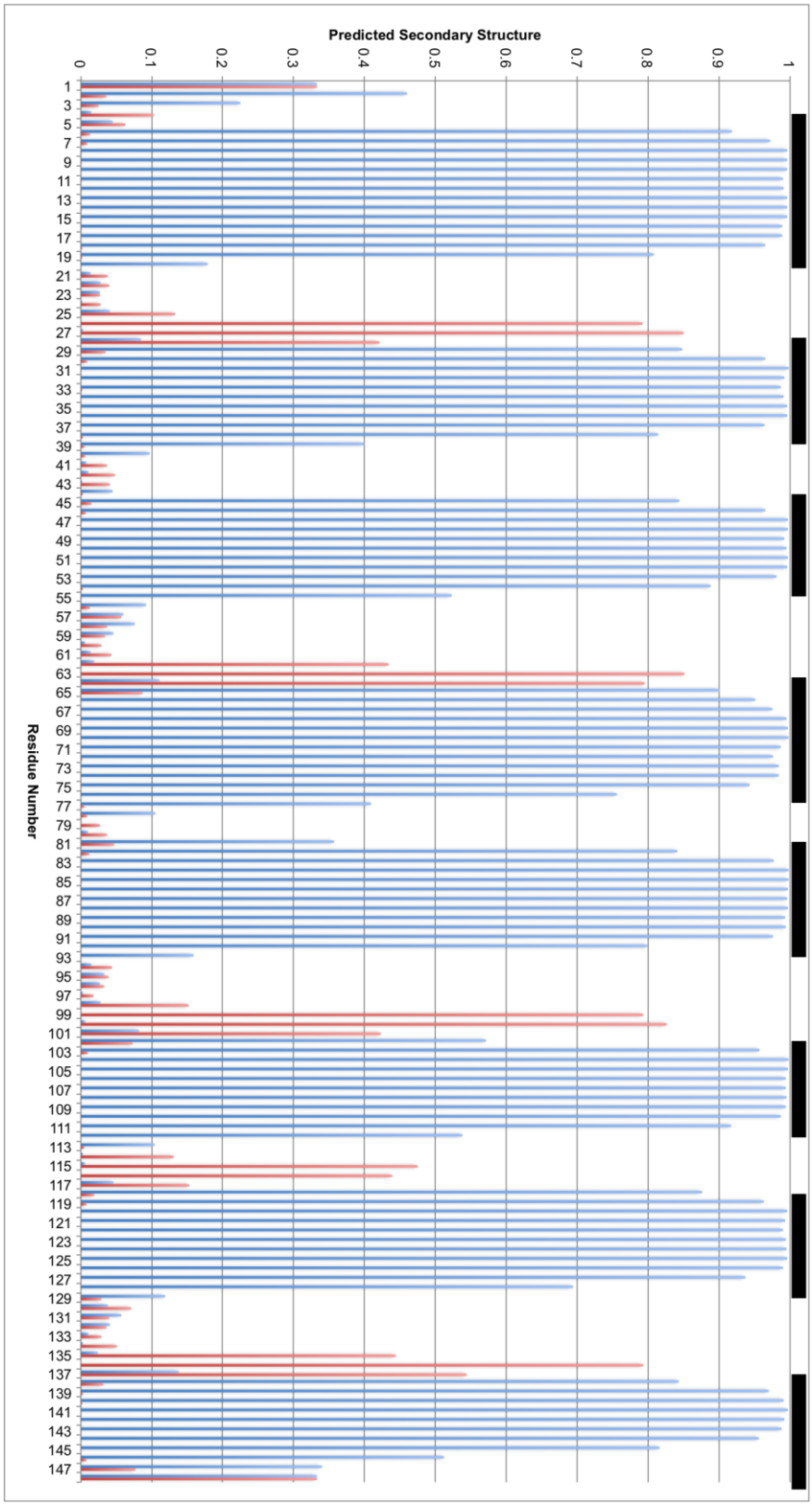

Figure 91. Predicted secondary structure of Ca^{2+}/CaM when bound to eEF2K$_{82\text{-}100}$, generated by TALOS-N.

Secondary structure predictions by TALOS-N (Shen and Bax, 2013). α-helices are shown by blue columns and β-strands are shown by red columns. Black bars at the top of the chart show the presence of the eight α-helices.

6.4 NOE assignment

Distance restraints are the key part of a structure calculation. They are determined from the assignment of NOE cross peaks, the intensity of which is proportional to the distance between two atoms. When determining distance restraints for a protein complex, two different approaches are needed that make use of different NMR experiments. Intra-protein NOEs within Ca^{2+}/CaM were assigned, as well as NOEs between Ca^{2+}/CaM and $eEF2K_{82-100}$.

6.4.1 Assignment of NOE distance restraints within Ca^{2+}/CaM

Standard NOESY experiments were used for the assignment of NOEs to provide distance restraints between the residues of Ca^{2+}/CaM. ^{13}C- and ^{15}N-NOESY experiments were used, spectra of which are shown in Figure 92.

In both of these spectra, strips of peaks from the diagonals represent an atom connectivity in the protein. In the case of the ^{15}N-NOESY, each strip represents an N-H. Those peaks present on the strip correspond to any atoms that are close in space to the atom on the diagonal. The chemical shift from the x-axis is representative of the atom itself, hence the vertical strip, whilst the chemical shift from the y-axis can come from the same residue or another residue located close to the atom itself. As mentioned in Section 6.2.1 the majority of atoms in Ca^{2+}/CaM have been assigned and so these assignments can be transferred onto the NOESY spectra. In this way, short and long range NOEs can be assigned.

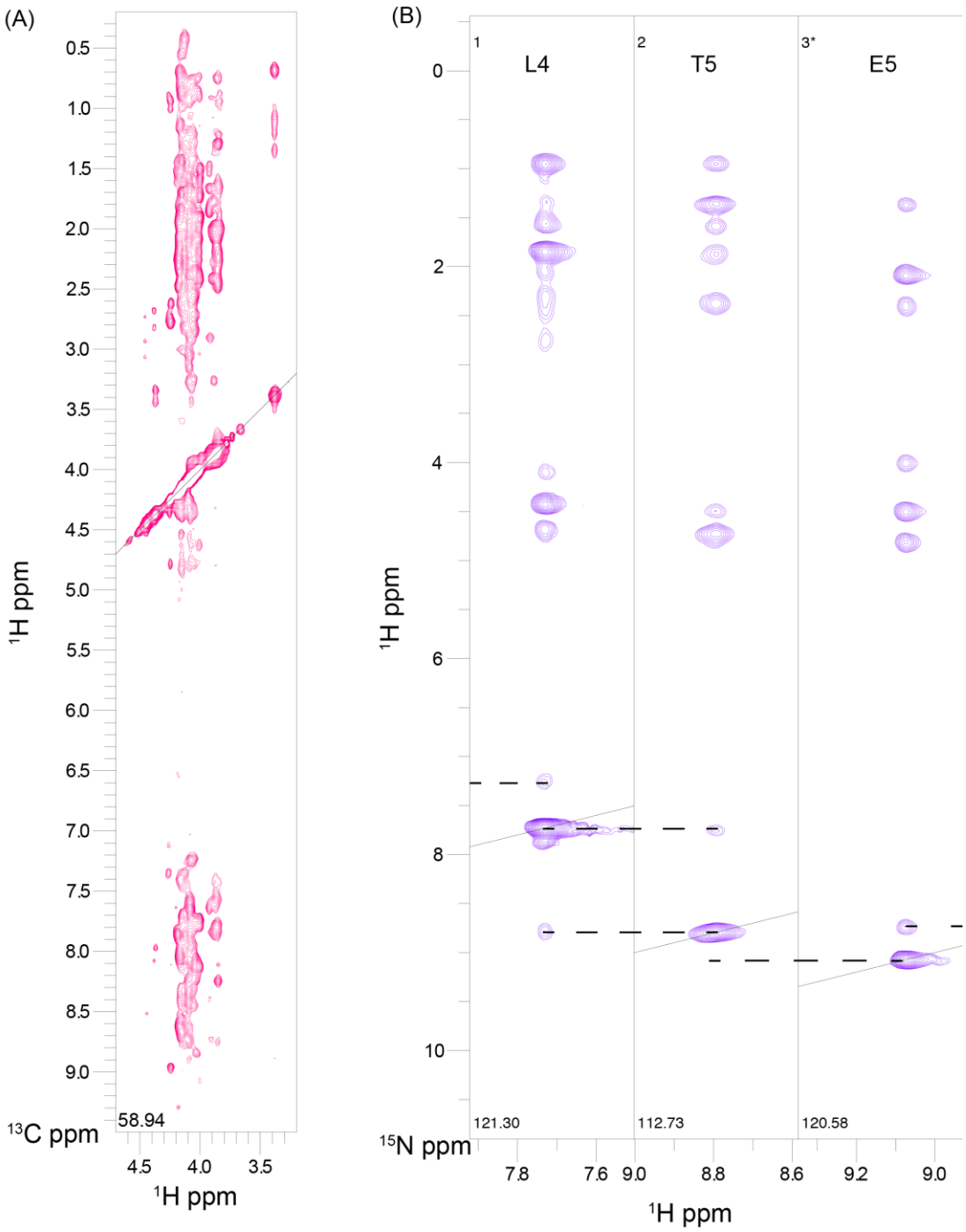

Figure 92. NOESY spectra for the NOE assignment of Ca^{2+}/CaM.

^{13}C-NOESY (A) and ^{15}N-NOESY (B) spectra used for the assignment of NOE cross peaks. A region of the ^{13}C-NOESY is shown from the Cα region. Three strips from the ^{15}N-NOESY are shown, that represent Leu^{4}, Thr^{5} and Glu^{6}. The connections between the adjacent residues between the N-H peaks on the diagonal line are shown with dashed lines.

6.4.2 Assignment of NOE distance restraints between Ca^{2+}/CaM and $eEF2K_{82-100}$

Similarly to the issues discussed in Section 6.2.2 for the resonance assignment of $eEF2K_{82-100}$, a different approach was required to determine distance restraints between Ca^{2+}/CaM and $eEF2K_{82-100}$.

NOEs were assigned for residues between the protein and peptide using a three-dimensional C-edited NOESY with ^{13}C and ^{15}N filtering in the F1 and F2 dimensions. This spectrum has cross peaks that represent those residues in Ca^{2+}/CaM that are close in space to residues in $eEF2K_{82-100}$. Those peaks are located with the chemical shift of the Ca^{2+}/CaM residue on the x-axis and the chemical shift of the $eEF2K_{82-100}$ residue on the y-axis.

The filters in the pulse sequence were not completely successful which meant that there were a number of extra peaks on the spectrum. These extra peaks overlay with peaks on the ^{13}C-NOESY discussed in the previous section and so they correspond to intra-protein NOEs. Whilst assigning the NOEs on this spectrum it was therefore important to try and ensure that only the inter-NOEs were assigned and not those peaks that were present due to inefficient filtering.

6.5 Three-dimensional structure of the Ca^{2+}/CaM: $eEF2K_{82-100}$ complex

The standard ARIA protocol for structure calculation was employed to generate structure ensembles. Four Ca^{2+} atoms were incorporated into the complex and restraints were used to obtain the correct geometry for calcium coordination and hydrogen bonds were also included. The method for structure calculation is described in Section 2.5.8.4. Several rounds of structure calculations were performed and violated NOE restraints analysed, as well as new NOEs assigned.

A three-dimensional structure ensemble (20 structures) of the Ca^{2+}/CaM: $eEF2K_{82-100}$ complex was solved, as described in Section 2.5.8. This ensemble can be seen in Figures 93 and 94. Eight clear α-helices are seen, connected by loop regions and there are four Ca^{2+} ion-binding sites, with a single Ca^{2+} ion coordinated in each site. This is as would be expected for a structure of Ca^{2+}/CaM and is in agreement with structures found in the PDB. Figure 94 shows an overlay between the structure of Ca^{2+}/CaM bound to the

hydrophobic IQ domain of the cardiac ca(v)1.2 calcium channel (PDB ID: 2F3Y) and the structure ensemble of the Ca^{2+}/CaM: $eEF2K_{82\text{-}100}$ complex. It is also shown overlaid with the lowest energy structure (RMSD 1.191 Å). The Ca^{2+} ions also overlay, indicating the correct geometry of calcium coordination has been maintained in the calculated structure.

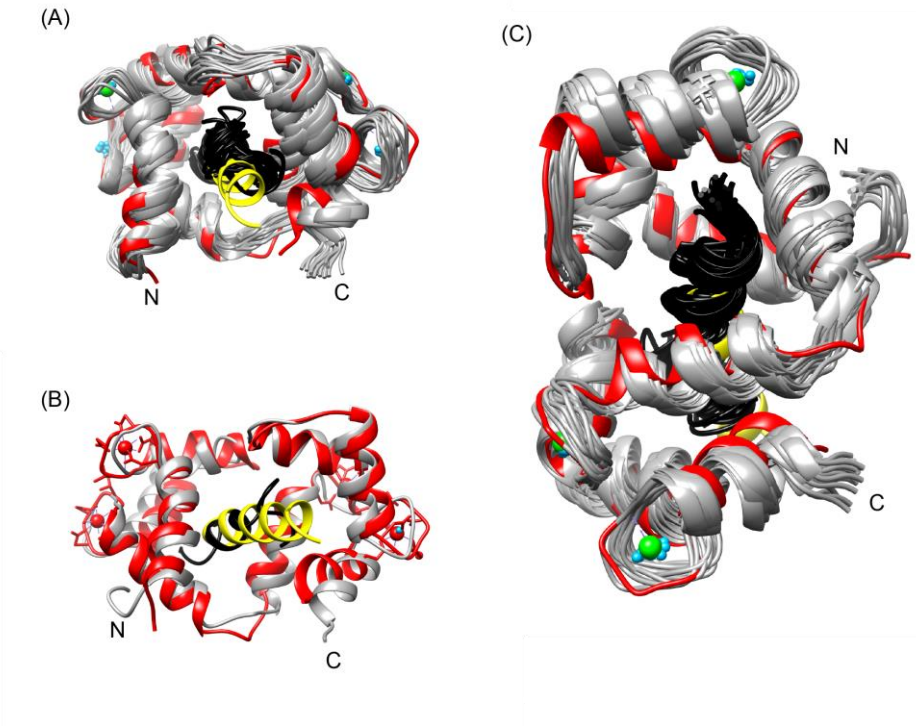

Figure 93. Overlay between the structure of Ca^{2+}/CaM bound to the hydrophobic IQ domain of the cardiac ca(v)1.2 calcium channel (PDB ID: 2F3Y) and the structure of the Ca^{2+}/CaM: $eEF2K_{82\text{-}100}$ complex.

Overlay of Ca^{2+}/CaM bound to the hydrophobic IQ domain of the cardiac ca(v)1.2 calcium channel (PDB ID: 2F3Y) with the calculated structure ensemble (A) and (C) and the lowest energy calculated structure (B) of the Ca^{2+}/CaM: $eEF2K_{82\text{-}100}$ complex . PDB ID: 2F3Y is shown in red, and the calculated structure in grey (CaM). The target peptide is shown in black (calculated structure) and yellow (PDB ID: 2F3Y).

The first observation to note from this structure is that it appears to be consistent with previously solved Ca^{2+}/CaM: target peptide structures. The two domains are folded at the linker region to engulf the peptide in a wrap-around structure. The peptide binds to both the N- and C-terminal domains through a tunnel in the centre of the structure. This differs from the models described in

Chapter 5, which were determined from SAXS and RDC data. As predicted from the NMR experiment using a modified eEF2K$_{82-100}$ peptide, with an ATCUN motif, the N-terminal domain of Ca^{2+}/CaM binds to the N-terminal region of eEF2$_{82-100}$ and consequently the C-terminal domain of Ca^{2+}/CaM to the C-terminal region of eEF2K$_{82-100}$.

The C-terminal part of eEF2K$_{82-100}$ is unstructured, and therefore differs from the majority of known target peptide structures, which are alpha helical. This region is likely unstructured due to the presence of two proline residues, which perturb the formation of a regular alpha helix due to the backbone NH being unavailable for hydrogen bonding.

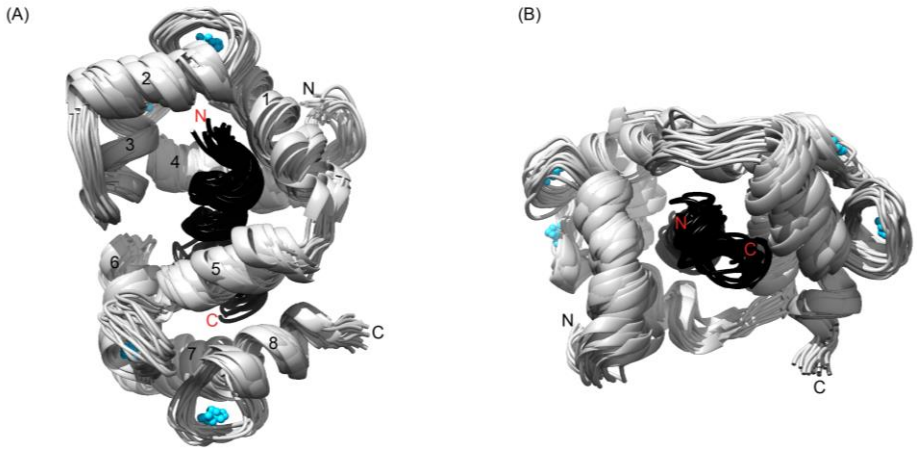

Figure 94. Structure ensemble of Ca^{2+}/CaM: eEF2K$_{82-100}$ complex.
Two representations of the Ca^{2+}/CaM: eEF2K$_{82-100}$ complex. Ca^{2+}/CaM is shown in grey, eEF2K$_{82-100}$ is shown in black and Ca^{2+} ions are shown in blue. The N- and C-termini of Ca^{2+}/CaM are labelled in black and the helices are numbered in (A). The N- and C-termini of eEF2K$_{82-100}$ are labelled in red.

The iCING server (Doreleijers et al., 2012) was used to validate the protein structure ensemble and the results are summarised in Table 14. A full report of the iCING analysis is shown in Appendix 19. The values obtained are in line with solution structures for Ca^{2+}/CaM structures in the PDB.

Table 14 also details the data included in the calculation, outlining the number of restraints used. A large amount of NOE restraints (2126) were included in the calculation initially, from iteration 1. Throughout the calculation, until iteration 8, the number of restraints used decreased in order to reach a converged structure. This meant that a total of 1385 NOE restraints

were included in the last step of the calculation and therefore used to produce the final structure ensemble. Of these, good proportions were medium (40) and long (136) range, which is important in a structure calculation to result in a correctly folded and globular protein structure. In addition, H-bond and calcium binding distance restraints were used, as well as torsion angle restraints.

There were few violations in the final structure ensemble. Across the 20 lowest energy structures for water refinement, constituting the final structure ensemble, there was a mean NOE violation of 0.2 and torsion angle violation of 1.6.

Table 14. Summary of restraints used in the structure calculation, violations and RMSD and Ramachandran analysis of structure ensemble.

NOE restraints	Ca^{2+}/CaM total	1935
	$eEF2K_{82\text{-}100}$ total	156
	Between Ca^{2+}/CaM and $eEF2K_{82\text{-}100}$ (intermolecular) total	35
	Intraresidue (s=0), sequential (s=1) and short range (2<s<3)**	1209
	Medium range (4<s<5)**	40
	Long range (s>5)**	136
Other distance (NOE-type) restraints	H-bonds	52
	Calcium	24
Torsion angle restraints	Total	278
	Phi	139
	Psi	139
Violations (Å)* **	Distance restraint >0.5 Å	0.2
	Torsion angle restraint >5°	1.6
RMSD (Å) backbone	Ca^{2+}/CaM: $eEF2K_{82\text{-}100}$	0.98 ± 0.18

	Ca^{2+}/CaM	0.92 ± 0.18
RMSD (Å) heavy atoms	Ca^{2+}/CaM: $eEF2K_{82-100}$	1.35 ±0.16
	Ca^{2+}/CaM	1.24 ± 0.15
Ramachandran****	Core (%)	85.9 (90.3)
	Allowed (%)	11.5 (8.6)
	Generous (%)	0.8 (0.2)
	Disallowed (%)	1.8 (0.9)

*Of total (unambiguous and ambiguous) restraints used in iteration 1

**Of unambiguous restraints used in iteration 8 (before final water refinement)

***Mean values across 20 lowest energy structures during water refinement

****Ca^{2+}/CaM: $eEF2K_{82-100}$ Ramachandran summary (Ca^{2+}/CaM Ramachandran summary)

Backbone RMSD values were obtained using MatchMaker (H, N, CO, Cα) in Chimera (Pettersen et al., 2004) for the N-terminal domain of CaM (0.721 Å), the C-terminal domain of CaM (0.820 Å) and $eEF2K_{82-100}$ (1.219 Å). The value for the peptide is higher than for the domains of CaM, which is consistent with the unstructured C-terminal end.

The locations of three key residues to be discussed in further sections are demonstrated in Figure 95. The side chain orientations are well defined for His^{87} and Trp^{99}, which along with the low RMSD values for CaM suggest that the lowest energy structure represents the atomic detail of the ensemble. It should be noted that Trp^{85} is less defined.

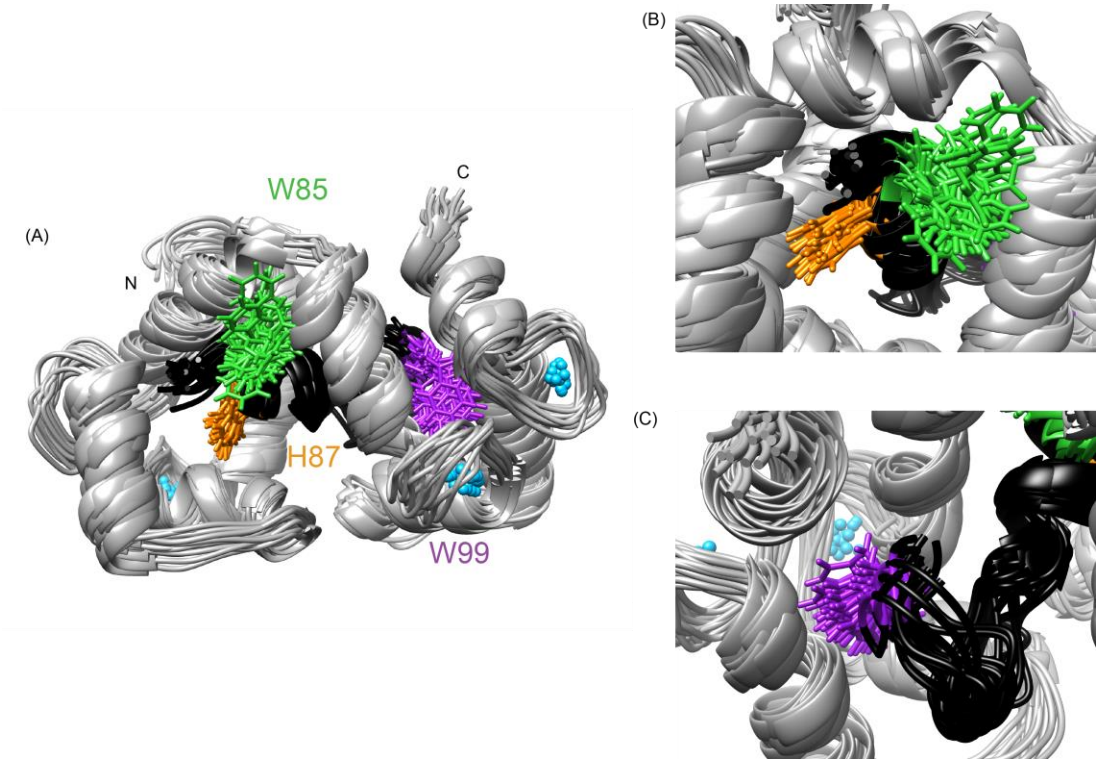

Figure 95. Overlay of structure ensemble highlighting the orientations of key residues across the different sructures.

The structure ensemble is shown in grey (CaM) and black (eEF2K$_{82-100}$). Three key residues in eEF2K$_{82-100}$ are highlighted – Trp^{85} (green), His^{87} (orange) and Trp^{99} (purple). Whole complex (A), close up views of Trp^{85} and His^{87} (B) and Trp^{99} (C).

The lowest energy structure of Ca^{2+}/CaM: eEF2K$_{82-100}$ will be used for further discussion and visualisation. The domains of Ca^{2+}/CaM fold around the peptide, as shown in Figure 96. When the surface of Ca^{2+}/CaM is shown, a clear empty space or "tunnel" is visible through the centre, which is where eEF2K$_{82-100}$ binds. The side chains of the amino acids stick out from the peptide, as the majority is structured as an alpha helix (residues 3-10), and contact specific Ca^{2+}/CaM residues. Table 15 below lists these interactions between Ca^{2+}/CaM and eEF2K$_{82-100}$. These contacts were determined in Chimera (Pettersen et al., 2004), using default distance values (0.4 negative cutoff value and an allowance of 0.0 Å) to find those atoms within favorable interaction distances. Those residues from CaM which appear in Table 15 are consistent with those determined to be important in the interaction by CSP analysis in Section 4.3.1. These residues are also present on the restraint list used for the structure

calculation. There are some additional CaM residues in Table 15, mostly from the N-terminal domain, which do not appear on the restraint list.

Table 15. Contacts between residues of eEF2K$_{82-100}$ and Ca^{2+}/CaM. Those residues of eEF2K which could not be assigned are shown in blue.

eEF2K$_{82-100}$ residue	Ca^{2+}/CaM residues
Lys^{82}	Glu^{54}, Arg^{74}
Glu^{83}	Met^{51}, Met^{71}, Leu^{32},
Ala^{84}	Met^{71}, Lys^{75}, Met^{72}
Trp^{85}	Glu^{87}, Glu^{84}, Lys^{75}, Arg^{86}, Glu^{83}
Lys^{86}	Gln^{41}, Glu^{87}
His^{87}	Met^{72}, Phe^{19}, Met^{36}, Phe^{68}, Leu^{32}
Ala^{88}	Met^{72}, Phe^{12},
Ile^{89}	Glu^{84}, Ala^{88}, Glu^{87}
Gln^{90}	Val^{91}, Leu^{112}, Leu^{39}
Lys^{91}	Glu^{11}, Glu^{14}, Ala^{15}
Ala^{92}	
Lys^{93}	Glu^{114}, Val^{108}, Leu^{112}, Met^{109}, Val^{91}
His^{94}	Leu^{112}, Glu^{114}, Leu^{18}, Met^{109}
Met^{95}	Met^{109}, Met^{124}, Leu^{116}, Glu^{114}, Glu^{120}
Pro^{96}	
Asp^{97}	Glu^{11}
Pro^{98}	
Trp^{99}	Leu^{105}, Met^{124}, Phe^{92}, Ala^{128}, Phe^{141}, Ile^{125}
Ala^{100}	

Two important interaction sites between Ca^{2+}/CaM and target peptides are hydrophobic patches in the N- and C-terminal domains. When the surface of Ca^{2+}/CaM is coloured according to hydrophobicity, it is clear that these sites are maintained in the Ca^{2+}/CaM: eEF2K$_{82-100}$ complex, also shown in Figure 96.

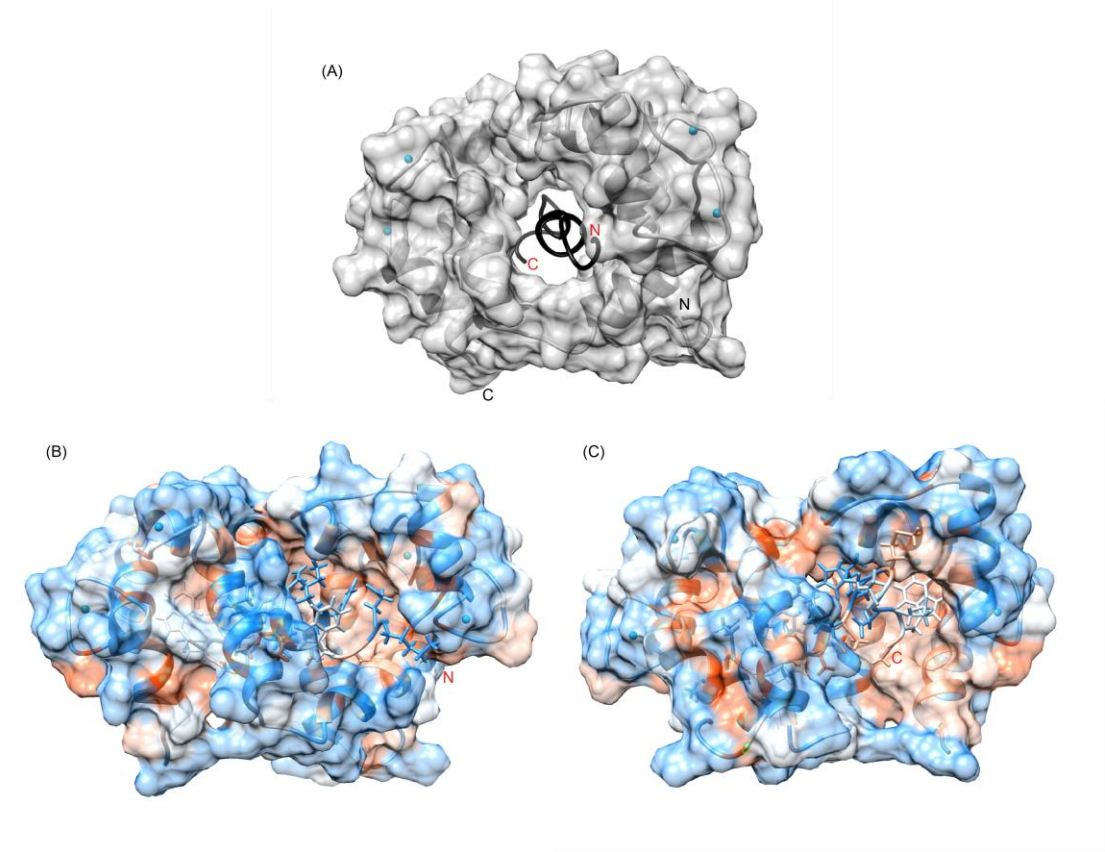

Figure 96. Surface representation of the Ca^{2+}/CaM: $eEF2K_{82-100}$ complex.
Ca^{2+}/CaM (grey) and $eEF2K_{82-100}$ (black) shown with a surface representation (A). Hydrophobic surface of Ca^{2+}/CaM and atoms of $eEF2K_{82-100}$ are coloured according to Kyte-Doolittle scale ranging from red (hydrophobic residues) to blue (hydrophilic residues). The hydrophobic binding pockets of the N-terminal domain (B) and C-terminal domain (C) of Ca^{2+}/CaM are shown.

6.5.1 SAXS modelling using the NOE-derived structure of the Ca^{2+}/CaM: $eEF2K_{82-100}$ complex

SAXS data collected for the Ca^{2+}/CaM: $eEF2K_{82-100}$ complex (Section 5.3) included an Rg value that indicated a more open structure than the compact, wraparound configuration seen for CaM: target peptide complexes in the Protein Data Bank.

Rigid body modelling using CORAL (Petoukhov and Svergun, 2005) was carried out using the NOE-derived structure of the complex to combine SAXS and NMR structural data. In this way, the NOE-derived structure was refined against the molecular envelope derived from SAXS experiments. Individual modelling of the Ca^{2+}/CaM: $eEF2K_{82-100}$ complex (no RDC derived domain orientations included) have shown that the SAXS data can fit the NMR

calculated structure of the complex. The model produced by SAXS modelling is slightly wider, in order to accommodate the shape dictated by the SAXS data. Despite this, the key residues discussed (Section 6.6) - $Trp^{85,}$ Trp^{99} and His^{87} - are positioned in the same locations to interact with the same residues of Ca^{2+}/CaM already described from the NMR structure itself. For example, Leu^{105}, Met^{124}, Phe^{92}, Ala^{128}, Phe^{141}, Ile^{125} of Ca^{2+}/CaM contact Trp^{99} of $eEF2K_{82-100}$, consistent with the results shown in Table 15. In addition Glu^{87}, Glu^{84}, Lys^{75}, Arg^{86}, Glu^{83} in the N-terminal domain of Ca^{2+}/CaM contact Trp^{85} of eEF2K, again consistent with Table 15. This is shown in Figure 97.

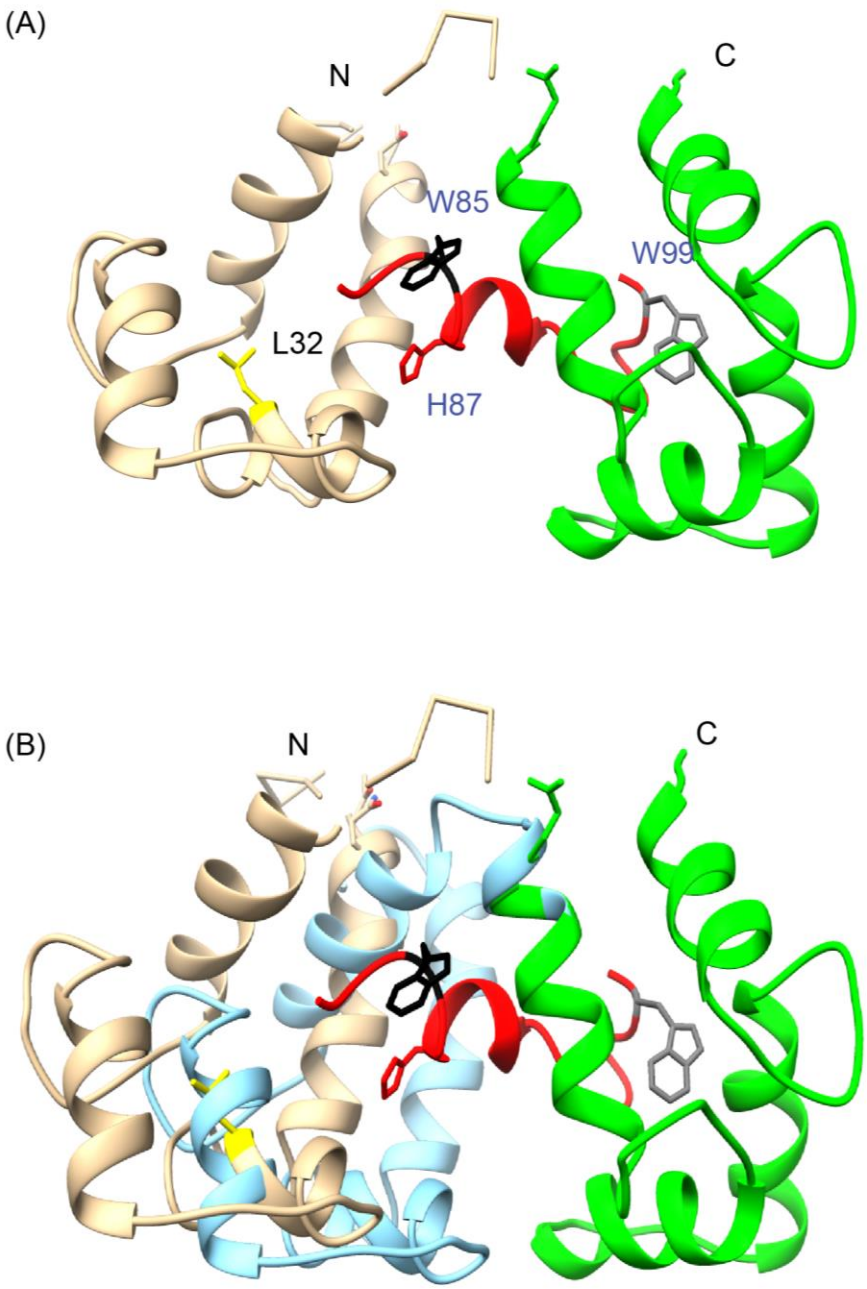

Figure 97. SAXS modelling of the Ca^{2+}/CaM: $eEF2K_{82\text{-}100}$ complex.

CORAL (Petoukhov and Svergun, 2005) was carried out with the calculated structure of the Ca^{2+}/CaM: $eEF2K_{82\text{-}100}$ complex (A). The structure was separated into the N- (brown) and C-terminal (green) domains and the peptide (red) separately. A contact was designated between Leu^{32} in the N-terminal domain and of Ca^{2+}/CaM and His^{87} of $eEF2K_{82\text{-}100}$, as determined in Section 6.5. The C-terminal domain was fixed and the N-terminal domain was not fixed in the simulation, allowing the N-terminal domain to move around, taking into consideration the contact. The resulting structure is also shown with the C-terminal domain overlaid with the NMR calculated structure, which is coloured blue (B). The residues corresponding to the linker region in the SAXS model is shown with a stick representation.

6.6 Implications for eEF2K activity from the structure of the Ca^{2+}/CaM: $eEF2K_{82-100}$ complex

The elucidation of the three-dimensional structure of the Ca^{2+}/CaM: $eEF2K_{82-100}$ complex from NMR and SAXS data provides a wealth of information on the interaction between the kinase and CaM. Combining this structure with further biochemical data on eEF2K is especially useful in describing the mechanism of activation. Importantly, the structure of the complex with $eEF2K_{82-100}$ has been used as a tool to study the eEF2K protein as a whole. The peptide complex provides a good representation of the interaction between eEF2K and Ca^{2+}/CaM.

6.6.1 Effect of pH on eEF2K activity – investigating the role of histidine residues

The effect of pH on eEF2K activity was described in Section 1.5.6.3. The activity of eEF2K is increased under acidic conditions. The CaM-binding region of eEF2K contains three highly conserved histidines, His^{80}, His^{87} and His^{94}, which are believed to play a role in the pH sensitivity of eEF2K activity. It should be noted that one of these histidine residues, His^{80}, is not present in $eEF2K_{82-100}$, which has been used for structural studies. A peptide containing all three histidine residues, $eEF2K_{78-100}$, was used to study the effects of pH.

An NMR chemical shift titration was used to determine the pKa values of these histidine residues of eEF2K and compare them to the pKa of free histidine, as described in Section 2.5.9. The control experiment determined a pKa of 6.13 for free histidine. The pKa values of the three histidine residues in $eEF2K_{78-100}$ were determined as 6.55 (His^{80}), 6.49 (His^{87}) and 6.45 (His^{94}). These values are slightly higher than for free histidine, meaning that the ionisation state of these side chains will be sensitive to changes in pH near physiological conditions. A higher percentage will therefore be protonated at near physiological pH than if their pKa values were closer to that of free histidine. The chemical shift titration curves for determining pKa values is shown in Figure 98.

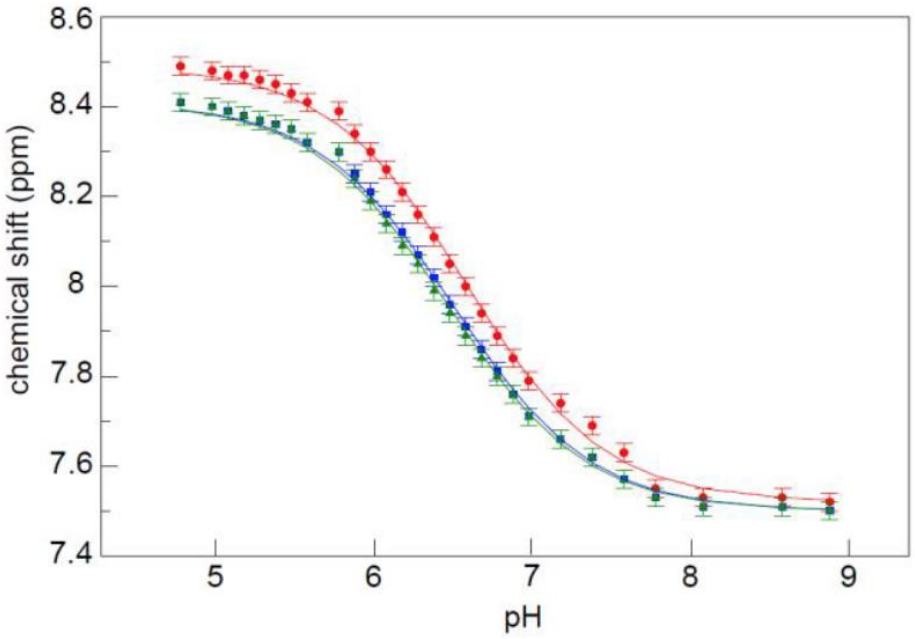

Figure 98. Chemical shift titration curves for the CH_2 protons of imidazole side chains of the 3 histidine residues in $eEF2K_{82-100}$.

Chemical shift titration curves for each histidine residue in $eEF2K_{78-100}$. His^{80} had a pKa of 6.55 and its curve is shown in red, His^{87} had a pKa of 6.49 and its curve is shown in blue and His^{94} had a pKa of 6.45 and is shown in green. NMR experiments were conducted at 298 K and samples were prepared in D_2O buffer containing 25 mM Bis-Tris, 150 mM KCl and 10 mM $CaCl_2$.

The role of pH in the activation of eEF2K was investigated using a combination of *in vitro* binding experiments (conducted by Dr Halina Mikolajek) and a set of activity assays (performed by Dr Jianling Xie). The three histidine residues in the CaM binding region of eEF2K (residues 78-100) play a particularly important role (Xie et al., 2015).

When all three histidine residues were mutated to alanine (H3A), the activation of eEF2K at acidic pH was greatly reduced. Conversely, when all three histidines were mutated to lysines (H3K), which are charged at both acidic (6.9) and physiological pH (7.4), eEF2K activity was enhanced at both pH values. Consistent with this, the affinity of H3A-$eEF2K_{78-100}$ for CaM was decreased (Kd = 97±9 nM) compared to that of WT eEF2K under acidic conditions (Kd = 38±3 nM), whereas CaM-binding to the H3K-$eEF2K_{78-100}$ was tighter (Kd = 32.5±3.2 nM) at physiological pH. These data strongly suggest that the protonation of all three histidines helps to promote binding of Ca^{2+}/CaM to eEF2K, resulting in stimulation of eEF2K at acidic pH (Xie et al., 2015).

The structure of the Ca^{2+}/CaM: $eEF2K_{82-100}$ complex revealed a possible explanation for the increased affinity between Ca^{2+}/CaM and eEF2K at acidic pH. $eEF2K_{82-100}$ does not contain His^{80} and so only His^{87} and His^{94} will be discussed. The locations of the two histidine residues are shown in Figure 99.

The first interesting observation is that His^{87} is facing the N-terminal domain binding pocket and thus interacts with the hydrophobic residues that line this pocket (Phe^{19}, Leu^{32}, Met^{36}, Phe^{68} and Met^{72}). This indicates that His^{87} is an important residue for mediating the interaction, as the N-terminal domain binding pocket is a critical interaction point between the two proteins. When this residue is mutated to a lysine, it is still able to occupy this pocket and makes the same contacts (Phe^{19}, Leu^{32}, Met^{36}, Phe^{68} and Met^{72}) with Ca^{2+}/CaM. However, when it is mutated to an alanine, this side chain is much shorter and so only Met^{72} of Ca^{2+}/CaM is able to make contact. It should be noted that the effects from these mutations could not be purely attributed to the protonation states of the amino acid residue side chains. The length of the side chain is very important, and in addition the alanine mutations could affect the helix formation.

His^{94} binds near the domain interface, making contact with residues from both the N- and C-terminal domains. Of the four residues it contacts, three are hydrophobic (Leu^{18}, Met^{109} and Leu^{112}), whilst one is polar and acidic (Glu^{114}). Figure 99 shows that a salt bridge can form between His^{94} and Glu^{114}. With a pKa value of 6.45, a proportion of His^{94} will be protonated at physiological pH. There are two titratable NH groups in histidine that can be protonated and as the pH decreases, the degree of protonation increases. There will therefore be a greater proportion of protonated histidine under acidic conditions. If only one of the NH groups is protonated then the side chain is neutral and can donate and accept protons but if both are protonated then the residue has an overall positive charge. This could facilitate the formation of a salt bridge between the now positively charged His^{94} and the negatively charged Glu^{114}, meaning that when His^{94} is protonated this salt bridge can form. This is a possible explanation as to why binding of eEF2K to Ca^{2+}/CaM and kinase activity increases at low pH. It could also be possible that the salt bridge

alters the interdomain arrangement and hence the overall conformation of CaM as part of the regulation of eEF2K activity.

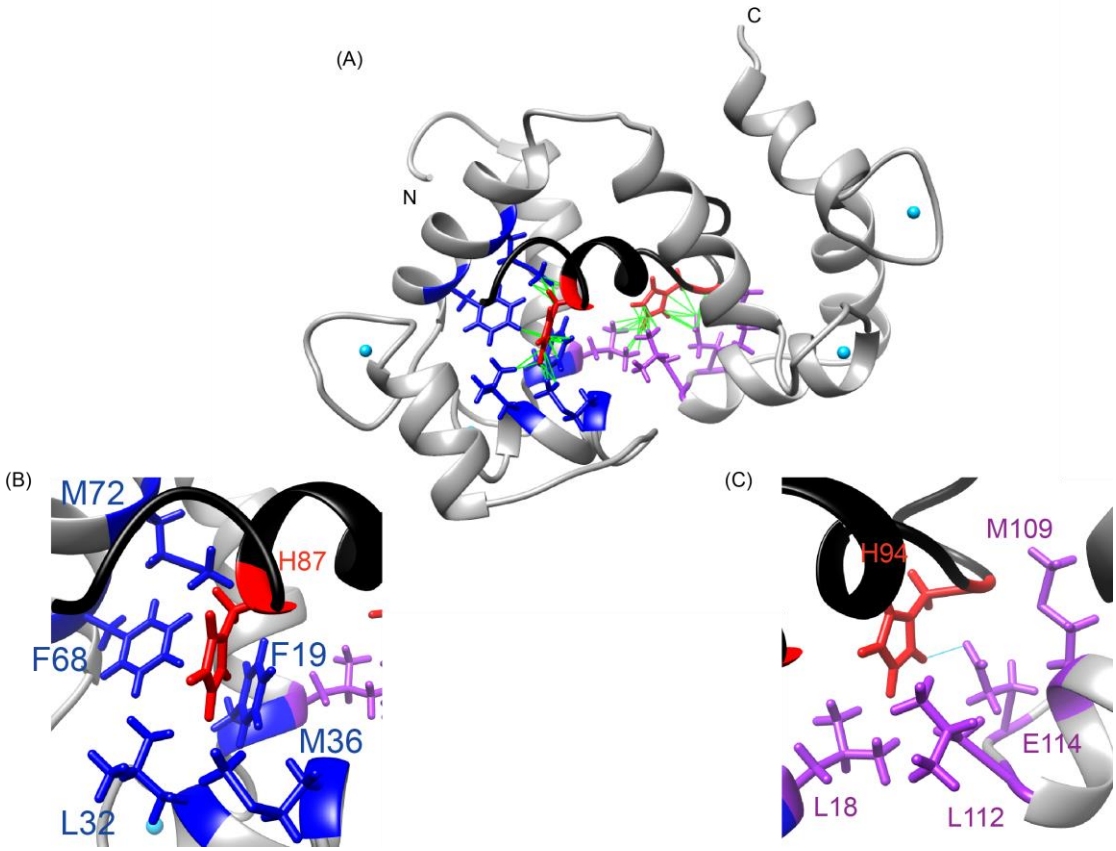

Figure 99. Histidine residues in the CaM-binding region of eEF2K.
Histidine residues in eEF2K interact with the N-terminal domain binding pocket and at the interface between the two domains of Ca^{2+}/CaM (A). Zoomed in views of interactions between His^{87} (A) and His^{94} (B) and residues of Ca^{2+}/CaM. The salt bridge is marked with a blue line and other contacts are shown with green lines. Histidine residues are coloured red and those residues that interact with His^{84} are coloured blue and those that interact with His^{94} are coloured purple.

There is a single, highly conserved histidine residue in CaM (His^{108}), which was predicted to also be involved in mediating the enhanced binding of Ca^{2+}/CaM to eEF2K under acidic conditions. Dr Jianling Xie found that there was a surprising reduction in eEF2K kinase activity at both acidic and physiological pH when the assay was performed with H108A-CaM. When the kinase assay was carried out using the H108K-CaM, eEF2K was no longer activated. However, both H108A-CaM and H108K-CaM were still able to bind eEF2K (at pH 6.8, K_d H108A-CaM = 42 nM; K_d H108K-CaM = 122 nM). Although, for H108K-CaM-binding affinity was not as strong as for wild-type CaM (K_d = 38 nM

at pH 6.8). Therefore, the decrease in ability of the H108A-CaM mutant to activate eEF2K cannot solely be due to the reduction in eEF2K binding. These data suggest that His^{108} in CaM is required for the activation of eEF2K.

The location of His^{108} in the Ca^{2+}/CaM: $eEF2K_{82-100}$ complex is consistent with the fact that it is not involved in binding to eEF2K but is critical for kinase activation. It is situated on the outside of the molecule, facing the solvent and making no contact with $eEF2K_{82-100}$, as shown in Figure 100.

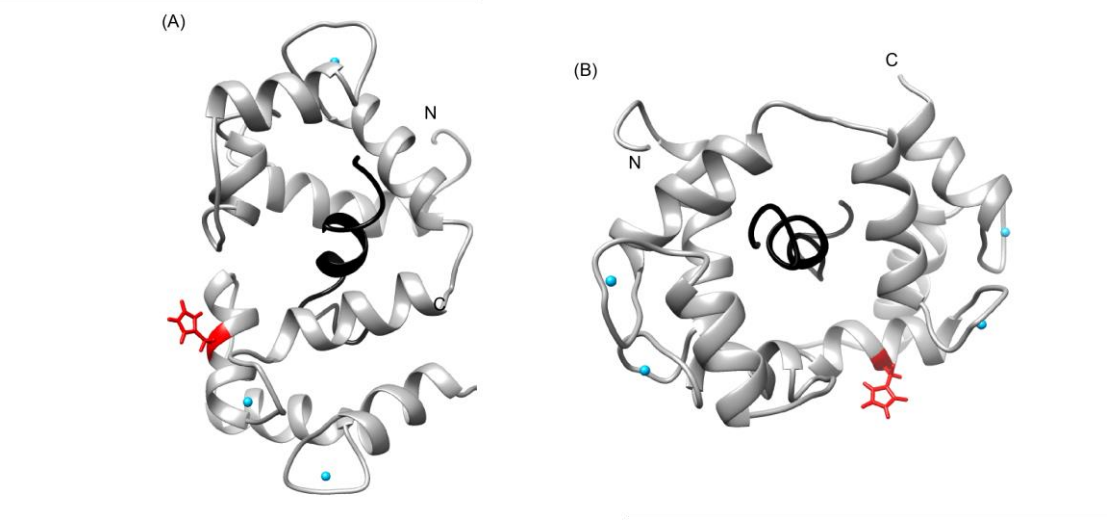

Figure 100. His^{108} of Ca^{2+}/CaM does not interact with $eEF2K_{82-100}$.
His^{108} is located on the outside of the complex, facing the solvent and making no contact with $eEF2K_{82-100}$. Viewed lengthways (A) and from the side (B). His^{108} is coloured red.

6.6.2 Effect of hydroxylation on eEF2K activity – investigating the role of proline residues in the CaM-binding region

Investigations by Dr Claire Moore *et al* found that eEF2K activity was decreased as a result of proline hydroxylation, as described in Section 1.5.7. Hydroxylation on Pro^{98} of eEF2K has been demonstrated using mass spectrometry (Moore et al., 2015), whilst hydroxylation could not be detected for the second proline residue in the CaM binding region of eEF2K - Pro^{96}.

The Ca^{2+}/CaM: $eEF2K_{82-100}$ complex shows that the two proline residues in the CaM-binding region of eEF2K, do not directly contact any CaM residues. However, there are some atoms that are located approximately 5 Å away from the atoms of these proline residues, and so may be affected by the addition of a hydroxyl group. The closest two residues to Pro^{96} are Glu^{14} and Glu^{114}; whilst for Pro^{98} the closest residues are Met^{109}, Met^{124} and Glu^{127}. The addition of a

hydroxyl group nearby is likely to affect the local structure in this region, which influences the binding or eEF2K to Ca^{2+}/CaM. ITC studies showed this with a decrease in affinity for binding a peptide containing hydroxylated Pro^{98} ($eEF2K_{78-100}$) as opposed to the wildtype peptide. Unmodified peptide bound to CaM with an affinity of 66 ± 9 nM, while binding to the hydroxylated form was somewhat weaker (K_d, 123 ± 3 nM), showing that the hydroxylation of Pro^{98} does interfere with CaM binding, but only modestly (Moore et al., 2015). Given the position of the proline residues in the complex, it is possible that these residues are involved in contacting the kinase domain of eEF2K. As the hydroxyproline residue is located near the start of the kinase domain of eEF2K its presence could shift the position of the CaM binding region and alter how CaM interacts with full-length eEF2K.

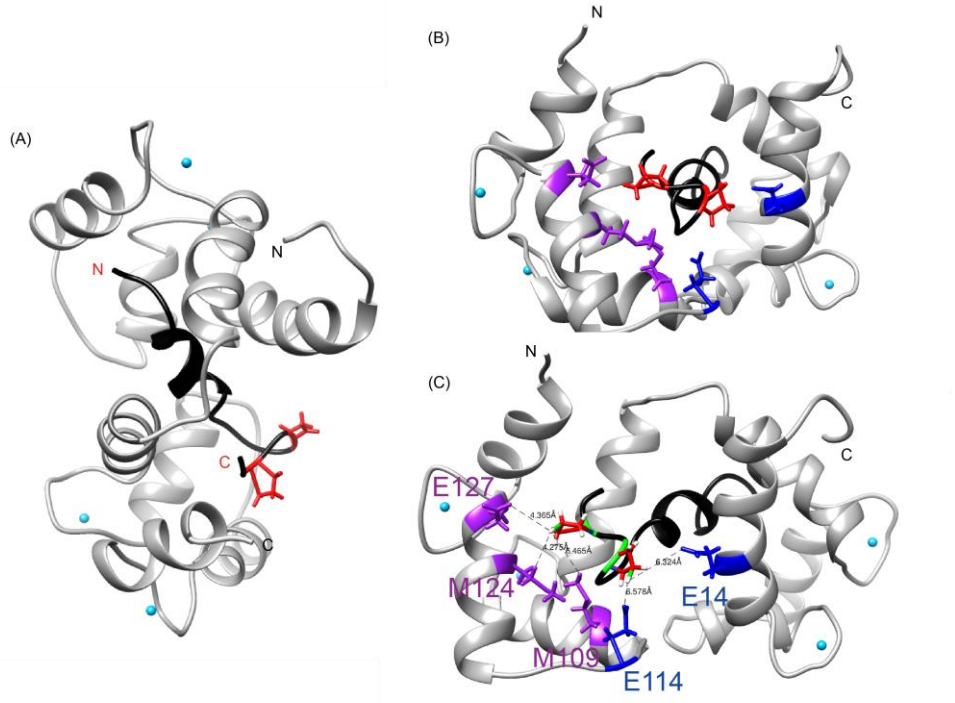

Figure 101. Location of two proline residues of $eEF2K_{82-100}$ in the Ca^{2+}/CaM: $eEF2K_{82-100}$ complex structure.

The two proline residues of $eEF2K_{82-100}$ are shown in red (A). Those residues which contact Pro^{96} are shown in blue and those residues which contact Pro^{98} are shown in purple (B) and labelled with residue number and distances (C).

6.6.3 eEF2K activation by Ca^{2+}/CaM - roles for Trp^{85} and Trp^{99} of eEF2K

As described in Section 1.4, the recognition sequences in CaM binding proteins contain hydrophobic anchor residues, which are primarily responsible for interacting with the N- and C-terminal domain binding pockets of Ca^{2+}/CaM. In the eEF2K CaM binding region there are two tryptophan residues, located at positions 85 and 99, which have been shown to be important for CaM recognition and binding.

ITC experiments performed by Dr Halina Mikolajek and the author, as well as kinase activity assays (Dr Claire Moore) were carried out to determine the roles these two key residues play in the activation of eEF2K by Ca^{2+}/CaM. For these experiments a slightly longer eEF2K peptide was used, $eEF2K_{78-100}$, which contained four extra residues at the N-terminal end and had higher affinity for Ca^{2+}/CaM than $eEF2K_{82-100.}$ A K_d of 247 nM +/- 2 nM was determined by ITC for $eEF2K_{82-100}$, compared to a K_d of 71 nM +/- 2.5 nM for $eEF2K_{78-100}$. Peptides were synthesised by China Peptides (Shanghai, China) with the Trp^{85} and Trp^{99} residues mutated to Alanine residues to create two mutant peptides – W85A-$eEF2K_{78-100}$ and W99A-$eEF2K_{78-100}$. An alanine mutation removes the aromatic ring and provides a much shorter side chain than a tryptophan residue. These peptides were used for ITC experiments, whilst a site directed mutagenesis protocol was used to make mutations to the full-length eEF2K protein for kinase activity assays (Dr Claire Moore). By comparison with WT-eEF2K, we could determine the effect of these mutations and the combination of ITC and kinase activity assays meant that we could investigate the binding of eEF2K to Ca^{2+}/CaM separately from the activity and so dissect the activation mechanism.

A summary of the results from the ITC experiments is shown in Table 16 and example calorimetric traces from two experiments are shown in Figure 102. The affinity for both mutants is lower than the wildtype, however the W99A mutation has a much larger effect on binding than the W85A mutation. When Trp^{99} is mutated to an alanine, the affinity of $eEF2K_{78-100}$ decreases more than ten-fold. However, when Trp^{85} is mutated to an alanine there is approximately a five-fold decrease in binding affinity to Ca^{2+}/CaM.

Kinase activity assays were performed by Dr Claire Moore with W99A-eEF2K mutants. Compared to WT-eEF2K, W99A-eEF2K has greatly reduced activity (Moore et al., 2015). Experiments involving the mutation of Trp^{85} have been previously published (Diggle et al., 1999). In this case the mutation was to a glycine residue and showed that kinase activity was completely abolished.

Table 16. K_d values for the binding of WT/W85A/W99A-eEF2K_{78-100} to Ca^{2+}/CaM.

Protein	Ligand	K_d (nM)
Ca^{2+}/CaM	WT-eEF2K_{78-100}	71 +/- 2.5
Ca^{2+}/CaM	W85A-eEF2K_{78-100}	364 +/- 49.8
Ca^{2+}/CaM	W99A-eEF2K_{78-100}	1036 +/- 402

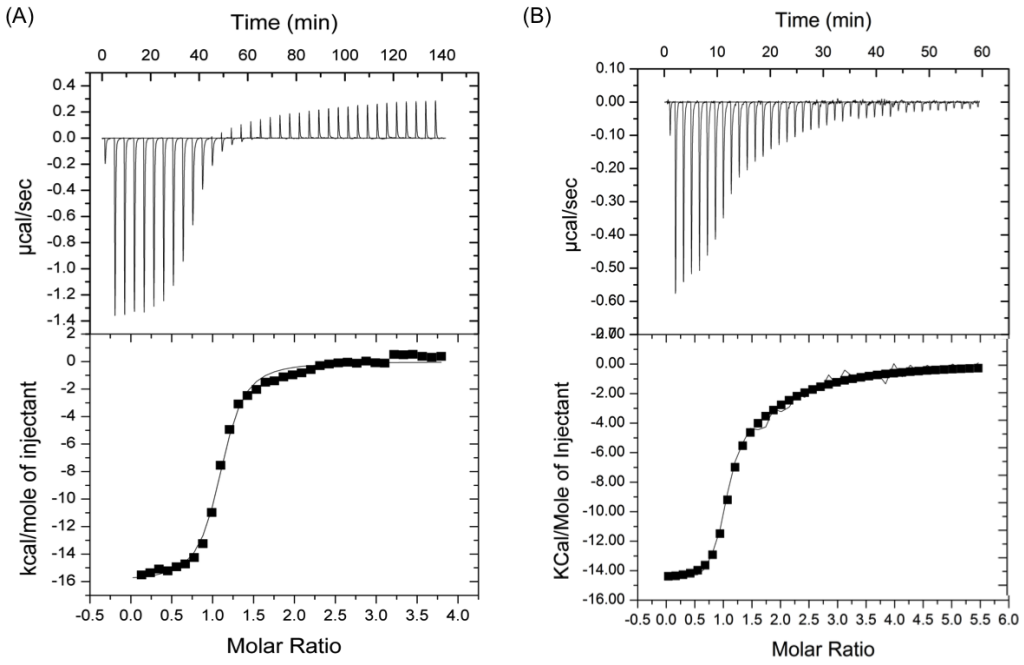

Figure 102. Binding of W85A-eEF2K_{78-100} and W99A-eEF2K_{78-100} to Ca^{2+}/CaM.

Calorimetric titrations of Ca^{2+}/CaM with W85A-eEF2K_{78-100} (A) and W99A-eEF2K_{78-100} (B) showing the original titration curve (top) and the binding isotherm obtained (bottom). Buffer conditions are as described in Section 2.4.4.

These two residues in eEF2K, Trp^{85} and Trp ^{99}, are therefore important for mediating the activation of eEF2K by Ca^{2+}/CaM and should be investigated

using the NOE-derived three-dimensional structure of the Ca^{2+}/CaM: $eEF2K_{82-100}$ complex.

Trp^{85} does not bind at the N-terminal hydrophobic pocket of Ca^{2+}/CaM. Trp^{99} interacts with residues lining the C-terminal domain pocket of Ca^{2+}/CaM (Phe^{92}, Leu^{105}, Met^{124}, Ile^{125}, Ala^{128} and Phe^{141}), which is expected when compared to other known structures of Ca^{2+}/CaM: target peptide complexes. However, Trp^{85} does not interact with corresponding residues in the N-terminal domain of Ca^{2+}/CaM. Instead, it contacts residues which are mostly located in helix 5 (Glu^{83}, Glu^{84}, Arg^{86} and Glu^{87}), as well as one residue from helix 4 (Lys^{75}). The majority of these residues actually belong to the C-terminal domain of CaM, except for Lys^{75}. Trp^{85} therefore binds at the interface between the two domains, as shown in Figure 103. The atoms in the 6-membered aromatic ring part of the indole group on Trp^{85}, have no contacts with Ca^{2+}/CaM and instead this ring faces out of the complex. It should be noted here that the side chain orientation of Trp^{85} is not as well defined by the NMR structural ensemble, as shown in Section 6.5. There is only 1 intermolecular NOE present for Trp^{85}, whereas there are 13 for Trp^{99}.

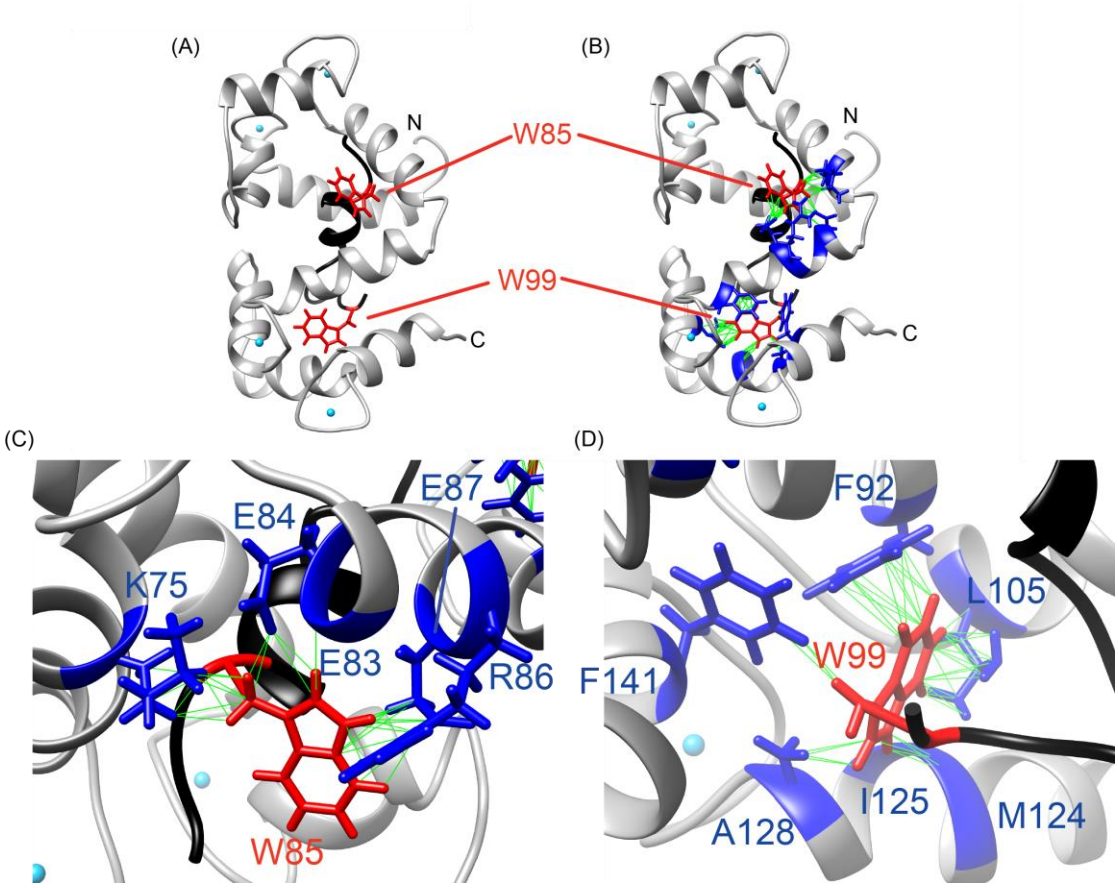

Figure 103. Roles of Trp^{85} and Trp^{99} in the activation of eEF2K by Ca^{2+}/CaM.

Trp^{99} binds to the hydrophobic binding pocket in the C-terminal domain of Ca^{2+}/CaM, whilst Trp^{85} binds at the interface between the two domains. Location of Trp^{85} and Trp^{99} shown on the structure of the Ca^{2+}/CaM: eEF2K$_{82\text{-}100}$ complex (A). Contacts between Trp^{85} and Trp^{99} also shown on the structure (B) and zoomed in areas showing those residues that interact with Trp^{85} (C) and Trp^{99} (D). Trp^{85} and Trp^{99} are shown in red and those residues of Ca^{2+}/CaM that contact the tryptophan residues are shown in blue. Contacts are shown with green lines.

A surface representation further demonstrates these observations and is shown in Figure 104. Trp^{85} does not sit within the N-terminal domain binding pocket, and instead the aromatic ring sticks out of the complex, making no contact with Ca^{2+}/CaM. His^{87} is positioned further into the N-terminal domain binding pocket and is therefore likely responsible for interacting with this region of Ca^{2+}/CaM. Trp^{99} however, is closely associated with the C-terminal binding pocket and sits within its pocket.

The presence of these two pockets of Ca^{2+}/CaM, and the positioning of interacting partners on eEF2K$_{82\text{-}100}$ are consistent with the regions of Ca^{2+}/CaM

identified in Chapter 4 as being important for binding. CSP analysis highlighted these two regions, one on each of the domains, as key interaction sites, which is now confirmed by structural analysis.

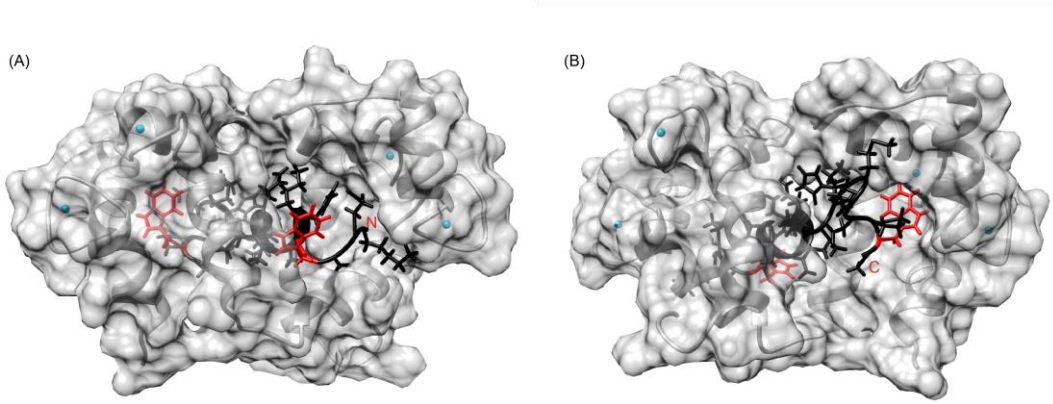

Figure 104. Surface representation of Trp^{85} and Trp^{99} binding to the N- and C-terminal domains of Ca^{2+}/CaM.

Trp^{99} is not located in the N-terminal domain binding pocket of Ca^{2+}/CaM (A). Trp^{99} is bound to the C-terminal domain binding pocket (B). Trp^{85} and Trp^{99} are shown in red, whilst all other $eEF2K_{82-100}$ residues are shown in black.

6.6.4 Model for eEF2K activation

As a result of the structural observations described here, we propose a model for the activation of eEF2K by Ca^{2+}/CaM. In addition, this model accounts for the results of CSP analysis of Ca^{2+}/CaM and apo-CaM binding to $eEF2K_{82-100}$, $eEF2K_{(74-342)(490-725)}$ and $eEF2K_{(100-336)(490-725)}$, including the peptide titration with $eEF2K_{82-100}$ and also the NMR experiment involving an ATCUN domain on $eEF2K_{82-100}$. Findings from ITC and activity assay experiments involving peptide with mutations at Trp^{85} and Trp^{99} were also crucial in proposing this model, shown in Figure 105.

CSP analysis of NMR experiments with apo-CaM showed that only the C-terminal domain of CaM can bind to $eEF2K_{82-100}$ and the affinity of this interaction was shown by MST to be weak. Therefore in the absence of Ca^{2+}, or at very low concentrations as in the resting cell, some apo-CaM may bind to eEF2K, albeit with a weak affinity. CSP analysis of NMR experiments with Ca^{2+}/CaM showed that there is a binding site in both the N- and C-terminal domains for $eEF2K_{82-100}$, demonstrating that in the presence of Ca^{2+}, both

domains of CaM interact with the peptide. These observations were confirmed with the elucidation of the three-dimensional structure of the Ca^{2+}/CaM: $eEF2K_{82-100}$ complex.

We know from the NMR experiment using ATCUN-$eEF2K_{82-100}$ and from the observed intermolecular NOEs that $eEF2K_{82-100}$ binds in a parallel fashion with CaM. The N-terminal end of the CaM binding site of eEF2K interacts with the N-terminal domain of CaM and the C-terminal end of the CaM binding site interacts with the C-terminal domain of CaM. Taken together with experiments involving W85A-$eEF2K_{78-100}$ and W99A-$eEF2K_{78-100}$, we suggest roles for Trp^{85} and Trp^{99}. Trp^{99} provides a binding site and significant binding energy to the C-terminal domain of Ca^{2+}/CaM. In contrast, Trp^{85} provides less interaction energy but plays a critical role in the activation of eEF2K, as shown by the fact that mutation of this residue results in no kinase activity. Examination of the structure showed that Trp^{87} binds near the interface between the two domains of CaM, making contact with residues in the linker region. This could suggest that the engagement of the N-terminal domain of CaM with eEF2K, which is only possible when Ca^{2+} is bound, is critical for eEF2K activation. This is consistent with findings by Dr Claire Moore that mutation of Trp^{99} results only in a reduction of kinase activity whilst mutation of Trp^{85} results in a kinase that cannot be activated.

Consequently, an activation model involves the C-terminal domain of apo-CaM able to contact and bind to the C-terminal end of the CaM binding region of eEF2K. This affinity is weak until the concentration of Ca^{2+} within the cell increases as a result of a Ca^{2+} signal, which increases the affinity. In the presence of Ca^{2+}, the N-terminal domain of Ca^{2+}/CaM binds to the N-terminal end of the CaM binding region of eEF2K. Trp^{85} binds near the domain interface of CaM, whilst residues including His^{87} interact with the hydrophobic binding patch of the N-terminal domain. As a result the kinase is activated. One possibility of this activation trigger, consistent with evidence from other CaM kinases and discussed in Section 1.6.6, could be that binding of Trp^{85} to the N-terminal domain of CaM relieves an autoinhibitory mechanism involving a pseudosubstrate to activate the kinase. The location of the CaM binding region when it is bound to Ca^{2+}/CaM (see below) and the observation that ATP

analogues can bind in the presence and absence of Ca^{2+}/CaM (Pigott et al., 2012) suggests that the CaM dependent activation of eeEF2 is mediated allosterically and not via removing an autoinhibitory pseudosubstrate. Investigations using eEF2K fragments showed that there are additional interactions between the kinase domain and Ca^{2+}/CaM, which are also likely to be required for activation.

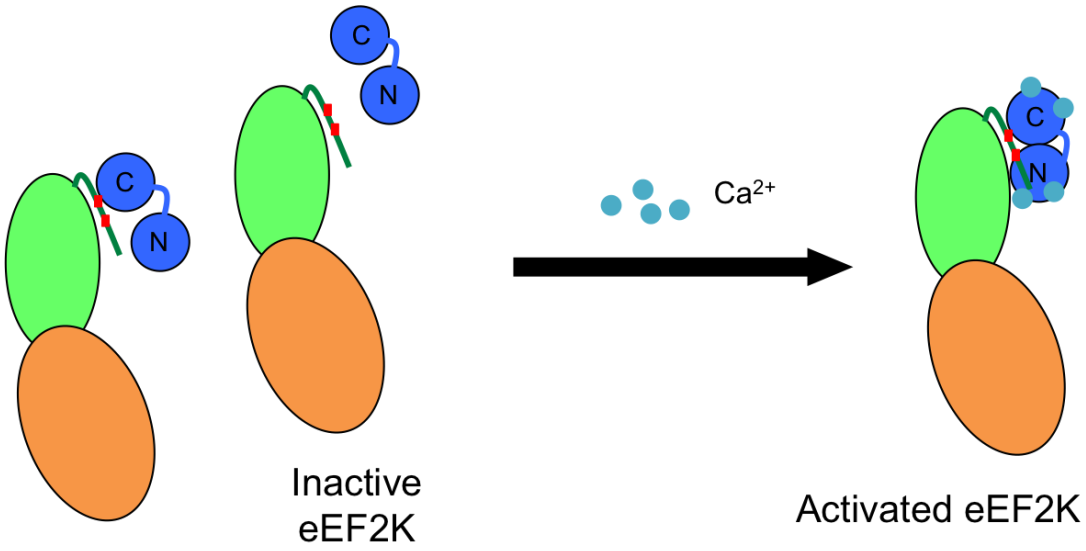

Figure 105. Proposed model for eEF2K activation by CaM.
The green shape represents the kinase domain of eEF2K and the yellow represents the Sel1-like region. The two key tryptophan residues are shown in red, whilst CaM is blue. Apo-CaM may bind to eEF2K, via its C-terminal domain. When the concentration of Ca^{2+} increases within the cell, four Ca^{2+} ions will bind to CaM, greatly increasing its affinity for eEF2K. The C-terminal domain of CaM is responsible for binding to eEF2K at the C-terminal end of the CaM binding sequence, including Trp^{99}. The engagement of the N-terminal domain of CaM to bind to the N-terminal domain of the CaM binding sequence of eEF2K, including Tr^{85}, is critical for the activation of eEF2K.

Given the differences between the purely NOE-derived structure and the structure that incorporates shape data from SAXS experiments (Section 6.5.1), it seems likely that there is an ensemble of CaM conformations present. The wraparound, compact structure is occupied, as shown by the NOE-derived structure, whilst SAXS data indicates a larger average shape, consistent with an open CaM conformation. SAXS modelling has been carried out with full-length eEF2K kinase fragments.

The activation model described is consistent with these findings by Dr. Halina Mikolajek from SAXS experiments using $eEF2K_{(74-342)(490-725)}$ and Ca^{2+}/CaM. A model was produced of the Ca^{2+}/CaM: $eEF2K_{(74-342)(490-725)}$ complex, which is shown in Figure 106 (Hooper and Mikolajek, manuscript in preparation). This SAXS modelling incorporated the NOE-derived structure from this thesis, highlighting that this structure is an important tool for studying eEF2K as a whole. The model fits the experimental molecular envelope well, with an NSD value of 0.97 and provides further evidence that the structure presented in this thesis for the Ca^{2+}/CaM: $eEF2K_{82-100}$ complex is applicable to the study of the interaction between CaM and full-length eEF2K.

The model showed that, in this active form of the kinase, the Sel-1 like domain is located with its N-terminal end contacting the C-terminal end of the kinase domain and there are few contacts between the two domains of eEF2K. CaM is positioned near the N-terminal lobe of the eEF2K kinase domain, away from the kinase active site. It is correctly located so that the peptide ($eEF2K_{82-100}$) binds to CaM in the right orientation (N-terminal end to N-terminal domain of CaM). It is also positioned optimally to reach the start of the eEF2K kinase domain, so that it can be seen how the CaM binding region and kinase domain are connected.

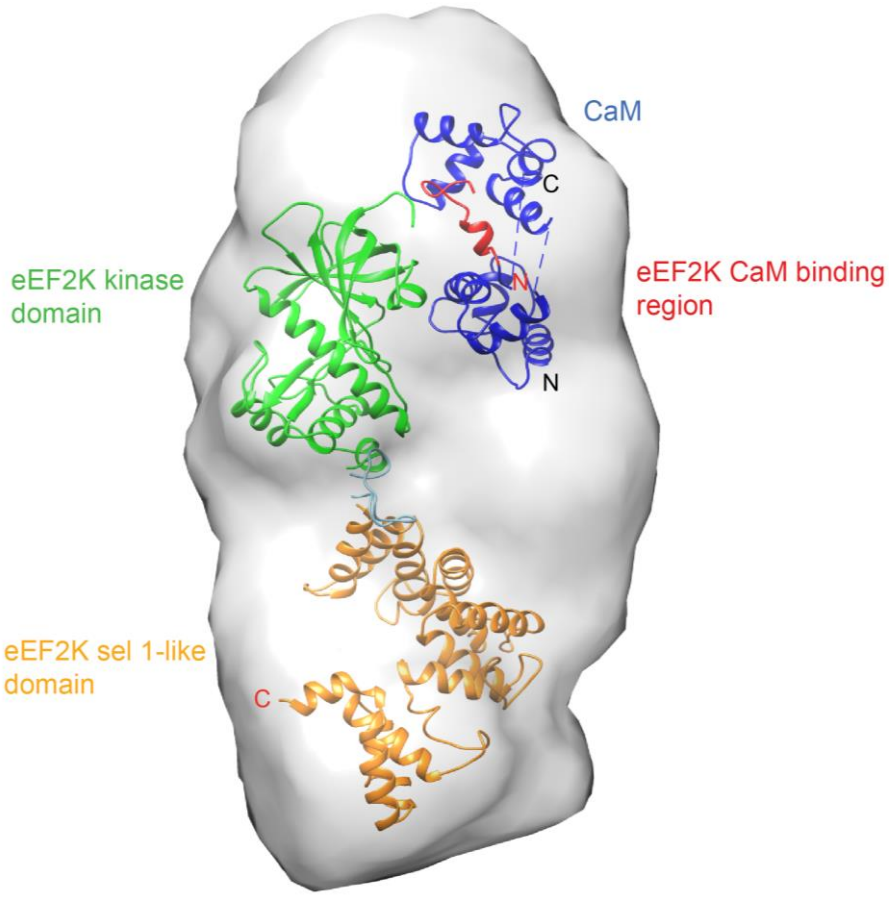

Figure 106. Model of the eEF2K and Ca^{2+}/CaM interaction based on findings from SAXS data.

The *Ab initio* averaged bead model envelope (semitransparent grey) of the Ca^{2+}/CaM: $eEF2K_{(74-342)(490-725)}$ are illustrated. The rigid body model with the best fit to the experimental data is overlaid with the molecular envelope. The kinase domain of eEF2K (green) and the Sel-1 like domain (orange) are displayed as ribbons. Ca^{2+}/CaM is shown in blue. The N- and C-termini of eEF2K (red) and CaM (black) are labeled. Data collected and analysed by Dr Halina Mikolajek, incorporating NOE-derived structure from this thesis (Hooper and Mikolajek, manuscript in preparation).

6.6 Discussion

The solution structure of $eEF2K_{82-100}$ in complex with Ca^{2+}/CaM was solved from NMR data. The quality of the structure is similar to other structures solved by NMR on the PDB, meaning that it can be used to investigate the interaction between these two proteins. In turn, the structure has also provided information on the activation mechanism of eEF2K by Ca^{2+}/CaM, which can be used together with data discussed in Chapter 4 and also recent observations by Drs Claire Moore and Jianling Xie, described in Section 1.5.

It was already known that the activity of eEF2K is increased under acidic conditions (at low pH) (Dorovkov et al., 2002). Three histidine residues (His^{80}, His^{87} and His^{94}) located within the CaM-binding domain of eEF2K are important for the association of CaM with eEF2K and hence the stimulation of eEF2K during acidosis. It was predicted that this likely reflects their ability to undergo protonation over this pH range, and the structure of the Ca^{2+}/CaM: $eEF2K_{82-100}$ complex is consistent with this idea. The two histidine residues in the complex have important roles in binding. For His^{94} especially, this role seems to be dependent on the protonation state of the histidine molecule, with a salt bridge forming upon histidine protonation.

It should be noted that this is not the only mechanism by which acidic pH activates eEF2K. Studies by Xie *et al.*, found that two further histidines in the eEF2K ATP-binding region (His^{227}, His^{230}) and the only histidine residue in CaM (His^{108}), have also been shown to be crucial for the activation of eEF2K at low pH; although they may also contribute to the activation of eEF2K under other conditions. These residues appear to be essential for the stimulation of eEF2K at low pH, since the disruption of any of them was enough to abolish eEF2K activation. These investigations also studied the role of H108K-CaM in the activation of a different CaM-dependent kinase, CaMK1. CaMK1 was activated to a similar extent by wild-type CaM, H108A-CaM and H108K-CaM, either at pH 7.4 or 6.8. Therefore, the effect of H108K-CaM on eEF2K activity is not a general one on CaM-dependent kinases (Xie et al., 2015).

The two tryptophan residues in the CaM binding region of eEF2K were thought to be important for the binding interaction and therefore for eEF2K activation. It was also thought that, as these residues are located at opposite ends of the peptide, one would bind to the N-terminal binding domain of Ca^{2+}/CaM and the other would bind to the C-terminal binding domain. However, elucidation of the structure showed that, whilst Trp^{99} did bind as expected to the C-terminal domain binding pocket, Trp^{85} binds at the interface between the two domains of CaM. Taking into account these observations, there should be some consideration of the activation model presented. In this model, it was

assumed that Trp^{85} would contact the N-terminal binding pocket whilst Trp^{99} would contact the C-terminal domain binding pocket.

With the elucidation of the three-dimensional structure of the Ca^{2+}/CaM: eEF2K complex, we now know that Trp^{85} does not sit within the N-terminal binding pocket. However, the premise of the model still stands. Mutation of Trp^{99} has a marked effect on Ca^{2+}/CaM binding (10-fold decrease in affinity), which is consistent with the fact that it binds to the C-terminal domain binding pocket. This pocket has been shown to exhibit high affinity binding with target, higher than the N-terminal domain binding pocket (Bayley et al., 1996). The preceding residue, Pro^{98}, has also been shown to be important for binding to Ca^{2+}/CaM (Moore et al., 2015). The binding affinity of W85A-eEF2K_{82-100} does not decrease to the same degree as W99A-eEF2K_{82-100}, likely because it does not bind to a site with as high an affinity. Mutation at Trp^{85}, however, affects the activity of eEF2K more severely than mutation at Trp^{99}. A binding role for Trp^{99} and activation role for Trp^{85} still stand. However, it does not seem that the trigger for activation is the binding of Trp^{85} to the N-terminal domain pocket and consequent engagement or "wrapping-around" of the N-terminal domain of Ca^{2+}/CaM. Trp^{85} does contact residues from both the N- and C-terminal domains of Ca^{2+}/CaM and so could still be influential in positioning the N-terminal domain to wrap around the CaM-binding region of eEF2K. However, given its position and the fact that the indole ring of Trp^{85} makes no contacts with Ca^{2+}/CaM, it also seems likely that this residue interacts with the kinase domain of eEF2K. Results presented in Chapter 4, showed that there were additional interactions between the kinase domain of eEF2K and Ca^{2+}/CaM. This has also been shown for other structures of CaM bound to full-length protein targets. In the case of DAPK, both domains of CaM also make extensive contacts with the DAPK catalytic domain, in addition to interactions with the CaM binding region.

An important point to consider is the fact that the molecular shape determined from SAXS data in Chapter 5 differs from the calculated structure of the Ca^{2+}/CaM: eEF2K_{82-100} complex. A compact, wraparound structure, remarkably similar to that seen for other Ca^{2+}/CaM: target peptide structures was elucidated from NMR data, whilst the overall shape of the complex in solution from SAXS data was more open. Combining the SAXS data with the

NOE-derived structure through rigid body modelling slightly widens the structure, as shown in Section 6.5.1. It is likely that this structure provides a more realistic representation of the solution state. This is because a three-dimensional structure calculation using NOE data only involves the process of simulated annealing and energy minimisation, which favours a compact structure. This is in order to satisfy Van der Waals forces and lower the energy of the system. In addition, NOEs strongly bias interatomic configurations towards the smallest possible distances, due to the $1/r^6$ dependence of the NOE (where r is the distance between two atoms). This means that in an ensemble of structures the ones with the shortest interatomic distances will disproportionally contribute to the observed NOEs. These can therefore bias the structure into a closed conformation. In contrast, SAXS data are particularly sensitive to the overall size of the protein with a bias towards larger objects within an ensemble. The most likely explanation of the slightly different conformations of the NOE and SAXS derived structures of CaM is that an ensemble of conformations is present, whereby the two domains of CaM can collapse and engulf the peptide but can also be in an open conformation. This in consistent with findings in the literature, described in Section 1.4.4, where NMR data from Gsponer et al. (2008) of Ca^{2+}/CaM showed an ensemble of different conformational states that included a range of structures that resembled the compact structure of Ca^{2+}/CaM bound to a target peptide from myosin light chain kinase (MLCK). It is also consistent with RDC data that showed there were dynamics between the two domains of CaM. The NOE-derived structure biases the compact structure, whilst the SAXS shape represents an average structure, which is slightly more open. SAXS modelling showed that the same interactions between $eEF2K_{82\text{-}100}$ and Ca^{2+}/CaM are maintained between the NOE-derived structure and the structure that included the SAXS data. It is therefore a good representation of the interaction.

As described in Section 6.6.4, Ca^{2+}/CaM binds near to the top of the N-terminal lobe of eEF2K, distal from the active site of the enzyme. This is consistent with a mechanism of allosteric control and differs from the mechanism of activation seen for other members of the Ca^{2+}/CaM-dependent kinases, as described in Section 1.6.6. For these kinases, an autoinhibitory

domain is present, adjacent to the CaM binding region that acts as a pseudosubstrate to keep the kinase inactive. Binding of Ca^{2+}/CaM relieves this autoinhibition to activate the kinases. It seems unlikely given the position of the CaM binding region and Ca^{2+}/CaM in the structural model presented in Section 6.6.4 that this mechanism of control occurs for eEF2K. Instead allosteric control seems a likely mechanism, similar to that seen for other kinases such as the epidermal growth factor (EGF) receptor kinase. In this case the C-terminal lobe of one receptor kinase domain binds to the N-terminal lobe of a second kinase receptor domain resulting in its activation. In turn, this kinase phosphorylated the tail of the first receptor kinase resulting in the recruitment of downstream signalling molecules (Zhang et al., 2006). In this mechanism the contact is not at the kinase active site, however still results in kinase activation.

In conclusion the elucidation of the Ca^{2+}/CaM: $eEF2K_{82\text{-}100}$ complex has aided in clarifying a number of observations concerning the activation of eEF2K. Previously, there has been little structural information to help explain these observations. However, with the availability of this structure some of these observations can now be explained.

Chapter 7. General Discussion and Outlook

8.1 Conclusions

The aim of this research project was to gain insight into the molecular mechanism of eEF2K activation by CaM. As discussed, the three-dimensional structure of eEF2K itself is unknown and despite CaM being one of the most well studied and understood proteins, there is little known about its interaction with eEF2K. Although there are a number of Ca^{2+}/CaM: target peptide complexes whose structures have been solved, previous to this thesis, the structure of Ca^{2+}/CaM bound to the eEF2K binding region remained unknown. Now that we have elucidated this structure, it can be applied to functional eEF2K studies. Indeed, we have used the three-dimensional structure to determine explanations for some known observations on the function of eEF2K from the laboratory of Prof. Chris Proud, and also to confirm our findings from initial experiments described in Chapters 3-5 of this thesis.

We initially defined the binding surfaces of Ca^{2+}/CaM and apo-CaM responsible for interacting with a peptide from eEF2K that corresponds to the CaM binding region. CSPs were calculated based on assigned ^{1}H-^{13}C-HSQC spectra collected in the peptide free and peptide bound states to determine those residues affected by the addition of $eEF2K_{82\text{-}100}$. We found that residues in both domains of Ca^{2+}/CaM are involved in binding to $eEF2K_{82\text{-}100}$ but that for apo-CaM only the C-terminal domain is involved.

In addition, we determined those residues of CaM which experienced a change in chemical shift or exchange characteristics upon addition of longer eEF2K fragments that represent the full-length kinase. The residues of Ca^{2+}/CaM that are involved in binding to an eEF2K fragment that contains both the CaM binding region and the kinase domain are conserved with those identified as binding to $eEF2K_{82\text{-}100}$. This is an important observation as it confirms that observations made from studies with $eEF2K_{82\text{-}100}$ can be applied to full-length eEF2K. The same is true for apo-CaM, whereby only C-terminal residues are involved in binding to $eEF2K_{82\text{-}100}$ and to an eEF2K fragment containing the CaM binding region and the kinase domain. It is interesting that

apo-CaM is still able to bind to $eEF2K_{82-100}$, although the affinity is weak at 1.38 mM. The CaM binding region of eEF2K is not recognised as conforming to a standard CaM binding motif, however, it does contain an isoleucine followed by a glutamine, which is a key feature of the IQ motif that is often attributed to calcium independent binding of CaM to target proteins.

Two eEF2K fragments, as well as $eEF2K_{82-100}$, were investigated to dissect those regions of the kinase important for the binding of CaM and also the consequent activation of eEF2K. Ca^{2+}/CaM is able to bind to a kinase fragment that does not contain the CaM binding region, showing that there are additional interactions between Ca^{2+}/CaM and the kinase domain of eEF2K. In contrast, apo-CaM did not bind to this eEF2K fragment, lacking the CaM binding region. It is therefore possible that apo-CaM is able to interact with eEF2K, via the CaM binding region only, but this is not sufficient to cause the activation of eEF2K. It seems possible that the additional interactions of Ca^{2+}/CaM with the kinase domain may be the trigger for activation of the kinase. Taken together these results lead to a possible mechanism of activation of eEF2K whereby interactions between the kinase domain of eEF2K and Ca^{2+}/CaM are responsible for the formation of a fully active eEF2K. The determination of the structure of the Ca^{2+}/CaM: $eEF2K_{82-100}$ complex are consistent with these observations, with some key residues known to heavily influence eEF2K activity, being located on the outside of the complex structure and therefore able to make contact with the kinase domain of eEF2K. In addition, combining structural information from the three-dimensional structure and the SAXS data derived structural model, as well as the observations just discussed, an activation model for eEF2K has been proposed. Binding of Ca^{2+}/CaM, predominantly via its C-terminal domain and the C-terminal end of the CaM binding region of eEF2K, is the first key step in triggering eEF2K activation. However, it seems that further engagement between the N-terminal domain of CaM and residues at the N-terminal end of the CaM binding region of eEF2K are necessary to initiate complete activation of eEF2K. In addition, some interactions between the kinase domain of eEF2K and CaM are important. This is also consistent with initial findings from analysis of the peptide titration, described in Section 4.3.2, where it was determined that the interaction

between $eEF2K_{82\text{-}100}$ and Ca^{2+}/CaM was complex. Preliminary analysis using SPINACH proved that a one-step binding model could not describe the interaction. Trp^{99} is the key residue of eEF2K for mediating the binding to Ca^{2+}/CaM, whilst Trp^{87} is critical for initiating further changes and interactions that fully activate the kinase.

Importantly, the elucidation of the structure of the complex was used to explain observations related to the effect of pH and proline hydroxylation on eEF2K activity, as outlined in sections 6.6.1 and 6.6.2. It will continue to be used for this purpose, aiding in understanding the interaction between eEF2K and CaM and kinase activation.

8.2 Outlook

Significant progress has been made in understanding the interaction between CaM and eEF2K, to help determine the mechanism of eEF2K activation. However, there still remains scope for further research on this project.

An important step in developing the understanding of the interaction further would be to complete the analysis of peptide titration data using SPINACH. This thesis described results for fitting of the simplest interaction model and showed that this was not suitable for the majority of residues of CaM. Further models should therefore be analysed to discover the steps involved in eEF2K binding to Ca^{2+}/CaM. The binding affinities of the different steps can also be determined using SPINACH. It may also be interesting to look at the LineshapeKin method (Kovrigin, 2012) for the analysis of the peptide titration data, especially for those peaks that can be easily traced in one dimension.

Now that the labour intensive task of resonance assignment for structure calculation has been performed for the Ca^{2+}/CaM: $eEF2K_{82\text{-}100}$ complex, it would be interesting to calculate the structures of Ca^{2+}/CaM bound to the W85A-$eEF2K_{82\text{-}100}$ and W99A-$eEF2K_{82\text{-}100}$ peptides. This would help to confirm the roles attributed to these two residues from the work outlined in this thesis. It

would also be interesting to study the N- and C-terminal domains of CaM in isolation to investigate if and how they bind individually to eEF2K, and also whether they are able to elicit eEF2K activity separately.

The significance of the Ca^{2+}/CaM: $eEF2K_{82-100}$ complex structure will come from its utility to studying the interaction with full-length eEF2K, something which has already started to be done, as discussed in Section 6.6.4. In the absence of a three-dimensional structure of eEF2K from X-ray crystallography or NMR, the structure of the target peptide complex is important for studying eEF2K. However, the ideal next step would be to determine the high resolution atomic structure of eEF2K, a task that has so far not been possible. *E. coli* may not be the best expression system for eEF2K and so some success could be possible using an insect cell expression system. The development of an inhibitor for eEF2K may also improve the success of structural studies on the kinase domain.

Appendix

Appendix 1. NMR experimental parameters for resonance assignment of Ca^{2+}/CaM

Data set	Experiment	Parameters		
		Acquisition times (s)	Heteronuclear decoupling	Mixing time (S)
Ca^{2+}/CaM	HNCACB	t_1^C=0.005 t_2^N=0.025 t_3^{NH}=0.051	wurst40N	
	CBCA(CO)NH	t_1^C=0.005 t_2^N=0.028 t_3^{NH}=0.051	wurst40N	
	H(CCO)NH	t_1^H=0.014 t_2^N=0.033 t_3^{NH}=0.050	wurst40N	0.012
	HCCH-TOCSY	t_1^H=0.010 t_2^C=0.005 t_3^H=0.050	wurst80	
	^{15}N-NOESY-HSQC	t_1^H=0.007 t_2^N=0.027 t_3^{NH}=0.050	wurst40N	0.15
	^{15}N-TOCSY-HSQC	t_1^H=0.013 t_2^N=0.027 t_3^{NH}=0.050	wurst40N	0.05

Appendix 2. NMR experimental parameters for the assignment of the Ca^{2+}/CaM: eEF2K$_{82-100}$ complex (1:10 ratio)

Data set	Experiment	Parameters		
		Acquisition times (s)	Heteronuclear decoupling	Mixing time (S)
Ca^{2+}/CaM: eEF2K$_{82-100}$ complex	HNCA	t_1^C=0.007 t_2^N=0.040 t_3^{NH}=0.051	wurst40N	
	HNCACB	t_1^C=0.005 t_2^N=0.044 t_3^{NH}=0.051	wurst40N	
	CBCA(CO)NH	t_1^C=0.004 t_2^N=0.033 t_3^{NH}=0.051	wurst40N	
	H(CCO)NH	t_1^H=0.006 t_2^N=0.027 t_3^{NH}=0.051	wurst40N	0.012
	HCCH-TOCSY	t_1^H=0.010 t_2^C=0.005 t_3^H=0.050	wurst80	
	^{15}N-NOESY-HSQC	t_1^H=0.009 t_2^N=0.032 t_3^{NH}=0.050	wurst40N	0.15

Appendix 3. NMR experimental parameters for the assignment of apo-CaM

Data set	Experiment	Parameters		
		Acquisition times (s)	Heteronuclear decoupling	Mixing time (S)
Apo-CaM	HNCACB	t_1^C=0.008 t_2^N=0.033 t_3^{NH}=0.050	wurst40N	
	H(CCO)NH	t_1^H=0.014 t_2^N=0.033 t_3^{NH}=0.050	wurst40N	0.012
	HCCH-TOCSY	t_1^H=0.010 t_2^C=0.006 t_3^H=0.050	wurst80	
	^{15}N-NOESY-HSQC	t_1^H=0.008 t_2^N=0.028 t_3^{NH}=0.050	wurst40N	0.15
	^{15}N-TOCSY-HSQC	t_1^H=0.014 t_2^N=0.033 t_3^{NH}=0.050	wurst40N	0.06

Appendix 4. NMR experimental parameters for the assignment of the apo-CaM: eEF2K$_{82-100}$ complex

Data set	Experiment	Parameters		
		Acquisition times (s)	Heteronuclear decoupling	Mixing time (S)
Apo-CaM: eEF2K$_{82-100}$ complex	HNCA	t_1^C=0.011 t_2^N=0.021 t_3^{NH}=0.107	wurst40N	
	HNCA (42 °C)	t_1^C=0.011 t_2^N=0.021 t_3^{NH}=0.050	wurst40N	
	HNCACB	t_1^C=0.007 t_2^N=0.021 t_3^{NH}=0.050	wurst40N	
	HNCACB (42 °C)	t_1^C=0.004 t_2^N=0.021 t_3^{NH}=0.050	wurst40N	
	CBCA(CO)NH	t_1^C=0.006 t_2^N=0.034 t_3^{NH}=0.064	wurst40N	
	H(CCO)NH	t_1^H=0.009 t_2^N=0.021 t_3^{NH}=0.050	wurst40N	0.012
	HCCH-TOCSY	t_1^H=0.010 t_2^C=0.005 t_3^H=0.050	wurst80	
	HCCH-TOCSY (42 °C)	t_1^H=0.010 t_2^C=0.005 t_3^H=0.050	wurst80	
	^{15}N-NOESY-HSQC	t_1^H=0.009 t_2^N=0.028 t_3^{NH}=0.050	wurst40N	0.15

Appendix 5. NMR experimental parameters for Ca^{2+}/CaM peptide titration and ATCUN-eEF2K$_{82-100}$ investigation

Data set	Experiment	Parameters		
		Acquisition times (s)	Heteronuclear decoupling	Mixing time (S)
Ca^{2+}/CaM	*Peptide titration* ^{1}H-^{15}N-HSQC	t_1^N=0.063 t_2^H=0.064	wurst40N	
	Peptide titration ^{1}H-^{13}C-HSQC	t_1^C=0.009 t_2^H=0.064	wurst40N	
	ATCUN-eEF2K$_{82-100}$ investigation ^{1}H-^{15}N-HSQC	t_1^N=0.063 t_2^H=0.064	wurst40N	
Apo-CaM	*Peptide titration* ^{1}H-^{15}N-HSQC	t_1^N=0.063 t_2^N=0.064	wurst40N	
	Peptide titration ^{1}H-^{13}C-HSQC	t_1^C=0.009 t_2^N=0.064	wurst40N	

Appendix 6. NMR experimental parameters for the assignment of the Ca^{2+}/CaM: eEF2K$_{82-100}$ complex at a 1:1 ratio and for the NOE assignment for the structure calculation

Data set	Experiment	Parameters		
		Acquisition times (s)	Heteronuclear decoupling	Mixing time (S)
Ca^{2+}/ CaM: eEF2K$_{82-100}$ complex (1:1 ratio)	HNCACB	t_1^C=0.008 t_2^N=0.027 t_3^{NH}=0.064	wurst40N	
	CBCA(CO)NH	t_1^C=0.006 t_2^N=0.034 t_3^{NH}=0.064	wurst40N	
	H(CCO)NH	t_1^H=0.013 t_2^N=0.027 t_3^{NH}=0.064	wurst40N	
	^{15}N-TOCSY HSQC	t_1^H=0.014 t_2^N=0.027 t_3^{NH}=0.064	wurst40N	0.05

	^{15}N-NOESY HSQC	t_1^H=0.008 t_2^N=0.027 t_3^{NH}=0.064	wurst40N	0.12
	HCCH-TOCSY	t_1^H=0.010 t_2^C=0.005 t_3^H=0.064	wurst80	
	hbCBcgcdceHE	t_1^C=0.008 t_2^H=0.064		
	hbCBcgcdHD	t_1^C=0.008 t_2^H=0.064		
	HNCO	t_1^C=0.011 t_2^N=0.027 t_3^{NH}=0.064		
	2D CN FIL NOESY	t_1^H=0.12 t_2^H=0.048		0.15
	2D CN FIL TOCSY	t_1^H=0.12 t_2^H=0.03		0.15
	^{13}C-NOESY HSQC	t_1^H=0.104 t_2^C=0.002 t_3^H=0.021		0.15
	3D NOESY CN FIL	t_1^H=0.011 t_2^C=0.005 t_3^H=0.064	Wurst40N	0.15

Appendix 7. Chemical shift Table for Ca^{2+}/CaM

	H	N	HA	HB	HG	HD	HE	CA	CB	CG	CD	CE
1	8.42	122.3	4.06	1.32	-	-	-	54.02	18.91	-	-	-
2	7.85	116.32	4.5	2.73,2.73	-	-	-	55.47	41.12	-	-	-
3	7.85	117.51	4.4	2.33,2.39	2.42,2.36	-	-	55.72	29.96	34.03	-	-
4	7.73	121.23	4.68	1.53,1.84	1.85	0.92,0.96	-	54.54	43.89	27.43	23.62,27.39	-
5	8.83	112.79	4.48	4.78	1.33	-	-	60.7	71.42	22.56	-	-
6	9.08	120.55	3.99	2.05,1.98	2.42,2.34	-	-	60.25	29.6	36.85	-	-
7	8.78	119.59	-	-	-	-	-	60.34	29.34	-	-	-
8	7.81	120.42	3.87	2.06,2.36	2.40,2.32	-	-	58.92	29.6	37.13	-	-
9	8.49	119.69	3.72	1.97	1.11,1.13,1.84	0.88	-	66.46	38.08	17.55,30.88	13.17	-
10	8.06	121.33	4.14	1.54	-	-	-	55.71	18.07	-	-	-
11	7.84	119.81	-	-	-	-	-	59.53	29.51	-	-	-
12	8.64	120.24	-	-	-	-	-	59.51	38.12	-	-	-
13	9.3	123.79	4.04	1.94,1.95	1.04,1.24	1.24,1.37	2.60,2.56	60.45	32.24	25.59	28.77	41.78
14	7.83	120.42	-	-	-	-	-	59.54	29.4	-	-	-
15	8.06	122.73	4.32	1.99	-	-	-	55.6	18.25	-	-	-
16	8.91	119.5	3.23	2.94,3.01	-	-	-	62.22	39.82	-	-	-
17	7.96	112.74	4.14	4.02,4.07	-	-	-	61.76	63.56	-	-	-
18	7.48	120.89	4.02	1.62,1.74	1.5	0.74,0.86	-	57.41	41.78	26.76	24.10,24.46	-
19	7.37	115.25	4.25	2.72,2.62	-	-	-	59.63	41.27	-	-	-
20	7.91	117.69	4.55	2.38,1.51	-	-	-	52.66	39.19	-	-	-
21	7.73	124.62	3.98	1.90,1.83	1.51,1.45	1.71,1.68	3.01,3.03	58.88	32.99	24.9	28.94	41.95
22	8.1	113.94	4.59	3.08,2.67	-	-	-	53.08	39.85	-	-	-
23	7.75	109.39	3.98,3.82	-	-	-	-	47.51	-	-	-	-
24	8.44	120.76	4.52	3.05,2.45	-	-	-	54.02	40.75	-	-	-
25	10.69	113.36	4.37,3.71	-	-	-	-	45.76	-	-	-	-

26	8.18	113.09	5.31	3.86	1.05	-	-	60.08	72.84	21.77	-	-
27	9.85	127.16	4.98	1.81	0.89,1.16,0.29	0.26	-	60.68	39.93	27.24,17.93	15.63	-
28	8.52	116.67	4.83	4.03	1.31	-	-	59.81	72.58	22.11	-	-
29	9.16	112.94	3.8	4.23	1.28	-	-	66.69	68.18	23.4	-	-
30	7.74	120.99	4.15	1.89,1.83	1.42,1.48	1.67,1.69	3.00,3.00	59.49	32.82	24.67	29.31	42.47
31	7.73	121.59	4.08	1.92,2.06	2.35,2.47	-	-	59.55	30.2	35.71	-	-
32	8.79	120.76	4.13	1.89,1.55	1.62	0.83,0.91	-	58.08	42.95	26.24	24.79,23.83	-
33	8.71	128.23	3.59,4.00	-	-	-	-	48.67	-	-	-	-
34	7.98	118.12	3.93	4.32	1.28	-	-	67.31	68.96	21.78	-	-
35	7.67	122.15	3.53	1.97	0.40,0.68	-	-	66.46	31.51	20.60,22.92	-	-
36	8.52	118.61	-	-	-	-	2.05	59.34	31.66	-	-	17.32
37	8.59	119.12	-	-	-	-	-	59.39	30.45	-	-	-
38	7.96	118.95	4.36	4.14,4.05	-	-	-	61.78	63.25	-	-	-
39	7.42	120.7	4.52	1.91,1.81	1.81	0.85,0.85	-	54.76	42.29	25.83	25.82,22.48	-
40	7.93	129.53	3.81,4.28	-	-	-	-	45.83	-	-	-	-
41	7.85	118.54	-	-	-	-	-	54.77	30.79	-	-	-
42	8.77	116.38	5.21	2.80,2.53	-	-	-	51.66	39.58	-	-	-
43	-	-	-	-	-	-	-	62.62	32.19	-	-	-
44	8.81	113.13	4.47	4.74	1.35	-	-	60.76	71.36	21.88	-	-
45	8.87	120.81	-	-	-	-	-	60.23	29.28	-	-	-
46	8.33	120.87	4.12	1.4	-	-	-	55.26	18.38	-	-	-
47	7.75	118.79	-	-	-	-	-	59.24	30.06	-	-	-
48	8.24	120.63	4.1	2.09,1.27	-	0.86,0.84	-	58.19	42.72	-	26.02,23.40	-
49	8.26	118.4	3.82	2.24,2.19	2.46,2.43	-	-	58.84	28.51	35.18	-	-
50	8.16	120.08	4.44	2.82,2.69	-	-	-	57.86	40.56	-	-	-
51	7.91	119.5	-	-	-	-	2.05	59.54	33.53	-	-	17.27
52	7.76	118.28	3.51	1.96	1.03,0.74,0.70	0.74	-	65.13	37.62	28.97,16.00	12.97	-
53	8.65	117.8	4.38	3.00,2.89	-	-	-	56.18	38.33	-	-	-
54	7.62	116.42	-	-	-	-	-	59.14	30.69	-	-	-
55	7.25	108.27	4.5	2.41	0.82,0.92	-	-	60.95	33.01	19.25,22.03	-	-
56	7.71	121.96	-	-	-	-	-	53.98	40.39	-	-	-
57	8.53	109.33	4.21	1.54	-	-	-	54.6	19.68	-	-	-
58	8.19	113.79	-	-	-	-	-	52.91	40.07	-	-	-
59	7.63	108.49	3.80,3.91	-	-	-	-	47.49	-	-	-	-
60	8.12	118.54	4.65	2.67,3.32	-	-	-	52.83	38.04	-	-	-
61	10.65	113.54	-	-	-	-	-	45.96	-	-	-	-
62	7.72	109.06	4.76	4.02	1.13	-	-	59.79	72.22	22.43	-	-
63	8.96	123.76	5.18	2.07	1.58,1.24,0.98	0.82	-	60.38	40.09	27.48,18.42	13.79	-
64	8.86	128.28	5.38	2.85,3.12	-	-	-	52.41	42.47	-	-	-

65	8.99	118.79	-	-	-	-	-	63.84	36.18	-	-	-
66	-	-	-	-	-	-	-	66.92	30.85	-	-	-
67	7.99	117.77	-	-	-	-	-	58.92	29.85	-	-	-
68	8.91	123.69	-	-	-	-	-	61.44	40.3	-	-	-
69	8.42	118.85	3.36	1.63,1.09	1.02	0.62,0.62	-	58.18	41.37	25.78	25.70,24.09	-
70	7.54	115.39	3.74	4.37	1.22	-	-	66.91	68.56	22.3	-	-
71	7.83	121.65	3.78	2.11,2.13	2.43	-	1.85	59.25	33.82	36.43	-	17.09
72	8.12	116.59	-	-	-	-	1.72	55.96	31.32	-	-	17.62
73	8.32	122.54	4.11	1.4	-	-	-	54.77	18.4	-	-	-
74	7.68	116.84	-	-	-	-	-	58.53	30.53	-	-	-
75	7.65	118.53	4.23	1.88,1.83	1.67,1.69	1.43,1.51	2.94,2.96	57.53	32.75	28.67	24.67	42.2
76	7.87	118.79	-	-	-	-	1.99	56.9	33.25	-	-	17.39
77	7.94	120.65	4.32	1.83,1.89	1.50,1.51	1.68,1.63	2.99,2.99	56.94	33.37	24.61	28.94	41.67
78	8.35	121.79	4.69	2.78,2.67	-	-	-	54.98	41.36	-	-	-
79	8.14	114.58	4.3	4.24	1.22	-	-	62.6	70.02	21.97	-	-
80	8.49	123.26	4.69	2.71,2.79	-	-	-	54.97	41.55	-	-	-
81	8.48	117.24	4.45	4.06,3.97	-	-	-	59.67	63.97	-	-	-
82	8.53	122.66	-	-	-	-	-	58.76	29.85	-	-	-
83	8.34	119.81	-	-	-	-	-	59.68	29.66	-	-	-
84	8.23	118.88	-	-	-	-	-	59.56	29.81	-	-	-
85	8.05	122.16	4.07	2.19	1.14,1.80,1.13	0.81	-	64.84	37.74	29.09,19.20	13.2	-
86	8.46	121.93	-	-	-	-	-	60.3	30.15	-	-	-
87	8.18	118.83	-	-	-	-	-	59.19	29.51	-	-	-
88	8.01	122.14	4.22	1.8	-	-	-	55.47	17.89	-	-	-
89	8.61	118.94	-	-	-	-	-	62.34	39.28	-	-	-
90	7.73	115.77	-	-	-	-	-	59.09	30.53	-	-	-
91	7.62	118.41	3.51	2.17	0.69,1.02	-	-	65.92	31.96	21.16,22.66	-	-
92	7.65	116.84	4.25	2.68,2.62	-	-	-	60.18	40.52	-	-	-
93	7.9	117.13	-	-	-	-	-	52.49	38.51	-	-	-
94	7.75	126.02	3.92	1.86,1.85	1.48,1.55	1.68,1.66	2.88,2.90	59.33	33.08	24.87	28.92	41.63
95	8.23	114.04	-	-	-	-	-	53.25	39.84	-	-	-
96	7.83	109.38	3.90,3.83	-	-	-	-	47.42	-	-	-	-
97	8.36	119.56	4.66	2.69,3.42	-	-	-	52.98	38.53	-	-	-
98	10.7	113.13	4.05,3.43	-	-	-	-	45.45	-	-	-	-
99	7.65	115.87	5.06	2.54,2.48	-	-	-	56.35	43.51	-	-	-
100	10.17	127.37	4.86	1.9	1.18,0.28,0.96	0.29	-	60.42	38.93	17.74,27.38	15.23	-
101	9	123.9	4.84	4.45,4.00	-	-	-	56.12	66.85	-	-	-
102	9.24	123.01	3.93	1.49	-	-	-	56.19	18.21	-	-	-
103	8.3	118.5	4.03	1.44	-	-	-	55.46	18.57	-	-	-

104	7.91	119.72	-	-	-	-	-	59.49	29.55	-	-	-
105	8.68	121.29	4.13	1.89,1.57	1.57	0.92,0.90	-	58.44	42.37	27.35	26.18,23.89	-
106	8.6	117.68	-	-	-	-	-	60.03	30.79	-	-	-
107	7.92	118.59	-	-	-	-	-	55.83	30.73	-	-	-
108	7.95	118.9	3.53	1.99	0.42,0.81	-	-	66.14	31.9	20.76,23.09	-	-
109	8.29	116.75	4.37	2.65,2.63	2.76,2.74	-	2.12	57.61	31.63	33.09	-	17.09
110	8.2	114.97	4.24	4.27	1.24	-	-	65.85	69.3	21.69	-	-
111	7.99	122.21	-	-	-	-	-	55.8	38.75	-	-	-
112	7.95	119.18	4.32	2.09,1.27	1.79	0.87,0.83	-	55.66	42.36	26.78	25.88,23.00	-
113	7.93	129.53	4.25,3.77	-	-	-	-	45.8	-	-	-	-
114	7.96	120.44	-	-	-	-	-	55.55	30.77	-	-	-
115	8.62	123.89	4.4	1.71,1.81	1.42,1.36	1.68,1.68	2.99,2.99	55.9	32.42	24.91	29.25	42.25
116	8.16	124.8	4.75	1.48,1.59	1.58	0.82,0.82	-	54.44	45.07	27.45	23.65,26.84	-
117	9.27	114.68	4.47	4.76	1.35	-	-	60.88	71.45	21.65	-	-
118	8.95	121.13	4.21	2.75,2.59	-	-	-	58.31	39.96	-	-	-
119	8.73	119.2	-	-	-	-	-	60.18	29.34	-	-	-
120	7.82	120.63	-	-	-	-	-	59.49	30.78	-	-	-
121	8.16	121.38	3.63	2.24	1.03,0.98	-	-	67.16	31.62	24.04,22.48	-	-
122	8.11	119.85	4.35	2.63,2.79	-	-	-	57.95	40.75	-	-	-
123	8.04	119.68	-	-	-	-	-	59.33	29.74	-	-	-
124	7.86	119.73	4.04	2.46,2.48	2.77,2.75	-	2.12	59.62	33.56	32.42	-	17.11
125	8.01	118.56	3.51	2.12	1.28,0.74,1.57	0.74	-	64.15	36.76	16.30,28.11	11.01	-
126	8.21	118.5	-	-	-	-	-	59.98	30.45	-	-	-
127	8	116.01	-	-	-	-	-	58.68	29.96	-	-	-
128	7.41	118.98	4.41	1.44	-	-	-	52.35	21.35	-	-	-
129	7.91	117.56	-	-	-	-	-	54.23	40.51	-	-	-
130	8.42	127.8	3.91	2.01	0.96,1.35,1.70	0.9	-	63.61	38.86	28.19,17.49	12.32	-
131	8.34	116.68	-	-	-	-	-	54.06	40.15	-	-	-
132	7.63	108.63	4.00,3.82	-	-	-	-	47.72	-	-	-	-
133	8.38	120.87	4.5	2.50,2.95	-	-	-	53.95	40.51	-	-	-
134	10.43	113.03	4.05,3.43	-	-	-	-	46.05	-	-	-	-
135	8	115.51	4.87	1.95,1.84	1.70,1.95	-	-	53.43	32.57	33.18	-	-
136	9.18	125.45	5.23	2.32	0.92,1.29	-	-	61.75	33.8	22.52,22.11	-	-
137	9.54	129.02	5.24	3.32,3.26	-	-	-	51.42	38.59	-	-	-
138	8.53	118.5	3.45	2.09,2.40	-	-	-	63.05	37.93	-	-	-
139	8.17	118.48	-	-	-	-	-	60.65	29.2	-	-	-
140	8.81	119.87	-	-	-	-	-	58.64	30.1	-	-	-
141	9.04	124.93	4.01	3.20,3.41	-	-	-	61.8	40.13	-	-	-
142	8.57	119.51	3.13	1.89	0.76,0.53	-	-	67.3	31.88	21.26,22.93	-	-

143	7.39	118.06	3.91	2.44,2.44	2.41,2.47	-	-	59.09	28.46	33.68	-	-
144	8.01	119.76	-	-	-	-	1.9	58.64	33.68	-	-	17.17
145	7.9	114.77	-	-	-	-	1.76	55.45	32.16	-	-	17.42
146	7.62	111.92	4.29	4.25	1.19	-	-	62.87	70.36	21.36	-	-
147	7.82	126.75	4.32	1.41	-	-	-	53.04	19.19	-	-	-
148	7.8	125.78	-	-	-	-	-	57.77	33.9	-	-	-

Appendix 8. Chemical shift Table for the Ca^{2+}/CaM: $eEF2K_{82-100}$ complex (1:10 ratio)

	H	N	HA	HB	HG	HD	HE	CA	CB	CG	CD	CE
1	-	-	-	-	-	-	-	-	-	-	-	-
2	7.84	116.48	-	-	-	-	-	-	-	-	-	-
3	7.87	117.68	-	-	-	-	-	-	-	-	-	-
4	7.76	121.41	4.67	1.79,1.51	1.79	0.90,0.92	-	54.24	43.59	27.27	23.60,27.16	-
5	8.71	112.82	4	4.04	1.16	-	-	60.6	71.36	22.54	-	-
6	9.05	120.57	-	-	-	-	-	60.25	29.51	-	-	-
7	8.74	119.49	-	-	-	-	-	60.16	29.32	-	-	-
8	7.75	120.57	-	-	-	-	-	58.8	29.25	-	-	-
9	8.3	119.16	3.6	1.91	0.86,1.08,1.09	0.86	-	66.48	37.95	30.38,17.52	13	-
10	8.04	121.17	4.11	1.51	-	-	-	55.68	18.11	-	-	-
11	7.8	120.02	-	-	-	-	-	59.54	29.37	-	-	-
12	8.57	120.59	-	-	-	-	-	58.93	37.5	-	-	-
13	9.25	123.71	-	-	-	-	-	60.22	32.11	-	-	-
14	7.98	120.77	-	-	-	-	-	59.5	29.5	-	-	-
15	7.98	121.94	4.28	1.98	-	-	-	55.52	18.2	-	-	-
16	8.68	118.98	-	-	-	-	-	62.17	40.04	-	-	-
17	8.17	113.5	-	-	-	-	-	61.69	63.54	-	-	-
18	7.38	120.35	3.93	1.66,1.45	1.47	0.67,0.80	-	57.4	41.54	26.89	23.94,24.92	-
19	7.05	112.85	-	-	-	-	-	59.2	41.71	-	-	-
20	7.6	116.47	-	-	-	-	-	52.33	39.36	-	-	-
21	7.6	124.43	-	-	-	-	-	58.36	32.47	-	-	-
22	8.24	114.23	-	-	-	-	-	53.05	39.74	-	-	-
23	7.72	109.44	-	-	-	-	-	47.5	-	-	-	-
24	8.51	120.97	-	-	-	-	-	54.01	40.66	-	-	-
25	10.6	113.15	-	-	-	-	-	45.63	-	-	-	-
26	8.29	112.73	5.49	3.87	1.07	-	-	59.93	73.01	22.34	-	-
27	9.97	127.04	4.78	1.76	0.99,1.20,1.25	0.4	-	61.57	40.49	17.59,26.79	15.67	-
28	8.3	116.38	-	-	-	-	-	59.39	72.61	-	-	-

29	9.24	114.35	3.77	4.19	1.26	-	-	66.97	68.28	23.29	-	-
30	7.84	121.11	-	-	-	-	-	59.52	32.77	-	-	-
31	7.81	121.94	-	-	-	-	-	59.88	29.93	-	-	-
32	8.64	119.81	4.09	1.30,1.80	1.35	0.49,0.54	-	58.36	42.65	26.89	23.67,26.07	-
33	8.75	105.66	-	-	-	-	-	48.74	-	-	-	-
34	8.03	118.49	3.92	4.41	1.27	-	-	67.2	69.09	21.5	-	-
35	8.1	122.8	3.43	2.21	0.97,0.89	-	-	66.95	31.93	22.13,23.80	-	-
36	8.78	118.39	-	-	-	-	1.85	58.97	31.09	-	-	17.17
38	8.04	119.31	-	-	-	-	-	61.76	62.76	-	-	-
39	7.48	120.55	4.33	1.61,1.90	-	0.74,0.81	-	55	42.18	-	22.97,26.03	-
40	7.94	107.18	-	-	-	-	-	45.74	-	-	-	-
41	7.78	118.01	-	-	-	-	-	54.47	30.87	-	-	-
42	8.73	116.64	-	-	-	-	-	51.53	39.62	-	-	-
43	-	-	-	-	-	-	-	62.37	31.9	-	-	-
44	8.76	113	4.42	4.74	1.33	-	-	60.78	71.34	21.92	-	-
45	8.85	120.81	-	-	-	-	-	60.24	29.22	-	-	-
46	8.29	120.92	4.1	1.38	-	-	-	55.23	18.65	-	-	-
47	7.72	119.11	-	-	-	-	-	59.23	30.01	-	-	-
48	8.11	120.09	3.88	1.18,1.65	-	0.62,0.79	-	57.85	42.21	-	25.98,23.42	-
49	8.27	118.59	-	-	-	-	-	58.72	28.42	-	-	-
50	8.19	119.96	-	-	-	-	-	57.86	40.56	-	-	-
51	7.82	119.31	-	-	-	-	1.82	60.16	33.6	-	-	17.04
52	7.99	119.78	3.9	2.17	0.80,1.49,1.63	0.73	-	63.97	36.88	16.58,28.49	10.89	-
53	8.9	118.65	-	-	-	-	-	56.03	38.22	-	-	-
54	7.7	116.81	-	-	-	-	-	59.07	30.57	-	-	-
55	7.22	113.27	4.11	1.95	0.77,0.66	-	-	61.29	33.57	23.41,22.23	-	-
56	7.9	120.63	-	-	-	-	-	54.2	40.9	-	-	-
57	8.22	131.88	4.21	1.52	-	-	-	54.68	20.01	-	-	-
58	8.28	114.14	-	-	-	-	-	52.98	40.05	-	-	-
59	7.64	108.64	-	-	-	-	-	47.27	-	-	-	-
60	8.24	118.95	-	-	-	-	-	52.96	37.72	-	-	-
61	10.54	113.42	-	-	-	-	-	45.79	-	-	-	-
62	7.7	108.57	-	-	-	-	-	59.49	72.59	-	-	-
63	8.76	123.81	5.2	2.09	0.98,1.20	0.98	-	59.5	40.06	27.59,18.88	14.08	-
64	8.84	128	-	-	-	-	-	52.12	42.53	-	-	-
65	9.01	118.52	-	-	-	-	-	63.23	-	-	-	-
67	8.25	118.13	-	-	-	-	-	59.56	29.81	-	-	-
68	8.53	123.82	-	-	-	-	-	62.29	40.58	-	-	-
69	9	119.88	3.32	1.16,1.23	1.02	0.63,0.67	-	58.1	41.48	26.12	24.90,25.54	-

70	7.72	114.81	3.63	4.12	1.15	-	-	66.88	68.74	21.85	-	-
71	7.18	120.4	-	-	-	-	1.85	58.69	31.01	-	-	17.13
72	8.5	118.93	-	-	-	-	1.68	59.56	30.27	-	-	17.45
73	8.26	120.96	4.1	1.39	-	-	-	54.45	18.43	-	-	-
74	7.41	117.26	-	-	-	-	-	58.31	30.54	-	-	-
75	7.98	119.13	-	-	-	-	-	57.37	32.61	-	-	-
76	7.95	119.05	-	-	-	-	1.89	56.64	32.87	-	-	16.83
77	7.87	120.36	-	-	-	-	-	56.81	33.17	-	-	-
78	8.27	121.63	-	-	-	-	-	54.89	41.33	-	-	-
79	8.12	114.56	-	-	-	-	-	62.45	70.04	-	-	-
80	8.47	123.21	-	-	-	-	-	54.93	41.68	-	-	-
81	8.51	117.4	-	-	-	-	-	59.49	64.02	-	-	-
82	8.55	122.45	-	-	-	-	-	59.09	29.77	-	-	-
83	8.34	119.46	-	-	-	-	-	59.93	29.83	-	-	-
85	7.99	121.71	3.96	2.2	1.83,1.13	0.8	-	65.34	37.67	19.02,29.14	13.39	-
86	8.45	121.5	-	-	-	-	-	60.28	30.37	-	-	-
87	8.35	118.07	-	-	-	-	-	59.4	29.72	-	-	-
88	7.91	121.59	4.23	1.88	-	-	-	55.48	18.32	-	-	-
89	8.59	118.72	-	-	-	-	-	62.44	39.54	-	-	-
90	7.84	115.72	-	-	-	-	-	58.72	30.57	-	-	-
91	7.38	118.4	3.41	2.12	0.98,0.42	-	-	66.14	31.48	22.84,20.88	-	-
92	6.89	113.98	-	-	-	-	-	60.1	41.8	-	-	-
93	7.79	115.86	-	-	-	-	-	52.15	38.89	-	-	-
94	7.63	125.46	-	-	-	-	-	58.98	32.5	-	-	-
95	8.37	114.2	-	-	-	-	-	53.2	39.93	-	-	-
96	7.81	109.34	-	-	-	-	-	47.32	-	-	-	-
97	8.43	119.91	-	-	-	-	-	52.89	38.51	-	-	-
98	10.67	112.8	-	-	-	-	-	45.31	-	-	-	-
99	7.74	116.49	-	-	-	-	-	56.64	42.93	-	-	-
100	10.18	127.6	4.68	1.96	1.1	0.58	-	61.62	39.8	17.63	16.1	-
101	9.01	123.94	-	-	-	-	-	55.91	67.08	-	-	-
102	9.4	123.42	3.94	1.5	-	-	-	56.14	18.11	-	-	-
103	8.31	118.64	4.05	1.44	-	-	-	55.49	18.55	-	-	-
104	7.96	120.31	-	-	-	-	-	59.71	29.39	-	-	-
105	8.57	120.31	4.14	1.40,1.89	1.32	0.69,0.59	-	58.67	42.29	27.41	26.24,24.34	-
106	8.72	117.71	-	-	-	-	-	60.22	30.69	-	-	-
107	7.98	119.86	-	-	-	-	-	60.17	30.85	-	-	-
108	8.59	120.22	3.65	2.12	1.01,0.58	-	-	67.04	31.97	23.34,20.72	-	-
109	8.55	115.78	-	-	-	-	2.11	57.51	29.67	-	-	17.11

110	8.1	115.99	4.05	4.29	1.22	-	-	66.95	68.75	21.67	-	-
111	7.93	123.35	-	-	-	-	-	56.24	38.36	-	-	-
112	7.96	118.47	4.48	1.90,1.75	1.8	0.75,0.84	-	54.97	42.02	26.37	22.53,26.01	-
113	7.87	107.18	-	-	-	-	-	45.78	-	-	-	-
114	8.02	120.28	-	-	-	-	-	54.89	30.95	-	-	-
115	8.58	124.4	-	-	-	-	-	55.7	32.06	-	-	-
116	8.15	125.57	4.68	1.40,1.58	1.55	0.71,0.68	-	54.49	44.85	27.9	24.15,27.07	-
117	9.26	114.62	4.07	-	1.33	-	-	60.95	71.28	22.02	-	-
118	8.95	121.27	-	-	-	-	-	58.22	39.84	-	-	-
119	8.66	119.47	-	-	-	-	-	60.14	29.35	-	-	-
120	7.76	120.86	-	-	-	-	-	59.36	30.66	-	-	-
121	8.08	121.69	3.52	2.11	0.54,1.12	-	-	67.17	31.8	21.09,23.85	-	-
122	8.04	119.74	-	-	-	-	-	57.9	40.78	-	-	-
123	8.16	119.62	-	-	-	-	-	59.57	29.63	-	-	-
124	7.77	119.87	-	-	-	-	2.11	60.46	33.06	-	-	17.1
125	8.07	120.21	3.8	2.32	1.55,0.78	0.8	-	64.12	36.38	16.38,27.92	10.11	-
126	8.49	118.29	-	-	-	-	-	59.94	30.57	-	-	-
127	8.01	116.74	-	-	-	-	-	59.14	30.44	-	-	-
128	7.21	117.48	4.47	1.17	-	-	-	51.89	21.97	-	-	-
129	8.05	117.92	-	-	-	-	-	54.72	40.96	-	-	-
130	8.33	128.1	3.91	1.95	0.91,1.24,0.86	0.86	-	63.67	39.14	17.54,27.82	12.71	-
131	8.37	116.77	-	-	-	-	-	54.16	40.14	-	-	-
132	7.7	108.69	-	-	-	-	-	47.61	-	-	-	-
133	8.41	120.89	-	-	-	-	-	53.86	40.25	-	-	-
134	10.25	112.77	-	-	-	-	-	46.04	-	-	-	-
135	8.05	115.48	-	-	-	-	-	53.46	33.03	-	-	-
136	9.18	125.6	5.17	2.34	1.04,1.09	-	-	61.86	34.31	22.86,21.54	-	-
137	9.59	129.26	-	-	-	-	-	51.2	38.66	-	-	-
138	8.22	118.59	-	-	-	-	-	62.66	37.93	-	-	-
139	8.07	118.49	-	-	-	-	-	60.35	29.07	-	-	-
140	8.71	120.04	-	-	-	-	-	59.01	29.65	-	-	-
141	-	-	-	-	-	-	-	62.08	40.97	-	-	-
141	8.56	123.86	-	-	-	-	-	-	-	-	-	-
142	8.69	119.22	3.1	1.79	0.70,0.44	-	-	67.09	31.77	21.44,23.14	-	-
143	7.62	118.66	-	-	-	-	-	58.89	28.27	-	-	-
144	7.36	117.07	-	-	-	-	2.05	57.39	32.01	-	-	17.11
145	7.81	116.46	-	-	-	-	1.35	56.63	32.18	-	-	19.3
146	7.67	108.81	4.3	4.26	1.15	-	-	62.43	70.54	21.31	-	-
147	7.51	126.65	4.1	1.43	-	-	-	53.23	19.35	-	-	-

148	8.01	126.62	-	-	-	-	-	58.17	34.11	-	-	-

Appendix 9. Chemical shift Table for apo-CaM

	H	N	HA	HB	HG	HD	HE	CA	CB	CG	CD	CE
1	-	122.75	4.11	1.32	-	-	-	53.55	18.9	-	-	-
2	7.86	116.91	-	-	-	-	-	55.12	40.84	-	-	-
3	7.81	117.4	-	-	-	-	-	55.71	30.04	-	-	-
4	7.74	120.78	4.61	1.39,1.78	1.71	0.92,0.86	-	54.26	43.45	27.26	27.25,23.55	-
5	8.74	112.81	4.44	4.77	1.33	-	-	60.26	71.17	21.95	-	-
6	8.97	120.42	-	-	-	-	-	60.2	29.36	-	-	-
7	8.67	119.4	-	-	-	-	-	60.2	29.13	-	-	-
8	7.74	120.72	-	-	-	-	-	58.71	29.24	-	-	-
9	8.2	118.49	3.44	1.83	1.78,0.81,1.12	0.81	-	66.7	38.1	30.38,17.42	13.42	-
10	7.9	120.53	4.14	1.51	-	-	-	55.35	17.99	-	-	-
11	7.74	120.4	-	-	-	-	-	59.42	29.55	-	-	-
12	8.71	120.37	-	-	-	-	-	58.36	37.05	-	-	-
13	9.23	121.6	3.76	1.80,1.93	0.75,1.13	1.27,1.18	2.62,2.63	59.81	32.11	24.81	28.53	41.73
14	8.05	120.69	-	-	-	-	-	59.56	29.4	-	-	-
15	7.56	120.9	4.32	1.71	-	-	-	55.1	19.32	-	-	-
16	8.46	118	-	-	-	-	-	61.82	40.98	-	-	-
17	8.41	111.16	-	-	-	-	-	61.71	63.11	-	-	-
18	7.29	121.25	3.93	1.12,1.72	1.62	0.90,0.76	-	57.04	41.75	26.5	24.86,23.25	-
19	7.33	114.84	-	-	-	-	-	58.38	39.79	-	-	-
20	7.26	122.71	-	-	-	-	-	52.64	40	-	-	-
21	8.03	123.78	-	-	-	-	-	58.43	32.53	-	-	-
22	8.67	117.16	-	-	-	-	-	54.47	41.35	-	-	-
23	7.99	110.38	-	-	-	-	-	46.92	-	-	-	-
24	8.75	121.04	-	-	-	-	-	53.89	41.49	-	-	-
25	10.17	112.21	-	-	-	-	-	45.98	-	-	-	-
26	7.54	110.05	5.54	4.06	1.08	-	-	59.92	73.22	21.72	-	-
27	8.21	110.6	4.76	1.69	1.05,0.75,-0.15	0.3	-	59.37	41.51	25.09,16.29	13.8	-
28	8.3	110.89	5.06	4.65	1.32	-	-	60.61	70.61	22.23	-	-
29	8.24	112.59	3.75	4.24	1.15	-	-	65.09	67.42	23.46	-	-
30	7.58	119.06	-	-	-	-	-	58.34	32.64	-	-	-
31	7.46	117.67	-	-	-	-	-	56.12	29.77	-	-	-
32	7.29	121.1	3.78	1.89,1.39	-	1.06,0.92	-	58.67	41.83	-	26.52,23.36	-
33	8.76	105.65	-	-	-	-	-	48.22	-	-	-	-
34	7.48	118.54	3.78	3.98	1.21	-	-	66.08	67.55	23.32	-	-

35	7.92	122.93	3.36	1.87	0.52,0.71	-	-	66.4	31.34	22.22,22.70	-	-
36	8.43	118.86	3.96	-	-	-	1.86	60.46	31.95	-	-	17.29
37	8.48	119.62	-	-	-	-	-	59.28	30.2	-	-	-
38	8.07	119.25	-	-	-	-	-	61.65	62.76	-	-	-
39	7.29	121.4	4.61	1.87	1.85	1.16,1.05	-	54.53	42.96	26.87	26.58,23.17	-
40	7.87	107.35	-	-	-	-	-	45.79	-	-	-	-
41	7.72	117.98	-	-	-	-	-	54.09	30.15	-	-	-
42	8.63	116.79	-	-	-	-	-	51.13	39.34	-	-	-
43	-	-	-	-	-	-	-	62.34	31.95	-	-	-
44	8.74	113.45	4.43	4.74	1.36	-	-	60.71	70.9	21.94	-	-
45	8.81	120.64	-	-	-	-	-	59.98	29.11	-	-	-
46	8.28	121.21	4.1	1.38	-	-	-	55	18.25	-	-	-
47	7.7	119.12	-	-	-	-	-	58.92	30.17	-	-	-
48	8.29	120.32	4.04	1.55,1.79	1.63	0.82,0.83	-	58	41.88	27.1	25.21,24.39	-
49	8.02	117.72	-	-	-	-	-	58.72	28.21	-	-	-
50	7.79	119.12	-	-	-	-	-	57.49	40.48	-	-	-
51	7.92	119.33	-	-	-	-	1.98	59.69	34.15	-	-	17.37
52	8.3	119.29	3.49	1.85	0.92,1.78,0.81	0.8	-	65.39	38.21	17.68,30.53	13.63	-
53	8.22	117.6	-	-	-	-	-	55.39	38.23	-	-	-
54	7.53	117.55	-	-	-	-	-	58.37	30.29	-	-	-
55	7.59	113.38	4.36	2.26	0.96,1.00	-	-	62.31	32.91	20.67,21.95	-	-
56	8.43	122.13	-	-	-	-	-	53.54	40.8	-	-	-
57	8.12	125.17	4.17	1.45	-	-	-	54.81	18.99	-	-	-
58	8.4	114.97	-	-	-	-	-	54.55	41.15	-	-	-
59	7.85	109.17	-	-	-	-	-	46.84	-	-	-	-
60	9.24	120.02	-	-	-	-	-	54.29	39.37	-	-	-
61	9.98	110.4	-	-	-	-	-	45.91	-	-	-	-
62	7.51	110.89	5.21	4.1	1.07	-	-	59.72	72.64	21.78	-	-
63	8.85	119.06	4.6	1.78	1.09,1.54,1.05	0.87	-	59.92	41.79	17.76,26.94	15.72	-
64	8.54	124.77	-	-	-	-	-	52.08	42.17	-	-	-
65	8.58	118.79	-	-	-	-	-	62.93	36.5	-	-	-
67	8.02	117.91	-	-	-	-	-	58.94	29.64	-	-	-
68	8.42	122.66	-	-	-	-	-	61.46	39.46	-	-	-
69	8.42	118.76	3.31	1.15,1.48	0.71	0.66,0.72	-	57.79	41.34	25.6	24.39,25.65	-
70	7.64	115.17	3.71	4.29	1.21	-	-	66.71	68.31	21.94	-	-
71	7.67	121.31	-	-	-	-	1.96	58.97	32.6	-	-	17.48
72	7.95	117.52	-	-	-	-	1.43	55.87	30.89	-	-	17.09
73	8.28	121.23	4.02	1.35	-	-	-	54.76	18.1	-	-	-
74	7.51	116.95	-	-	-	-	-	58.87	30.35	-	-	-

75	7.64	118.23	-	-	-	-	-	56.67	31.73	-	-	-
76	7.9	118.14	-	-	-	-	2.1	56.8	33.26	-	-	17.04
77	7.69	120.43	4.3	1.47,1.86	1.68,1.45	1.69	3.00,3.00	56.78	33.05	24.42	29.13	42.27
78	8.26	122.29	-	-	-	-	-	54.83	41.13	-	-	-
79	-	-	-	-	-	-	-	-	-	-	-	-
79	8.06	115.21	4.3	4.31	1.25	-	-	62.66	69.75	21.92	-	-
80	8.41	123.4	-	-	-	-	-	54.97	41.33	-	-	-
81	8.42	117.41	-	-	-	-	-	60.07	63.61	-	-	-
82	8.36	122.1	-	-	-	-	-	59.59	30.01	-	-	-
83	8.13	118.68	-	-	-	-	-	59.24	29.59	-	-	-
84	7.84	118.88	-	-	-	-	-	59.22	34.01	-	-	-
85	8.27	118.5	3.75	1.96	0.86	0.75	-	65.29	37.97	17.15	13.75	-
86	7.91	119.93	-	-	-	-	-	59.31	30.36	-	-	-
87	7.8	117.18	-	-	-	-	-	57.2	29.83	-	-	-
88	7.54	121.72	4.35	1.56	-	-	-	52.53	19.82	-	-	-
89	8.33	119.87	-	-	-	-	-	54.29	40.22	-	-	-
90	7.79	121.3	-	-	-	-	-	60.86	39.23	-	-	-
91	8.09	120.3	3.64	2.2	0.93,1.02	-	-	67.04	31.59	22.15,24.37	-	-
92	8.32	119.38	-	-	-	-	-	54.28	40.48	-	-	-
93	7.79	121.49	-	-	-	-	-	52.54	40.25	-	-	-
94	8.38	124.58	-	-	-	-	-	58.75	32.51	-	-	-
95	8.57	116.42	-	-	-	-	-	54.48	41.34	-	-	-
96	7.95	110.54	-	-	-	-	-	46.95	-	-	-	-
97	8.97	119.01	-	-	-	-	-	53.39	39.27	-	-	-
98	8.35	118.78	-	-	-	-	-	45.69	-	-	-	-
99	8.27	120.46	-	-	-	-	-	54.59	41.35	-	-	-
100	7.89	120.49	3.67	1.95	0.99	0.82	-	64.61	37.67	19.26	13.61	-
101	8.92	117.53	-	-	-	-	-	57.97	65.09	-	-	-
102	8.73	124.56	3.87	1.4	-	-	-	55.51	17.92	-	-	-
103	8.21	119.33	3.87	1.4	-	-	-	54.99	18.3	-	-	-
104	7.7	120.72	-	-	-	-	-	56.76	28.71	-	-	-
105	8.19	120.9	3.78	1.31,1.85	1.28	0.32,0.25	-	58.66	41.91	26.81	25.65,24.70	-
106	7.99	117.47	-	-	-	-	-	59.97	30.2	-	-	-
107	7.69	119.39	-	-	-	-	-	59.41	29.78	-	-	-
108	8.08	119.65	3.57	1.72	0.83,0.38	-	-	66.46	32.01	20.60,21.76	-	-
109	8.14	115.44	-	-	-	-	2.06	58.3	-	-	-	17.1
110	7.89	110.84	4.22	4.31	1.26	-	-	64.65	69.37	21.76	-	-
111	7.57	119.86	-	-	-	-	-	54.65	39.51	-	-	-
112	7.67	120.13	4.34	1.61,1.73	0.92	0.75,0.81	-	55.32	42.87	25.07	23.39,26.41	-

113	8.13	108.26	-	-	-	-	-	46.29	-	-	-	-
114	8.14	120.57	-	-	-	-	-	56.54	29.73	-	-	-
115	8.2	120.23	-	-	-	-	-	57.05	32.48	-	-	-
116	7.75	121.36	4.71	1.58,1.53	1.62	0.90,0.86	-	54.05	44.59	27.69	23.80,26.48	-
117	8.95	113.73	4.46	4.72	1.35	-	-	60.79	71.22	22.08	-	-
118	8.77	121.16	-	-	-	-	-	57.85	40.16	-	-	-
119	8.53	118.16	-	-	-	-	-	59.91	29.34	-	-	-
120	8.19	118.11	-	-	-	-	-	59.12	30.43	-	-	-
121	8.15	120.96	3.54	2.38	1.14,0.97	-	-	66.88	31.64	21.65,23.58	-	-
125	8.32	119.46	5.01	2.4	1.49,0.96,1.52	0.69	-	57.77	40.5	18.54,24.30	13.94	-
126	7.81	119.43	-	-	-	-	-	59.25	29.61	-	-	-
127	7.96	119.31	-	-	-	-	-	58.98	29.46	-	-	-
128	7.45	121.51	-	-	-	-	-	54.68	18.3	-	-	-
130	8	123.77	4.47	1.85	0.96,1.51,1.15	0.87	-	60.73	39.07	17.62,26.91	13.43	-
131	8.57	124.52	-	-	-	-	-	53.7	41.44	-	-	-
132	8.33	108.11	-	-	-	-	-	46.52	-	-	-	-
133	8.24	119.6	-	-	-	-	-	54.11	41.48	-	-	-
134	8.27	109.53	-	-	-	-	-	45.7	-	-	-	-
136	-	-	4.54	1.91	0.83,0.83	-	-	60.51	35.21	21.05,21.79	-	-
137	8.77	125.34	-	-	-	-	-	52.32	38.42	-	-	-
138	7.47	122.57	-	-	-	-	-	-	-	-	-	-
139	8.12	126.21	-	-	-	-	-	-	-	-	-	-
142	-	-	3.46	-	0.97,0.10	-	-	66.2	-	21.16,23.50	-	-
144	7.71	118.29	-	-	-	-	1.9	58.59	33.38	-	-	17.03
145	7.93	116.22	-	-	-	-	2.14	57.34	33.73	-	-	17.67
146	7.66	110.64	-	-	-	-	-	62.61	69.78	-	-	-
147	7.56	125.6	4.35	1.42	-	-	-	52.78	19.12	-	-	-
148	7.65	125.61	-	-	-	-	-	-	33.74	-	-	-

Appendix 10. Chemical shift Table for the apo-CaM: eEF2K$_{82-100}$ complex

	H	N	HA	HB	HG	HD	HE	CA	CB	CG	CD	CE
1	-	-	-	-	-	-	-	-	-	-	-	-
2	7.84	116.48	-	-	-	-	-	-	-	-	-	-
3	7.87	117.68	-	-	-	-	-	-	-	-	-	-
4	7.76	121.41	4.67	1.79,1.51	1.79	0.92,0.90	-	54.24	43.59	27.27	23.60,27.16	-
5	8.71	112.82	4	4.04	1.16	-	-	60.6	71.36	22.54	-	-
6	9.05	120.57	-	-	-	-	-	60.25	29.51	-	-	-
7	8.74	119.49	-	-	-	-	-	60.16	29.32	-	-	-

8	7.75	120.57	-	-	-	-	-	58.8	29.25	-	-	-
9	8.3	119.16	3.6	1.91	1.09,1.08,0.86	0.86	-	66.48	37.95	30.38,17.52	13	-
10	8.04	121.17	4.11	1.51	-	-	-	55.68	18.11	-	-	-
11	7.8	120.02	-	-	-	-	-	59.54	29.37	-	-	-
12	8.57	120.59	-	-	-	-	-	58.93	37.5	-	-	-
13	9.25	123.71	-	-	-	-	-	60.22	32.11	-	-	-
14	7.98	120.77	-	-	-	-	-	59.5	29.5	-	-	-
15	7.98	121.94	4.28	1.98	-	-	-	55.52	18.2	-	-	-
16	8.68	118.98	-	-	-	-	-	62.17	40.04	-	-	-
17	8.17	113.5	-	-	-	-	-	61.69	63.54	-	-	-
18	7.38	120.35	3.93	1.45,1.66	1.47	0.80,0.67	-	57.4	41.54	26.89	23.94,24.92	-
19	7.05	112.85	-	-	-	-	-	59.2	41.71	-	-	-
20	7.6	116.47	-	-	-	-	-	52.33	39.36	-	-	-
21	7.6	124.43	-	-	-	-	-	58.36	32.47	-	-	-
22	8.24	114.23	-	-	-	-	-	53.05	39.74	-	-	-
23	7.72	109.44	-	-	-	-	-	47.5	-	-	-	-
24	8.51	120.97	-	-	-	-	-	54.01	40.66	-	-	-
25	10.6	113.15	-	-	-	-	-	45.63	-	-	-	-
26	8.29	112.73	5.49	3.87	1.07	-	-	59.93	73.01	22.34	-	-
27	9.97	127.04	4.78	1.76	1.20,1.25,0.99	0.4	-	61.57	40.49	26.79,17.59	15.67	-
28	8.3	116.38	-	-	-	-	-	59.39	72.61	-	-	-
29	9.24	114.35	3.77	4.19	1.26	-	-	66.97	68.28	23.29	-	-
30	7.84	121.11	-	-	-	-	-	59.52	32.77	-	-	-
31	7.81	121.94	-	-	-	-	-	59.88	29.93	-	-	-
32	8.64	119.81	4.09	1.80,1.30	1.35	0.54,0.49	-	58.36	42.65	26.89	23.67,26.07	-
33	8.75	105.66	-	-	-	-	-	48.74	-	-	-	-
34	8.03	118.49	3.92	4.41	1.27	-	-	67.2	69.09	21.5	-	-
35	8.1	122.8	3.43	2.21	0.89,0.97	-	-	66.95	31.93	23.80,22.13	-	-
36	8.78	118.39	-	-	-	-	1.85	58.97	31.09	-	-	17.17
38	8.04	119.31	-	-	-	-	-	61.76	62.76	-	-	-
39	7.48	120.55	4.33	1.61,1.90	-	0.81,0.74	-	55	42.18	-	22.97,26.03	-
40	7.94	107.18	-	-	-	-	-	45.74	-	-	-	-
41	7.78	118.01	-	-	-	-	-	54.47	30.87	-	-	-
42	8.73	116.64	-	-	-	-	-	51.53	39.62	-	-	-
43	-	-	-	-	-	-	-	62.37	31.9	-	-	-
44	8.76	113	4.42	4.74	1.33	-	-	60.78	71.34	21.92	-	-
45	8.85	120.81	-	-	-	-	-	60.24	29.22	-	-	-
46	8.29	120.92	4.1	1.38	-	-	-	55.23	18.65	-	-	-
47	7.72	119.11	-	-	-	-	-	59.23	30.01	-	-	-

48	8.11	120.09	3.88	1.18,1.65	-	0.62,0.79	-	57.85	42.21	-	25.98,23.42	-
49	8.27	118.59	-	-	-	-	-	58.72	28.42	-	-	-
50	8.19	119.96	-	-	-	-	-	57.86	40.56	-	-	-
51	7.82	119.31	-	-	-	-	1.82	60.16	33.6	-	-	17.04
52	7.99	119.78	3.9	2.17	0.80,1.49,1.63	0.73	-	63.97	36.88	16.58,28.49	10.89	-
53	8.9	118.65	-	-	-	-	-	56.03	38.22	-	-	-
54	7.7	116.81	-	-	-	-	-	59.07	30.57	-	-	-
55	7.22	113.27	4.11	1.95	0.66,0.77	-	-	61.29	33.57	23.41,22.23	-	-
56	7.9	120.63	-	-	-	-	-	54.2	40.9	-	-	-
57	8.22	131.88	4.21	1.52	-	-	-	54.68	20.01	-	-	-
58	8.28	114.14	-	-	-	-	-	52.98	40.05	-	-	-
59	7.64	108.64	-	-	-	-	-	47.27	-	-	-	-
60	8.24	118.95	-	-	-	-	-	52.96	37.72	-	-	-
61	10.54	113.42	-	-	-	-	-	45.79	-	-	-	-
62	7.7	108.57	-	-	-	-	-	59.49	72.59	-	-	-
63	8.76	123.81	5.2	2.09	0.98,1.20	0.98	-	59.5	40.06	18.88,27.59	14.08	-
64	8.84	128	-	-	-	-	-	52.12	42.53	-	-	-
65	9.01	118.52	-	-	-	-	-	63.23	-	-	-	-
67	8.25	118.13	-	-	-	-	-	59.56	29.81	-	-	-
68	8.53	123.82	-	-	-	-	-	62.29	40.58	-	-	-
69	9	119.88	3.32	1.16,1.23	1.02	0.63,0.67	-	58.1	41.48	26.12	25.54,24.90	-
70	7.72	114.81	3.63	4.12	1.15	-	-	66.88	68.74	21.85	-	-
71	7.18	120.4	-	-	-	-	1.85	58.69	31.01	-	-	17.13
72	8.5	118.93	-	-	-	-	1.68	59.56	30.27	-	-	17.45
73	8.26	120.96	4.1	1.39	-	-	-	54.45	18.43	-	-	-
74	7.41	117.26	-	-	-	-	-	58.31	30.54	-	-	-
75	7.98	119.13	-	-	-	-	-	57.37	32.61	-	-	-
76	7.95	119.05	-	-	-	-	1.89	56.64	32.87	-	-	16.83
77	7.87	120.36	-	-	-	-	-	56.81	33.17	-	-	-
78	8.27	121.63	-	-	-	-	-	54.89	41.33	-	-	-
79	8.12	114.56	-	-	-	-	-	62.45	70.04	-	-	-
80	8.47	123.21	-	-	-	-	-	54.93	41.68	-	-	-
81	8.51	117.4	-	-	-	-	-	59.49	64.02	-	-	-
82	8.55	122.45	-	-	-	-	-	59.09	29.77	-	-	-
83	8.34	119.46	-	-	-	-	-	59.93	29.83	-	-	-
85	7.99	121.71	3.96	2.2	1.83,1.13	0.8	-	65.34	37.67	29.14,19.02	13.39	-
86	8.45	121.5	-	-	-	-	-	60.28	30.37	-	-	-
87	8.35	118.07	-	-	-	-	-	59.4	29.72	-	-	-
88	7.91	121.59	4.23	1.88	-	-	-	55.48	18.32	-	-	-

89	8.59	118.72	-	-	-	-	-	62.44	39.54	-	-	-
90	7.84	115.72	-	-	-	-	-	58.72	30.57	-	-	-
91	7.38	118.4	3.41	2.12	0.42,0.98	-	-	66.14	31.48	20.88,22.84	-	-
92	6.89	113.98	-	-	-	-	-	60.1	41.8	-	-	-
93	7.79	115.86	-	-	-	-	-	52.15	38.89	-	-	-
94	7.63	125.46	-	-	-	-	-	58.98	32.5	-	-	-
95	8.37	114.2	-	-	-	-	-	53.2	39.93	-	-	-
96	7.81	109.34	-	-	-	-	-	47.32	-	-	-	-
97	8.43	119.91	-	-	-	-	-	52.89	38.51	-	-	-
98	10.67	112.8	-	-	-	-	-	45.31	-	-	-	-
99	7.74	116.49	-	-	-	-	-	56.64	42.93	-	-	-
100	10.18	127.6	4.68	1.96	1.1	0.58	-	61.62	39.8	17.63	16.1	-
101	9.01	123.94	-	-	-	-	-	55.91	67.08	-	-	-
102	9.4	123.42	3.94	1.5	-	-	-	56.14	18.11	-	-	-
103	8.31	118.64	4.05	1.44	-	-	-	55.49	18.55	-	-	-
104	7.96	120.31	-	-	-	-	-	59.71	29.39	-	-	-
105	8.57	120.31	4.14	1.40,1.89	1.32	0.69,0.59	-	58.67	42.29	27.41	26.24,24.34	-
106	8.72	117.71	-	-	-	-	-	60.22	30.69	-	-	-
107	7.98	119.86	-	-	-	-	-	60.17	30.85	-	-	-
108	8.59	120.22	3.65	2.12	0.58,1.01	-	-	67.04	31.97	20.72,23.34	-	-
109	8.55	115.78	-	-	-	-	2.11	57.51	29.67	-	-	17.11
110	8.1	115.99	4.05	4.29	1.22	-	-	66.95	68.75	21.67	-	-
111	7.93	123.35	-	-	-	-	-	56.24	38.36	-	-	-
112	7.96	118.47	4.48	1.90,1.75	1.8	0.75,0.84	-	54.97	42.02	26.37	26.01,22.53	-
113	7.87	107.18	-	-	-	-	-	45.78	-	-	-	-
114	8.02	120.28	-	-	-	-	-	54.89	30.95	-	-	-
115	8.58	124.4	-	-	-	-	-	55.7	32.06	-	-	-
116	8.15	125.57	4.68	1.40,1.58	1.55	0.68,0.71	-	54.49	44.85	27.9	27.07,24.15	-
117	9.26	114.62	4.07	-	1.33	-	-	60.95	71.28	22.02	-	-
118	8.95	121.27	-	-	-	-	-	58.22	39.84	-	-	-
119	8.66	119.47	-	-	-	-	-	60.14	29.35	-	-	-
120	7.76	120.86	-	-	-	-	-	59.36	30.66	-	-	-
121	8.08	121.69	3.52	2.11	0.54,1.12	-	-	67.17	31.8	21.09,23.85	-	-
122	8.04	119.74	-	-	-	-	-	57.9	40.78	-	-	-
123	8.16	119.62	-	-	-	-	-	59.57	29.63	-	-	-
124	7.77	119.87	-	-	-	-	2.11	60.46	33.06	-	-	17.1
125	8.07	120.21	3.8	2.32	0.78,1.55	0.8	-	64.12	36.38	27.92,16.38	10.11	-
126	8.49	118.29	-	-	-	-	-	59.94	30.57	-	-	-
127	8.01	116.74	-	-	-	-	-	59.14	30.44	-	-	-

128	7.21	117.48	4.47	1.17	-	-	-	51.89	21.97	-	-	-
129	8.05	117.92	-	-	-	-	-	54.72	40.96	-	-	-
130	8.33	128.1	3.91	1.95	0.86,1.24,0.91	0.86	-	63.67	39.14	17.54,27.82	12.71	-
131	8.37	116.77	-	-	-	-	-	54.16	40.14	-	-	-
132	7.7	108.69	-	-	-	-	-	47.61	-	-	-	-
133	8.41	120.89	-	-	-	-	-	53.86	40.25	-	-	-
134	10.25	112.77	-	-	-	-	-	46.04	-	-	-	-
135	8.05	115.48	-	-	-	-	-	53.46	33.03	-	-	-
136	9.18	125.6	5.17	2.34	1.04,1.09	-	-	61.86	34.31	21.54,22.86	-	-
137	9.59	129.26	-	-	-	-	-	51.2	38.66	-	-	-
138	8.22	118.59	-	-	-	-	-	62.66	37.93	-	-	-
139	8.07	118.49	-	-	-	-	-	60.35	29.07	-	-	-
140	8.71	120.04	-	-	-	-	-	59.01	29.65	-	-	-
141	8.56	123.86	-	-	-	-	-	-	-	-	-	-
141	-	-	-	-	-	-	-	62.08	40.97	-	-	-
142	8.69	119.22	3.1	1.79	0.70,0.44	-	-	67.09	31.77	23.14,21.44	-	-
143	7.62	118.66	-	-	-	-	-	58.89	28.27	-	-	-
144	7.36	117.07	-	-	-	-	2.05	57.39	32.01	-	-	17.11
145	7.81	116.46	-	-	-	-	1.35	56.63	32.18	-	-	19.3
146	7.67	108.81	4.3	4.26	1.15	-	-	62.43	70.54	21.31	-	-
147	7.51	126.65	4.1	1.43	-	-	-	53.23	19.35	-	-	-
148	8.01	126.62	-	-	-	-	-	58.17	34.11	-	-	-

Appendix 11. Chemical shift differences between resonances collected under isotropic and anisotropic collections with a 1:1 ratio of Ca^{2+}/CaM and $eEF2K_{82-100}$. Those highlighted in yellow have been used in the RDC analysis.

Residue	H	N	d
1Ala*	0.0007	0.0044	0.001719128
2Asp	0.00175	0.00496	0.002230577
3Gln	0.00513	0.02388	0.009643343
4Leu	0.00378	6E-05	0.002672958
5Thr	0.00184	0.00901	0.003613587
6Glu	0.00091	0.01101	0.004169516
7Glu	0.00423	0.01241	0.005523367
8Gln	0.00086	0.01865	0.007004638
9Ile	0.00037	0.00572	0.00215616
10Ala	0.00161	0.00918	0.003618589
11Glu	0.00672	0.02233	0.009611828
12Phe	0.00577	0.0267	0.010791249
13Lys	0.00357	0.0219	0.008574255

14Glu	0.00766	0.00348	0.00557075
15Ala	0.00602	0.0084	0.00529137
16Phe	0.00253	0.00756	0.003346932
17Ser	0.00974	0.00713	0.007385863
18Leu	0.00024	0.01668	0.006243391
19Phe	0.00633	0.07549	0.028598218
20Asp	0.0172	0.02012	0.014303636
21Lys	0.00452	0.03243	0.012548063
22Asp	0.00913	0.03171	0.013507473
23Gly	0.00566	0.03806	0.014792454
24Asp	0.00582	0.04347	0.016777542
25Gly	0.00464	0.03209	0.012447182
26Thr	0.00244	0.03411	0.012878886
27Ile	0.00083	0.05153	0.019289691
28Thr	0.00344	0.0198	0.007797589
29Thr	0.00145	0.06264	0.023460158
30Lys	0.00758	0.00544	0.00573335
31Glu	0.00411	0.01373	0.00590236
32Leu	0.00773	0.01574	0.008034993
33Gly	0.00135	0.02295	0.00864
34Thr	0.00221	0.0224	0.008525752
35Val			
36Met	0.00905	0.01455	0.008401762
37Arg	0.00169	0.03426	0.012874499
38Ser	0.01078	0.04056	0.016982936
39Leu	0.00725	0.0101	0.006368881
40Gly	0.00824	0.02127	0.009863397
41Gln	0.00525	0.00287	0.003864507
42Asn	0.00128	0.00705	0.002788826
43Pro			
44Thr	0.01224	0.05139	0.021086472
45Glu	0.00323	0.05331	0.020077109
46Ala	0.00033	0.01879	0.007034446
47Glu	0.00446	0.03997	0.015284303
48Leu	0.00084	0.03009	0.011274304
49Gln	0.00087	0.00715	0.002745105
50Asp	0.0006	0.02453	0.009188086
51Met	0.00205	0.00617	0.002725967
52Ile	0.0033	0.10387	0.038934583
53Asn	0.00545	0.04206	0.016202387
54Glu	0.00169	0.02851	0.010734191
55Val	0.00428	0.14881	0.055761792
56Asp			
57Ala	0.00217	0.03569	0.013441842
58Asp	0.0061	0.02448	0.010124369

59Gly	0.00163	0.01203	0.004646437
60Asn	0.00692	0.00578	0.005349801
61Gly	0.00128	0.02675	0.010049774
62Thr	0.00087	0.08756	0.032767727
63Ile	0.00776	0.00417	0.005704669
64Asp	0.00157	0.00987	0.00385627
65Phe	0.00489	0.00265	0.00359711
66Pro			
67Glu	0.00673	0.01967	0.008764342
68Phe	0.01279	0.04124	0.017885618
69Leu	0.0103	0.00585	0.007605008
70Thr	0.02385	0.17936	0.069196912
71Met	0.0059	0.02099	0.008893043
72Met	0.00865	0.03137	0.013235634
73Ala	0.00341	0.05915	0.022262866
74Arg	0.00145	0.00891	0.00348792
75Lys	0.0195	0.01227	0.014532804
76Met	0.00572	0.00255	0.004155665
77Lys	0.00535	0.03637	0.014124447
78Asp	0.0063	0.00026	0.004455835
79Thr	0.00522	0.03611	0.014006238
80Asp	0.00298	0.01157	0.004814695
81Ser	0.00016	0.01541	0.005767004
82Glu	0.0045	0.05355	0.020287665
83Glu	0.00138	0.00083	0.001024034
84Glu	0.01055	0.0065	0.007846416
85Ile	0.00958	0.03169	0.013655916
86Arg	0.0044	0.02437	0.009634603
87Glu	0.00524	0.00076	0.003716136
88Ala	0.00338	0.00568	0.003198271
89Phe	0.00645	0.03675	0.014487236
90Arg	0.00389	0.00366	0.003072692
91Val	0.00163	0.02612	0.009840938
92Phe	0.00061	0.004	0.001557578
93Asp	0.00715	0.00576	0.005496009
94Lys	0.00188	0.02284	0.008648722
95Asp	0.004	0.04904	0.018565803
96Gly	0.00342	0.04608	0.017410327
97Asn	0.00416	0.04907	0.018594458
98Gly	0.00091	0.0043	0.001732816
99Tyr	0.00255	0.05551	0.020848061
100Ile	0.00056	0.04076	0.015256135
101Ser	0.00264	0.03087	0.011700375
102Ala	0.00391	0.00552	0.003451073
103Ala	0.001	0.01333	0.005037504

104Glu	0.00544	0.05014	0.019150967
105Leu	0.00579	0.01356	0.006519536
106Arg	0.00445	0.01237	0.00559675
107 His	0.00355	0.11911	0.044637519
108Val	0.01117	0.03764	0.016147204
109Met	0.00418	0.00705	0.003961635
110Thr	0.00016	0.02506	0.009377276
111Asn	0.00262	0.01387	0.005510442
112Leu	0.00642	0.01476	0.007149004
113Gly	0.00537	0.07395	0.027928888
114Glu	0.00061	0.06937	0.025959461
115Lys	0.00455	0.00062	0.003225688
116Leu	0.00471	0.03587	0.013828377
117Thr	0.01176	0.04007	0.017144489
118Asp	0.00102	0.00372	0.001567666
119Glu	0.00667	0.00237	0.004799043
120Glu	0.00094	0.02443	0.009165003
121Val	0.00395	0.00798	0.004088582
122Asp	0.00426	0.01302	0.005727709
123Glu	0.00067	0.00228	0.000975821
124Met	0.00402	0.00758	0.004015482
125Ile	0.00732	0.03738	0.014913357
126Arg	0.00226	0.02728	0.010331581
127Glu	0.00516	0.00461	0.004035851
128Ala	0.00367	0.03209	0.012284217
129Asp	0.00673	0.00736	0.005498199
130Ile	0.00751	0.0081	0.006114364
131Asp	0.00404	0.01288	0.005602322
132Gly	0.00611	0.10151	0.038226499
133Asp	0.00371	0.00193	0.002720944
134Gly	0.00123	0.0292	0.010960203
135Gln	0.00263	0.00554	0.002784829
136Val	0.00243	0.03221	0.012173751
137Asn	0.00377	0.00081	0.002682966
138Tyr	0.0147	0.0501	0.021434701
139Glu	0.00215	0.02626	0.00994251
140Glu	0.00321	0.06327	0.023782032
141Phe	0.01747	0.01251	0.013210241
142Val	4E-05	0.02338	0.008748041
143Gln	0.0018	0.03144	0.011832426
144Met	0.00055	0.05505	0.020601495
145Met	0.00133	0.04683	0.017547401
146Thr	0.00079	0.03732	0.013975034
147Ala	9E-05	0.01297	0.004853347
148Lys	0.00321	0.00218	0.002411926

Appendix 12. Chemical shift differences between resonances collected under isotropic and anisotropic collections with a 1:1 ratio of Ca^{2+}/CaM and $eEF2K_{82-100}$. Those highlighted in yellow have been used in the RDC analysis.

Residue	H	N	d
1Ala			
2Asp			
3Gln			
4Leu	0.01933	0.03229	0.018242659
5Thr	0.04631	0.17819	0.074280164
6Glu	0.00627	0.0815	0.030815117
7Glu	0.00156	0.16226	0.060722153
8Gln			
9Ile			
10Ala			
11Glu			
12Phe			
13Lys	0.01656	0.07156	0.029223852
14Glu			
15Ala			
16Phe			
17Ser			
18Leu	0.02413	0.29108	0.11024059
19Phe			
20Asp	0.01471	0.00301	0.010462335
21Lys	0.07087	0.05147	0.053685761
22Asp	0.09411	0.06575	0.070947691
23Gly			
24Asp	0.02042	0.01219	0.015142379
25Gly	0.02358	0.12645	0.050165252
26Thr	0.03844	0.1001	0.046277621
27Ile	0.03487	0.01664	0.025430749
28Thr	0.06966	0.0451	0.052067449
29Thr	0.01167	0.8908	0.333408974
30Lys			
31Glu	0.01244	0.09362	0.036116969
32Leu			
33Gly	0.05877	0.51947	0.19876073
34Thr			
35Val			
36Met	0.03883	0.02564	0.029084735
37Arg			
38Ser			

39Leu	0.05352	0.40638	0.156692226
40Gly	0.04076	0.1241	0.054651644
41Gln	0.02766	0.31442	0.119259922
42Asn			
43Pro			
44Thr	0.02732	0.13636	0.054556009
45Glu	0.00406	0.06918	0.026043501
46Ala			
47Glu			
48Leu			
49Gln			
50Asp	0.0389	0.06821	0.037522921
51Met	0.06542	0.07285	0.053692507
52Ile			
53Asn			
54Glu			
55Val			
56Asp			
57Ala	0.02481	0.35254	0.133069874
58Asp	0.02075	0.15834	0.061035228
59Gly			
60Asn	0.05841	0.11846	0.060584256
61Gly	0.02707	0.07898	0.035209233
62Thr			
63Ile	0.00197	0.04317	0.016212689
64Asp	0.04672	0.27923	0.109576887
65Phe			
66Pro			
67Glu			
68Phe	0.00463	0.40169	0.150334289
69Leu			
70Thr	0.09327	0.46007	0.184343872
71Met			
72Met			
73Ala			
74Arg			
75Lys			
76Met			
77Ala			
78Asp			
79Thr	0.0084	0.01113	0.007254155
80Asp			
81Ser	0.0068	0.18039	0.067666811
82Glu			
83Glu	0.01354	0.08098	0.031776599

84Glu			
85Ile			
86Arg	0.00221	0.17104	0.064016384
87Glu			
88Ala			
89Phe			
90Arg	0.00705	0.15901	0.059704577
91Val	0.01989	0.09697	0.038913383
92Phe			
93Asp	0.01656	0.15257	0.05827505
94Lys	0.02813	0.00934	0.02019558
95Asp	0.01175	0.01828	0.010761665
96Gly	0.00713	0.0997	0.037643473
97Asn	0.00203	0.07613	0.028521382
98Gly	0.02147	0.0474	0.02334581
99Tyr			
100Ile	0.01113	0.08064	0.031182235
101Ser	0.03137	0.03197	0.025201781
102Ala	0.01183	0.00963	0.009108107
103Ala			
104Glu			
105Leu			
106Arg	0.01655	0.07761	0.031308385
107His			
108Val			
109Met	0.01188	0.25395	0.095389997
110Thr	0.00208	0.02547	0.009642828
111Asn	0.00939	0.05914	0.023102848
112Leu	0.01832	0.04499	0.021241121
113Gly	0.0079	0.12892	0.048559822
114Glu			
115Lys	0.00793	0.23005	0.086259277
116Leu	0.00628	0.09542	0.035977992
117Thr	0.01236	0.11191	0.042775268
118Asp	0.00737	0.08619	0.032667701
119Glu	0.00214	0.12251	0.045864014
120Glu			
121Val			
122Asp			
123Glu	0.03622	0.00509	0.025682121
124Met			
125le			
126Arg	0.05265	0.03907	0.039996454
127Glu			
128Ala			

129Asp	0.00889	0.00314	0.006395029
130Ile	0.01592	0.16206	0.061673376
131Asp	0.02041	0.05644	0.025578318
132Gly			
133Asp	0.00493	0.16693	0.062556694
134Gly	0.01431	0.00112	0.010127372
135Gln	0.0058	0.07256	0.027457485
136Val	0.00024	0.03739	0.013991086
137Asn	0.00258	0.09667	0.03621658
138Tyr	0.02788	0.09368	0.040215409
139Glu	0.02176	0.05419	0.025453225
140Glu	0.02472	0.02336	0.019543176
141Phe	0.04455	0.45662	0.173731421
142Val			
143Gln			
144Met			
145Met	0.04261	0.03712	0.033176969
146Thr			
147Ala	0.00129	0.07494	0.028054813
148Lys	0.00835	0.0564	0.021913367

Appendix 13. MATLAB scripts used for analysis of RDC data.

```
%% Jmod fit example
% Amended by A.Bailey from original by Neil Dalchau, Microsoft
Research
% 8th October 2013

% Clear the workspace and close any figures
close all
clear all

%% Load in the data, delcare the variables and estimate the
parameters

tic % Start timing how long it takes
load('jmod_rdc_all.mat'); % Here's one I made earlier
ta = dataIN.ca_1to1_iso(1,:)'; % Time points
yaErr = dataIN.ca_1to1_iso(2:end,:)'; % Data points
resid = dataIN.ca_1to1_iso_id; % Residue number
n = length(resid); % Find out how many residues to fit

% Estimate the parameters for each residue and use to create
predicted data
[yhat,a0est,a1est,a2est,a3est] = separateFit2(ta,yaErr);
fname = 'jmod_ca_1to1_iso_fit'; % Name for the file
toc % Print how long it took

% Create a matrix with resid and parameter estimates
jmods_ca_1to1_iso = [resid a0est a1est a2est a3est];

% Write a comma separtated variable output of the jmods
csv = 'jmod_ca_1to1_iso.csv';
dlmwrite(csv,jmods_ca_1to1_iso,'delimiter',',');

%% Plot the fits for all the residues

nc = 12; % Number of columns for figure
nr = 12; % Number of rows for figure

fh1 = figure(3); % Make a figure
set(fh1,'position',[100 100 1000 900]); % Set the size and position

% Now plot the data and each fit for each residue
% It's an exercise for the reader to figure out what the code means!
for i = 1:n
  r = nr-ceil(i/nc);
  c = mod(i-1,nc);
  subplot('position',[(0.15+c)/nc (0.1+r)/nr 0.8/nc 0.8/nr])
  plot(ta,yaErr(:,i),'x')
  hold on
  plot(ta,yhat(:,i),'r-')
  hold off
  xlim([0 0.025])
  box off
  set(gca,'Xtick',[],'Ytick',[])
  drawnow;
  ylims = get(gca,'Ylim');
  xlims = get(gca,'Xlim');
  text(xlims(1)+0.01,ylims(2),num2str(resid(i)),'FontSize',8) % Add
the resid
end
box off

% Save the figure
figuresave(fh1,[fname 'datasim'],300)
```

```
%% Load in the data, delcare the variables and estimate the
parameters

tic % Start timing how long it takes
load('jmod_rdc_all.mat'); % Here's one I made earlier
ts = dataIN.ca_1to1_aniso(1,:)'; % Time points
ysErr = dataIN.ca_1to1_aniso(2:end,:)'; % Data points
resid = dataIN.ca_1to1_aniso_id; % Residue number
n = length(resid); % Find out how many residues to fit

%% Estimate the parameters for each residue and use to create
predicted data
[yhat,a0est,a1est,a2est,a3est] = separateFit2(ts,ysErr);
fname = 'jmod_ca_1to1_aniso_fit'; % Name for the file
toc % Print how long it took

% Create a matrix with resid and parameter estimates
jmods_ca_1to1_aniso = [resid a0est a1est a2est a3est];

% Write a comma separtated variable output of the jmods
csv = 'jmod_ca_1to1_aniso.csv';
dlmwrite(csv,jmods_ca_1to1_aniso,'delimiter',',');

%% Plot the fits for all the residues

nc = 12; % Number of columns for figure
nr = 12; % Number of rows for figure

fh1 = figure(3); % Make a figure
set(fh1,'position',[100 100 1000 900]); % Set the size and position

% Now plot the data and each fit for each residue
% It's an exercise for the reader to figure out what the code means!
for i = 1:n
  r = nr-ceil(i/nc);
  c = mod(i-1,nc);
  subplot('position',[(0.15+c)/nc (0.1+r)/nr 0.8/nc 0.8/nr])
  plot(ts,ysErr(:,i),'x')
  hold on
  plot(ts,yhat(:,i),'r-')
  hold off
  xlim([0 0.025])
  box off
  set(gca,'Xtick',[],'Ytick',[])
  drawnow;
  ylims = get(gca,'Ylim');
  xlims = get(gca,'Xlim');
  text(xlims(1)+0.01,ylims(2),num2str(resid(i)),'FontSize',8) % Add
the resid
end
box off

% Save the figure
figuresave(fh1,[fname 'datasim'],300)

return

% Jmod error calculation example script
% A. Bailey 8th October 2013

% This takes a while to run depending on how many iterations you do.
```

```
% Clear workspace
clear all

%% Load in some data
load('jmod_rdc_all.mat'); % Here's one I prepared earlier

% Assign variables
ts = dataIN.ca_1to1_iso(1,:)'; % Time points
ys = dataIN.ca_1to1_iso(2:end,:)'; % Data points
resid = dataIN.ca_1to1_iso_id; % Residue ids

n = length(ys); % Find number of data points
r = 100; % Choose number of iterations
sig = 1179.37; % Noise for ISO = 1179.37 Noise for ANISO = 1729.42
Nt = length(ts); % Find number of timepoints

% Create structure for my errors
ysErr = cell(n,1);

%% Generate some data plus errors over iterations

%  randn Normally distributed pseudorandom numbers.
%  R = randn(N) returns an N-by-N matrix containing pseudorandom
values drawn
%  from the standard normal distribution.  randn(M,N) or randn([M,N])
returns
%  an M-by-N matrix.
for i = 1:r
    ysErr{i} = ys + sig*randn(Nt,n); % Add a normal distribution of
noise
end

% Save output
save('fakedata_ca_1to1_iso.mat','ts','ysErr')

%% Now estimate some parameters using the fake data
dataIn = load('fakedata_ca_1to1_iso.mat');

% Preallocate some arrays for the parameters for speed
a0est = cell(n,1); % parameter 0
a1est = cell(n,1); % parameter 1
a2est = cell(n,1); % parameter 2
a3est = cell(n,1); % parameter 3
yhat = cell(n,1);  % data prediction
sdr = cell(n,1);   % standard deviation of the residuals

% Estimate the parameters using the separateFit2 and objective
functions
for i = 1:r
    disp(['Fit ' num2str(i)]) % Display the iteration
    [yhat{i},a0est{i},a1est{i},a2est{i},a3est{i},sdr{i}] =
separateFit2(ts,ysErr{i});
end

% Save fits
save('fakefits_ca_1to1_iso.mat','yhat','a0est','a1est','a2est','a3est
','sdr');

% Extract all the estimates
for i = 1:r
    a0_allest(1:n,i) = a0est{i}(1:n,:);
    a1_allest(1:n,i) = a1est{i}(1:n,:);
    a2_allest(1:n,i) = a2est{i}(1:n,:);
```

```
    a3_allest(1:n,i) = a3est{i}(1:n,:);
end

% Calculate std. deviation
for j = 1:n
    a0err(j,1) = std(a0_allest(j,:));
    a1err(j,1) = std(a1_allest(j,:));
    a2err(j,1) = std(a2_allest(j,:));
    a3err(j,1) = std(a3_allest(j,:));
end

% % Write out the file to Excel
% xl = 'jmod_err_test_iso.xlsx';
%
xlswrite(xl,{'RESID','a0err','a1err','a2err','a3err'},'Sheet1','A1');
% xlswrite(xl,resid,'A2:A112');
% xlswrite(xl,a0err,'B2:B112');
% xlswrite(xl,a1err,'C2:C112');
% xlswrite(xl,a2err,'D2:D112');
% xlswrite(xl,a3err,'E2:E112');

% Create a matrix with resid and parameter estimates
jmods_errors_ca_1to1_iso = [resid a0err a1err a2err a3err];

% Write a comma separtated variable output of the jmods
csv = 'jmod_errors1_ca_1to1_iso.csv';
dlmwrite(csv,jmods_errors_ca_1to1_iso,'delimiter',',');

return
```

Appendix 14. J-coupling and RDC values for Ca^{2+}/CaM at a 1:1 ratio of Ca^{2+}/CaM and $eEF2K_{82-100}$. Initial intensity (a) and value for the imperfection of π pulses (b) and r2 relaxation are also shown.

RESIDUE	ISOTROPIC				ANISOTROPIC				RDC
	a	b	J	r2	a	b	J	r2	
1	278300.00	0.03	95.16	0.07	283450.00	0.05	93.06	0.08	2.10
2	327210.00	0.03	94.58	0.10	357050.00	0.03	96.12	0.09	-1.54
3	306970.00	0.03	93.83	0.06	316130.00	0.05	93.04	0.08	0.80
4	233570.00	0.02	94.64	0.05	216150.00	0.03	90.22	0.04	4.42
5	136690.00	0.03	94.75	0.04	105820.00	0.04	96.23	0.04	-1.48
6	153330.00	0.02	94.80	0.05	127160.00	0.03	94.85	0.04	-0.05
7	172290.00	0.03	94.82	0.05	161240.00	0.03	93.45	0.04	1.38
8	119470.00	0.04	95.01	0.04	88899.00	0.05	98.23	0.03	-3.22
9	194880.00	0.04	94.46	0.04	156060.00	0.03	91.68	0.03	2.78
10	193520.00	0.03	95.66	0.04	165080.00	0.04	93.38	0.03	2.28
11	199160.00	0.04	95.14	0.04	177610.00	0.02	96.09	0.03	-0.95
12	242910.00	0.03	95.49	0.04	207430.00	0.05	93.27	0.03	2.23
13	139800.00	0.03	95.48	0.04	112010.00	0.03	94.50	0.04	0.98
14	113970.00	0.03	95.08	0.05	90571.00	0.07	89.34	0.04	5.74
15	121870.00	0.03	95.09	0.03	88435.00	0.05	95.82	0.03	-0.73
16	69800.00	0.03	94.72	0.04	58640.00	0.02	95.76	0.03	-1.04
17	92400.00	0.02	94.56	0.03	78839.00	0.04	90.72	0.03	3.85
18	154610.00	0.04	94.28	0.03	116590.00	0.05	93.11	0.04	1.16
19	78323.00	0.03	93.44	0.03	66751.00	0.05	97.38	0.02	-3.94
20	47421.00	0.04	94.16	0.03	38168.00	-0.02	88.72	0.02	5.43

21	90511.00	0.03	93.78	0.05	78307.00	0.06	95.56	0.04	-1.78
22	107660.00	0.04	95.81	0.05	92797.00	0.03	99.17	0.05	-3.37
23	117060.00	0.02	96.46	0.05	90891.00	0.04	95.34	0.05	1.12
24	119490.00	0.02	96.73	0.04	104780.00	0.02	99.26	0.04	-2.53
25	97849.00	0.03	94.76	0.04	79660.00	0.06	95.05	0.04	-0.28
26	106840.00	0.01	95.04	0.04	87922.00	0.03	97.60	0.04	-2.56
27	80531.00	0.03	93.19	0.04	53757.00	0.03	96.94	0.03	-3.76
28	67543.00	0.01	95.25	0.04	59766.00	0.01	98.58	0.03	-3.33
29	74857.00	0.03	94.42	0.02	67817.00	0.04	91.10	0.02	3.32
30	86338.00	0.04	94.36	0.05	83117.00	0.03	91.45	0.03	2.91
31	96011.00	0.04	95.14	0.03	69182.00	0.03	97.89	0.03	-2.75
32	202190.00	0.03	95.37	0.04	201780.00	0.04	92.60	0.03	2.76
33	69716.00	0.03	96.33	0.04	57544.00	0.06	90.62	0.03	5.71
34	168340.00	0.04	94.67	0.04	153860.00	0.04	93.58	0.03	1.08
36	79348.00	0.03	95.40	0.03	69188.00	0.04	93.33	0.03	2.07
37	91302.00	0.04	95.21	0.04	90120.00	0.04	91.39	0.03	3.82
38	116010.00	0.04	95.45	0.04	148080.00	0.04	95.57	0.04	-0.12
39	109160.00	0.05	93.85	0.03	92250.00	0.03	92.41	0.03	1.44
40	119980.00	0.02	94.21	0.05	120650.00	0.05	91.28	0.04	2.93
41	201870.00	0.03	94.76	0.04	166180.00	0.07	95.88	0.03	-1.12
42	137130.00	0.02	93.69	0.05	133080.00	0.03	93.24	0.04	0.44
44	82907.00	0.05	94.62	0.04	64848.00	0.03	94.31	0.04	0.31
45	144470.00	0.03	94.40	0.04	112910.00	0.03	96.23	0.04	-1.83
46	183040.00	0.03	95.54	0.04	152410.00	0.03	98.38	0.04	-2.84
47	122510.00	0.03	94.95	0.04	80878.00	0.05	99.69	0.04	-4.74
48	97031.00	0.02	95.51	0.03	82755.00	0.01	97.26	0.03	-1.75
49	152760.00	0.03	94.87	0.04	129820.00	0.04	96.95	0.04	-2.08
50	143280.00	0.02	95.58	0.03	125210.00	0.02	99.19	0.03	-3.61
51	93866.00	0.03	95.48	0.04	70408.00	0.05	98.43	0.04	-2.95
52	48282.00	0.05	94.91	0.04	36880.00	0.10	96.33	0.02	-1.42
53	77751.00	0.02	94.85	0.04	63395.00	0.05	97.94	0.04	-3.08
54	159050.00	0.03	95.25	0.05	150650.00	-0.01	101.04	0.03	-5.79
55	51712.00	0.03	91.73	0.01	43607.00	0.01	93.97	0.02	-2.24
57	106180.00	0.02	94.47	0.04	86292.00	0.03	94.55	0.05	-0.08
58	128530.00	0.02	95.13	0.04	112210.00	0.02	99.38	0.04	-4.26
59	120850.00	0.03	95.35	0.05	106650.00	0.04	89.98	0.04	5.37
60	95800.00	0.04	96.46	0.03	93067.00	0.03	91.64	0.03	4.82
61	85151.00	0.02	94.86	0.05	72816.00	0.04	93.55	0.05	1.31
62	186180.00	0.01	95.38	0.04	143790.00	0.06	98.23	0.04	-2.85
63	63012.00	0.03	93.59	0.03	41091.00	0.04	98.13	0.03	-4.54
64	80420.00	0.02	95.50	0.04	62559.00	0.03	100.37	0.03	-4.87
65	69466.00	0.03	93.89	0.04	57365.00	0.04	91.35	0.03	2.53
67	118330.00	0.03	94.43	0.04	100360.00	0.03	91.45	0.03	2.98
68	105770.00	0.02	95.25	0.04	73072.00	0.03	102.45	0.03	-7.20
69	47525.00	0.04	95.22	0.03	36210.00	0.03	90.11	0.02	5.11
71	72677.00	0.02	94.56	0.05	40399.00	0.02	92.41	0.03	2.16
72	90363.00	0.05	95.08	0.03	66098.00	0.08	88.67	0.02	6.41
73	57851.00	0.03	95.93	0.03	57458.00	0.03	90.12	0.02	5.82
74	92372.00	0.02	95.07	0.05	84532.00	0.02	88.27	0.04	6.80
75	37119.00	0.05	93.17	0.03	34177.00	0.05	89.63	0.05	3.54
76	118600.00	0.04	94.53	0.04	164860.00	0.08	94.92	0.03	-0.39

77	134790.00	0.03	94.51	0.05	133540.00	0.04	91.70	0.03	2.81
78	88428.00	0.04	94.66	0.03	84181.00	0.04	94.83	0.03	-0.17
79	115670.00	0.03	94.24	0.05	114710.00	0.02	96.17	0.05	-1.93
80	160640.00	0.03	94.64	0.05	162860.00	0.04	96.91	0.05	-2.27
81	140220.00	0.03	94.60	0.04	123800.00	0.04	94.96	0.04	-0.36
82	119770.00	0.03	94.22	0.05	97091.00	0.03	93.24	0.05	0.98
83	194970.00	0.04	94.49	0.04	156060.00	0.03	91.68	0.03	2.80
84	111240.00	0.05	95.57	0.04	66501.00	0.06	96.17	0.04	-0.61
85	103880.00	0.03	94.41	0.04	83503.00	0.03	94.25	0.03	0.15
86	106280.00	0.03	95.00	0.04	86871.00	0.04	90.75	0.04	4.24
87	143260.00	0.03	94.75	0.04	130970.00	0.02	92.46	0.03	2.30
88	129880.00	0.03	95.23	0.04	102040.00	0.03	96.00	0.03	-0.78
89	117720.00	0.03	94.90	0.04	96860.00	0.05	92.56	0.03	2.34
90	220720.00	0.03	94.31	0.04	163600.00	0.06	89.25	0.03	5.05
91	143200.00	0.03	94.41	0.05	108410.00	0.03	96.72	0.03	-2.31
92	98770.00	0.04	93.85	0.03	74951.00	0.12	94.29	0.02	-0.44
93	205480.00	0.03	94.41	0.04	163600.00	0.06	89.25	0.03	5.16
94	141710.00	0.02	93.44	0.04	105960.00	0.04	97.18	0.04	-3.73
95	140500.00	0.02	95.51	0.04	115640.00	0.03	94.72	0.04	0.79
96	112340.00	0.01	96.67	0.04	71560.00	0.06	104.62	0.11	-7.96
97	123710.00	0.04	96.81	0.05	104600.00	0.03	101.13	0.03	-4.32
98	85330.00	0.01	94.38	0.04	73414.00	0.03	90.95	0.04	3.43
99	264170.00	0.03	94.79	0.05	196910.00	0.02	101.15	0.04	-6.36
100	81872.00	0.04	93.43	0.05	60080.00	0.02	97.24	0.04	-3.81
101	88060.00	0.03	96.28	0.04	68889.00	0.01	95.41	0.03	0.87
102	128820.00	0.03	94.88	0.04	95957.00	0.04	88.21	0.04	6.67
103	176380.00	0.04	95.32	0.04	139290.00	0.04	94.23	0.03	1.08
104	110410.00	0.04	95.23	0.04	84768.00	0.04	93.70	0.03	1.54
105	202190.00	0.03	95.37	0.04	201780.00	0.04	92.60	0.03	2.76
106	136240.00	0.03	94.86	0.04	100920.00	0.03	91.22	0.03	3.64
107	130190.00	0.03	94.90	0.04	84521.00	0.02	95.47	0.03	-0.57
108	69054.00	0.02	95.28	0.04	67167.00	0.07	92.28	0.03	3.00
109	100410.00	0.02	95.52	0.04	74863.00	0.04	87.93	0.03	7.59
110	80647.00	0.05	94.33	0.04	57479.00	0.08	93.77	0.04	0.57
111	118760.00	0.03	95.75	0.04	85943.00	0.02	95.80	0.04	-0.05
112	137470.00	0.05	94.62	0.04	110360.00	0.09	87.41	0.03	7.21
113	134130.00	0.04	94.51	0.05	119230.00	0.03	95.44	0.04	-0.94
114	168260.00	0.03	94.68	0.04	148880.00	0.02	101.14	0.03	-6.46
115	236880.00	0.02	93.74	0.06	215390.00	0.02	98.17	0.06	-4.43
116	217660.00	0.03	94.53	0.05	191890.00	0.03	100.00	0.06	-5.47
117	120720.00	0.04	94.51	0.04	80941.00	0.03	100.48	0.04	-5.98
118	138830.00	0.03	94.97	0.04	104840.00	0.03	95.62	0.04	-0.66
119	170160.00	0.03	94.68	0.05	143350.00	0.03	97.31	0.04	-2.62
120	133930.00	0.03	95.28	0.03	97337.00	0.02	97.30	0.03	-2.02
121	148960.00	0.03	94.86	0.05	126240.00	0.02	94.56	0.03	0.30
122	169120.00	0.02	95.35	0.03	129260.00	0.02	97.28	0.03	-1.93
123	165660.00	0.02	95.13	0.04	123520.00	0.03	97.54	0.04	-2.42
124	171720.00	0.03	95.55	0.04	133450.00	0.01	98.08	0.03	-2.53
125	119580.00	0.03	94.72	0.04	95088.00	0.05	96.52	0.03	-1.80
126	140060.00	0.02	95.23	0.04	110450.00	0.02	97.11	0.03	-1.88
127	161140.00	0.02	95.23	0.04	122750.00	0.03	97.66	0.04	-2.44

128	163240.00	0.03	94.40	0.04	125520.00	0.03	95.80	0.04	-1.40
129	140270.00	0.02	94.99	0.05	109680.00	0.00	98.34	0.03	-3.36
130	122330.00	0.02	93.36	0.05	98907.00	0.02	88.56	0.04	4.79
131	128150.00	0.03	95.04	0.03	111810.00	0.03	89.68	0.03	5.36
132	172120.00	0.01	95.51	0.05	148500.00	0.04	90.68	0.04	4.83
133	144490.00	0.03	96.28	0.04	135590.00	0.04	89.48	0.03	6.80
134	115150.00	0.03	94.69	0.04	83189.00	0.04	99.87	0.05	-5.19
135	170230.00	0.02	94.39	0.05	152220.00	0.03	95.99	0.04	-1.60
136	116080.00	0.03	93.65	0.05	76850.00	0.05	94.92	0.04	-1.28
137	94260.00	0.03	95.37	0.04	73333.00	0.03	96.09	0.03	-0.72
138	110060.00	0.02	93.98	0.04	77484.00	0.02	99.13	0.03	-5.15
139	205930.00	0.02	94.73	0.04	171170.00	0.05	95.32	0.03	-0.60
140	120400.00	0.03	95.14	0.03	75545.00	0.04	99.91	0.03	-4.77
141	50595.00	0.04	94.90	0.03	38343.00	0.04	93.16	0.03	1.74
142	115540.00	0.04	94.50	0.04	93763.00	0.06	99.52	0.04	-5.01
143	150830.00	0.03	95.01	0.04	110310.00	0.03	95.95	0.04	-0.94
144	111550.00	0.03	94.76	0.03	70282.00	0.00	104.05	0.03	-9.29
145	264170.00	0.03	94.79	0.05	196910.00	0.02	101.15	0.04	-6.36
146	158960.00	0.04	94.09	0.05	159080.00	0.03	89.73	0.04	4.36
147	247880.00	0.03	95.34	0.06	242440.00	0.05	95.99	0.06	-0.66
148	411200.00	0.02	93.52	0.10	443210.00	0.04	93.40	0.12	0.12

Appendix 15. J-coupling and RDC values for Ca^{2+}/CaM at a 1:10 ratio of Ca^{2+}/CaM and $eEF2K_{82-100}$. Initial intensity (a), value for the imperfection of π pulses (b) and r2 relaxation are also shown.

RESIDUE	ISOTROPIC				ANISOTROPIC				RDC
	a	b	J	r2	a	b	J	r2	
4	135802.22	0.22	91.85	0.04	312093.67	0.04	92.30	0.05	-0.45
5	93100.68	0.20	92.88	0.03	362382.68	0.03	98.79	0.03	-5.91
6	75451.27	0.20	92.90	0.03	595349.15	0.04	96.73	0.04	-3.82
7	105406.66	0.20	93.08	0.03	670013.80	0.04	86.64	0.04	6.44
13	114412.88	0.18	94.46	0.03	292738.57	0.04	95.64	0.04	-1.19
18	114058.01	0.23	92.86	0.03	435552.17	0.02	83.46	0.03	9.39
20	82943.32	0.24	93.36	0.02	201917.15	0.00	111.67	0.05	-18.31
21	125910.46	0.22	92.71	0.03	292609.48	0.02	94.09	0.04	-1.39
22	97498.73	0.22	94.03	0.04	301821.84	0.04	96.50	0.06	-2.46
24	98578.72	0.21	95.75	0.03	474322.03	0.03	103.70	0.04	-7.95
25	76279.46	0.20	92.89	0.04	340605.84	0.03	109.52	0.05	-16.63
26	86191.09	0.20	93.66	0.04	320264.19	0.02	90.08	0.05	3.58
27	61404.46	0.21	90.11	0.03	242834.89	0.05	96.62	0.04	-6.52
28	50877.55	0.22	92.18	0.03	172671.05	0.01	101.93	0.04	-9.75
29	78849.68	0.18	92.56	0.03	231881.28	0.04	101.19	0.02	-8.63
31	65444.41	0.27	94.05	0.03	244915.98	0.04	110.49	0.04	-16.44
33	68771.36	0.24	94.54	0.04	152652.89	-0.01	96.74	0.03	-2.21
36	66840.29	0.06	93.82	0.04	141767.49	0.00	104.14	0.04	-10.32
39	81246.64	0.23	92.73	0.04	302102.96	0.10	98.06	0.02	-5.34
40	79930.51	0.24	94.07	0.04	570406.12	0.07	83.68	0.02	10.40
41	73528.78	0.20	95.08	0.04	245421.39	0.06	93.02	0.05	2.05
44	95524.11	0.20	92.10	0.03	420821.09	0.05	86.76	0.02	5.34
45	70545.87	0.19	92.48	0.03	442480.31	0.00	97.60	0.05	-5.11

50	131095.85	0.25	94.87	0.04	386065.63	0.04	99.37	0.03	-4.50
51	104877.83	0.25	91.94	0.03	178255.91	0.04	98.31	0.02	-6.37
57	114684.33	0.21	92.83	0.04	334545.67	0.03	97.58	0.04	-4.75
58	122765.03	0.23	94.83	0.03	424593.49	0.05	106.09	0.05	-11.26
60	87510.35	0.22	92.30	0.03	306714.42	0.06	91.80	0.05	0.49
61	82522.18	0.22	93.89	0.03	219082.15	0.02	79.02	0.05	14.87
63	55159.98	0.22	92.32	0.04	133437.80	0.01	101.10	0.02	-8.78
64	64165.47	0.22	93.25	0.03	221078.80	0.03	99.64	0.04	-6.40
68	67526.40	0.24	95.26	0.04	114906.12	-0.01	96.51	0.17	-1.25
79	61041.29	0.19	93.14	0.04	638160.99	0.02	94.42	0.05	-1.29
81	27262.65	0.33	97.92	0.02	607577.58	0.04	95.84	0.05	2.08
83	92913.54	0.24	91.93	0.04	320163.65	0.03	64.30	0.03	27.64
86	95477.66	0.18	92.31	0.03	189453.27	0.07	64.93	0.02	27.39
90	100122.75	0.21	93.48	0.03	138597.29	-0.06	60.89	0.15	32.58
91	109420.97	0.22	94.11	0.04	292938.59	0.04	95.87	0.03	-1.77
93	123432.63	0.24	93.28	0.03	567675.05	0.39	62.85	0.01	30.43
94	111649.99	0.23	92.79	0.04	278747.20	0.02	90.25	0.03	2.54
95	116790.97	0.19	94.38	0.03	296605.30	0.04	100.89	0.05	-6.50
96	92732.96	0.23	95.74	0.03	309037.15	0.05	114.63	0.03	-18.89
97	88509.48	0.26	96.63	0.03	420134.21	0.03	92.92	0.04	3.71
98	70777.16	0.22	93.96	0.05	280394.30	0.02	106.46	0.04	-12.51
100	60761.96	0.21	90.99	0.04	203128.25	0.01	108.36	0.03	-17.36
101	55274.15	0.22	94.62	0.03	101803.02	-0.01	109.36	0.04	-14.74
102	98701.52	0.16	92.93	0.03	287977.12	0.02	96.54	0.04	-3.61
106	91534.78	0.20	94.15	0.04	220353.16	0.00	100.32	0.04	-6.16
109	89471.67	0.21	94.14	0.03	181909.80	0.02	98.22	0.03	-4.08
110	75628.54	0.23	93.49	0.03	232813.71	0.04	105.74	0.03	-12.26
111	97030.82	0.24	94.16	0.04	227850.89	0.01	110.79	0.05	-16.63
112	153992.54	0.25	93.59	0.03	291263.05	0.02	99.35	0.03	-5.76
113	104860.56	0.25	93.41	0.03	563721.41	0.05	96.15	0.02	-2.74
115	104519.28	0.18	91.31	0.03	346025.50	0.03	106.61	0.04	-15.31
116	159874.34	0.20	92.61	0.05	549283.13	0.01	103.91	0.04	-11.30
117	84522.93	0.15	92.83	0.04	243246.59	0.04	109.21	0.04	-16.38
118	56549.73	0.21	92.50	0.03	407637.12	0.04	79.03	0.03	13.47
119	122933.85	0.19	90.95	0.03	420828.81	0.03	89.99	0.03	0.96
123	133267.22	0.22	92.79	0.03	338917.00	0.07	95.22	0.02	-2.43
126	129602.42	0.23	94.38	0.03	288355.74	0.09	87.72	0.03	6.66
129	101780.58	0.17	94.30	0.03	321133.42	0.02	92.79	0.03	1.51
130	97331.14	0.22	92.40	0.04	245328.82	0.02	84.64	0.03	7.76
131	97643.91	0.21	93.36	0.04	246420.77	0.03	98.50	0.03	-5.13
133	94664.84	0.26	96.17	0.03	337871.42	0.10	65.41	0.02	30.76
134	85534.85	0.17	92.92	0.03	346920.70	0.03	106.18	0.05	-13.26
135	131751.11	0.22	92.97	0.03	440506.57	0.04	107.72	0.04	-14.76
136	61860.70	0.19	91.95	0.04	193881.41	0.03	109.02	0.04	-17.06
137	70167.64	0.16	93.73	0.03	224858.59	-0.01	111.57	0.04	-17.84
138	59897.17	0.27	94.42	0.03	156737.88	0.03	105.25	0.03	-10.83
139	204315.75	0.24	93.99	0.03	614967.29	0.03	103.00	0.03	-9.02
140	75501.27	0.17	90.78	0.02	188364.20	0.01	108.22	0.03	-17.44
141	73414.64	0.21	92.65	0.03	114906.12	-0.01	96.51	0.17	-3.86
145	167102.08	0.23	93.65	0.06	683912.72	0.03	97.80	0.06	-4.15
147	114731.39	0.24	95.00	0.05	466718.80	0.03	90.93	0.04	4.07

148	308127.98	0.21	92.33	0.07	1029887.38	0.02	99.92	0.05	-7.59

Appendix 16. CSP analysis (1:1 ratio)

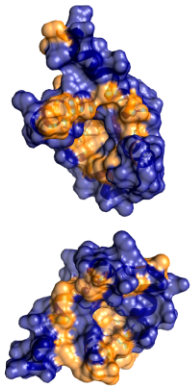

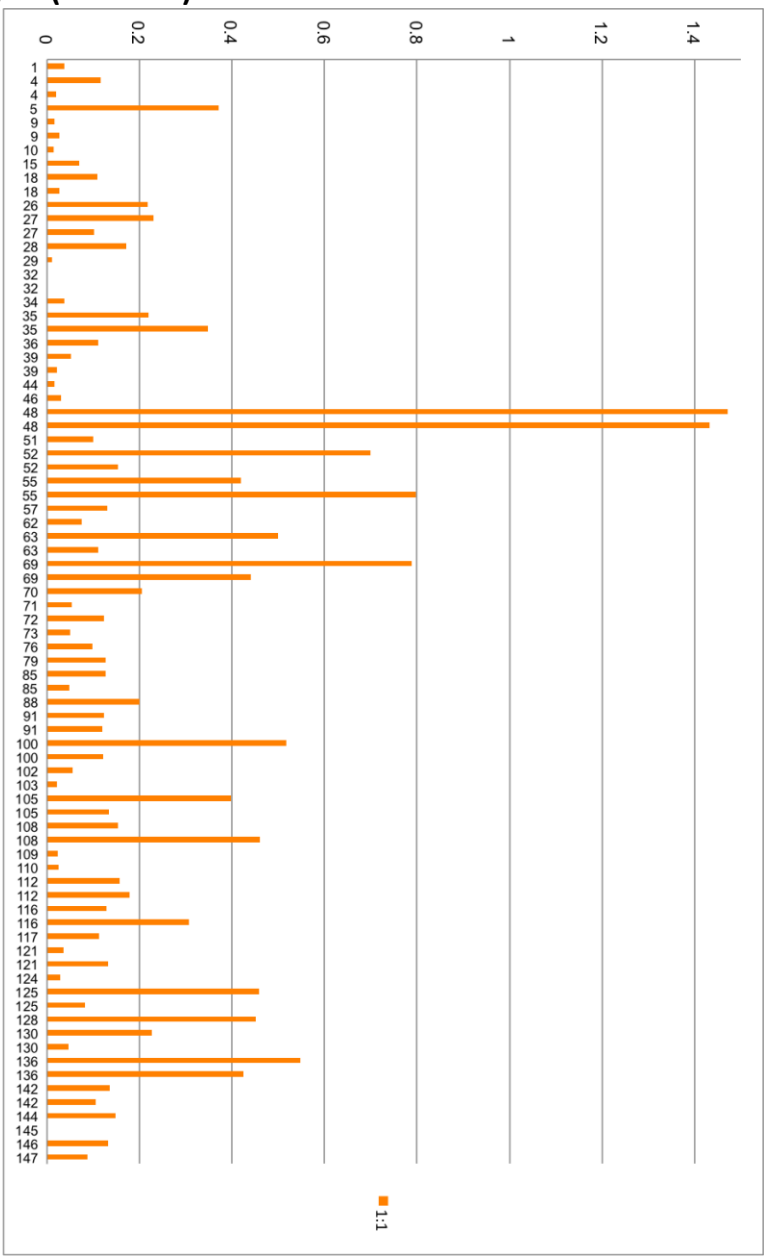

Appendix 17. Chemical shift Table for the Ca^{2+}/CaM: $eEF2K_{82-100}$ complex (1:1 ratio).

	H	N	HA	HB	HG	HD	HE	C	CA	CB	CG	CD	CE	ND	NE
1	-	122.46	4.09	1.35	-	-	-	177	53.83	18.72	-	-	-	-	-
2	7.85	116.4	4.52	2.75, 2.75	-	-	-	177.99	55.3	40.85	-	-	-	-	-
3	7.85	117.55	4.42	2.26, 2.07	2.42,2.42	-	-	176.39	55.55	29.63	34.12	-	-	-	-
4	7.73	121.29	4.7	1.85, 1.56	1.86	0.95, 0.98	-	175.89	54.33	43.65	27.26	27.19, 23.68	-	-	-
5	8.79	112.73	4.5	4.82	1.37	-	-	177.51	60.49	71.25	21.94	-	-	-	-

6	9.08	120.58	4.01	2.09, 2.09	2.44,2.38	-	-	175.54	60.16	29.29	37.13	-	-	-	-
7	8.74	119.55	4.1	1.97, 2.09	2.37,2.32	-	-	179.54	60.02	29.07	37.69	-	-	-	-
8	7.78	120.47	3.83	-	-	-	7.51, 6.80	179.21	58.79	29.22	-	-	-	-	111.35
9	8.42	119.38	3.69	1.98	1.15,1.86,1.12	0.91	-	178.23	66.36	37.87	17.57,30.40	13.04	-	-	-
10	8.07	121.27	4.16	1.56	-	-	-	177.83	55.51	17.95	-	-	-	-	-
11	7.86	119.89	-	-	-	-	-	181.13	59.49	29.17	-	-	-	-	-
12	8.63	120.39	5.07	3.53, 3.49	-	7.17	7.25	178.79	58.97	37.6	-	-	-	-	-
13	9.3	123.84	4.06	1.95, 1.95	1.05,1.22	1.24, 1.38	2.60, 2.60	178.77	60.11	31.91	25.65	28.8	41.81	-	-
14	7.89	120.62	4.18	2.49, 2.36	2.35,2.49	-	-	179.34	59.43	29.14	36.56	-	-	-	-
15	8.03	122.62	4.35	2.04	-	-	-	179.61	55.45	18.24	-	-	-	-	-
16	8.83	119.25	4.06	2.96, 3.27	-	6.58	7.38	179.04	62.27	39.89	-	-	-	-	-
17	8.13	113.38	4.15	4.07, 4.07	-	-	-	177.68	61.56	63.24	-	-	-	-	-
18	7.41	120.83	4.01	1.69, 1.61	1.48	0.86, 0.73	-	-	57.25	41.5	26.84	24.14, 24.54	-	-	-
19	7.11	113.67	4.25	-	-	7.41	7.26	177.6	59.45	41.49	-	-	-	-	-
20	7.82	117.09	4.62	2.38, 1.55	-	-	-	-	52.38	39.18	-	-	-	-	-
21	7.73	124.48	4.01	1.90, 1.91	1.58,1.51	1.72, 1.72	3.05, 3.04	177.3	58.55	32.66	24.5	28.38	41.73	-	-
22	8.13	114.08	4.62	3.11, 2.69	-	-	-	178.26	52.92	39.73	-	-	-	-	-
23	7.74	109.49	3.90, 3.94	-	-	-	-	177.77	47.25	-	-	-	-	-	-
24	8.5	120.98	4.56	2.50, 3.10	-	-	-	175.24	53.81	40.5	-	-	-	-	-
25	10.65	113.17	4.41, 3.76	-	-	-	-	177.46	45.53	-	-	-	-	-	-
26	8.25	112.55	5.45	3.89	1.09	-	-	173.89	59.73	72.86	22.13	-	-	-	-
27	9.98	127.02	4.9	1.82	0.28,0.94,0.44	0.45	-	173.25	61.1	40.24	17.64,26.75	15.82	-	-	-
28	8.39	116.49	4.85	4.05	1.17	-	-	176.18	59.37	72.49	22.55	-	-	-	-
29	9.21	113.16	3.77	4.22	1.29	-	-	176.51	66.42	68.01	23.4	-	-	-	-
30	7.7	121.01	4.16	1.85, 1.74	1.45,1.53	1.71, 1.71	3.02, 3.02	177.17	59.27	32.64	24.88	29.23	40.22	-	-
31	7.78	121.92	4.06	2.25, 2.41	2.57,2.40	-	-	179.97	59.58	29.8	35.95	-	-	-	-
32	8.64	120.38	-	-	-	-	-	179.13	58.3	42.34	-	-	-	-	-
33	8.7	105.65	4.00, 3.57	-	-	-	-	178.96	48.6	-	-	-	-	-	-
34	8.05	118.35	3.96	4.38	1.31	-	-	175.11	67.01	68.91	21.75	-	-	-	-
35	7.8	122.39	3.67	2.09	0.56,0.90	-	-	-	66.64	31.6	23.50,20.88	-	-	-	-
36	8.67	118.71	4.15	1.91, 2.06	2.60,2.60	-	2.01	179.4	59.14	31.5	32.76	-	17.52	-	-
37	8.6	118.87	4.83	1.89, 1.93	-	3.16, 3.36	-	-	59.28	30.14	-	43.26	-	-	-
38	7.98	119.06	4.45	4.13, 4.11	-	-	-	-	61.52	62.77	-	-	-	-	-
39	7.45	121	4.53	1.85, 1.95	1.85	0.86, 0.89	-	174.97	54.69	42.13	25.97	22.54, 26.00	-	-	-
40	7.91	106.97	4.31, 3.84	-	-	-	-	177.53	45.66	-	-	-	-	-	-
41	7.84	118.46	4.54	2.28, 2.28	2.28,2.28	-	6.79, 7.46	-	54.54	30.62	33.98	-	-	-	112.25
42	8.78	116.44	5.23	2.55, 2.81	-	6.76, 7.59	-	174.19	51.38	38.93	-	-	-	112.29	-

43	-	-	-	-	-	-	-	-	62.46	31.94	-	-	-	-	-
44	8.83	113.1	4.47	4.78	1.38	-	-	177.65	60.67	71.16	21.94	-	-	-	-
45	8.86	120.71	4.03	2.37, 2.38	2.38	-	-	175.14	60.04	29.02	36.51	-	-	-	-
46	8.32	120.95	4.14	1.43	-	-	-	178.97	55.05	18.27	-	-	-	-	-
47	7.75	118.94	4.02	2.36, 1.91	1.89	-	-	180.29	59.11	29.69	37.69	-	-	-	-
48	8.22	120.23	4.05	1.22, 2.09	1.9	0.86, 0.77	-	180.14	57.89	42.54	27.69	25.98, 23.61	-	-	-
49	8.25	118.35	3.85	2.21, 2.21	2.47,2.47	-	-	178.59	58.66	28.33	34.14	-	-	-	-
50	8.11	120.12	4.46	2.73, 2.84	-	-	-	178.55	57.63	40.35	-	-	-	-	-
51	7.95	119.57	4.09	2.81, 2.53	-	-	1.91	178.74	59.64	33.68	-	-	17.26	-	-
52	7.82	118.99	3.76	2.08	1.29,1.60,0.77	0.7	-	179.34	64.03	36.83	16.37,28.14	11.6	-	-	-
53	8.76	118.26	4.45	2.93, 3.06	-	7.02, 7.92	-	178.17	56.02	38.14	-	-	-	111.91	-
54	7.69	116.43	4.09	2.25, 2.10	2.38,2.25	-	-	177.44	58.91	30.21	38.84	-	-	-	-
55	7.25	111.42	4.34	2.28	0.96,0.88	-	-	177.23	61.04	33.03	22.68,20.89	-	-	-	-
56	7.73	121.53	4.55	2.59, 2.79	-	-	-	-	53.89	40.48	-	-	-	-	-
57	8.25	106.25	4.25	1.58	-	-	-	176.07	54.43	19.87	-	-	-	-	-
58	8.27	113.98	4.61	2.72, 3.10	-	-	-	178.73	52.84	39.91	-	-	-	-	-
59	7.65	108.62	3.95, 3.83	-	-	-	-	177.95	47.22	-	-	-	-	-	-
60	8.2	118.87	4.66	2.69, 3.35	-	6.99, 7.56	-	174.97	52.77	37.69	-	-	-	113.26	-
61	10.65	113.55	4.30, 3.53	-	-	-	-	176.9	45.72	-	-	-	-	-	-
62	7.71	108.64	4.83	4.06	1.17	-	-	173.27	59.48	72.28	22.65	-	-	-	-
63	8.89	123.94	5.3	2.25	1.33,1.60,1.64	0.96	-	173.26	59.05	39.49	27.61,18.60	12.86	-	-	-
64	8.89	128.24	5.52	2.88, 3.19	-	-	-	175.73	52.03	42.24	-	-	-	-	-
65	9.04	118.59	-	-	-	6.81	7.24	176.07	63.17	35.98	-	-	-	-	-
66	-	-	-	-	-	-	-	-	66.94	30.75	-	-	-	-	-
67	8.29	118.09	-	-	-	-	-	-	58.65	29.64	-	-	-	-	-
68	8.53	123.67	3.87	3.21, 3.51	-	6.93	-	179.32	61.56	40.55	-	-	-	-	-
69	8.9	119.71	3.39	1.21, 1.36	1.07	0.68, 0.70	-	176.82	57.94	41.36	25.91	25.70, 24.80	-	-	-
70	7.76	115.5	3.72	4.24	1.22	-	-	178.7	66.81	68.61	21.84	-	-	-	-
71	7.41	121.02	-	-	-	-	1.92	-	58.77	31.99	-	-	16.94	-	-
72	8.03	117.83	-	-	-	-	1.69	178.05	55.98	30.35	-	-	17.51	-	-
73	8.45	121.93	4.09	1.41	-	-	-	-	54.78	18.26	-	-	-	-	-
74	7.57	117.05	4.09	1.92, 1.98	1.69,1.69	3.16, 3.16	-	179.88	58.66	30.21	27.69	43.56	-	-	-
75	7.65	118.4	4.2	2.11	-	-	-	178.11	57.68	32.57	-	-	-	-	-
76	7.8	118.36	4.36	2.18, 2.24	2.69,2.78	-	1.98	177.94	56.94	33.06	32.35	-	17.58	-	-
77	7.87	120.36	4.36	1.87, 1.92	1.51,1.51	1.71, 1.71	3.03, 3.03	176.75	56.54	33.12	24.68	29.21	42.12	-	-
78	8.21	120.8	4.74	2.83, 2.69	-	-	-	176.54	54.68	41.16	-	-	-	-	-
79	8.05	114.95	4.37	4.25	1.25	-	-	176.38	62.13	70.11	21.62	-	-	-	-

80	8.56	123.5	4.77	2.80, 2.71	-	-	-	174.2	54.24	41.58	-	-	-	-	-
81	8.52	117.59	4.44	4.01, 4.14	-	-	-	176.38	59.49	64.15	-	-	-	-	-
82	8.64	122.48	4.42	-	-	-	-	175.59	59.26	29.43	-	-	-	-	-
83	8.38	119.39	4.11	2.39, 2.39	2.39,2.39	-	-	178.26	59.42	29.31	36.58	-	-	-	-
84	8.04	118.69	4.16	2.13, 2.13	2.36,2.36	-	-	178.7	59.37	29.87	36.31	-	-	-	-
85	8.06	121.69	4	2.24	1.89,2.24,1.18	0.84	-	179.52	65.14	37.57	28.85,18.97	13.38	-	-	-
86	8.42	121.54	4.19	1.88, 2.09	1.89,1.61	3.01, 3.00	-	178.11	60.3	29.89	27.6	43.19	-	-	-
87	8.31	118.18	4.09	-	-	-	-	179.35	59.3	29.32	-	-	-	-	-
88	8	121.85	4.25	1.88	-	-	-	178.98	55.31	18.17	-	-	-	-	-
89	8.61	118.65	4.19	3.25, 2.97	-	7.17	6.86	178.9	62.23	39.04	-	-	-	-	-
90	7.84	115.84	3.88	2.00, 2.00	1.75,1.71	3.27, 3.27	-	177.18	58.56	30.47	28.55	43.64	-	-	-
91	7.42	118.59	3.46	2.2	1.08,0.53	-	-	177.56	65.81	31.4	23.03,20.92	-	-	-	-
92	6.89	114.1	4.3	2.67, 2.87	-	7.39	-	176.36	60.15	41.48	-	-	-	-	-
93	7.85	115.87	4.63	1.34, 2.18	-	-	-	176.22	51.99	38.8	-	-	-	-	-
94	7.64	125.41	3.92	1.86, 1.86	1.47,1.52	1.67, 1.67	2.86, 2.91	177.78	58.94	32.5	25.55	27.69	41.53	-	-
95	8.4	114.27	4.59	2.70, 3.12	-	-	-	178.25	53.16	39.78	-	-	-	-	-
96	7.84	109.4	3.92, 3.86	-	-	-	-	177.93	47.18	-	-	-	-	-	-
97	8.44	120.01	4.68	3.45, 2.72	-	-	-	175.13	52.75	38.27	-	-	-	-	-
98	10.7	112.87	4.15, 3.51	-	-	-	-	176.14	45.08	-	-	-	-	-	-
99	7.74	116.48	5.06	2.59, 2.63	-	6.83	6.96	-	56.39	42.84	-	-	-	-	-
100	10.22	127.63	4.73	2.03	1.13,1.49,1.49	0.64	-	174.8	61.38	39.48	17.72	16.1	-	-	-
101	9.01	123.98	5.01	4.03, 4.51	-	-	-	175.62	55.87	66.8	-	-	-	-	-
102	9.42	123.42	3.98	1.54	-	-	-	175.23	55.99	18.17	-	-	-	-	-
103	8.33	118.65	4.07	1.47	-	-	-	179.36	55.26	18.49	-	-	-	-	-
104	7.98	120.14	4.07	2.60, 2.77	2.38,2.38	-	-	181.52	59.62	29.21	37.88	-	-	-	-
105	8.63	120.38	4.17	1.94, 1.52	-	0.70, 0.78	-	180.45	58.39	42.18	-	24.43, 26.49	-	-	-
106	8.7	117.65	3.83	2.00, 2.00	1.68,1.68	3.30, 3.19	-	178.41	60.05	30.75	28.27	43.86	-	-	-
107	7.98	118.82	4.38	3.44, 3.34	-	-	-	178.97	59.42	29.96	-	-	-	-	-
108	8.72	120.43	3.59	2.13	0.56,1.16	-	-	177.63	66.89	31.96	23.84,21.03	-	-	-	-
109	8.55	116.08	4.37	2.15, 2.15	2.43,2.43	-	2.16	178.25	57.44	29.61	32.18	-	17.09	-	-
110	8.01	115.86	4.09	4.34	1.27	-	-	179.32	66.78	68.65	21.67	-	-	-	-

111	7.93	123.19	4.5	2.82, 2.88	-	7.43, 6.64	-	178.29	56.15	38.26	-	-	-	111.11	-
112	7.99	118.31	4.37	1.96, 1.68	1.92	0.79, 0.83	-	176.54	55.05	42.24	26.22	26.07, 22.72	-	-	-
113	7.88	107.13	4.21, 3.79	-	-	-	-	176.98	45.7	-	-	-	-	-	-
114	8.05	120.33	4.5	1.97, 1.74	2.19,2.07	-	-	174.48	54.75	30.79	35.39	-	-	-	-
115	8.6	124.34	4.37	1.69, 1.79	1.32,1.32	1.68, 1.68	3.00, 3.00	175.12	55.62	31.94	24.71	29.42	42.15	-	-
116	8.2	125.64	4.77	1.45, 1.61	1.6	0.74, 0.76	-	175.34	54.2	44.67	27.65	24.20, 26.95	-	-	-
117	9.24	114.53	4.47	4.78	1.37	-	-	178.25	60.81	71.2	21.49	-	-	-	-
118	8.97	121.29	4.25	2.62, 2.78	-	-	-	175.59	58.09	39.64	-	-	-	-	-
119	8.68	119.47	4.12	-	-	-	-	176.85	59.96	29.11	-	-	-	-	-
120	7.79	120.8	-	-	-	-	-	179.19	59.32	30.51	-	-	-	-	-
121	8.1	121.66	3.48	2.24	1.01,0.94	-	-	180.04	67.01	31.51	23.95,23.88,24.01,22.36	-	-	-	-
122	8.07	119.83	4.39	2.82, 2.68	-	-	-	177.45	57.73	40.52	-	-	-	-	-
123	8.15	119.66	4.05	2.40, 2.40	2.39,2.39	-	-	179.18	59.34	29.4	38.84	-	-	-	-
124	7.81	119.87	4.2	-	-	-	2.16	178.68	60.25	33.11	-	-	17.09	-	-
125	8.1	120.34	3.83	2.37	1.60,0.82,1.60	0.84	-	180.16	63.89	36.08	16.50,27.80	10.18	-	-	-
126	8.45	118.23	4.1	1.90, 1.96	1.72,1.72	3.26, 3.26	-	177.53	59.79	30.45	28.84	43.53	-	-	-
127	8.09	116.75	4.05	2.26, 2.41	2.59,2.59	-	-	178.94	58.91	30.15	36.27	-	-	-	-
128	7.23	117.62	4.49	1.2	-	-	-	177	51.78	21.94	-	-	-	-	-
129	8.08	117.79	4.53	2.55, 2.55	-	-	-	177.75	54.53	40.71	-	-	-	-	-
130	8.37	128.19	3.96	2	0.96,1.30,1.70	0.91	-	175.91	63.43	38.91	27.50,17.52	12.72	-	-	-
131	8.38	116.8	4.57	3.12, 2.70	-	-	-	177.95	54.01	39.99	-	-	-	-	-
132	7.7	108.82	3.86, 4.03	-	-	-	-	178.26	47.54	-	-	-	-	-	-
133	8.43	120.95	4.53	2.55, 3.03	-	-	-	175.39	53.7	40.19	-	-	-	-	-
134	10.3	112.82	4.10, 3.48	-	-	-	-	177.62	45.9	-	-	-	-	-	-
13	8.06	115.5	5.04	2.07, 2.07	2.06,2.06	-	6.59, 6.03	176.87	53.29	32.82	33.51	-	-	-	108.93

5															
136	9.2	125.57	5.22	2.39	1.12,1.09	-	-	175.12	61.73	34	21.86,22.88	-	-	-	-
137	9.6	129.3	5.38	3.17, 3.20	-	6.87, 7.54	-	175.91	51.05	38.57	-	-	-	112.57	-
138	8.28	118.54	3.33	2.41, 2.09	-	6.25	6.52	174.82	62.44	37.95	-	-	-	-	-
139	8.09	118.34	3.67	-	-	-	-	176.11	60.3	28.91	37.02	-	-	-	-
140	8.73	120.12	3.91	2.31	2.45	-	-	180.28	58.62	29.64	-	-	-	-	-
141	8.78	123.95	4.25	2.62, 2.78	-	6.72	7.34	179.39	61.82	40.34	-	-	-	-	-
142	8.68	119.13	3.13	1.84	0.50,0.75	-	-	178.71	66.85	31.57	23.18,21.48	-	-	-	-
143	7.59	118.56	3.88	-	-	-	6.82, 7.41	179.56	58.67	28.04	-	-	-	-	111.58
144	7.35	116.96	4.21	2.07, 2.07	-	-	2.09	177.94	56.88	31.61	-	-	17.16	-	-
145	7.74	116.47	4.09	2.06, 2.19	-	-	-	-	56.87	32.24	-	-	-	-	-
146	7.66	108.9	4.32	4.3	1.19	-	-	177.33	61.92	70.24	21.55	-	-	-	-
147	7.54	126.72	4.31	1.46	-	-	-	174.28	52.92	19.25	-	-	-	-	-
148	8.06	126.67	4.16	1.86, 1.73	-	-	3.02, 3.02	176.91	57.74	33.69	-	-	42.26	-	-

Appendix 18. ϕ/ψ angles used in the structure calculation of the Ca^{2+}/CaM: $eEF2K_{82-100}$ complex.

(resid 1 and name C) (resid 2 and name N)
(resid 2 and name CA) (resid 2 and name C) 1.0 -70.2 20.0 2
(resid 2 and name N) (resid 2 and name CA)
(resid 2 and name C) (resid 3 and name N) 1.0 -17.8 20.0 2
(resid 2 and name C) (resid 3 and name N)
(resid 3 and name CA) (resid 3 and name C) 1.0 -93.1 20.0 2
(resid 3 and name N) (resid 3 and name CA)
(resid 3 and name C) (resid 4 and name N) 1.0 -6.0 20.0 2
(resid 3 and name C) (resid 4 and name N)
(resid 4 and name CA) (resid 4 and name C) 1.0 -91.8 21.0 2
(resid 4 and name N) (resid 4 and name CA)
(resid 4 and name C) (resid 5 and name N) 1.0 146.9 21.7 2
(resid 4 and name C) (resid 5 and name N)
(resid 5 and name CA) (resid 5 and name C) 1.0 -80.8 20.0 2
(resid 5 and name N) (resid 5 and name CA)
(resid 5 and name C) (resid 6 and name N) 1.0 165.1 20.0 2
(resid 5 and name C) (resid 6 and name N)
(resid 6 and name CA) (resid 6 and name C) 1.0 -58.7 20.0 2
(resid 6 and name N) (resid 6 and name CA)
(resid 6 and name C) (resid 7 and name N) 1.0 -39.0 20.0 2
(resid 6 and name C) (resid 7 and name N)
(resid 7 and name CA) (resid 7 and name C) 1.0 -65.5 20.0 2
(resid 7 and name N) (resid 7 and name CA)
(resid 7 and name C) (resid 8 and name N) 1.0 -42.7 20.0 2
(resid 7 and name C) (resid 8 and name N)
(resid 8 and name CA) (resid 8 and name C) 1.0 -64.6 20.0 2

(resid 8 and name N) (resid 8 and name CA)
(resid 8 and name C) (resid 9 and name N) 1.0 -41.6 20.0 2
(resid 8 and name C) (resid 9 and name N)
(resid 9 and name CA) (resid 9 and name C) 1.0 -63.0 20.0 2
(resid 9 and name N) (resid 9 and name CA)
(resid 9 and name C) (resid 10 and name N) 1.0 -43.3 20.0 2
(resid 9 and name C) (resid 10 and name N)
(resid 10 and name CA) (resid 10 and name C) 1.0 -64.7 20.0 2
(resid 10 and name N) (resid 10 and name CA)
(resid 10 and name C) (resid 11 and name N) 1.0 -40.3 20.0 2
(resid 10 and name C) (resid 11 and name N)
(resid 11 and name CA) (resid 11 and name C) 1.0 -65.6 20.0 2
(resid 11 and name N) (resid 11 and name CA)
(resid 11 and name C) (resid 12 and name N) 1.0 -41.9 20.0 2
(resid 11 and name C) (resid 12 and name N)
(resid 12 and name CA) (resid 12 and name C) 1.0 -67.8 20.0 2
(resid 12 and name N) (resid 12 and name CA)
(resid 12 and name C) (resid 13 and name N) 1.0 -36.4 20.0 2
(resid 12 and name C) (resid 13 and name N)
(resid 13 and name CA) (resid 13 and name C) 1.0 -64.8 20.0 2
(resid 13 and name N) (resid 13 and name CA)
(resid 13 and name C) (resid 14 and name N) 1.0 -39.6 20.0 2
(resid 13 and name C) (resid 14 and name N)
(resid 14 and name CA) (resid 14 and name C) 1.0 -65.9 20.0 2
(resid 14 and name N) (resid 14 and name CA)
(resid 14 and name C) (resid 15 and name N) 1.0 -42.5 20.0 2
(resid 14 and name C) (resid 15 and name N)
(resid 15 and name CA) (resid 15 and name C) 1.0 -64.8 20.0 2
(resid 15 and name N) (resid 15 and name CA)
(resid 15 and name C) (resid 16 and name N) 1.0 -41.3 20.0 2
(resid 15 and name C) (resid 16 and name N)
(resid 16 and name CA) (resid 16 and name C) 1.0 -62.8 20.0 2
(resid 16 and name N) (resid 16 and name CA)
(resid 16 and name C) (resid 17 and name N) 1.0 -42.1 20.0 2
(resid 16 and name C) (resid 17 and name N)
(resid 17 and name CA) (resid 17 and name C) 1.0 -63.8 20.0 2
(resid 17 and name N) (resid 17 and name CA)
(resid 17 and name C) (resid 18 and name N) 1.0 -36.5 20.0 2
(resid 17 and name C) (resid 18 and name N)
(resid 18 and name CA) (resid 18 and name C) 1.0 -67.7 20.0 2
(resid 18 and name N) (resid 18 and name CA)
(resid 18 and name C) (resid 19 and name N) 1.0 -36.6 20.0 2
(resid 18 and name C) (resid 19 and name N)
(resid 19 and name CA) (resid 19 and name C) 1.0 -81.0 20.0 2
(resid 19 and name N) (resid 19 and name CA)
(resid 19 and name C) (resid 20 and name N) 1.0 -31.0 20.0 2
(resid 19 and name C) (resid 20 and name N)
(resid 20 and name CA) (resid 20 and name C) 1.0 -79.6 20.0 2
(resid 20 and name N) (resid 20 and name CA)
(resid 20 and name C) (resid 21 and name N) 1.0 77.0 20.0 2
(resid 20 and name C) (resid 21 and name N)
(resid 21 and name CA) (resid 21 and name C) 1.0 -66.0 20.0 2
(resid 21 and name N) (resid 21 and name CA)
(resid 21 and name C) (resid 22 and name N) 1.0 -33.7 20.0 2
(resid 21 and name C) (resid 22 and name N)
(resid 22 and name CA) (resid 22 and name C) 1.0 -89.0 20.0 2
(resid 22 and name N) (resid 22 and name CA)
(resid 22 and name C) (resid 23 and name N) 1.0 -2.9 20.0 2
(resid 22 and name C) (resid 23 and name N)
(resid 23 and name CA) (resid 23 and name C) 1.0 60.8 20.0 2
(resid 23 and name N) (resid 23 and name CA)
(resid 23 and name C) (resid 24 and name N) 1.0 30.7 20.0 2
(resid 23 and name C) (resid 24 and name N)
(resid 24 and name CA) (resid 24 and name C) 1.0 -89.8 20.0 2
(resid 24 and name N) (resid 24 and name CA)
(resid 24 and name C) (resid 25 and name N) 1.0 0.3 20.0 2
(resid 24 and name C) (resid 25 and name N)
(resid 25 and name CA) (resid 25 and name C) 1.0 85.5 20.0 2
(resid 25 and name N) (resid 25 and name CA)
(resid 25 and name C) (resid 26 and name N) 1.0 4.7 20.0 2

(resid 25 and name C) (resid 26 and name N)
(resid 26 and name CA) (resid 26 and name C) 1.0 -132.8 34.9 2
(resid 26 and name N) (resid 26 and name CA)
(resid 26 and name C) (resid 27 and name N) 1.0 147.7 28.0 2
(resid 26 and name C) (resid 27 and name N)
(resid 27 and name CA) (resid 27 and name C) 1.0 -100.9 24.9 2
(resid 27 and name N) (resid 27 and name CA)
(resid 27 and name C) (resid 28 and name N) 1.0 123.8 20.0 2
(resid 27 and name C) (resid 28 and name N)
(resid 28 and name CA) (resid 28 and name C) 1.0 -104.3 41.6 2
(resid 28 and name N) (resid 28 and name CA)
(resid 28 and name C) (resid 29 and name N) 1.0 169.5 20.0 2
(resid 28 and name C) (resid 29 and name N)
(resid 29 and name CA) (resid 29 and name C) 1.0 -60.5 20.0 2
(resid 29 and name N) (resid 29 and name CA)
(resid 29 and name C) (resid 30 and name N) 1.0 -34.2 20.0 2
(resid 29 and name C) (resid 30 and name N)
(resid 30 and name CA) (resid 30 and name C) 1.0 -65.2 20.0 2
(resid 30 and name N) (resid 30 and name CA)
(resid 30 and name C) (resid 31 and name N) 1.0 -40.9 20.0 2
(resid 30 and name C) (resid 31 and name N)
(resid 31 and name CA) (resid 31 and name C) 1.0 -66.3 20.0 2
(resid 31 and name N) (resid 31 and name CA)
(resid 31 and name C) (resid 32 and name N) 1.0 -42.3 20.0 2
(resid 31 and name C) (resid 32 and name N)
(resid 32 and name CA) (resid 32 and name C) 1.0 -63.5 20.0 2
(resid 32 and name N) (resid 32 and name CA)
(resid 32 and name C) (resid 33 and name N) 1.0 -43.5 20.0 2
(resid 32 and name C) (resid 33 and name N)
(resid 33 and name CA) (resid 33 and name C) 1.0 -61.8 20.0 2
(resid 33 and name N) (resid 33 and name CA)
(resid 33 and name C) (resid 34 and name N) 1.0 -42.2 20.0 2
(resid 33 and name C) (resid 34 and name N)
(resid 34 and name CA) (resid 34 and name C) 1.0 -63.7 20.0 2
(resid 34 and name N) (resid 34 and name CA)
(resid 34 and name C) (resid 35 and name N) 1.0 -42.7 20.0 2
(resid 34 and name C) (resid 35 and name N)
(resid 35 and name CA) (resid 35 and name C) 1.0 -64.5 20.0 2
(resid 35 and name N) (resid 35 and name CA)
(resid 35 and name C) (resid 36 and name N) 1.0 -43.4 20.0 2
(resid 35 and name C) (resid 36 and name N)
(resid 36 and name CA) (resid 36 and name C) 1.0 -63.6 20.0 2
(resid 36 and name N) (resid 36 and name CA)
(resid 36 and name C) (resid 37 and name N) 1.0 -41.8 20.0 2
(resid 36 and name C) (resid 37 and name N)
(resid 37 and name CA) (resid 37 and name C) 1.0 -64.7 20.0 2
(resid 37 and name N) (resid 37 and name CA)
(resid 37 and name C) (resid 38 and name N) 1.0 -37.9 20.0 2
(resid 37 and name C) (resid 38 and name N)
(resid 38 and name CA) (resid 38 and name C) 1.0 -66.5 20.0 2
(resid 38 and name N) (resid 38 and name CA)
(resid 38 and name C) (resid 39 and name N) 1.0 -26.2 20.0 2
(resid 38 and name C) (resid 39 and name N)
(resid 39 and name CA) (resid 39 and name C) 1.0 -87.8 20.0 2
(resid 39 and name N) (resid 39 and name CA)
(resid 39 and name C) (resid 40 and name N) 1.0 -0.8 20.0 2
(resid 39 and name C) (resid 40 and name N)
(resid 40 and name CA) (resid 40 and name C) 1.0 86.6 20.2 2
(resid 40 and name N) (resid 40 and name CA)
(resid 40 and name C) (resid 41 and name N) 1.0 15.1 20.0 2
(resid 41 and name C) (resid 42 and name N)
(resid 42 and name CA) (resid 42 and name C) 1.0 -124.4 22.2 2
(resid 42 and name N) (resid 42 and name CA)
(resid 42 and name C) (resid 43 and name N) 1.0 79.1 25.0 2
(resid 42 and name C) (resid 43 and name N)
(resid 43 and name CA) (resid 43 and name C) 1.0 -67.5 20.0 2
(resid 43 and name N) (resid 43 and name CA)
(resid 43 and name C) (resid 44 and name N) 1.0 147.0 25.5 2
(resid 43 and name C) (resid 44 and name N)
(resid 44 and name CA) (resid 44 and name C) 1.0 -84.0 24.7 2

(resid 44 and name N) (resid 44 and name CA)
(resid 44 and name C) (resid 45 and name N) 1.0 166.5 20.0 2
(resid 44 and name C) (resid 45 and name N)
(resid 45 and name CA) (resid 45 and name C) 1.0 -60.4 20.0 2
(resid 45 and name N) (resid 45 and name CA)
(resid 45 and name C) (resid 46 and name N) 1.0 -38.4 20.0 2
(resid 45 and name C) (resid 46 and name N)
(resid 46 and name CA) (resid 46 and name C) 1.0 -64.5 20.0 2
(resid 46 and name N) (resid 46 and name CA)
(resid 46 and name C) (resid 47 and name N) 1.0 -39.9 20.0 2
(resid 46 and name C) (resid 47 and name N)
(resid 47 and name CA) (resid 47 and name C) 1.0 -66.7 20.0 2
(resid 47 and name N) (resid 47 and name CA)
(resid 47 and name C) (resid 48 and name N) 1.0 -40.7 20.0 2
(resid 47 and name C) (resid 48 and name N)
(resid 48 and name CA) (resid 48 and name C) 1.0 -64.5 20.0 2
(resid 48 and name N) (resid 48 and name CA)
(resid 48 and name C) (resid 49 and name N) 1.0 -41.7 20.0 2
(resid 48 and name C) (resid 49 and name N)
(resid 49 and name CA) (resid 49 and name C) 1.0 -63.2 20.0 2
(resid 49 and name N) (resid 49 and name CA)
(resid 49 and name C) (resid 50 and name N) 1.0 -39.5 20.0 2
(resid 49 and name C) (resid 50 and name N)
(resid 50 and name CA) (resid 50 and name C) 1.0 -65.5 20.0 2
(resid 50 and name N) (resid 50 and name CA)
(resid 50 and name C) (resid 51 and name N) 1.0 -39.9 20.0 2
(resid 50 and name C) (resid 51 and name N)
(resid 51 and name CA) (resid 51 and name C) 1.0 -64.8 20.0 2
(resid 51 and name N) (resid 51 and name CA)
(resid 51 and name C) (resid 52 and name N) 1.0 -43.0 20.0 2
(resid 51 and name C) (resid 52 and name N)
(resid 52 and name CA) (resid 52 and name C) 1.0 -65.9 20.0 2
(resid 52 and name N) (resid 52 and name CA)
(resid 52 and name C) (resid 53 and name N) 1.0 -40.9 20.0 2
(resid 52 and name C) (resid 53 and name N)
(resid 53 and name CA) (resid 53 and name C) 1.0 -65.3 20.0 2
(resid 53 and name N) (resid 53 and name CA)
(resid 53 and name C) (resid 54 and name N) 1.0 -35.5 20.0 2
(resid 53 and name C) (resid 54 and name N)
(resid 54 and name CA) (resid 54 and name C) 1.0 -70.0 20.0 2
(resid 54 and name N) (resid 54 and name CA)
(resid 54 and name C) (resid 55 and name N) 1.0 -27.1 20.0 2
(resid 54 and name C) (resid 55 and name N)
(resid 55 and name CA) (resid 55 and name C) 1.0 -102.4 26.5 2
(resid 55 and name N) (resid 55 and name CA)
(resid 55 and name C) (resid 56 and name N) 1.0 -1.3 21.0 2
(resid 56 and name C) (resid 57 and name N)
(resid 57 and name CA) (resid 57 and name C) 1.0 -68.5 20.0 2
(resid 57 and name N) (resid 57 and name CA)
(resid 57 and name C) (resid 58 and name N) 1.0 -21.4 20.0 2
(resid 57 and name C) (resid 58 and name N)
(resid 58 and name CA) (resid 58 and name C) 1.0 -93.9 20.0 2
(resid 58 and name N) (resid 58 and name CA)
(resid 58 and name C) (resid 59 and name N) 1.0 -2.2 20.0 2
(resid 58 and name C) (resid 59 and name N)
(resid 59 and name CA) (resid 59 and name C) 1.0 59.2 20.0 2
(resid 59 and name N) (resid 59 and name CA)
(resid 59 and name C) (resid 60 and name N) 1.0 31.8 20.0 2
(resid 59 and name C) (resid 60 and name N)
(resid 60 and name CA) (resid 60 and name C) 1.0 -89.4 20.0 2
(resid 60 and name N) (resid 60 and name CA)
(resid 60 and name C) (resid 61 and name N) 1.0 0.4 20.0 2
(resid 60 and name C) (resid 61 and name N)
(resid 61 and name CA) (resid 61 and name C) 1.0 84.5 20.0 2
(resid 61 and name N) (resid 61 and name CA)
(resid 61 and name C) (resid 62 and name N) 1.0 6.7 20.0 2
(resid 61 and name C) (resid 62 and name N)
(resid 62 and name CA) (resid 62 and name C) 1.0 -133.3 26.7 2
(resid 62 and name N) (resid 62 and name CA)
(resid 62 and name C) (resid 63 and name N) 1.0 155.4 21.7 2

(resid 62 and name C) (resid 63 and name N)
(resid 63 and name CA) (resid 63 and name C) 1.0 -107.7 20.0 2
(resid 63 and name N) (resid 63 and name CA)
(resid 63 and name C) (resid 64 and name N) 1.0 119.1 20.0 2
(resid 63 and name C) (resid 64 and name N)
(resid 64 and name CA) (resid 64 and name C) 1.0 -93.9 37.4 2
(resid 64 and name N) (resid 64 and name CA)
(resid 64 and name C) (resid 65 and name N) 1.0 175.2 20.0 2
(resid 64 and name C) (resid 65 and name N)
(resid 65 and name CA) (resid 65 and name C) 1.0 -58.7 20.0 2
(resid 65 and name N) (resid 65 and name CA)
(resid 65 and name C) (resid 66 and name N) 1.0 -44.7 20.0 2
(resid 65 and name C) (resid 66 and name N)
(resid 66 and name CA) (resid 66 and name C) 1.0 -58.8 20.0 2
(resid 66 and name N) (resid 66 and name CA)
(resid 66 and name C) (resid 67 and name N) 1.0 -40.6 20.0 2
(resid 66 and name C) (resid 67 and name N)
(resid 67 and name CA) (resid 67 and name C) 1.0 -69.1 20.0 2
(resid 67 and name N) (resid 67 and name CA)
(resid 67 and name C) (resid 68 and name N) 1.0 -36.9 20.0 2
(resid 67 and name C) (resid 68 and name N)
(resid 68 and name CA) (resid 68 and name C) 1.0 -63.7 20.0 2
(resid 68 and name N) (resid 68 and name CA)
(resid 68 and name C) (resid 69 and name N) 1.0 -45.2 20.0 2
(resid 68 and name C) (resid 69 and name N)
(resid 69 and name CA) (resid 69 and name C) 1.0 -64.0 20.0 2
(resid 69 and name N) (resid 69 and name CA)
(resid 69 and name C) (resid 70 and name N) 1.0 -42.1 20.0 2
(resid 69 and name C) (resid 70 and name N)
(resid 70 and name CA) (resid 70 and name C) 1.0 -62.7 20.0 2
(resid 70 and name N) (resid 70 and name CA)
(resid 70 and name C) (resid 71 and name N) 1.0 -41.4 20.0 2
(resid 70 and name C) (resid 71 and name N)
(resid 71 and name CA) (resid 71 and name C) 1.0 -65.8 20.0 2
(resid 71 and name N) (resid 71 and name CA)
(resid 71 and name C) (resid 72 and name N) 1.0 -42.7 20.0 2
(resid 71 and name C) (resid 72 and name N)
(resid 72 and name CA) (resid 72 and name C) 1.0 -68.8 20.0 2
(resid 72 and name N) (resid 72 and name CA)
(resid 72 and name C) (resid 73 and name N) 1.0 -37.3 20.0 2
(resid 72 and name C) (resid 73 and name N)
(resid 73 and name CA) (resid 73 and name C) 1.0 -64.2 20.0 2
(resid 73 and name N) (resid 73 and name CA)
(resid 73 and name C) (resid 74 and name N) 1.0 -37.7 20.0 2
(resid 73 and name C) (resid 74 and name N)
(resid 74 and name CA) (resid 74 and name C) 1.0 -68.1 20.0 2
(resid 74 and name N) (resid 74 and name CA)
(resid 74 and name C) (resid 75 and name N) 1.0 -39.6 20.0 2
(resid 74 and name C) (resid 75 and name N)
(resid 75 and name CA) (resid 75 and name C) 1.0 -67.8 20.0 2
(resid 75 and name N) (resid 75 and name CA)
(resid 75 and name C) (resid 76 and name N) 1.0 -34.6 20.0 2
(resid 75 and name C) (resid 76 and name N)
(resid 76 and name CA) (resid 76 and name C) 1.0 -69.5 20.0 2
(resid 76 and name N) (resid 76 and name CA)
(resid 76 and name C) (resid 77 and name N) 1.0 -25.5 20.0 2
(resid 79 and name C) (resid 80 and name N)
(resid 80 and name CA) (resid 80 and name C) 1.0 -71.8 20.0 2
(resid 80 and name N) (resid 80 and name CA)
(resid 80 and name C) (resid 81 and name N) 1.0 150.1 38.0 2
(resid 81 and name C) (resid 82 and name N)
(resid 82 and name CA) (resid 82 and name C) 1.0 -63.5 20.0 2
(resid 82 and name N) (resid 82 and name CA)
(resid 82 and name C) (resid 83 and name N) 1.0 -37.1 20.0 2
(resid 82 and name C) (resid 83 and name N)
(resid 83 and name CA) (resid 83 and name C) 1.0 -68.7 20.0 2
(resid 83 and name N) (resid 83 and name CA)
(resid 83 and name C) (resid 84 and name N) 1.0 -41.4 20.0 2
(resid 83 and name C) (resid 84 and name N)
(resid 84 and name CA) (resid 84 and name C) 1.0 -66.7 20.0 2

(resid 84 and name N) (resid 84 and name CA)
(resid 84 and name C) (resid 85 and name N) 1.0 -40.1 20.0 2
(resid 84 and name C) (resid 85 and name N)
(resid 85 and name CA) (resid 85 and name C) 1.0 -65.6 20.0 2
(resid 85 and name N) (resid 85 and name CA)
(resid 85 and name C) (resid 86 and name N) 1.0 -41.4 20.0 2
(resid 85 and name C) (resid 86 and name N)
(resid 86 and name CA) (resid 86 and name C) 1.0 -63.0 20.0 2
(resid 86 and name N) (resid 86 and name CA)
(resid 86 and name C) (resid 87 and name N) 1.0 -41.9 20.0 2
(resid 86 and name C) (resid 87 and name N)
(resid 87 and name CA) (resid 87 and name C) 1.0 -64.6 20.0 2
(resid 87 and name N) (resid 87 and name CA)
(resid 87 and name C) (resid 88 and name N) 1.0 -41.2 20.0 2
(resid 87 and name C) (resid 88 and name N)
(resid 88 and name CA) (resid 88 and name C) 1.0 -66.3 20.0 2
(resid 88 and name N) (resid 88 and name CA)
(resid 88 and name C) (resid 89 and name N) 1.0 -41.0 20.0 2
(resid 88 and name C) (resid 89 and name N)
(resid 89 and name CA) (resid 89 and name C) 1.0 -62.2 20.0 2
(resid 89 and name N) (resid 89 and name CA)
(resid 89 and name C) (resid 90 and name N) 1.0 -42.2 20.0 2
(resid 89 and name C) (resid 90 and name N)
(resid 90 and name CA) (resid 90 and name C) 1.0 -65.4 20.0 2
(resid 90 and name N) (resid 90 and name CA)
(resid 90 and name C) (resid 91 and name N) 1.0 -34.4 20.0 2
(resid 90 and name C) (resid 91 and name N)
(resid 91 and name CA) (resid 91 and name C) 1.0 -67.4 20.0 2
(resid 91 and name N) (resid 91 and name CA)
(resid 91 and name C) (resid 92 and name N) 1.0 -37.5 20.0 2
(resid 91 and name C) (resid 92 and name N)
(resid 92 and name CA) (resid 92 and name C) 1.0 -79.5 20.1 2
(resid 92 and name N) (resid 92 and name CA)
(resid 92 and name C) (resid 93 and name N) 1.0 -30.7 20.0 2
(resid 92 and name C) (resid 93 and name N)
(resid 93 and name CA) (resid 93 and name C) 1.0 -79.6 20.0 2
(resid 93 and name N) (resid 93 and name CA)
(resid 93 and name C) (resid 94 and name N) 1.0 76.1 20.0 2
(resid 93 and name C) (resid 94 and name N)
(resid 94 and name CA) (resid 94 and name C) 1.0 -65.2 20.0 2
(resid 94 and name N) (resid 94 and name CA)
(resid 94 and name C) (resid 95 and name N) 1.0 -33.6 20.0 2
(resid 94 and name C) (resid 95 and name N)
(resid 95 and name CA) (resid 95 and name C) 1.0 -89.0 20.0 2
(resid 95 and name N) (resid 95 and name CA)
(resid 95 and name C) (resid 96 and name N) 1.0 -2.9 20.0 2
(resid 95 and name C) (resid 96 and name N)
(resid 96 and name CA) (resid 96 and name C) 1.0 59.8 20.0 2
(resid 96 and name N) (resid 96 and name CA)
(resid 96 and name C) (resid 97 and name N) 1.0 32.3 20.0 2
(resid 96 and name C) (resid 97 and name N)
(resid 97 and name CA) (resid 97 and name C) 1.0 -89.7 20.0 2
(resid 97 and name N) (resid 97 and name CA)
(resid 97 and name C) (resid 98 and name N) 1.0 0.2 20.0 2
(resid 97 and name C) (resid 98 and name N)
(resid 98 and name CA) (resid 98 and name C) 1.0 86.4 20.0 2
(resid 98 and name N) (resid 98 and name CA)
(resid 98 and name C) (resid 99 and name N) 1.0 3.9 20.0 2
(resid 98 and name C) (resid 99 and name N)
(resid 99 and name CA) (resid 99 and name C) 1.0 -133.6 28.8 2
(resid 99 and name N) (resid 99 and name CA)
(resid 99 and name C) (resid 100 and name N) 1.0 152.8 26.0 2
(resid 99 and name C) (resid 100 and name N)
(resid 100 and name CA) (resid 100 and name C) 1.0 -99.3 20.0 2
(resid 100 and name N) (resid 100 and name CA)
(resid 100 and name C) (resid 101 and name N) 1.0 116.8 20.0 2
(resid 100 and name C) (resid 101 and name N)
(resid 101 and name CA) (resid 101 and name C) 1.0 -93.0 20.0 2
(resid 101 and name N) (resid 101 and name CA)
(resid 101 and name C) (resid 102 and name N) 1.0 168.2 20.0 2

(resid 101 and name C) (resid 102 and name N)
(resid 102 and name CA) (resid 102 and name C) 1.0 -58.4 20.0 2
(resid 102 and name N) (resid 102 and name CA)
(resid 102 and name C) (resid 103 and name N) 1.0 -38.1 20.0 2
(resid 102 and name C) (resid 103 and name N)
(resid 103 and name CA) (resid 103 and name C) 1.0 -64.4 20.0 2
(resid 103 and name N) (resid 103 and name CA)
(resid 103 and name C) (resid 104 and name N) 1.0 -38.9 20.0 2
(resid 103 and name C) (resid 104 and name N)
(resid 104 and name CA) (resid 104 and name C) 1.0 -66.0 20.0 2
(resid 104 and name N) (resid 104 and name CA)
(resid 104 and name C) (resid 105 and name N) 1.0 -41.7 20.0 2
(resid 104 and name C) (resid 105 and name N)
(resid 105 and name CA) (resid 105 and name C) 1.0 -63.6 20.0 2
(resid 105 and name N) (resid 105 and name CA)
(resid 105 and name C) (resid 106 and name N) 1.0 -42.2 20.0 2
(resid 105 and name C) (resid 106 and name N)
(resid 106 and name CA) (resid 106 and name C) 1.0 -63.5 20.0 2
(resid 106 and name N) (resid 106 and name CA)
(resid 106 and name C) (resid 107 and name N) 1.0 -41.4 20.0 2
(resid 106 and name C) (resid 107 and name N)
(resid 107 and name CA) (resid 107 and name C) 1.0 -65.7 20.0 2
(resid 107 and name N) (resid 107 and name CA)
(resid 107 and name C) (resid 108 and name N) 1.0 -41.1 20.0 2
(resid 107 and name C) (resid 108 and name N)
(resid 108 and name CA) (resid 108 and name C) 1.0 -63.8 20.0 2
(resid 108 and name N) (resid 108 and name CA)
(resid 108 and name C) (resid 109 and name N) 1.0 -44.4 20.0 2
(resid 108 and name C) (resid 109 and name N)
(resid 109 and name CA) (resid 109 and name C) 1.0 -65.2 20.0 2
(resid 109 and name N) (resid 109 and name CA)
(resid 109 and name C) (resid 110 and name N) 1.0 -36.4 20.0 2
(resid 109 and name C) (resid 110 and name N)
(resid 110 and name CA) (resid 110 and name C) 1.0 -63.0 20.0 2
(resid 110 and name N) (resid 110 and name CA)
(resid 110 and name C) (resid 111 and name N) 1.0 -41.3 20.0 2
(resid 110 and name C) (resid 111 and name N)
(resid 111 and name CA) (resid 111 and name C) 1.0 -65.7 20.0 2
(resid 111 and name N) (resid 111 and name CA)
(resid 111 and name C) (resid 112 and name N) 1.0 -29.5 20.0 2
(resid 111 and name C) (resid 112 and name N)
(resid 112 and name CA) (resid 112 and name C) 1.0 -80.8 20.0 2
(resid 112 and name N) (resid 112 and name CA)
(resid 112 and name C) (resid 113 and name N) 1.0 -7.4 20.0 2
(resid 112 and name C) (resid 113 and name N)
(resid 113 and name CA) (resid 113 and name C) 1.0 94.1 20.0 2
(resid 113 and name N) (resid 113 and name CA)
(resid 113 and name C) (resid 114 and name N) 1.0 10.9 20.0 2
(resid 113 and name C) (resid 114 and name N)
(resid 114 and name CA) (resid 114 and name C) 1.0 -83.4 24.2 2
(resid 114 and name N) (resid 114 and name CA)
(resid 114 and name C) (resid 115 and name N) 1.0 137.9 29.3 2
(resid 114 and name C) (resid 115 and name N)
(resid 115 and name CA) (resid 115 and name C) 1.0 -89.1 23.9 2
(resid 115 and name N) (resid 115 and name CA)
(resid 115 and name C) (resid 116 and name N) 1.0 121.5 35.4 2
(resid 115 and name C) (resid 116 and name N)
(resid 116 and name CA) (resid 116 and name C) 1.0 -125.5 48.6 2
(resid 116 and name N) (resid 116 and name CA)
(resid 116 and name C) (resid 117 and name N) 1.0 137.8 21.6 2
(resid 116 and name C) (resid 117 and name N)
(resid 117 and name CA) (resid 117 and name C) 1.0 -77.4 20.0 2
(resid 117 and name N) (resid 117 and name CA)
(resid 117 and name C) (resid 118 and name N) 1.0 162.7 20.0 2
(resid 117 and name C) (resid 118 and name N)
(resid 118 and name CA) (resid 118 and name C) 1.0 -60.0 20.0 2
(resid 118 and name N) (resid 118 and name CA)
(resid 118 and name C) (resid 119 and name N) 1.0 -37.3 20.0 2
(resid 118 and name C) (resid 119 and name N)
(resid 119 and name CA) (resid 119 and name C) 1.0 -66.2 20.0 2

(resid 119 and name N) (resid 119 and name CA)
(resid 119 and name C) (resid 120 and name N) 1.0 -39.5 20.0 2
(resid 119 and name C) (resid 120 and name N)
(resid 120 and name CA) (resid 120 and name C) 1.0 -66.7 20.0 2
(resid 120 and name N) (resid 120 and name CA)
(resid 120 and name C) (resid 121 and name N) 1.0 -41.5 20.0 2
(resid 120 and name C) (resid 121 and name N)
(resid 121 and name CA) (resid 121 and name C) 1.0 -64.6 20.0 2
(resid 121 and name N) (resid 121 and name CA)
(resid 121 and name C) (resid 122 and name N) 1.0 -41.6 20.0 2
(resid 121 and name C) (resid 122 and name N)
(resid 122 and name CA) (resid 122 and name C) 1.0 -63.6 20.0 2
(resid 122 and name N) (resid 122 and name CA)
(resid 122 and name C) (resid 123 and name N) 1.0 -39.9 20.0 2
(resid 122 and name C) (resid 123 and name N)
(resid 123 and name CA) (resid 123 and name C) 1.0 -64.2 20.0 2
(resid 123 and name N) (resid 123 and name CA)
(resid 123 and name C) (resid 124 and name N) 1.0 -40.7 20.0 2
(resid 123 and name C) (resid 124 and name N)
(resid 124 and name CA) (resid 124 and name C) 1.0 -65.2 20.0 2
(resid 124 and name N) (resid 124 and name CA)
(resid 124 and name C) (resid 125 and name N) 1.0 -43.5 20.0 2
(resid 124 and name C) (resid 125 and name N)
(resid 125 and name CA) (resid 125 and name C) 1.0 -64.7 20.0 2
(resid 125 and name N) (resid 125 and name CA)
(resid 125 and name C) (resid 126 and name N) 1.0 -40.9 20.0 2
(resid 125 and name C) (resid 126 and name N)
(resid 126 and name CA) (resid 126 and name C) 1.0 -65.3 20.0 2
(resid 126 and name N) (resid 126 and name CA)
(resid 126 and name C) (resid 127 and name N) 1.0 -36.6 20.0 2
(resid 126 and name C) (resid 127 and name N)
(resid 127 and name CA) (resid 127 and name C) 1.0 -74.2 20.0 2
(resid 127 and name N) (resid 127 and name CA)
(resid 127 and name C) (resid 128 and name N) 1.0 -32.8 20.0 2
(resid 127 and name C) (resid 128 and name N)
(resid 128 and name CA) (resid 128 and name C) 1.0 -99.4 20.0 2
(resid 128 and name N) (resid 128 and name CA)
(resid 128 and name C) (resid 129 and name N) 1.0 -9.5 22.8 2
(resid 128 and name C) (resid 129 and name N)
(resid 129 and name CA) (resid 129 and name C) 1.0 -76.4 20.0 2
(resid 129 and name N) (resid 129 and name CA)
(resid 129 and name C) (resid 130 and name N) 1.0 105.7 39.5 2
(resid 129 and name C) (resid 130 and name N)
(resid 130 and name CA) (resid 130 and name C) 1.0 -67.3 20.0 2
(resid 130 and name N) (resid 130 and name CA)
(resid 130 and name C) (resid 131 and name N) 1.0 -29.9 20.7 2
(resid 130 and name C) (resid 131 and name N)
(resid 131 and name CA) (resid 131 and name C) 1.0 -90.5 20.0 2
(resid 131 and name N) (resid 131 and name CA)
(resid 131 and name C) (resid 132 and name N) 1.0 -5.3 20.0 2
(resid 132 and name C) (resid 133 and name N)
(resid 133 and name CA) (resid 133 and name C) 1.0 -90.4 20.0 2
(resid 133 and name N) (resid 133 and name CA)
(resid 133 and name C) (resid 134 and name N) 1.0 1.6 20.0 2
(resid 133 and name C) (resid 134 and name N)
(resid 134 and name CA) (resid 134 and name C) 1.0 83.7 20.0 2
(resid 134 and name N) (resid 134 and name CA)
(resid 134 and name C) (resid 135 and name N) 1.0 6.9 20.0 2
(resid 134 and name C) (resid 135 and name N)
(resid 135 and name CA) (resid 135 and name C) 1.0 -137.0 20.3 2
(resid 135 and name N) (resid 135 and name CA)
(resid 135 and name C) (resid 136 and name N) 1.0 153.0 24.1 2
(resid 135 and name C) (resid 136 and name N)
(resid 136 and name CA) (resid 136 and name C) 1.0 -107.8 20.0 2
(resid 136 and name N) (resid 136 and name CA)
(resid 136 and name C) (resid 137 and name N) 1.0 116.1 20.0 2
(resid 136 and name C) (resid 137 and name N)
(resid 137 and name CA) (resid 137 and name C) 1.0 -86.3 20.0 2
(resid 137 and name N) (resid 137 and name CA)
(resid 137 and name C) (resid 138 and name N) 1.0 173.8 20.0 2

(resid 137 and name C) (resid 138 and name N)
(resid 138 and name CA) (resid 138 and name C) 1.0 -60.9 20.0 2
(resid 138 and name N) (resid 138 and name CA)
(resid 138 and name C) (resid 139 and name N) 1.0 -42.8 20.0 2
(resid 138 and name C) (resid 139 and name N)
(resid 139 and name CA) (resid 139 and name C) 1.0 -63.7 20.0 2
(resid 139 and name N) (resid 139 and name CA)
(resid 139 and name C) (resid 140 and name N) 1.0 -43.4 20.0 2
(resid 139 and name C) (resid 140 and name N)
(resid 140 and name CA) (resid 140 and name C) 1.0 -67.3 20.0 2
(resid 140 and name N) (resid 140 and name CA)
(resid 140 and name C) (resid 141 and name N) 1.0 -38.1 20.0 2
(resid 140 and name C) (resid 141 and name N)
(resid 141 and name CA) (resid 141 and name C) 1.0 -63.8 20.0 2
(resid 141 and name N) (resid 141 and name CA)
(resid 141 and name C) (resid 142 and name N) 1.0 -42.8 20.0 2
(resid 141 and name C) (resid 142 and name N)
(resid 142 and name CA) (resid 142 and name C) 1.0 -62.4 20.0 2
(resid 142 and name N) (resid 142 and name CA)
(resid 142 and name C) (resid 143 and name N) 1.0 -43.6 20.0 2
(resid 142 and name C) (resid 143 and name N)
(resid 143 and name CA) (resid 143 and name C) 1.0 -64.8 20.0 2
(resid 143 and name N) (resid 143 and name CA)
(resid 143 and name C) (resid 144 and name N) 1.0 -40.0 20.0 2
(resid 143 and name C) (resid 144 and name N)
(resid 144 and name CA) (resid 144 and name C) 1.0 -68.1 20.0 2
(resid 144 and name N) (resid 144 and name CA)
(resid 144 and name C) (resid 145 and name N) 1.0 -36.7 20.0 2
(resid 144 and name C) (resid 145 and name N)
(resid 145 and name CA) (resid 145 and name C) 1.0 -69.6 20.0 2
(resid 145 and name N) (resid 145 and name CA)
(resid 145 and name C) (resid 146 and name N) 1.0 -23.8 20.0 2
(resid 145 and name C) (resid 146 and name N)
(resid 146 and name CA) (resid 146 and name C) 1.0 -89.3 20.0 2
(resid 146 and name N) (resid 146 and name CA)
(resid 146 and name C) (resid 147 and name N) 1.0 -6.2 20.0 2
(resid 146 and name C) (resid 147 and name N)
(resid 147 and name CA) (resid 147 and name C) 1.0 -68.7 20.0 2
(resid 147 and name N) (resid 147 and name CA)
(resid 147 and name C) (resid 148 and name N) 1.0 138.0 20.0 2

Appendix 19. iCING server reports for validating quality of protein structure

Summary: all

Home Help

---------- CING SUMMARY project all ----------

Because there were no experimental data, this project was not fully validated.
All applicable programs/checks for the coordinate data were performed.

---------- <RmsdResult Ranges A.1-148,B.1-19,C.1-4> ----------

```
backboneAverage:      0.98 +- 0.18
heavyAtomsAverage:    1.35 +- 0.16
models:                  0    1    2    3    4    5    6    7    8    9   10   11   12   13   14   15   16   17   18   19
backbone   (n= 512): [0.77 1.13 1.06 0.93 0.96 1.44 0.92 1.09 0.86 1.15 0.87 0.97 0.70 0.90 0.80 1.25 0.82 0.89 1.10 1.09 ]
heavyAtoms (n=1565): [1.18 1.51 1.45 1.33 1.30 1.71 1.28 1.49 1.24 1.58 1.17 1.33 1.19 1.28 1.18 1.62 1.21 1.26 1.38 1.39 ]
closestToMean:        model 10
```

---------- CING ROG analysis (all residues) ----------

```
Red:      65  ( 38%)
Orange:   64  ( 37%)
Green:    42  ( 25%)
          ----------
Total    171  (100%)
```

---------- WHAT IF Summary ----------

```
WHATIF summary report of molecule "all", ranges "all"

- This is an overall summary of the quality of the structure as
  compared with current reliable structures.
- The first part of the table shows a number of constraint-independent
  quality indicators.
- The second part of the table mostly gives an impression of how well
  the model conforms to common refinement constraint values.
- The standard deviation shows the variation over models in the ensemble
  where appropriate.

Structure Z-scores, positive is better than average:
    1st generation packing quality :   0.051 +/-   0.413
    2nd generation packing quality :   5.083 +/-   1.535
    Ramachandran plot appearance   :  -4.391 +/-   0.292 (bad)
    chi-1/chi-2 rotamer normality  :  -7.737 +/-   0.282
    Backbone conformation          :  -0.940 +/-   0.478

RMS Z-scores, should be close to 1.0:
    Bond lengths                   :   1.034 +/-   0.001
    Bond angles                    :   0.370 +/-   0.006 (tight)
    Omega angle restraints         :   0.739 +/-   0.040 (tight)
    Side chain planarity           :   0.329 +/-   0.032 (tight)
    Improper dihedral distribution :   0.985 +/-   0.047
    Inside/Outside distribution    :   1.076 +/-   0.009
```

---------- Procheck Summary ----------

```
molecule:     <Molecule "all" (C:3,R:171,A:3369,H:20)>
ranges:       None
ramachandran
  core:       85.9%
  allowed:    11.5%
  generous:    0.8%
  disallowed:  1.8%
```

Validation report for all using CING (r1240)

Summary: all

Home Help

---------- CING SUMMARY project all ----------

Because there were no experimental data, this project was not fully validated.
All applicable programs/checks for the coordinate data were performed.

---------- <RmsdResult Ranges A.1-148> ----------

```
backboneAverage:       0.92 +- 0.18
heavyAtomsAverage:     1.24 +- 0.15
models:                   0    1    2    3    4    5    6    7    8    9   10   11   12   13   14   15   16   17   18   19
backbone    (n= 455): [0.74 1.11 0.88 0.86 0.95 1.41 0.90 1.08 0.73 1.03 0.86 0.75 0.64 0.86 0.73 1.20 0.82 0.84 0.92 1.03 ]
heavyAtoms  (n=1363): [1.10 1.46 1.26 1.24 1.27 1.61 1.19 1.36 1.11 1.35 1.13 1.14 0.98 1.22 1.08 1.50 1.18 1.17 1.20 1.31 ]
closestToMean:         model 12
```

---------- CING ROG analysis (all residues) ----------

```
Red:      65  ( 38%)
Orange:   62  ( 36%)
Green:    44  ( 26%)
          ------------
Total    171  (100%)
```

---------- CING ROG analysis (A.1-148) ----------

```
Red:      53  ( 36%)
Orange:   60  ( 41%)
Green:    35  ( 24%)
          ------------
Total    148  (100%)
```

---------- WHAT IF Summary ----------

```
WHATIF summary report of molecule "all", ranges "A.1-148" (148 residues)

- This is an overall summary of the quality of the structure as
  compared with current reliable structures.
- The first part of the table shows a number of constraint-independent
  quality indicators.
- The second part of the table mostly gives an impression of how well
  the model conforms to common refinement constraint values.
- The standard deviation shows the variation over models in the ensemble
  where appropriate.

Structure Z-scores, positive is better than average:
    1st generation packing quality :   0.553 +/-   0.487
    2nd generation packing quality :   6.956 +/-   1.774
    Ramachandran plot appearance   :  -3.942 +/-   0.289 (poor)
    chi-1/chi-2 rotamer normality  :  -7.726 +/-   0.264
    Backbone conformation          :  -0.727 +/-   0.379

RMS Z-scores, should be close to 1.0:
    Bond lengths                   :   1.032 +/-   0.001
    Bond angles                    :   0.357 +/-   0.006 (tight)
    Omega angle restraints         :   0.693 +/-   0.029 (tight)
    Side chain planarity           :   0.333 +/-   0.035 (tight)
    Improper dihedral distribution :   0.929 +/-   0.036
    Inside/Outside distribution    :   1.051 +/-   0.012
```

---------- Procheck Summary ----------

(ranges A.1-148)

```
molecule:     <Molecule "all" (C:1,R:171,A:3369,M:20)>
ranges:       A.1-148

ramachandran
  core:       90.3%
  allowed:     8.6%
  generous:    0.2%
  disallowed:  0.9%
```

Validation report for all using CING (r1240)

References

ANDREW, E. R. 1984. Nuclear Magnetic-Resonance and Its Clinical-Application - a Historical Review of Nmr and Its Clinical-Applications. *British Medical Bulletin,* 40**,** 115-&.

ANTHIS, N. J., DOUCLEFF, M. & CLORE, G. M. 2011. Transient, sparsely populated compact states of apo and calcium-loaded calmodulin probed by paramagnetic relaxation enhancement: interplay of conformational selection and induced fit. *Journal of the American Chemical Society,* 133**,** 18966-74.

ARORA, S., YANG, J. M. & HAIT, W. N. 2005. Identification of the ubiquitin-proteasome pathway in the regulation of the stability of eukaryotic elongation factor-2 kinase. *Cancer Research,* 65**,** 3806-10.

BABER, J. L., SZABO, A. & TJANDRA, N. 2001. Analysis of slow interdomain motion of macromolecules using NMR relaxation data. *Journal of the American Chemical Society,* 123**,** 3953-9.

BABU, Y. S., SACK, J. S., GREENHOUGH, T. J., BUGG, C. E., MEANS, A. R. & COOK, W. J. 1985. Three Dimensional Structure of Calmodulin. *Nature,* 315**,** 37-40.

BAGAGLIO, D. M., CHENG, E. H. C., GORELICK, F. S., MITSUI, K., NAIRN, A. C. & HAIT, W. N. 1993. Phosphorylation of elongation factor-ii in normal and malignant rat glial-cells. *Cancer Research,* 53**,** 2260-2264.

BAHLER, M. & RHOADS, A. 2002. Calmodulin signaling via the IQ motif. *Febs Letters,* 513**,** 107-13.

BARBATO, G., IKURA, M., KAY, L. E., PASTOR, R. W. & BAX, A. 1992. Backbone Dynamics of Calmodulin Studied by N-15 Relaxation Using Inverse Detected 2-Dimensional Nmr-Spectroscopy - the Central Helix Is Flexible. *Biochemistry,* 31**,** 5269-5278.

BAX, A. & GRISHAEV, A. 2005. Weak alignment NMR: a hawk-eyed view of biomolecular structure. *Current Opinion in Structural Biology,* 15**,** 563-70.

BAYLEY, P. M., FINDLAY, W. A. & MARTIN, S. R. 1996. Target recognition by calmodulin: Dissecting the kinetics and affinity of interaction using short peptide sequences. *Protein Science,* 5**,** 1215-1228.

BERNSTEIN, F. C., KOETZLE, T. F., WILLIAMS, G. J. B., MEYER, E. F., BRICE, M. D., RODGERS, J. R., KENNARD, O., SHIMANOUCHI, T. & TASUMI, M. 1977. Protein Data Bank - Computer-Based Archival File for Macromolecular Structures. *European Journal of Biochemistry,* 80**,** 319-324.

BERRIDGE, M. J., LIPP, P. & BOOTMAN, M. D. 2000. The versatility and universality of calcium signalling. *Nature Reviews Molecular Cell Biology,* 1**,** 11-21.

BERTINI, I., DEL BIANCO, C., GELIS, I., KATSAROS, N., LUCHINAT, C., PARIGI, G., PEANA, M., PROVENZANI, A. & ZORODDU, M. A. 2004. Experimentally exploring the conformational space sampled by domain reorientation in calmodulin. *Proceedings of the National Academy of Sciences of the United States of America,* 101**,** 6841-6.

BIEKOFSKY, R. R., MARTIN, S. R., BROWNE, J. P., BAYLEY, P. M. & FEENEY, J. 1998. Ca2+ coordination to backbone carbonyl oxygen atoms in calmodulin and other EF-hand proteins: N-15 chemical shifts as probes for monitoring individual-site Ca2+ coordination. *Biochemistry,* 37**,** 7617-7629.

BLACK, D. J., TRAN, Q. K. & PERSECHINI, A. 2004. Monitoring the total available calmodulin concentration in intact cells over the physiological range in free Ca2+. *Cell Calcium,* 35**,** 415-425.
BLOCH, F., HANSEN, W. W. & PACKARD, M. 1946. The Nuclear Induction Experiment. *Physical Review,* 70**,** 474-485.
BOSSEMEYER, D. 1995. Protein-Kinases - Structure and Function. *Febs Letters,* 369**,** 57-61.
BROWNE, G. J., FINN, S. G. & PROUD, C. G. 2004. Stimulation of the AMP-activated protein kinase leads to activation of eukaryotic elongation factor 2 kinase and to its phosphorylation at a novel site, Serine 398. *Journal of Biological Chemistry,* 279**,** 12220-12231.
BROWNE, G. J. & PROUD, C. G. 2004. A novel mTOR-regulated phosphorylation site in elongation factor 2 kinase modulates the activity of the kinase and its binding to calmodulin. *Molecular and Cellular Biology,* 24**,** 2986-2997.
BRUNGER, A. T., ADAMS, P. D., CLORE, G. M., DELANO, W. L., GROS, P., GROSSE-KUNSTLEVE, R. W., JIANG, J. S., KUSZEWSKI, J., NILGES, M., PANNU, N. S., READ, R. J., RICE, L. M., SIMONSON, T. & WARREN, G. L. 1998. Crystallography & NMR system: A new software suite for macromolecular structure determination. *Acta Crystallographica Section D-Biological Crystallography,* 54**,** 905-921.
CAVANAGH, J. 1996. *Protein NMR Spectroscopy: Principles and Practice*, Academic Press.
CHEEK, S., GINALSKI, K., ZHANG, H. & GRISHIN, N. V. 2005. A comprehensive update of the sequence and structure classification of kinases. *Bmc Structural Biology,* 5.
CHEN, K. & TJANDRA, N. 2012. The use of residual dipolar coupling in studying proteins by NMR. *Topics in current chemistry,* 326**,** 47-67.
CHEUNG, M. S., MAGUIRE, M. L., STEVENS, T. J. & BROADHURST, R. W. 2010. DANGLE: A Bayesian inferential method for predicting protein backbone dihedral angles and secondary structure. *Journal of Magnetic Resonance,* 202**,** 223-33.
CHIN, D. & MEANS, A. R. 2000. Calmodulin: a prototypical calcium sensor. *Trends in Cell Biology,* 10**,** 322-328.
CHOU, J. J., LI, S. P., KLEE, C. B. & BAX, A. 2001. Solution structure of Ca2+-calmodulin reveals flexible hand-like properties of its domains. *Nature Structural Biology,* 8**,** 990-997.
CLARK, K., MIDDELBEEK, J., DOROVKOV, M. V., FIGDOR, C. G., RYAZANOV, A. G., LASONDER, E. & VAN LEEUWEN, F. N. 2008. The alpha-kinases TRPM6 and TRPM7, but not eEF-2 kinase, phosphorylate the assembly domain of myosin IIA, IIB and IIC. *Febs Letters,* 582**,** 2993-7.
COTE, G. P., LUO, X., MURPHY, M. B. & EGELHOFF, T. T. 1997. Mapping of the novel protein kinase catalytic domain of Dictyostelium myosin II heavy chain kinase A. *Journal of Biological Chemistry,* 272**,** 6846-6849.
CRAWLEY, S. W. & COTE, G. P. 2009. Identification of dimer interactions required for the catalytic activity of the TRPM7 alpha-kinase domain. *Biochemical Journal,* 420**,** 115-122.
CRAWLEY, S. W., GHARAEI, M. S., YE, Q. L., YANG, Y. D., RAVEH, B., LONDON, N., SCHUELER-FURMAN, O., JIA, Z. C. & COTE, G. P. 2011. Autophosphorylation Activates Dictyostelium Myosin II Heavy Chain Kinase A by Providing a

Ligand for an Allosteric Binding Site in the alpha-Kinase Domain. *Journal of Biological Chemistry,* 286**,** 2607-2616.
CRIVICI, A. & IKURA, M. 1995. Molecular and Structural Basis of Target Recognition by Calmodulin. *Annual Review of Biophysics and Biomolecular Structure,* 24**,** 85-116.
CSERMELY, P., PALOTAI, R. & NUSSINOV, R. 2010. Induced fit, conformational selection and independent dynamic segments: an extended view of binding events. *Trends in Biochemical Sciences,* 35**,** 539-46.
CUERVO, A. M., BERGAMINI, E., BRUNK, U. T., DROGE, W., FFRENCH, M. & TERMAN, A. 2005. Autophagy and aging: the importance of maintaining "clean" cells. *Autophagy,* 1**,** 131-40.
DE DIEGO, I., KUPER, J., BAKALOVA, N., KURSULA, P. & WILMANNS, M. 2010. Molecular basis of the death-associated protein kinase-calcium/calmodulin regulator complex. *Science Signaling,* 3**,** ra6.
DELAGLIO, F., GRZESIEK, S., VUISTER, G. W., ZHU, G., PFEIFER, J. & BAX, A. 1995. Nmrpipe - a Multidimensional Spectral Processing System Based on Unix Pipes. *Journal of Biomolecular Nmr,* 6**,** 277-293.
DIGGLE, T. A., SEEHRA, C. K., HASE, S. & REDPATH, N. T. 1999. Analysis of the domain structure of elongation factor-2 kinase by mutagenesis. *Febs Letters,* 457**,** 189-192.
DORELEIJERS, J. F., SOUSA DA SILVA, A. W., KRIEGER, E., NABUURS, S. B., SPRONK, C. A., STEVENS, T. J., VRANKEN, W. F., VRIEND, G. & VUISTER, G. W. 2012. CING: an integrated residue-based structure validation program suite. *Journal of Biomolecular Nmr,* 54**,** 267-83.
DOROVKOV, M. V., PAVUR, K. S. & PETROV, A. G. 2002. Regulation of elongation factor-2 kinase by pH. *Biochemistry,* 41**,** 13444-13450.
DOSSET, P., HUS, J. C., MARION, D. & BLACKLEDGE, M. 2001. A novel interactive tool for rigid-body modeling of multi-domain macromolecules using residual dipolar couplings. *Journal of Biomolecular Nmr,* 20**,** 223-231.
DRENNAN, D. & RYAZANOV, A. G. 2004. Alpha-kinases: analysis of the family and comparison with conventional protein kinases. *Progress in Biophysics & Molecular Biology,* 85**,** 1-32.
DRUM, C. L., YAN, S. Z., BARD, J., SHEN, Y. Q., LU, D., SOELAIMAN, S., GRABAREK, Z., BOHM, A. & TANG, W. J. 2002. Structural basis for the activation of anthrax adenylyl cyclase exotoxin by calmodulin. *Nature,* 415**,** 396-402.
FALLON, J. L., HALLING, D. B., HAMILTON, S. L. & QUIOCHO, F. A. 2005. Structure of calmodulin bound to the hydrophobic IQ domain of the cardiac Ca(v)1.2 calcium channel. *Structure,* 13**,** 1881-6.
FISCHER, E. H. & KREBS, E. G. 1955. Conversion of phosphorylase b to phosphorylase a in muscle extracts. *The Journal of biological chemistry,* 216**,** 121-32.
FITTS, R. H. 1994. Cellular mechanisms of muscle fatigue. *Physiological reviews,* 74**,** 49-94.
FRANKE, D. & SVERGUN, D. I. 2009. DAMMIF, a program for rapid ab-initio shape determination in small-angle scattering. *Journal of Applied Crystallography,* 42**,** 342-346.
FREEMAN, R. 1987. *A handbook of nuclear magnetic resonance*, Longman Scientific & Technical.

GOLDBERG, J., NAIRN, A. C. & KURIYAN, J. 1996. Structural basis for the autoinhibition of calcium calmodulin-dependent protein kinase I. *Cell,* 84**,** 875-887.
GRABAREK, Z. 2005. Structure of a trapped intermediate of calmodulin: Calcium regulation of EF-hand proteins from a new perspective. *Journal of Molecular Biology,* 346**,** 1351-1366.
GRZESIEK, S. & BAX, A. 1992a. Correlating Backbone Amide and Side-Chain Resonances in Larger Proteins by Multiple Relayed Triple Resonance Nmr. *Journal of the American Chemical Society,* 114**,** 6291-6293.
GRZESIEK, S. & BAX, A. 1992b. An Efficient Experiment for Sequential Backbone Assignment of Medium-Sized Isotopically Enriched Proteins. *Journal of Magnetic Resonance,* 99**,** 201-207.
GSPONER, J., CHRISTODOULOU, J., CAVALLI, A., BUI, J. M., RICHTER, B., DOBSON, C. M. & VENDRUSCOLO, M. 2008. A coupled equilibrium shift mechanism in calmodulin-mediated signal transduction. *Structure,* 16**,** 736-46.
HANKS, S. K. & HUNTER, T. 1995. Protein Kinases .6. The Eukaryotic Protein-Kinase Superfamily - Kinase (Catalytic) Domain-Structure and Classification. *Faseb Journal,* 9**,** 576-596.
HANKS, S. K., QUINN, A. M. & HUNTER, T. 1988. The Protein-Kinase Family - Conserved Features and Deduced Phylogeny of the Catalytic Domains. *Science,* 241**,** 42-52.
HELLER, W. T., KRUEGER, J. K. & TREWHELLA, J. 2003. Further insights into calmodulin-myosin light chain kinase interaction from solution scattering and shape restoration. *Biochemistry,* 42**,** 10579-88.
HIGMAN, V. A., BOYD, J., SMITH, L. J. & REDFIELD, C. 2011. Residual dipolar couplings: are multiple independent alignments always possible? *Journal of Biomolecular Nmr,* 49**,** 53-60.
HOEFLICH, K. P. & IKURA, M. 2002. Calmodulin in action: Diversity in target recognition and activation mechanisms. *Cell,* 108**,** 739-742.
HOGBEN, H. J., KRZYSTYNIAK, M., CHARNOCK, G. T., HORE, P. J. & KUPROV, I. 2011. Spinach--a software library for simulation of spin dynamics in large spin systems. *Journal of Magnetic Resonance,* 208**,** 179-94.
HOOK, S. S. & MEANS, A. R. 2001. Ca2+/CaM-dependent kinases: From activation to function. *Annual Review of Pharmacology and Toxicology,* 41**,** 471-505.
HORE, P. J. 1995. *Nuclear magnetic resonance,* Oxford; New York, Oxford University Press.
IKURA, M. 1996. Calcium binding and conformational response in EF-hand proteins. *Trends in Biochemical Sciences,* 21**,** 14-17.
IKURA, M. & BAX, A. 1992. Isotope-filtered 2D NMR of a protein-peptide complex: study of a skeletal muscle myosin light chain kinase fragment bound to calmodulin. *Journal of the American Chemical Society,* 114**,** 2433-2440.
JOHNSON, L. N., LOWE, E. D., NOBLE, M. E. M. & OWEN, D. J. 1998. The structural basis for substrate recognition and control by protein kinases. *Febs Letters,* 430**,** 1-11.
JORGENSEN, R., MERRILL, A. R. & ANDERSEN, G. R. 2006. The life and death of translation elongation factor 2. *Biochemical Society Transactions,* 34**,** 1-6.

JORGENSEN, R., ORTIZ, P. A., CARR-SCHMID, A., NISSEN, P., KINZY, T. G. & ANDERSEN, G. R. 2003. Two crystal structures demonstrate large conformational changes in the eukaryotic ribosomal translocase. *Nature Structural Biology,* 10**,** 379-385.

KAY, L. E., IKURA, M., TSCHUDIN, R. & BAX, A. 1990. 3-Dimensional Triple-Resonance Nmr-Spectroscopy of Isotopically Enriched Proteins. *Journal of Magnetic Resonance,* 89**,** 496-514.

KEELER, J. 2010. *Understanding NMR Spectroscopy*, Wiley.

KIM, S. A., HEINZE, K. G., WAXHAM, M. N. & SCHWILLE, P. 2004. Intracellular calmodulin availability accessed with two-photon cross-correlation. *Proceedings of the National Academy of Sciences of the United States of America,* 101**,** 105-10.

KNEBEL, A., MORRICE, N. & COHEN, P. 2001. A novel method to identify protein kinase substrates: eEF2 kinase is phosphorylated and inhibited by SAPK4/p38 delta. *Embo Journal,* 20**,** 4360-4369.

KNIGHTON, D. R., XUONG, N. H., TAYLOR, S. S. & SOWADSKI, J. M. 1991a. Crystallization Studies of Camp-Dependent Protein-Kinase - Cocrystals of the Catalytic Subunit with a 20 Amino-Acid Residue Peptide Inhibitor and Mgatp Diffract to 3.0 a Resolution. *Journal of Molecular Biology,* 220**,** 217-220.

KNIGHTON, D. R., ZHENG, J. H., TENEYCK, L. F., ASHFORD, V. A., XUONG, N. H., TAYLOR, S. S. & SOWADSKI, J. M. 1991b. Crystal-Structure of the Catalytic Subunit of Cyclic Adenosine-Monophosphate Dependent Protein-Kinase. *Science,* 253**,** 407-414.

KNIGHTON, D. R., ZHENG, J. H., TENEYCK, L. F., XUONG, N. H., TAYLOR, S. S. & SOWADSKI, J. M. 1991c. Structure of a Peptide Inhibitor Bound to the Catalytic Subunit of Cyclic Adenosine-Monophosphate Dependent Protein-Kinase. *Science,* 253**,** 414-420.

KONAREV, P. V., PETOUKHOV, M. V., VOLKOV, V. V. & SVERGUN, D. I. 2006. ATSAS 2.1, a program package for small-angle scattering data analysis. *Journal of Applied Crystallography,* 39**,** 277-286.

KOSHLAND, D. E. 1958. Application of a Theory of Enzyme Specificity to Protein Synthesis. *Proceedings of the National Academy of Sciences of the United States of America,* 44**,** 98-104.

KOVALEVSKAYA, N., WATERBEEMD, M., BOKHOVCHUK, F., BATE, N., BINDELS, R. J. M., HOENDEROP, J. J. & VUISTER, G. 2013. Structural analysis of calmodulin binding to ion channels demonstrates the role of its plasticity in regulation. *Pfl√¯°gers Archiv - European Journal of Physiology***,** 1-13.

KOVRIGIN, E. L. 2012. NMR line shapes and multi-state binding equilibria. *Journal of Biomolecular Nmr,* 53**,** 257-70.

KOZIN, M. B. & SVERGUN, D. I. 2001. Automated matching of high- and low-resolution structural models. *Journal of Applied Crystallography,* 34**,** 33-41.

KRAUT, J. A. & MADIAS, N. E. 2010. Metabolic acidosis: pathophysiology, diagnosis and management. *Nature reviews. Nephrology,* 6**,** 274-85.

KREZEL, A. & BAL, W. 2004. A formula for correlating pKa values determined in D2O and H2O. *Journal of inorganic biochemistry,* 98**,** 161-6.

KRUEGER, J. K., GALLAGHER, S. C., ZHI, G., GEGUCHADZE, R., PERSECHINI, A., STULL, J. T. & TREWHELLA, J. 2001. Activation of myosin light chain kinase

requires translocation of bound calmodulin. *The Journal of biological chemistry,* 276**,** 4535-8.
KRUISWIJK, F., YUNIATI, L., MAGLIOZZI, R., LOW, T. Y., LIM, R., BOLDER, R., MOHAMMED, S., PROUD, C. G., HECK, A. J., PAGANO, M. & GUARDAVACCARO, D. 2012. Coupled activation and degradation of eEF2K regulates protein synthesis in response to genotoxic stress. *Science Signaling,* 5**,** ra40.
KUBONIWA, H., TJANDRA, N., GRZESIEK, S., REN, H., KLEE, C. B. & BAX, A. 1995. Solution Structure of Calcium-Free Calmodulin. *Nature Structural Biology,* 2**,** 768-776.
KUMAR, V., CHICHILI, V. P., ZHONG, L., TANG, X., VELAZQUEZ-CAMPOY, A., SHEU, F. S., SEETHARAMAN, J., GERGES, N. Z. & SIVARAMAN, J. 2013. Structural basis for the interaction of unstructured neuron specific substrates neuromodulin and neurogranin with Calmodulin. *Scientific Reports,* 3**,** 1392.
KUPROV, I. 2008. Polynomially scaling spin dynamics II: further state-space compression using Krylov subspace techniques and zero track elimination. *Journal of Magnetic Resonance,* 195**,** 45-51.
LAPORTE, D. C., WIERMAN, B. M. & STORM, D. R. 1980. Calcium-Induced Exposure of a Hydrophobic Surface on Calmodulin. *Biochemistry,* 19**,** 3814-3819.
LEAVITT, S. & FREIRE, E. 2001. Direct measurement of protein binding energetics by isothermal titration calorimetry. *Current Opinion in Structural Biology,* 11**,** 560-6.
LEPRIVIER, G., REMKE, M., ROTBLAT, B., DUBUC, A., MATEO, A. R., KOOL, M., AGNIHOTRI, S., EL-NAGGAR, A., YU, B., SOMASEKHARAN, S. P., FAUBERT, B., BRIDON, G., TOGNON, C. E., MATHERS, J., THOMAS, R., LI, A., BAROKAS, A., KWOK, B., BOWDEN, M., SMITH, S., WU, X., KORSHUNOV, A., HIELSCHER, T., NORTHCOTT, P. A., GALPIN, J. D., AHERN, C. A., WANG, Y., MCCABE, M. G., COLLINS, V. P., JONES, R. G., POLLAK, M., DELATTRE, O., GLEAVE, M. E., JAN, E., PFISTER, S. M., PROUD, C. G., DERRY, W. B., TAYLOR, M. D. & SORENSEN, P. H. 2013. The eEF2 kinase confers resistance to nutrient deprivation by blocking translation elongation. *Cell,* 153**,** 1064-79.
LEVITT, M. H. 2001. *Spin Dynamics: Basics of Nuclear Magnetic Resonance*, Wiley.
LI, X., ALAFUZOFF, I., SOININEN, H., WINBLAD, B. & PEI, J. J. 2005. Levels of mTOR and its downstream targets 4E-BP1, eEF2, and eEF2 kinase in relationships with tau in Alzheimer's disease brain. *Febs Journal,* 272**,** 4211-4220.
LIPFERT, J. & DONIACH, S. 2007. Small-angle X-ray scattering from RNA, proteins, and protein complexes. *Annual Review of Biophysics and Biomolecular Structure,* 36**,** 307-27.
LUBYPHELPS, K., HORI, M., PHELPS, J. M. & WON, D. 1995. Ca2+-Regulated Dynamic Compartmentalization of Calmodulin in Living Smooth-Muscle Cells. *Journal of Biological Chemistry,* 270**,** 21532-21538.
MA, B., KUMAR, S., TSAI, C. J. & NUSSINOV, R. 1999. Folding funnels and binding mechanisms. *Protein engineering,* 12**,** 713-20.
MADHUSUDAN, TRAFNY, E. A., XUONG, N. H., ADAMS, J. A., TEN EYCK, L. F., TAYLOR, S. S. & SOWADSKI, J. M. 1994. cAMP-dependent protein kinase:

crystallographic insights into substrate recognition and phosphotransfer. *Protein science : a publication of the Protein Society,* 3**,** 176-87.
MAL, T. K., IKURA, M. & KAY, L. E. 2002. The ATCUN domain as a probe of intermolecular interactions: Application to calmodulin-peptide complexes. *Journal of the American Chemical Society,* 124**,** 14002-14003.
MANNING, G., PLOWMAN, G. D., HUNTER, T. & SUDARSANAM, S. 2002a. Evolution of protein kinase signaling from yeast to man. *Trends in Biochemical Sciences,* 27**,** 514-520.
MANNING, G., WHYTE, D. B., MARTINEZ, R., HUNTER, T. & SUDARSANAM, S. 2002b. The protein kinase complement of the human genome. *Science,* 298**,** 1912-1934.
MARION, D., DRISCOLL, P. C., KAY, L. E., WINGFIELD, P. T., BAX, A., GRONENBORN, A. M. & CLORE, G. M. 1989a. Overcoming the Overlap Problem in the Assignment of H-1-Nmr Spectra of Larger Proteins by Use of 3-Dimensional Heteronuclear H-1-N-15 Hartmann-Hahn Multiple Quantum Coherence and Nuclear Overhauser Multiple Quantum Coherence Spectroscopy - Application to Interleukin-1-Beta. *Biochemistry,* 28**,** 6150-6156.
MARION, D., KAY, L. E., SPARKS, S. W., TORCHIA, D. A. & BAX, A. 1989b. 3-Dimensional Heteronuclear Nmr of N-15-Labeled Proteins. *Journal of the American Chemical Society,* 111**,** 1515-1517.
MARKLEY, J. L. 1973. Nuclear magnetic resonance studies of trypsin inhibitors. Histidines of virgin and modified soybean trypsin inhibitor (Kunitz). *Biochemistry,* 12**,** 2245-50.
MARQUARDT, D. W. 1963. An Algorithm for Least-Squares Estimation of Nonlinear Parameters. *Journal of the Society for Industrial and Applied Mathematics,* 11**,** 431-441.
MCLEOD, L. E. & PROUD, C. G. 2002. ATP depletion increases phosphorylation of elongation factor eEF2 in adult cardiomyocytes independently of inhibition of mTOR signalling. *Febs Letters,* 531**,** 448-452.
MEADOR, W. E., MEANS, A. R. & QUIOCHO, F. A. 1992. Target Enzyme Recognition by Calmodulin - 2.4-Angstrom Structure of a Calmodulin-Peptide Complex. *Science,* 257**,** 1251-1255.
MEIJER, A. J. & CODOGNO, P. 2004. Regulation and role of autophagy in mammalian cells. *The international journal of biochemistry & cell biology,* 36**,** 2445-62.
MIDDELBEEK, J., CLARK, K., VENSELAAR, H., HUYNEN, M. A. & VAN LEEUWEN, F. N. 2010. The alpha-kinase family: an exceptional branch on the protein kinase tree. *Cellular and Molecular Life Sciences,* 67**,** 875-890.
MILLET, O., LORIA, J. P., KROENKE, C. D., PONS, M. & PALMER, A. G. 2000. The static magnetic field dependence of chemical exchange linebroadening defines the NMR chemical shift time scale. *Journal of the American Chemical Society,* 122**,** 2867-2877.
MITSUI, K., BRADY, M., PALFREY, H. C. & NAIRN, A. C. 1993. Purification and Characterization of Calmodulin-Dependent Protein Kinase-Iii from Rabbit Reticulocytes and Rat Pancreas. *Journal of Biological Chemistry,* 268**,** 13422-13433.
MITTL, P. R. E. & SCHNEIDER-BRACHERT, W. 2007. Sel1-like repeat proteins in signal transduction. *Cellular Signalling,* 19**,** 20-31.

MONTELIONE, G. T., LYONS, B. A., EMERSON, S. D. & TASHIRO, M. 1992. An Efficient Triple Resonance Experiment Using C-13 Isotropic Mixing for Determining Sequence-Specific Resonance Assignments of Isotopically-Enriched Proteins. *Journal of the American Chemical Society,* 114**,** 10974-10975.
MOORE, C. E., MIKOLAJEK, H., REGUFE DA MOTA, S., WANG, X., KENNEY, J. W., WERNER, J. M. & PROUD, C. G. 2015. Elongation factor 2 kinase is regulated by proline hydroxylation and protects cells during hypoxia. *Molecular and Cellular Biology*.
MORRIS, G. A. & FREEMAN, R. 1979. Enhancement of Nuclear Magnetic-Resonance Signals by Polarization Transfer. *Journal of the American Chemical Society,* 101**,** 760-762.
MURZIN, A. G., BRENNER, S. E., HUBBARD, T. & CHOTHIA, C. 1995. Scop - a Structural Classification of Proteins Database for the Investigation of Sequences and Structures. *Journal of Molecular Biology,* 247**,** 536-540.
NAIRN, A. C. & PALFREY, H. C. 1987. Identification of the major Mr 100,000 substrate for calmodulin-dependent protein kinase III in mammalian cells as elongation factor-2. *The Journal of biological chemistry,* 262**,** 17299-303.
NANOTEMPER 2013a. MST Demo Report.
NANOTEMPER 2013b. MST Internal Measurements Report.
NELDER, J. A. & MEAD, R. 1965. A Simplex Method for Function Minimization. *The Computer Journal,* 7**,** 308-313.
NERI, D. & SUPURAN, C. T. 2011. Interfering with pH regulation in tumours as a therapeutic strategy. *Nature reviews. Drug discovery,* 10**,** 767-77.
OGIER-DENIS, E. & CODOGNO, P. 2003. Autophagy: a barrier or an adaptive response to cancer. *Biochimica et biophysica acta,* 1603**,** 113-28.
OSAWA, M., TOKUMITSU, H., SWINDELLS, M. B., KURIHARA, H., ORITA, M., SHIBANUMA, T., FURUYA, T. & IKURA, M. 1999. A novel target recognition revealed by calmodulin in complex with Ca2+-calmodulin-dependent kinase kinase. *Nature Structural Biology,* 6**,** 819-824.
OTTING, G. & WUTHRICH, K. 1990. Heteronuclear filters in two-dimensional [1H, 1H]-NMR spectroscopy: combined use with isotope labelling for studies of macromolecular conformation and intermolecular interactions. *Quarterly reviews of biophysics,* 23**,** 39-96.
PADRE, R. C. & STULL, J. T. 2000. Conformational requirements for Ca2+/calmodulin binding and activation of myosin light chain kinase. *Febs Letters,* 472**,** 148-152.
PALFREY, H. C. 1983. Presence in Many Mammalian-Tissues of an Identical Major Cytosolic Substrate (Mr-100000) for Calmodulin-Dependent Protein-Kinase. *Febs Letters,* 157**,** 183-190.
PARMER, T. G., WARD, M. D., YURKOW, E. J., VYAS, V. H., KEARNEY, T. J. & HAIT, W. N. 1999. Activity and regulation by growth factors of calmodulin dependent protein kinase III (elongation factor 2-kinase) in human breast cancer. *British Journal of Cancer,* 79**,** 59-64.
PAVUR, K. S., PETROV, A. N. & RYAZANOV, A. G. 2000. Mapping the functional domains of elongation factor-2 kinase. *Biochemistry,* 39**,** 12216-12224.
PEERSEN, O. B., MADSEN, T. S. & FALKE, J. J. 1997. Intermolecular tuning of calmodulin by target peptides and proteins: differential effects on Ca2+

binding and implications for kinase activation. *Protein science : a publication of the Protein Society,* 6**,** 794-807.
PERSECHINI, A. & CRONK, B. 1999. The relationship between the free concentrations of Ca2+ and Ca2+-calmodulin in intact cells. *The Journal of biological chemistry,* 274**,** 6827-30.
PETOUKHOV, M. V., KONAREV, P. V., KIKHNEY, A. G. & SVERGUN, D. I. 2007. ATSAS 2.1 - towards automated and web-supported small-angle scattering data analysis. *Journal of Applied Crystallography,* 40**,** s223-s228.
PETOUKHOV, M. V. & SVERGUN, D. I. 2005. Global rigid body modeling of macromolecular complexes against small-angle scattering data. *Biophysical Journal,* 89**,** 1237-1250.
PETTERSEN, E. F., GODDARD, T. D., HUANG, C. C., COUCH, G. S., GREENBLATT, D. M., MENG, E. C. & FERRIN, T. E. 2004. UCSF Chimera--a visualization system for exploratory research and analysis. *Journal of computational chemistry,* 25**,** 1605-12.
PIGOTT, C. R., MIKOLAJEK, H., MOORE, C. E., FINN, S. J., PHIPPEN, C. W., WERNER, J. M. & PROUD, C. G. 2012. Insights into the regulation of eukaryotic elongation factor 2 kinase and the interplay between its domains. *Biochemical Journal,* 442**,** 105-118.
PRICE, N. T., REDPATH, N. T., SEVERINOV, K. V., CAMPBELL, D. G., RUSSELL, J. M. & PROUD, C. G. 1991. Identification of the Phosphorylation Sites in Elongation Factor-Ii from Rabbit Reticulocytes. *Febs Letters,* 282**,** 253-258.
PROUD, C. G. 2007. Signalling to translation: how signal transduction pathways control the protein synthetic machinery. *Biochemical Journal,* 403**,** 217-234.
PURCELL, E. M., TORREY, H. C. & POUND, R. V. 1946. Resonance Absorption by Nuclear Magnetic Moments in a Solid. *Physical Review,* 69**,** 37-38.
PUTNAM, C. D., HAMMEL, M., HURA, G. L. & TAINER, J. A. 2007. X-ray solution scattering (SAXS) combined with crystallography and computation: defining accurate macromolecular structures, conformations and assemblies in solution. *Quarterly reviews of biophysics,* 40**,** 191-285.
PYR DIT RUYS, S., WANG, X. M., SMITH, E. M., HERINCKX, G., HUSSAIN, N., RIDER, M. H., VERTOMMEN, D. & PROUD, C. G. 2012. Identification of autophosphorylation sites in eukaryotic elongation factor-2 kinase. *Biochemical Journal,* 442**,** 681-692.
RAKHILIN, S. V., OLSON, P. A., NISHI, A., STARKOVA, N. N., FIENBERG, A. A., NAIRN, A. C., SURMEIER, D. J. & GREENGARD, P. 2004. A network of control mediated by regulator of calcium/calmodulin-dependent signaling. *Science,* 306**,** 698-701.
RATTLE, H. W. E. 1995. *An NMR Primer for Life Scientists*, Partnership Press.
REDPATH, N. T., PRICE, N. T. & PROUD, C. G. 1996. Cloning and expression of cDNA encoding protein synthesis elongation factor-2 kinase. *Journal of Biological Chemistry,* 271**,** 17547-17554.
REDPATH, N. T., PRICE, N. T., SEVERINOV, K. V. & PROUD, C. G. 1993. Regulation of elongation factor-ii by multisite phosphorylation. *European Journal of Biochemistry,* 213**,** 689-699.
RELLOS, P., PIKE, A. C. W., NIESEN, F. H., SALAH, E., LEE, W. H., VON DELFT, F. & KNAPP, S. 2010. Structure of the CaMKII delta/Calmodulin Complex Reveals the Molecular Mechanism of CaMKII Kinase Activation. *Plos Biology,* 8.

RHOADS, A. R. & FRIEDBERG, F. 1997. Sequence motifs for calmodulin recognition. *Faseb Journal,* 11**,** 331-340.
RIEPING, W., HABECK, M., BARDIAUX, B., BERNARD, A., MALLIAVIN, T. E. & NILGES, M. 2007. ARIA2: Automated NOE assignment and data integration in NMR structure calculation. *Bioinformatics,* 23**,** 381-382.
ROBERTSON, I., SPYRACOPOULOS, L. & SYKES, B. 2009. The Evaluation of Isotope Editing and Filtering for Protein, Ligand Interaction Elucidation by Nmr. *In:* PUGLISI, J. (ed.) *Biophysics and the Challenges of Emerging Threats.* Springer Netherlands.
ROESSLE, M. 2012. EMBO Course 2012. *Fach Hochshule Lubeck*.
RUCKERT, M. & OTTING, G. 2000. Alignment of biological macromolecules in novel nonionic liquid crystalline media for NMR experiments. *Journal of the American Chemical Society,* 122**,** 7793-7797.
RYAZANOV, A. G., PAVUR, K. S. & DOROVKOV, M. V. 1999. Alpha-kinases: a new class of protein kinases with a novel catalytic domain. *Current Biology,* 9**,** R43-R45.
RYAZANOV, A. G., RUDKIN, B. B. & SPIRIN, A. S. 1991. Regulation of Protein-Synthesis at the Elongation Stage - New Insights into the Control of Gene-Expression in Eukaryotes. *Febs Letters,* 285**,** 170-175.
RYAZANOV, A. G., WARD, M. D., MENDOLA, C. E., PAVUR, K. S., DOROVKOV, M. V., WIEDMANN, M., ERDJUMENTBROMAGE, H., TEMPST, P., PARMER, T. G., PROSTKO, C. R., GERMINO, F. J. & HAIT, W. N. 1997. Identification of a new class of protein kinases represented by eukaryotic elongation factor-2 kinase. *Proceedings of the National Academy of Sciences of the United States of America,* 94**,** 4884-4889.
RYAZANOVA, L. V., DOROVKOV, M. V., ANSARI, A. & RYAZANOV, A. G. 2004. Characterization of the protein kinase activity of TRPM7/ChaK1, a protein kinase fused to the transient receptor potential ion channel. *Journal of Biological Chemistry,* 279**,** 3708-3716.
RYAZANOVA, L. V., PAVUR, K. S., PETROV, A. N., DOROVKOV, M. V. & RYAZANOV, A. G. 2001. Novel type of signaling molecules: Protein kinases covalently linked with ion channels. *Molecular Biology,* 35**,** 271-283.
SANABRIA, H., DIGMAN, M. A., GRATTON, E. & WAXHAM, M. N. 2008. Spatial diffusivity and availability of intracellular calmodulin. *Biophysical Journal,* 95**,** 6002-15.
SCHEEFF, E. D. & BOURNE, P. E. 2005. Structural evolution of the protein kinase-like superfamily. *Plos Computational Biology,* 1**,** 359-381.
SCHESCHONKA, A., FINDLOW, S., SCHEMM, R., EL FAR, O., CALDWELL, J. H., CRUMP, M. P., HOLDEN-DYE, K., O'CONNOR, V., BETZ, H. & WERNER, J. M. 2008. Structural determinants of calmodulin binding to the intracellular c-terminal domain of the metabotropic glutamate receptor 7A. *Journal of Biological Chemistry,* 283**,** 5577-5588.
SCHUMACHER, M. A., RIVARD, A. F., BACHINGER, H. P. & ADELMAN, J. P. 2001. Structure of the gating domain of a Ca2+-activated K+ channel complexed with Ca2+/calmodulin. *Nature,* 410**,** 1120-4.
SEATON, B. A., HEAD, J. F., ENGELMAN, D. M. & RICHARDS, F. M. 1985. Calcium-induced increase in the radius of gyration and maximum dimension of calmodulin measured by small-angle X-ray scattering. *Biochemistry,* 24**,** 6740-3.

SEIDEL, S. A., DIJKMAN, P. M., LEA, W. A., VAN DEN BOGAART, G., JERABEK-WILLEMSEN, M., LAZIC, A., JOSEPH, J. S., SRINIVASAN, P., BAASKE, P., SIMEONOV, A., KATRITCH, I., MELO, F. A., LADBURY, J. E., SCHREIBER, G., WATTS, A., BRAUN, D. & DUHR, S. 2013. Microscale thermophoresis quantifies biomolecular interactions under previously challenging conditions. *Methods,* 59**,** 301-15.

SHEN, Y. & BAX, A. 2013. Protein backbone and sidechain torsion angles predicted from NMR chemical shifts using artificial neural networks. *Journal of Biomolecular Nmr,* 56**,** 227-41.

SMITH, E. M. & PROUD, C. G. 2008. cdc2-cyclin B regulates eEF2 kinase activity in a cell cycle- and amino acid-dependent manner. *Embo Journal,* 27**,** 1005-1016.

SONENBERG, N. & HINNEBUSCH, A. G. 2009. Regulation of Translation Initiation in Eukaryotes: Mechanisms and Biological Targets. *Cell,* 136**,** 731-745.

SPAHN, C. M. T., GOMEZ-LORENZO, M. G., GRASSUCCI, R. A., JORGENSON, R., ANDERSEN, G. R., BECKMANN, R., PENCZEK, P. A., BALLESTA, J. P. G. & FRANK, J. 2004. Domain movements of elongation factor eEF2 and the eukaryotic 80S ribosome facilitate tRNA translocation. *Embo Journal,* 23**,** 1008-1019.

SPERA, S. 1991. Measurement of the exchange rates of rapidly exchanging amido protons: Application to the study of calmodulin and its complex with a myosin light chain kinase fragment. *Journal of Biomolecular Nmr***,** 155-165.

STEINBERG, R. A., CAUTHRON, R. D., SYMCOX, M. M. & SHUNTOH, H. 1993. Autoactivation of catalytic (C alpha) subunit of cyclic AMP-dependent protein kinase by phosphorylation of threonine 197. *Molecular and Cellular Biology,* 13**,** 2332-41.

STRYNADKA, N. C. J. & JAMES, M. N. G. 1989. Crystal-Structures of the Helix-Loop-Helix Calcium-Binding Proteins. *Annual Review of Biochemistry,* 58**,** 951-998.

SUTHERLAND, E. W., JR. & WOSILAIT, W. D. 1955. Inactivation and activation of liver phosphorylase. *Nature,* 175**,** 169-70.

SVERGUN, D., BARBERATO, C. & KOCH, M. H. J. 1995. CRYSOL - A program to evaluate x-ray solution scattering of biological macromolecules from atomic coordinates. *Journal of Applied Crystallography,* 28**,** 768-773.

SVERGUN, D. I. 1992. Determination of the Regularization Parameter in Indirect-Transform Methods Using Perceptual Criteria. *Journal of Applied Crystallography,* 25**,** 495-503.

SWINDELLS, M. B. & IKURA, M. 1996. Pre-formation of the semi-open conformation by the apo-calmodulin C-terminal domain and implications for binding IQ-motifs. *Nature Structural Biology,* 3**,** 501-504.

SWULIUS, M. T. & WAXHAM, M. N. 2008. Ca(2+)/calmodulin-dependent protein kinases. *Cellular and Molecular Life Sciences,* 65**,** 2637-2657.

TAVARES, C. D., FERGUSON, S. B., GILES, D. H., WANG, Q., WELLMANN, R. M., O'BRIEN, J. P., WARTHAKA, M., BRODBELT, J. S., REN, P. & DALBY, K. N. 2014. The molecular mechanism of eukaryotic elongation factor 2 kinase activation. *The Journal of biological chemistry,* 289**,** 23901-16.

TAVARES, C. D. J., O'BRIEN, J. P., ABRAMCZYK, O., DEVKOTA, A. K., SHORES, K. S., FERGUSON, S. B., KAOUD, T. S., WARTHAKA, M., MARSHALL, K. D., KELLER, K. M., ZHANG, Y., BRODBELT, J. S., OZPOLAT, B. & DOLBY, K. N. 2012.

Calcium/Calmodulin Stimulates the Autophosphorylation of Elongation Factor 2 Kinase on Thr-348 and Ser-500 To Regulate Its Activity and Calcium Dependence. *Biochemistry,* 51**,** 2232-2245.
TAYLOR, D. J., NILSSON, J., MERRILL, A. R., ANDERSEN, G. R., NISSEN, P. & FRANK, J. 2007. Structures of modified eEF2.80S ribosome complexes reveal the role of GTP hydrolysis in translocation. *Embo Journal,* 26**,** 2421-2431.
TAYLOR, S. S., KNIGHTON, D. R., ZHENG, J., TEN EYCK, L. F. & SOWADSKI, J. M. 1992. Structural framework for the protein kinase family. *Annual review of cell biology,* 8**,** 429-62.
TIDOW, H. & NISSEN, P. 2013. Structural diversity of calmodulin binding to its target sites. *The FEBS journal,* 280**,** 5551-65.
TJANDRA, N. & BAX, A. 1997. Direct measurement of distances and angles in biomolecules by NMR in a dilute liquid crystalline medium. *Science,* 278**,** 1111-4.
TJANDRA, N., GRZESIEK, S. & BAX, A. 1996. Magnetic field dependence of nitrogen-proton J splittings in N-15-enriched human ubiquitin resulting from relaxation interference and residual dipolar coupling. *Journal of the American Chemical Society,* 118**,** 6264-6272.
VACHETTE, P. 2010. EMBO practical course on solution scattering from biological macromolecules.
VOLKOV, V. V. & SVERGUN, D. I. 2003. Uniqueness of ab initio shape determination in small-angle scattering. *Journal of Applied Crystallography,* 36**,** 860-864.
VRANKEN, W. F., BOUCHER, W., STEVENS, T. J., FOGH, R. H., PAJON, A., LLINAS, P., ULRICH, E. L., MARKLEY, J. L., IONIDES, J. & LAUE, E. D. 2005. The CCPN data model for NMR spectroscopy: Development of a software pipeline. *Proteins-Structure Function and Bioinformatics,* 59**,** 687-696.
WALTERSSON, Y., LINSE, S., BRODIN, P. & GRUNDSTROM, T. 1993. Mutational Effects on the Cooperativity of Ca2+ Binding in Calmodulin. *Biochemistry,* 32**,** 7866-7871.
WANG, X., XIE, J., DA MOTA, S. R., MOORE, C. E. & PROUD, C. G. 2015. Regulated stability of eukaryotic elongation factor 2 kinase requires intrinsic but not ongoing activity. *The Biochemical journal,* 467**,** 321-31.
WANG, X. M., CAMPBELL, L. E., MILLER, C. M. & PROUD, C. G. 1998. Amino acid availability regulates p70 S6 kinase and multiple translation factors. *Biochemical Journal,* 334**,** 261-267.
WANG, X. M., LI, W., WILLIAMS, M., TERADA, N., ALESSI, D. R. & PROUD, C. G. 2001. Regulation of elongation factor 2 kinase by p90(RSK1) and p70 S6 kinase. *Embo Journal,* 20**,** 4370-4379.
WILDEN, B., SAVELSBERGH, A., RODNINA, M. V. & WINTERMEYER, W. 2006. Role and timing of GTP binding and hydrolysis during EF-G-dependent tRNA translocation on the ribosome. *Proceedings of the National Academy of Sciences of the United States of America,* 103**,** 13670-13675.
WILLIAMSON, M. P. 2013. Using chemical shift perturbation to characterise ligand binding. *Progress in Nuclear Magnetic Resonance Spectroscopy,* 73**,** 1-16.

WU, H., YANG, J. M., JIN, S., ZHANG, H. Y. & HAIT, W. N. 2006. Elongation factor-2 kinase regulates autophagy in human glioblastoma cells. *Cancer Research,* 66**,** 3015-3023.

XIE, J., MIKOLAJEK, H., PIGOTT, C. R., HOOPER, K. J., MELLOWS, T., MOORE, C. E., MOHAMMED, H., WERNER, J. M., THOMAS, G. J. & PROUD, C. G. 2015. Molecular Mechanism for the Control of Eukaryotic Elongation Factor 2 Kinase by pH: Role in Cancer Cell Survival. *Molecular and Cellular Biology,* 35**,** 1805-24.

YAMAGUCHI, H., MATSUSHITA, M., NAIRN, A. C. & KURIYAN, J. 2001. Crystal structure of the atypical protein kinase domain of a TRP channel with phosphotransferase activity. *Molecular Cell,* 7**,** 1047-1057.

YAMAZAKI, T., FORMANKAY, J. D. & KAY, L. E. 1993. 2-Dimensional Nmr Experiments for Correlating C-13-Beta and H-1-Delta/Epsilon Chemical-Shifts of Aromatic Residues in C-13-Labeled Proteins Via Scalar Couplings. *Journal of the American Chemical Society,* 115**,** 11054-11055.

YAMNIUK, A. P. & VOGEL, H. J. 2004. Calmodulin's flexibility allows for promiscuity in its interactions with target proteins and peptides. *Molecular Biotechnology,* 27**,** 33-57.

YE, Q. L., CRAWLEY, S. W., YANG, Y. D., COTE, G. P. & JIA, Z. C. 2010. Crystal Structure of the alpha-Kinase Domain of Dictyostelium Myosin Heavy Chain Kinase A. *Science Signaling,* 3.

ZHANG, M., TANAKA, T. & IKURA, M. 1995. Calcium-Induced Conformational Transition Revealed by the Solution Structure of Apo Calmodulin. *Nature Structural Biology,* 2**,** 758-767.

ZHANG, X., GUREASKO, J., SHEN, K., COLE, P. A. & KURIYAN, J. 2006. An allosteric mechanism for activation of the kinase domain of epidermal growth factor receptor. *Cell,* 125**,** 1137-49.

ZHENG, J. H., KNIGHTON, D. R., PARELLO, J., TAYLOR, S. S. & SOWADSKI, J. M. 1991. Crystallization of Catalytic Subunit of Adenosine Cyclic Monophosphate-Dependent Protein-Kinase. *Methods in Enzymology,* 200**,** 508-521.

ZWAHLEN, C., LEGAULT, P., VINCENT, S. B. J. F., GREENBLATT, J., KONRAT, R. & KAY, L. E. 1997. Methods for Measurement of Intermolecular NOEs by Multinuclear NMR Spectroscopy:‚Äâ Application to a Bacteriophage Œª N-Peptide/boxB RNA Complex. *Journal of the American Chemical Society,* 119**,** 6711-6721.